Cerebrovascular alterations associated with 16p11.2 deletion autism syndrome

Julie Ouellette

Thesis submitted to the University of Ottawa in partial fulfillment
of the requirements for the Doctorate in Philosophy in Neuroscience

Department of Cellular & Molecular Medicine
Faculty of Medicine
University of Ottawa

Abstract

Brain development and function are highly reliant on adequate establishment and maintenance of vascular networks. As such, early impairments in vascular health can lead to neurodevelopmental anomalies. Despite a wealth of knowledge on neuronal underpinnings of autism spectrum disorders (ASD), vascular contributions to ASD have remained largely overlooked. ASD are neurodevelopmental conditions associated with genetic origins such as the common 16p11.2 deletion, which leads to a haploinsufficiency of ~30 genes on chromosome 16 in humans and chromosome 7 in mice. We revealed 16p11.2 deletion-induced endothelial-dependent structural and functional vascular abnormalities in the mouse brain, establishing a novel link between cerebrovascular impairments and ASD. We demonstrated that endothelial cells (ECs) contribute cell-autonomously to 16p11.2-deficient phenotypes. Furthermore, we unmasked the molecular mechanisms involved in 16p11.2-deficient EC dysfunctions. We identified a reduced mitochondrial density with a bioenergetic failure, a lack of ATP availability, in 16p11.2-deficient ECs. Interestingly, *in vitro* ATP supplementation rescued 16p11.2-deficient EC dysfunctions. We discovered that this response was P2-class purinergic receptor dependent, particularly P2Y2 mediated. These findings underscore energy metabolism and purinergic receptors as vascular targets in ASD. Furthermore, we showed that *Rock2* haploinsufficiency, a downstream effector of RhoA, improves 16p11.2-deficient endothelial network formation *in vitro* and ameliorates 16p11.2 deletion-associated adult mouse behaviors. Overall, this thesis revealed unsuspected cerebrovascular underpinnings in ASD as well as highlights the critical role of ECs in brain health. Taken together, this work provides insight into new players and mechanisms of ASD pathogenesis, which is a pre-requisite for the development of transformative therapeutics.

Acknowledgements

This thesis would of not have been possible without the continuous contribution, help and support from numerous people along the way.

I would first and foremost like to express my gratitude to my supervisor, Dr. Baptiste Lacoste, who works diligently in advancing brain vascular research in development and neurological disorders. Thank you for accepting to be my advisor and taking a chance on a young graduate student who had very little experience in the scientific world. You taught me vital lessons to succeed in research and in life. You have given me your trust in taking this research project far beyond any graduate student's dream. You showed me how to manage multiple projects and tasks at once as well as become a better scientific communicator. I can sincerely say that you have made me a stronger person and researcher. These skills will forever stay with me.

Next, I would like to thank Dr. Moises Freitas-Andrade, you have been a consistent help, advocate and source of motivation. I could always count on you to think outside the box for solutions when I had very thought provoking problems. All graduate students are lucky to have you in their vicinity. I also wish to express my gratitude to all members of the Lacoste Lab. Nicole Blakeley, Pavel Kotchetkov, Leya Aubert-Tandon, Nour El Khatib and Joanna Raman-Nair, you have all found a way to make long and difficult days enjoyable and incredibly funny. I am sure you will all keep future students entertained. I want to sincerely say thank you for your friendship.

To all our incredible collaborators, thank you for your hard work and help with completing this research. I would also like to thank my thesis advisory committee, Dr. Pierre Mattar, Dr. Maxime Rousseaux and Dr. Antonio Colavita for their guidance and feedback throughout my studies. Thank you for the University of Ottawa for their financial support through an Admission and Excellence Scholarships. I am grateful to the Canadian Institutes of Health Research for the

Frederick Banting and Charles Best Doctoral Scholarships and the Canadian Vascular Network Scholar Award.

To my friends and family, this thesis could not have been possible without your unwavering support throughout the good and the challenging times. I will forever be grateful for the multiple pep talks and constant advice that you have provided me. A special thanks to my parents, who have patiently and continuously endured my constant practicing and prepping for talks. You always knew the right words to say when I needed them. Thank you for encouraging me every step of the way, supporting me to follow my dreams and for your endless faith in my abilities.

Lastly, to my four legged friends, you are the best stress relievers I can ask for. I can always count on you to keep it light and funny and to be beside me late in the night as I worked.

To everyone, thank you for your constant support.

Table of Contents

List of Publications (most recent first)

Ouellette J., Warsi S., Khare P., Naz S., Aubert-Tandon L., Pileggi C., Yandiev S., Freitas-Andrade M., Comin C.H., Harper M-E., Manickam D.S., Saghatelyan A. and Lacoste B. P2 purinergic receptor activation rectifies autism-associated brain endothelial cell dysfunction. *Submitted*.

Ouellette J. and Lacoste B. *Rock2* heterozygosity improves behavior and endothelial function in a mouse model of 16p11.2 deletion autism syndrome. (2024) *Neuroscience Letters.* 837:137904. doi: 10.1016/j.neulet.2024.137904.

Ouellette J., Crouch E.E., Morel J-L., Coelho-Santos V., Lacoste B. A Vascular-Centric Approach to Autism Spectrum Disorders. (2024) *Neuroscience Insights*. 19. doi: 10.1177/26331055241235921.

Ghorbani P., Kim S.Y., Smith T.K.T, Minarrieta L., Robert-Gostlin V., Kilgour M.K., Ilijevska M., Alecu I., Snider S.A., Margison K.D., Nunes J.R.C., Woo D., Pember C., O'Dwyer C., **Ouellette J.,** Kotchetkov P., St-Pierre J., Bennett S.A.L., Lacoste B., Blais A., Nair M.G., and Fullerton M.G. (2023) Choline metabolism underpins macrophage IL-4 polarization and RELMa up-regulation in helminth infection. *PLoS Pathogens.* 19(9):e1011658. doi: 10.1371/journal.ppat.1011658

Freitas-Andrade M, Comin CH, Van Dyken P, **Ouellette J**, Raman-Nair J, Blakeley N, Liu QY, Leclerc S, Pan Y, Liu Z, Carrier M, Thakur K, Savard A, Rurak GM, Tremblay MÈ, Salmaso N, da F Costa L, Coppola G, Lacoste B. (2023) Astroglial Hmgb1 regulates postnatal astrocyte morphogenesis and cerebrovascular maturation. *Nature Communications* 214(1):4965. doi: 10.1038/s41467-023-40682-3.

Béland-Millar A., Kirby A., Truong Y., **Ouellette J.**,Yandiev S., Bouyakdan K., Pileggi C., Naz S., Yin M., Carrier M., Kotchetkov P., St-Pierre M-K., Tremblay M-E., Courchet J., Harper M-E., Alquier T., Messier C., Shuhendler A. and Lacoste B. (2023). 16p11.2 haploinsufficiency reduces mitochondrial biogenesis in brain endothelial cells and alters brain metabolism in adult mice. *Cell Reports.* 30;42(5):112485. doi: 10.1016/j.celrep.2023.112485.

Lithopoulos MA., Toussay X., Zhong S., Xu L., Mustafa SB., **Ouellette J.,** Freitas-Andrade M., Comin CC., Bassam HA., Baker AN.., Sun Y, Wakem M., Moreira AG., Blanco CL., Vadivel A., Tsilfidis C., Seidner SR., Slack RS., Lagace DC., Wang J., Lacoste B. and Thébaud B. (2022) Neonatal hyperoxia in mice triggers long-term cognitive deficits via impairments in cerebrovascular function and neurogenesis. *Journal of Clinical Investigation* 22:e146095. doi: 10.1172/JCI146095.

da Silva M., **Ouellette J.**, Lacoste B. and Comin C.H. (2022) An Analysis of the Influence of Transfer Learning When Measuring the Tortuosity of Blood Vessels. *Computer Methods and Programs in Biomedicine*, 225:107021. doi: 10.1016/j.cmpb.2022.107021.

Ouellette J. and Lacoste B. (2021) Isolation and functional characterization of primary endothelial cells from mouse cerebral cortex. *STAR Protocols*, 11;2(4):101019. doi: 10.1016/j.xpro.2021.101019.

Ouellette J. and Lacoste B. (2021) From neurodevelopmental to neurodegenerative disorders: the vascular continuum. *Frontiers in Aging Neuroscience,* 20;13:749026. doi: 10.3389/fnagi.2021.749026.

Ouellette J., Toussay X., Comin C.H., Costa L., Ho M., Lacalle-Aurioles M., Freitas-Andrade M., Liu Q., Leclerc S., Pan Y., Liu Z., Thibodeau J-F., Yin M., Carrier M., Morse C., Van Dyken P., Bergin C., Baillet S., Kennedy C., Tremblay M-E., Benoit Y., Stanford W., Burger D., Stewart D. and Lacoste B. (2020) Vascular contributions to 16p11.2 deletion autism syndrome modeled in mice. *Nature Neuroscience*, 23(9):1090-1101. doi: 10.1038/s41593-020-0663-1.

List of Figures

List of Appendix Figures

Supplementary Figure 1. Additional information on gene expression between male WT and *16p11.2*$^{df/+}$ brain endothelial cells. Related to Figure 6.

Supplementary Figure 2. Additional information on behavioral changes between WT and *16p11.2*$^{df/+}$ mice, and between control and in *16p11.2*$^{\Delta EC}$ mice. Related to Figure 8.

Appendix B: Supplemental for Manuscript II

Figure S1. No change in mitochondrial dynamics and biogenesis in 16p11.2-deficient brain endothelial cells and additional altered metabolites. Related to Fig 1.

Figure S2. Additional altered energy-related metabolites and mitochondrial function assessment in 16p11.2-deficient brain endothelial cells. Related to Fig 1.

Figure S3. *In vitro* network formation assay of 16p11.2-deficient ECs with treatment of 5mM ATP-LNPs and confirmation of colloidal stability of ATP-LNPs. Related to Fig 2.

Figure S4. Additional treatment conditions of extracellular ATP in 16p11.2-deficient brain ECs. Related to Fig 3.

Figure S5. Adenosine supplementation does not improve 16p11.2-deficient primary brain ECs network formation *in vitro*. Related to Fig 3.

Figure S6. Additional treatment conditions of non-selective antagonist (PPADs) and representative dose response curves. Related to Fig 3.

Figure S7. Gene expression level of other P2-class receptors and steady-calcium profile of 16p11.2-deficient brain endothelial cells. Related to Fig 4.

List of Appendix Tables

List of Abbreviations

Aβ	β- amyloid peptide
ACh	Acetylcholine
AD	Alzheimer's disease
ADHD	Attention deficit/ hyperactivity disorder
AD-DS	Alzheimer's disease-dementia
α-SMA	alpha-smooth muscle actin
AMPA	α–amino-3-hydroxy-5-methyl-4-isoxazolepropionic acid
AMPK	Adenosine monophosphate activated protein kinase
Angpt2	Angiopoietin 2
ANOVA	Analysis of variance
Apln	Apelin
ApoE	Apolipoprotein E
APP	Amyloid precursor protein
ASD	Autism spectrum disorder
ASL	Arterial Spin Labeling
ATEC	Autism Treatment Evaluation Checklist
ATP	Adenosine triphosphate
BACHD	Bacterial artificial chromosome-mediated transgenic mouse model
BBB	Blood brain barrier
BCAA	Branched chain amino acid
BDNF	Brain-derived neurotrophic factor
bFGF	Basic fibroblast growth factor

BMEC	Brain microvascular endothelial cells
BOLD	Blood oxygen level-dependent
BSA	Bovine serum albumin
BTBR	Black and Tan Brachyury *T+tf/J* model
CAA	Cerebral amyloid angiopathy
CADASIL	Cerebral autosomal dominant arteriopathy with subcortical infarcts and leukoencephalopathy
CARS	Childhood Autism Rating Scale
CBF	Cerebral blood flow
CBV	Cerebral blood volume
CCM	Cavernous malformations
Cdh5-Cre$^{tg/+}$	Vascular endothelial-cadherin Cre expressing transgenic mice
CDR	Cellular danger response
CD31	Cluster of differentiation 31
CD45	Lymphocyte common antigen
cECs	Cortical endothelial cells
cGMP	cyclic guanosine monophosphate
CIH	Chronic intermittent hypoxia
CLDN	Claudin
c-MYC	cellular myelocytomatosis oncogene
CNS	Central nervous system
CNV	Copy number variation
COX	Cyclooxygenase

Cx43	Connexin 43
Da	Dalton
DCE-MRI	Dynamic contrast enhanced- magnetic resonance imaging
DEACMP	Delayed encephalopathy after acute carbon monoxide poisoning
DEL	deletion
DNA	Deoxyribonucleic acid
Dll4	Delta-like 4
DMSO	Dimethylsulfoxide
DS	Down Syndrome
DRP1	Dynamin-related protein 1
DQS	Diquafosol tetrasodium
EAAT	Excitatory amino acid transporters
EAE	Experimental autoimmune encephalomyelitis
EC	Endothelial cell
ECAR	Extracellular acidification rate
ECoG	Electrocorticography
EDHF	Endothelium-derived hyperpolarizing factor
EdU	5-Ethynyl-2-deoxyuridine
EEG	Electroencephalography
EETs	Epoxyeicosatrienoic acids
ETC	Electron transport chain
ET-1	Endothelin-1
EGF	Epidermal growth factor

eNOS	Endothelial nitric oxide synthase
Erk1	Extracellular signal-regulated kinase 1
E2	Estradiol
FOXO1	Forkhead box protein O1
FMR1	Fragile X messenger ribonucleoprotein 1
FMRI	Functional magnetic resonance imaging
FRET	Fluorescence resonance energy transfer
GABA	Gamma-aminobutyric acid
GBA	Glucocerebrosidase
GDNF	Glial cell-line derived neurotrophic factor
GFAP	Glial fibrillary acidic protein
GLUT1	Glucose transporter 1
GLUT-1 DS	Glucose transporter-1 deficiency syndrome
GMH	Germinal matrix hemorrhage
GO terms	Gene Ontology terms
Grem1	Gremlin 1
GSH	Glutathione reduced
GSSG	Glutathione oxidized
G1 phase	Growth
G2/S phase	Proliferation
HBOT	Hyperbaric oxygen therapy
HBSS	Hank’s balanced salt solution
HD	Huntington’s disease

hiECs	Human induced endothelial cells
HIF1A	Hypoxia-inducible factor 1a
HUVECs	Human umbilical vein endothelial cells
Htt	Huntingtin
Hz	Hertz
Iba1	Ionized calcium binding adaptor molecule 1
Icam1	Intercellular adhesion molecular 1
IGF-1	Insulin-like Growth Factor 1
INVP	Intraneural vascular plexus
iPSCs	Induced pluripotent stem cells
Kb	Kilobase
LAM	Leukocyte adhesion molecules
LAT1	Large neutral amino acid transporter
LDF	laser Doppler flowmetry
L-NNA	NG-nitro-L-arginine
LNP	Lipid nanoparticles
LRP	Low density lipoprotein receptor
LRRK2	Leucine-rich repeat kinase 2
Mapk3	Mitogen-activated protein kinase 3
MARVD2	Tricellulin
MCA	Middle cerebral artery
MCT	Monocarboxylate transporters
MEOX2	Mesenchyme Homeobox 2

MFN	Mitofusin
mGluR	metabotropic glutamate receptors
MMP	Matrix metalloproteinase
MPTP	1-methyl-4-phenyl-1,2,3,6-tetrahydropyridine
MRI	Magnetic resonance imaging
MS	Multiple sclerosis
MVP	Major vault protein
MRA	Magnetic resonance angiopathy
NAc	Nucleus accumbens
NAWM	Normal appearing white matter
NDD	Neurodevelopmental disorder
NeuN	Neuronal nuclear antigen
NG2	Neural/glial antigen 2
NMDA	N-methyl-D-aspartate
nNOS	neuronal nitric oxide synthase
NO	Nitric oxide
NOR	Novel object recognition
NOTCH	Neurogenic locus notch homolog protein
NPCs	Neural progenitor cells
NT-PGC-1α	Truncated variant of peroxisome proliferator-activated receptor gamma coactivator 1- alpha
NVU	Neurovascular unit
NVC	Neurovascular coupling

OCR	Oxygen consumption rate
OPA1	Optic atrophy gene 1
P-	Postnatal day
PARK2	Parkin RBR E3 ubiquitin protein ligase
PARK7	Parkinson protein 7
PBS	Phosphate-buffered saline
PBST	Phosphate-buffered saline and triton
PCW	Post-conception week
PD	Parkinson's disease
PDGF	Platelet-derived growth factor
PDGFRβ	Platelet-derived growth factor receptor beta
pD_2	Potency of a competitive irreversible or non-competitive antagonist
PE	Phenylephrine
PECAM-1	Platelet endothelial cell adhesion molecule-1
PET	Positron emission tomography
PGC1α	Peroxisome proliferator-activated receptor-gamma coactivator-1 alpha
PGE_2	Prostaglandin E2
PICALM	Phosphatidylinositol-binding clathrin assembly protein
Piezo1	Piezo type mechanosensitive ion channel component 1
PINK1	Phosphatase and tensing homolog-induced kinase-1
PIP_2	Phosphatidylinositol 4,5-biphosphate
PFA	Paraformaldehyde
PFKFB3	6-phosphofructo-2-kinase/fructose-2,6-bisphosphatase

PGE_2	Astrocyte-derived prostaglandins
PKC	Protein kinase C
PLS-DA	Partial least square – discriminant analysis
PNVP	Perineural vascular plexus
PPADs	Pyridoxalphosphate-6-azophenyl-2',4'-disulfonic acid
PP-MS	Primary progressive multiple sclerosis
PPP	Pentose phosphate pathway
PS1	Amyloidogenic presenilin
P2-class	Purinergic receptors
Shh	Sonic Hedgehog
SNc	Substantia nigra pars compacta
SNCA	Alpha-synuclein
SNP	Sodium nitroprusside
SPECT	Single-photon emission computed tomography
SP-MS	Secondary progressive multiple sclerosis
STRING	Search tool for retrieval of interacting genes/proteins
SVD	Small vessel disease
RAS	Renin angiotensin system
rCBF	Regional cerebral blood flow
RhoA	Ras homolog family member A
RH-PAT	Non-invasive peripheral arterial tonometry
RNA	Ribonucleic acid
RNAseq	RNA sequencing

ROCK	Rho associated coiled-coil containing protein kinase
ROI	Region of interest
ROS	Reactive oxygen species
RR-MS	Relapsing-remitting multiple sclerosis
RT-qPCR	Reverse transcription-quantitative polymerase chain reaction
Taok2	TAO Kinase 2
TBI	Traumatic brain injury
TBR1	T-box brain transcription factor 1
TCA	Tricarboxylic acid cycle
TGFβ	Transforming growth factor beta
TJ	Tight junction
TNF-α	Tumor necrosis factor alpha
TRP	Transient receptor potential
TRPV4	Transient receptor potential vanilloid-type 4
USV	Ultrasonic vocalizations
VE-cadherin	Vascular endothelial-cadherin
VEGF-A	Vascular endothelial growth factor A
VEGFR2	Vascular endothelial growth factor receptor 2
VIP score	Variable importance plot
VPS35	Vacuolar protein sorting-associated protein 35
VSMCs	Vascular smooth muscle cells
WNT	Wingless-related integration site
WT	Wild type

ZO-1	Zonula occludens-1
16p11.2$^{df/+}$	16p11.2 deletion
16p11.2$^{\Delta EC}$	Endothelium-specific 16p11.2 hemizygosity
20-HETE	20-Hydroxyeicosatetraenoic acid
3D	Three-dimensional

Authorizations

Manuscript I: This article was published in *Nature Neuroscience* in 2020. “Ownership of copyright in original research articles remains with the Author, and provided that, when reproducing the contribution or extracts from it or from the Supplementary Information, the Author acknowledges first and reference publication in the Journal, the Author retains the following non-exclusive rights: To reproduce the contribution in whole or in part in any printed volume (book or thesis) of which they are the author(s).”

Manuscript II is submitted and thus carries no copyright.

Manuscript III: This article was published in *Neuroscience Letters* in 2024*,* under a Creative Commons Attribution-Non Commercial-No Derivatives (CC-BY-NC-ND) 4.0 license and permits non-commercial use of the work as published, without adaptation or alteration provided the work is fully attributed. “Please note that, as the author of this Elsevier article, you retain the right to include it in a thesis or dissertation, provided it is not published commercially. Permission is not required.”

Manuscript IV: This article was published in *Star Protocols* in 2021*,* under a Creative Commons Attribution-Non Commercial- No Derivatives (CC-BY-NC-ND) 4.0 license and permits non-commercial use of the work as published, without adaptation or alteration provided the work is fully attributed. “Please note that, as the author of this Elsevier article, you retain the right to include it in a thesis or dissertation, provided it is not published commercially. Permission is not required.”

Manuscript V: This article was published in *Frontiers in Aging Neuroscience* in 2021 under the terms of the Creative Commons Attribution License (CC-BY) 4.0 license and permits anyone to copy, re-publish, adapt, and/or re-use the content and create derivate work from it, for commercial or non-commercial purposes.

Manuscript VI: This article was published in *Neuroscience Insights* in 2024 under a Creative Commons Attribution-Non Commercial (CC-BY-NC) 4.0 license: "Content may be copied, adapted, displayed, distributed, republished or otherwise reused provided the purpose of these activities is not for commercial use. Commercial use means use of the content by a commercial organisation or individual for direct (including through sale, loan or license) or indirect (including through marketing campaigns, promotional materials or presentations) commercial gain or remuneration. You may use the final published PDF or Accepted Manuscript in your dissertation or thesis, including where the dissertation or thesis will be posted in any electronic Institutional Repository or database."

Chapter 1- Introduction

1.1. Brain vasculature in health

The brain is an expensive organ in energetic terms as it accounts for 2% of the body mass and consumes a quarter of the body's energy when at rest[1,2]. Its elevated energy consumption and limited energy storage makes the brain exceptionally reliant on the adequate supply of oxygen and nutrients from the blood stream[3,4]. In the human brain, the cerebrovasculature reaches approximately 600 km in length to maintain the metabolic demand of the brain's 86 billion neurons during development and throughout life[5,6]. To maintain a healthy brain, the vascular system entails key features such as a functional blood-brain barrier (BBB) for brain homeostasis, a dense vascular network for proper perfusion as well as regulation of cerebral blood flow (CBF) to match neuronal metabolic demands[3,4,7-9]. These essential vascular features ensure brain function and maturation throughout all critical periods of life[9]. Consequently, tight regulation of brain energy dynamics is maintained by many cell types collectively forming the neurovascular unit (NVU). This multicellular complex includes neurons, mural cells (pericytes and smooth muscle cells), astrocytes, and endothelial cells (ECs). Cells forming the NVU have specific roles for upholding proper brain function and metabolism[1,2,6,8,10,11] (Figure 1). Together, the NVU provides the cellular architecture to establish functional neurovascular coupling (NVC) where increased neural activity will lead to a concomitant increase of CBF [2,12,13].

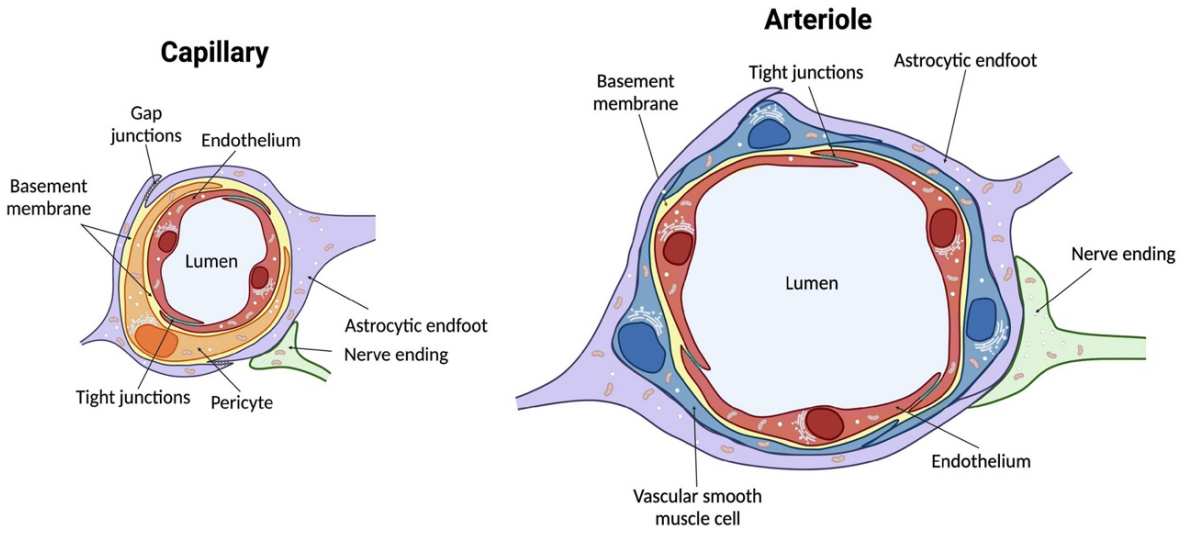

Figure 1. Cellular architecture of the neurovascular unit.
Endothelial cells are surrounded by mural cells which are involved in maintaining vascular integrity. Intracerebral capillaries (*left*) and intracerebral arterioles (*right*) differ from on another by the presence of vascular smooth muscle cells (VSMCs) to mediate vascular tone. Adopted from Ouellette and Lacoste (2021*). Frontiers in Aging Neuroscience*.

1.2. Cells of the neurovascular unit

1.2.1. Neurons

The close collocation of neuronal and vascular systems support the notion that they are mutually interdependent[14-16]. While these cells are unique in the sense that they can send electrical or chemical signals throughout the body to complete a plethora of functions, neurons are highly dependent on cells of the NVU (*i.e*. astrocytes and ECs). In general, neurons are characterized by dendrites, fibrous roots that branch out from the cell body, and an axon, a long and slender projection from the soma. Dendrites receive afferent signals, while an axon carry out efferent signals. The axon terminal releases neurotransmitters or neuromodulators to propagate a message through the synapse that is then converted into an electrical signal. The electrical signal can propagate via ion movement through voltage-gated ion (potassium, sodium and chloride) channels.

These functions makes neurons highly energy consuming, and thus extremely dependent on the constant supply of energy by the brain vasculature[3].

Neurons inherently send signals to astrocytes and ECs to modulate CBF through the phenomenon of NVC[17]. NVC consist of a sequence of highly coordinated multicellular events, orchestrated by the cellular components of the NVU. NVC is highly specific, localized spatially as well as temporally to areas of elevated neuronal activity, and thus can act as an indicator of brain function[18-20]. This is highly relevant when studying neurological diseases and understanding the region-specific changes of neuronal activity. This mechanism is fully functional as of ~3 weeks of age in rodents and ~7 to 8 weeks in humans[9,21,22].

Active neurons signal to adjacent cells in time of decreased oxygen and glucose availability to consequently alter vascular tone. For instance, the discovery of neurotransmitter-mediated signaling, such as by glutamate, is shown to have a major role in regulating CBF by acting on astrocytes[2]. Neurons synaptically release glutamate to act on N-methyl-D-aspartate receptors (NMDAR) to increase intracellular calcium concentration. This increase in calcium activates neuronal nitric oxide synthase (nNOS) to release nitric oxide (NO). NO will activate smooth muscle guanylate cyclase inhibiting VSMC-mediated constriction leading to vasodilation[2]. Inhibition of nNOS in turn reduces the CBF increase associated with neural activity[23]. Moreover, the release in glutamate from neurons will raise intracellular calcium in astrocytes by activating metabotropic glutamate receptors (mGluR), generating prostaglandins (COX1/3) and epoxyeicosatrienoic acids (EETs). Production of these vasoactive factors by astrocytes will induce vasodilation. In addition, increased calcium concentration in astrocytic end-feet will activate Ca^{2+} - gated K^+ channels, releasing K^+. This will in turn dilate vessels, increasing CBF[2]. Conversely, astrocytes will also generate 20-hydroxyeicosatetraenoic acid (20-HETE), a potent

vasoconstrictor, that activates protein kinase C (PKC), mitogen-activated protein kinase (MAPK), tyrosine kinase and Rho kinase to promote calcium entry through depolarization of VSMCs[2].

Another neurotransmitter involved in modulating CBF is gamma-aminobutyric acid (GABA). GABA acts through $GABA_A$ receptors to mediate vasodilation in the cortex following basal forebrain stimulation. Vaucher et al. has demonstrated that cortical blood vessels receive rich GABAerigc input. They suggest that GABA with its colocalization of cholinoceptive intracortical neurons has a vasodilatory effect by stimulating cholinergic neurons to release acetylcholine (ACh)[24]. ACh will have a downstream impact by activating muscarinic receptors on ECs, increasing intracellular calcium concentration, and as a result activation of endothelial nitric oxide synthase (eNOS). NO is then released by ECs to act on VSMCs leading to vasodilation[25].

In addition to neurotransmitters modulating CBF, adenosine has been shown to be a neuronal signal involved in regulating NVC. Notably, blocking adenosine receptors reduces the parallel increase in CBF evoked by neuronal activity[26]. Adenosine may act as a vasodilator or a vasoconstrictor. Whether CBF is decreased or increased will dependent on availability of oxygen, the mechanism mediating this switch is currently unknown[26].

All excitatory synapses are equally influential in controlling blood flow. These inputs can lead to the activation of interneurons that release vasoactive peptides (*i.e.* cortical vasoactive intestinal peptide) acting on VSMCs to modulate CBF[27,28]. While neuronal activity can lead to the release of vasoactive factors (*i.e.* NO, 20-HETE), it can also alter oxygen concentration within the tissue which will in turn modulate availability of these factors. For example, low oxygen concentration will reduce vasoconstriction due to generation of vasoactive factor arachidonic acid in astrocytes. Additionally, hypoxia can result in increased NO production as well as increased

arachidonic acid metabolism for production of vasodilatory epoxyeicosatrienoic acids (EETs) and prostaglandins by ECs[29-31].

Furthermore, neurons have an important role in initiating BBB properties during development. Neural stem cells activate the Wnt/ β-catenin signaling pathway by releasing Wnt ligands (Wnt7, Wnt1, and Wnt3) which bind to Frizzled receptor and co-receptor LRP5 on ECs to activate β-catenin. β-catenin will migrate to the nucleus to mediate gene expression of BBB properties including tight junctions (claudin-5) and glucose transporter 1 (GLUT1). Furthermore, β-catenin downregulates Snail, a transcription factor, to stabilize adherens and tight junctions (VE-cadherin, occludin and claudin-5)[32]. Thus, the interaction between the brain vasculature and neurons is essential for proper brain function. Highlighting the importance of the uninterrupted supply of oxygen and nutrients from the blood stream.

1.2.2. Astrocytes

Astrocytes are strategically located to enable bidirectional communication between the vasculature and neural cells[2,33]. Astrocytes are a subtype of glial cells that comprise the majority of the cells in the brain. Structurally, the shape of these cells give reason to their name as the radially-arranged foot-processes create a star-like appearance. Astrocytic end-feet ensure communication with surrounding cells. The brain entails two main types of astrocytes including protoplasmic and fibrous astrocytes[34]. Protoplasmic astrocytes are large astrocytes mostly found in the cortical gray matter of the brain. These cells are organized to project to surrounding blood vessels and synapses. As a result, these extended processes can modulate blood flow depending on neuronal activity[35]. Fibrous astrocytes express fewer end-feet, and are located within the white matter tracts. As

opposed to protoplasmic astrocytes, fibrous astrocytes are not dependent on neuronal activity but mediate metabolic and ionic homeostasis in the brain via communication with the vasculature[34].

Astrocytes have a number of functions to ensure a healthy brain, these include signal propagation between neurons, removal of free radicals in the brain, regeneration of CNS damage and injury, neurotransmitter uptake mediated by excitatory transporters 1 and 2, neuronal survival and development support, maintenance of fluid levels, establishment of BBB properties as well as regulation of CBF[17,36-38]. Astrocytes also consist of gap junctions to allow for intercellular communication with other cells to monitor, coordinate their responses to different stimuli, and interact with the extracellular environment[34]. These gap junctions, comprising connexins 30 and 43, are calcium dependent, and enable cell-cell communication to maintain brain homeostasis[34].

Although astrocytes have many roles in ensuring brain health, one of their primary functions consist of modulating CBF to deliver energy to neurons. This is established by astrocytic end-feet processes surrounding the arterioles and capillaries to innately respond to neurotransmitters such as glutamate to help mediate CBF[17]. The close relationship of astrocytes with synapses and blood vessels in the brain is evident with end-feet processes completely surrounding all cerebral blood vessels. Astrocytic end-feet cover ~99% of the vascular surface, including ECs and pericytes, to facilitate rapid transfer of glucose through the presence of glucose transporters for energy demanding dendrites[39].

Astrocytes regulate CBF depending on neuronal activity, and as previously depicted, by the release of neuronal glutamate. Electrical stimulation of neuronal processes in brain slices leads to an increase of intracellular calcium in astrocytic end-feet, subsequent slow-developing dilation of cerebral arterioles, and in some instances vasoconstriction. Of note, the mechanism distinguishing the two are yet to be fully understood. Moreover, pharmaceutically inhibiting

metabotropic glutamate receptors on astrocytes prevented the vasodilation response. The vasodilation response was reinstated following removal of the antagonist, and increased neuronal stimulation[39].

Another mediator of the vascular changes during NVC by astrocytes is cyclooxygenase 1 (COX-1). COX-1 has been shown to be highly expressed in astrocytic end-feet of adult mice. COX-1 leads to the production of prostaglandin E2 (PGE_2) in astrocytes which increases intracellular calcium concentration, and so leading to subsequent vasodilation. One study in mice demonstrated that COX inhibition via indomethacin attenuated the vascular response *in vivo* despite increases in neural activity and in intracellular calcium[40]. These findings emphasize the role of astrocytes in modulating blood flow to increase energy availability. In periods of high demand, astrocytes can also provide energy sources to neurons through their glycogen storage while priming the vasculature to alter blood flow to respond to the increase in energy required by the brain[41]. While astrocytes respond to changes in neuronal activity, they can also support synaptic transmission. For instance, glutamate produced by astrocytes can be utilised by neurons to form synapses[42]. Therefore, the interaction of astrocytes with both neurons and ECs will have a strong downstream impact on brain health.

In addition to modulating CBF, astrocytes are essential for maintaining BBB integrity and function. Astrocytic end-feet express aquaporin 4 and gap junction connexin43 (Cx43) to support the BBB. Aquaporin 4 is involved in interstitial fluid resorption, neuroinflammation, cell migration and calcium signaling. Its enrichment at astrocytic end-feet allows for mediation of water exchange across the BBB[43]. Cx43 channels mediate intercellular signaling involving calcium to maintain BBB integrity. For example, astrocyte-specific Cx43 deletion downregulates aquaporin 4 expression and increased BBB permeability[44]. Astrocytes also produce laminins which are major

constituents of the basement membrane at the BBB; however, their role in BBB development is unclear. Laminin α2 produced by astrocytes has been associated with maintaining astrocytic end-feet polarization as well as polarizing aquaporin 4 channels[45]. Moreover, astrocytes release growth factors like VEGF, glial cell-line derived neurotrophic factor (GDNF), basic fibroblast growth factor (bFGF) and angiopoietin 1 (Ang-1). These factors are important for the formation of tight junctions, and the polarization of transporters to support BBB integrity[46]. Notably, astrocytes maintain BBB integrity after induction of BBB properties by neural stem cells. Astrocytes activate the Sonic hedgehog (Shh) signaling cascade on brain ECs. Shh receptors, Patched-1, expressed by ECs activate transcription factor Gli to induce the expression of junctional proteins (*i.e.* claudin-5) to promote the BBB phenotype[32].

1.2.3. Vascular smooth muscle cells

Vascular smooth muscles cells (VSMCs) are located throughout the vascular tree with the exception of endothelial capillaries (Figure 2). Their main role is to regulate vascular tone by depending on signals from adjacent cells (neurons, astrocytes, and ECs). VSMCs express contractile proteins including smooth muscle actin, myosin heavy chain and myosin light chain which together alter blood vessel diameter[47]. In the event of altered oxygen or nutrient requirements, chemical signals from adjacent cells (neurons, astrocytes, and ECs) are converted into mechanical constriction or relaxation signals by VSMCs. These signals increase intracellular calcium concentration and activate potassium channels leading to conformational changes of myosin light chain[48].

Mechanical constriction is a process through which mechanical signaling by VSMC alters gene transcription and regulate cellular function resulting in a faster response to mediate vascular

tone[47]. Increased blood flow or pressure, activates transmembrane proteins such as mechanosensitive ion channels primarily including piezo-type mechanosensitive ion channel component 1 (Piezo1) and transient receptor potential (TRP). These channels are activated transiently by increased blood flow stretching the vessel wall resulting in VSMC constriction following calcium influx[47]. Retailleau et al. demonstrated that VSMC-specific knockout of Piezo1 in mice led to a reduced vessel tone resulting in decreased hypertension. Thus, supporting the role of stretch-activated cationic channel activity in mediating vessel tone[49]. In addition, enhanced membrane stretch can also mediate TRP family channel proteins leading to nonselective cation currents, elevated calcium, and resulting in contraction of VSMCs[47]. Calcium influx in VSMCs is also regulated by voltage-dependent L-type Ca^{2+} channels[50]. Consequently, calcium influx leads to vasoconstriction by forming a complex with ubiquitous calcium binding protein calmodulin, and subsequently increasing the activity of myosin light chain kinase[50].

Smooth muscle relaxation produced by local release of vasoactive factors from neurons and astrocytes propagates upstream through the intercellular gap junctions that link neighbouring ECs and VSMCs. As blood flow increases in upstream vessels, the increase in shear stress on ECs produces further vasodilation through the release of a endothelium-dependent vasodilator (NO)[47].

VSMCs are considered one of the primary regulators of vascular tone in the brain to quickly respond to the increasing need in energy to support brain function.

1.2.4. Pericytes

Pericytes are perivascular cells that wrap around endothelial capillaries, and are embedded within the basement membrane. These cells are characterized by a prominent nucleus with long processes surrounding the abluminal wall of ECs. The long processes ensure that pericytes can contact

several capillaries, pre-capillary arterioles and post-capillary venules to support signal propagation[51]. Pericyte processes form cellular adhesions with the endothelium at discrete points, known as peg-and-socket junctions, which are mediated by adhesion molecule N-cadherin. In addition, other pericyte-endothelial cellular adhesions have been identified including adhesion plaques, gap junctions, and tight junctions. Thus, signals coming from adjacent cells are processed in pericytes to generate multiple responses to maintain brain health. These responses include regulation of BBB permeability, angiogenesis, clearance of toxic metabolites and modulation of capillary vascular tone[51]. Being in close proximity with the endothelium and extending along the microvasculature in every capillary ensures the involvement of pericytes in BBB development and integrity[6]. Pericytes play an important role in the inhibition of properties associated with leaky vessels by regulating *Mfsd2a* expression and transcellular permeability[52-56]. For example, analysis of the BBB in platelet-derived growth factor receptor beta (PDGFRβ) null mice during embryogenesis revealed a leaky BBB demonstrating that pericytes are required to regulate BBB permeability[53,54]. Furthermore, pericytes can clear tissue debris and foreign proteins which has been a topic of interest in the context of disease[53,57].

While pericytes have been described by many as support cells with a limited involvement in neurovascular function, studies have demonstrated that they mediate capillary tone[51,58,59]. While this notion is still debated in the literature, pericytes express contractile proteins and cystoskeletal proteins (α-smooth muscle actin, tropomyosin and myosin, vimentin, desmin and nestin) suggesting they have a basal level of contractility[17]. Only a subset of pericytes can mediate vascular tone. These include ensheathing pericytes at the arteriolar end of the capillary bed as they express high levels of α-smooth muscle actin compared to thin-strand pericytes at the venous end of the

capillary bed[60]. As pericytes mediate vascular tone, and so CBF, they are suggested to take part in regulating NVC with astrocytes, neurons and ECs[51].

In addition to mediating vascular tone, pericytes express cell surface antigens such as transmembrane chondroitin sulfate proteoglycan neural/glial antigen 2 (NG2), platelet-derived growth factor receptor-b (PDGFRb), aminopeptidase A and N (CD13), and cell surface glycoprotein MUC18 (CD146). These antigens contribute to blood vessel formation, maintenance and development by regulating pericyte-EC interaction and promoting cell proliferation[61-63]. Adult pericyte-deficient mice were characterized with vascular dysfunctions, including reduced brain microcirculation, reduced capillary perfusion, loss of blood flow responses during brain activation and accumulation of neurotoxic serum molecules due to BBB breakdown[52]. In addition to stabilizing the vessel wall during development, pericytes migrate to new vessels following the release of growth factors from ECs which include transforming growth factor beta (TGF-β) and platelet-derived growth factor-BB (PDGF-BB)[64]. In capillaries, pericytes control the cell cycle of ECs and contribute to the formation of the basement membrane. These cells also modulate angiogenesis by regulating VEGF signaling and secreting angiogenic-promoting factor neurogenic locus notch homolog protein (Notch) 3[65]. Angiogenic defects including vascular hyperplasia, microvessel dilation, and upregulation of VEGF-A expression have been identified following pericyte depletion. Therefore, pericytes mediate the expression and activity of VEGF-A during development to ensure proper balance of endothelial cell proliferation[66].

1.2.5. Brain endothelial cells

The main component of the brain vasculature are the endothelial cells (ECs) as they line the vessel wall and regulate vascular tone[3,67]. Brain ECs are distinct to those in the periphery as they must

maintain brain homeostasis through the establishment of BBB properties to protect the brain from toxins. Anatomically, these cells are highly polarized with distinct luminal and abluminal partitions[68]. The luminal surface is covered by glycoproteins, proteoglycans, and glycosaminoglycans forming a structure known as the glycocalyx. This inner layer of the vessel extend from the membrane of ECs to the vascular lumen acting as a barrier preventing leukocytes and platelets from interacting with ECs while maintaining a stable environment[69,70]. On the abluminal side, ECs sit on the basement membrane which acts as a cellular scaffold contributing to the integrity of the brain vasculature. This basement membrane is composed of laminin, collagen IV, nidogen and heparan sulfate proteoglycans which support the interaction with pericytes and astrocytes[71]. Specifically, ECs are characterized by a lack of fenestrations as well as junctional complexes that include tight junctions and adherens junctions to seal the paracellular pathways between adjacent ECs[72-75]. Additionally, brain ECs have a low number of pinocytic vesicles that limit endocytosis and transcytosis as well as an increased number of mitochondria compared to peripheral ECs[30,76]. These specific brain EC characteristics regulate the influx or efflux of molecules making them the anatomic site of the BBB[30,77].

The BBB unique properties allow to tightly regulate the movement of ions, molecules and cells between blood and brain. Brain ECs are considered as the primary gatekeepers of the BBB, as they take part in protecting the brain from metabolic, environmental, and toxic insults all while maintaining the adequate delivery of nutrients and oxygen to neurons to uphold their activity[78]. As previously described, brain ECs comprise junctional complexes consisting of tight junction proteins including claudins and occludin as well as adhesion molecules such as VE-Cadherin and E-cadherin. Adaptor proteins such as zonula occludens allow these transmembrane proteins to be

stabilized and linked to the cytoskeleton[79]. Moreover, brain ECs express connexin hemichannels which act as communication channels between the cytoplasm and extracellular milieu[80-82].

While the BBB is a selective barrier, it allows for gases including carbon dioxide to enter the blood, and oxygen to exit the blood to be utilized by the brain. In addition, lipophilic and small molecules (< 400 Da) can freely enter the brain without the need of transporters. To allow influx of proteins and circulating nutrients to by-pass the BBB, brain ECs comprise several different transmembrane transporters. Brain ECs express facilitative transporters to transport ions, macromolecules and proteins from the blood to the brain. These facilitative transporters consist of sugar transporters including glucose transporter 1 (SCL2A1), lactate and pyruvate transporters (SLC16A1), large amino acid transporters (SLC7A5; transport of neutral amino acids) as well as cationic amino acid transporters (SLC7A1; transport of ornithine, lysine, and arginine)[74,83]. Glucose, lactate and pyruvate transporters are crucial in maintaining energy metabolism and homeostasis in the brain during increased energy demands. Large amino acid transporters are imperative for entry of neurotransmitter precursors such as dopamine, serotonin and histamine in the brain[84]. Cationic amino acid transporters aid with NO synthesis in brain ECs which is essential for ECs to mediate vascular tone[85]. Furthermore, brain ECs lack expression of leukocyte adhesion molecules (LAMs) including E-selectin and Icam1[86]. The lack of these molecules prevent entry of immune cells from the blood into the brain. In addition to facilitative transporters, brain ECs express active transporters. For instance, ECs consist of excitatory amino acid transporters (EAAT) for the transport of glutamine and aspartate from the brain to the blood as well as taurine transporters (SLC6A6). The latter ensure that the brain receives enough taurine in order to act as an osmoregulator and neurotransmitter[87]. As opposed to facilitative transporters, active transporters are voltage-dependent.

Brain ECs also consist of active efflux transporters and transport proteins to remove toxic waste products. At the luminal side of ECs, a major class of efflux transporters consist of ATP-binding cassette (ABC) transporters. These transporters are dependent on the hydrolysis of ATP to transport substrates against the concentration gradient into the blood [88]. These transporters play a critical role in neuroprotection and pharmacoresistance, a topic in BBB research that is highly important for drug delivery in the brain[89].

Particularly, BBB characteristics are not innate in brain ECs but are dependent on neural environmental cues to activate genetic programs to acquire these properties. Although the specific programs eliciting BBB characteristics are not fully known, the Wnt/β-catenin signaling and Shh signaling pathways modulated by neurons and astrocytes are forefront in activating BBB properties[90,91]. These pathways highlight the interdependence of ECs, astrocytes and neurons in maintaining brain function and barrier integrity.

While brain ECs have a major role in maintaining BBB properties, they also modulate vascular tone depending on neural cell energy demands. Brain ECs can release various relaxing and constricting factors on VSMCs to alter vessel tone. Vasoactive mediators produced by brain ECs include NO, endothelium-derived hyperpolarizing factor (EDHF), eicosanoids and endothelin-1 (ET-1). Maintaining vascular tone is considered a balancing act as the proper signals must be released in response to energy demands. NO is a vasodilator produced by endothelial NO synthase (eNOS). NO production via eNOS is in part dependent on intracellular calcium levels which implicates calcium-dependent binding protein calmodulin. In order to alter vascular tone, NO acts on VSMCs changing intracellular calcium of these cells leading to vasorelaxation[92]. Outside of the involvement of calcium, eNOS is also regulated by sphingolipid ceramide acting as a secondary messenger to transduce cellular signals. Although EDHF has been involved in

regulating CBF, the precise mechanisms are yet to be fully elucidated. EDHF has been shown to hyperpolarize VSMCs to induce vasorelaxation[93]. Eicosanoids, derived from arachidonic acid, are a family of bioactive signaling lipids comprised of three essential enzymes such as cyclooxygenase (COX), lipoxygenase and epoxygenase[94]. Metabolites produced by these enzymes include thromboxane, prostacyclins, prostaglandins and epoxyeicosatrienoic acids which take part in mediating vascular tone. These metabolites can act as vasoconstrictors or vasodilators depending on their concentration[95]. ET-1 is a peptide released by the endothelium that acts as a vasoconstrictor to reduce CBF via activation of endothelin receptor type A of VSMCs[96].

Although the vasoactive mediators previously described are mostly released by the endothelium of arteries and arterioles, capillary ECs can regulate CBF in absence of VSMCs by mechanoreceptors and shear stress[97]. The endothelium forming the capillaries can modulate CBF using inward-rectifier K^+ channels which signal upstream to arterioles to alter CBF. In addition, brain ECs express transient receptor potential vanilloid-type 4 (Trpv4) channels, calcium-permeable cation channel, that also signal upstream to arterioles to alter blood flow[98]. Given the critical role ECs play in the brain, the dependency of the brain on an extensive endothelium throughout life underscores the need of functional endothelial networks during development as well as properly established vascular cells throughout each vascular segment.

1.3. Cerebrovascular tree

Along the surface of the brain, large cerebral arteries, known as pial arteries, branch into smaller arteries and arterioles. These arteries entail an EC layer, a VSMC layer and an outer layer of leptomeningeal cells, called adventitia, separated from the brain by the Virchow-Robin space. As the arterioles penetrate into the brain, this space disappears, and the vascular basement membrane

comes into contact with astrocytic end-feet in intracerebral arterioles and capillaries[99]. Across the cerebrovascular tree, there is cellular diversity within each vascular segments (Figure 2). Upstream of blood flow, arteries and their corresponding arterioles are enwrapped by VSMCs which ensure changes in vascular tone and modulate downstream CBF in capillaries[9,100,101]. Brain capillaries comprise 85% of the vasculature[6]. The capillary bed of the brain is the primary site of oxygen and nutrient exchange. This exchange is dependent on path length and transit time of red blood cells. The endothelium capillary bed provides a large surface area facilitating solute transport exchange between blood and brain[77]. Each neuron has its own capillary, highlighting the essential relationship between neuronal and vascular systems[102]. In healthy conditions, brain capillary density varies within different region of the brain depending on energy requirements. For instance, gray matter has a higher capillary density than white matter[103]. Brain capillary density can also vary depending on the local microenvironment, physiological and pathological stresses. For example, hypoxia can activate different processes via hypoxia inducible factor-1 (HIF-1) and vascular endothelial growth factor (VEGF) to increase capillary density. This is in response to the increase need in oxygen to support brain tissue metabolism[104]. On the other hand, hypertension can lead to decreased capillary density and altered vascular networks[105]. From the capillaries, the blood drains into venules and veins which comprise the smallest fraction of the brain vasculature. Although ECs found in venules have a similar composition as in arterial ECs, venous ECs have a passive function. VSMCs within the venous system also have a more passive function compared to arterial VSMCs[106,107]. The proper juxtaposition of these cells to ensure brain function are dependent on processes established during brain development.

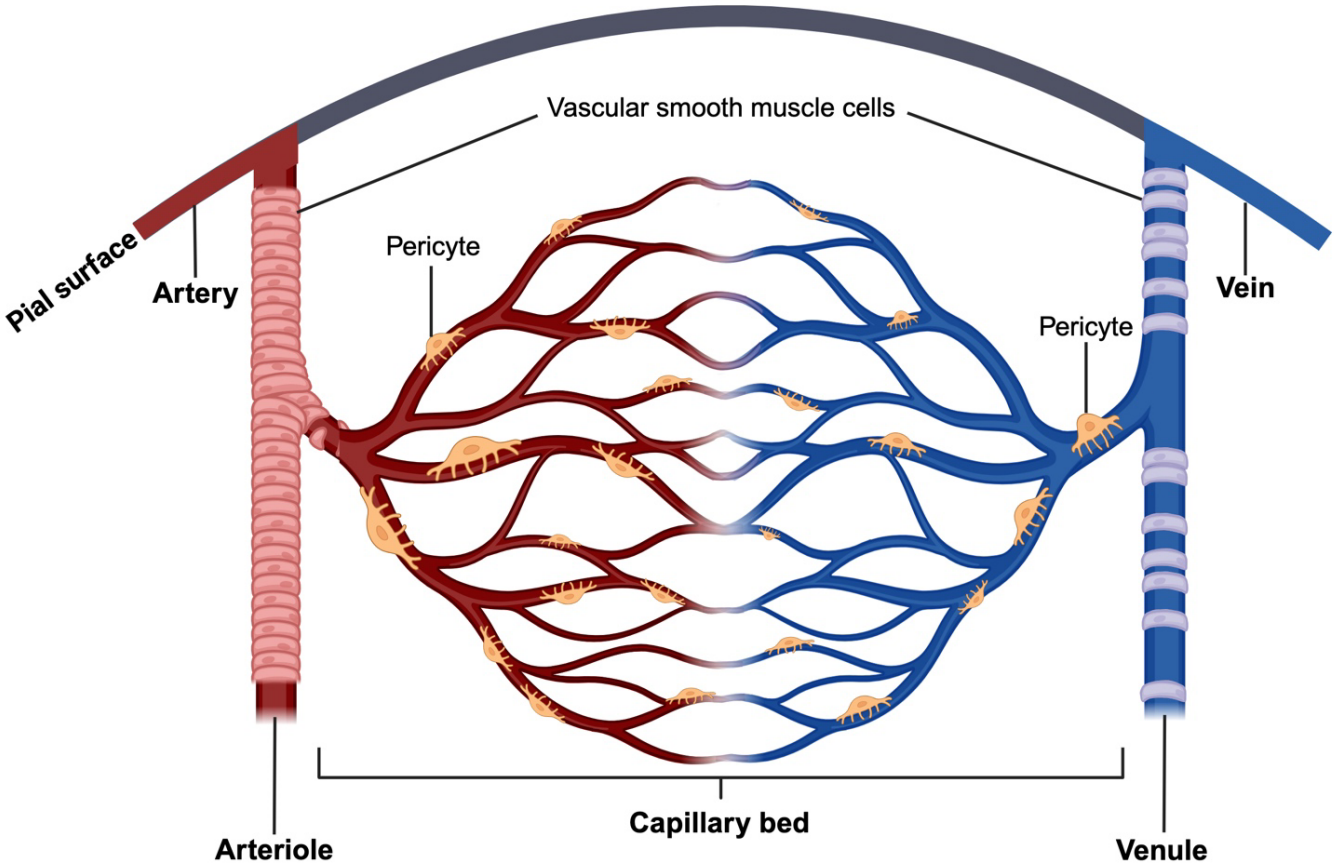

Figure 2. Cellular diversity across the cerebrovascular tree.
Arteries ensheathed by contractile VSMCs line the surface of the brain and descend into the brain parenchyma, branching to become penetrating arterioles. These arterioles are covered by VSMCs until they branch further to form a dense network of capillaries. VSMCs found on venules are molecularly distinct from VSMCs found on arteries. This figure was created with BioRender and is based on the following references[13,108,109].

1.4. Brain vasculature during development

Brain development consist of complex highly demanding processes that require constant support and synchronization[110]. The proper establishment of the brain vasculature is essential for brain development. During developmental neurogenesis, several high energy processes are underway comprising of cell division, migration and differentiation of neuroblasts as well as integration of newborn neurons with mature neurons into the neural circuit[111,112]. As these newborn neurons take up oxygen and nutrients, the vasculature must be able to maintain the metabolic needs of these

cells[113]. Thus, both neuronal and vascular systems are required to be coordinated early in life to support brain function (Figure 3).

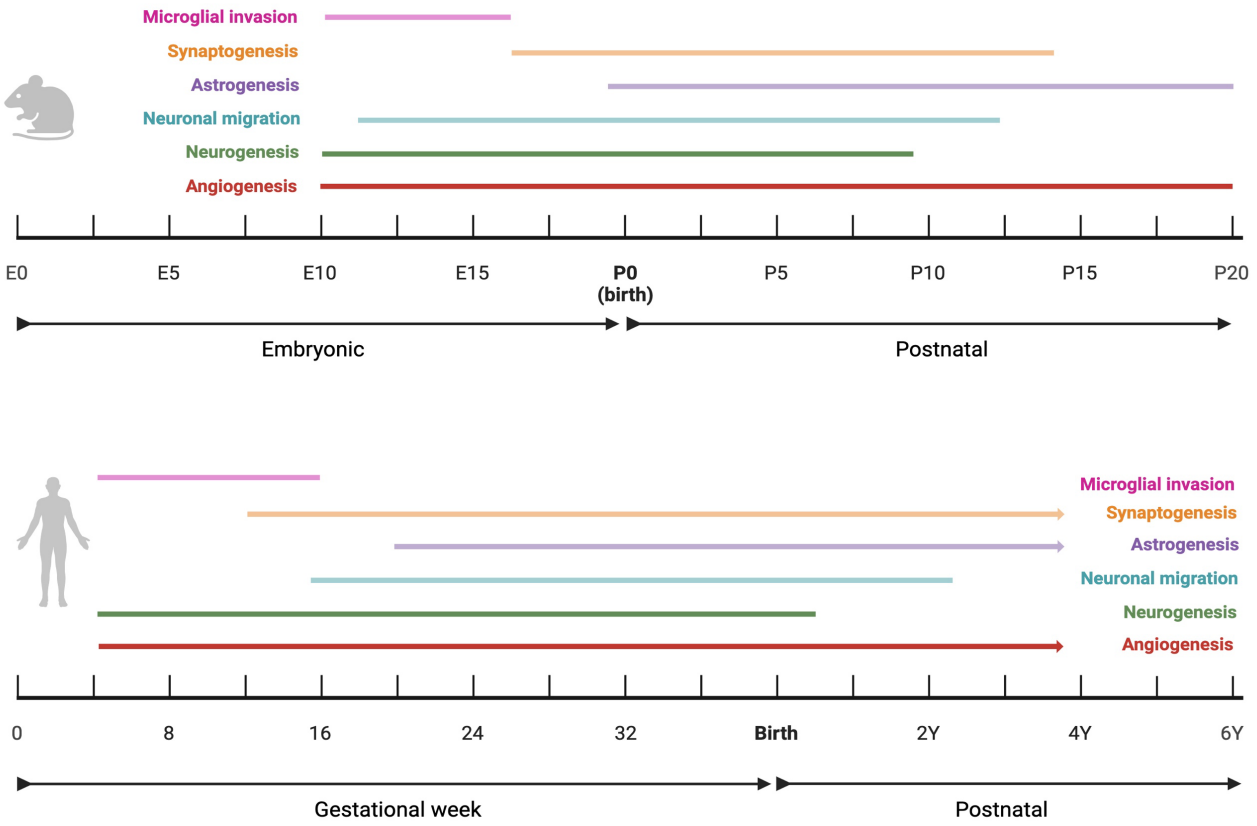

Figure 3. Summarized developmental timeline of neuronal and vascular systems. In mice (*top*) and humans (*bottom*), angiogenesis and neurogenesis begin within the same timeframe; highlighting the interdependence of the vascular and neuronal systems throughout development. In addition, several other processes take part after or during the start of angiogenesis, emphasizing the need of a functional vasculature to support the energy requirements for maintaining brain function. Y= years old. This figure was created with BioRender and is based on the following references[114-121].

During early embryonic development, vasculogenesis is underway. This process entails *de novo* formation of blood vessels via differentiation of angioblasts (ECs progenitors) into ECs. Following closure of the neural tube, angioblasts are recruited from the pre-somitic mesoderm to surround the neural tube with a vascular mesh, known as perineural vascular plexus (PNVP). This is established around E8.5 and E10.5 in mice. These early vessels, sprout radially into the neural tube developing a ramified vascular network known as intraneural vascular plexus (INVP) which takes place at E10.5[122]. As of E10.5 in mice and approximately 4 weeks post-conception (PCW)

in humans, neurogenesis starts which coincides with angiogenesis. During this stage, resident brain macrophages, microglia, migrate from the yolk sac and infiltrate the brain at E9.5 until E14.5-16.5 in mice[119]. In humans, microglia migrate into the developing brain from 4 PCW to 16 PCW. Neurogenesis continues until approximately 8 days after birth in mice and 18 months after birth in humans. In humans, there are discrepancies in the literature regarding the age at which neurogenesis decreases or stops but most are hinting at neurogenesis persisting past birth. During neurogenesis, key developmental processes take place, such as astrogenesis, proliferation and maturation of astrocytes, which is initiated around E18.5 in mice and 20 PCW in humans. Synaptogenesis, synapse formation, is initiated around E16.5 until 14 days after birth in mice and 12 PCW until after birth in humans[117,120]. During this developmental period, continuous delivery of oxygen and nutrients are critical to fuel the different growth processes occurring simultaneously in the brain. Therefore, angiogenesis must continue throughout the duration of brain development, and past birth to support the metabolic requirements of neural cells.

The process of angiogenesis entails the formation of new blood vessels from pre-existing vessels to assemble a vascular network[114,123]. Angiogenesis is a highly coordinated process where ECs undergo differentiation into specialized EC subtypes to establish newly perfused blood vessels. These include migratory tip cells and proliferating stalk cells to elongate the sprout. Once the new vessel has been established, ECs return to their quiescent phalanx cell state[29,124,125].

In development, neurons have key roles in cerebrovascular organization as neural activity determines vascular development and density in the brain[17,126]. Therefore, making the processes of neurogenesis and angiogenesis mutually dependent. During neurogenesis, newborn neurons and neuron maturation increase energy consumption as well as oxygen utilization creating an hypoxic area[113]. HIF1A is highly expressed by neural progenitor cells (NPCs) during brain vascularization,

and is suggested to regulate vascular endothelial growth factor-A (VEGF-A) expression to drive angiogenesis into avascular regions[127]. Other neuronal cues are also known to regulate brain vascularization[122]. For instance, neural progenitor cells secrete cues such as VEGF, Wnt ligands and TGFβ to promote vascular ingression and radial outgrowth as well as support vascular maturation and stability[128,129]. This angiogenesis process entails VEGF signals to stimulate, detach and loosen intercellular tight junctions, and so plasma proteins extravasate as well as build an extracellular matrix[130]. Migratory tip cells with the expression of vascular endothelial growth factor receptor 2 (VEGFR2) migrate to the extracellular matrix to direct the newly developing sprout. Activation of VEGFR2 in tip cells induce expression of delta-like 4 (Dll4) gene which will subsequently activate the Notch signaling pathway in neighbouring cells, inhibiting proliferating stalk cells to adopt a tip cell phenotype[131,132]. Once the new vessel is lumenized, the vessel becomes functional and ECs return to their quiescent state[133]. After birth, neuronal activity continues to direct angiogenesis during critical developmental periods to support the energy demand of the expanding brain[126].

While neurogenesis stimulates vascularization of the brain, the communication between neurons and ECs during this process is bidirectional suggesting a neurovascular crosstalk[127]. Although very little is known about this concept, ECs can modulate neuronal processes by releasing VEGF and increasing Reelin signaling, a mediator of neuronal migration, to stimulate and regulate neurogenesis[122,134,135]. This interdependence highlights that the vasculature must develop symbiotically with neural cells to establish a proper functioning brain (Figure 3). As the vascular network must maintain a constant supply of energy to the brain, it emphasizes the role of the cerebrovasculature at being forefront in regulating brain energy metabolism.

1.5. Involvement of the cerebrovasculature in brain metabolism

Brain metabolism consists of intricate mechanisms not only at the gross anatomical scale, but also at the cellular level[136]. Accordingly, the brain is highly dynamic, and changes in neuronal activity drives the increase in energy consumption leading to compensatory metabolic processes to maintain functional integrity[1]. As previously depicted, a striking feature of brain energy metabolism is the tight coupling that is required between energy demand and the adequate glucose and oxygen delivery from the vasculature[137]. Glucose and oxygen metabolism are key in maintaining brain plasticity and cognition[138]. As such, glucose is the principal metabolic substrate for living cells, and is rich in potential energy[139]. Glucose enters the brain mainly through glucose transporter 1 (GLUT1). Notably, GLUT1 is predominantly expressed in ECs, and to a lesser extent in astrocytes, while GLUT3 is primarily expressed in neurons[10]. In addition to glucose, several substrates may be consumed by the brain to generate energy such as lactate, acetate, ketone bodies and fatty acids. These substrates are transported via different transporters mediated by monocarboxylate transporters (MCTs), expressed by astrocytes and neurons[10,140].

Brain metabolism is dependent on the adequate production of adenosine triphosphate (ATP), main energy currency of cells, by the multicellular NVU. ATP can be generated via different biochemical pathways and depends on the availability of oxygen. In the presence of oxygen (aerobic metabolism), oxidative phosphorylation involving mitochondria is the main pathway to produce ATP. Oxidative phosphorylation harnesses the reduction of oxygen to produce a large number of ATP molecules[141]. Aerobic cellular respiration is made of three major steps: 1) glycolysis; 2) tricarboxylic acid cycle (TCA); 3) oxidative phosphorylation. Glycolysis takes place within the cytosol, and does not require oxygen. Notably, in the absence of oxygen, glycolysis is initiated for the rapid production of ATP. In this pathway, glucose is broken down into two

molecules of pyruvate with an output of ATP and nicotinamide adenine dinucleotide (NADH)[142]. Of note, pyruvate can be further metabolized to lactate. In events of high energy demand and low energy output, lactate can act as a gluconeogenic precursor to support energy supply[141]. In non-high energy demanding conditions, pyruvate molecules are oxidized into acetyl CoA, NADH and carbon dioxide (CO_2). Acetyl CoA enters the TCA cycle, taking place in the matrix of the mitochondria, to undergo a chain of chemical reactions to produce CO_2, NADH, flavin adenine dinucleotide ($FADH_2$), and ATP[143]. Electrons derived from NADH and $FADH_2$ combine with O_2, releasing energy for the electron transport chain (ETC) of oxidative phosphorylation. This pathway consist of complex enzymatic reactions at the inner mitochondrial membrane. ETC proteins comprise complex I, complex II, coenzyme Q, complex III (cytochrome C), complex IV and complex V. Complex I oxidizes NADH transferring electrons to coenzyme Q. Complex II accepts electrons from succinate, an intermediate of the TCA cycle, by FAD which transfers the electrons to coenzyme Q. Coenzyme Q acts as an electron carrier, and transfers electrons to complex III. Complex III, known as cytochrome C, accepts the electrons and transfers them to complex IV while also releasing 4 protons contributing to the proton gradient. Complex IV oxidizes cytochrome C, and transfers electrons to oxygen, the final electron carrier in aerobic cellular respiration. Complex V, ATP synthase, uses the proton gradient generated across the inner mitochondrial membrane to form ATP through the process of chemiosmosis[144].

With the brain's massive energy consumption, a synergistic function of the cells forming the NVU (ECs, astrocytes and neurons) is required to maintain brain metabolism[1,137]. These cells function in a complex network regulating energy production and oxygen metabolism[145]. While in this thesis we focus primarily on EC metabolism, it is important to note the essential association between neurons and astrocytes in mediating brain metabolism.

Elevated neuronal activity will severely alter availability of ATP, neurons produce the bulk of their energy through oxidative phosphorylation at baseline. During increased energy demands, neurons can become dependent on glycolysis[146]. As such, the brain must be able to respond to these changes in ATP, and proper signals must be sent to increase ATP production. For instance, neuronal mitochondria can increase ATP synthesis to support elevated activity, however this is highly dependent on the vasculature[147]. Increased neuronal activity prompts changes in blood flow through the process of NVC to increase glucose uptake and oxygen consumption[2,12]. In parallel, NO is produced by neurons leading to an elevated glutamatergic excitation. Active neurons release glutamate which will lead to astrocytic uptake[148]. In 1994, Pellegrin and Magistretti suggested that astrocytes switch from oxidative metabolism to glycolysis during glutamate uptake[149]. Notably, astrocytes generate ATP mostly through glycolysis and partly through oxidative phosphorylation. As a result, a raised glycolytic rate within astrocytes leads to an increased lactate production that is shuttled to neurons for energy production[149,150]. The astrocytic-derived lactic acid is converted to pyruvate in neurons, and transported to the mitochondria to produce ATP through oxidative phosphorylation[151]. The astrocytic metabolic switch can help respond to the increased metabolic demand of neurons as lactate can act as a substrate for oxidative metabolism[150]. Although the concept of the astrocyte-neuron lactate shuttle is widely supported, this hypothesis is still a matter of debate within the field[152]. Furthermore, astrocytes can alter vascular tone by triggering vasodilation via calcium release in pericytes surrounding capillaries. As a result, there is increased glucose and oxygen availability[1,151]. Glucose entering the brain can be taken up by astrocytes through GLUT1 expressed at the astrocytic end-feet to support their glycolytic metabolism. In times of decreased glucose availability, ketone bodies become the main source of energy which is dependent on MCT1 transporters expressed by astrocytes. While astrocytes are dependent on

signals from neurons to increase energy availability during elevated metabolic demand, neurons must also dependent on ECs to support their energetic needs by modulating vascular tone and activating angiogenesis[133,137].

ECs have a high glycolytic activity to efficiently support brain metabolism. Glucose from the blood stream enters the brain via GLUT1, mainly expressed by ECs. Notably, inhibition of GLUT1 leads to energy depletion due to the decreased glucose uptake and glycolysis. Lack of GLUT1 activity decreases EC proliferation without having an impact on migration[153]. Moreover, GLUT1 deletion results in reduced lactate production in ECs which leads to the loss of pericyte coverage, BBB breakdown and increased permeability[154]. Interestingly, GLUT1 deletion often leads to severe seizures, neuronal loss and CNS inflammation[153]. While brain ECs reside in a high-oxygen environment with an elevated mitochondria number compared to peripheral ECs, glycolysis is their main source of energy as it allows for fast production of ATP to ensure migration and proliferation of cells to rapidly form new sprouts[155,156]. Consequently, the dependency of ECs on glycolysis (86% of metabolism) rather than mitochondrial oxidative metabolism (14% of metabolism) enables sprouting ECs in avascular regions to generate energy independent of oxygen[133,157]. Additionally, glycolysis reduces the production of reactive oxygen species that are formed during oxidative phosphorylation[141]. The final step in glycolysis consist of the conversion of pyruvate to lactate by lactate dehydrogenase. Lactate produced by ECs can be utilized as an energy source by other cells found within the NVU (*i.e.* pericytes, neurons and astrocytes). For instance, lactate production by ECs is essential for pericyte metabolism to support oxidative phosphorylation[154]. Of note, although pericytes produce energy via oxidative phosphorylation, they are also dependent on glycolysis to generate ATP. Moreover, lactate from ECs can signal to neurons to suppress neuronal activity in times of reduced energy availability[158]. While lactate can

reduce neuronal activity, it can also stimulate angiogenesis by activating PI3K/Akt and MAPK/ERK pathways to upregulate VEGF. Furthermore, glycolysis intermediates may be taken up by the pentose phosphate pathway (PPP) as a source of nucleotides during cell division or redox agents during cell homeostasis[133]. Once ECs are quiescent, glycolysis activity is reduced as less energy is required. This change in metabolism is regulated by transcriptional factor forkhead box protein O1 (FOXO1) which reduces signaling by cellular myelocytomatosis oncogene (c-MYC), a regulator of anabolic metabolism and growth. Additionally, laminar shear stress, downregulates 6-phosphofructo-2-kinase/fructose-2,6-bisphosphatase (PFKFB3), a key regulator of glycolysis, which decreases glycolysis in ECs and leads to quiescence[133]. The increased mitochondrial number in these cells, making up for 8-11% of cytoplasmic volume, allows to support the high metabolism and transport properties of the BBB in order to account for the sensitivity of the BBB to oxidative stress[159]. The numerous roles of the endothelium in brain function highlights the importance of these cells in maintaining a healthy brain. Any vascular discrepancies can lead to detrimental effects, and even onset or progression of neurological disorders.

1.6. Brain vasculature in neurological diseases

The brain vasculature is involved in several pathologies[7]. Often, defective vascular mechanisms are present before the appearance of symptoms, and so has been hinted to be a biomarker of disease progression[7]. Most studies investigating the vascular perspective in neurological diseases are focusing on neurodegenerative disorders including multiple sclerosis (MS), Huntington's (HD), Parkinson's (PD) and Alzheimer's (AD) diseases[160-164]. In these diseases, common vascular discrepancies are emerging such as altered CBF, impaired cerebrovascular reactivity as well as changes in vascular network density.

MS, a chronic autoimmune disease of the CNS occurring when the immune system attacks its own nerve fibers and myelin sheaths, has been associated with functional cerebrovascular abnormalities including decreased cerebral perfusion and reduced CNS venous blood drainage[165,166]. MS imaging studies have reported decreased CBF in both gray and white matter of MS patients[165,167]. For example, hypoperfusion in the gray matter has been suggested to lead to a reduced metabolism due to loss of cortical neurons[168]. Furthermore, impaired energy metabolism of astrocytes is associated with MS and is suggested to contribute to altered CBF. Reactive astrocytes secrete ET-1, a vasoconstrictor, which can also dysregulate CBF[166,169]. Interestingly, decreased CBF was identified in patients prior to symptom onset[170], suggesting that vascular abnormalities may be a factor in precipitating MS progression. In MS, the BBB has been described as highly permeable with decreased expression of tight junctions including ZO-1 and occludin[171]. Furthermore, MS is characterized with increased angiogenesis which is suggested to contribute to disease progression and MS relapses[172].

HD is an hereditary, autosomal dominant and neurodegenerative disorder that entails trinucleotide CAG repeats on chromosome 4 in the Huntingtin gene (HTT). HD has been mostly associated with cerebral hypoperfusion[173]. As in MS, changes in CBF are often present prior to gross structural changes with altered NVC leading to cognitive impairments[174,175]. In addition, HD progression is associated with elevated transcytosis and paracellular permeability due to decreased tight junction molecules in the BBB as well as increased vessel density[176,177].

PD is the second most common neurodegenerative disorder after AD[178]. PD is characterized by the progressive degeneration of the nigrostriatal system namely dopaminergic neurons, resulting in rigidity, bradykinesia, postural instability, and resting tremor[178]. PD patients are often associated with hypoperfusion as well as increased BBB dysfunction with decreased tight

junctions and vascular degeneration which includes string vessel formation in brain capillaries. String capillaries are a type of degenerating vessels characterized by thin connective tissue strands with no ECs and without blood flow[179]. In addition to this vessel abnormality, a collapsed basement membrane without an endothelium is considered a common feature in PD[180,181]. Structural alterations of the basement membrane can lead to compromised nutrient transport and cognitive disturbances[182]. Other vascular abnormalities such as reduced capillary density, basement membrane thickening and pericyte degradation are observed in PD patients[182].

As for AD, this neurodegenerative disease manifests with memory, attention, executive, visuospatial and perceptual impairments. This disease is characterized by amyloid deposition, neuroinflammation and cerebrovascular pathology. Furthermore, vascular features including hypercholesterolemia, hypertension and ischemic strokes have been shown to increase the risk of AD development[163,183,184]. As AD leads to amyloid (Aβ) deposition in the brain, Aβ deposits have been associated with alterations in the vessel wall (cerebral amyloid angiopathy) with degeneration of ECs[102]. As in other neurodegenerative disorders, AD is associated with reduced CBF that premediates cognitive decline and Aβ deposition[185]. Notably, many cerebrovascular dysfunctions have been detected early in AD which are associated with decreased Aβ clearance, vascular oxidative stress, inflammatory damage and impaired BBB function[102]. These include altered vascular reactivity and increased production of ROS such as peroxynitrite, a known contributor to endothelial dysfunction[186]. In addition, decreased CBF is often associated with poor cognitive function and a faster cognitive decline in AD[187]. While decreased CBF is at the forefront of AD pathology, the underlying cellular mechanisms are only starting to emerge. A known contributing factor involve pericytes, these cells are linked to hypoperfusion and increased capillary constriction in AD[52,188]. Neutrophils, immune cells, have been demonstrated to block capillaries

leading to altered CBF[189]. Impaired capillary endothelial inward rectifying Kir2.1 channel which plays a role in mediating blood delivery has been associated with AD[190]. In addition, early signs of BBB leakage have been detected in AD[185]. As in other neurodegenerative disorders, AD is characterized with reduced expression of tight junctions such as claudin-5, ZO-1 and occludin as well as infiltration of circulating leukocytes, reduced capillary length and basement membrane thickening[191,192]. Angiogenesis is also altered in patients with AD due to reduced expression of a regulator of vascular differentiation (MEOX2)[193].

While the vascular mechanisms linked with neurodegenerative disorders are being investigated, vascular deficits are starting to be deciphered in other conditions. Endothelial dysfunction has been shown to have a pivotal role in small vessel disease (SVD)[194]. SVD is characterized with ECs losing BBB properties, tight junction disruptions, and difficulties in mediating vascular tone, which is often associated with changes in CBF[194]. Repetitive traumatic brain injuries (TBI) have been associated with BBB disruptions through elevated vascular shear stress and CBF alterations[195]. Furthermore, a growing number of recent studies indicate chronic stress and depression to be linked with BBB leakiness through loss of tight junction expression[196-198].

The commonality of vascular deficits in neurodegenerative disorders, injury and conditions, namely dysregulated CBF and BBB as well as EC dysfunction, underlines the requirement of proper functional vascular networks for maintaining brain health. Therefore, a functional cerebrovasculature is key in supporting brain development and maturation. As such, early vascular impairments may exacerbate and/or lead to onset of neurodevelopmental disorders. This being a main focus of this thesis as we investigated the contribution of the brain vasculature to a neurodevelopmental disorder.

1.7. Altered cerebrovasculature in neurodevelopmental disorders

Neurodevelopmental disorders (NDDs) define a group of conditions with early onset symptoms preceding adulthood[199]. In general terms, these conditions impact the typical functioning of the brain, leading to lifelong adverse effects. Globally, almost everyone if not all, have been impacted by conditions pertaining to brain development[200]. NDDs have been shown to encompass complex multifaceted etiologies with elevated individual variability, adding to the intricacy of aiding these individuals on a day-to-day basis[201]. NDDs consist of several conditions including, but not limited to, attention-deficit/hyperactivity disorder (ADHD), GLUT1 deficiency syndrome, Down syndrome, schizophrenia, and autism spectrum disorders (ASD)[201].

Vascular discrepancies have been very little studied in the context of NDD. For example, children with ADHD, hyperactivity and impulsivity often have concomitant altered CBF where both hypo- and hyper-perfusion have been found[202]. GLUT1 deficiency syndrome, severely affects EC function, leading to a reduced capacity of brain angiogenesis, disrupting glucose entry into the brain, and dysregulating brain metabolism[67]. Down syndrome which results from trisomy of chromosome 21 has been associated with cerebrovascular disease including enlarged perivascular spaces and cerebral microbleeds[203]. Schizophrenia, on the other hand, is described with behavioral and cognitive symptoms that arise progressively with positive (psychotic episodes) and negative (social and motivational deficits) symptoms[204]. Studies have linked altered CBF with schizophrenia-related symptoms[205,206]. For instance, positive symptoms correlated with increased CBF while severe negative symptoms were related with decreased CBF[207,208]. Furthermore, as schizophrenia symptoms persist with age, there is a parallel with decreased CBF and degenerative changes in these patients[209,210]. In accordance with altered CBF, altered NVC responses have been identified in schizophrenia patients[211,212]. As with neurodegenerative diseases, dysfunctional BBB

with increased permeability and reduced expression of tight junctions in ECs have been reported in schizophrenia. More specifically, schizophrenia patients present with microvascular abnormalities including thickening and deformation of the basal lamina, vacuolation of cytoplasm in ECs, swelling of astrocytic end-feet, microglial activation and atypical vascular arborization[213,214]. Furthermore, ASD have also been associated with cerebrovascular discrepancies, this will be discussed in more detail in the following sections, as it is the main topic of this thesis. Thus, the vascular alterations in these disorders could suggest a cerebrovascular contribution to NDDs pathophysiology.

1.8. Autism spectrum disorders (ASD)

1.8.1. ASD characteristics, diagnostic and origins

ASD are a group of neurodevelopmental disorders characterized with social interaction and communication deficits as well as stereotypic behaviors often present early in life[215,216]. ASD have a prevalence of 1.5% worldwide, and is suggested to be 4 times more common in boys than girls[201,217]. However, the diagnosis criteria are mostly geared towards boys which could lead to a misrepresentation of these disorders in girls[201]. In the last twenty years, there has been an increase in diagnosis in ASD, in part from the more inclusive standards by clinicians as well as increased awareness by the overall population[218]. As ASD are classified as a spectrum, they entail a variety of symptoms, ranging from mild and high functional individuals to severely impaired cases requiring long-term support[219]. The variability of these disorders increases the difficulty of diagnosis as no medical test can discriminately diagnose ASD[219]. Since the first description of ASD in 1943 by Leo Kanner, there are now standardized techniques including screening tools to better identify these disorders[220,221]. Medical professionals establish an ASD diagnosis with the

developmental history and behavior of a child[222]. The Diagnostic and Statistical Manual of Mental Illnesses (DSM-5) indicates that an ASD diagnosis can only be made if the individual presents with persistent deficits in social-emotional reciprocity, and nonverbal communicative behaviors for social interaction (DSM-5, 5th edition, American Psychiatric Association, 2013). According to the Centers for Disease Control and Prevention, ASD can be detected as early as 12 months of age; however, a definitive diagnosis is usually made by the age of 2[223]. In some rare instances, individuals with very mild symptoms are only diagnosed in early adulthood[224]. In order to receive an ASD diagnosis, individuals must present altered behaviors early in development. Diagnosis of ASD is completed in two steps: 1) developmental screening and 2) comprehensive diagnostic evaluation. In the first step, children are screened during regular doctor visits at 18 months of age and at 24 months of age where the pediatrician examines how the child learns, behaves, moves and interacts. If there are any signs of developmental delay, the child undergoes a second screening step by completing a comprehensive diagnostic evaluation which includes genetic and neurological testing[225] (Centers for Disease Control and Prevention, 2018).

Considering the variability in the presentation of ASD between individuals, the added element of medical co-morbidities increases the complexity of these disorders. Medical co-morbidities are more common in individuals with ASD than in the general population[226]. Often, these include skin allergies, asthma, ear infections, severe headaches, gastrointestinal problems, sleep disorders, diabetes and heart disease[221,227]. These added health burdens can exacerbate the core ASD symptoms. Although, co-morbidities can be treated or at least managed to ameliorate the quality of life of individuals, the core symptoms of ASD are very difficult to mediate[228]. Currently, there are no treatments for ASD. However, there are methods to reduce debilitating symptoms such as aggression, self-injurious behaviors, agitation and hyperactivity. For instance,

pharmacological treatments including antipsychotics, anticonvulsants, antidepressants and mood stabilizers can help moderate some of these symptoms[223].

From the day of symptom presentation, these individuals often require elevated care, treatment and/or rehabilitation depending on symptom severity[223]. With a definitive need for improvement of the quality of life of these individuals, potential targets must be identified to tackle the core symptoms. This represents a knowledge gap that research must address. While the causes of ASD are unknown, a starting point in unraveling these potential targets is understanding the two main origins of ASD: environmental and genetic origins[220,229,230]. Exposure to several chemical stressors including lead, valproic acid, heavy metals as well as prenatal viral infections and maternal diabetes can all be considered contributors to ASD onset[231-235]. Research is now in the process of unraveling their contributions to ASD pathophysiology. Although these environmental factors increase the susceptibility of an individual to have an ASD diagnosis, the main risk factors are genetic variants as they account for up to 80% of ASD onset[230].

The establishment of genetic predisposition to ASD was first suggested when monozygotic twins were more likely to receive a diagnosis compared to dizygotic twins[236]. This not only points to genetics but heritability of these disorders. Over 100 candidate genes have been related to ASD which often include genes involved in synapse formation (e.g. synaptic Ras GTPase activating protein 1 (*Syngap1*), and SH3 and multiple ankyrin repeat domains 3 (*Shank3*)) and transcription/chromatin remodeling pathways (e.g. methyl-CpG binding protein 2 (*Mecp2*), ubiquitin-protein ligase E3A (*Ube3a*))[237]. In addition, copy number variations (CNVs) account for 10% of ASD cases[230,238]. These CNVs consist of recurrent chromosomal abnormalities that lead to microduplications, microdeletions, inversion or translocations[239]. Notably, many genes can be implicated within these CNVs. However, they may not always be involved in disease pathology.

The most common CNVs associated with ASD include the 15q11-13, 22q11-13, 1q21.1 and 16p11.2 regions[230], the latter being the mutation of interest for this thesis. Notably, individuals can share similar mutations but present symptoms differently[230]. Therefore, increasing the difficulty in managing these disorders as well as leading to the question of why these individuals present symptoms differently. An answer that is currently unknown. These genetic components will allow research to further understand these disorders with a goal of identifying specific targets when developing therapies.

1.8.2. Non-vascular features of ASD

The majority of studies focus on the neuronal contributions to the pathology of ASD. Neuroanatomical studies have identified macrocephaly and abnormal neuronal connectivity in ASD. In the ASD population, 20% of individuals have been characterized with brain overgrowth as well as elevated neuronal density. Architectural organization abnormalities are mostly in the frontal lobe, cerebellum and subcortical limbic area[240,241]. The amygdala is a region of interest in ASD as it is one of the main regions with an overabundance of neurons, and it regulates emotions. Further along these lines, a study made an association between increased amygdala size and social interaction and communication deficits in ASD[242]. Neuroanatomical changes are also found in the cortex such as irregular cortical thickness, altered neuronal morphology and increased number of neurons. In superficial and deep cortical layers of the frontal, temporal and parietal lobe, increased spine densities on pyramidal neurons are often described in ASD. In addition, the prefrontal cortex of ASD children is frequently characterized with 67% more neurons when compared to typically-developing children[243,244].

Neocortex functions dependent on proper neuronal networks for connectivity. Altered

functional connectivity is a common feature in ASD patients[245]. A study has been able to make early predictions of ASD diagnosis by using functional connectivity MRI (fcMRI) data of 6-month-old infants with high familial risk for ASD. Brain metrics from these infants were associated with functional connectivity taken at 24 months of age, a time when ASD can be diagnosed[246]. These brain metrics showed a correlation between functional connectivity and ASD-related behavior scores[246]. Furthermore, dysregulated functional connectivity has been identified in the cerebral cortex in individuals with ASD, and is thought to be associated with increased short to medium distance axons and branching[247]. In addition, the overconnectivity of the sensorimotor, frontal and cerebellar regions could in part explain the altered sensory integration and emotional regulation in ASD[248]. The relationship between overconnectivity and ASD-related behaviors has been demonstrated in a mouse model of ASD which consisted of an overproduction of excitatory neurons in neocortical layer 2/3[249]. This model displayed abnormal neuronal morphology as well as ASD-like behaviors including deficits in social interactions and compulsive/repetitive behaviors[249]. On the other hand, the ASD prefrontal cortex is characterized with reduced network integration (*i.e.* underconnectivity). The underconnectivity of this region was correlated with ASD-related cognitive behaviors, this is of interest as this brain region is essential for decision making and task-related information in working memory[250].

As ASD entail increased neuronal density with widespread changes in connectivity, it has been suggested that these changes are related to abnormal proliferation/apoptosis as well as abnormal early and late neuronal migration[251,252]. These findings have prompted research to investigate the neuronal underpinnings of ASD. With the association of ASD with increased electroencephalogram (EEG) activity in the cerebral cortex, there is evidence that elevated cortical excitability correlates with altered expression of genes involved in GABAergic and glutamatergic

neurotransmission systems[253]. For instance, a reduction of GABA-related genes as well as lower counts of GABAergic neurons in ASD patients can lead to an increased neuronal excitability[254]. Further along these lines, increased glutamate receptors and mRNA levels of AMPA, related to glutamatergic system, have been reported in ASD[255]. This emphasizing the role of an excitatory/inhibitory imbalance in these disorders[256]. Consequently, the reduction of inhibitory signaling and higher expression of excitatory genes influence overall cortical activity in ASD. This excitability impacts neural synchronization, habituation and adaption, all of which can create disruptions in temporal processing, stimulus intensity coding, seizure susceptibility, and/or lead to sensory hyper- or hypo-sensitivity[257]. These changes are consistent with documented clinically-observed perceptual differences in ASD patients[257]. The imbalance between excitatory (glutamatergic) and inhibitory (GABAergic) mechanisms in the brain has been suggested to underlie ASD symptomatology[258].

Furthermore, the altered functional connectivity could be in part contributed to defects in synaptic structure and function, suggesting a synaptopathy in ASD. In ASD patients, excess synaptic protein synthesis and a reduced synaptic pruning may contribute to developmental deficits in these patients[259]. While studies have shown a strong neuronal contribution to ASD pathophysiology, the dependence of neuronal health on brain vasculature warrants a detailed investigation of the cerebrovasculature in these disorders.

1.8.3. Cerebrovascular features of ASD

While ASD are mostly studied from a neuronal point of view, in the last several years, research has started to unravel cerebrovascular alterations in ASD. The most common observation being changes in CBF in ASD patients. Different regions of the ASD brain have been associated with

either hypo-, hyper-perfusion or both[260,261]. These brain regions include, and are not limited to, the frontotemporal regions, bilateral insula, superior temporal gyri and supramarginal gyrus[261,262]. Importantly, altered CBF has been linked with ASD-related behaviors including language deficits and impaired executive function[260,263]. CBF responses were lower in children with ASD during different tasks compared to the control group[264]. In addition, ASD are also described with widespread hyperperfusion in frontotemporal regions including the orbitofrontal cortex, temporal gyrus and precentral gyrus[261]. The medial orbitofrontal cortex is known to have extensive connections with the limbic system, a system involved in socio-emotional cognition. Hyperperfusion has also been detected in frontal white matter and subcortical gray matter in ASD children. This is of interest as it correlated with severity of social deficits[265]. As such, CBF abnormalities appear to be associated with clinical manifestations[261]. While ASD are highly heterogenous, there are discrepancies between studies in regards to the specific changes in CBF. However, the commonality that CBF is altered in these individuals is a step towards the identification of novel cellular and molecular mechanisms in ASD pathophysiology.

Although the vascular component of ASD is not often the main goal in studies, there is one study which indirectly suggested impaired angiogenesis in young ASD post-mortem brain tissue[266]. In addition, few have investigated BBB aspects in the context of ASD. From the available literature, ASD patients are characterized with reduced tight junctions. As previously described, these are essential for maintaining BBB integrity[267,268]. Thus, altered BBB components may be at play in ASD pathophysiology. While there are no treatments for the core symptoms of ASD, hyperbaric oxygen treatment (HBOT) has been a suggested as a therapy that may improve cerebral hypoperfusion in ASD patients[269]. Although certain studies describe improvement in ASD

behavioral parameters, the variability in symptoms within each individual and different protocols did not lead to consistent benefits following this treatment[270].

Notably, animal models of ASD have shown similar vascular inconsistencies. A mouse model of idiopathic autism (Black and Tan Brachyury (BTBR) *T+tf/J* model) displayed decreased CBF[271]. In addition, a mouse model lacking solute carrier transporter 7a5 (*Slc7a5*) gene, a large neutral amino acid transporter expressed at the BBB, presented with ASD-related behaviors including motor dysfunctions. Administration of branched-chain amino acids was enough to improve these behaviors[272]. Moreover, a valproic acid ASD model revealed increased BBB permeability[273]. Taken together, these animal models of ASD present with similar cerebrovascular alterations found in patients with ASD inferring that they are great assets to unravel vascular mechanism(s) in ASD. Throughout this thesis, we provide a detailed body of work unraveling the vascular contributions to ASD using an animal model. This ASD animal model will help underline the importance of considering the vasculature in these disorders.

1.8.4. Altered metabolism in ASD

The brain requires adequate delivery of oxygen and nutrients via the blood stream to support its metabolic demand. As recent studies are demonstrating a link between altered CBF and ASD, it is expected that these changes will affect metabolic mechanisms in the brain. In the ASD population, 30% of individuals with ASD have metabolic abnormalities[274]. At first glance, mitochondrial disease is often considered the main culprit leading to metabolic alterations in ASD. Notably, the mitochondria are central in generating energy in the form of ATP through oxidative phosphorylation[275]. The ETC in the inner mitochondrial membrane has been key in identifying mitochondrial dysfunction. Evidence has shown that frontal and temporal cortices are associated

with decreased levels of respiratory chain complexes in children aged between 4-10 years old, these changes were not identified in older age groups[276]. Different brain regions have been associated with lower levels of ETC complexes, these include the cerebellum, frontal and temporal cortices[276]. Moreover, misshapen mitochondria and impaired ETC activity are described in ASD[277]. Further along these lines, ASD-linked conditions have been coupled with increased number of mitochondria with reduced energy output. Interestingly, the contrary has also been shown where less mitochondria is found in ASD[278,279].

Although ASD are most often characterized with mitochondrial alterations, the impact of these changes are not fully elucidated[274]. Metabolite quantifications using different sample types, including plasma, blood, urine and brain tissue, highlighted elevated lactate, pyruvate, carnitine, and creatine phosphokinase, as well as inconsistencies in the glutathione pathway, which is crucial for redox capacity[280,281]. Moreover, stem cells from ASD patients exhibited diminished expression of glycolysis-associated transcripts and metabolites, overall reduced ATP-production and reduced cell respiration[282]. A similar observation was made in the plasma from ASD patients with reduced ATP levels[283]. Taken together, these markers indicate that ASD are linked with an altered metabolic profile[284].

In some ASD patients, there is evidence of brain cells (*i.e.* astrocytes) having altered glucose transport, impaired release and production of ATP, abnormal mitochondria morphology and increased oxidative stress[141]. For example, a model of ASD (mutation in inositol 1,4,5-triphosphate receptor type 2 (*Ip3r2*) gene) revealed impaired astrocyte-derived ATP production which was associated with ASD-related behaviors such as social interaction deficits and repetitive behaviors. Providing systemic ATP improved social behaviors in these mice[285]. However, there are discrepancies in these findings as the opposite has also been found where increased extracellular

ATP leads to a cellular danger response in ASD. In this case, elevated ATP acts as a regulator of the cellular danger response signaling, in turn altering whole system function and shown to contribute to ASD-like behaviors[286]. Based on this finding, ASD has been broadly linked with changes in purinergic metabolism. Transcriptional changes of purinergic receptors have been identified in plasma from patients with ASD[287]. As these findings suggest elevated ATP to be detrimental in ASD, several studies have completed a multisystem treatment using anti-purinergic therapies to inhibit purinergic signaling. This treatment improved core behaviors associated with ASD in certain individuals[286,288,289].

As ameliorating core symptoms of ASD has been the goal in many studies, identifying new metabolic biomarkers will allow for the development of potential therapies. Metabolite supplementation and a change in diet have been suggested to improve core symptoms of ASD. For instance, supplementation of vitamin B, co-enzyme Q10 and creatine monohydrate have shown to ameliorate mitochondrial disease ASD-related symptoms as they stimulate function of the ETC and increase energy production[290]. A ketogenic diet consisting of high-fat and low-carbohydrates has been suggested to improve sociability, learning and memory, motor coordination as well as restrictive behaviors in the Autism Treatment Evaluation Test and Childhood Autism Rating Scale[291,292]. The suggested mechanism for this improvement is that ketone bodies increase ATP production and regulate mitochondrial function[293]. While this diet may improve core symptoms in certain individuals, often, children with ASD are selective eaters, and so this diet can be difficult to maintain[294]. Although most patients with ASD have been associated with metabolic dysfunction, whether it is primary to the onset of these disorders is unknown. However, the literature provides strong evidence that these dysfunctions contribute at least secondarily to ASD pathophysiology, establishing metabolism as having a pivotal role in ASD pathogenesis.

Despite the contradicting views on ASD metabolism, energy metabolism must be further investigated to resolve these inconsistencies. Currently, the literature insinuates that energy balance and availability are key in ASD pathophysiology. Moreover with the importance of the cerebrovasculature in mediating brain metabolism, the vascular system must be taking into consideration to have the full picture of these metabolic alterations. A significant portion of this thesis is concerned with unraveling endothelium-based metabolic alterations in a model of ASD to obtain a deeper understanding of energy metabolism in these disorders.

1.8.5. 16p11.2 deletion syndrome

The focus of this thesis is on one of the most common CNVs associated with neurodevelopmental disorders and ASD, the 16p11.2 deletion syndrome. Within the 16p11.2 locus, both microdeletions and microduplications increases the risk of intellectual disability and psychiatric disorders. Most cases of the 16p11.2 duplication are familial (70%) while 16p11.2 microdeletion are mostly *de novo* (71%)[295]. The 16p11.2 duplication is associated with schizophrenia and ASD, while the deletion primarily relates to ASD. Compared to the microduplication, the 16p11.2 deletion has a more severe phenotype with a more serious impact on function[296]. This mutation accounts for 1% of ASD cases, and is considered one of the most common genetic links of ASD with a prevalence of 3 in 10,000 in the general population[297-299]. This heterozygous mutation consist of the loss of 550-600 kb and entails ~30 genes. It encompasses a range of clinical presentations including neurocognitive phenotypes such as developmental and language delay, cognitive impairment, macrocephaly and epilepsy. In addition to the typical ASD characteristics such as communication difficulties and expressive language (emotional outburst), the population with this mutation also has a high prevalence of ADHD as well as mood and anxiety disorders[300]. Other than behavioral

alterations, the 16p11.2 deletion is linked with several co-morbidities which can exacerbate symptoms including obesity, hyperinsulinaemic hypoglyceamia, cardiac malformations (narrowing of the aorta and ventricular septal defect), congenital heart disease, diabetes and sleep disturbances[301-304]. Structurally, 16p11.2 deletion carriers are often associated with an overall increased brain volume as well as increased thalamic, hippocampal, cerebellum, cortical surface area and overall white and gray matter[305]. In addition, abnormalities in the basal ganglia (striatum and globus pallidus) and decreased volume of the corpus callosum have been observed in carriers of this deletion[306].

Within the 16p11.2 locus, no single gene has been identified as the main cause for ASD-related phenotypes. However, several genes within this locus are essential for neural functions. For instance, proline-rich transmembrane protein 2 (*Prrt2*) is required for synaptic transmission and neuronal excitability. Serine/threonine-protein kinase 2 (*Taok2*) and potassium channel tetramerization domain containing 13 (*Kctd13*) are essential for neuronal differentiation and maturation[307,308]. Dysregulation of these genes is related to increased proliferation of cells as well as altered brain size and neurite morphogenesis[306]. Furthermore, *Kctd13* deletion is associated with reduced synaptic transmission as well as increased levels of Ras homolog family member A (RhoA). This protein is essential for maintaining the cytoarchitecture. Elevated levels of RhoA contributes to several neurological disorder pathogenesis[309]. This thesis provides evidence of the involvement of Rho associated coiled-coil containing protein kinase 2 (*Rock2*) expression, a downstream target of RhoA, in 16p11.2 deletion syndrome. Kinesin-like protein 22 (*Kif22*) mediates cell proliferation especially in neural progenitors as it regulates microtubule stability and cell division[307]. Major vault protein (*Mvp*), on the other hand, is an important regulator for cellular

motility, proliferation and differentiation[310]. Therefore, several genes found within this locus are essential for neural development and function.

Furthermore, the 16p11.2 locus entails the aldolase A (*Aldoa*) gene, a gene important for regulating glycolysis as well as mitochondrial function and cytoskeleton stability[311]. Changes in *Aldoa* dosage in the developing brain can perturb energy metabolism[307]. Moreover, the 16p11.2 locus comprise genes associated with EC function including *Mapk3*, myc-associated zinc finger protein (*Maz1*), transmembrane protein 219 (*Tmem219*) and coronin 1A (*Coro1A*). *Mapk3* is part of the MAPK/ERK signaling cascade. This cascade promotes cell proliferation, differentiation and angiogenesis by increasing expression of VEGF[312]. *Maz1* is a transcription factor that promotes expression of VEGF and in turn angiogenic activity. *Tmem219* is a receptor that binds to IGFBP3, insulin like growth factor binding protein 3, to induce caspase-dependent EC apoptosis. Similarly, *Coro1a* regulates TNFα-induced apoptosis of ECs[313-315]. Overall, genes within this locus are required for key cellular processes where altered dosage will have a detrimental impact on health. To examine the cellular and molecular mechanisms affecting 16p11.2 deletion on the vasculature, a validated pre-clinical mouse model has been generated[316].

1.8.6. 16p11.2 deletion syndrome modeled in mice

The murine model of 16p11.2 deletion syndrome allows for a more in depth investigation of the mechanisms pertaining to ASD pathophysiology. In the mouse model of 16p11.2 deletion syndrome, the deletion is located on chromosome 7 in the qf3 region and consist of 440kb[316]. Importantly, this area consist of a region of synteny with the 16p11.2 deletion found in the human condition (Figure 4). As such, this murine model entails the loss of the same genes found in the human deletion.

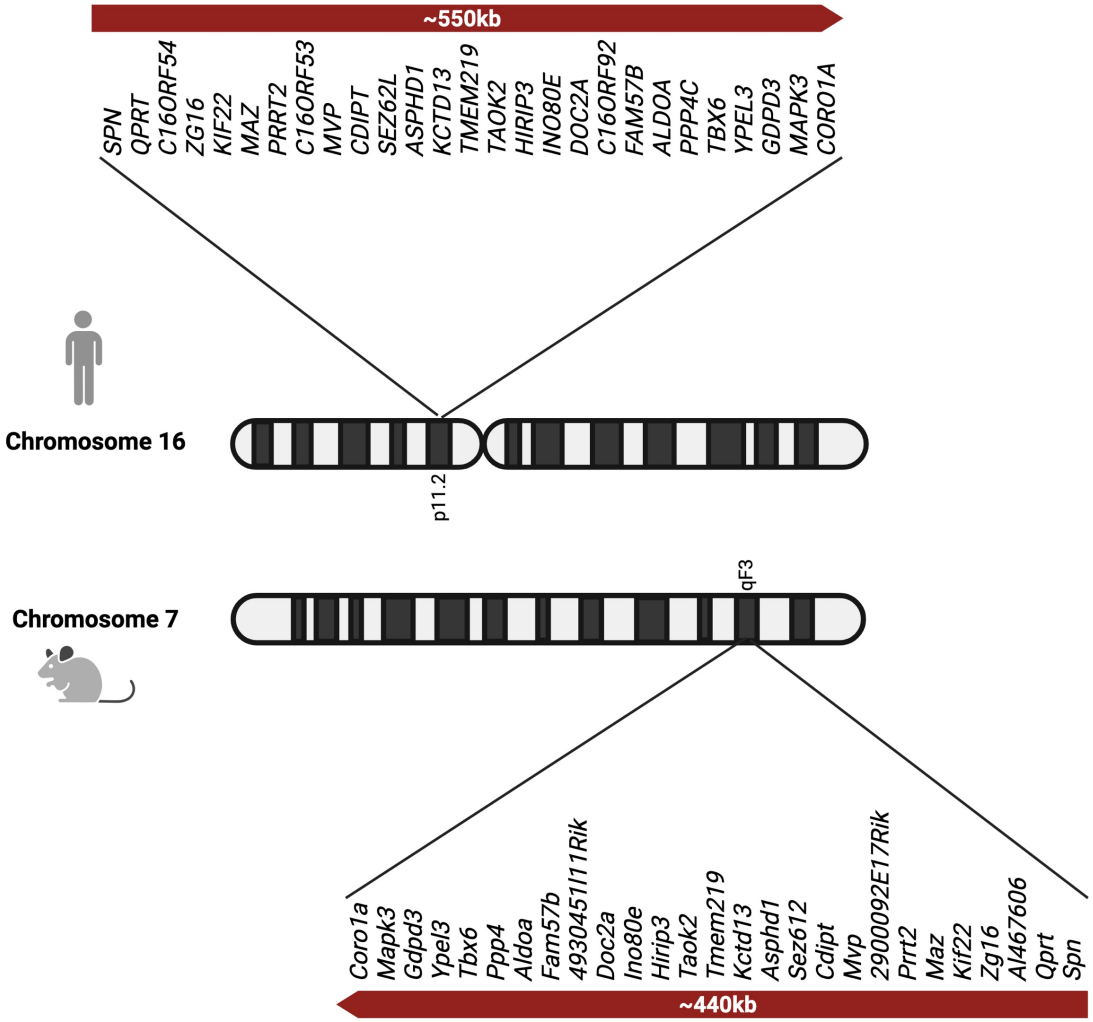

Figure 4. Genes mapping the human 16p11.2 deletion are conserved in the mouse qF3 locus on chromosome 7. Figure made with BioRender and based on the following references[306,316].

Furthermore, this 16p11.2 deletion mouse model has been confirmed to depict ASD-related behaviors including hyperactivity, stereotypic behaviors, severe motor coordination defects, lack of novelty-seeking behavior, and cognitive deficits[306,316]. Structurally, 16p11.2-deficient (*16p11.2*$^{df/+}$) mice have an increased basal forebrain, hypothalamus, midbrain, striatum and globus pallidus volume, as well as altered dopamine signaling and striatal circuitry[306]. Mice with the 16p11.2 deletion have a low body weight as well as exhibit normal general health and neurological reflexes[316]. These studies support the validity of this model for 16p11.2 deletion ASD research,

and is a valuable model to identify markers to target. In this thesis, we are focusing on this mouse model to investigate the vascular contributions to ASD.

1.9. Rational and hypothesis

Autism spectrum disorders (ASD) are complex neurodevelopmental disorders mostly studied from a neuronal point of view. However, the concomitant neuronal and vascular development paired with the crucial role of the vasculature in maintaining a functioning brain brings into question the role of the cerebrovasculature in these disorders. Moreover, alterations of critical cerebrovascular mechanisms during development can lead to lifelong consequences. Although previous studies highlight altered vascular parameters in the brain of individuals with ASD and animal models of ASD, the cerebrovascular contribution to these disorders are unknown. Furthermore, the lack of efficient treatments for core symptoms in ASD underscores the requirement for identifying new targets or biomarkers relating to ASD pathophysiology. In this thesis, we focus on one of the most common genetic risk factors for neurodevelopmental disorders and ASD, the 16p11.2 deletion. We hypothesize that: 1) cerebrovascular abnormalities represent structural and/or functional determinants in ASD pathophysiology, and 2) the 16p11.2 deletion leads to specific endothelial dysfunctions that are substantial contributors to neurodevelopmental alterations.

The main objectives of Manuscript I were to: 1) determine whether there is a cerebrovascular contribution to 16p11.2 deletion autism syndrome, 2) assess the cellular and molecular players underlying 16p11.2 deletion-associated brain vascular deficits, and 3) investigate the neurodevelopmental consequences of endothelium-specific 16p11.2 haploinsufficiency. These objectives were accomplished by assessing cerebrovascular function and structure in a 16p11.2 deletion mouse model *in vivo* and *in vitro*. The main objectives of Manuscript II were to: 1) identify

the specific endothelial dysfunctions related to the 16p11.2 deletion, 2) rescue 16p11.2 deletion-associated endothelial dysfunctions, and 3) validate the mechanism through which the rescue takes place. This was accomplished by assessing and modulating metabolic parameters of primary brain endothelial cells isolated from 16p11.2-deficient mice. The main objective of Manuscript III was to investigate the involvement of reduced *Rock2* expression, Rho kinase essential for vascular function, on 16p11.2 deletion-associated endothelial dysfunction and 16p11.2 deletion-associated adult mouse behaviors. This objective was accomplished by generating a novel mouse model of 16p11.2 deletion with *Rock2* heterozygosity.

Preface to Manuscripts

The manuscripts presented in this thesis were produced and written during my graduate studies in the Neuroscience Program at the University of Ottawa. For each manuscript, figures, figure legends, as well as references follow the formatting of the respective journals. The references pertaining to each manuscript can be found within the corresponding manuscript chapter while introduction and discussion references are found at the end of the thesis. Supplemental information for each manuscript is found in the Appendices section. While three manuscripts comprise the main body of this thesis, three additional manuscripts covering important supplementary topics relating to this work can be located in the Appendices section. Each thesis chapter is preceded with a contribution, connection to thesis topic and status statement.

Manuscripts found in Main Text:

Manuscript I is published at *Nature Neuroscience* (2020); co-first author.

Manuscript II is submitted; first author. Manuscript is subject to change.

Manuscript III is published at *Neuroscience Letters* (2024); first author.

Manuscripts found in Appendix:

Manuscript IV is published at *Star Protocols* (2021); first author.

Manuscript V is published at *Frontiers in Aging Neuroscience* (2021); first author.

Manuscript VI is published at *Neuroscience Insights* (2024); first author.

Chapter 2- Manuscript I

Association to hypothesis: This manuscript uncovers cerebrovascular contributions to autism spectrum disorder (ASD) including a novel association between endothelial dysfunction and 16p11.2 deletion syndrome using a well-known mouse model of ASD.

Current manuscript status: This manuscript is published in *Nature Neuroscience* in 2020.

Author contributions: J.O. completed experiments, analyzed data/images and produced manuscript draft. J.O. performed all mouse husbandry and genotyping. J.O. conducted all behavioral testing and analysis as well as completed the analysis of contrast imaging. Contrast imaging was conducted by M.Y. LDF and ECoG experiments were performed by X.T. S.B. provided expertise for the ECoG data analysis. Middle cerebral artery vascular reactivity was performed and analyzed by M.L-A. Mesenteric artery vascular reactivity was completed and analyzed by J-F.T. J.O. completed and analyzed blood pressure data, performed immunohistochemistry and imaging of vascular network and NVU. Vascular images were analyzed by C.H.C. and L.d.F.C. J.O. analyzed NVU cell density and coverage. M.F.A completed cortical thickness data. M.C. and M-È.T. completed the TEM images. P.V.D. analyzed TEM images. C.J.M. performed western blots and ELISA. J.O. completed mouse brain endothelial cell isolation, immunocytochemistry and RNA extraction. Q.Y.L., S.L., Y.P., Z.L., Y.D.B. and B.L. generated and/or analyzed transcriptomic data. J.O. performed mouse brain endothelial cell characterization. J.O. completed the tube formation assay on murine ECs and hiECs with M.H. J.O. performed hiPSCs differentiation with the help of M.H. W.L.S. provided healthy donor iPSC lines and expertise in stem cell research. D.J.S. (supervisor of M.H.) provided expertise in endothelial differentiation of iPSCs. C.J.B. and Y.D.B completed apoptosis experiments. B.L.

conceived and led the project, designed experiments and wrote manuscript from draft produced by J.O. with input from X.T., M.F.-A., M.L.-A., M.-È.T., D.B., C.R.K., S.B., Y.D.B., D.J.S. and W.L.S.

Manuscript contribution to thesis statement: Experiments for this manuscript were started during my Master's program. However, the bulk of the experiments were completed during my PhD studies. These experiments include behavioral assays, *in vitro* endothelial cell characterization and functional assessment, as well as *in vivo* assays. For this manuscript, I performed: the analysis for contrast imaging of baseline cerebral blood flow; immunohistochemistry (imaging and analysis) of NVU; immunohistochemistry and imaging of endothelial networks; primary cell isolation of endothelial cells; endothelial cell characterization and functional assays; endothelial cell RNA extraction for RNA sequencing; all behavioral assays; blood pressure and heart rate measurements; iPSCs differentiation and functional assay; and generated the draft for this manuscript. Furthermore, the manuscript was written, reviewed and published during my PhD program.

Vascular contributions to 16p11.2 deletion autism syndrome modeled in mice

Julie Ouellette[1*], Xavier Toussay[1*], Cesar H. Comin[2], Luciano da F. Costa[3], Mirabelle Ho[4], María Lacalle-Aurioles[5], Moises Freitas-Andrade[1], Qing Yan Liu[6,7], Sonia Leclerc[6], Youlian Pan[8], Ziying Liu[8], Jean-François Thibodeau[9], Melissa Yin[10], Micaël Carrier[11], Cameron J. Morse[1], Peter Van Dyken[1], Christopher J. Bergin[12], Sylvain Baillet[5], Christopher R. Kennedy[9,12], Marie-Ève Tremblay[11], Yannick D. Benoit[12], William L. Stanford[4,12], Dylan Burger[9,12], Duncan J. Stewart[4,12], and Baptiste Lacoste†[1,12,13]

Institutions:

[1] Ottawa Hospital Research Institute, Neuroscience Program, Ottawa, ON, Canada
[2] Federal University of São Carlos, Department of Computer Science, São Carlos, Brazil
[3] São Carlos Institute of Physics, FCM-USP, University of São Paulo, Brazil
[4] Ottawa Hospital Research Institute, Regenerative Medicine Program, Ottawa, ON, Canada
[5] Montreal Neurological Institute, McGill University, Montréal, QC, Canada
[6] National Research Council of Canada, Human Health and Therapeutics, Ottawa, ON, Canada
[7] University of Ottawa, Faculty of Medicine, Department of Department of Biochemistry Microbiology and Immunology, Ottawa, ON, Canada
[8] Digital Technologies, National Research Council of Canada, Ottawa, ON, Canada
[9] Kidney Research Center, Ottawa Hospital Research Institute, Ottawa, ON, Canada
[10] FUJIFILM VisualSonics, Inc., Toronto, ON, Canada
[11] Centre de recherche du CHU de Québec, Université Laval, Axe neurosciences, Québec, QC, Canada
[12] University of Ottawa, Faculty of Medicine, Department of Cellular and Molecular Medicine, Ottawa, ON, Canada
[13] University of Ottawa Brain and Mind Research Institute, Ottawa, ON, Canada

***** *These authors contributed equally to the work*

† *Lead contact*

Correspondence to:
Dr. Baptiste Lacoste
Faculty of Medicine, Department of Cellular and Molecular Medicine
University of Ottawa & Ottawa Hospital Research Institute
451 Smyth Road, Ottawa (ON) K1H 8M5, Ottawa, Canada
Phone: +1 (613) 562-5800 ext. 7124
Email: blacoste@uottawa.ca

Classification: Article

Number of figures:
Main figures: 8
Extended Data Figures: 10
Supplementary Figure: 2

Number of words:
Abstract: 149
Main text: 4496

Key words: autism spectrum disorders; 16p11.2 deletion; cerebrovascular; angiogenesis; cerebral blood flow; neurodevelopment.

Abstract

While the neuronal underpinnings of autism spectrum disorder (ASD) are being unraveled, vascular contributions to ASD remain elusive. Here, we investigated postnatal cerebrovascular development in the *16p11.2*$^{df/+}$ mouse model of 16p11.2 deletion ASD syndrome. We discover that 16p11.2 hemizygosity leads to male-specific, endothelium-dependent structural and functional neurovascular abnormalities. In *16p11.2*$^{df/+}$ mice, endothelial dysfunction results in impaired cerebral angiogenesis at postnatal day 14, and in altered neurovascular coupling and cerebrovascular reactivity at postnatal day 50. Moreover, we show that there is defective angiogenesis in primary *16p11.2*$^{df/+}$ mouse brain endothelial cells and in induced-pluripotent-stem-cell-derived endothelial cells from human carriers of the 16p11.2 deletion. Finally, we find that mice with an endothelium-specific 16p11.2 deletion (*16p11.2*$^{\Delta EC}$) partially recapitulate some of the behavioral changes seen in 16p11.2 syndrome, specifically hyperactivity and impaired motor learning. By showing that developmental 16p11.2 haploinsufficiency from endothelial cells results in neurovascular and behavioral changes in adults, our results point to a potential role for endothelial impairment in ASD.

Introduction

While neuronal mechanisms underlying ASD, including the 16p11.2 deletion syndrome, have been extensively investigated[1,2], vascular contributions to these conditions have been largely overlooked. This discrepancy in research focus is surprising given that the interplay between vascular and neuronal systems is critical for the normal growth and function of neurons[3,4]. Indeed, brain development relies heavily on proper cerebrovascular maturation. Brain vascular beds not only support the proliferation, differentiation and migration of neural progenitors[5] but they also ensure brain homeostasis and a steady supply of oxygen and nutrients for healthy neuronal function[6]. Hence, alterations in cerebrovascular processes during development may have long-lasting neurodevelopmental consequences, but direct evidence supporting this notion is missing. Classically, deficiencies in cerebrovascular networks are not associated with neurodevelopmental disorders, but rather with neurodegenerative conditions such as Alzheimer's disease. Vascular endothelium dysfunction is indeed recognized as an underlying mechanism of altered cerebral blood flow (CBF) and blood–brain barrier breakdown in Alzheimer's disease[7,8]. Recently, a postmortem study of brains of young patients with ASD indirectly suggested an impairment in cerebral angiogenesis[9], and a functional imaging study proposed a possible link between ASD and altered CBF[10]. Yet, contributions of cerebrovascular deficits to the pathophysiology of neurodevelopmental disorders and ASD remain to be explored. Accumulating evidence from ASD research supports the importance of copy number variations[11], which are found at higher frequency in the human 16p11.2 locus[12]. While 16p11.2 microduplications were linked to schizophrenia[13], reciprocal microdeletions are common etiological factors in ASD[14]. Approximately 2% of patients diagnosed with ASD harbor a 16p11.2 microdeletion, making it a common genetic cause of ASD[15]. A 16p11.2 deletion leads to a loss of approximately 500kb of DNA and haploinsufficiency of about

30 genes, which gives rise to a syndrome characterized by a large head size, speech and language problems, intellectual disability, an increased prevalence of seizures and a movement coordination disorder. The brains of 16p11.2 deletion carriers display cortical thickness anomalies, a dysmorphic cerebellum and an abnormal microstructure in white matter tracts[16–18]. It is now possible to study the 16p11.2 deletion syndrome in mice. Heterozygous *16p11.2*$^{df/+}$ mice possess a deletion (440kb, 27 genes) of the 7qF3 region of synteny conservation with the human 16p11.2 locus[19]. Compared with their wild-type (WT) littermates, *16p11.2*$^{df/+}$ mice display alterations in basal ganglia volume and cytoarchitecture, synaptic defects, sensory and social interaction deficits, hyperactivity and stereotypic movements, and a sleep disorder[19–22].

Despite the characterization of the above-mentioned features, to date, no investigation has focused on the role of the cerebrovasculature in ASD etiology. To address this important knowledge gap, we investigated the maturation of cerebrovascular networks in *16p11.2*$^{df/+}$ mice[19], a robust mouse model of the 16p11.2 deletion ASD syndrome. In addition, we achieved endothelial-specific 16p11.2 (7qF3) deletion by CRE-mediated recombination under the control of the endothelial promoter for vascular endothelial cadherin (*Cdh5-Cre*$^{tg/+}$*;16p11.2*$^{flox/+}$*).* We demonstrate the effects of endothelial 16p11.2 haploinsufficiency on postnatal neurovascular development, revealing a novel link between ASD and neurovascular abnormalities.

Results

Constitutive 16p11.2 haploinsufficiency leads to cerebrovascular dysfunction in vivo.

Task-induced blood oxygen level-dependent (BOLD) magnetic resonance imaging (MRI), which is commonly used as a surrogate of neural activation, shows reduced signals in the cerebral cortex of patients with ASD and is predictive of symptom severity[23]. BOLD–MRI relies on neurovascular coupling mechanisms, whereby neural activity regulates the interplay between cells that form the

neurovascular unit. Neurovascular coupling ultimately leads to constrictions or relaxations of vascular smooth muscle cells (VSMCs) around endothelial cells (ECs), which lead to changes in blood vessel diameter in the brain. Here, we first assessed activity-dependent regulation of CBF in *16p11.2*$^{df/+}$ mice and their age-matched WT littermates. CBF responses to whisker stimulation were measured using laser Doppler flowmetry (LDF) over the primary somatosensory cortex at postnatal day 14 (P14) and P50, two key ages of postnatal cerebrovascular maturation. Indeed, endothelial capillary networks rapidly develop from birth to P14, and then enter a remodeling phase from P50[4]. Evoked CBF responses were substantially attenuated in young adult (P50) *16p11.2*$^{df/+}$ male mice, but not females (n = 5–6; Fig. 1a and Extended Data Fig. 1a). CBF traces recorded in P50 mutant males appeared right-shifted, with reduced response amplitudes from baseline during stimulation and slower kinetics compared with P50 WT males. No difference was evidenced between *16p11.2*$^{df/+}$ and WT males at P14 (n = 4; Fig. 1a) or between female *16p11.2*$^{df/+}$ and WT mice at both ages (Extended Data Fig. 1a,c,d). Since higher tissue perfusion units could be reliably detected by LDF in P50 *16p11.2*$^{df/+}$ males at baseline (Extended Data Fig. 2a,b), we next sought to obtain an absolute measure of resting-state brain perfusion in male mice. Of note, an arterial spin labeling MRI study showed that elevated resting-state cerebral cortex perfusion was found in patients with ASD and correlated with symptom severity[10]. We assessed resting-state CBF in P50 male *16p11.2*$^{df/+}$ mice and WT littermates using non-invasive ultrasound imaging of intravenously injected microbubbles. This contrast imaging method, which relies on the detection of nonlinear subharmonic signals generated by microbubbles when exposed to ultrasound[24,25], quantified significantly higher resting-state CBF in anesthetized adult *16p11.2*$^{df/+}$ males than in age-matched WT males (n = 6–8; Fig. 1b and Extended Data Fig. 1b).

Differences in baseline and evoked CBF may result from chronically elevated or reduced peripheral blood pressure, a classic confounder in brain perfusion analyses. However, the above-reported cerebrovascular deficits could not be attributed to gross cardiovascular dysfunction, as systolic blood pressures and heart rates appeared normal in *16p11.2*$^{df/+}$ mice (n = 6–7; Extended Data Fig. 1e).

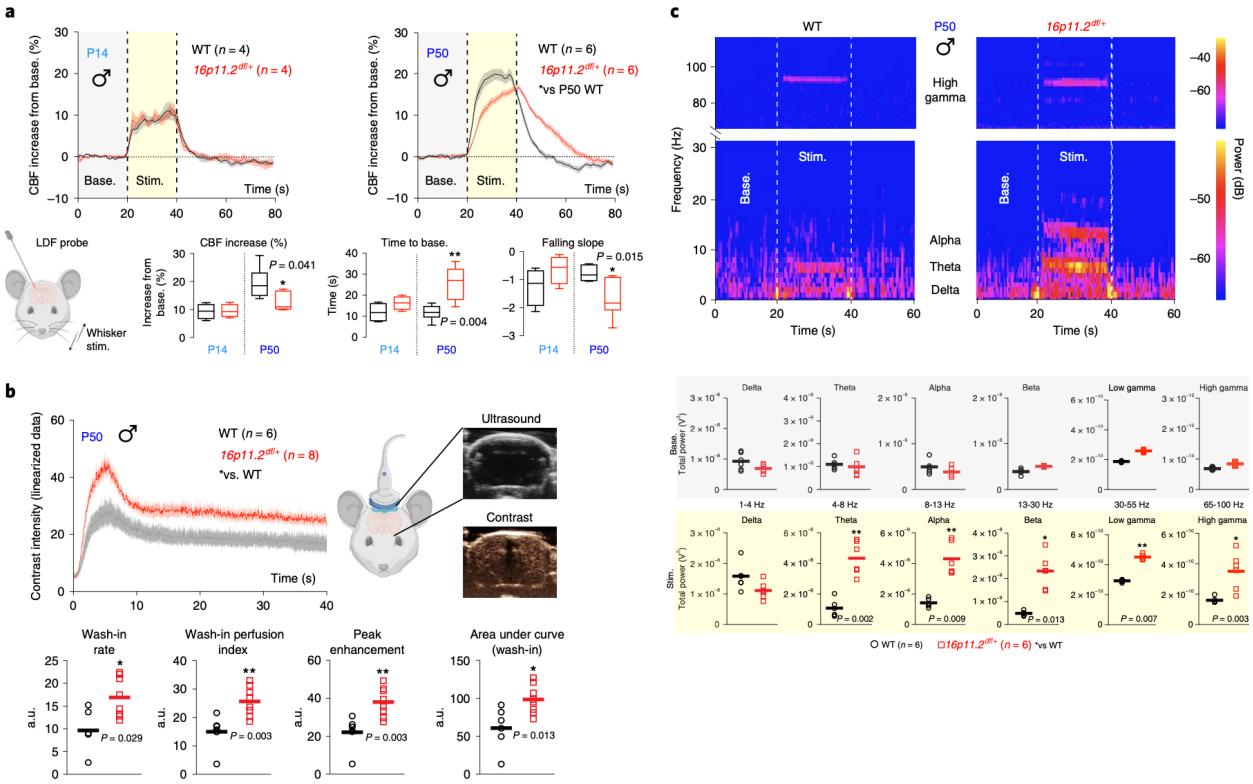

Fig. 1 | Adult male *16p11.2*$^{df/+}$ mice exhibit altered neurovascular function. a, LDF coupled to whisker stimulation (schematic shown on bottom left) in male mice at P14 and P50. Top: traces of normalized CBF responses. Bottom: whisker boxes showing averaged CBF parameters. Data represent hemodynamic parameters of evoked CBF monitored over the primary somatosensory cortex. A neurovascular coupling defect is evidenced in *16p11.2*$^{df/+}$ mice at P50, but not P14. Base., baseline; Stim., stimulation. **b**, Top right: schematic of ultrasound contrast imaging of intravenously injected microbubbles in anesthetized male mice at P50 (contrast imaging kinetics at resting state). Top left: the traces illustrate time–intensity values over a 40-s wash-in/ wash-out period in the somatosensory cortex. Bottom: these graphs show parameters of microbubble resonance kinetics (presented as arbitrary units (a.u.)). Quantifications demonstrate higher resting-state CBF in *16p11.2*$^{df/+}$ males compared with WT controls. **c**, eCoG recordings in the somatosensory cortex from WT and *16p11.2*$^{df/+}$ males before, during and after whisker stimulation. Top: selected spectrogram of eCoG traces representative of signaling power changes in higher (upper panel) and lower (lower panel) frequency bands. Bottom: average absolute power in delta (1–4 Hz), theta (4–8 Hz), alpha (8–13 Hz), beta (13–30 Hz), low gamma (35–55 Hz) and high gamma (65–100 Hz) frequency bands at resting-state (upper panel) and during stimulation (lower panel). While no change was observed in baseline eCoG power between *16p11.2*$^{df/+}$ and WT males, stimulus-evoked eCoG signals were increased in mutant mice (n = 5 animals per group, 6 stimulations per animal). Data are presented as whisker boxes showing minimum to maximum values, with the center line indicating the median (**a**) or mean with individual values (**b** and **c**). Traces in **a** and **b** represent the mean ± s.e.m. (n = 4–8 animals per group). *P < 0.05, **P < 0.01 (two-tailed Mann–Whitney test).

During mature neurovascular coupling, neuronal activity drives increased CBF[26]. In light of the attenuated CBF responses and enhanced resting-state CBF in *16p11.2*$^{df/+}$ male mice at P50, one would expect that the underlying neuronal activity is reduced or prolonged in response to sensory stimulation, and/or higher at baseline, in these animals. To test this, we used electrocorticographic (ECoG) measurements of somatosensory cortex activity before, during and after whisker stimulation in anesthetized males and females. At P50, ECoG power was not significantly different at baseline compared with controls in *16p11.2*$^{df/+}$ males (n = 6) and females (n = 5). However, the steady-state ECoG response to whisker stimulation was significantly more pronounced across multiple frequency bands in *16p11.2*$^{df/+}$ males at P50 with respect to age-matched WT controls, with similar onset/offset kinetics (Fig. 1c). This effect was absent in *16p11.2*$^{df/+}$ males at P14 (n = 4–5; Extended Data Fig. 2c), and was not found in female mice at P50 (n=5; Extended Data Fig. 2d). These data demonstrate a form of uncoupling between stimulus-evoked neurophysiological signaling and CBF responses in adult male *16p11.2*$^{df/+}$ mice.

This finding led us to hypothesize that neurovascular coupling phenotypes may have a vascular origin. We therefore sought to dissect the contribution of brain ECs and VSMCs to 16p11.2-deletion-associated cerebrovascular alterations and quantified the reactivity of middle cerebral arteries (MCAs) to increasing concentrations of known vasomodulators (Fig. 2 and Extended Data Fig. 3a). Using pressure myography coupled to video microscopy, we found an endothelium-dependent deficit in both male and female *16p11.2*$^{df/+}$ MCAs compared with WT MCAs at P50 (n = 5), as evidenced by reduced vessel relaxation in response to acetylcholine (ACh) (Fig. 2a), impaired vessel constriction to endothelial nitric oxide synthase (eNOS) inhibition (Fig. 2b) and reduced vessel relaxation by adenosine (Fig. 2c). The endothelial nature of this deficit was further confirmed by intact VSMC function, as evidenced by normal vasorelaxation by exogenous

nitric oxide (NO) donor sodium nitroprusside (SNP) (Fig. 2d) and normal vasoconstriction by phenylephrine (PE) (Fig. 2e). A similar phenotype was evidenced at P50 in peripheral (mesenteric) arteries (n = 6–7) when sexes were combined, hence further outside the influence of the cerebral cortex milieu (Extended Data Fig. 3b). Finally, as shown by unchanged p$D2$ values, which is a measure of vascular sensitivity to agonists (see Methods), this endothelium-dependent phenotype was not attributed to altered endothelial responses to vasomodulators in *16p11.2*$^{df/+}$ vessels (Extended Data Fig. 3b,c).

Therefore, our data demonstrate a correlation between global CBF dysregulation and endothelial dysfunction in *16p11.2*$^{df/+}$ male mice.

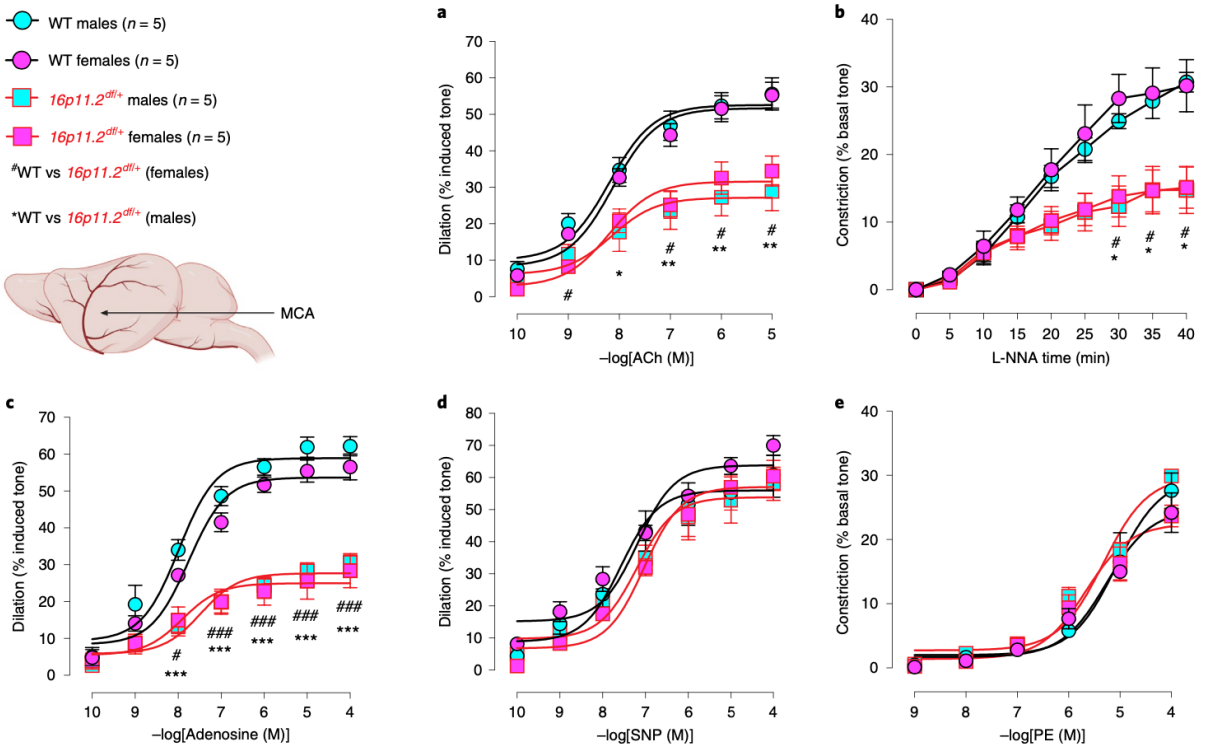

Fig. 2 | *16p11.2*$^{df/+}$ mice exhibit impaired endothelium-dependent vasodilation of pial arteries. a–**e**, The key applies to all panels. Vascular reactivity of pressurized middle cerebral artery (MCA, illustrated in the diagram) segments ex vivo revealed an endothelium-dependent vasodilation deficit, but normal smooth muscle function in *16p11.2*$^{df/+}$ mice at P50. Changes in lumen diameter were measured in response to ACh (**a**), L-NNA (**b**), adenosine (**c**), SNP(**d**) and PE (**e**). All data are shown as the mean ± s.e.m. (n = 5 animals per group). $^{*/\#}P < 0.05$, $^{**/\#\#}P < 0.01$, $^{***/\#\#\#}P < 0.001$ (two-way repeated measure ANOVA and Tukey's post-hoc test).

Constitutive 16p11.2 haploinsufficiency alters cerebrovascular growth in vivo.

As ECs are building blocks for the vessel wall and play crucial roles in CBF regulation[27,28], early alteration of endothelial growth and function might subsequently affect endothelium-dependent CBF regulation. Early after birth in mice, the brain microvasculature undergoes rapid maturation until P14 and then remodels from P50[4]. Past P14, a critical neurodevelopmental milestone, neurovascular coupling mechanisms progressively mature until adulthood[26]. To test the possibility that CBF alterations in P50 *16p11.2*$^{df/+}$ mice are subsequent to delayed endothelial maturation, we next sought to assess endothelial network development *in vivo* at P14 and P50 in three major subdivisions (anterior, parietal and occipital) of the cerebral cortex. Combining three-dimensional (3D) imaging of immunostained tissue to unbiased computational image analysis[4], we found that both the density and the branching of CD31-immunoreactive endothelial networks were lower in *16p11.2*$^{df/+}$ males at P14 throughout the cerebral cortex (n = 6; Fig. 3a,b and Extended Data Fig. 4a–c). At this age, the neuronal cytoarchitecture assessed in the parietal (that is, somatosensory) cortex by the markers NeuN and TBR1 appeared identical between WT and *16p11.2*$^{df/+}$ mice (n = 5; Fig. 3c and Extended Data Fig. 4k). At P50, the endothelial network structure appeared globally normal in *16p11.2*$^{df/+}$ mice (Fig. 3b), but mild cytoarchitectural defects emerged (n = 5; Fig. 3c and Extended Data Fig. 4k), which is concurrent to the ECoG phenotypes in males (Fig. 1c). Interestingly, mutant males failed to display the characteristic endothelial remodeling in parietal cortex layer IV (Extended Data Fig. 4b), whereby vascular density and branching normally decrease at P50[4]. Remarkably, the effect of genotype on endothelial growth from P14 to P50 was only apparent in males, as WT and *16p11.2*$^{df/+}$ females displayed similar patterns (Extended Data Fig. 4d–i).

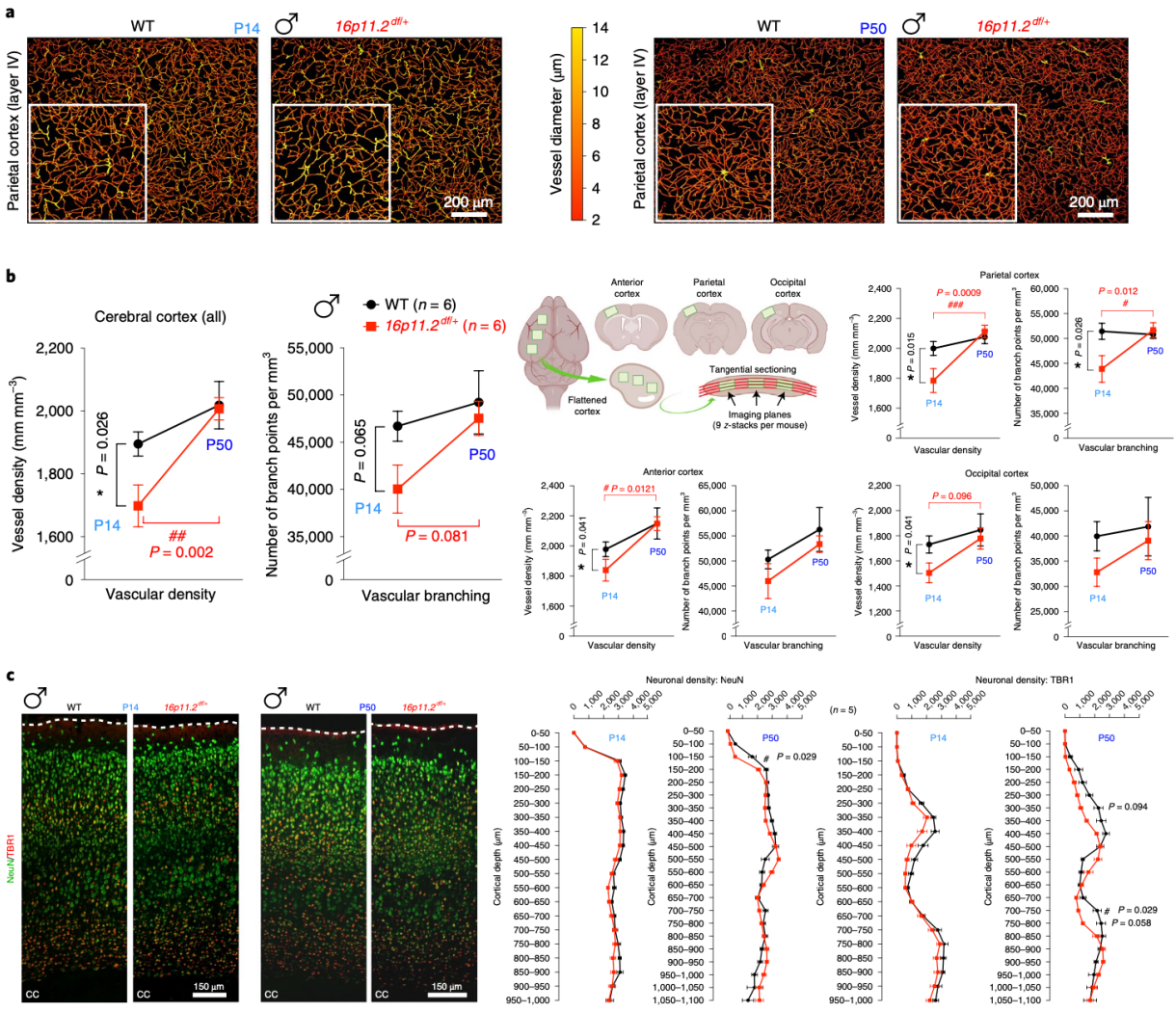

Fig. 3 | Male *16p11.2*$^{df/+}$ mice exhibit delayed endothelial network maturation in the cerebral cortex. a, *Z*-projection images of 3D endothelial network computational reconstructions (color-code indicated), illustrating lower vessel density overall at P14 (left) and higher vessel density in layer IV of the parietal (that is, the somatosensory) cortex of *16p11.2*$^{df/+}$ males at P50 (right). Displayed reconstructions are representative of experiments repeated in a total 24 male mice with similar results obtained. **b**, Quantifications by computational image analysis across three major subdivisions of the cerebral cortex at P14 and P50. Left: average of data from the entire cerebral cortex. Right: details for the three cortical ROIs. The center cartoon summarizes the image locations. A widespread delay in vascular network formation was measured at P14 in the cerebral cortex of *16p11.2*$^{df/+}$ males. Cortical layers in which most significant differences were found are shown in extended Data Fig. 4a–c. **c**, Representative images (left) and quantification (right) of neuronal densities in the somatosensory cortex following immunostaining for the neuronal markers NeuN and TBR1. All data are from male mice and are shown as the mean ± s.e.m. (n = 5–6 mice per group). White-outlined insets show higher-magnification images of computational reconstruction of endothelial networks. cc, corpus callosum. *P < 0.05 (two-tailed Mann–Whitney test). $^{\#}P$ < 0.05, $^{\#\#}P$ < 0.01, $^{\#\#\#}P$ < 0.001 (two-way ANOVA and Sidak's post hoc test).

The endothelial dependence of 16p11.2-associated delayed vascular growth was supported by normal development of mural cells (that is, pericytes, astrocytes and VSMCs) between P14 and P50; these cells interact closely with brain ECs to control vascular development, integrity and function[6] (*n*=3–7; Extended Data Fig. 5). Moreover, cerebral cortex levels of vascular endothelial growth factor A (VEGFA), which contributes to both neuronal and vascular development, were identical in WT and *16p11.2*$^{df/+}$ mice at both P14 and P50 (*n* = 3–6; Extended Data Fig. 4l), which suggests that there is normal release of this canonical angiogenesis regulator within the cerebral cortex of mutant mice. These results demonstrate that faulty endothelial maturation precedes neuronal abnormalities in the cerebral cortex of male *16p11.2*$^{df/+}$ mice during postnatal development.

Endothelium-specific 16p11.2 haploinsufficiency *in vivo* alters cerebral angiogenesis and neurovascular function.

The timing at which vascular versus neuronal phenotypes arise, as reported above, may reflect a contribution of early endothelial dysfunction to 16p11.2-deletion-associated neuronal abnormalities. Normal vascular development is critical to ensure proper establishment of neural circuits[5], but the impact of endothelial 16p11.2 haploinsufficiency on brain maturation is currently unknown. To test whether ECs contribute cell-autonomously to 16p11.2-deletion-associated alterations, we generated mice with endothelium-specific 7qF3 hemizygosity (*Cdh5-Cre*$^{tg/+}$*;16p11.2*$^{flox/+}$ or *16p11.2*$^{\Delta EC}$; Fig. 4a,b). This resulted in a mosaic pattern with partial expression of the excision reporter mCherry (Fig. 4c,d), which is probably subsequent to the limited excision efficiency of the large *loxP* 7qF3 region[20] (Fig. 4b). Remarkably, we measured significantly higher excision efficiency in female compared to male *16p11.2*$^{\Delta EC}$ mutants at P0

(*n*=4–5; Fig. 4c). While sex differences in excision efficiency remain unexplained, the mosaic pattern allowed for side-by-side phenotyping of WT ($CD31^{+}mCherry^{-}$) versus hemizygous ($CD31^{+}mCherry^{+}$) cortical ECs (cECs).

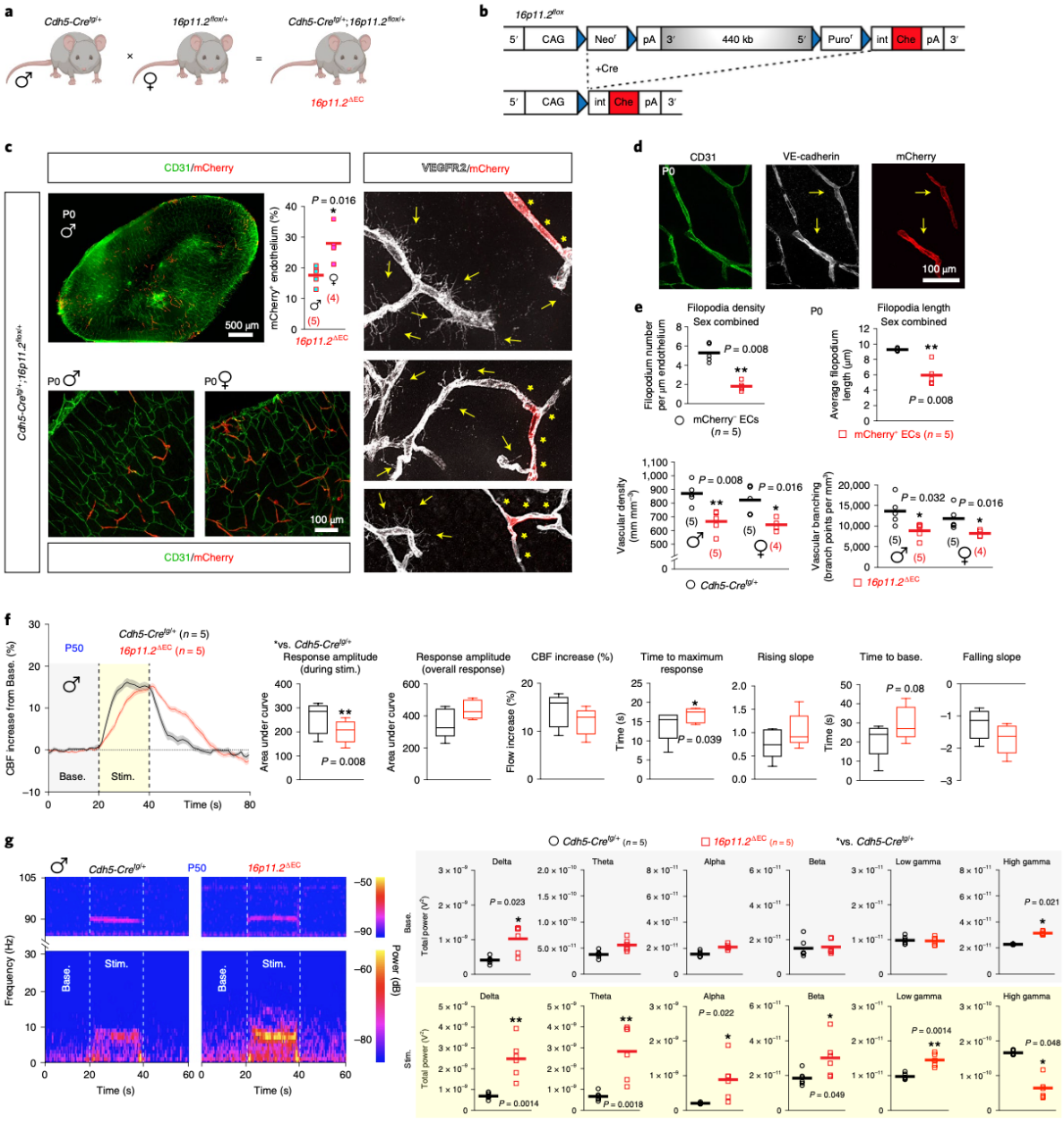

Fig. 4 | See next page for caption.

Fig. 4 | Effect of endothelium-specific 16p11.2 hemizygosity on neurovascular maturation *in vivo*. a,**b**, Breeding scheme (**a**) and mouse genetics (**b**)to obtain conditional deletion of the syntenic region from the 7qF3 locus in mouse eCs. **c**, Immunohistochemical characterization of CD31-positive endothelial networks in the cerebral cortex of male and female *16p11.2* $^{\Delta eC}$ newborns (P0). Left: in *16p11.2*$^{\Delta eC}$ newborns, CD31^{+} (green) mCherry^{+}(red) haploinsufficient cECs coexist with CD31^{+}mCherry^{-} WT cECs in a mosaic pattern. Center: the graph shows the proportion of CD31^{+}mCherry+(that is, excision efficiency) staining in the cerebral cortex of male versus female *16p11.2* $^{\Delta eC}$ newborns (representative images are shown for each sex). Right: VeGFR2^{-}mCherry double-immunostaining revealed that haploinsufficient cECs (depicted by yellow asterisks) display fewer filopodium extensions (arrows), as quantified in **e**. **d**, Confirmation of the expression of VE-cadherin (*Cdh5* gene product) in both CD31^{+}and mCherry^{+} cECs (arrows). Displayed images are representative of experiments repeated in five male newborn mice with similar results obtained. **e**, Quantification of endothelial structures in the cortex of *16p11.2* $^{\Delta eC}$ animals compared with littermate controls at P0. Top: quantifications of endothelial filopodia density and length. Bottom: quantifications of vessel density and branching in male versus female newborns. **f**, LDF coupled to whisker stimulation in anesthetized P50 males demonstrated reduced response amplitudes and slower kinetics in *16p11.2* $^{\Delta eC}$ mutants compared with *Cdh5-Cre*$^{tg/+}$littermates. For the chart on the far left, shaded areas represent 20 s of normalized CBF at baseline (gray) and during stimulation (yellow). **g**, eCoG recordings in the somatosensory cortex from *Cdh5-Cre* $^{tg/+}$ and *16p11.2* $^{\Delta eC}$ males at P50 before, during and after whisker stimulation. Left: spectrogram of selected eCoG traces representative of signaling power changes with stimulation in higher (upper panel) and lower (lower panel) frequency bands. Right: average neurophysiological signaling power in delta (1–4 Hz), theta (4–8 Hz), alpha (8–13 Hz), beta (13–30 Hz), low gamma (35–55 Hz) and high gamma (65–100 Hz) frequency bands at baseline (top) and during whisker stimulation (bottom). eCoG signal responses were globally increased in mutant mice during stimulation, with the exception of high-gamma power. Baseline activity in the delta and high-gamma frequency ranges were also increased in conditional mutants compared with age-matched control littermates. Data are shown as whisker boxes showing minimum to maximum values, with the center line indicating the median (**f**) or mean with individual values (**c**, **e** and **g**) (n = 4–5 animals per group). *P < 0.05, **P < 0.01 (two-tailed Mann–Whitney test).

Since our in vivo experiments demonstrated delayed endothelial network growth at P14 in male *16p11.2*$^{df/+}$ mice, we next sought to assess sprouting angiogenesis in the early developing brain of *16p11.2*$^{\Delta EC}$ mice using VEGF receptor 2 (VEGFR2) immunostaining (VEGFR2 is abundantly expressed by sprouting cECs[29]). At birth (P0), when endothelial sprouting is highly active in the cerebral cortex[4,30], CD31^{+}mCherry^{+} cECs displayed reduced sprouting, as evidenced by significantly decreased densities and lengths of filopodium extensions compared with neighboring CD31^{+}mCherry^{-} cECs (n = 5; Fig. 4c,e). In addition, the cerebral cortex of *16p11.2*$^{\Delta EC}$ newborns (males and females) displayed significantly reduced endothelial network density and branching compared with control littermates (n = 4–5; Fig. 4e).

At P50, while the cortical cytoarchitecture and neuronal patterning appeared normal in both male and female *16p11.2*$^{\Delta EC}$ animals (n=4–5; Extended Data Fig. 6a,b), hemodynamic responses

measured in conditional *16p11.2*$^{\Delta EC}$ males (n = 5) partially recapitulated the defects identified in *16p11.2*$^{df/+}$ mice, including right-shifted reduced response amplitudes during the stimulation and slightly slower kinetics (Fig. 4f). Systolic blood pressures and heart rates also appeared unaltered in *16p11.2*$^{\Delta EC}$ mutants at P50 (n=6–8; Extended Data Fig. 6c).

Finally, recordings in the somatosensory cortex revealed significant differences in all frequency bands of ECoG signaling power between male *16p11.2*$^{\Delta EC}$ mice and age-matched controls at P50 (n=5; Fig. 4g) during whisker stimulation. These findings align with the ECoG phenotypes we reported in constitutive *16p11.2*$^{df/+}$ mutants (Fig. 1c), with the exceptions of high-gamma band signals that appeared lower than in WT controls during stimulation, and a higher baseline level. The neurophysiological ECoG signals in female *16p11.2*$^{\Delta EC}$ mutants were similar to controls at P50, again with the exception of lower signaling power in the high-gamma band during whisker stimulation (Extended Data Fig. 6d). Akin to *16p11.2*$^{df/+}$ mice, the transient onset/offset kinetics of ECoG signaling responses to whisker stimulation were similar between adult *16p11.2*$^{\Delta EC}$ mutants and their controls.

Altogether, these results demonstrate that 16p11.2 (7qF3) homozygosity is required in ECs to ensure proper neurovascular maturation in the mouse cerebral cortex.

16p11.2 haploinsufficiency alters endothelial angiogenic activity in vitro.

Evidence obtained from conditional *16p11.2*$^{\Delta EC}$ animals confirmed an important role of the 16p11.2 locus in endothelial maturation, which warrants further examination of EC behavior. Brain endothelial network expansion and remodeling rely on EC differentiation, proliferation and tubularization, which are all processes that are highly regulated at the cellular and molecular levels. To investigate cEC behavior, we isolated and characterized primary cECs from *16p11.2*$^{df/+}$ and

WT males at P14 and P50 (Fig. 5 and Extended Data Fig. 7). Mutant cECs appeared healthy in primary cultures, with normal levels of the endothelial markers eNOS, vascular endothelial (VE)-cadherin and GLUT1 ($n = 4$; Extended Data Fig. 7a), normal apoptosis rates ($n = 4$; Extended Data Fig. 7b) and normal motility in a scratch wound-healing assay ($n = 3–4$; Fig. 5b). Sequencing of the cEC transcriptome also quantified normal expression of numerous core endothelial genes (Extended Data Fig. 7c and Supplementary Fig. 1a) and high enrichment of endothelial genes (Extended Data Fig. 7d) in *16p11.2*$^{df/+}$ cECs. To test the angiogenic activity of these primary cECs, we performed an in vitro Matrigel-based network-formation assay. In growth-factor-reduced conditions, which best isolate cell-autonomous behaviors, endothelial network formation appeared dramatically impaired with *16p11.2*$^{df/+}$ compared with WT cECs that were isolated at P14 ($n = 5$; Fig. 5c), but not at P50 ($n = 5$, Extended Data Fig. 8a). This phenotype suggests that there is an intrinsic endothelial deficit in sprout initiation and elongation at P14. The defects measured with P14 mutant cECs were independent of their proliferative state, as the cell cycle was normal ($n = 5$; Fig. 5d and Extended Data Fig. 8b). The angiogenic activity deficit observed in growth-factor-reduced conditions using P14 cECs was partially rescued in growth-factor-supplemented conditions (n=4–5; Extended Data Fig. 8c). These observations support the cell-autonomous nature of 16p11.2-deletion-induced endothelial dysfunction and the need for a permissive environment to compensate for this dysfunction.

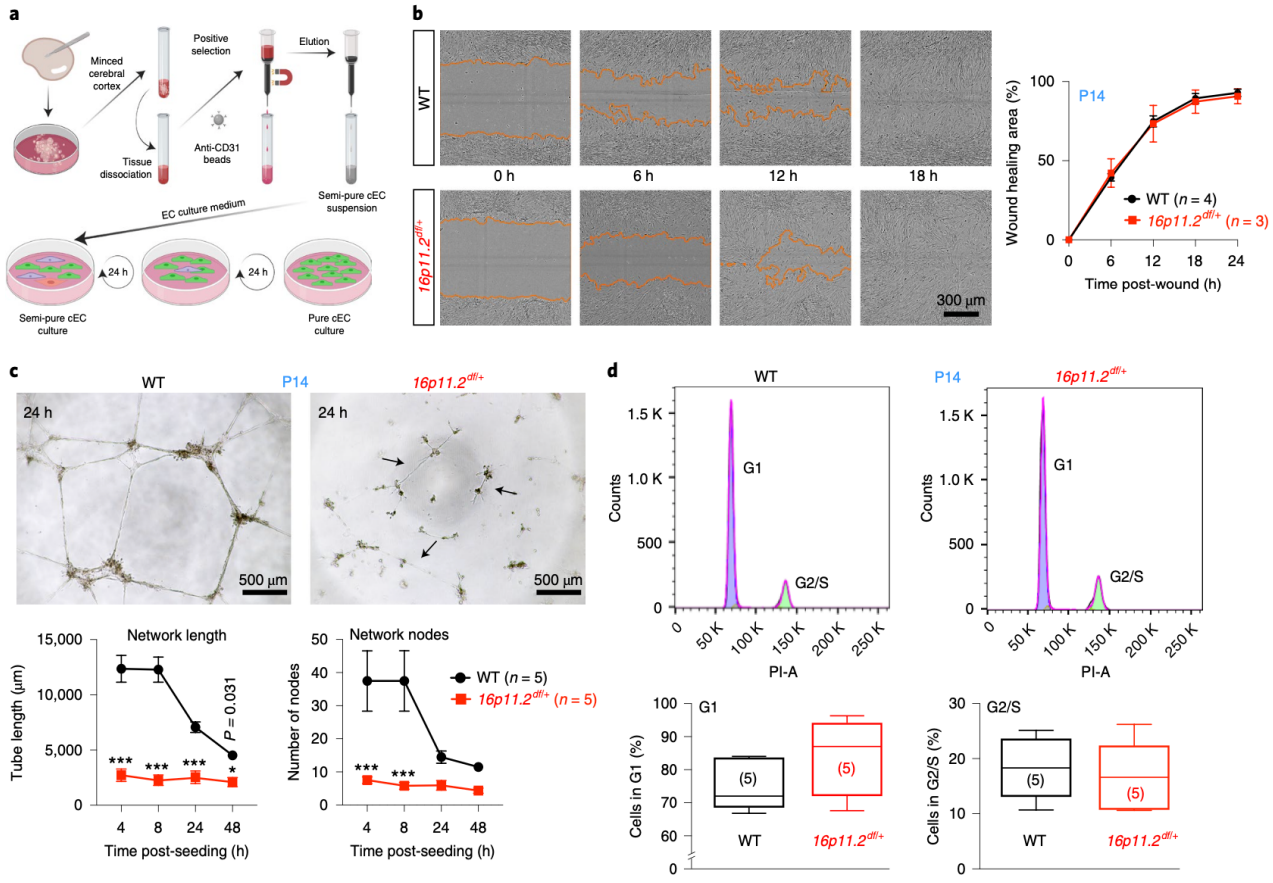

Fig. 5 | Brain ECs from P14 *16p11.2*$^{df/+}$ males display reduced angiogenic activity. a, Summary of the method used to isolate and culture primary cerebral cECs. **b**, Scratch wound-healing assays were used to measure cEC migration. Images (left) and quantification (right) showed no difference between WT and mutant cECs. Orange lines indicate cellular migration fronts. **c**, In vitro network-formation assays using primary cECs from P14 brains were used to assess vascular network formation and remodeling over 48 h in a growth-factor-reduced Matrigel (eGF < 0.5 ng ml–1, PDGF < 5 pg ml–1, IGF1 = 5 ng ml–1, TGF-β = 1.7 ng ml–1). Defective endothelial tube formation is evidenced in *16p11.2df/+* cECs compared with WT cECs. Top: representative images at the 24 h time point. Arrows indicate residual vascular branches and sprouts. Bottom: quantifications of network densities (that is, total endothelial tube length) and network nodes (that is, the total number of branching hubs). **d**, Flow-cytometry-based assessment of cellular proliferation using cell cycle analysis with cECs from P14 brains. The proportion of cells in G2/S (proliferation) or G1 (growth) phases was identical between *16p11.2*$^{df/+}$ and WT cECs. Data are shown as the mean ± s.e.m. (**b** and **c**) or whisker boxes showing minimum to maximum values, with the center line indicating the median (**d**) (n = 3–5 animals per group). *P < 0.05, ***P < 0.001 (two-way repeated measure ANOVA and Sidak's post-hoc test in **c**).

Next, we tested whether the endothelial cell-autonomous reduction in angiogenesis is associated with downstream gene expression changes in cECs harboring the 16p11.2 deletion compared with WT cECs. In addition to confirming 7qF3 hemizygosity in primary *16p11.2*$^{df/+}$ cECs (Extended Data Fig. 7f), deep sequencing of cEC RNA libraries (n=3–4 samples per group,

n=30 mice in total) revealed a significant upregulation of numerous genes related to developmental processes (Fig. 6), including 19 genes involved in "blood circulation" or "blood vessel development" (Gene Ontology (GO) terms) (Fig. 6c–e and Supplementary Fig. 1b). Other core endothelial genes involved in angiogenesis, vascular remodeling or blood–brain barrier maintenance remained unaffected by genotype, but were upregulated or downregulated in function with age (that is, between P14 and P50; Supplementary Fig. 1a). Of note, *Grem1* (which encodes Gremlin) was upregulated at both P14 and P50 in *16p11.2*$^{df/+}$ cECs. Gremlin is a secreted bone morphogenic protein antagonist acting as a proangiogenic factor in part through binding and activating VEGFR2[31]; however, this concept was recently challenged[32]. A protein interaction analysis for the 19 upregulated gene products revealed functional networks centered around the VEGFA signaling pathway (Fig. 6f–h). Interestingly, epidermal growth factor (EGF) and transforming growth factor-β (TGF-β; encoded by *Tgfb2*), both important components of the growth-factor-supplemented Matrigel (see Methods), were identified as close functional interactors in our dataset. *Tgfb2* also appeared to functionally interact with Gremlin (Fig. 6f–h), which is consistent with published work showing that TGF-β2 increases *Grem1* expression and Gremlin production, which in turn activates TGF-β2 signaling[33,34]. Further investigation is required to test whether increased *Grem1* expression in *16p11.2*$^{df/+}$ cECs is pathogenic or whether it represents a compensatory response to decreased angiogenic function.

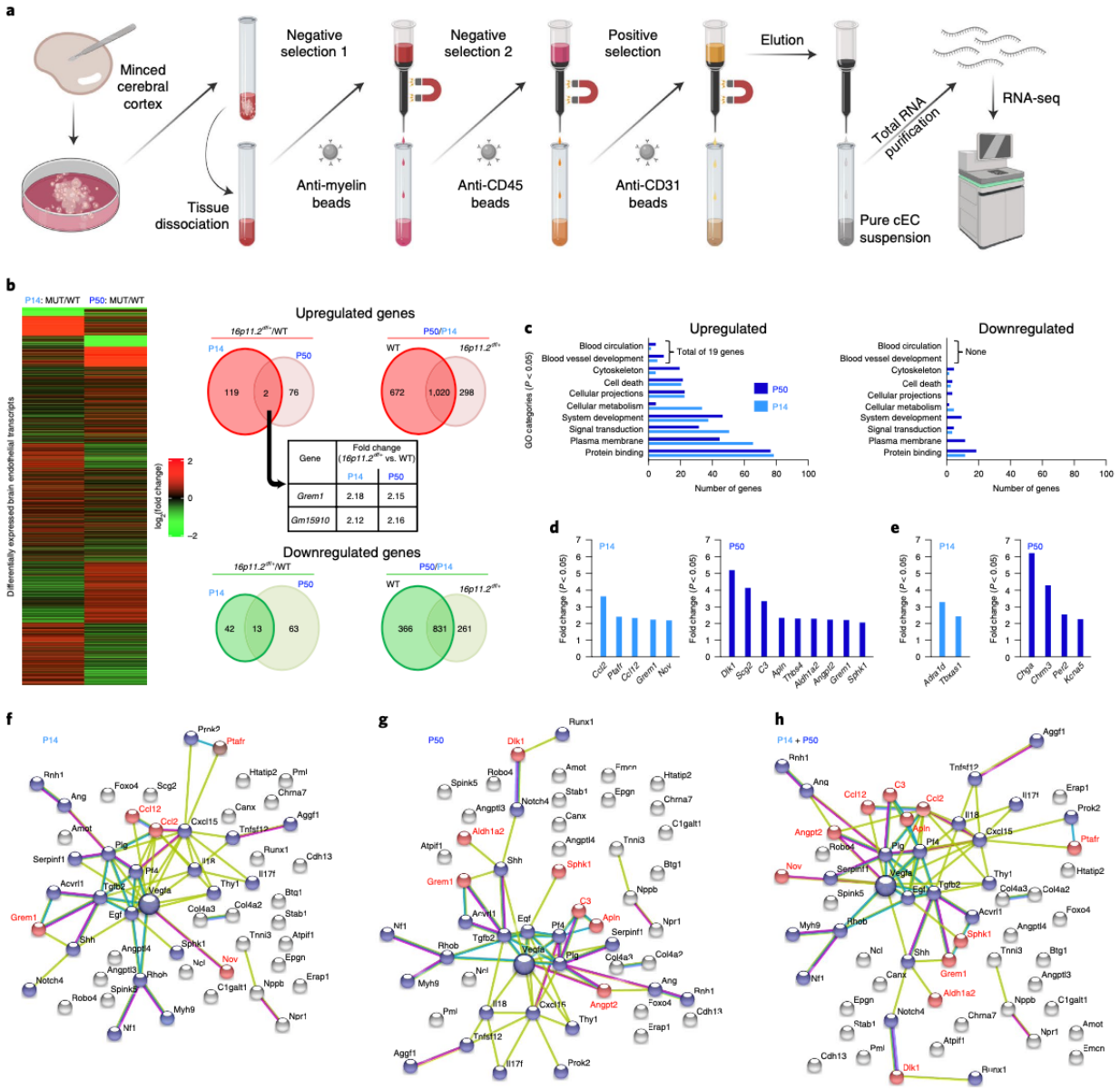

Fig. 6 | Transcriptional consequences of 16p11.2 haploinsufficiency in primary mouse brain ECs. a, Summary of the procedure to acutely purify total cEC RNA for deep sequencing analysis. Following microdissection and dissociation of the cerebral cortex, series of selections (negative followed by positive) allow for isolation of a pure cEC population (see Methods for details). **b**, A heatmap (left) and Venn diagrams illustrating (right) the number of DEGs between mutant (MUT) and WT mice. Deep sequencing of the cEC transcriptome (n = 3–4 samples per group, 4 groups, P14 and P50, RNA from 2 mice pooled per sample) identified a prominent upregulation of genetic programs in *16p11.2*$^{df/+}$ cECs. **c**, Genes upregulated (left) or downregulated (right) in *16p11.2*$^{df/+}$ cECs. **d**,**e**, GO analysis. Pathway enrichment P values (n = number of genes indicated in **c** computed using Fisher's exact test via the hypergeometric distribution). Among the upregulated genes, 19 were specifically involved in 'blood vessel development' (**d**) or 'blood circulation' (**e**), including *Grem1*, *Angpt2* and *Apln*, all known regulators of angiogenesis. **f**–**h**, Functional protein interaction networks for upregulated gene products identified in **c** versus the 'angiogenesis' gene expression signature (GO_0001525). Members of the 'blood vessel development' GO category at P14 (**f**), P50 (**g**) and P14 + P50 (**h**) are highlighted in red. First-degree interactors are emphasized with blue shells. Network maps were generated using the STRING database with a medium confidence interaction score (0.400). evidence of an interaction was based on experimental determination (magenta), curated databases (cyan) and text-mining (green).

Finally, to translate our findings to human 16p11.2 hemizygosity, we characterized human-induced ECs (hiECs) derived from induced pluripotent stem cells (iPSCs) obtained from carriers of the 16p11.2 deletion (n = 5 lines) and from healthy donors (n = 6 lines), and performed an *in vitro* Matrigel-based network-formation assay in growth-factor-reduced conditions (Fig. 7, Extended Data Fig. 9 and Supplementary Table 1). We found that, while being healthy in culture (Fig. 7b and Extended Data Fig. 9), hiECs harboring the 16p11.2 deletion displayed significant network-forming defects compared with control hiECs (Fig. 7c–e), which is reminiscent of the reduced angiogenic activity measured with P14 mouse cECs. While these data command further investigation, they strongly suggest that 16p11.2-haploinsufficient hiECs can phenocopy abnormalities found with *16p11.2*$^{df/+}$ mouse cECs.

Altogether, these results demonstrate the existence of endothelial cell-autonomous angiogenic deficits associated with 16p11.2 hemizygosity and reveal a novel cellular abnormality linked to ASD.

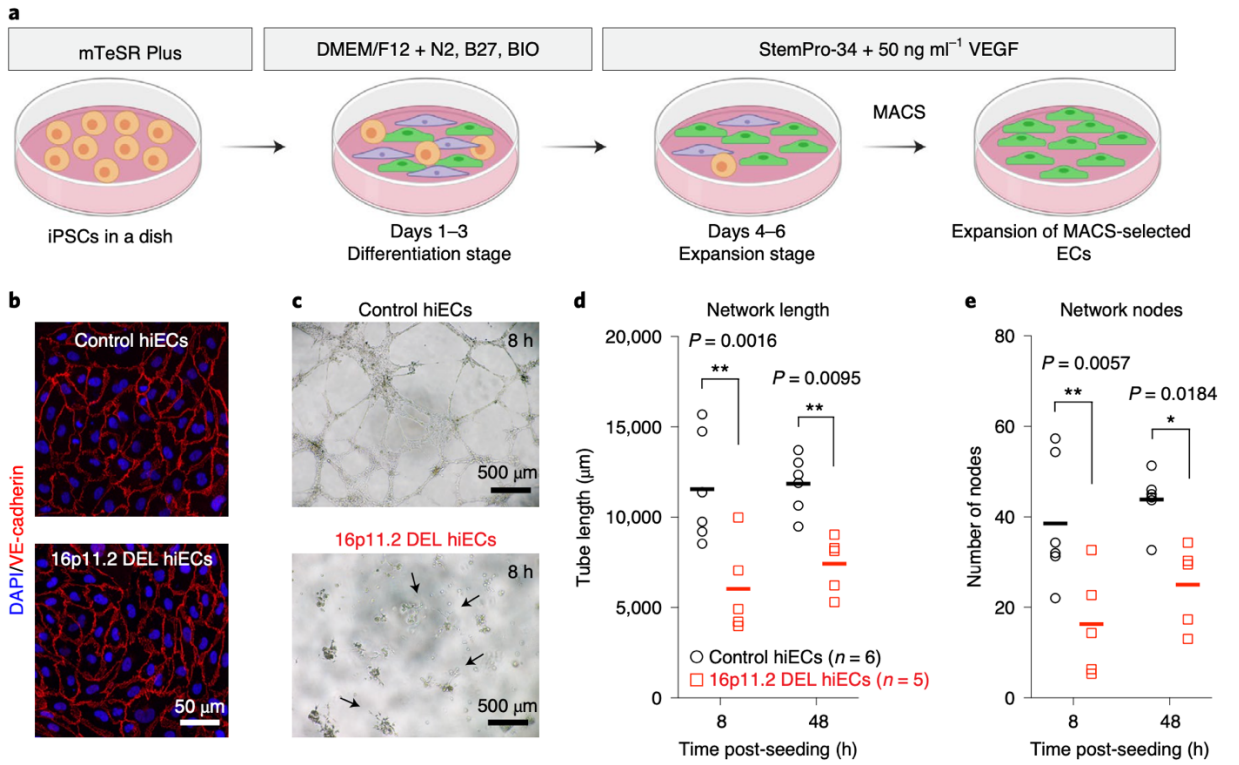

Fig. 7 | 16p11.2-haplodeficient human-derived ECs display faulty angiogenic activity. a, Schematic of the culture steps and conditions involved in differentiating hiECs from human iPSCs.. **b**, Sample images of immunocytochemical staining for the endothelial marker VE-cadherin in hiEC cultures (control and 16p11.2 deletion (DEL)). Images are representative of three independent experiments using three hiEC lines per genotype, with similar results obtained (see also extended Data Fig. 9). **c**–**e**, In vitro network-formation assays were performed using hiECs in a growth-factor-reduced Matrigel. **c**, Sample images illustrating the phenotype observed using control (healthy) versus 16p11.2 deletion hiECs after 8 h in Matrigel. Arrows indicate residual vascular branches and sprouts. Sample images are representative of three independent experiments using five to six hiEC lines per genotype, with similar results obtained. **d**,**e**, Defective endothelial tube formation, including defects in length (**d**) and nodes (**e**), was evidenced when comparing hiECs from 16p11.2 deletion carriers to control hiECs. Data are shown as the mean with individual values in **d** and **e** (n = 5–6 hiEC lines per group, 3 experimental replicates per line). *P < 0.05, **P < 0.01 (two-way ANOVA and Sidak's post hoc test).

Endothelium-specific 16p11.2 haploinsufficiency in vivo leads to behavioral changes.

Our findings thus far establish the importance of 16p11.2 homozygosity in ECs for proper neurovascular maturation in the mouse cerebral cortex. Whether developmental endothelial 16p11.2 haploinsufficiency affects brain function into adulthood remains to be investigated. The majority of human carriers of the 16p11.2 deletion display behavioral features including hyperactivity, repetitive behaviors, deficits in social interaction and difficulties with motor

learning. Likewise, although globally healthy, constitutive *16p11.2*$^{df/+}$ mutant mice are characterized by behavioral changes including hyperactivity (males and females), novel-object recognition deficits, repetitive movements (males and females) and altered communication during social interactions (males)[20,35].

Here, we observed that P50 *16p11.2*$^{\Delta EC}$ females (n = 14) exhibited significantly higher home-cage activity than control mice (n = 12) during their active phase (Fig. 8a and Extended Data Fig. 10a), which was to a level comparable to constitutive *16p11.2*$^{df/+}$ males (n=18; Fig. 8b and Supplementary Fig. 10b). During the first 12h (habituation) of this home-cage beam-break activity test, *16p11.2*$^{\Delta EC}$ males (n=15) were slightly slower to acclimatize than *Cdh5-Cre*$^{tg/+}$ littermates (n=12), while *16p11.2*$^{df/+}$ males were already more active than their WT counterparts (n = 18; Extended Data Fig. 10a,b).

In addition, a previously unknown behavioral trait of constitutive *16p11.2*$^{df/+}$ mice was evidenced using a 1-week rotarod test. Previous work with these mice did not find motor coordination or learning abnormalities in a 2-day rotarod task[20]. Here, altered motor coordination and learning (that is, improved performance but lack of plateau) was measured in both *16p11.2*$^{df/+}$ males (n=11) and *16p11.2*$^{\Delta EC}$ females (n=15) compared with their respective controls (Fig. 8c,d). This phenotype appeared particularly significant in *16p11.2*$^{df/+}$ mice when sexes were combined (n=22–25; Extended Data Fig. 10c,d and Supplementary Fig. 2a,b).

Furthermore, *16p11.2*$^{\Delta EC}$ females showed significantly increased marble-burying behavior compared with female controls (n = 14–16; Fig. 8e and Extended Data Fig. 10e), which is an indicator of stereotypic and/or repetitive behavior that was not evidenced in constitutive *16p11.2*$^{df/+}$ females (n = 10; Fig. 8g).

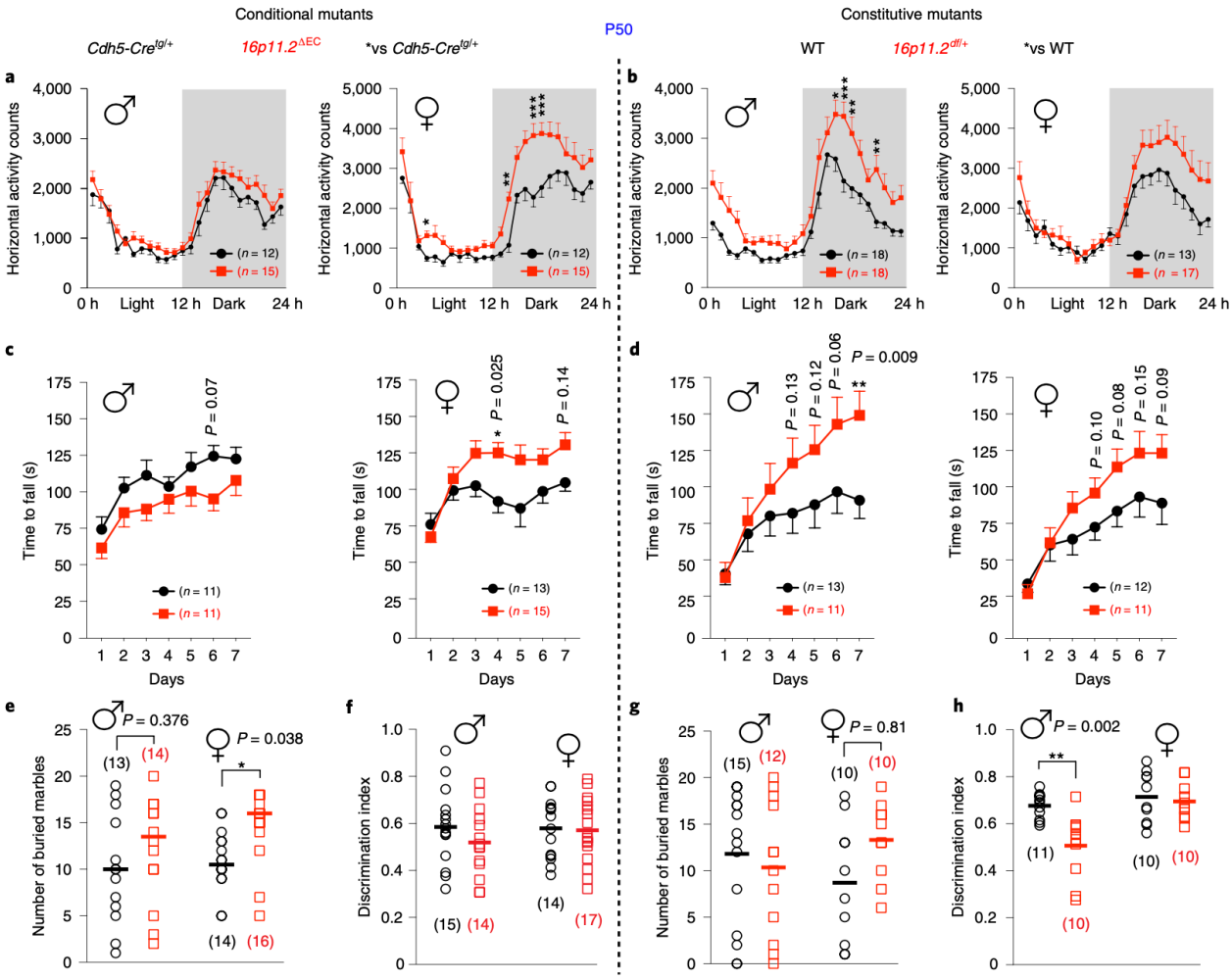

Fig. 8 | Impact of developmental endothelium-specific 16p11.2 haploinsufficiency on adult mouse behavior. a–**h**, Left: behavioral assessments of *16p11.2*$^{\Delta eC}$ and control littermates at P50 demonstrated home-cage hyperactivity in the beam break test (**a**), motor coordination/learning alterations in the rotarod test (**c**) and increased marble burying (**e**) in female *16p11.2*$^{\Delta eC}$ mice compared with *Cdh5-Cre*$^{tg/+}$ controls. No phenotype was found in the novel-object recognition task (**f**). Right: identical tests conducted using P50 WT and *16p11.2*$^{df/+}$ mice measured home-cage hyperactivity (**b**), motor coordination/learning abnormalities (**d**) and impaired novel-object recognition (**h**) in male *16p11.2df/+* mice compared with WT littermates. No phenotype was found in the marble-burying test (**g**). Data are shown as the mean ± s.e.m. (**a**–**d**) or mean with individual values (**e**–**h**) (n = 10–18 animals per group). *P < 0.05, **P < 0.01, ***P < 0.001 (two-way repeated measure ANOVA and Sidak's post hoc test in **a-d**; two-way ANOVA and Sidak's post hoc test in **e**–**h**).

As opposed to the marble-burying test, a novel-object recognition task showed altered performance in *16p11.2*$^{df/+}$ males (n=10; Fig. 8h and Extended Data Fig. 10f), which is consistent with the literature[20], but not in *16p11.2*$^{\Delta EC}$ animals (n = 14–17; Fig. 8f).

Finally, assessment of male–female interactions (with concomitant ultrasonic vocalizations (USVs)) in *16p11.2*$^{\Delta EC}$ animals and their controls (n = 9) failed to uncover previously published[21] phenotypes characteristic of *16p11.2*$^{df/+}$ mice (Supplementary Fig. 2c).

These findings demonstrate that developmental endothelial 16p11.2 haploinsufficiency is able to cause a subset of behaviors reminiscent of certain aspects of ASD.

Discussion

By uncovering a novel association between endothelial dysfunction and the 16p11.2 deletion syndrome, our findings establish a vascular link to ASD. In addition, our findings emphasize the importance of ECs in brain development.

To date, research on ASD and 16p11.2 copy number variations has mostly focused on neuronal mechanisms. Several 16p11.2 genes, conserved at the mouse 7qF3 locus, control critical features of neuronal development and function. For instance, *Taok2* regulates neuronal maturation[36] and *Mvp* regulates experience-dependent plasticity[37]. ECs also express 16p11.2 genes that modulate angio- genesis. A classic example is *Mapk3*, which encodes ERK1, a downstream effector of VEGFR2 signaling[38]. We now reveal that 16p11.2 (7qF3) hemizygosity leads to downstream transcriptional changes in mouse brain ECs, including the upregulation of genes involved in cerebrovascular maturation. While the underpinnings of such genetic upregulation are unknown, our findings unveil the existence of a 16p11.2-locus-dependent repressor mechanism normally present in WT mouse ECs.

In the cerebral cortex of *16p11.2*$^{df/+}$ males, we measured a delayed endothelial network growth compared with sex/age-matched WT littermates at P14. At this age, cortical cytoarchitecture (neurons and glia) and activity (ECoG) appeared normal in mutant mice.

Moreover, P14 cECs failed to initiate and/or elongate endothelial networks in vitro, a defect absent at P50. While endothelial network density and branching normalized in *16p11.2*$^{df/+}$ males by P50, vascular (neurovascular coupling and endothelium-dependent vasodilation) and neuronal (cytoarchitecture and activity) abnormalities emerged at this age in males. Hence, endothelial defects exist before neuronal alterations. First, this suggests that the *16p11.2*$^{df/+}$ cerebral cortex still provides compensatory support for vascular network expansion, yet leaves core features of endothelial function compromised, which translates into late-onset functional deficits. This influence of the cortical environment in constitutive mutants is also supported by more pronounced phenotypes *in vitro*, in which artificial matrices do not recapitulate the in vivo environment (for example, cells, proteins, stiffness and growth factors, among others). Second, this discrepancy in the timing of phenotypes points to the necessity of normal endothelial function, from early stages, for proper brain maturation. The early requirement for a functionally intact endothelium is supported by our comparison between conditional *16p11.2*$^{\Delta EC}$ and control mice. Despite a relatively low 7qF3 excision efficiency, imputed to locus size, *16p11.2*$^{\Delta EC}$ mutants partially recapitulated key phenotypes, including reduced cerebrovascular density (P0), altered neurovascular function (P50) and behavioral changes (P50). Nonetheless, we cannot exclude that the absence of neurovascular coupling phenotypes in *16p11.2*$^{df/+}$ mice at P14 may result from incomplete neurovascular unit maturation. Indeed, neurovascular coupling mechanisms are not fully functional at P14, and it is generally accepted that positive hemodynamic responses to neuronal activation are reliably measured only from ~2 to 3 weeks of age in mice[26] and from 7 to 8 weeks in humans[39].

Our data show a global increase of neurophysiological signaling power during whisker stimulation in constitutive mutant males under isoflurane anesthesia. This is in alignment with

similar results from other rodent models under the same anesthesia conditions[40]. A broad effect of increased neural activity was recently reported in anesthetized *Fmr1* knockout mice at P60, but not at P21, also in a sensory (auditory) cortex[40]. Aberrant neurophysiological activity has been reported in human ASD research, with a large variety of effects from sensory responses to neural oscillations and interactions in brain networks. Early sensory responses are delayed or attenuated in pediatric carriers of the 16p11.2 deletion compared to neurotypical controls[41], which is compatible with our observations of delayed CBF responses in mutant mice. We note that somatosensory neurophysiological responses in human ASD exhibit remarkable idiosyncrasies, the precise origins of which remain to be investigated.

We measured striking sex differences *in vivo* in structural, physiological and behavioral features between *16p11.2*$^{df/+}$ and WT mice and between *16p11.2*$^{\Delta EC}$ mutants and their controls. Interestingly, as opposed to males, WT and *16p11.2*$^{df/+}$ females displayed similar rates of cerebral angiogenesis between P14 and P50, hence revealing differences between WT males and WT females. This could reflect fundamental sex differences in endothelial biology that could mask phenotypes in females. Studies have demonstrated a role for steroid hormones in the regulation of eNOS (encoded by *Nos3*) expression, whereby 17β-estradiol (also known as E2), the most abundant estrogen in mammals, signals through estrogen receptor-α to increase NO production via the upregulation of eNOS[42]. Our results demonstrated normal *Nos3* expression in male *16p11.2*$^{df/+}$ cECs and broad transcriptional changes compared with WT cECs. However, further investigation is needed to elucidate the sex-specific regulation of the EC transcriptome and cell behavior.

Phenotypes were prominently evident in *16p11.2*$^{df/+}$ males; however, defective endothelium-dependent vasodilation *ex vivo* was found in both sexes. The latter observation reveals that core impairments in EC function are found in males and females outside the brain

milieu. However, behavioral phenotypes quantified in *16p11.2*$^{\Delta EC}$ mutants were found only in females. While this may seem counterintuitive in light of the more pronounced phenotypes in *16p11.2*$^{df/+}$ males, this is likely inherent to our conditional mouse model (for example, resulting from a higher 7qF3 excision efficiency in female cECs). Importantly, sex differences have often been reported between *16p11.2*$^{df/+}$ and WT mice. For instance, a sleep-wake cycle deficit was identified in *16p11.2*$^{df/+}$ males but not females[35]. More recently, male-specific impairments in operant learning[43] was measured in *16p11.2*$^{df/+}$ mice. Our results in *16p11.2*$^{df/+}$ mice are therefore in agreement with published observations, as we demonstrated male-specific impairments in neurovascular structure and function as well as in behavior. Interestingly, while the precise causes of these sex differences are unknown, sex-specific disparities in brain structure and function have been previously attributed to cerebrovascular aspects. Women show a higher resting CBF compared to men, as well as higher perfusion rates during cognitive tasks[44]. Furthermore, steroid hormones regulate vascular function and brain perfusion[45]. Therefore, the sex differences described in our study may relate to the modulation of neurovascular maturation by sex hormones and/or sex-linked genes. ASD is more commonly (three-to-four times) diagnosed in males than in females. While the reasons behind this sex bias remain undetermined, theories suggest that a heavier genetic burden is required to diagnose ASD in women, and that estrogen may be protective in ASD[46]. Further research is needed to elucidate whether sex differences measured in ASD originate, at least in part, from vascular features.

We demonstrated that 16p11.2-deletion-induced endothelial dysfunction manifests as a developmental phenotype at P14 (angiogenesis) and as a functional phenotype at P50 (impaired endothelium-dependent vasodilation). While this reveals novel cell-autonomous deficits linked to ASD, the mechanisms by which 16p11.2-deletion-induced endothelial dysfunction drives neuronal

abnormalities remain to be elucidated. One possibility is the lack of proper cell–cell communication in vascular niches of neurogenesis. Indeed, reciprocal relationships between brain ECs and neural progenitor cells (NPCs) regulate neuronal differentiation, migration and proliferation in the developing and adult brain[5,47]. NPCs secrete proangiogenic factors that promote brain vascularization, and brain ECs instruct NPCs to divide or differentiate through release of 'angiocrine' signals (for example, BDNF)[48]. 16p11.2 hemizygosity might affect the angiocrine function of ECs and/or their response to NPC cues.

Altogether, our study unmasked unsuspected vascular aspects of the 16p11.2 deletion syndrome and raises a number of corollary implications. For one, commonly observed functional MRI BOLD alterations in 16p11.2 deletion carriers and other patients with ASD may stem in part from endothelial-dependent vascular deficits rather than from sole neuronal abnormalities. This warrants further caution for interpretations of functional MRI data. Furthermore, these findings echo an emerging body of literature that documents a higher prevalence of vascular-associated conditions in patients with ASD, including cardiovascular risk factors (for example, hypertension, diabetes and obesity)[49,50], thereby raising the possibility of causal relationships. Identifying the full complement of vascular players involved in ASD pathogenesis may lead to transformative strategies for diagnosis, prevention and/or early treatment.

Methods

Animals. All animal procedures were approved by the University of Ottawa Animal Care Committee and conducted in accordance to guidelines of the Canadian Council on Animal Care.

Mouse husbandry. All mice were bred in-house and housed at a maximum of five per cage with free access to water and food. Males *16p11.2*$^{df/+}$ (Jackson laboratory, stock number (no.) 013128;

mixed B6/129 background)[19] were crossed with WT females of the same background (Jackson laboratory, stock no. 101043) to obtain hemizygous *16p11.2*$^{df/+}$ offspring and WT littermates. Conditional *Cdh5-Cre*$^{tg/+}$;*16p11.2*$^{flox/+}$ mutants (that is, *16p11.2*$^{\Delta EC}$; mixed B6/129 background) and littermate controls were obtained from breeding between *Cdh5-Cre*$^{tg/+}$ males (Jackson laboratory, stock no. 006137; B6 background)[51] and *16p11.2*$^{flox/+}$ females (Jackson laboratory, stock no. 025330; 129 background)[20]. As recommended by the Jackson Laboratory to improve *16p11.2*$^{df/+}$ pup survival, breeding cages (both constitutive and conditional mutants) were supplemented with breeding chow (no. 2019, Envigo Teklad) and DietGel (no. 76A, ClearH2O) up to weaning age. To assess astrocyte coverage and number in 16p11.2 hemizygous mice, *16p11.2*$^{df/+}$ males were crossed with *Aldh1l1-eGFP* (BAC) females (Jackson laboratory, stock no. 026033; B6 background)[52].

Genotyping. 16p11.2$^{df/+}$ mice and WT littermates were genotyped using the following two primers: 5′-CCTCATGGACTAATTATGGAC-3′ (forward) and 5′-CCAGTTTCACTAATGACACA-3′ (reverse), with a PCR product of 2.2 kb for *16p11.2*$^{df/+}$ mice[19]. Conditional *16p11.2*$^{\Delta EC}$ mutants (*Cdh5-Cre*$^{tg/+}$;*16p11.2*$^{flox/+}$) were genotyped as follows. For *16p11.2*$^{flox/+}$ genotyping[20], the following three primers were used: 5′-TTCGGCTTCTGGCGTGTGAC-3′ (p26, forward), 5′-TTGGACA GACCCTGGTTCAGTC-3′ (p301, forward) and 5′-GGTGGATGTGGAATGT GTGCGAG-3′ (p132, reverse), with two PCR products of 431 bp and 341 bp in length. For Cre genotyping, the following primers were used: 5′-GCAAGTTGAA TAACCGGAAATGGTT-3′ (forward) and 5′-AGGGTGTTATAAGCAATCCCC AGAA-3′ (reverse), with a 250-bp PCR product. For *Aldh1l1-eGFP* genotyping, the following primers were used: 5′-GAACAGGCGAAAGCGTTAAG-3′ (23136, forward), 5′-GTAAACCTCCTGGCCAAACA-3′(18707,reverse), 5′-CTAGGCC ACAGAATTGAAAGATCT-3′ (oIMR7338, forward) and 5′-

GTAGGTGGAAA TTCTAGCATCATCC-3′ (oIMR7339, reverse), with PCR products of 550 bp (transgene) and 324 bp (internal positive control) in length. To determine the sex of newborn (P0) mice, genotyping of the *Rbm31x/y* genes was conducted with the following primers: 5′-CACCTTAAGAACAAGCCAATACA-3′ (forward), 5′-GGCTTGTCCTGAAAACATTTGG-3′ (reverse), yielding a 269-bp product from the X chromosome and a 353-bp product from the Y chromosome[53].

Ultrasound contrast imaging. Nonlinear contrast imaging was performed using a Vevo 3100 high-frequency ultrasound imaging system (Fujifilm VisualSonics)[24,25,54] to assess resting-state cerebral cortex perfusion. All images were acquired using a MX250 21M-Hz linear array transducer. Animals were first anesthetized with a xylazine/ketamine cocktail (0.1 ml per 100 g). The head of each animal was then secured and stabilized using a stereotactic frame attached to the imaging platform. Key physiological parameters such as heart rate, respiratory rate and temperature were monitored throughout the imaging session. The transducer was positioned in the transverse plane so that coronal sections of the mouse brain could be visualized. Using B-mode images as a reference, the scan plane was adjusted to encompass the hippocampus. For nonlinear contrast imaging, a 50-µl bolus of MicroMarker (Fujifilm VisualSonics) contrast agents was administered through the lateral tail vein. Images were acquired before, during and after contrast-agent injection. Data analysis was completed offline using Vevo CQ, a dedicated contrast analysis software. Regions of interest (ROIs) were selected to encompass the cerebral cortex. A time–intensity curve was then plotted, and parameters related to blood volume and flow (peak enhancement, wash-in rate and rise time) were obtained from each ROI.

LDF. LDF measurements (Transonic Systems) of evoked CBF in response to sensory stimulation were carried out in anesthetized mice (ketamine given at 100 mg per kg intraperitoneally; Bimeda) fixed in a stereotaxic frame, as previously described[55]. In brief, CBF was recorded over the contralateral somatosensory cortex before, during and after unilateral stimulation of the right whiskers with an electric tooth brush (20 s at 8–10 Hz). Recordings from four to six stimulations (every 60 s) were acquired and averaged for each mouse. Quantifications of hemodynamic parameters (percentage increase from baseline, rising slope, time to maximum response and falling slope) were inspired from a reference hemodynamic study using multispectral optical intrinsic signal imaging[27].

ECoG. Concordantly with the CBF measurements, ECoG was recorded over the contralateral somatosensory cortex in response to whisker stimulation in anesthetized mice (isoflurane), fixed in a stereotaxic frame at P14 (males) and P50 (males and females). Needle electrodes (29 gauge; MLA1213, ADInstruments) were accurately implanted through a burr hole, one electrode in the contralateral (to stimulated whiskers) primary somatosensory cortex (distance from the brain surface: anterior–posterior, −0.9; medial–lateral, −3.0; dorsal–ventral, −0.4 mm), and the second electrode implanted at the same coordinates in the ipsilateral hemisphere. The ground electrode was placed in the body of the animal. Six consecutive epochs were acquired over 60 s (20-s baseline, 20-s stimulation, 20-s after stimulation). Labchart was used to collect the ECoG data with high-pass (>1 Hz) and low-pass (<120 Hz) filters set on ECoG acquisition amplifiers. Data were sampled at a rate of 1 kHz. For the analysis, ECoG data were notch-filtered at 60 Hz to remove residual line noise from recordings. Each of the six ECoG epochs were then divided into segments of 20 s, each corresponding to the following conditions: baseline before stimulation, whisker

stimulation and a post-stimulation period. The ECoG traces were then processed with a short-term fast Fourier transform (FFT) computed over sliding time windows of 1-s length yielding a 1-Hz frequency resolution. The squared modulus of FFT coefficients were averaged over the six epochs to estimate the total power of ECoG signals (in V2) in each of the following frequency bands of interest: delta (1–4 Hz), theta (4–8 Hz), alpha (8–13 Hz), beta (13–30 Hz) and gamma (30–100 Hz), excluding the bins within the 55–65 Hz range to account for the 60-Hz powerline notch. The gamma band was further separated into low gamma (30–55 Hz) and high gamma (65–100 Hz) ranges, inspired by recent studies of fragile-X-syndrome with a *Fmr1* knockout mouse model[40,56].

Cardiovascular monitoring. Systolic blood pressure and heart rate were measured by tail-cuff plethysmography (Visitech BP-2000, Apex). Mice were trained for five consecutive days before the actual recordings for 5 days. Measurements were acquired each day (five preliminary readings followed by ten recordings) at fixed times. The 5-day average of systolic blood pressure and heart rate was then calculated.

Pressure myography. *Compounds.* Adenosine, ACh, PE, sodium nitroprusside (SNP) and l-*N*G-nitroarginine (L-NNA) were purchased from Sigma-Aldrich. Compounds for Krebs solution were purchased from Sigma-Aldrich ($MgSO_4$, KH_2PO_4 , $NaHCO_3$ and glucose) or Fisher Chemical ($CaCl_2$, NaCl and KCl).

Procedure. Mice were decapitated and the brains were immediately immersed in cold (4 °C) oxygenated (5% CO) Krebs buffer solution (37 ± 0.5 °C, pH 7.4 ± 0.1) containing (in mM):118 NaCl, 4.5 KCl, 2.5 $CaCl_2$, 1 $MgSO_4$, 1 KH_2PO_4, 25 $NaHCO_3$ and 6 glucose. As described elsewhere[57], segments (~2-mm long) of the middle or posterior cerebral arteries were carefully

dissected and cannulated with a glass pipette (~40 μM in diameter) at one end and sealed to another glass pipette on the other end. The intraluminal pressure was maintained at 60 mmHg using a pressure-servo controller (PS-200) (Living Systems Instrumentation). Vessels were superfused (6 ml min^{-1}) with oxygenated Krebs solution in a chamber for online video microscopy. All compounds were applied extraluminally, and changes in lumen diameter were measured using a closed-circuit video system (National Electronics). Dilatory responses to adenosine (10−10 to 10−4 mol per liter), ACh (10^{-10} to 10^{-5} mol per liter) and SNP (10^{-10} to 10^{-4} mol per liter) were tested on vessels submaximally pre-constricted with PE (2×10^{-7} mol per liter). Contractile responses to PE (10^{-9} to 10^{-4} mol per liter) and the tonic production of the vasodilator NO were measured in vessels at basal tone, the latter after inhibition of NOS with L-NNA (10^{-5} mol per liter, 40 min).

Analysis. Dose–response curves were generated as percentages of change from pre-constricted tone (vasodilators) or basal tone (PE and L-NNA). Percentages of change were plotted as a function of agonist concentration or incubation time (L-NNA). pD_2 values (that is, the parameter of vascular sensitivity to drugs) were calculated as the negative logarithm to base 10 of the half maximal effective concentration of a drug (EC_{50}).

Wire myography. Mesenteric arteries isolated from both WT and *16p11.2*$^{df/+}$ mice were used to assess peripheral vascular reactivity *ex vivo* as previously described[58]. Briefly, second-order branches were obtained and carefully cleaned of adipose and connective tissue. Segments (~2 mm) were mounted on a Multi-Wire Myograph system (DMT) and equilibrated in Krebs solution with 95% O_2 and 5% CO_2. Vasoconstriction or endothelium-dependent vasorelaxation were examined

in response to PE or Ach (1 nM to 10 μM), respectively. Analysis was performed as for pressure myography (see above).

Immunohistochemistry. For immunohistochemistry experiments, all mice were euthanized by cervical dislocation. Whole brains or dissected cortices were fixed in 4% paraformaldehyde (PFA) overnight at 4 °C. For two-dimensional (2D) imaging experiments, following fixation, all brains were rinsed in PBS, submerged in 15% sucrose overnight, followed by 30% sucrose overnight, then embedded in OCT medium and cut coronally into 25-μm-thick serial sections using a cryostat (HM525 NX, ThermoScientific), and finally mounted on charged glass slides. For 3D vascular reconstructions, flattened cortices were embedded in agarose and cut tangentially into serial 120-μm-thick sections with a vibratome (VT1000S, Leica) and processed free-floating, as previously described[4]. Sections were blocked using a solution containing 10% donkey serum, 0.5% Triton X-100 in PBS (0.5% PBT) and 0.5% cold water fish skin gelatin, and incubated overnight at room temperature with combinations of primary antibodies including anti-CD31 (1:200, BD Pharmingen), anti-VGLUT2 (1:500, Cedarlane), anti-IBA1 (1:1,000, Cedarlane), anti-PDGFR-β (1:200, Cedarlane), anti-α-SMA (1:200, Abcam), anti-GFP (1:500, Invitrogen), anti-VEGFR2 (1:500, R&D systems) anti-mCherry (1:500, Abcam), anti-NeuN (1:1500, Millipore Sigma) or anti-TBR1 (1:400, Abcam). On the next day, sections were washed with 0.5% PBT and incubated with species-specific AlexaFluor secondary antibodies (1:300, Invitrogen) for 3 h at room temperature. Sections were washed with 0.5% PBT and PB (floating sections mounted) then coverslipped in Fluoromount G (EMS).

Image acquisition. Immunostained sections were examined using a Zeiss Axio Imager M2 microscope equipped with a digital camera (Axiocam 506 mono) and the Zeiss ApoTome.2 module for optical sectioning. For 3D reconstruction of vascular networks at P14 and P50, tangential flattened cortex sections comprising layer IV of the primary somatosensory barrel cortex were used as a landmark: layer IV was located with VGLUT2-immunofluorescent barrels under a 5x objective. Nine 60-µm-deep *z*-stacks were then acquired at 10x in three major subdivisions of the cortex (anterior, parietal and occipital) for representative sampling of the cerebral cortex (see Fig. 3b). The parietal subdivision corresponded to the primary somatosensory cortex. Tangential sections above and below layer IV were considered as layer II/III and V, respectively, as previously described4. At P0 (*16p11.2*$^{\Delta EC}$ mice and controls), only six *z*-stacks were acquired due to the smaller size of the cortex (two cortical regions, three depths). For 2D imaging, a 10x, 20x or 40x objective was used to acquire 20-µm- (10x), 15-µm- (20x) or 10-µm-deep (40x) *z*-stacks that were subsequently transformed into maximal intensity projections for 2D quantifications.

Computational morphometric analysis of 3D vascular images. Computational image analysis was performed using a method we previously developed[4]. In brief, a Gaussian smoothing filter with unit standard deviation was applied to each 3D image. Then, a circular-window adaptive threshold with a radius of 36 µm was used to binarize the images. Connected components with a volume smaller than 375 µm were removed from the image. The Palágyi–Kuba thinning algorithm was used to calculate the medial lines of the blood vessels, which were then represented as a graph. Each termination and bifurcation of a blood vessel becomes a node, and nodes are connected when there is a blood vessel segment between them. The length of each blood vessel segment was calculated, and segments shorter than 9 µm were removed. The blood vessel density in the stack

was calculated as the sum of the lengths of all blood vessel segments divided by the volume of the stack. The number of bifurcation nodes (that is, branch points) was also calculated and divided by the volume of the stack. All data are expressed as the vessel length or branch point number per cubic mm.

Quantification of neuronal density from 2D neuronal images. Neurons were identified using the following approach. The Laplacian of Gaussian (LoG) filter was applied at different scales. Standard deviations in the range [3.5 μm, 5.5 μm] were used for the filters. The results were stacked to define a 3D image in which local maxima represent candidate neurons[59]. Maxima with LoG values smaller than 0.05 were discarded. Maxima that were too close to each other were also removed using the following criterion. Each maximum is associated with a scale and, therefore, with a typical radius. Maxima were removed when the disks defined by their radius had an overlapping area that was larger than 25% of the area of the smaller disk. The remaining maxima were understood as neuron locations in the image. The channel corresponding to the NeuN marker was subtracted from the TBR1 marker channel to remove staining crosstalk. Calculating the neuron density critically relies on the adopted definition of the ROI, which was obtained as follows. The surface of the cortex was manually marked in each image. A smoothing spline interpolation was applied to the cortex surface to obtain a smoother curve, parametrized by a parameter t going from 0 to 1. The normals of this curve were calculated at $t = 0.2$ and $t = 0.8$. The two normals define respective straight lines, which, together with the manually marked cortex surface, delimit the ROI. The ROI was subdivided into 50-μm strips (Extended Data Fig. 4j) according to the distance from the cortex surface[60]. That is, the first strip is composed of all points inside the ROI with a distance between 0 μm and 50 μm from the cortex surface, the second strip

contains all points with a distance between 50 μm and 100 μm, and so on. The neuron density was then calculated for each strip.

Quantification of mural cell coverage/number from 2D images. For cellular coverage quantifications (VSMCs, astrocytes, microglia and pericytes), a 10x objective was used, while a 20x objective was used for counting 4,6-diamidino- 2-phenylindole (DAPI)-counterstained cell bodies. Image analysis was completed using Fiji-ImageJ. Coverage was determined by converting the image to 8-bit, running the Z-Project with the Max Intensity setting to obtain a 2D image. The image threshold was determined using the Moments pre-set to acquire a binary image. Analyze Particles, with size set to 5-infinity, was used to find the proportion of the image containing the signal of interest. Pericyte coverage of cortical vessels was quantified by analyzing the proportion of the total CD31-positive endothelial surface area also positive for the pericyte marker PDGFR-β. For cellular coverage by glial cells, the cortical area occupied by IBA1-positive or eGFP(ALDH1L1)-positive cells was quantified as the surface occupied by labeling within the image. For artery quantification, the proportion of CD31/α-SMA-double-positive cortical vessels was quantified. The number of cell bodies (pericytes, microglia and astrocytes) were manually counted using the Cell Counter plugin. For each animal, nine images were used (three images per brain section, three sections per brain).

Quantification of cortical layers in *16p11.2*$^{\Delta EC}$ mutants and controls from 2D images. Images of DAPI-stained coronal brain sections were acquired using the tile feature of the Zeiss Axio Imager M2 microscope. Measurements of cortical layer/thickness were performed as described elsewhere[61,62]. In brief, quantification of layer thickness was assessed by measuring the length

along several points (at least eight points) of a given cortical layer using Fiji-Image J. The average cortical layer thickness was obtained from three sections per mouse (n = 5 mice) within the somatosensory cortex.

Quantification of endothelial filopodia in *16p11.2*$^{\Delta EC}$ mutants at P0 from 2D images. For quantification of VEGFR2-positive filopodium extensions in P0 *16p11.2*$^{\Delta EC}$ brains, 40x ApoTome images were used. Filopodia were quantified first on mutant endothelium ($CD31^{+}mCherry^{+}$) and then on the same length of neighboring WT endothelium ($CD31^{+}mCherry^{-}$). Using Fiji-Image J, the endothelial length of each cell type was quantified first by manual tracing on scaled images using the Segmented line tool and the Measure function. Then, filopodia were manually traced to obtain their length using the same method. Individual filopodia were also manually counted using the of Cell Counter plugin of Fiji-ImageJ. All data are expressed as the filopodium number or length per micrometer of $CD31^{+}$ endothelium.

Transmission electron microscopy (TEM). Mice were anesthetized with a ketamine/xylazine cocktail (1 mg per kg, intraperitoneally) and perfused through the aortic arch with 3.5% acrolein and 4% PFA. Coronal sections (50-µm thick) of the brains were cut in sodium phosphate buffer (PBS 50 mM, pH 7.4) using a Leica VT1000S vibratome (Leica Biosystems) and stored at −20 °C in cryoprotectant until further processing[63]. Sections were post-fixed and embedded using variations of the protocol by Deerinck et al. (https://ncmir.ucsd.edu/sbem-protocol). In brief, the sections were washed three times in PBS for 10 min, and were incubated in 1.5% potassium ferrocyanide and 2% aqueous osmium tetroxide in 0.1 M PB (pH 7.4) for 1 h at room temperature. The sections were subsequently washed five times with double-distilled water (ddH2O) for 3 min,

then incubated 20 min in a fresh solution of thiocarbohydrazide (1% w/v) at room temperature. Sections were washed again five times with ddH2O for 3 min, incubated 30 min in 2% aqueous osmium tetroxide, and washed five times with ddH2O for 3 min. Sections were dehydrated using increasing ethanol concentrations followed by propylene oxide, and then embedded in Durcupan resin (Sigma-Aldrich) between ACLAR sheets at 55 °C for 3 days, as previously described64. Ultrathin sections were generated at ~65 nm using a Leica UC7 ultramicrotome. Imaging was performed in the antero-frontal (2.8 to 1.98 mm Bregma) and parieto-somatosensory (−0.70 to −1.82 mm Bregma) areas. In each region, ten capillaries per animal, ranging in diameter between 3 and 6 μm, were randomly photographed using a FEI Tecnai Spirit G2 transmission electron microscope operating at 80 kV and equipped with a Hamamatsu ORCA-HR digital camera (10 MP). For each capillary, an image at 4,800x was acquired, in addition to 1–3 images at 13,000x to generate a high-resolution mosaic of the capillary.

TEM image analysis. Quantifications were completed using Fiji-Image J. The averaged diameter of the vessel lumen was calculated using the Line tool in both horizontal and vertical orientations. To analyze astrocyte endfeet, a ROI was drawn around each astrocyte endfoot in contact with the blood vessel. The Measure function was used to calculate the area of the each endfoot. For each image, the total endfoot number in contact with the vessel was tallied, as was the combined area of all endfeet. The length of basement membrane (BM) surrounding the endothelium, and of the astrocytic membrane in direct contact with the BM, was measured to obtain the proportion of BM (that is, capillary) covered by astrocyte endfeet.

ELISA. Levels of soluble VEGF were measured in protein extracts from microdissected cerebral cortex (*16p11.2*$^{df/+}$ and WT mice, P14 and P50) using a commercially available ELISA kit (mouse VEGF PicoKine cat. no. EK0541, Boster Biological Technology). In brief, brain tissue was homogenized in a lysis buffer containing 10 mM Tris-HCl, 150 mM NaCl, 1% Triton X-100, 1% glycerol as well as protease and phosphatase inhibitors. The resulting supernatant underwent a Bradford assay to measure the soluble protein concentration. All protein samples were normalized to 0.25 μg μl^{-1}. Soluble levels of VEGF were measured following the manufacturer's instructions, and results expressed as picograms of protein per milliliter of supernatant.

Primary mouse brain EC isolation. All mice were euthanized by cervical dislocation. Cell isolation procedures were completed following the manufacturer's instructions. The cortex was dissected in cold HBSS (without calcium and magnesium) using tools that were autoclaved and submerged in 100% ethanol before dissection. Cortical tissue was minced and incubated in Neural Tissue Dissociation compounds (Kit P, Miltenyi Biotec) to obtain a cell suspension.

Cell culture. cECs were isolated by incubation with CD31-coated magnetic microbeads (130-097-418, Miltenyi Biotec) and placed in the magnetic MACS separator for positive selection. To obtain a pure EC population, cECs were cultured in an EC culture medium (MV2, PromoCell) that was replaced 24 h post-seeding and every 48 h until an appropriate level of confluence was reached (40–60% for immunocytochemistry; 90–100% for Matrigel experiments).

Acute RNA isolation. ECs were isolated as above, but with additional steps to deplete myelin (using myelin removal beads II, Miltenyi Biotec) and CD45-positive cells (CD45 microbeads, 130-052-301, Miltenyi Biotec) to obtain a pure CD31-positive cell suspension. Cell suspensions from two animals were pooled into one biological sample. RNA was acutely extracted using this cell

suspension (E.Z.N.A. HP Total RNA kit, Omega Bio-tek), with an additional DNase step (E1091, Omega Bio-tek), following the manufacturer's protocol. A total of 16 RNA samples (that is, 16 samples) from 32 mice were produced in total for RNA deep sequencing (see the "RNA sequencing" section below). RNA quality and purity (optical density 260/280 ratio; RNA quality number) were measured using a bioanalyzer, and RNA samples passing quality standards (optical density 260/280 between 1.8 and 2, RNA quality number > 9) were used for sequencing.

PCR with reverse transcription. Total cEC RNA was extracted as for RNA sequencing (RNA-seq; see above). RNA was converted to complementary DNA using a High-Capacity cDNA Reverse Transcription kit (Life Technologies) with 200–500 ng starting material per reaction. Quantitative PCR (qPCR) was performed using an ABI Prism 7000 Sequence Detection System with SYBR Advantage qPCR Premix (Cedarlane). Amplicons were separated by agarose gel (1%) electrophoresis. The following primers were used: 5′-CAACGCTACCACGA GGACATT-3′ (forward) and 5′-CTCCTGCAAAGAAAAGCTCTGG-3′ (reverse) for *eNOS*; 5′-CTGCCAGTCCGAAAATGGAAC-3′ (forward) and 5′-CTTCATC CACCGGGGCTATC-3′ (reverse) for *CD31*; 5′-CTCATGTCTGAACTCAAGA TCC-3′ (forward) and 5′-CCAGAATCCTCTTCCATGCTCA-3′ (reverse) for *VEGFR2*; 5′-GGCAAATTCAACGGCACAGT-3′ (forward) and 5′-AGATGGTG ATGGGCTTCCC-3′ (reverse) for *GAPDH*. A no reverse transcriptase control was used by carrying out the reverse transcription (RT) step of the qRT–PCR experiment in the absence of reverse transcriptase to assess the amount of DNA contamination present in a RNA preparation.

Immunocytochemistry. Primary cECs were cultured until 40–60% confluence (3 days post-isolation) on a cover glass for subsequent mounting for microscopy. Before staining, cECs were washed twice in pre-warmed PBS and fixed for 10 min in cold 4% PFA. Fixed cells were permeabilized in a blocking solution containing 10% donkey serum, 0.1% PBT and 0.5% cold water fish skin gelatin. The primary antibodies anti-CD31 (1:200, BD Pharmingen), anti-VE-cadherin (1:500, Fisher Scientific), anti-eNOS (1:200, Abcam) and anti-GLUT1 (1:200, Abcam) were diluted in blocking solution and incubated for 2 h at room temperature. Cells were rinsed with 0.2% PBT. AlexaFluor species-specific secondary antibodies were diluted in blocking solution and incubated with cells for 60 min. Cells were washed with 0.2% PBT then 0.1 M PB. Cover glasses with stained cECs were mounted on slides in Fluoromount G and imaged (×40 objective) with a Zeiss Axio Imager M2 microscope equipped with a digital camera and ApoTome.2 module.

To quantify VE-cadherin, eNOS and GLUT1 immunostaining, 40x ApoTome images (16-bit Tiff files) were loaded into Fiji-Image J. For VE-cadherin staining, a 20 × 10-µm ROI was centered on a cell–cell junction (15 cell–cell contacts per genotype, $n = 4$ mice per genotype), and average intensity plots were obtained across junctions using the Plot Profile function of Image J. For eNOS and GLUT1 staining, four 10 × 10-µm cytoplasmic ROIs were equally distributed around the nucleus, and the immunofluorescence intensity (gray value) was quantified (10 cells per animal, $n = 4$ animals per genotype) using the Measure function.

Deep RNA-seq. RNA-seq libraries were generated using a TruSeq strand mRNA kit (Illumina). The RNA-seq libraries were quantified by Qbit and qPCR according to the Illumina Sequencing Library qPCR Quantification Guide, and the quality of the libraries was evaluated on an Agilent

Bioanalyzer 2100 using the Agilent DNA-100 chip. The RNA-seq library sequencing was performed using Illumina Next-Seq500. FASTQ file formats were processed by trimming the adaptor sequences, filtering low-quality reads (Phred score ≤ 20) and eliminating short reads (length ≤ 20 bps) using the software package FASTX-toolkit (http://hannonlab.cshl.edu/fastx_toolkit/). STAR (v.2.5.3a)65 was used for alignment of the reads to the reference genome and to generate gene-level read counts. The mouse (*Mus musculus*) reference genome (v.GRCm38.p5)66 and the corresponding annotation were used as reference for the RNA-seq data alignment process. DESeq2 was used for data normalization and differentially expressed gene identification for each pair-wise comparison67. Differentially expressed genes (DEGs) were defined as those with a *q*-value (adjusted *P* value based on Benjamini–Hochberg procedure) of less than 0.05 and twofold of changes in ratio (abs(log2 fold-change) ≥ 1). A total of 4,089 DEGs were identified across 4 comparisons. These genes were used to generate the heatmap. KEGG pathway enrichment analyses were done using GOAL software68. Pathway enrichment *P* values were computed using Fisher's exact test via hypergeometric distribution and then Bonferroni corrected.

Four DEG analyses were performed among 15 samples (*n* = samples):

1. P14_Mut (*n* = 4) versus P14_WT (*n* = 4)
2. P50_Mut (*n* = 3)* versus P50_WT (*n* = 4)
3. P50_Mut (*n* = 3)* versus P14_Mut (n = 4)
4. P50_WT (*n* = 4) versus P14_WT (*n* = 4)

An asterisk indicates analyses where elimination of one P50_Mut sample was decided due to lower overall fragments mapped (94% versus 97% average), almost double the number of

unmapped reads (4.97% versus 2.52% average), and significantly lower correlation with other three replicates (0.70 ± 0.09 versus 0.89 ± 0.02).

Cell cycle analysis. EC suspensions were pelleted at 1,000 × *g* for 5 min and resuspended, then fixed in increasing concentrations of ethanol (up to 70%) for 60 min at 4°C. Fixed cells were pelleted at 1,000 × *g* for 10 min and resuspended in a Krishian buffer (0.1% sodium citrate, 0.02 mg ml^{-1} RNAse A, 0.3% NP-40 and 0.05 mg ml^{-1} propidium iodide). Cells were pelleted again and incubated in fresh Krishian buffer for another 60 min on ice in the dark. Finally, cell suspensions were filtered using a 25-gauge needle and analyzed for propidium iodide labeling of DNA by flow cytometry (LSR Fortessa).

EdU incorporation assay. Rates of hiEC proliferation were determined using a Click-iT 5-ethynyl-2'-deoxyuridine (EdU) assay (Invitrogen) according to the manufacturer's instructions. Briefly, hiECs were plated on coverslips at a density of 5×10^3 cells per well. Cells were allowed to grow until ~70% confluence at which time EdU (10 μM) was added to each well. After 48 h of incubation with EdU, cells were fixed with 4% PFA and processed according to manufacturer's protocol. ECs were then immunofluorescently labeled, as described above, with anti-VE-cadherin (1:400 Abcam) diluted in PBS solution (0.5% Triton X-100 supplemented with 10% normal donkey serum and 0.5% gelatin). Nuclear labeling of the samples was performed by incubating cells with 1 mg ml^{-1} Hoechst 33342 for 30 min at room temperature. Coverslips were washed and mounted onto microscope slides. Samples were examined using a Zeiss Axio Imager M2 microscope equipped with a digital camera (Axiocam 506 mono) and the Zeiss ApoTome.2 module. Ten 20x images were acquired per cell line (n = 3 lines per group). Images were analyzed

by an examiner blinded to the experimental conditions, and cells were counted using the Cell Counter plugin in Fiji-Image J. Data are expressed as the percentage of VE-cadherin^{+}Hoechst^{+}EdU^{+} ECs from the total of VE-cadherin^{+}Hoechst^{+} cells.

In vitro Matrigel network-formation assay. EC network-formation assays were performed using growth-factor-reduced Matrigel (BD Bioscience, cat. no. C354230) or growth-factor supplemented Matrigel (BD Bioscience, cat. no. 356234). Growth-factor-reduced conditions were as follows: EGF < 0.5 ng ml^{-1}, PDGF < 5 pg ml^{-1}, IGF1 = 5 ng ml^{-1} and TGF-β = 1.7 ng ml^{-1}. Growth-factor-supplemented conditions were as follows: EGF = 0.7 ng ml–1,PDGF = 12 pg ml^{-1}, IGF1 = 16 ng ml^{-1} and TGF-β = 2.3 ng ml^{-1}. In brief, each well of a 96-well plate was coated with 50 µl of Matrigel and incubated at 37 °C for 30 min to promote polymerization. ECs were collected and counted using Trypan Blue exclusion. Approximately 2 × 10^{4} cells were seeded in each well with 200 µl EGM-MV2 + 0.5% FBS media. TIFF images of capillary-like networks were captured using a Nikon TE2000 inverted microscope at 4, 8, 24 and 48 h post-seeding (mouse cECs) or at 8 and 48 h post-seeding (human ECs). Images were processed using the Angiogenesis function of ImageJ.

In vitro apoptosis detection assay. Basal apoptosis levels in WT and 16p11.2 mutant primary cultures were determined using CellEvent caspase-3/7 green detection reagent (ThermoFisher Scientific, no. C10423), according to the manufacturer's recommendations. Mouse primary cEC cultures were plated at 5 × 10^{3} cells per well in 96-well plates and maintained for 2 days in a MV2 endothelial cell growth media formulation (PromoCell, cat. no. C-22221). Human-derived hiEC cultures were plated at 5 × 10^{3} cells per well in 96-well plates and maintained for 2 days in an

EBM-2 endothelial cell basal media formulation (Lonza, cat. no. CC-3156). Then, 5 μM of caspase-3/7 green was added to each well and incubated for 30 min at 37 °C. Cells were washed twice with PBS and fixed with 2% formaldehyde for 30 min. Hoechst 33342 was used to stain nuclei. As a positive control, cells were treated with 1 μM of staurosporine for 6 h before caspase-3/7 green incubation. Images were acquired using a Cellomics ArrayScan VTI high-content imaging platform running on the HCS Studio software.

In vitro scratch wound-healing assay. Following cell isolation, cECs were plated in coated 6-well plates. Once 90% confluent, cells were collected using TrypLE (Life Technologies) and counted using a hemocytometer. A 96-well ImageLock plate (Essen Bioscience) was coated with an attachment factor (Life Technologies) before cEC seeding. cECs were seeded at a density of 20,000 cells per well. After 48 h of seeding, a WoundMaker (Essen BioScience) was used to create uniform scratches in each well according to the manufacturer's protocol. After creating the scratch, the medium was aspirated and replaced by fresh medium. The plate was placed into an IncuCyte Zoom apparatus where cell migration was recorded every 2 h for a total duration of 24 h.

iPSC culture and differentiation. 16p11.2-deletion iPSC lines (SV0001442, SV0001453, SV0001459, SV0001455 and SV0001481) were obtained from the Simons Foundation (SFARI) following approval from the Ottawa Hospital Research Institute Ethics Committee (REB no. 20170708-01H). Healthy iPSC lines, which include the 090-iPSC, EPC-iPSC Clone B, EPC-iPSC Clone C, EPC-iPSC-106, BJ1D, GM01650E and 168 1d2, were from W. L. Stanford's laboratory (see Supplementary Table 1 for details). Matrigel (BD Bioscience, cat. no. C354230) was subjected to 1:30 dilution before coating culture plates. All iPSC lines were maintained on

Matrigel-coated plates in mTeSR media (Stem Cell Technologies, cat. no. 085850) with daily media changes. Routine passage of iPSC lines was performed mechanically with a fine-gauge needle under a dissection microscope to obtain smaller cell clumps for transfer using a p200 pipette into new culture dishes.

Differentiation of all lines into hiECs was performed using an adapted protocol from Tatsumi et al.[69]. Briefly, cells were cultured in DMEM/F12 (Life Technologies, cat. no. 11320033) supplemented with B27 (Life Technologies, cat. no. 17504044), N2 (Life Technologies, cat. no. 17502048) and 5 μM BIO (Sigma, cat. no. B1686-5MG) for 72 h, with daily media changes performed. Cells were then cultured in StemPro-34 (Life Technologies, cat. no. 10639-011) supplemented with 50 ng ml^{-1} of VEGF165 (R&D Systems, cat. no. 293-VE-050) for 72 h before MAC selection with CD144 microbeads (Miltenyi Biotec, cat. no. 130-097-857). CD144-enriched cells were then expanded to confluence (~48 h) in StemPro-34 media supplemented with 50 ng ml^{-1} VEGF165, and flow cytometry characterization was performed on an Attune acoustic focusing cytometer (Life Technologies) using the endothelial surface markers CD31 (BD Bioscience, cat. no. 340297), CD34 (BD Bioscience, cat. no. 345802) and CD144 (BD Bioscience, cat. no. 560411). Briefly, 2×10^5 cells were stained with the aforementioned antibodies and incubated on ice for 30 min before flow cytometry analysis. Approximately 20,000 events were collected for each sample, and cells were gated against an isotype control and results analyzed using FlowJo V10.

Whole-transcript expression analysis using Clariom S. Total hiEC RNA ($n = 3$ lines per group) was quantified using a NanoDrop Spectrophotometer ND-1000 (NanoDrop Technologies) and its integrity was assessed using a 2100 Bioanalyzer (Agilent Technologies). Sense-strand cDNA was

synthesized from 100 ng of total RNA, and fragmentation and labeling were performed to produce single-stranded DNA with a GeneChip whole transcriptome Terminal Labeling kit according to manufacturer's instructions (Thermo Fisher Scientific). After fragmentation and labeling, 3.5 µg of DNA target was hybridized on a GeneChip Clariom S human (Thermo Fisher Scientific) and incubated at 45 °C in a GeneChip Hybridization oven 640 (Affymetrix) for 17 h at 60 r.p.m. GeneChips were then washed in a GeneChips Fluidics Station 450 (ThermoFisher) using a GeneChip Hybridization Wash and Stain kit according to the manufacturer's instructions (ThermoFisher). The microarrays were finally scanned on a GeneChip scanner 3000 (ThermoFisher). The signal was analyzed using Transcript Analysis Console 4.0 (TAC) software from Applied Biosystems (Thermo Fisher Scientific.)

Behavioral assays. Before behavioral testing, all animals were left to acclimatize to an inverted light cycle housing room for 10 days and handled once a day for 1 week. Behavioral tests were completed at the University of Ottawa's Behavior Core Facility between 9:00 and 17:00 under dim red light. On the testing day, before the task, animals were habituated to the testing room for 60 min. Behavior tests were performed with all mice in the following order: novel-object recognition (2 days); rotarod (7 days); beam break (7 days); and male–female interaction with USV (1 day). The marble-burying test (1 day) was performed on different cohorts of mice. All tests were directly inspired or slightly modified from published studies[20,21,70,71].

Novel-object recognition test. A 2-day novel-object recognition test was performed as described elsewhere[20]. On day one, 24 h before the actual experiment, each animal was habituated to an empty open-field arena (45 × 45 × 45 cm) for 30 min. On the experimental day, mice were habituated for a second time to the open field for 10 min. Following habituation, each mouse was

removed from the open field and placed in a clean holding cage for 2 min. Two identical objects (red cup or white funnel) were placed in the arena and the mouse returned to the arena for a 10-min familiarization period. The mouse was removed from the arena and placed in a clean holding cage for 1 h. After this hour, the object-recognition test consisted of one cleaned familiar object and one cleaned novel object (red cup or white funnel switched). The mouse was returned to the arena for a 5-min recognition period. All interactions with the objects were recorded using Ethovision 7 XT software (Noldus). Object recognition was scored as the time during which the nose of the animal was located within 2 cm of the object. A discrimination index was calculated as follows: [time spent sniffing novel object/(time spent sniffing novel object + time spent sniffing familiar object)].

Rotarod test. Motor coordination was assessed using a rotarod apparatus equipped with automatic timers and falling sensors using the protocol from Cao et al.[70]. Each mouse was placed on a textured rod (IITC Life Science) and left for 5 min to acclimatize. The rod accelerated gradually from 4 to 40 r.p.m. for 300 s. When the mouse fell, the magnetic triggers recorded the rotational speed (r.p.m.), duration (seconds) and distance traveled (meters). The test was repeated for a period of 7 days with a total of 6 trials per day, with 15-min inter-trial intervals.

Beam-break test. Locomotor activity was monitored using an infrared beam-break system (Micromax Analyzer with Fusion 5.3 Software, Omnitech Electronics) similar to a recent study using *16p11.2*$^{df/+}$ mice35. Mice were individually housed in separate cages (27 × 16 × 13 cm) with clean bedding. A maximum of 24 animals were tested at once. Each cage was placed in a metal frame and general motor activity was measured during seven consecutive days for 24 h per day using Micromax analyzer software (Omnitech Electronics). The first day was considered habituation and not included in the locomotor activity average. Horizontal activity counts (beam

breaks) were recorded. At the end of the paradigm, mice were removed from the testing cages and returned to their home cages.

Male–female interaction test with USVs. A three-phase male–female interaction test with USVs was performed as described in Yang et al.[21]. Before testing, males *16p11.2*$^{\Delta EC}$ subjects and stimulus *Cdh5-Cre*$^{tg/+}$ females were group-housed by sex, and sexually naive. Females were visually inspected for estrus cycle[71]. Only females in proestrus or estrus were used as stimulus mice. A control (*Cdh5-Cre*$^{tg/+}$) estrus female was placed in a small rectangular wire mesh enclosure at one side of an open-field box (45 × 45 × 45 cm). Interactions with the control female mouse were video recorded and monitored using Ethovision 7 XT software. The test consisted of three phases: phase 1, the male interacts with an unfamiliar female for 5 min; phase 2, the female is removed for 3 min, leaving the male alone in the arena; phase 3, the same female is returned for 3min. One female interacted with two males per testing day, with 30 min between each interaction. The time spent by the male in the rectangular interaction zone (2 cm from the female enclosure), as well as the time spent in two open-field corners away from the female, were recorded. USVs were continuously recorded during the test by an ultrasonic microphone (Ultravox XT by Noldus) mounted on the outside of the wire-mesh female enclosure. As explained in Yang et al.[20], USVs are produced by the male in this context.

Marble-burying test. This test, performed as described elsewhere[72], consisted of a 30-min trial per mouse. For each trial, a standard polycarbonate rat cage (26 × 48 × 20 cm) filled with 5-cm-thick SANI-chip bedding was used on which 20 marbles were evenly distributed (5 rows of 4 marbles). Each mouse was placed at the bottom-left corner of the cage. During the test, the cage was covered by transparent Plexiglas. Once the trial was completed, the number of marbles that were either fully buried or at least two-thirds covered by bedding were counted as buried.

Statistical analyses. No statistical methods were used to predetermine sample sizes, but our sample sizes were similar to those reported in previous publications[4,20,21,25,27,35,40,56–58,62,70,72]. All animal, sample and biological replicate numbers in this study are in line with well-accepted standards from the literature for each method. All data presented in this work were obtained from experimental replicates (for example, multiple animal cohorts from different litters, at least three experimental repeats for each assay, multiple RNA extractions and production of biological replicates). All attempts of replication were successful. All data analyses were conducted blinded to the genotype and experimental condition. Groups were reassembled following completion of the data analysis according to genotype, age and sex. Randomization of individual samples/animals was performed by numbering. All statistical tests were performed using GraphPad Prism 8.0 Software. Data distributions were assumed to be normal, but this was not formally tested. Further information can be found in the Nature Research Reporting Summary. A Mann–Whitney *U*-test (appropriate for small sample sizes, each animal being considered as a sample) was used for two-group comparisons between WT and *16p11.2*$^{df/+}$ mice (and between *Cdh5-Cre*$^{tg/+}$ and *16p11.2*$^{\Delta EC}$ mice) for metrics including CBF kinetics, vascular density and branching at a specific age, filopodia extension number, number/coverage of cellular types, mean capillary diameter and cerebral cortex anatomical indices. A two-way analysis of variance (ANOVA) (for example, genotype × age or genotype × time), with repeated measure when appropriate, and a post-hoc test (Sidak's or Tukey's multicomparison) was used for ECoG, vascular reactivity, endothelial network growth and behavioral readouts. $P < 0.05$ was considered significant.

Data availability

Source data for the bulk RNA-seq experiments are available (GSE147790), and information on iPSC lines can be found in Supplementary Table 1. More details on control lines are available from the Stanford Lab (wstanford@ohri.ca). ANOVA tables are given as statistics source data files. All other data and protocols are available from the corresponding author upon reasonable request. Source data are provided with this paper.

Code availability

The custom scripts for blood vessel and neuronal quantifications, written in Python, are available on GitHub (https://github.com/chcomin/NatNeurosci2020) and from the Comin Lab (chcomin@gmail.com).

Acknowledgements

We thank J.-C. Béïque, C.D. Harvey, P. Kaeser and C. Gu for their valuable comments on the manuscript; E. Hamel for generously sharing pressure myography equipment from her laboratory; D. Lagace, K. Ure and their assistant M. Barclay for training and guidance on behavioral assays; T. Portmann for advice on mouse genetics; C. Boisvert and K. Slodki for technical assistance on mouse husbandry and genotyping; A. Gagné and N. Vernoux for technical assistance on TEM; F. Xiao and M. Munkonda for training J. Ouellette on cell cycle analysis and tail-cuff plethysmography; L. Zhu for technical assistance; D.B. Stanimirovic for facilitating the collaboration with the National Research Council of Canada; A. Heinmiller for sharing equipment from the Fujifilm VisualSonics facility and for guidance on acoustic contrast imaging; S. Thompson for guidance on the marble-burying test; and C. Doré for helping organize experiments

using control iPSC lines. For this work, B.L. was supported by start-up funds from the Ottawa Hospital Research Institute, by research grants from the Canadian Institutes of Health Research (CIHR) (grant no. 388805), the Scottish Rite Charitable Foundation of Canada (grant no. 17112), and the J. P. Bickell Foundation. C.H.C. thanks FAPESP (grant no. 15/18942-8). L.d.F.C. thanks CNPq (grant no. 307333/2013-2), FAPESP (grant no. 11/50761-2 and no. 2015/22308-2) and NAP-PRP-USP.

Competing interests

The authors declare no competing interests.

Additional information

Extended data is available for this paper at https://doi.org/10.1038/s41593-020-0663-1 and can be found in Appendix A.

Supplementary information is available for this paper at https://doi.org/10.1038/s41593-020-0663-1 and can be found in Appendix A.

Peer review information *Nature Neuroscience* thanks Anusha Mishra and the other, anonymous, reviewer(s) for their contribution to the peer review of this work.

References

1. Walsh, J. J. et al. 5-HT release in nucleus accumbens rescues social deficits in mouse autism model. *Nature* **560**, 589–594 (2018).
2. Ebert, D. H. & Greenberg, M. E. Activity-dependent neuronal signalling and autism spectrum disorder. *Nature* **493**, 327–337 (2013).
3. Attwell, D. & Laughlin, S. B. An energy budget for signaling in the grey matter of the brain. J. Cereb. Blood Flow. Metab. 21, 1133–1145 (2001).
4. Lacoste, B. et al. Sensory-related neural activity regulates the structure of vascular networks in the cerebral cortex. Neuron 83, 1117–1130 (2014).
5. Segarra, M. et al. Endothelial Dab1 signaling orchestrates neuro–glia–vessel communication in the central nervous system. Science 361, eaao2861 (2018).
6. Andreone, B. J., Lacoste, B. & Gu, C. Neuronal and vascular interactions. Annu. Rev. Neurosci. 38, 25–46 (2015).
7. Kisler, K., Nelson, A. R., Montagne, A. & Zlokovic, B. V. Cerebral blood flow regulation and neurovascular dysfunction in Alzheimer disease. Nat. Rev. Neurosci. 18, 419–434 (2017).
8. Sweeney, M. D., Sagare, A. P. & Zlokovic, B. V. Blood–brain barrier breakdown in Alzheimer disease and other neurodegenerative disorders. Nat. Rev. Neurol. 14, 133–150 (2018).
9. Azmitia, E. C., Saccomano, Z. T., Alzoobaee, M. F., Boldrini, M. & Whitaker-Azmitia, P. M. Persistent angiogenesis in the autism brain: an immunocytochemical study of postmortem cortex, brainstem and cerebellum. J. Autism Dev. Disord. 46, 1307–1318 (2016).
10. Jann, K. et al. Altered resting perfusion and functional connectivity of default mode network in youth with autism spectrum disorder. Brain Behav. 5, e00358 (2015).
11. Cook, E. H. Jr & Scherer, S. W. Copy-number variations associated with neuropsychiatric conditions. Nature 455, 919–923 (2008).
12. Steinberg, S. et al. Common variant at 16p11.2 conferring risk of psychosis. Mol. Psychiatry 19, 108–114 (2014).
13. Zheng, X. et al. The association between rare large duplication of 16p11.2 and schizophrenia in the Singaporean Chinese population. Schizophr. Res. 146, 368–369 (2013).
14. Weiss, L. A. et al. Association between microdeletion and microduplication at 16p11.2 and autism. N. Engl. J. Med. 358, 667–675 (2008).
15. Simons VIP Connect Study Team. 16p11.2 Deletion Syndrome Guidebook https://diazatienza.es/wp-content/uploads/2017/12/16p_GUIDEBOOK_ FINAL_VERSION.pdf (Simons VIP Connect, 2015).
16. Hippolyte, L. et al. The number of genomic copies at the 16p11.2 locus modulates language, verbal memory, and inhibition. Biol. Psychiatry 80, 129–139 (2016).
17. Blackmon, K. et al. Focal cortical anomalies and language impairment in 16p11.2 deletion and duplication syndrome. Cereb. Cortex 28, 2422–2430 (2018).
18. Owen, J. P. et al. Aberrant white matter microstructure in children with 16p11.2 deletions. J. Neurosci. 34, 6214–6223 (2014).
19. Horev, G. et al. Dosage-dependent phenotypes in models of 16p11.2 lesions found in autism. Proc. Natl Acad. Sci. USA 108, 17076–17081 (2011).
20. Portmann, T. et al. Behavioral abnormalities and circuit defects in the basal ganglia of a mouse model of 16p11.2 deletion syndrome. Cell Rep. 7, 1077–1092 (2014).

21. Yang, M. et al. 16p11.2 Deletion syndrome mice display sensory and ultrasonic vocalization deficits during social interactions. Autism Res. 8, 507–521 (2015).
22. Tian, D. et al. Contribution of mGluR5 to pathophysiology in a mouse model of human chromosome 16p11.2 microdeletion. Nat. Neurosci. 18, 182–184 (2015).
23. Reynell, C. & Harris, J. J. The BOLD signal and neurovascular coupling in autism. Dev. Cogn. Neurosci. 6, 72–79 (2013).
24. Needles, A. et al. Nonlinear contrast imaging with an array-based micro-ultrasound system. Ultrasound Med. Biol. 36, 2097–2106 (2010).
25. Fischer, K. et al. Testing the efficacy of contrast-enhanced ultrasound in detecting transplant rejection using a murine model of heart transplantation. Am. J. Transplant. 17, 1791–1801 (2017).
26. Kozberg, M. G., Ma, Y., Shaik, M. A., Kim, S. H. & Hillman, E. M. Rapid postnatal expansion of neural networks occurs in an environment of altered neurovascular and neurometabolic coupling. J. Neurosci. 36, 6704–6717 (2016).
27. Chen, B. R., Kozberg, M. G., Bouchard, M. B., Shaik, M. A. & Hillman, E. M. A critical role for the vascular endothelium in functional neurovascular coupling in the brain. J. Am. Heart Assoc. 3, e000787 (2014).
28. Hillman, E. M. Coupling mechanism and significance of the BOLD signal: a status report. Annu. Rev. Neurosci. 37, 161–181 (2014).
29. Mannell, H. K. et al. ARNO regulates VEGF-dependent tissue responses by stabilizing endothelial VEGFR-2 surface expression. Cardiovasc. Res. 93, 111–119 (2012).
30. Harb, R., Whiteus, C., Freitas, C. & Grutzendler, J. In vivo imaging of cerebral microvascular plasticity from birth to death. J. Cereb. Blood Flow. Metab. 33, 146–156 (2013).
31. Mitola, S. et al. Gremlin is a novel agonist of the major proangiogenic receptor VEGFR2. Blood 116, 3677–3680 (2010).
32. Dutton, L. R., O'Neill, C. L., Medina, R. J. & Brazil, D. P. No evidence of Gremlin1-mediated activation of VEGFR2 signaling in endothelial cells. J. Biol. Chem. 294, 18041–18045 (2019).
33. Ma, B., Kang, Q., Qin, L., Cui, L. & Pei, C. TGF-β2 induces transdifferentiation and fibrosis in human lens epithelial cells via regulating gremlin and CTGF. Biochem. Biophys. Res. Commun. 447, 689–695 (2014).
34. Zode, G. S., Clark, A. F. & Wordinger, R. J. Bone morphogenetic protein 4 inhibits TGF-β2 stimulation of extracellular matrix proteins in optic nerve head cells: role of gremlin in ECM modulation. Glia 57, 755–766 (2009).
35. Angelakos, C. C. et al. Hyperactivity and male-specific sleep deficits in the 16p11.2 deletion mouse model of autism. Autism Res. 10, 572–584 (2017).
36. Yadav, S. et al. TAOK2 kinase mediates PSD95 stability and dendritic spine maturation through septin7 phosphorylation. Neuron 93, 379–393 (2017).
37. Ip, J. P. K. et al. Major vault protein, a candidate gene in 16p11.2 microdeletion syndrome, is required for the homeostatic regulation of visual cortical plasticity. J. Neurosci. 38, 3890–3900 (2018).
38. Shin, M. et al. Vegfa signals through ERK to promote angiogenesis, but not artery differentiation. Development 143, 3796–3805 (2016).
39. Anderson, A. W. et al. Neonatal auditory activation detected by functional magnetic resonance imaging. Magn. Reson. Imaging 19, 1–5 (2001).

40. Wen, T. H., Lovelace, J. W., Ethell, I. M., Binder, D. K. & Razak, K. A. Developmental changes in EEG phenotypes in a mouse model of fragile X syndrome. Neuroscience 398, 126–143 (2019).
41. Berman, J. I. et al. Relationship between M100 auditory evoked response and auditory radiation microstructure in 16p11.2 deletion and duplication carriers. Am. J. Neuroradiol. 37, 1178–1184 (2016).
42. Miyazaki-Akita, A. et al. 17β-estradiol antagonizes the down-regulation of endothelial nitric-oxide synthase and GTP cyclohydrolase I by high glucose: relevance to postmenopausal diabetic cardiovascular disease. J. Pharmacol. Exp. Ther. 320, 591–598 (2007).
43. Grissom, N. M. et al. Male-specific deficits in natural reward learning in a mouse model of neurodevelopmental disorders. Mol. Psychiatry 23, 544–555 (2018).
44. Gur, R. C. et al. Sex and handedness differences in cerebral blood flow during rest and cognitive activity. Science 217, 659–661 (1982).
45. Ospina, J. A., Duckles, S. P. & Krause, D. N. 17β-estradiol decreases vascular tone in cerebral arteries by shifting COX-dependent vasoconstriction to vasodilation. Am. J. Physiol. Heart Circ. Physiol. 285, H241–H250 (2003).
46. Robinson, E. B., Lichtenstein, P., Anckarsater, H., Happe, F. & Ronald, A. Examining and interpreting the female protective effect against autistic behavior. Proc. Natl Acad. Sci. USA 110, 5258–5262 (2013).
47. Goldman, S. A. & Chen, Z. Perivascular instruction of cell genesis and fate in the adult brain. Nat. Neurosci. 14, 1382–1389 (2011).
48. Tata, M. & Ruhrberg, C. Cross-talk between blood vessels and neural progenitors in the developing brain. Neuronal Signal. 2, NS20170139 (2018).
49. Flygare Wallen, E., Ljunggren, G., Carlsson, A. C., Pettersson, D. & Wandell, P. High prevalence of diabetes mellitus, hypertension and obesity among persons with a recorded diagnosis of intellectual disability or autism spectrum disorder. J. Intellect. Disabil. Res. 62, 269–280 (2018).
50. Sigmon, E. R., Kelleman, M., Susi, A., Nylund, C. M. & Oster, M. E. Congenital heart disease and autism: a case–control study. Pediatrics 144, e20184114 (2019).
51. Alva, J. A. et al. VE-cadherin-Cre-recombinase transgenic mouse: a tool for lineage analysis and gene deletion in endothelial cells. Dev. Dyn. 235, 759–767 (2006).
52. Tsai, H. H. et al. Regional astrocyte allocation regulates CNS synaptogenesis and repair. Science 337, 358–362 (2012).
53. Tunster, S. J. Genetic sex determination of mice by simplex PCR. Biol. Sex. Differ. 8, 31 (2017).
54. Munoz, N. M. et al. Comparison of dynamic contrast-enhanced magnetic resonance imaging and contrast-enhanced ultrasound for evaluation of the effects of sorafenib in a rat model of hepatocellular carcinoma. Magn. Reson. Imaging 57, 156–164 (2019).
55. Lacoste, B., Tong, X. K., Lahjouji, K., Couture, R. & Hamel, E. Cognitive and cerebrovascular improvements following kinin B1 receptor blockade in Alzheimer's disease mice. J. Neuroinflammation 10, 57 (2013).
56. Lovelace, J. W., Ethell, I. M., Binder, D. K. & Razak, K. A. Translation-relevant EEG phenotypes in a mouse model of fragile X syndrome. Neurobiol. Dis. 115, 39–48 (2018).
57. Tong, X. K., Nicolakakis, N., Kocharyan, A. & Hamel, E. Vascular remodeling versus amyloid β-induced oxidative stress in the cerebrovascular dysfunctions associated with Alzheimer's disease. J. Neurosci. 25, 11165–11174 (2005).

58. Thibodeau, J. F. et al. Vascular smooth muscle-specific EP4 receptor deletion in mice exacerbates angiotensin II-induced renal injury. Antioxid. Redox Signal. 25, 642–656 (2016).
59. Lindeberg, T. Feature detection with automatic scale selection. Int. J. Comput. Vis. 30, 79–116 (1998).
60. Travencolo, B. A. et al. A new method for quantifying three-dimensional interactions between biological structures. J. Anat. 210, 221–231 (2007).
61. Woodworth, M. B. et al. Ctip1 regulates the balance between specification of distinct projection neuron subtypes in deep cortical layers. Cell Rep. 15, 999–1012 (2016).
62. Pinto, L. et al. AP2γ regulates basal progenitor fate in a region- and layer-specific manner in the developing cortex. Nat. Neurosci. 12, 1229–1237 (2009).
63. Tremblay, M. E., Riad, M. & Majewska, A. Preparation of mouse brain tissue for immunoelectron microscopy. J. Vis. Exp. https://doi.org/10.3791/2021 (2010).
64. Bisht, K., El Hajj, H., Savage, J. C., Sanchez, M. G. & Tremblay, M. E. Correlative light and electron microscopy to study microglial interactions with beta-amyloid plaques. J. Vis. Exp. https://doi.org/10.3791/54060 (2016).
65. Dobin, A. et al. STAR: ultrafast universal RNA-seq aligner. Bioinformatics 29, 15–21 (2013).
66. Zerbino, D. R. et al. Ensembl 2018. Nucleic Acids Res. 46, D754–D761 (2018).
67. Love, M. I., Huber, W. & Anders, S. Moderated estimation of fold change and dispersion for RNA-seq data with DESeq2. Genome Biol. 15, 550 (2014).
68. Tchagang, A. B. et al. GOAL: a software tool for assessing biological significance of genes groups. BMC Bioinf. 11, 229 (2010).
69. Tatsumi, R. et al. Simple and highly efficient method for production of endothelial cells from human embryonic stem cells. Cell Transplant. 20, 1423–1430 (2011).
70. Cao, V. Y. et al. Motor learning consolidates arc-expressing neuronal ensembles in secondary motor cortex. Neuron 86, 1385–1392 (2015).
71. Behringer, R., Gertsenstein, M., Nagy, K. V. & Nagy, A. Selecting female mice in estrus and checking plugs. Cold Spring Harb. Protoc. https://doi. org/10.1101/pdb.prot092387 (2016).
72. Angoa-Perez, M., Kane, M. J., Briggs, D. I., Francescutti, D. M. & Kuhn, D. M. Marble burying and nestlet shredding as tests of repetitive, compulsive-like behaviors in mice. J. Vis. Exp. https://doi.org/10.3791/50978 (2013).

Chapter 3- Manuscript II

Association to hypothesis: This manuscript provides a detailed investigation of the impact of the 16p11.2 deletion on brain endothelial cells while determining a vascular mechanism to target in ASD. Furthermore, this manuscript strengthened the notion that healthy brain endothelial cells are required during brain development and for brain function.

Current manuscript status: This manuscript was originally submitted in June 2024 and is subject to change.

Author contributions: J.O. designed experiments, led the project (with guidance from B.L.) and wrote the manuscript. J.O. isolated and cultured all primary ECs, completed and analyzed all tube formation assays and performed immunocytochemistry, extracted metabolites as well as completed and analyzed mitochondrial function. Mitochondrial density and fragmentation were quantified by C.H.C. Western blots were completed by M.F.A , C.P. (supervised by M-E.H.) and S.Y. Adenosine and PPADs experiments were completed by L.A.T with the guidance of J.O. Metabolomics was completed by S.N. P.K. generated lipid nanoparticles. D.S.M. provided expertise for the lipid nanoparticles. Calcium steady state and dynamics experiments were completed by S.W. A.S. provided expertise for calcium assessment. B.L. generated figures for the manuscript. B.L. edited the manuscript with input from A.S. and D.S.M.

P2 purinergic receptor activation rectifies autism-associated brain endothelial cell dysfunction

Julie Ouellette[1,2], Sareen Warsi[1,2], Purva Khare[3], Shama Naz[4], Leya Aubert-Tandon[1], Chantal Pileggi[5], Sozerko Yandiev[1], Moises Freitas-Andrade[1], Cesar H. Comin[6], Mary-Ellen Harper[5], Devika S. Manickam[3], Armen Saghatelyan[1,2,7], and Baptiste Lacoste[1,2,7*].

Affiliations:

[1] Neuroscience Program, The Ottawa Hospital Research Institute, Ottawa, ON, Canada.
[2] Cellular & Molecular Medicine, University of Ottawa, Ottawa, ON, Canada.
[3] Graduate School of Pharmaceutical Sciences, Duquesne University, Pittsburgh, PA, USA.
[4] University of Ottawa Metabolomics Core Facility, Faculty of Medicine, Ottawa, ON, Canada.
[5] Department of Biochemistry Microbiology and Immunology, Faculty of Medicine, University of Ottawa, Ottawa, Ontario, Canada.
[6] Federal University of São Carlos, Department of Computer Science, São Carlos, SP, Brazil.
[7] University of Ottawa Brain and Mind Research Institute, Ottawa, ON, Canada.

***Correspondence to:**

Dr. Baptiste Lacoste
Faculty of Medicine, Department of Cellular and Molecular Medicine
University of Ottawa & Ottawa Hospital Research Institute
451 Smyth Road, Ottawa (ON) K1H 8M5, Ottawa, Canada
Email: blacoste@uottawa.ca

Competing Interest Statement:

The authors have no competing interest to declare.

Manuscript type:

RESEARCH ARTICLE - direct submission

Number of words:

Abstract: 184
Significance statement: 106

Number of figures:

Main: 4
Supplementary: 7

Key words:

Endothelium, autism, metabolism, ATP, postnatal, brain, angiogenesis, mice, P2 receptors.

ABSTRACT

Brain development and function are reliant on a continuous supply of oxygen, nutrients and growth factors from its vasculature. Early cerebrovascular dysfunction can affect brain maturation by impacting trophic support and/or energy availability. Recent evidence in a mouse model of 16p11.2 deletion autism spectrum disorder (ASD) revealed neurovascular abnormalities associated with brain endothelial dysfunction postnatally, and a compensatory shift in adult brain metabolism. However, the endothelial alterations eliciting these changes remain unknown. Here, we isolated brain endothelial cells (ECs) from 14-day old 16p11.2-deficient male mice and wild-type littermates to assess endothelial parameters *in vitro*. We discover that 16p11.2 deletion-induced endothelial dysfunction is linked to a bioenergetic failure in ECs, including reduced intracellular ATP. We show that intra- or extra-cellularly ATP supplementation rescues the angiogenic capacity of 16p11.2-deficient ECs via P2 purinergic receptor activation. We also demonstrate that selective P2Y2 receptor activation can rescue endothelial cell function in 16p11.2-deficient ECs. Finally, we find that 16p11.2-deficient ECs display distinct Ca^{2+} responses following administration of extracellular ATP. Taken together, we propose that metabolic reprogramming of brain ECs may represent a new therapeutic avenue for ASD-associated cerebrovascular deficits.

SIGNIFICANCE STATEMENT

A healthy vasculature is required for the brain to properly develop and regulate its metabolism. While the neuronal underpinnings of autism spectrum disorders (ASD) are extensively studied, recent findings of neurovascular alterations in ASD, particularly brain endothelial dysfunction, highlighted the need to unravel vascular components underlying these deficits. This study offers the first detailed characterization of brain endothelial cells (ECs) from a mouse model of ASD

syndrome and finds a new strategy to rescue their function. We discover that a 16p11.2 deletion results in brain endothelial metabolic failure, and we identify P2 purinergic signaling as a vascular target for the development of transformative therapies for ASD.

MAIN TEXT

Introduction

The brain is highly reliant on metabolic health (1), which includes uninterrupted delivery of nutrients and oxygen from its vasculature. This synergy between vascular and neuronal systems must be established early during development to support the elevated metabolic demands of expanding cellular networks (2-5). As such, a healthy brain requires normal vascular structure and function, as well as metabolic processes that are tightly regulated from a regional level down to single cells and tripartite synapses (1). While neurons are responsible for massive energy consumption, the brain's highly specialized endothelium takes part in modulating essential functions such as vascular permeability and tone, maintenance of brain homeostasis, and promotion of neurogenesis (6). Although the metabolic characteristics of brain endothelial cells (ECs) are not fully elucidated, these specialized cells are known to meet their own metabolic needs predominantly through glycolysis, and in part via oxidative phosphorylation, to generate ATP (7). While brain ECs exist in an oxygen-rich environment, glycolytic metabolism enables fast ATP production for rapid proliferation and migration to efficiently vascularize and/or revascularize tissues and maintain brain energy balance (8, 9).

Energy requirements during critical periods of brain development further increase the vulnerability of the brain to metabolic failures (10, 11). During development, brain ECs help guide and coordinate neurogenesis, while neuronal cues regulate vascularization of the central nervous

system (12). As such, brain endothelial dysfunction can compromise metabolic support to neuronal cells, leading to the progression and/or onset of neurological conditions. Recent evidence revealed a causal link between altered brain EC function and autism spectrum disorders (ASD) (13-16). Also, in the ASD-associated glucose transporter-1 (GLUT-1) deficiency syndrome, lack of ECs GLUT-1 was linked to neuroinflammation and defective endothelial tip cells that are crucial for brain angiogenesis (17). Moreover, several neurodegenerative diseases have been associated with elevated oxidative stress in ECs, decreased expression of endothelial tight junction molecules, as well as altered endothelium-dependent regulation of cerebral blood flow, altogether contributing to cognitive decline (13, 18).

In the context of neurodevelopmental disorders, disturbances in EC physiology have been largely overlooked. We recently uncovered an association between brain endothelial dysfunction and ASD onset in a mouse model of the 16p11.2 deletion syndrome which mimics a mutation commonly found in human ASD (14). While 16p11.2-deficient mouse brain ECs were healthy at baseline (*i.e.*, normal survival, migration and proliferation), they were unable to respond to functional challenges both *in vitro* (*i.e.*, lack of angiogenic capacity in a Matrigel®-based tube formation assay) and *in vivo* (*e.g.*, lack of endothelial-dependent vasodilation). These results were consistent with delayed endothelial network growth at postnatal (P) day 14 and reduced neurovascular coupling at P50 *in vivo*, underscoring that 16p11.2-deficient ECs fail to execute intrinsic functions when triggered. As a result, endothelium-specific 16p11.2 haploinsufficiency was sufficient to drive a subset of ASD-associated behaviors in mice (14). Since ECs are fundamental for regulating energy allocation to the brain (19), we also recently assessed brain metabolism in adult 16p11.2-deficient male mice (15). We identified reduce mitochondrial biogenesis as a possible player in 16p11.2 deletion-induced endothelial dysfunctions and found

that endothelium-specific 16p11.2 haploinsufficiency led to compensatory shifts in adult brain metabolism (15).

Accumulating evidence implicate metabolic disturbances in ASD (20). These pervasive neurodevelopmental disorders are characterized by early-onset social interaction deficits, communication impairments, repetitive behaviors and restricted interests (21). And while ASD are generally depicted by neuronal features that are highly contingent on brain metabolism (21-27), the recent association with endothelial dysfunction warrants further inquiry. Here, we investigated the impact of a 16p11.2 deletion on brain EC metabolism at a key milestone of cerebrovascular development (P14) to unveil new mechanisms underlying ASD pathophysiology. We demonstrate that 16p11.2 deletion-induced endothelial dysfunction is caused by a bioenergetic failure, with reduced intracellular ATP, and that activation of ATP signaling via endothelial P2-class purinergic receptors, more specifically P2Y2 receptors, can rescue EC dysfunction. Altogether, these findings open new avenues for the development of therapies for ASD.

Results

Dysfunction of brain endothelial cells from P14 *16p11.2*$^{df/+}$ mice is associated with a bioenergetic failure.

In previous work, we demonstrated that the 16p11.2 deletion is associated with male-specific endothelial dysfunction characterized by defective angiogenesis and lack of endothelium-dependent vasodilation *in vivo*, coinciding with the emergence of ASD-related phenotypes (14). Here, we focused on 16p11.2-deficient ECs *in vitro* parameters as a screening platform. We first confirmed that 16p11.2-deficient ECs isolated from 14-day old mice, a landmark of cerebrovascular maturation (28), do not establish a vascular network *in vitro.* This is evidenced by

absence of endothelial tubes following seeding of 16p11.2-deficent ECs in an extracellular matrix. (Figs. 1*A*, 2*D* and E, 3*A,B* and *D,* 4*C, SI Appendix,* Fig. S5). Our prior work also identified reduced mitochondria number in adult 16p11.2-deficent brain ECs *in vivo* (15). Here, we tested whether mitochondrial density was also reduced *in vitro* in P14 brain ECs isolated from *16p11.2*$^{df/+}$ male mice and found a similar phenotype, without apparent change in mitochondrial fragmentation (Fig. 1*B*). This suggests that mitochondrial discrepancies are present before adulthood and may impact EC function early. Despite reduced mitochondrial network density in *16p11.2*$^{df/+}$ ECs at P14, levels of proteins involved in mitochondrial fusion (MFN1, MFN2 and OPA1) and fission (DRP1), as well as mitochondrial biogenesis (PGC-1α), appeared unchanged (*SI Appendix*, Fig. S1*A*). Altogether, these findings lead us to hypothesize that 16p11.2 haploinsufficiency may cause metabolic alterations in P14 mouse brain ECs.

To test this, we investigated the bioavailability of intracellular metabolites in P14 brain ECs from *16p11.2*$^{df/+}$ and WT male mice by performing targeted metabolomics analysis. Distinct metabolite profiles were identified between *16p11.2*$^{df/+}$ and WT brain ECs, as shown by cluster separation following a partial least square-discriminant analysis (PLS-DA) (Fig. 1*D*). We measured overall decreased metabolite abundance in *16p11.2*$^{df/+}$ ECs compared to WT ECs, which was consistent in two independent cohorts (Fig. 1*C*). With no exception, changes observed were reductions in metabolite abundance in *16p11.2*$^{df/+}$ ECs (Fig. 1*F*). Remarkably, the top 20 metabolites driving cluster separation comprised high energy molecules including ATP, as well as co-factors involved in glycolysis and energy utilization (e.g., glutamine, pyruvic acid and aspartic acid) (Fig. 1*E*). These results indicate that energy metabolism is altered in 16p11.2-deficient ECs. Specifically, a bioenergetic failure in 16p11.2-deficient ECs was evidenced by 50% reduction in abundance of ATP and by lower abundance of metabolites including high energy donors (UDP-

glucose/UDP galactose), co-enzymes required for the Krebs cycle and oxidative phosphorylation (NAD^+, FAD), and amino acids essential for balancing energy dynamics (alanine/sarcosine and creatine) (Fig. 1*G* , *SI Appendix*, Fig. S1*B* and *SI Appendix,* Fig. S2*A*). *16p11.2*$^{df/+}$ ECs also displayed a significant reduction in both ATP:ADP ratio and adenylate energy charge, which are indicators of cellular energy status (Fig. 1*H*). Notably, no difference in the reduced glutathione-to-oxidized glutathione ratio (GSH:GSSG) was found between *16p11.2*$^{df/+}$ and WT ECs, indicating that changes in metabolite abundance were not attributed to poor cellular health at the time of the metabolite extraction (29, 30), which is consistent with our previous work showing normal baseline endothelial health (*i.e.*, survival, proliferation and migration) in P14 *16p11.2*$^{df/+}$ brain ECs (14). Although no difference was seen in the GSH:GSSG ratio, both GSH and GSSG were individually reduced in *16p11.2*$^{df/+}$ ECs compared to WT ECs, consistent with decreased gamma-glu-cys (31) (Fig. 1*G* and *SI Appendix,* Fig. S2*A*). Given that 16p11.2-deficient ECs showed a 50% reduction in ATP abundance and a lower ATP:ADP ratio, we next sought to determine whether ATP-sensing AMP-activated protein kinase (AMPK) (32) activity was enhanced. Unexpectedly, no difference was measured in AMPK activity between 16p11.2-deficient and WT ECs (*SI Appendix,* Fig. S2*A*). Of note, abundance of the main regulators of AMPK activity (*i.e.,* AMP and ADP) were not significantly changed in 16p11.2-deficient ECs (*SI Appendix,* Fig. S2*A*).

To test whether the observed bioenergetic failure was related to alterations in mitochondrial function, we used a Seahorse Cell Mito stress test. No difference was observed between P14 WT and *16p11.2*$^{df/+}$ ECs in oxygen consumption rate (OCR), extracellular acidification rate (ECAR), as well as additional parameters of mitochondrial function including ATP production (*SI Appendix,* Fig. S2*B*). These findings suggest that the bioenergetic failure evidenced in 16p11.2-deficient ECs might be a direct contributor to endothelial dysfunction, independent of the function of individual

mitochondria. While at this stage the direct cause of reduced intracellular ATP in 16p11.2-deficient ECs remain to be elucidated, it raises the possibility of restoring ATP bioavailability as a rescue strategy.

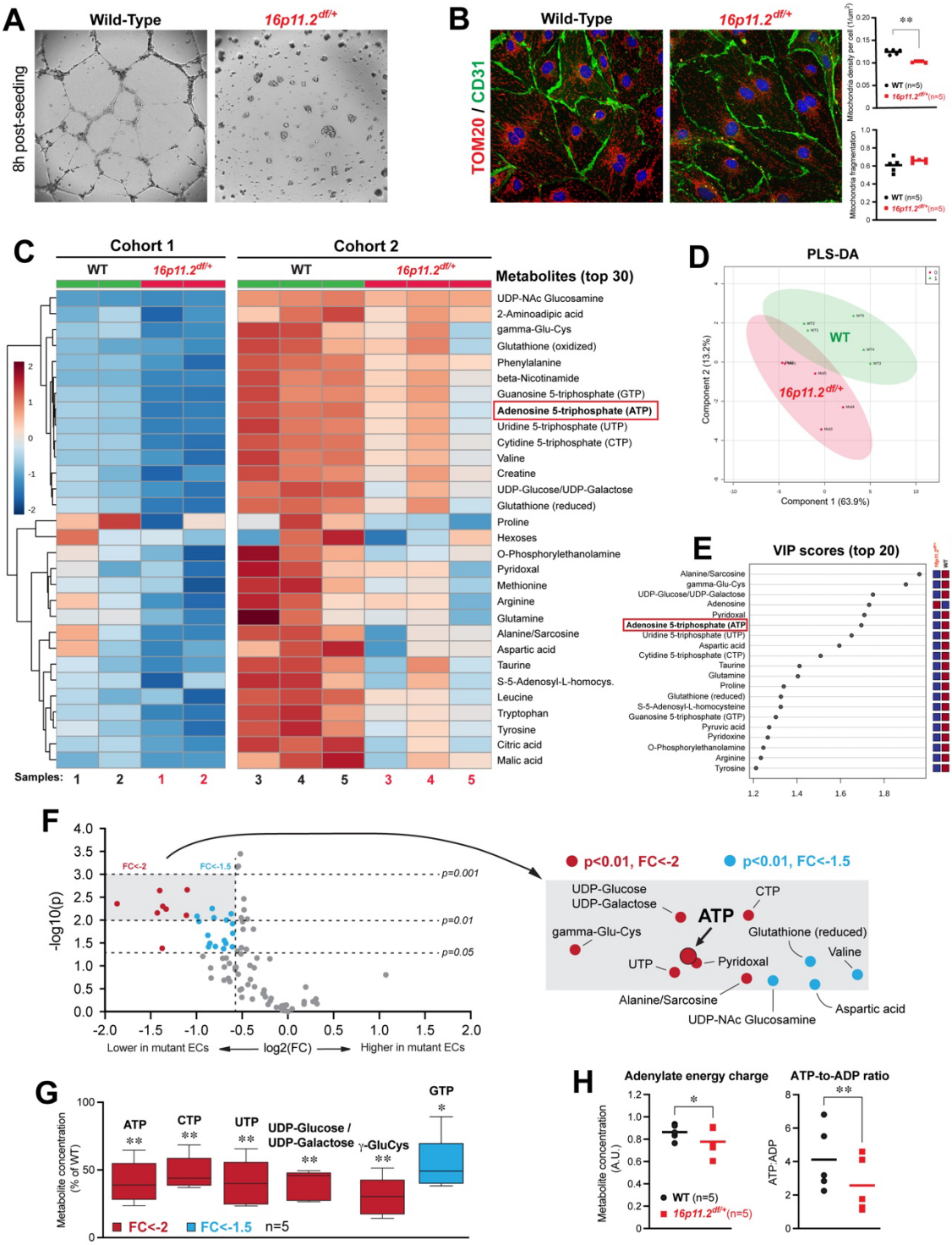

Fig 1. See caption on next page.

Fig 1. Primary 16p11.2-deficient brain endothelial cells isolated from P14 mice exhibit reduced mitochondrial density with a bioenergetic failure. *(A)* Representative images of primary brain wild-type (WT) and 16p11.2-deficient ECs angiogenic ability. *(B)* Representative images (*left*) and quantification (*right*) of mitochondria density (*top right*) and mitochondria fragmentation (*bottom right*) in WT (n=5 mice) and 16p11.2-deficient (n=5 mice) ECs following immunostaining for mitochondrial marker TOM20 (red), endothelial marker CD31 (green) and nuclei marker DAPI (blue). *(C)* Heatmap (multivariate statistical analysis) of two distinct cohorts displaying the top 30 metabolites significantly altered by genotype. *(D)* Partial least-square discriminant analysis (PLS-DA) of metabolomics data from 16p11.2-deficient (n=5) and WT (n=5) ECs. Each data point represents pooled ECs isolated from three mice. Supervised PLS-DA was obtained with 2 components. The explained variances are shown in parentheses. *(E)* Variable importance projection (VIP) score showing the top 20 (score > 1) most important metabolites contributing to the separation of metabolic profiles identified by PLS-DA. *(F)* Volcano plot showing most significantly altered metabolites ($p<0.01$) with a fold change (FC)<-2 (red) and FC<-1.5 (blue). Plot summarizes both fold-change and t-test criteria. Scatter-plot of the negative log10-transformed p-values from the t-test plotted against the log2 fold change is shown. *(G)* Energy-related metabolites detected as most significantly altered by univariate statistical analysis. Metabolites displayed consist of a fold-change FC<-2 (red) or FC<-1.5 (blue) (n=5 samples, ECs pooled from 3 mice per sample). *(H)* Quantitative assessment of energy-related metabolite ratio (adenylate energy charge and ATP-to-ADP ratio, n=5 n=5 samples, ECs pooled from 3 mice per sample). All data shown are from ECs isolated from P14 male mice. Data in *B* and *H* are mean with individual values (n=animals). Data in *H* are whisker boxes (min to max, center line indicating median) and represented as percentage of Wild-Type (WT). *P<0.05, **P<0.01 (two-tailed Mann-Whitney test in *B;* two-tailed paired t test in *G,H*.

Intracellular delivery of ATP rescues 16p11.2 deletion-associated endothelial dysfunction.

Considering the findings above, and in light of recent work showing that mitochondrial ATP is required to maintain cerebrovascular tone (33), we next sought to test whether intracellular ATP supplementation could normalize the cell-autonomous angiogenic capacity of 16p11.2-deficient ECs in a Matrigel®-based assay (14). Our previous work revealed that *16p11.2*$^{df/+}$ ECs isolated from P14 male mice were unable to form capillary-like networks in this assay, without changes in proliferation or migration (14). Here, we opted to deliver ATP intracellularly in cultured ECs via lipid nanoparticles (LNPs) (34). Since physico-chemical properties of nanoparticles, such as colloidal stability, determine their biological efficiency (35, 36), we first assessed particle size and dispersity indices of ATP-loaded LNPs (ATP-LNPs) over 14 days upon intermittent storage at 2-8^{o}C. While particle diameters and dispersity indices of ATP-LNPs increased over 14 days (*SI Appendix*, Fig. S3*B-C*), theses size changes were indicative of colloidally stable dispersions (particle sizes <200 nm and dispersity indices ~0.3). Additionally, LNPs exhibited sphere-like morphologies over two weeks of storage, further supporting colloidal stability (*SI Appendix,* Fig.

S3*A*). The cellular uptake of LNPs containing AF647-labeled ATP (34) compared to blank LNPs was confirmed using fluorescence microscopy (Fig. 2*A*). 16p11.2-deficient and WT ECs were then treated with 1mM of ATP-LNPs from cell isolation for 7 days (6 days in culture and 24-hour tube formation assay) (Fig. 2*B*). Total capillary tube length (*i.e.,* branches) and network nodes (*i.e.,* intersection of three or more branches) were quantified. 16p11.2-deficient ECs treated with 1mM of ATP-LNPs displayed a dramatic increase in tube length at the 4- and 8-hour timepoints compared to *16p11.2*$^{df/+}$ ECs treated with blank-LNPs (Fig. 2*C-E*). These results demonstrate that intracellular delivery of ATP can boost the angiogenic capacity of 16p11.2-deficient brain ECs *in vitro*. Interestingly, increasing ATP-LNP concentration to 5mM did not confer rescue, but further hindered the ability of *16p11.2*$^{df/+}$ ECs to establish a network in the same assay (*SI Appendix*, Fig. S3*D*). These data thus support that 16p11.2 deletion-induced endothelial dysfunction can be rescued by intracellular ATP supplementation below a concentration threshold.

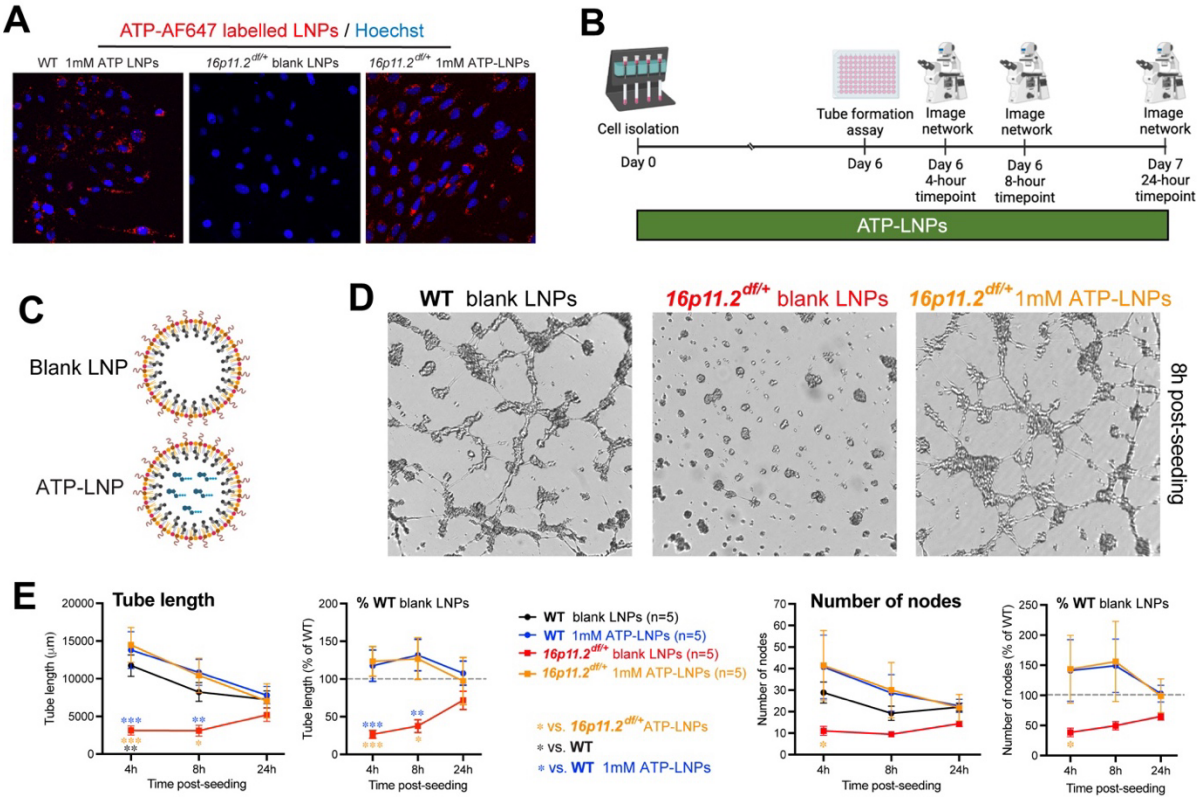

Fig 2. See caption on next page.

Fig 2. Intracellular delivery of ATP rescues 16p11.2-deficient primary brain EC angiogenic activity. *(A)* Representative images confirming intracellular delivery of ATP (red) via lipid nanoparticles (LNPs). *(B)* Experimental timeline for treatment of 16p11.2-deficient ECs with ATP-LNPs following cell isolation and during a 24-hour *in vitro* network formation assay. *(C-E) In vitro* network formation assay was used to assess angiogenic activity over 24 hours in a growth-factor-reduced Matrigel®. *(C)* Schematic representation of blank LNPs (without ATP) and ATP-LNP structures. *(D)* Representative images at the 8h post-seeding time point of WT and 16p11.2-deficient ECs treated with blank LNPs and 16p11.2-deficient ECs treated with 1mM of ATP-LNPs during a network formation assay. *(E)* Quantifications of network densities (total endothelial tube length) and network nodes (total number of branching hubs) with representative percent of untreated WT. Dotted line represents 100% of untreated WT values. All data shown are from ECs isolated from P14 male mice, and are mean ± s.e.m. (n=5 animals per group) *P<0.05, **P<0.01, ***P<0.001 (two-way repeated measure ANOVA and Sidak's multicomparison *post hoc* test).

Extracellular exposure to ATP rescues 16p11.2 deletion-associated endothelial dysfunction *in vitro* via P2-class purinergic receptor-mediated signaling.

The question remains what mechanisms underlie ATP-mediated rescue. In addition to being the main energy source for the cell, ATP also acts as a signaling molecule on brain ECs (37). Brain ECs are sensitive to ATP via expression of P2-class purinergic receptors (38). Recent work by Thakore et al. also demonstrated that intracellular ATP can exit brain ECs through pannexin-1 (Panx1) channels to subsequently activate membrane P2 purinergic receptors on adjacent ECs to regulate vascular tone (39). We thus tested whether extracellular ATP can also rescue the angiogenic capacity of 16p11.2-deficient ECs *in vitro*. ECs were treated with exogenous ATP at 1μM, 10 μM and 100 μM from cell isolation for 7 days (6 days in culture and 24-hour tube formation assay), as previously described (Fig. 3*A*). We found that extracellular ATP supplementation was also able to rescue capillary network formation, in a dose-dependent manner (100μM shown in Fig. 3*A*; 1μM and 10μM shown in *SI Appendix*, Fig. S*4*). These findings indicate that dysfunction of 16p11.2-deficient ECs might result from lack of ATP signaling, rather than lack of ATP itself. Of note, adenosine, a by-product of ATP hydrolysis, failed to influence endothelial network growth (*SI Appendix*, Fig. S*5*).

Brain ECs are known to express various purinergic receptors that are activated by ATP, namely most ionotropic P2X isoforms and several metabotropic P2Y isoforms, all of which take

part in maintaining vascular function (39, 40). Considering this, we next sought to test whether rescue of endothelial function by extracellular ATP is indeed receptor-mediated. To test this, ECs were treated with a non-selective P2 purinergic antagonist (pyridoxalphosphate-6-azophenyl-2',4'-disulfonic acid, PPADS) for 10 minutes prior to each ATP administration (*i.e.,* each culture medium change) (*SI Appendix,* Fig. S6*A*). Administration of 50μM of PPADs abolished the extracellular ATP-mediated rescue in *16p11.2*$^{df/+}$ ECs (Fig. 3*B*). At a concentration of 10μM or 100μM, PPADs was less efficient at preventing ATP-mediated rescue (*SI Appendix*, Fig. S6*B,C*). These results demonstrate that extracellular ATP acts on purinergic P2 receptors to rescue the angiogenic ability of 16p11.2-deficient brain ECs. Lastly, we explored the possibility that ATP delivered intracellularly via LNPs can exit ECs to subsequently act on membrane P2 receptors (39). Mouse brain ECs express Panx1, as confirmed here (Fig. 3*C*). We find that co-administration of 1mM of ATP-LNPs and 50 μM of PPADs abolishes the rescue mediated by intracellular ATP delivery (Fig. 3*D*). These findings demonstrate that LNP-delivered intracellular ATP can indeed exit ECs to then act on P2 receptors to mediate functional rescue similar to free extracellular ATP.

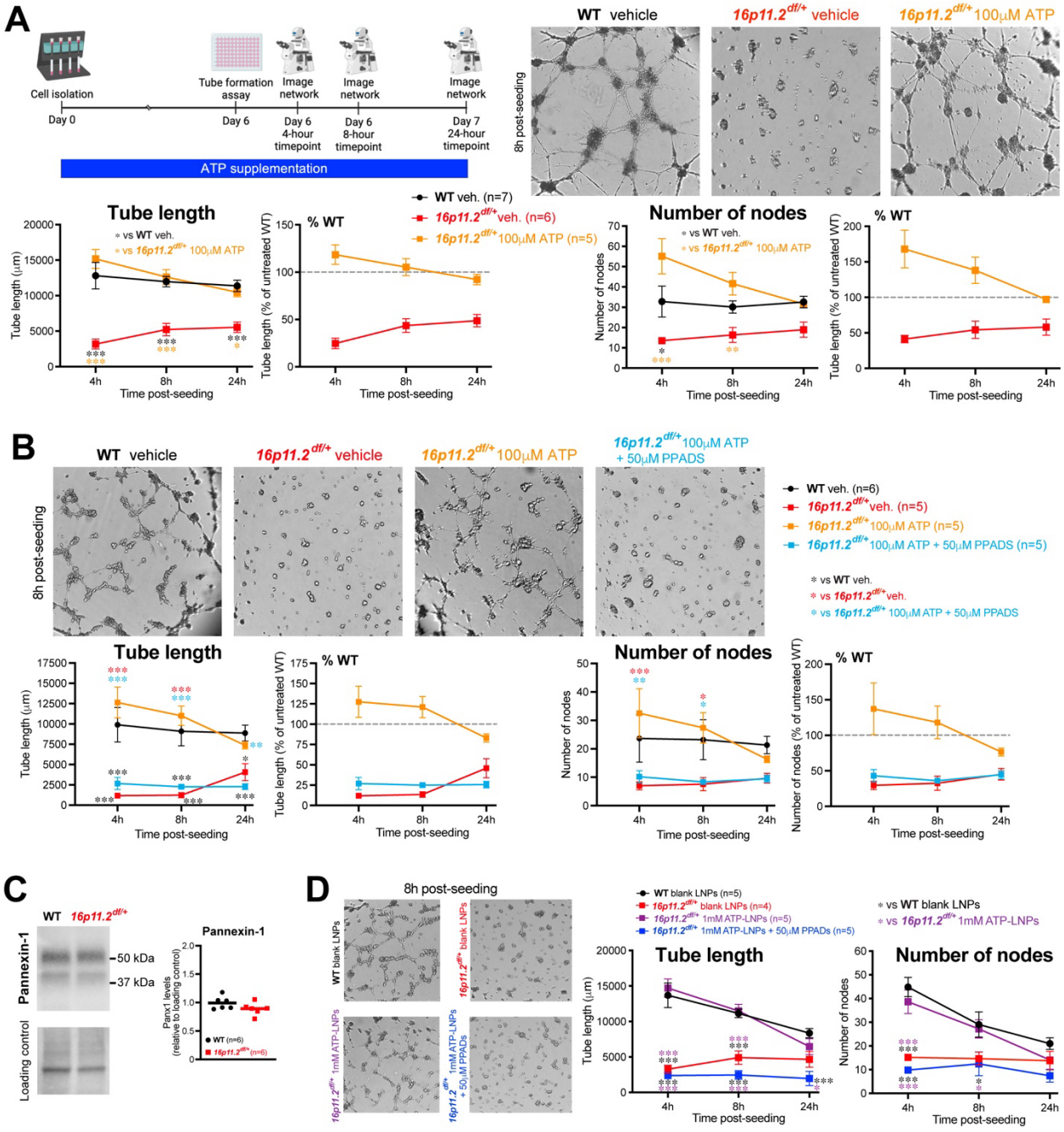

Fig 3. See next page for caption.

Fig 3. Angiogenic activity is rescued in 16p11.2-deficient primary brain ECs via extracellular ATP and mediated by P2-class purinergic receptors. *(A)* Extracellular ATP rescues 16p11.2-deficient network formation ability. *Top left,* experimental timeline for treatment of 16p11.2-deficient ECs with extracellular ATP following cell isolation and during a 24-hour *in vitro* network formation assay. *Top right,* representative images at the 8h post-seeding time point of WT and 16p11.2-deficient untreated ECs and 16p11.2-deficient ECs treated with 100μM of extracellular ATP. *Bottom,* quantifications of network densities (total endothelial tube length) and network nodes (total number of branching hubs) with representative percent of WT panels. *(B)* Non selective P2 receptor antagonist (PPADs) prevents rescue of 16p11.2-deficient EC network formation via extracellular ATP. *Top,* representative images at the 8h post-seeding time point. *Bottom,* quantifications of network densities (total endothelial tube length) and network nodes (total number of branching hubs) with representative percent of WT panels. *(C)* Western blot quantification of relative level of Pannexin-1 protein in 16p11.2-deficient (n=6 mice) and WT (n=6 mice) primary brain ECs. *(D)* Administration of PPADs prevented rescue of 16p11.2-deficient EC angiogenic activity by intracellular delivery of ATP. *Left,* representative images of capillary-like networks at the 8h post-seeding time point. *Right,* quantifications of network densities (total endothelial tube length) and network nodes (total number of branching hubs). Dotted line represents 100 % of WT values in *A* and *B*. All data shown are from ECs isolated from P14 male mice, and are mean ± s.e.m in *A,B* and *D,* or mean with individual values in *C*. (n=4-7 animals per group) *P<0.05, **P<0.01, ***P<0.001 (two-way repeated measure ANOVA and Sidak's multicomparison *post hoc* test in *A,B* and *D*).

Activation of purinergic P2Y2 receptors restores the angiogenic function of 16p11.2-deficient endothelial cells.

When consulting our previously published RNAseq database (14), we could detect the expression of several purinergic receptors expressed in both WT and *16p11.2*$^{df/+}$ brain ECs at P14. Messenger RNAs (mRNAs) encoding P2-class receptors were found at high expression levels in both genotypes, including *P2rx1*, *P2rx4*, *P2rx7* and *P2ry14* (*SI Appendix,* Fig. S7*A*). The mRNA encoding P2Y2 (*P2ry2)*, a metabotropic receptor important for angiogenesis (40), was found at relatively low expression levels in WT mice, however its expression nearly doubled in 16p11.2-deficient brain ECs (Fig. 4*A*). A slight, albeit non-significant, increase in P2Y2 protein levels was seen in 16p11.2-deficient ECs (Fig. 4*B*). Considering this, we decided to engage P2Y2 to test its ability to modulate endothelial function in 16p11.2-deficient ECs. We proceeded to treat 16p11.2-deficient ECs with a selective P2Y2 agonist, Diquafosol tetrasodium (DQS), a compound with efficacy in treating Dry Eye Syndrome post-cataract surgery (41, 42) and clinically-approved in Japan and South Korea (Diquas®). Activation of P2Y2 receptors with 100μM of DQS rescued capillary network formation in *16p11.2*$^{df/+}$ ECs (Fig. 4*C*). These results suggest that P2Y2 receptor

activation may represent a strategy to maintain brain EC function in the 16p11.2 deletion ASD syndrome via metabolic rescue.

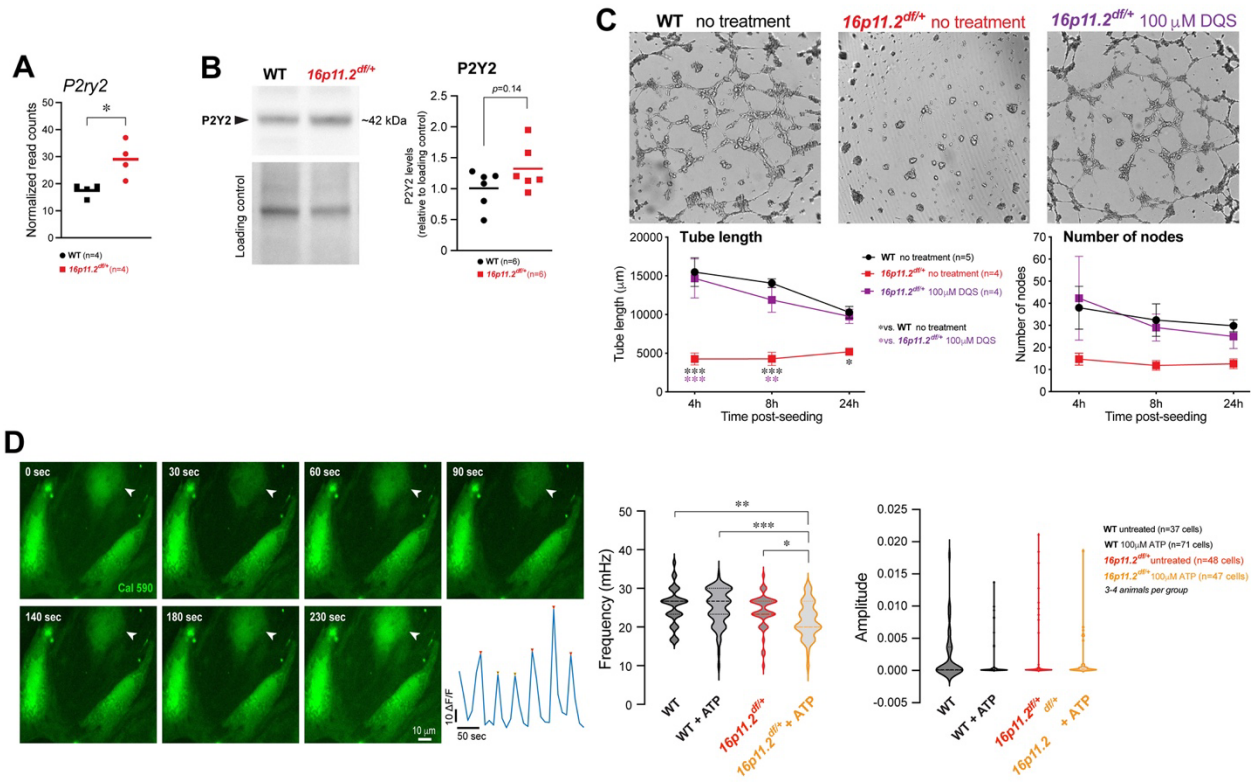

Fig 4. Mechanisms of purinergic receptor activation in functional rescue of 16p11.2-deficient mouse brain endothelial cells. *(A)* Expression level of genes encoding P2-class receptors in WT and 16p11.2-deficient ECs from our previously generated RNAseq database (Ouellette et al., 2020). A high expression level of the gene encoding P2Y2 receptors was identified in 16p11.2-deficient ECs. *(B)* Western blot quantification of relative P2Y2 protein levels in primary mouse brain ECs (n=6) isolated from 16p11.2-deficient and WT littermates. *(C)Top,* representative images at the 8h post-seeding time point of the *in vitro* network formation assay. *Bottom,* quantification of network densities (total endothelial tube length) and network nodes (total number of branching hubs). *(D) Left,* Example of time-lapse Ca^{2+} imaging in 16p11.2-deficient ECs and dF/F trace showing Ca^{2+} transients for the cell labeled with white arrowhead. *Right,* quantification of the frequency and amplitude of Ca^{2+} transients in 16p11.2 deficient and WT ECs. Note, larger decrease in the frequency of Ca^{2+} transients in 16p11.2-deficient, as compared to WT ECs. All data shown are from ECs isolated from P14 male mice. Data are mean with individual values in *A* and *B* or mean ± s.e.m. in *C*. Data in *D* are violin plots, center line indicating median, n=3-4 animals per group. *P<0.05, **P<0.01, ***P<0.001 (two-tailed Mann-Whitney test in *A*; two-way repeated measure ANOVA and Sidak's multicomparison *post hoc* test in *C;* one-way ANOVA and Tukey multicomparison *post hoc* test in *D*).

Ca^{2+}-mediated responses to ATP are altered in 16p11.2-deficient brain ECs.

Purinergic receptor signaling relies on G protein-coupled receptors resulting in IP_3-mediated Ca^{2+} release from internal stores (P2Y class) (43) as well as Ca^{2+} permeable ligand-gated ion channels

(P2X class) (44) to establish its function. To gain further insight into ATP-mediated cellular responses, we measured both steady-state intracellular Ca^{2+} levels and Ca^{2+} transients. To assess the steady-state Ca^{2+} level, we used Twitch-2B, a FRET-based ratiometric Ca^{2+} indicator. Our analysis revealed similar steady-state intracellular Ca^{2+} levels under baseline conditions, in non-treated WT and *16p11.2*$^{df/+}$ ECs (*SI Appendix,* Fig. S7*B* and *C*). Interestingly, while ATP supplementation significantly increased intracellular steady-state Ca^{2+} level in WT ECs as compared to WT ECs without ATP, no difference was observed between *16p11.2*$^{df/+}$ ECs and *16p11.2*$^{df/+}$ with ATP supplementation (*SI Appendix*, Fig. S7*C*).

We next loaded ECs derived from WT and *16p11.2*$^{df/+}$ mice with Cal590-AM organic Ca^{2+} indicator to record Ca^{2+} transients (Fig. 4*D*). No difference in the frequency and amplitude of Ca^{2+} transients were observed under baseline conditions, in non-treated WT and *16p11.2*$^{df/+}$ ECs (Fig. 4*D*). Interestingly, however, while supplementation with ATP decreased the frequency in both WT and *16p11.2*$^{df/+}$ ECs, the effect was larger in *16p11.2*$^{df/+}$ ECs (Fig. 4*D*), revealing statistically significant differences in WT + ATP vs. *16p11.2*$^{df/+}$ + ATP conditions (Fig. 4*D*). Altogether, our data suggest distinct Ca^{2+} signatures in WT and *16p11.2*$^{df/+}$ ECs in response to extracellular ATP supplementation.

Discussion

This study focuses on the impact of a 16p11.2 deletion on brain endothelial cell (ECs) metabolism and function. We find that endothelial dysfunction caused by 16p11.2 haplodeficiency is associated to a bioenergetic failure in ECs, with reduced intracellular ATP levels. When ATP is made bioavailable, intra- or extra-cellularly, it acts on P2-class purinergic receptors at the plasma membrane to reinstate endothelial function, distinctly affecting Ca^{2+} signaling.

We previously revealed a reduced mitochondrial mass in adult mouse brain 16p11.2-deficient ECs *in vivo* (15), a result replicated here *in vitro* using ECs isolated from 14-day old mice, thus reiterating the findings from prior work. This suggest that mitochondria parameters altered early in development might have an early impact on brain EC metabolism, however, we do not have causal evidence for this link. No change in mitochondrial fusion or fission markers was identified in P14 16p11.2-deficient ECs. Thus, reduced mitochondrial density in P14 16p11.2-deficient ECs cannot be attributed to altered mitochondrial dynamics. Moreover, PGC-1α, a master regulator of mitochondrial biogenesis, was also unchanged. Of note, we were not able to detect the truncated variant NT- PGC-1α in both WT and 16p11.2-deficient brain ECs at P14 (data not shown), yet this splicing isoform was selectively absent from 16p11.2-deficient brain ECs at P50 (15). This suggests that other mechanisms might be at play to downregulate mitochondrial biogenesis postnatally and/or that NT-PGC-1α is not produced by WT brain ECs at P14. While the precise connection between 16p11.2 haploinsufficiency and reduced mitochondrial density is not known at this time, mitochondrial alterations represent a valid candidate to explain functional disturbances in a wide range of physiological systems, especially as these organelles are essential for energy-demanding cellular responses.

Our investigation into 16p11.2-deficient ECs metabolism revealed a significant reduction in intracellular metabolites. Although metabolomics studies have been performed in the context of ASD, namely using blood, serum, urine or brain tissues (45-47), this work provides the first metabolomics approach focused on brain ECs in ASD, unraveling the cell-specific endothelial metabolic changes that contribute to 16p11.2 deletion-related dysfunctions. Metabolite profiling of 16p11.2-deficient ECs helped us identify a reduction of high-energy molecules such as ATP, reduced adenylate energy charge, and reduced ATP-to-ADP ratio, as well as reduced energy

donors (*i.e.* UDP-glucose/UDP-galactose), all indicative of a lack of available energy. The reduced intracellular ATP could be in part attributed to the reduced mitochondrial density; however, despite having less mitochondria, ATP production, measured by the Seahorse assay, was not different between 16p11.2-deficient and WT ECs. Since cumulative mitochondria output per cell was measured, we can hypothesize that each mitochondrion within 16p11.2-deficient ECs may be producing more energy to compensate for their reduced numbers. Yet, considering that intracellular ATP was decreased in 16p11.2-deficient ECs and ATP production was unchanged, 16p11.2-deficient ECs may require more energy to function properly. This is in line with our recent findings that adult *16p11.2*$^{df/+}$ mice display an elevated brain glucose uptake compared to WT mice (15).

Despite the bioenergetic failure measured in 16p11.2-deficient brain ECs, these cells were healthy at baseline as indicated by unchanged GSH:GSSG ratio, in agreement with our previous observations of normal migration, survival and proliferation for 16p11.2-deficient brain ECs at P14 (14). Impact of lack of bioavailable energy was revealed when these cells were challenged, or, in other words, when a functional task is required (*i.e.* angiogenesis, vascular reactivity) (14). It has been recently shown that mitochondrial ATP is essential for endothelial control of vascular tone. When ATP production is blocked *in vivo* or *ex vivo*, ECs do not respond to vasodilator acetylcholine in both cerebral and mesenteric arteries (33). This is in line with our prior work demonstrating that middle cerebral and mesenteric arteries isolated from 16p11.2-deficient mice respond poorly to acetylcholine (14). Thus, considering decreased intracellular ATP, this suggests that 16p11.2 deletion-associated bioenergetic failure is a culprit in endothelial dysfunction. While the reduced mitochondrial density was slight, albeit significant, in 16p11.2-deficent ECs, recent evidence has shown that even a small dose of one mitochondrion, following mitochondrial

transplantation, can significantly increase ATP levels in cells (48), highlighting the possible impact of the minor changes in mitochondrial density on intracellular ATP levels.

While output of individual mitochondria in 16p11.2-deficient ECs was not different from WT ECs, intracellular metabolites related to mitochondrial function were altered. Most of the reduced metabolites in 16p11.2-deficient ECs are dependent on or involved in ATP metabolism. For instance, glutathione reduced (GSH) and its precursor (γ-glu-cys) are synthesized in steps requiring ATP hydrolyzation (49). Creatine is required for ATP production and the brain can use creatine for additional energy production when demand is elevated (50). Therefore, reduced ATP stores may lead 16p11.2-deficient ECs to utilize creatine for energy production (ATP) and so decreasing availability of creatine. Alanine/sarcosine are indirectly involved in energy metabolism, formed from the hydrolysis of creatine, suggesting a downstream impact of reduced ATP in 16p11.2-deficient ECs (51). In addition, NAD^+ and FAD play a role in mitochondrial function and takes part in oxidative phosphorylation resulting in the generation of ATP. It is thus possible that the additional energy requirements to maintain 16p11.2-deficient ECs function is consuming available metabolites.

As ATP is required for EC function, we raised the possibility of rescuing 16p11.2-deficient EC associated phenotypes by increasing ATP bioavailability intra- or extra-cellularly. Strikingly, both intra- and extra-cellular delivery of ATP rescued 16p11.2-deficient EC function, suggesting that lack of ATP might be causing deficits. However, extracellular ATP has emerged as a signaling regulator in several cellular processes including proliferation, angiogenesis, and vessel homeostasis. Brain ECs release ATP in response to various stimuli, triggering signaling events via ligand gated (P2X) and/or G-protein-coupled (P2Y) purinergic receptors (52, 53). In line with ATP regulating key vascular features via activation of purinergic receptors, we provide novel evidence

that ATP-mediated rescue of 16p11.2-related dysfunction relies on P2-class receptors expressed by ECs. Indeed, non-selective pharmacological blockade of P2 receptors abolished the extracellular ATP-mediated rescue. The fact that 16p11.2-deficient EC function was also reinstated following intracellular ATP delivery brings into question whether this effect was mediated in similar manner as extracellular ATP. It has recently been established that ATP can exit brain ECs through pannexin-1 channels to activate P2 receptors on adjacent ECs (39). Here, we show that inhibition of P2-class receptors with PPADs prior to intracellular delivery of ATP prevented rescue of 16p11.2-deficient EC function. These findings demonstrate that ATP acts on membrane-bound P2 receptors in both treatment conditions (extra- and intra-cellular ATP), and pannexin-1 channel activity may be involved in this response.

We specifically highlight the involvement of P2Y2 receptor activation as a mechanism to rescue 16p11.2-related endothelial dysfunction. P2Y2 receptors have been associated with vascular function (40). Mice with endothelial P2Y2-knockout displayed dysregulated vasodilatory responses during increased blood flow (54). Furthermore, P2Y2 receptors have a prominent role in angiogenesis, as their activation promotes endothelial sprouting and vascular tube formation. Inhibition of P2Y2 with a selective antagonist reduced tube length in human umbilical vein endothelial cells (HUVECs) (40). These findings emphasize that lack of P2Y2 activation in 16p11.2-deficient ECs due to decreased ATP availability might be sufficient to drive functional changes.

The purinergic system has been linked to ASD; however, anti-purinergic therapies improved autism-like behavior (47, 55). In certain instances, elevated extracellular ATP in the blood of ASD patients have been associated with metabolic changes and suggested to activate the cellular danger response (CDR), leading to detrimental stress responses (*i.e.* changes in

mitochondrial function, oxidative stress and innate immune activation) (47). As we have demonstrated that ATP exits the cells to act on adjacent P2 receptors, the CDR could explain the lack of rescue following delivery of a higher dose of intracellular ATP (*i.e.* 5mM ATP-LNPs). As such, higher extracellular ATP may negatively impact EC function. These findings show that an ATP delivery threshold should be taken into consideration when designing purinergic signaling therapies. Furthermore, we confirmed that functional rescue was specifically conferred by ATP and not by adenosine, a by-product of ATP hydrolysis, acting on P1-class receptors. Indeed, administration of adenosine to 16p11.2-deficient cultured ECs failed to promote angiogenic ability of these cells. Of note, adenosine was recently associated with improved social novelty behaviors in adult female *16p11.2*$^{df/+}$ mice (56). It thus possible that the beneficial effects of adenosine in female mice behavior are independent of vascular features.

P2-class purinergic receptor activation via ATP can modulate steady-state intracellular Ca^{2+} levels as well as Ca^{2+} transients. Interestingly, we observed marked differences in Ca^{2+} responses in 16p11.2-deficient ECs, as compared to WT ECs, in response to extracellular ATP. In contrast to WT ECs, supplementation with ATP did not affect the steady-state intracellular Ca^{2+} level in 16p11.2-deficient ECs. Furthermore, the decrease in frequency of Ca^{2+} transients was more pronounced in 16p11.2-deficient ECs, as compared to WT ECs. While it is yet unclear how these distinct Ca^{2+} responses to ATP may underlie the rescue effects observed in 16p11.2-deficient ECs, our data hint on Ca^{2+} as a possible signaling molecule mechanistically linking purinergic receptor activation to intracellular pathways leading to restoration of angiogenic ability of 16p11.2-deficient ECs. Notably, Pannexin-1 channels are activated by increases in intracellular calcium leading to the release of ATP from the cell and so ATP acting on P2 receptors (39). Here, our

findings emphasize the possible role of Ca^{2+} signaling and pannexin-1 in mediating the intracellular ATP rescue response in 16p11.2-deficient ECs.

ATP being at the epicenter of EC dysfunction in the 16p11.2 deletion syndrome brings into question whether other factors can modulate ATP metabolism/activity. Magnesium (Mg^{2+}) is a known crucial cofactor of ATP which regulates enzymatic activity and is essential for all ATPase reactions (57). In ASD, there is only limited evidence that Mg^{2+} supplements in children can improve hyperactivity and attention (58). Further investigation is thus required to test the possible involvement of Mg^{2+} in 16p11.2 deletion-induced brain endothelial dysfunction.

In this study, we emphasize the importance of studying ASD with a holistic lens, as these disorders remain predominantly considered a result of neuronal malfunction. The fact we reveal new disease hallmarks specific to endothelial metabolism should help broaden therapeutic strategies for ASD. In the future, identifying the downstream consequences of targeting endothelial metabolism on other neural cells will provide a full picture of the influence of cerebrovascular health in ASD.

MATERIALS AND METHODS

Animals. All animal procedures were approved by the University of Ottawa Animal Care Committee and conducted in accordance with guidelines of the Canadian Council on Animal Care. *Mouse husbandry.* All mice were bred in house and housed maximum five per cage with free access to water and food. Males *16p11.2*$^{df/+}$ (Jackson laboratory, stock #013128; mixed B6/129 background) were crossed with WT females of the same background (Jackson laboratory, stock #101043) to obtain hemizygous *16p11.2*$^{df/+}$ offspring as well as WT littermates. As recommended by Jackson Laboratory to improve *16p11.2*$^{df/+}$ pup survival, breeding cages were supplemented with breeding chow (#2019, Envigo Teklad) and DietGel (#76A, ClearH_2O) up to weaning age. All experiments were conducted using P14 mice.

Genotyping. 16p11.2$^{df/+}$ mice and WT littermates were genotyped using the following primers: 5′-CCTCATGGACTAATTATGGAC-3′ (forward) and 5′-CCAGTTTCACTAATGACACA-3′ (reverse), with a PCR product of 2.2 kb for *16p11.2*$^{df/+}$ mice (59).

Primary mouse brain EC isolation. All mice were euthanized by cervical dislocation. The cerebral cortex was dissected in cold HBSS without calcium and magnesium using autoclaved tools submerged in 100% ethanol for 30 minutes prior dissections. The cortex was minced in 2-3 mm pieces and dissociated in Neural Tissue Dissociation Kit P compounds (Miltenyi Biotec, 130-092-628) to obtain a cell suspension. Cell isolation procedures were completed according to the manufacturer's instructions. The cell suspension was incubated with CD31-coated magnetic microbeads (Miltenyi Biotec, 130-097-418) and placed on a magnetic MACs separator to isolate ECs. ECs isolated from one mouse were seeded in a plate coated with attachment factor protein 1X (ThermoFisher Scientific, S006100). For a pure EC population, ECs were cultured in an EC specific medium (Lonza, CC-3202) which was replaced 48 hours post-seeding and every 48 hours

until appropriate level of confluency was reached for subsequent processing (40-60% for immunocytochemistry; 90-100% for metabolomics, protein extraction, tube formation and 80% for calcium experiments).

Immunocytochemistry. Primary ECs were cultured until 40–60% confluence (3 days post-isolation) on glass coverslip for microscopy analysis. Before staining, ECs were washed twice in pre-warmed PBS and fixed for 10 min in cold 4% PFA. Fixed cells were permeabilized in a blocking solution containing 10% donkey serum, 0.1% PBT and 0.5% cold water fish skin gelatin. The primary antibodies anti-CD31 (1:200, BD Pharmingen) and anti-TOM20 (1:2000, Proteintech) were diluted in blocking solution and incubated for 2 hours at room temperature. Cells were then rinsed with 0.2% PBT. AlexaFluor species-specific secondary antibodies were diluted in blocking solution at 1:300 and incubated with cells for 60 minutes. Cells were washed with 0.2% PBT then 0.1 M PB. Glass coverslips, with stained ECs, were mounted on slides using Fluoromount G and imaged (40x objective) with a Zeiss Axio Imager M2 microscope equipped with a digital camera and ApoTome.2 module. Images consisted of 4uM thick z-stacks (0.250uM/slice) in which 5-10 ECs were visible per image, a total of 10 images were taken per animal. To quantify TOM20 and CD31 immunostaining, 40X ApoTome images (16-bit Tiff files) were processed using custom scripts written in the Python programming language. Mitochondria were detected using scale-space maxima of the Laplacian of Gaussian (LoG) operator (60). Specifically, the images were first convolved with four LoG filters with standard deviations of 1.0, 1.33, 1.66, and 2.0 pixels. Peaks having a value larger than 0.03 on the scale-space representation were considered to represent mitochondria. ECs nuclei were also automatically identified to avoid mitochondria detection inside the nuclei. Pixels having an intensity smaller than 10 on nuclei (DAPI) images were considered to belong to the background. Connected components with less

than 75 pixels were removed, and remaining holes were filled. The obtained connected components were associated with nuclei of the ECs. Mitochondria detected inside the identified nuclei were then removed by masking. ECs within each image were manually outlined and mitochondria density per cell was calculated as the number of mitochondria divided by cell area. The values were then averaged among the outlined cells. To calculate fragmentation, a mitochondria neighborhood graph was created to identify their spatial relationship. To do so, the highest affinity paths between all pairs of mitochondria having a distance smaller than 15 pixels between them were identified. The affinity of a path consists of the sum of the image intensities of a connected sequence of pixels between two mitochondria. The lowest intensity value along the highest affinity path between two mitochondria defined their affinity. Intuitively, if there is a connected sequence of pixels between two mitochondria such that no pixel in the sequence has a low-intensity value, the two mitochondria likely belong to a single, non-fragmented, structure. A graph having mitochondria as nodes was constructed, two nodes were connected if the affinity between the respective mitochondria was larger than 0.25 times the average intensity of the two mitochondria. The fragmentation was then calculated as the number of connected components in the graph divided by the number of mitochondria.

Western blots.

Protein extraction. For endothelial proteins, primary brain endothelial cells were isolated and cultured as previously described (15, 61). To lyse cells, 50µL of RIPA buffer (NaCl 150mM, Sodium Deoxycholate 0.5%, SDS 1%, NP-40 1% in Tris 50mM pH 8.0) with protease and phosphatase inhibitors was added to each well and left on ice for 30 min. The cells were scraped off the culture dish and transferred to a 1.5mL tube then sonicated for 1 minute on ice. Tubes were stored at -20 ^{o}C overnight and then centrifuged at 13,000rpm for 10 min. The protein concentration

of the collected supernatant was quantified using Pierce BCA Protein assay (kit #23227, ThermoScientific, Illinois, USA).

Protein extraction for AMPK samples. For endothelial proteins, primary brain ECs were isolated and cultured as previously described. To lyse cells, 100uL of AMPK extraction buffer (50 mM Tris-HCL, pH 7.5, 1 mM EDTA, 1 mM EGTA, 0,27M sucrose, 1% Triton X-100 and 10mM DTT with protease and phosphatase inhibitors) was added to each well. The bottom of the well was scraped for one minute. The supernatant was transferred to 1.5mL tubes and then sonicated, incubated on ice for 15 minutes and centrifuged at 13 000 rpm for 15 minutes at 4 °C to remove cell debris. The protein concentration of the collected supernatant was quantified using Pierce BCA Protein assay (kit #23227, ThermoScientific, Illinois, USA).

Immunoblotting. Twelve (12) µg of protein (MFN1, MFN2, OPA1 and DRP1) or forty (40) µg of protein (AMPK and phospho-AMPK) were loaded into the wells of SDS-acrylamide gels (GX Stain-free FastCast 12% Biorad gels, Bio-Rad, ON, CAN, #1610184) and separated by a constant current of 100 V for 120 min in running buffer (SDS 35mM, Tris 250mM, Glycine 1865mM). After UV activation of the gels, the proteins were then transferred to a nitrocellulose membrane in ice-cold transfer buffer (Tris 48mM, Glycine 38mM, methanol 20% v/v) for 30 min at 100 V. After the transfer, the nitrocellulose membranes and gels were imaged to quantify the total protein transferred. The membranes were then blocked with 5% skim milk in 1M PBS (or 5% BSA in TBST for AMPK samples) for 1 h at room temperature and incubated with primary antibodies raised against either AMPK (1:1000, Cell Signaling, 2532), phospho-AMPK (1:800, Cell Signaling, 2535), DRP1 (1:2000, BD Biosciences, 611113), MFN1 (Abcam, ab126575, 1:1000), MFN2 (1:1000, Abcam, ab56889), OPA1 (1:2000, Abcam, ab42364), PGC-1a (1:1500, Millipore,

ST1202) in TBST (Tris 50mM, NaCl 150mM, Tween 20 1% v/v) overnight at 4°C. The membranes were then washed with TBST (3 x 10 min) and incubated at room temperature for 1 h with the secondary antibody (1/10,000, Fisher Scientific, #PR-W4011), also diluted in TBST. After a final wash (TBST, 3 x 10 min), the proteins were detected by enhanced chemiluminescence (ECL; 1⁄4, Fisher Scientific, #34579) and imaged with the Odyssey Imaging system. The samples were normalized to the total protein content (AMPK) and to a loading control (OPA1, DRP1, MFN1&2, PGC1a) and calculated as relative to group average.

Immunoblotting for Pannexin-1. Thirty (30) µg protein was separated on a 10% SDS-PAGE gel according to manufacturer's protocol (TGX Stain-Free FastCast, BioRad) and transferred to polyvinylidene difluoride (PVDF) membranes. Membranes were processed according to manufacturer's protocol (TGX Stain-Free FastCast, BioRad) and incubated overnight at 4^{o}C with primary antibody anti-Pannexin-1 (1:500, Cell Signaling, Cat# 91137) in Tris-buffered saline (Tris 50 mM and NaCl 150 mM, pH 8.0) containing 0.05% Tween (TBST) in 1% non-fat dry milk. The membranes were washed and incubated with horseradish peroxidase–conjugated secondary antibody: Anti-Rabbit HRP or Anti-mouse HRP (Promega or Thermo Fisher Scientific) 1:2000 in TBST containing 5% non-fat dry milk. Immunoreactive proteins were visualized by chemiluminescent solution (SuperSignal West Dura; Pierce Biotechnology). Densitometric, semiquantitative analysis of Western blots was performed using Image Lab software and normalized to total protein.

Targeted metabolomics. Primary ECs were split once and cultured until 90-100% confluency was reached. ECs from 3 mice were pooled to have at minimum 1.5million cells per sample (n). Prior sample collection, cells were washed 3 times with 1mL of ammonium formate per well of a 6-well

plate. For sample collection, 80uL of ice cold methanol:water (1:1) was added to each well and cells were collected using a cell scraper. The cell slurry was transferred to a pre-chilled 2 mL tube containing 6 washed ceramic beads (1.4 mm) and kept at -80 °C until the day of metabolite extraction.

On the day of extraction, samples were vortexed 10s, followed by adding 220 µL of acetonitrile and vortexed a second time for 10s. Cell lysis was done by bead beating for 60 s at 2000 rpm (bead beating was done twice). Samples were then incubated with a 2:1 dichloromethane:water solution on ice for 10 minutes. The polar and non-polar phases were separated by centrifugation at 4000g for 10 minutes at 1°C. The upper polar phase was dried using a refrigerated CentriVap Vacuum Concentrator at -4°C (LabConco Corporation, Kansas City, MO). Samples were resuspended in water and run on an Agilent 6470A tandem quadruple mass spectrometer equipped with a 1290 Infinity II ultra-high performance LC (Agilent Technologies) utilizing the Metabolomics Dynamic MRM Database and Method (Agilent), which uses an ion-pairing reverse phase chromatography. This method was further optimized for phosphate-containing metabolites with the addition of 5 µM InfinityLab deactivator (Agilent) to mobile phases A and B, which requires decreasing the backflush acetonitrile to 90%. Multiple reaction monitoring (MRM) transitions were optimized using authentic standards and quality control samples. Metabolites were quantified by integrating the area under the curve of each compound using external standard calibration curves with Mass Hunter Quant (Agilent). No corrections for ion suppression or enhancement were performed, as such, uncorrected metabolite concentrations are presented. Multivariate statistical modelling was performed on log-transformed, mean-centered and pareto-scaled data using MetaboAnalyst 5.0 (www.metaboanalyst.ca). Partial least squares discriminant analysis (PLS-DA) was performed on the identified metabolites. The variables highly contributing to the group separation were selected

with a variable importance in projection (VIP)≥1. The clustering analysis and pathway analysis were performed as well using MetaboAnalyst 5.0. Statistical analysis was performed by one-way analysis of variance (ANOVA) followed by Tukey's post hoc test. P values <0.05 were considered statistically significant. Pairwise comparisons were completed to eliminate batch effect. Data for genotype comparison is presented as box and whisker plots and statistical analysis was performed by unpaired t test. The box plot analysis was performed using Prism 10 (GraphPad Software, La Jolla, CA, USA).

Seahorse Cell Mito Stress test assay. Agilent Seahorse Cell Mito Stress test XF96 kit was prepared according to the manufacturer's instructions. 24 hours before the start of the assay, ECs were harvested and seeded at a density of 10,000 cells per well in a Seahorse XFe96 well plate coated with 1X attachment factor. The sensor cartridge was submerged in XFe calibration buffer overnight in a non-CO_2 incubator at 37°C. On the day of assay, Seahorse XF Base Medium was supplemented with 1mM pyruvate, 10mM glucose and 2mM glutamine. Chemical compounds were reconstituted using assay medium. Cells were washed twice with assay medium and incubated for 1 hour in a non-CO_2 incubator at 37°C. Reconstituted compounds were loaded onto a sensor cartridge at the following final concentrations: Oligomycin (port A, 1.0μM), FCCP (port B, 1.0μM) and Rotenone/antimycin A (port C, 0.5μM). Sensor cartridge with loaded compounds were placed in a pre-heated Seahorse XFe96 analyzer for calibration. Following the 1 hour incubation and sensor cartridge calibration, the cells are placed in the Seahorse XFe96 analyzer for subsequent mitochondrial function assessment. Once assay was completed, cells were fixed with 4% PFA, washed twice with 1X PBS and stained with DAPI for cell counting. Cells within each well was counted using a EVOS FL Auto imaging system for normalization of parameters. Assay was completed and analyzed with the Agilent Seahorse Wave Software.

ATP-LNPs.

Materials. Adenosine triphosphate (ATP) (150266) was purchased from MP Biomedicals (Solon, OH). Cholesterol (8667) was procured from Sigma-Aldrich (St. Louis, MO). 1,2-Dimyristoyl-rac–glycero-3-methoxypolyethylene glycol-2000 (PEG-DMG) (8801518) and 1, 2-distearoyl-sn-glycero-3-phosphocholine (DSPC) (850365P) were obtained from Avanti Polar Lipids (Alabaster, AL). The ionizable cationic lipidoid, 1,1‘-((2-(4-(2-((2-(bis (2 hydroxy dodecyl) amino) ethyl) (2hydroxydodecyl) amino) ethyl) piperazin1yl) ethyl) azanediyl) bis(dodecan-2-ol) (C12-200) was obtained as a generous gift from Dr. Muthiah Manoharan, Alnylam Pharmaceuticals (Cambridge, MA). Alexa Fluor 647-labeled ATP (AF647-ATP) (A22362) was obtained from ThermoFisher Scientific (Waltham, MA). Phosphate-buffered saline (PBS) was procured from Hyclone Laboratories (Logan, UT). All reagents were used as obtained unless stated otherwise.

Preparation of ATP-loaded LNPs (ATP-LNPs). Lipid nanoparticles (LNPs) were prepared using previously reported methods (34, 62). Briefly, C12-200 (ionizable cationic lipid), cholesterol, PEG-DMG, and DSPC were dissolved in ethanol at a molar ratio of 50/10/38.5/1.5. The representative scheme for the formulation of ATP-LNPs is depicted in **Table 1**. The aqueous phase consisted of an ATP solution at 33.73 mg/mL prepared in 1*x* PBS, pH 7.4. The ethanolic phase was gradually added into the aqueous phase under continuous vortexing for 30 seconds using a Fisher benchtop vortexer knob at position ‘7’. The resulting ATP-LNP formulations were prepared with a final ATP concentration of 40 mM. Alexa fluor 647-labeled ATP-LNPs were prepared by volumetrically spiking unlabeled ATP with Alexa fluor 647-labeled ATP at a ratio of 1:1000 (Alexa fluor 647-labeled ATP: unlabeled ATP).

Table 1. Formulation scheme of ATP-LNPs (34)

Component	w/w% in LNP mixture	Stock concentration (mg/mL)	Volume of the stock solution (µL)
Ethanolic phase			
C12-200	50	1	12.5
Cholesterol	38.5	1	3.1
PEG-DMG	1.5	0.1	13.6
DSPC	10	0.1	16.9
Ethanol	-	-	78.9
Total ethanolic phase volume			125
Aqueous phase			
ATP	40 mM	33.73	300.7
1*x* PBS	-	-	74.3
Total aqueous phase volume			375
Final volume of LNPs prepared (µL)			500

Dynamic Light Scattering. The particle characteristics and colloidal stability of ATP-LNPs were studied by measuring their average particle diameters and dispersity indices using dynamic light scattering on a Malvern Zetasizer Pro (Malvern Panalytical Inc., Westborough, PA). Particle sizes and dispersity indices of ATP-LNPs were measured over 14 days with intermittent storage at 2-8ºC. For dynamic light scattering measurements, LNPs were diluted to a final ATP concentration of 40 mM in 1*x* PBS pH 7.4. The data are depicted as the mean value along with the standard deviation (SD) derived from triplicate measurements.

Transmission Electron Microscopy. LNPs were prepared for negative stain electron microscopy by depositing a 3 µL volume onto a freshly glow-discharged continuous carbon-coated copper grid and subsequently treating it with a 1% uranyl acetate solution for staining purposes. Grids were introduced into a Thermofisher TF20 electron microscope, outfitted with a field emission gun, and

imaged using a TVIPS XF416 CMOS camera to visualize LNP dimensions. The electron microscope was operated at 200 kV and the contrast was enhanced using a 40 µm objective aperture. Electron micrographs were captured at a nominal 19,000*x* magnification using a post-column magnification of 1.3*x*, corresponding to a calibrated pixel size of 5.6 Ångstroms at the sample level. The images were acquired utilizing TVIPS Emplified software in movie mode to correct for drift.

ATP-LNPs uptake. Primary brain ECs were cultured until 80% confluency on a cover-glass and treated with AF647-labeled ATP-LNPs or blank-LNPs following cell isolation. Primary ECs were washed twice with pre-warmed PBS and stained with Hoechst (Invitrogen, C10339 G) for 5 minutes. The stain was removed and cells were washed twice with PBS. Cover glasses were mounted on slides and imaged with a Zeiss Axio Imager M2 microscope equipped with a digital camera and ApoTome.2 module.

In vitro treatment protocols.

Intracellular ATP supplementation (ATP-LNPs). Primary ECs were treated with 1mM or 5mM of ATP-LNPs or blank-LNPs following cell isolation and once cells reached 90-100% confluency, they underwent an *in vitro* network-formation assay. ATP-LNPs were directly added to EC specific culture media (Lonza, CC-3202) and was replaced every 48hrs until required confluency was reached.

Extracellular ATP supplementation. Primary ECs were treated with 1µM, 10µM or 100µM of ATP (Sigma Aldrich, A7699) following cell isolation and once cells reached 90-100% confluency, underwent an *in vitro* network-formation assay. ATP was directly added to EC specific culture media (Lonza, CC-3202) and was replaced every 48hrs until required confluency was reached.

Adenosine supplementation. Primary ECs were treated with 100μM of adenosine (Sigma Aldrich, A4036) or NH_4OH (vehicle, Sigma Aldrich, 09859) following cell isolation, once cells reached 90-100% confluency, underwent an *in vitro* network-formation assay. Adenosine was prepared according to the manufacturers. Briefly, adenosine was dissolved in 1M NH_4OH using heat (70°C) for 5 mins and maintained at room temperature protected from light. Adenosine was directly added to EC specific culture media (Lonza, CC-3202) and was replaced every 48hrs until required confluency was reached.

Non-selective P2 antagonist treatment. Primary ECs were treated with 10μM, 50μM or 100μM of pyridoxalphosphate-6-azophenyl-2',4'-disulfonic acid (PPADs) tetrasodium salt (Tocris, 0625) for 10 minutes prior to addition of 100μM of ATP and replaced every 48hours until cells reached 90-100% confluency. Once confluency was reached, ECs underwent an *in vitro* network-formation assay.

Non-selective P2 antagonist (PPADs) and ATP-LNP treatment. Primary ECs were treated with 50μM of PPADs for 10 minutes prior administration of 1mM of ATP-LNPs. Cell cyulture media was replaced every 48 hours until cells reached 90-100% confluency. Once confluency was reached, ECs underwent an *in vitro* network-formation assay.

P2Y2 agonist (diquafosol tetrasodium, DQS) treatment. Primary ECs were treated with 100μM of DQS (Sigma Aldrich, SML3058) following cell isolation, throughout culturing and during the tube formation assay. DQS was directly added to EC specific culture media (Lonza, CC-3202) and was replaced every 48hrs until required confluency was reached (90-100%).

In vitro network-formation assay. EC network-formation assays were performed using growth-factor-reduced Matrigel (BD Bioscience, cat. no. C354230). Growth-factor-reduced condition includes: EGF < 0.5 ng ml^{-1}, PDGF < 5 pg ml^{-1}, IGF1 = 5 ng ml^{-1} and TGF-β = 1.7 ng ml^{-1}. In brief, each well of a 96-well plate was coated with 50 µl of Matrigel and incubated at 37 °C for 30 min to promote polymerization. ECs were collected with TryplE (Gibco, 12604013) and counted. A total of 2×10^4 cells were seeded in each well with 150 µl EC specific media (Lonza, CC-3202) or EC media supplemented with ATP-LNPs, ATP, Adenosine, ATP+PPADs, ATP-LNPs+ PPADs or DQS. TIFF images of capillary-like networks were captured using a Zeiss Axio Image M2 microscope equipped with a digital camera at 4, 8, and 24h post-seeding (mouse ECs). Images were processed using the Angiogenesis function of ImageJ (63).

Steady-state cytosolic Ca^{2+} level. To assess the cytosolic levels of intracellular Ca^{2+} in endothelial cells we used a ratiometric FRET-based Ca^{2+} indicator Twitch-2B, driven by the CMV promoter. Primary brain ECs were isolated and seeded in a 12-well plate on 12mm glass coverslips and maintained in an EC specific medium (Lonza, CC-3202) with or without 100uM of ATP at 37 °C and 5% CO_2 atmosphere, replacing the growth medium every 48 hours. Transfection with CMV-Twitch-2B was performed when cell cultures were at ~80% confluency. On the day of transfection, Lipofectamine/DNA complexes were prepared in 100ul of opti-MEM (Invitrogen) for each well of 12-well plates by mixing 1.5 µg of plasmid with 3 µl of Lipofectamine LTX and 1ul of Plus transfection reagent according to manufacturer's instructions (Invitrogen) and added dropwise to each well (100 µl/well). Cells were incubated at 37 °C in a CO_2 incubator for 24 h, followed by fixation in 4% PFA. The images were acquired using the CBIA Core Facility confocal microscope (LSM880 AxioObserver Z1; Zeiss) at the University of Ottawa with a 20x air objective (Plan-Apochromat 20x/NA 0.8; Zeiss). Images were acquired using a 458 nm laser to excite CFP, and

the fluorescence signals were collected at the CFP and YFP emission wavelengths (461-519 and 522-578 nm bandwidth, respectively). The fluorescence signals from the regions of interest (ROIs) were calculated as a ratio of YFP to CFP emissions.

Analysis of Ca^{2+} transients. To assess spontaneous Ca^{2+} activity in primary mouse cerebral cortex endothelial cells we used Cal-590™ AM, a membrane-permeable organic dye that allows detection of intracellular Ca^{2+} fluctuation (64). ECs were cultured in an EC specific medium (Lonza, CC-3202) with or without 100uM of ATP at 37 °C and 5% CO_2. EC medium was replaced every second day up until 80% confluence was reached (~6 days). On the day of experiment once ECs were 80% confluent, cells were treated with 2 μM of Cal-590™ AM (AAT Bioquest, CA, USA) and were further incubated for about 1 hour in a humidified incubator at 37 °C and 5% CO_2. After incubation, the culture dish was transferred on the stage of fluorescent microscope (DeltaVision Elite Olympus XI-71) of the CBIA Core Facility at the University of Ottawa. The microscope was equipped with an incubation chamber allowing to maintain the temperature at 37°C and CO_2 at 5%. Images were acquired every 10 s for 5 min using a 40x oil objective, (UPLFLN 40x/NA 1.3; Olympus) and the recorded videos were analyzed using a custom-written script (65) in MATLAB (MathWorks). Briefly, regions of interests (ROI)s were traced around the entire cell and the fluorescence intensity in each ROI and for each time point was extracted. Ca^{2+} activity was calculated as relative changes in the percentage of $\Delta F/F = (F-F_{back})/ F_{back}$, where F is the Cal-590™ AM intensity in the ROI and F_{back} is the background signal taken in a "cell-free" region of the imaging field. Analysis of spontaneous Ca^{2+} activity was performed using a multiple threshold algorithm (66, 67). Briefly, mean standard deviation (SD) of Ca^{2+} trace for each cell was first calculated, and all peaks with an amplitude greater than 1.5 times the SD were measured. These peaks were then removed from the Ca^{2+} traces, and the mean SD of Ca^{2+} trace was re-calculated

to depict events greater than 1.5 times the new SD. This procedure allowed us to depict all Ca^{2+} events regardless of their amplitudes. Ca^{2+} frequency was calculated as the number of peaks over video duration**.** The statistical analysis was performed in a total number of n videos collected from n wells for n cells in total in Cal-590 treated cells for 4 distinct conditions.

Statistical analyses. No statistical methods were used to predetermine sample sizes. Sample sizes were similar to those reported in previous publications (14, 15). All sample numbers in this study are in line with well-accepted standards from the literature for each method. All data presented in this work were obtained from experimental replicates (e.g. multiple animal cohorts from different litters, at least three experimental repeats for each assay). All attempts of replication were successful. All data analyses were conducted blinded to the genotype and experimental condition. Groups were reassembled following completion of the data analysis according to genotype and experimental condition. Randomization of individual samples was performed by numbering. Statistical tests were performed using GraphPad Prism 10.0 software and MetaboAnalyst 5.0 (for metabolomics). Data distribution was assumed to be normal, but this was not formally tested. A Mann-Whitney *U*-test or t test (appropriate for small sample sizes) was used for two-group comparisons between WT and 16p11.2-deficient ECs isolated from mice for metrics including mitochondrial density and fragmentation, mitochondrial function, Western blot quantifications and metabolite abundance. A two-way ANOVA (e.g. 'genotype x condition') and Sidak's multicomparisons *post-hoc* test was used for *in vitro* network formation assay. A one-way ANOVA and Tukey's multicomparison *post-hoc* test was used for steady state Ca^{2+} readouts and Ca^{2+} transients. $P<0.05$ was considered significant. Statistical details of each experiment can be found in figure legends.

REFERENCES

1. M. E. Watts, R. Pocock, C. Claudianos, Brain Energy and Oxygen Metabolism: Emerging Role in Normal Function and Disease. *Front Mol Neurosci* **11**, 216 (2018).
2. P. Carmeliet, R. K. Jain, Molecular mechanisms and clinical applications of angiogenesis. *Nat Review* **473**, 298-307 (2011).
3. M. Belanger, I. Allaman, P. J. Magistretti, Brain energy metabolism: focus on astrocyte-neuron metabolic cooperation. *Cell Metab* **14**, 724-738 (2011).
4. B. J. Andreone, B. Lacoste, C. Gu, Neuronal and vascular interactions. *Annu Rev Neurosci* **38**, 25-46 (2015).
5. D. a. Attwell, S. Laughlin, An Energy Budget for Signaling in the Grey Matter of the Brain. *Journal of Cerebral Blood Flow and Metabolism* **21**, 1133-1145 (2001).
6. M. Tata, C. Ruhrberg, Cross-talk between blood vessels and neural progenitors in the developing brain. *Neuronal Signaling* 10.1042/NS20170139 (2018).
7. K. Veys *et al.*, Role of the GLUT1 Glucose Transporter in Postnatal CNS Angiogenesis and Blood-Brain Barrier Integrity. *Circ Res* **127**, 466-482 (2020).
8. M. Potente, P. Carmeliet, The Link Between Angiogenesis and Endothelial Metabolism. *Annu Rev Physiol* **79**, 43-66 (2017).
9. L. Bierhansl, L. C. Conradi, L. Treps, M. Dewerchin, P. Carmeliet, Central Role of Metabolism in Endothelial Cell Function and Vascular Disease. *Physiology (Bethesda)* **32**, 126-140 (2017).
10. P. Steiner, Brain Fuel Utilization in the Developing Brain. *Ann Nutr Metab* **75 Suppl 1**, 8-18 (2019).
11. A. A. Baburamani, C. J. Ek, D. W. Walker, M. Castillo-Melendez, Vulnerability of the developing brain to hypoxic-ischemic damage: contribution of the cerebral vasculature to injury and repair? *Front Physiol* **3**, 424 (2012).
12. J. Vogenstahl, M. Parrilla, A. Acker-Palmer, M. Segarra, Vascular Regulation of Developmental Neurogenesis. *Front Cell Dev Biol* **10**, 890852 (2022).
13. J. Ouellette, B. Lacoste, From Neurodevelopmental to Neurodegenerative Disorders: The Vascular Continuum. *Front Aging Neurosci* **13**, 749026 (2021).
14. J. Ouellette *et al.*, Vascular contributions to 16p11.2 deletion autism syndrome modeled in mice. *Nat Neurosci* **23**, 1090-1101 (2020).
15. A. Beland-Millar *et al.*, 16p11.2 haploinsufficiency reduces mitochondrial biogenesis in brain endothelial cells and alters brain metabolism in adult mice. *Cell Rep* **42**, 112485 (2023).
16. J. Ouellette, E. E. Crouch, J. L. Morel, V. Coelho-Santos, B. Lacoste, A Vascular-Centric Approach to Autism Spectrum Disorders. *Neurosci Insights* **19**, 26331055241235921 (2024).
17. M. Tang *et al.*, An early endothelial cell-specific requirement for Glut1 is revealed in Glut1 deficiency syndrome model mice. *JCI Insight* **6** (2021).
18. F. Wang *et al.*, Dysfunction of Cerebrovascular Endothelial Cells: Prelude to Vascular Dementia. *Front Aging Neurosci* **10**, 376 (2018).
19. M. T. Rizzo, H. A. Leaver, Brain endothelial cell death: modes, signaling pathways, and relevance to neural development, homeostasis, and disease. *Mol Neurobiol* **42**, 52-63 (2010).

20. N. Cheng, J. M. Rho, S. A. Masino, Metabolic Dysfunction Underlying Autism Spectrum Disorder and Potential Treatment Approaches. *Front Mol Neurosci* **10**, 34 (2017).
21. N. T. Vijayakumar, M. V. Judy, Autism spectrum disorders: Integration of the genome, transcriptome and the environment. *J Neurol Sci* **364**, 167-176 (2016).
22. H. R. Park *et al.*, A Short Review on the Current Understanding of Autism Spectrum Disorders. *Exp Neurobiol* **25**, 1-13 (2016).
23. W. J. Bosl, H. Tager-Flusberg, C. A. Nelson, EEG Analytics for Early Detection of Autism Spectrum Disorder: A data-driven approach. *Sci Rep* **8**, 6828 (2018).
24. Y. Takarae, J. Sweeney, Neural Hyperexcitability in Autism Spectrum Disorders. *Brain Sci* **7** (2017).
25. E. Courchesne *et al.*, Neuron Number and Size in Prefrontal Cortex of Children With Autism. *JAMA* **306**, 2001-2010 (2011).
26. G. Kaushik, K. S. Zarbalis, Prenatal Neurogenesis in Autism Spectrum Disorders. *Frontiers in Chemistry* **4** (2016).
27. A. P. Donovan, M. A. Basson, The neuroanatomy of autism - a developmental perspective. *J Anat* **230**, 4-15 (2017).
28. B. Lacoste *et al.*, Sensory-Related Neural Activity Regulates the Structure of Vascular Networks in the Cerebral Cortex. *Neuron* **83**, 1117-1130 (2014).
29. J. B. a. B. Owen, A., Measurement of Oxidized/Reduced Glutathione Ratio. *Protein Misfolding and Cellular Stress in Disease and Aging*, 269-277 (2010).
30. G. Bjorklund *et al.*, The role of glutathione redox imbalance in autism spectrum disorder: A review. *Free Radic Biol Med* **160**, 149-162 (2020).
31. M. Muraoka *et al.*, Reactivity of gamma-glutamyl-cysteine with intracellular and extracellular glutathione metabolic enzymes. *FEBS Lett* **596**, 180-188 (2022).
32. D. Grahame Hardie, AMP-activated protein kinase: a key regulator of energy balance with many roles in human disease. *J Intern Med* **276**, 543-559 (2014).
33. C. Wilson, M. D. Lee, C. Buckley, X. Zhang, J. G. McCarron, Mitochondrial ATP Production is Required for Endothelial Cell Control of Vascular Tone. *Function (Oxf)* **4**, zqac063 (2023).
34. P. Khare, J. F. Conway, S. M. D, Lipidoid nanoparticles increase ATP uptake into hypoxic brain endothelial cells. *Eur J Pharm Biopharm* **180**, 238-250 (2022).
35. S. Chen *et al.*, Influence of particle size on the in vivo potency of lipid nanoparticle formulations of siRNA. *J Control Release* **235**, 236-244 (2016).
36. P. R. Cullis, M. J. Hope, Lipid Nanoparticle Systems for Enabling Gene Therapies. *Mol Ther* **25**, 1467-1475 (2017).
37. A. W. Lohman, M. Billaud, B. E. Isakson, Mechanisms of ATP release and signalling in the blood vessel wall. *Cardiovasc Res* **95**, 269-280 (2012).
38. Y. Wang *et al.*, Purinergic signaling: A gatekeeper of blood-brain barrier permeation. *Front Pharmacol* **14**, 1112758 (2023).
39. P. Thakore *et al.*, Brain endothelial cell TRPA1 channels initiate neurovascular coupling. *Elife* **10** (2021).
40. S. Muhleder *et al.*, Purinergic P2Y(2) receptors modulate endothelial sprouting. *Cell Mol Life Sci* **77**, 885-901 (2020).
41. K. Yamazaki, J. Yoneyama, R. Kimoto, Y. Shibata, T. Mimura, Prevention of Surgery-Induced Dry Eye by Diquafosol Eyedrops after Femtosecond Laser-Assisted Cataract Surgery. *J Clin Med* **11** (2022).

42. S. Kim, J. Shin, J. E. Lee, A randomised, prospective study of the effects of 3% diquafosol on ocular surface following cataract surgery. *Sci Rep* **11**, 9124 (2021).
43. W. Bintig *et al.*, Purine receptors and Ca(2+) signalling in the human blood-brain barrier endothelial cell line hCMEC/D3. *Purinergic Signal* **8**, 71-80 (2012).
44. B. S. Khakh, R. A. North, Neuromodulation by extracellular ATP and P2X receptors in the CNS. *Neuron* **76**, 51-69 (2012).
45. K. a. E. Glinton, S., Untargeted Metabolomics for Autism Spectrum Disorders: Current Status and Future Directions. *Front in Psychiatry* **10** (2019).
46. N. Likhitweerawong *et al.*, Profiles of urine and blood metabolomics in autism spectrum disorders. *Metab Brain Dis* **36**, 1641-1671 (2021).
47. S. S. Lingampelly *et al.*, Metabolic network analysis of pre-ASD newborns and 5-year-old children with autism spectrum disorder. *Commun Biol* **7**, 536 (2024).
48. R. Z. Lin *et al.*, Mitochondrial transfer mediates endothelial cell engraftment through mitophagy. *Nature* **629**, 660-668 (2024).
49. R. Quintana-Cabrera *et al.*, gamma-Glutamylcysteine detoxifies reactive oxygen species by acting as glutathione peroxidase-1 cofactor. *Nat Commun* **3**, 718 (2012).
50. A. Gordji-Nejad *et al.*, Single dose creatine improves cognitive performance and induces changes in cerebral high energy phosphates during sleep deprivation. *Sci Rep* **14**, 4937 (2024).
51. M. Wyss, R. Kaddurah-Daouk, Creatine and Creatinine Metabolism. *Physiological Reviews* **80**, 1107-1213 (2000).
52. K. Losenkova *et al.*, Endothelial cells cope with hypoxia-induced depletion of ATP via activation of cellular purine turnover and phosphotransfer networks. *Biochim Biophys Acta Mol Basis Dis* **1864**, 1804-1815 (2018).
53. G. Burnstock, V. Ralevic, Purinergic signaling and blood vessels in health and disease. *Pharmacol Rev* **66**, 102-192 (2014).
54. S. Wang *et al.*, P2Y(2) and Gq/G(1)(1) control blood pressure by mediating endothelial mechanotransduction. *J Clin Invest* **125**, 3077-3086 (2015).
55. L. Babiec, A. Wilkaniec, E. Gawinek, W. Hilgier, A. Adamczyk, Inhibition of purinergic P2 receptors prevents synaptic and behavioral alterations in a rodent model of autism spectrum disorders. *Research in Autism Spectrum Disorders* **112** (2024).
56. J. Ju *et al.*, Adenosine mediates the amelioration of social novelty deficits during rhythmic light treatment of 16p11.2 deletion female mice. *Mol Psychiatry* 10.1038/s41380-024-02596-4 (2024).
57. R. M. Touyz, J. H. F. de Baaij, J. G. J. Hoenderop, Magnesium Disorders. *N Engl J Med* **390**, 1998-2009 (2024).
58. M. Mousain-Bosc, C. Siatka, J. P. Bali (2011) Magnesium, hyperactivity and autism in children. ed R. N. Vink, M. (University of Adelaide Press).
59. G. Horev *et al.*, Dosage-dependent phenotypes in models of 16p11.2 lesions found in autism. *Proc Natl Acad Sci U S A* **108**, 17076-17081 (2011).
60. T. Lindeberg, Feature detection with automatic scale selection. *International journal of computer vision* **30**, 79-116 (1998).
61. M. Freitas-Andrade *et al.*, Astroglial Hmgb1 regulates postnatal astrocyte morphogenesis and cerebrovascular maturation. *Nat Commun* **14**, 4965 (2023).
62. K. A. Whitehead *et al.*, Degradable lipid nanoparticles with predictable in vivo siRNA delivery activity. *Nature communications* **5**, 4277 (2014).

63. G. Carpentier (2012) Angiogenesis Analyzer for ImageJ. in *ImageJ News*.
64. C. H. Tischbirek, A. Birkner, A. Konnerth, In vivo deep two-photon imaging of neural circuits with the fluorescent Ca(2+) indicator Cal-590. *J Physiol* **595**, 3097-3105 (2017).
65. J. Ropa, S. Cooper, M. L. Capitano, W. Van't Hof, H. E. Broxmeyer, Human Hematopoietic Stem, Progenitor, and Immune Cells Respond Ex Vivo to SARS-CoV-2 Spike Protein. *Stem Cell Rev Rep* **17**, 253-265 (2021).
66. A. Gengatharan *et al.*, Adult neural stem cell activation in mice is regulated by the day/night cycle and intracellular calcium dynamics. *Cell* **184**, 709-722 e713 (2021).
67. S. Malvaut *et al.*, CaMKIIalpha Expression Defines Two Functionally Distinct Populations of Granule Cells Involved in Different Types of Odor Behavior. *Curr Biol* **27**, 3315-3329 e3316 (2017).

Chapter 4- Manuscript III

Association to hypothesis: This manuscript identifies a pathway of interest to improve 16p11.2 deletion-associated behaviors and endothelial dysfunctions. These findings underlined a potential target in 16p11.2 deletion syndrome.

Current manuscript status: This manuscript is published in *Neuroscience Letters* in 2024.

Author contributions: J.O. performed experiments, analyzed the data/images in a blinded manner and wrote the manuscript. B.L. generated figures for the manuscript and edited the manuscript.

Rock2 heterozygosity improves recognition memory and endothelial function in a mouse model of 16p11.2 deletion autism syndrome

Julie Ouellette[1,2] and Baptiste Lacoste[1,2,3*]

Affiliations:

[1] Neuroscience Program, The Ottawa Hospital Research Institute, Ottawa, ON, Canada.
[2] Cellular & Molecular Medicine, University of Ottawa, Ottawa, ON, Canada.
[3] University of Ottawa Brain and Mind Research Institute, Ottawa, ON, Canada.

***Correspondence to:**

Dr. Baptiste Lacoste
Faculty of Medicine, Department of Cellular and Molecular Medicine
University of Ottawa & Ottawa Hospital Research Institute
451 Smyth Road, Ottawa (ON) K1H 8M5, Ottawa, Canada
Email: blacoste@uottawa.ca

Manuscript type:

Short Communication

Numbers:

Words in Abstract: 132
Words in Main text: 1955
References: 25
Figures: 2

Key words:

Autism, 16p11.2 deletion, ROCK2, endothelium, brain, angiogenesis, behavior, mice.

Abstract

Rho-associated protein kinase-2 (ROCK2) is a critical player in many cellular processes and was incriminated in cardiovascular and neurological disorders. Recent evidence has shown that non-selective pharmacological blockage of ROCKs ameliorates behavioral alterations in a mouse model of 16p11.2 haploinsufficiency. We had revealed that 16p11.2-deficient mice also display cerebrovascular abnormalities, including endothelial dysfunction. To investigate whether genetic blockage of ROCK2 also exerts beneficial effects on cognition and angiogenesis, we generated mice with both 16p11.2 and *Rock2* haploinsufficiency (*16p11.2*$^{df/+}$*;Rock2*$^{+/-}$). We find that *Rock2* heterozygosity on a *16p11.2*$^{df/+}$ background significantly improved recognition memory. Furthermore, brain endothelial cells from *16p11.2*$^{df/+}$*;Rock2*$^{+/-}$ mice display improved angiogenic capacity compared to cells from *16p11.2*$^{df/+}$ littermates. Overall, this study implicates *Rock2* gene as a modulator of 16p11.2-associated alterations, highlighting its potential as a target for treatment of autism spectrum disorders.

1. Introduction

Rho-associated kinases (ROCK) are downstream effectors of RhoA GTPases [1]. The RhoA/ROCK pathway is involved in cell migration, morphogenesis, survival, cytoskeleton regulation [2] and vascular function [3, 4]. ROCK consist of two isoforms (ROCK-1 and -2), with ROCK2 being primarily expressed in the brain and its vasculature [1].

A growing body of literature highlights the therapeutic potential of pharmacological ROCK inhibition in neurological disorders [5-9]. In a mouse model of 16p11.2 deletion autism syndrome, Lorenzo et al. demonstrated that treatment with Fasudil, a non-selective ROCK inhibitor, improved cognitive performance [10]. The 16p11.2 deletion is a common genetic risk factor for autism

spectrum disorders (ASD). This locus comprises genes linked to neuropsychiatric conditions, including *Kctd13* [10, 11]. *Kctd13* is crucial for late stages of brain development as it regulates levels of RhoA to control actin cytoskeleton and cell motility [12]. Lorenzo et al. demonstrated that *Kctd13*$^{+/-}$ mice phenocopied cognitive deficits identified in their 16p11.2 deletion mouse model, and these cognitive changes were improved by Fasudil [10].

Using another mouse model of the 16p11.2 deletion syndrome, namely *16p11.2*$^{df/+}$ mice [13], we have previously established a causal relationship between 16p11.2 deletion and altered cerebrovascular maturation, leading to lasting brain endothelial dysfunction and behavioral changes [14]. Elevated ROCK2 is associated with endothelial dysfunction as it inhibits endothelial nitric oxide synthase (eNOS), an essential modulator of vascular tone, increases endothelial cell (EC) apoptosis and promotes vascular permeability [4, 6]. Whether selective reduction of *Rock2* gene expression corrects 16p11.2 deletion-related deficits remained to be tested. Here, we investigate the impact of *Rock2* heterozygosity (*Rock2*$^{+/-}$) on two behaviors and brain endothelial function in *16p11.2*$^{df/+}$ mice.

2. Methods

2.1. Animals

Procedures were approved by University of Ottawa's Animal Care Committee, and conducted in accordance with the Canadian Council on Animal Care's guidelines.

Mice were bred in-house and housed 5/cage with free access to water and food. Experimental animals (F5) were on mixed B6/129/CD1 genetic background. Males *16p11.2*$^{df/+}$ (Jackson stock #013128; B6/129 background) were crossed with WT females of the same background (stock #101043) to maintain a WT and *16p11.2*$^{df/+}$ littermate colony. As recommended

by Jackson Laboratory, cages were supplemented with breeding chow (#2019, Envigo Teklad) and DietGel (#76A, ClearH_2O) up to weaning age. Female *Rock2*$^{+/-}$ were crossed with CD1 WT males to maintain a heterozygous *Rock2*$^{+/-}$ colony (*Rock2*$^{-/-}$ mice die *in utero*). *Rock2*$^{+/-}$ mice were on a standard chow diet (#2018, Envigo Teklad). *Rock2*$^{+/-}$ breeders were a gift from Dr. Zhengping Jia (University of Toronto). To obtain experimental animals, *16p11.2*$^{df/+}$ males were crossed with *Rock2*$^{+/-}$ females and maintained on the *16p11.2*$^{df/+}$ mouse diet. All assays were performed on offspring past the 5th generation. *16p11.2*$^{df/+}$;*Rock2*$^{+/-}$, *Rock2*$^{+/-}$, *16p11.2*$^{df/+}$ and WT littermates were genotyped with the following primers: 5′-CCTCATGGACTAATTATGGAC-3′ (forward) and 5′-CCAGTTTCACTAATGACACA-3′ (reverse), with a PCR product of 2.2 kb for *16p11.2*$^{df/+}$ mice[13]. *Rock2*$^{+/-}$ mice were genotyped with the following primers: 5′-CATACATGTGCCAAAATCTGCTAAC-3′ and 5′-GGGGGAACTTCCTGACTAGG-3′.

2.2. Behavioral assays.

All animals (2-month-old males) were left to acclimatize to inverted light cycle for 10 days prior to behavior testing. During this time, animals were handled once a day for 7 days. Behavioral tests were completed at the University of Ottawa's Behavior Core Facility between 9:00 and 17:00 under dim red light. Before testing was started, animals were habituated in the testing room for 60 minutes (min). Tests were adapted from our previous work [14-16].

2.2.1. Novel-object recognition (NOR) test

On day 1, animals were habituated for 30 min in an empty open-field arena (45 x 45 x 45 cm). On day 2, mice were habituated in the same open field for 10 min. After habituation, each mouse was removed from the open field and placed in a clean home cage for 2 min. Two identical objects were placed in the arena. The mouse was returned and left to explore for 10 min of familiarization. The mouse was then removed and placed in a clean holding cage for 1 hr. After,

the object-recognition test entailed one cleaned familiar object (FO) and one cleaned novel object (NO). The mouse was then returned to the arena for a 5-min recognition period. Interactions with objects were recorded using Ethovision XT (Noldus). Object recognition was scored as the amount of time the nose of the animal was within 2 cm of the object. A discrimination index (DI) was calculated for NO: [time spent interacting with NO / (time spent interacting with NO + time spent interacting with FO)].

2.2.2. Marble-burying test

This test entailed a 30-min trial per mouse in a standard polycarbonate rat cage (26 x 48 x 20 cm) filled with 5-cm thick SANI-chip bedding. 20 marbles were evenly distributed (5 rows of 4) on the bedding. At start, each mouse was placed in the bottom left corner and left to navigate while the cage is covered by a transparent Plexiglas. After the trial, the number of marbles either fully buried or at least two-thirds covered by bedding were counted as buried.

2.3. Primary mouse brain endothelial cell isolation.

Mice were euthanized by cervical dislocation and the cerebral cortex was dissected in cold HBSS. The cortex cut in 2-3 mm pieces was dissociated in Neural Tissue Dissociation Kit P compounds (Miltenyi Biotec, 130-092-628) to obtain a cell suspension. This suspension was incubated with CD31-coated magnetic microbeads (Miltenyi Biotec, 130-097-418) and placed on a magnetic MACs separator to isolate endothelial cells (ECs). ECs from each mouse were seeded in 2 wells of a plate coated with attachment factor protein 1X (ThermoFisher Scientific, S006100). For a pure EC population, an EC-specific medium (Lonza, CC-3202) was every 48 hrs until cells were at least 90% confluent [14].

2.4. In vitro network-formation assay

Each well of a 96-well plate was coated with 50 µl of growth-factor-reduced Matrigel (BD Bioscience, cat. no. C354230) and incubated at 37°C for 30 mins to promote polymerization. ECs were collected with TryplE (Gibco, 12604013) and counted using a hemocytometer. A total of 2 $\times 10^4$ cells were seeded in each well with 150 µl EC specific media (Lonza, CC-3202). TIFF images of capillary-like networks were captured using a Nikon TE2000 inverted microscope at 4, 8, and 24 hrs post-seeding. Images were processed with Angiogenesis function in ImageJ [14, 17].

2.5. Statistical analyses.

Sample sizes fit our published report [14]. Data analysis was conducted blind. Statistical tests were performed in GraphPad Prism 10.2 software. Normal data distribution was verified using a Shapiro-Wilk test. A one-way analysis of variance (ANOVA) and a Tukey's *post-hoc* test were used for the NOR and marble burying tests. A two-way ANOVA ('genotype x time') and a Tukey's *post-hoc* test were used for the *in vitro* network formation assay. $P<0.05$ was considered significant.

3. Results

3.1. Rock2 heterozygosity improves 16p11.2 deletion-associated cognitive deficits

We subjected *16p11.2*$^{df/+}$;*Rock2*$^{+/-}$ mice and control littermates (WT, *Rock2*$^{+/-}$ and *16p11.2*$^{df/+}$) to two behavioral tests: novel object recognition task (NOR, assessing recognition memory) and a marble burying task (repetitive behaviors). Consistent with previous findings [14], *16p11.2*$^{df/+}$ mice exhibited a significant preference for the familiar, not novel, object. However, *16p11.2*$^{df/+}$;*Rock2*$^{+/-}$ mice displayed a similar discrimination index as WT and *Rock2*$^{+/-}$ mice. Notably, *16p11.2*$^{df/+}$;*Rock2*$^{+/-}$ mice showed increased discrimination for the novel object compared

to *16p11.2*$^{df/+}$ littermates (Fig. 1A). While *16p11.2*$^{df/+}$ mice buried significantly more marbles, *16p11.2*$^{df/+}$;*Rock2*$^{+/-}$ mice showed a reduction, albeit non-significant, in repetitive behaviors (Fig. 1B). These results suggest that *Rock2* heterozygosity has the potential to improve 16p11.2-deletion induced behavioral deficits.

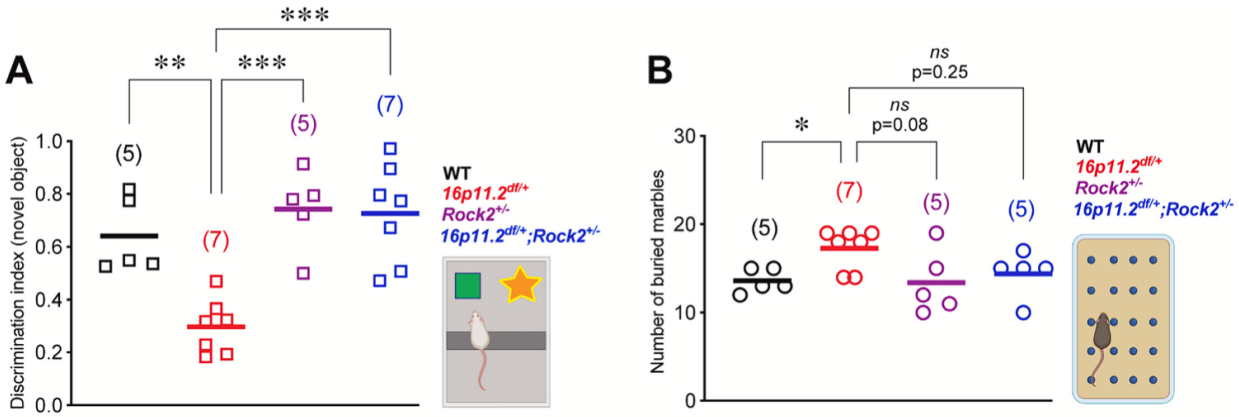

Fig. 1. *Rock2* heterozygosity improves 16p11.2 deletion-associated behavioral deficits. Behavioral assessment was conducted in *16p11.2*$^{df/+}$; *Rock2*$^{+/-}$, *16p11.2*$^{df/+}$, *Rock2*$^{+/-}$ and WT littermates at P50. (A) The novel object recognition task revealed improved recognition memory in *16p11.2*$^{df/+}$;*Rock2*$^{+/-}$ mice compared to *16p11.2*$^{df/+}$ littermates. (B) Marble burying task demonstrated a slight decrease in the number of marbles buried by *16p11.2*$^{df/+}$;*Rock2*$^{+/-}$ mice compared to *16p11.2*$^{df/+}$ littermates. Data are mean ± s.e.m. ns: not significant, *P < 0.05, **P < 0.01, ***P < 0.001 (one-way ANOVA and Tukey's *post-hoc* test).

3.2. Rock2 heterozygosity ameliorates 16p11.2 deletion-associated brain endothelial dysfunction

We have reported that brain ECs from *16p11.2*$^{df/+}$ mice are unable to form a capillary-like network *in vitro* [14]. Here, we seeded primary brain ECs from WT, *Rock2*$^{+/-}$, *16p11.2*$^{df/+}$ and *16p11.2*$^{df/+}$;*Rock2*$^{+/-}$ littermates in Matrigel® and evaluated capillary-like network formation 4-, 8- and 24-hrs post-seeding (Fig. 2A). ECs from WT mice showed an expected increase in tube length and node number (Fig. 2B-D). In addition, ECs isolated from *Rock2*$^{+/-}$ mice displayed similar network forming abilities compared to WT cells (Fig. 2D). In line with previous work [14], 16p11.2-deficient ECs were unable to form a capillary-like network compared to WT cells. However, *16p11.2*$^{df/+}$;*Rock2*$^{+/-}$ ECs showed an overall increased angiogenic ability compared to

16p11.2-deficient ECs (Fig. 2B-D). At 24 hrs post-seeding, *16p11.2*$^{df/+}$;*Rock2*$^{+/-}$ EC tube length returned closer to *16p11.2*$^{df/+}$ ECs network values, consistent with lack of trophic support at the end of the assay. Both *16p11.2*$^{df/+}$;*Rock2*$^{+/-}$ and *16p11.2*$^{df/+}$ ECs had similar node numbers whereas WT network nodes increased throughout the assay (Fig. 2D). Finally, *16p11.2*$^{df/+}$;*Rock2*$^{+/-}$ ECs displayed an increased number of angiogenic sprouts throughout the 24-hour assay compared to *16p11.2*$^{df/+}$ ECs (Fig. 2D). These results demonstrate that *Rock2* heterozygosity can partially alleviate 16p11.2 deletion-induced brain EC dysfunction.

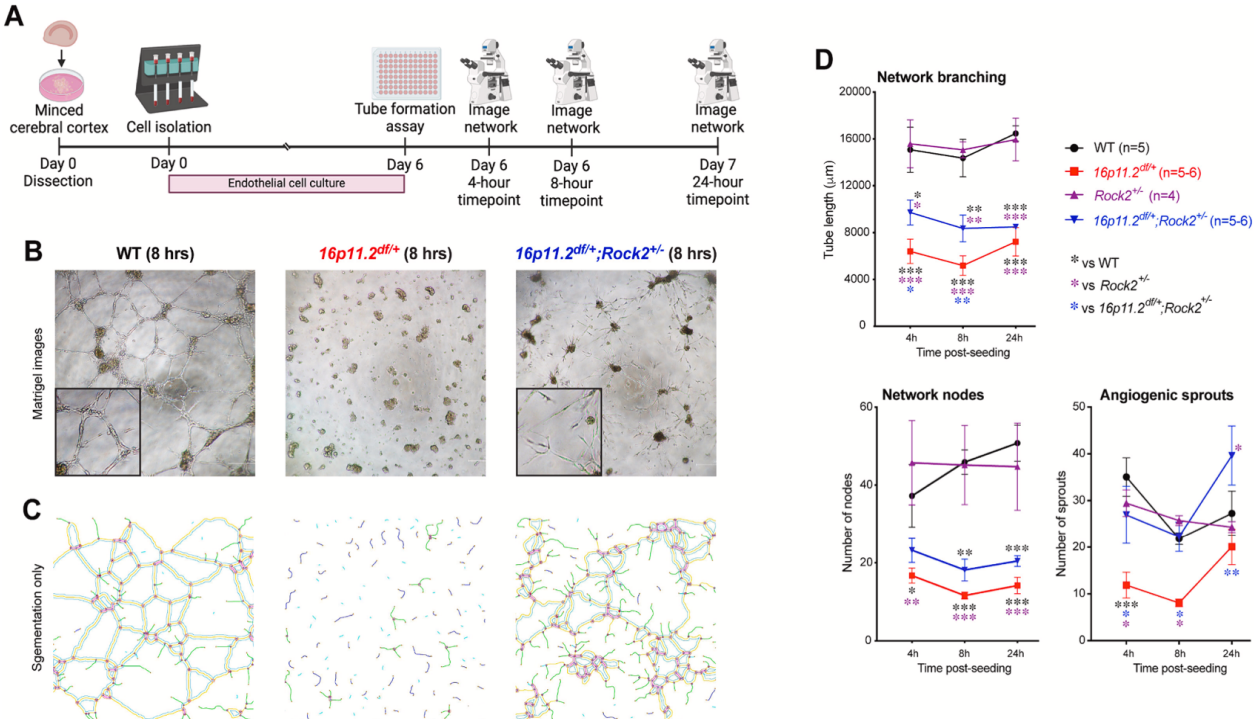

Fig. 2. *Rock2* heterozygosity improves the function of 16p11.2-deficient endothelial cells. (A) Experimental design for the Matrigel®-based tube formation assay. (B) Representative images of the tube formation assay 8 hrs after seeding mouse brain endothelial cells. (C) Respective network traces obtained in ImageJ. (D) Quantification of network branching, network nodes, and angiogenic sprouts. Increased angiogenic capacity was seen in *16p11.2*$^{df/+}$; *Rock2*$^{+/-}$ ECs compared to *16p11.2*$^{df/+}$ ECs. Data are mean ± s.e.m. *P < 0.05, **P < 0.01, ***P < 0.001 (two-way ANOVA and Tukey's *post-hoc* test).

4. Discussion

Pharmacological modulation of ROCK activity is a recognized disease-modifying strategy [7, 10]. ROCK inhibitor Fasudil can modulate α-synuclein aggregation and ameliorate motor function in a Parkinson's disease mouse model [18]. In a rat model of delayed encephalopathy following acute carbon monoxide poisoning (DEACMP), inhibition of ROCK2 with Y-27632 reduced neuronal damage and improved cognitive and motor ability [19]. Mutations in *Ccm-1*, *-2*, or *-3* are associated with endothelial defects often leading to cerebral cavernous malformations (CCM). While RhoA was upregulated in cells lines of *Ccm-1*, -2 or -3 knockdown, ROCK inhibitor Y-27632 or ROCK2 knockdown rescued tube formation in this model [20]. Here, we provide evidence supporting the involvement of the RhoA/ROCK pathway in neurodevelopmental disorders.

Data obtained with *16p11.2*$^{df/+}$*;Rock2*$^{+/-}$ mice reveal that developmental reduction of *Rock2* expression triggers long-term beneficial effects, such as improved recognition memory. This is in line with a recent study demonstrating that chronic ROCK inhibition with Fasudil ameliorated recognition memory in 16p11.2 deletion mice [10]. Beneficial effects of *Rock2* ablation may be related to decreased RhoA signaling as *Kctd13* expression, a 16p11.2 locus gene regulator of RhoA protein level, is reduced [21]. Without proper regulation of RhoA/ROCK pathway by *Kctd13*, elevated RhoA/ROCK activity may be involved in 16p11.2 deletion-associated phenotypes.

The improved angiogenic response of *16p11.2*$^{df/+}$*;Rock2*$^{+/-}$ ECs highlights the beneficial effects of decreased ROCK2. A previous study using a model of hindlimb ischemia showed enhanced endothelial tube formation using a ROCK inhibitor [22]. Increased endothelial branching and sprouting measured in *16p11.2*$^{df/+}$*;Rock2*$^{+/-}$ ECs may be in part attributed to role of the RhoA/ROCK pathway in cytoskeletal reorganization [23].

We demonstrated that endothelium-specific 16p11.2 haploinsufficiency drives ASD-related mouse behaviors [14]. Here, we report improved endothelial function in *16p11.2*$^{df/+}$*;Rock2*$^{+/-}$ mice, suggesting that improved behaviors may result, at least in part, from improved vascular function. However, other factors could contribute to improved cognitive performance and endothelial function. In cortical organoids derived from 16p11.2 deletion carriers, ROCK inhibition rescued delayed migration of neurons [24]. In a mouse model deficient for *Kctd13*, increased RhoA levels were associated with altered synaptic transmission, which was recovered following ROCK inhibition [25]. Hence, *Rock2* heterozygosity in 16p11.2-deficient mice may not only impact the vasculature but also neuronal cells, and future research is required to unmask the underlying mechanisms.

Significance statement

Elevated ROCK2 was linked to neurological disorders, and pharmacological blockage of ROCK2 was shown to ameliorate behaviors in a mouse model of autism spectrum disorders (ASD). Here, we show that reduced *Rock2* gene expression improves cognitive behavior and endothelial function in a mouse model of 16p11.2 deletion syndrome. This new work highlights the beneficial aspects of *Rock2* heterozygosity in an ASD mouse model, supporting the RhoA/ROCK pathway as a potential therapeutic target in neurodevelopmental disorders.

Declaration of competing interest

The authors declare that they have no known competing financial interests or personal relationships that could have appeared to influence the work reported in this paper.

Acknowledgements

This research was funded by two grants from the Canadian Institutes of Health Research (#388805, #506513) to B.L., and a Scholarship from the Canadian Institutes of Health Research to J.O.

REFERENCES

[1] Noma K, Kihara Y, Higashi Y. Striking crosstalk of ROCK signaling with endothelial function. J Cardiol. (2012);60(1):1-6. https://doi.org/10.1016/j.jjcc.2012.03.005

[2] Hall A. Rho family GTPases. Biochem Soc Trans. (2012);40(6):1378-82. https://doi.org/10.1042/bst20120103

[3] Strassheim D, Gerasimovskaya E, Irwin D, Dempsey EC, Stenmark K, Karoor V. RhoGTPase in Vascular Disease. Cells. (2019);8(6). https://doi.org/10.3390/cells8060551

[4] Yao L, Romero MJ, Toque HA, Yang G, Caldwell RB, Caldwell RW. The role of RhoA/Rho kinase pathway in endothelial dysfunction. J Cardiovasc Dis Res. (2010);1(4):165-70. https://doi.org/10.4103/0975-3583.74258

[5] Rikitake Y, Liao JK. ROCKs as therapeutic targets in cardiovascular diseases. Expert Rev Cardiovasc Ther. (2005);3(3):441-51. https://doi.org/10.1586/14779072.3.3.441

[6] Beckers CM, Knezevic N, Valent ET, Tauseef M, Krishnan R, Rajendran K, et al. ROCK2 primes the endothelium for vascular hyperpermeability responses by raising baseline junctional tension. Vascul Pharmacol. (2015);70:45-54. https://doi.org/10.1016/j.vph.2015.03.017

[7] Koch JC, Tatenhorst L, Roser AE, Saal KA, Tonges L, Lingor P. ROCK inhibition in models of neurodegeneration and its potential for clinical translation. Pharmacol Ther. (2018);189:1-21. https://doi.org/10.1016/j.pharmthera.2018.03.008

[8] Weber AJ, Herskowitz JH. Perspectives on ROCK2 as a Therapeutic Target for Alzheimer's Disease. Front Cell Neurosci. (2021);15:636017. https://doi.org/10.3389/fncel.2021.636017

[9] Shimizu T, Fukumoto Y, Tanaka S, Satoh K, Ikeda S, Shimokawa H. Crucial role of ROCK2 in vascular smooth muscle cells for hypoxia-induced pulmonary hypertension in mice. Arterioscler Thromb Vasc Biol. (2013);33(12):2780-91. https://doi.org/10.1161/atvbaha.113.301357

[10] Martin Lorenzo S, Nalesso V, Chevalier C, Birling MC, Herault Y. Targeting the RHOA pathway improves learning and memory in adult Kctd13 and 16p11.2 deletion mouse models. Mol Autism. (2021);12(1):1. https://doi.org/10.1186/s13229-020-00405-7

[11] Crepel A, Steyaert J, De la Marche W, De Wolf V, Fryns JP, Noens I, et al. Narrowing the critical deletion region for autism spectrum disorders on 16p11.2. Am J Med Genet B Neuropsychiatr Genet. (2011);156(2):243-5. https://doi.org/10.1002/ajmg.b.31163

[12] Lin P, Yang J, Wu S, Ye T, Zhuang W, Wang W, et al. Current trends of high-risk gene Cul3 in neurodevelopmental disorders. Frontiers in Psychiatry. (2023);14. https://doi.org/10.3389/fpsyt.2023.1215110

[13] Horev G, Ellegood J, Lerch JP, Son YE, Muthuswamy L, Vogel H, et al. Dosage-dependent phenotypes in models of 16p11.2 lesions found in autism. Proc Natl Acad Sci U S A. (2011);108(41):17076-81. https://doi.org/10.1073/pnas.1114042108

[14] Ouellette J, Toussay X, Comin CH, Costa LDF, Ho M, Lacalle-Aurioles M, et al. Vascular contributions to 16p11.2 deletion autism syndrome modeled in mice. Nat Neurosci. (2020);23(9):1090-101. https://doi.org/10.1038/s41593-020-0663-1

[15] Angoa-Pérez M, Kane MJ, Briggs DI, Francescutti DM, Kuhn DM. Marble Burying and Nestlet Shredding as Tests of Repetitive, Compulsive-like Behaviors in Mice. J Vis Exp. (2013)(82):e50978. https://doi.org/10.3791/50978

[16] Portmann T, Yang M, Mao R, Panagiotakos G, Ellegood J, Dolen G, et al. Behavioral abnormalities and circuit defects in the basal ganglia of a mouse model of 16p11.2 deletion syndrome. Cell Rep. (2014);7(4):1077-92. https://doi.org/10.1016/j.celrep.2014.03.036

[17] Carpentier G. Angiogenesis Analyzer for ImageJ 2012 [Available from: http://image.bio.methods.free.fr/ImageJ/?Angiogenesis-Analyzer-for-ImageJ#outil_sommaire_0.

[18] Tatenhorst L, Eckermann K, Dambeck V, Fonseca-Ornelas L, Walle H, Lopes da Fonseca T, et al. Fasudil attenuates aggregation of alpha-synuclein in models of Parkinson's disease. Acta Neuropathol Commun. (2016);4:39. https://doi.org/10.1186/s40478-016-0310-y

[19] Xu L, Liu X, Guo C, Wang C, Zhao J, Zhang X, et al. Inhibition of ROCK2 kinase activity improved behavioral deficits and reduced neuron damage in a DEACMP rat model. Brain Res Bull. (2022);180:24-30. https://doi.org/10.1016/j.brainresbull.2021.12.018

[20] Borikova AL, Dibble CF, Sciaky N, Welch CM, Abell AN, Bencharit S, et al. Rho kinase inhibition rescues the endothelial cell cerebral cavernous malformation phenotype. J Biol Chem. (2010);285(16):11760-4. https://doi.org/10.1074/jbc.c109.097220

[21] Richter M, Murtaza N, Scharrenberg R, White SH, Johanns O, Walker S, et al. Altered TAOK2 activity causes autism-related neurodevelopmental and cognitive abnormalities through RhoA signaling. Mol Psychiatry. (2018). https://doi.org/10.1038/s41380-018-0025-5

[22] Fayed HS, Bakleh MZ, Ashraf JV, Howarth A, Ebner D, Al Haj Zen A. Selective ROCK Inhibitor Enhances Blood Flow Recovery after Hindlimb Ischemia. Int J Mol Sci. (2023);24(19). https://doi.org/10.3390/ijms241914410

[23] Amano M, Nakayama, M. and Kaibuchi, K. Rho-Kinase/ROCK: A Key Regulator of the Cytoskeleton and Cell Polarity. Cytoskeleton. (2010);67:545-56. https://doi.org/10.1002/cm.20472

[24] Urresti J, Zhang P, Moran-Losada P, Yu NK, Negraes PD, Trujillo CA, et al. Cortical organoids model early brain development disrupted by 16p11.2 copy number variants in autism. Mol Psychiatry. (2021);26(12):7560-80. https://doi.org/10.1038/s41380-021-01289-6

[25] Sundberg M, Pinson H, Smith RS, Winden KD, Venugopal P, Tai DJC, et al. 16p11.2 deletion is associated with hyperactivation of human iPSC-derived dopaminergic neuron networks and is rescued by RHOA inhibition in vitro. Nat Commun. (2021);12(1):2897. https://doi.org/10.1038/s41467-021-23113-z

Chapter 5- General discussion

5.1. Summary of results

This thesis focused on unraveling the cerebrovascular contributions to autism spectrum disorders (ASD). It provided compelling evidence that the underlining phenotypes characterizing ASD are not solely neuronal in nature but are also driven by the brain vasculature. Manuscript I established a vascular link with ASD, uncovering functional and structural vascular discrepancies including altered hemodynamics and dysfunctional brain endothelial cells (ECs) (*i.e.* impaired endothelium-dependent vasodilation; delayed and reduced angiogenic capacity) in a model of 16p11.2 deletion syndrome. Strikingly, these findings translated to the human disease. We found similar endothelial dysfunctions in human induced ECs from 16p11.2 deletion carriers. Furthermore, Manuscript I revealed that ECs can cell-autonomously contribute to 16p11.2 deletion phenotypes as shown in a mouse model harboring an endothelium-specific 16p11.2 deletion. The endothelial-specific 16p11.2 deletion was enough to drive ASD-related behaviors as well as cerebrovascular phenotypes identified in 16p11.2-deficient mice. Manuscript II unmasked the molecular mechanisms linked with endothelial dysfunctions. It demonstrated that the 16p11.2 deletion induced a bioenergetic failure (*i.e.* lack of available ATP) and a reduced mitochondrial density in brain ECs. Intracellular and extracellular delivery of ATP rescued the angiogenic capacity in 16p11.2-deficient ECs. Providing extracellular ATP generated a distinct Ca^{2+} response in 16p11.2-deficient brain ECs such as decreased frequency of Ca^{2+} transients. The altered energy metabolism in brain 16p11.2-deficient ECs is considered the main driver of the reduced angiogenic capacity. Targeting ATP signaling via P2-class receptors, specifically P2Y2 receptors, rescued the angiogenic ability of 16p11.2-deficient ECs, pinpointing a possible therapeutic strategy for ASD. Manuscript III identified an indirect target for improving 16p11.2 deletion-associated phenotypes. This manuscript demonstrated that *Rock2* heterozygosity in a 16p11.2 deletion mouse model

increased angiogenic capacity of 16p11.2-deficient ECs as well as rescued recognition memory. Taken together, these manuscripts present a large body of work that highlight the importance of a healthy vasculature for brain development and function. The data presented here significantly adds to the growing body of literature emphasizing the contribution of the brain vasculature and EC metabolism to ASD pathophysiology.

5.2. Brain endothelial cells are contributors to neurodevelopmental disorder pathophysiology - a paradigm shift in ASD research

Brain vascular research is mostly focused on late-onset conditions with few studies investigating vascular alterations during development. Interestingly, vascular discrepancies in neurodegenerative disorders are preceding disease symptom onset. Multiple sclerosis, Alzheimer's, Parkinson's and Huntington's diseases as well as vascular dementia and cerebral small vessel disease are all examples of disorders with early cerebrovascular dysfunctions[7]. These disorders share similar early vascular changes including endothelial dysfunctions at the BBB and altered CBF, suggesting a possible common dysfunctional feature[317-319]. These findings raise the possibility that vascular alterations during critical periods of brain development can contribute to the onset of neurodevelopmental disorders.

During brain development, both neuronal and vascular systems are coordinated to ensure proper brain growth and function[113]. Neurons depend on signaling cues from ECs for neurogenesis and neuronal network formation, while ECs rely on neuronal signaling cues for angiogenesis and vascular network establishment[17,126]. This relationship, established during development and conserved throughout life, ensures that energy metabolism in the brain is maintained through NVC. Given the important role of the cerebrovasculature in brain function, vascular abnormalities during

development will severely impact the brain in the long-term. Little evidence is available for the contribution of EC dysfunctions in neurodevelopmental disorders. For instance, GLUT1 deficiency syndrome, which entails the inactivation of a single copy of the *Glut1* gene, consist of a rare disease that impairs brain metabolism before 6 months of age. GLUT1 deficiency syndrome shares a common vascular alteration with neurodegenerative disorders such as reduced angiogenesis, and is associated with movement disorders as well as cognitive impairments[67,320]. Moreover, a recent study using brain organoids from iPSCs obtained from schizophrenic patients identified endothelial alterations such as enrichment of genes important for vessel formation and vascular regulation as well as vessel-like structural changes and enhanced permeability of ECs[321]. Taken together, these endothelial alterations highlight the potential of ECs in contributing to disease pathology, in particular, neurodevelopmental disorders.

Despite the interdependence of neuronal and vascular systems for brain health and these previous vascular findings in neurodevelopmental disorders, ASD are still mostly studied from the neuronal point of view. With the increasing ASD incidence, there is an urgent need for exploring novel avenues of research to better understand the pathophysiology of these disorders.

Manuscript I unraveled the vascular contributions to one ASD using a mouse model of 16p11.2 deletion syndrome. Adult 16p11.2-deficient mice demonstrated elevated baseline cerebral blood flow with impaired vascular reactivity, suggesting possible altered cerebrovascular parameters in ASD. This initial finding prompt us to dissect what was contributing to these CBF alterations. VSMC and EC functional assessments were completed as these cells modulate vessel tone to regulate CBF. Upon vascular reactivity assessment, VSMC responses to vasomodulators were unchanged between 16p11.2-deficient and wild-type (WT) mice. However, endothelium-dependent vasodilation was impaired in 16p11.2 deficient mice. This was the first evidence of

brain EC involvement in 16p11.2 deletion phenotypes. Further along these lines, no structural changes were found in other cell types of the NVU (*i.e.* astrocytes, pericytes and VSMCs). EC networks *in vivo* were reduced only in young 14-day old mice. These findings adding to the evidence that ECs are important for 16p11.2 deletion pathophysiology.

Given that young 16p11.2-deficient mice have altered vascular parameters that are endothelial in nature, we proceeded to isolate brain ECs from P14 16p11.2-deficient mice to have a better understanding of their contributions to these disorders. These cells were characterized with reduced angiogenesis during functional assessment with no change in baseline parameters (*i.e.* no difference in migration, proliferation, and apoptosis compared to wild-type ECs). This of interest as 16p11.2-deficient ECs present with healthy features; however, they are not able to respond in times of a challenge (*i.e.* forming a network of tubes and responding to endothelial-specific vasomodulators for vascular reactivity). This finding suggest that the EC machinery may be disrupted in 16p11.2 deletion syndrome. We investigated the transcriptional consequence of the 16p11.2 deletion on brain ECs. Interestingly, we identified upregulation of genes in 16p11.2-deficient ECs found in GO categories: blood circulation and vessel development. This is surprising considering the 16p11.2 deletion entails an haploinsufficiency of ~30 genes. Within these categories, we identified an upregulation of *Angpt2* in P50 brain ECs isolated from 16p11.2-deficient mice. This gene promotes vessel destabilization by weakening cell-cell interaction among ECs, a prerequisite for EC proliferation[322]. Thus, the upregulation of this gene may be responsible for the increase in vessel density in P50 16p11.2-deficient mice, and in turn returning to WT values. *Angpt2* was not upregulated at P14, the age we identified a delay in angiogenesis in 16p11.2-deficient mice. In addition, *Grem1* was upregulated in both P14 and P50 ECs. *Grem1* overexpression is associated with inhibition of angiogenesis, proliferation and migration[323].

Therefore, the upregulation of this gene may contribute to the delayed angiogenesis in P14 brain 16p11.2-deficient ECs. However, the opposite has also been suggested where knockdown of *Grem1* suppresses angiogenesis[324]. Further studies are required to unravel the involvement of *Grem1* in brain 16p11.2-deficient EC angiogenesis. While we identified endothelial alterations in 16p11.2 deletion, we next tackled the question of whether ECs can cell-autonomously contribute to 16p11.2 deletion-related phenotypes.

Remarkably, a mouse model comprising the 16p11.2 deletion specifically in ECs provided compelling evidence that ECs are significant contributors to ASD pathophysiology. This model presented with ASD-related behaviors (*i.e.* repetitive behaviors, motor coordination/learning alterations and hyperactivity), altered neuronal activity following electrocorticography measurements, and recapitulated vascular dysfunctions (*i.e.* altered hemodynamics, and early reduced angiogenesis) found in the 16p11.2 deletion syndrome mouse model. Thus, further highlighting ECs as being involved in 16p11.2 deletion pathophysiology. In addition, these findings show that early endothelial discrepancies translate into late-onset functional deficits. These results demonstrate that altered EC function during development will have a severe impact on later brain function and behavior.

While this study is a first of its kind, the outcomes of Manuscript I demonstrated the requirement for investigating brain vascular ECs in brain development, but also their involvement in disease progression and onset. It raises the question of whether neuronal alterations often described in ASD as being possible consequences of endothelial dysfunction or whether the vascular discrepancies are consequences of neuronal modifications. Our endothelial-specific 16p11.2 deletion model suggest that endothelial alterations at least contribute along with neurons to ASD phenotypes. To have a clearer understanding, a mouse model harboring the 16p11.2

deletion only in neurons would reveal whether similar phenotypes are identified. This model would also dissect the specific neuronal from endothelial contributions to 16p11.2 deletion phenotypes. However, this falls beyond the scope of this thesis.

Whether neurons are the primary drivers or are initially impacted by dysfunctional ECs is not known. Manuscript I, however, provided strong evidence that brain ECs are significant contributors to early brain development, and have a profound effect on phenotypes associated with ASD.

5.3. 16p11.2 deletion alters brain endothelial cell metabolism highlighting potential therapeutic targets

ASD are often depicted with an altered brain metabolism suggesting it is crucial to their pathophysiology. ASD are also characterized with dysregulated energy metabolism mostly attributed to dysfunctional mitochondria[275]. While brain ECs mediate entry of nutrients and glucose for brain metabolism, dysfunctional ECs may severely impact brain homeostasis. Given that Manuscript I demonstrated dysfunctional brain ECs in 16p11.2 deletion syndrome as well as a vascular link to ASD, it raised the question of the impact of the 16p11.2 deletion on brain EC machinery. With ASD mostly associated with mitochondrial discrepancies, we quantified mitochondria density in ECs isolated from 14 day old (P14) 16p11.2-deficient mice. Supporting the mitochondrial alterations in the literature[275], 16p11.2-deficient ECs were characterized with a reduced mitochondrial density *in vitro*. Interestingly, we recently demonstrated that adult 16p11.2-deficient ECs also presented with reduced mitochondrial density *in vivo*[325]. This suggests that early endothelial alterations are long lasting, and have a continuous impact on brain function. Indeed, the turnover rate for ECs is ~0.1% per day as opposed to other cell types (erythrocytes-65%,

neutrophils-18% and gastrointestinal epithelial cells-12%)[326]. Therefore ECs are long-lived suggesting they will carry early structural and functional impairments into aging. Notably, the reduced mitochondrial density in adult mice was attributed to reduced mitochondrial biogenesis[325]. However, this was not the case for P14 16p11.2-deficient ECs. We identified no change in mitochondrial dynamics (fission and fusion) as well as no change in a key regulator of mitochondrial biogenesis (PGC1α). Currently, it is unknown what is contributing to the reduced mitochondria in P14 16p11.2-deficient ECs. We can hypothesize that brain ECs from 16p11.2-deficient mice may have elevated mitophagy. Postmortem studies found that children and adolescents with ASD have excessive pro-apoptotic (p53, caspase-3 and cathepsin D) and decreased anti-apoptotic (Bcl-2) proteins on the mitochondrial membrane which may suggest increased mitophagy[327]. While the decreased mitochondrial density was slight in 16p11.2-deficient ECs, a recent study demonstrated that a minimal dose of one additional mitochondrion per cell could produce a 40% increase in levels of ATP[328]. Therefore, the reduced mitochondrial density in 16p11.2-deficient ECs can have an immense impact on EC metabolism, and in turn function. To determine whether this mitochondrial phenotype contributes to 16p11.2-associated EC dysfunction, further studies will have to be performed. For instance, performing mitochondrial delivery in 16p11.2-deficient ECs using microvesicles loaded with mitochondria could increase the number of mitochondria in 16p11.2-deficient ECs. 16p11.2-deficient brain ECs treated with microvesicles loaded with mitochondria can undergo functional assessment (*in vitro* tube formation assay) to determine if increased mitochondria will improve 16p11.2-deficient EC function. Previous evidence has demonstrated in human brain EC lines that microvesicles are a viable method to transfer mitochondria, and this method leads to an increased ATP production[329]. In addition, a second potential method to increase mitochondrial numbers in 16p11.2-deficient

ECs is through stimulation mitochondrial biogenesis via overexpression of PGC1α. PGC1α being a main regulator of mitochondrial biogenesis[330].

Considering that reduced mitochondria can significantly alter metabolism, we assessed brain endothelial metabolite profile to have an overview of the metabolic machinery of these cells. We demonstrated that 16p11.2-deficient ECs have a distinct metabolite profile compared to WT ECs. Although two cohorts were presented in this study with different abundance of metabolites, often due to batch effects commonly associated with metabolomics, both cohorts demonstrated the same result. ECs from 16p11.2-deficient mice have an overall reduction in metabolite abundance, and an extensive bioenergetic failure. The bioenergetic failure in 16p11.2-deficient ECs was classified by reduced ATP, UTP, GTP, CTP, adenylate energy charge and ATP-to-ADP ratio. These findings are in line with the literature associating ASD with dysregulated energy metabolism, including reduced ATP[278,279,282]. While the findings in the literature were not in the context of brain ECs in ASD, it suggested that the lack of energy in ECs could be contributing to ASD pathophysiology.

Despite the lack of ATP, AMPK activity, the internal sensor of ATP availability that is activated when ATP is decreased, was not different between 16p11.2-deficient and WT ECs. It is unknown why AMPK was not activated. As a possible explanation, AMP and ADP, regulators of AMPK, were not found at a different abundance in 16p11.2-deficient and WT ECs. Thus, AMP and ADP concentrations may not reach the threshold to induce activation of AMPK in 16p11.2-deficient ECs. The ratio of AMP-to-ATP is of importance for AMPK activation. Therefore, an increased level of AMP relative to ADP is required to activate AMPK[331]. We identified no difference between AMP and ADP levels in 16p11.2-deficient ECs, which can possibly explain the lack of AMPK activation despite the decreased ATP in 16p11.2-deficient ECs.

The 50% reduction of ATP in 16p11.2-deficient ECs was of interest, as ATP is the energy currency of the cell. One would expect that these cells were unhealthy. However, in Manuscript I, we demonstrated that 16p11.2-deficient ECs have normal migration, proliferation and apoptosis. Furthermore, in Manuscript II, we established no difference in the glutathione reduced-to-glutathione oxidized ratio between 16p11.2-deficient and WT ECs, an indicator of cellular health[332,333]. These findings suggested that the altered metabolite profile in 16p11.2-deficient ECs was not related to poor cellular health.

We further demonstrated that energy metabolism was dysregulated in 16p11.2-deficient ECs by the reduction of several metabolites that are essential for ATP generation. For instance, creatine was found to be reduced in 16p11.2-deficient ECs. Given that ATP was reduced, 16p11.2-deficient ECs may require other energy generating pathways to compensate for the lack of energy. Creatine is considered to have an important role in brain health and function. For example, in times of elevated energy requirement, creatine will generate ATP in the phosphocreatine system to support neuronal energy demands[334]. The lack of ATP could be exhausting creatine stores in the brain of 16p11.2-deficient ECs, and contributing to 16p11.2-deficient EC bioenergetic failure. Interestingly, creatine deficiency syndrome shares ASD-related characteristics such as developmental delay, intellectual disability, speech and language impairments as well as extrapyramidal movements[335]. Therefore, a lack of energy production in creatine deficiency syndrome may be contributing to the altered behaviors. As such, we can hypothesize that the bioenergetic failure is involved in 16p11.2 deletion phenotypes. Moreover, the dysregulated energy metabolism was supported by decreased metabolites important for the TCA cycle and glycolysis, including glutamine, aspartic acid and glutamic acid. These metabolites are required for energy producing pathways.

In 16p11.2-deficient ECs, we also identified reduced hexose and pyroxidine. The latter generates fuel such as glucose which will be needed for glycolysis to produce ATP[336]. Consequently, this demonstrates that energy producing pathways lack required fuels for ATP generation. Indeed, most metabolites which produce ATP or energy fuels for ATP producing pathways were found to be reduced in 16p11.2-deficient ECs. As we demonstrated that 16p11.2-deficient ECs were characterized with reduced ATP, we assessed mitochondrial function. It is well-known that mitochondria are the primary location for producing ATP. However, no difference in mitochondrial function was identified between 16p11.2-deficient and WT ECs following modulation of activity of the ETC. Surprisingly, ATP production was not altered in 16p11.2-deficient ECs. For this measure, it is important to note that the parameters in mitochondrial function (*i.e.* ATP production, proton leak, basal respiration, non-mitochondrial oxygen consumption and maximal respiration) represented the total value for each cell. Therefore, despite the reduced mitochondrial density, 16p11.2-deficient cells were able to sustain basal ATP levels. We can hypothesize that mitochondria in 16p11.2-deficient ECs may be more efficient in producing energy considering their reduced numbers. However, in times of a challenge (*i.e.* angiogenesis), we could suggest that: 1) 16p11.2-deficient ECs are not able to produce enough energy to support their elevated function, or 2) 16p11.2-deficient ECs require excessive energy to support their function. Interestingly, we previously demonstrated that endothelial dysfunction leads to compensatory altered brain metabolism in 16p11.2-deficient mice. Adult 16p11.2-deficient mice revealed an increased glucose uptake in the brain compared to WT mice as well as increased systemic energy expenditure, which could suggest elevated energy requirement to support the function of these mice[325,337].

Since the bioenergetic failure in 16p11.2-deficient ECs was central to the altered EC metabolism, we next targeted the decreased ATP in 16p11.2-deficient ECs. We provided ATP intracellularly via lipid nanoparticles as the reduced ATP was representative of intracellular ATP. Strikingly, intracellular delivery of ATP rescued angiogenic capacity of 16p11.2-deficient ECs *in vitro*. This finding supported the lack of energy (ATP) in 16p11.2-deficient ECs as being crucial for 16p11.2 deletion associated EC dysfunction. Notably, this response was only evident with a low concentration of intracellular ATP delivery (1mM), as increasing the concentration to 5mM did not improve angiogenic activity of 16p11.2-deficient ECs. Previous evidence has demonstrated that elevated ATP can activate the cellular danger response which entails changes in cellular metabolism, namely mitochondrial dysfunction[286]. Therefore elevated ATP concentration (5mM) via lipid nanoparticles may be activating this response. This underlining the need for awareness if ATP is to be used as a potential therapy. An ATP threshold will need to be established to understand at which concentration ATP activates the cellular danger response.

With ASD being associated with dysregulated energy discrepancies, an alternate diet has been suggested to increase ATP production and improve ASD-related behaviors[292]. For instance, a ketogenic diet can increase levels of ATP and mitochondrial biogenesis[292]. In an animal model of ASD, a ketogenic diet improved social exploration and social interaction[338]. These findings support the notion that energy metabolism is a possible contributor to ASD-related behaviors. While modifying diets of individuals with ASD is non-invasive, these individuals can be difficult eaters making this therapy difficult to maintain[294]. To our knowledge, there is no evidence of available diets specifically improving vascular function in ASD.

While ATP is the energy currency for cells, it also acts as a signaling molecule. For example, extracellular ATP can propagate calcium signals from the capillary level to larger arteries

to modulate vascular tone by acting on purinergic receptors[98]. We provided extracellular ATP to 16p11.2-deficient ECs to determine if ATP signaling contributed to 16p11.2-deficient EC phenotypes. Indeed, extracellular ATP rescued angiogenic capacity in 16p11.2-deficient ECs. Moreover, we demonstrated that the extracellular ATP rescue of 16p11.2-deficient ECs was dose-dependent. We identified a mild increase of network branches in 1μM and 10μM of ATP, while 100μM of ATP was the optimal concentration for rescuing network formation in 16p11.2-deficient ECs. We did not treat 16p11.2-deficient ECs with a higher concentration of ATP. This could be of interest to determine if excessive ATP (>100 μM) would activate the cellular danger response, and hinder the ability of 16p11.2-deficient ECs to form networks, as was observed following the treatment of 5mM ATP-LNPs in 16p11.2-deficient ECs.

While Manuscript II revealed that both intra- and extra-cellular ATP rescued 16p11.2-deficient angiogenic capacity, we further assessed the mechanism of this rescue. Brain ECs express ligand gated (P2X) and G-protein-coupled (P2Y) purinergic receptors. These receptors are triggered by ATP for activation of calcium signaling[339,340]. As extracellular ATP acts as a signaling molecule, we inhibited P2-class purinergic receptors using a non-selective P2 receptor antagonist (PPADs). The P2 receptor antagonist prevented the ATP-mediated rescue in 16p11.2-deficient ECs. Therefore, we can suggest that extracellular ATP acts on P2 purinergic receptors to establish its angiogenic rescue in 16p11.2-deficient ECs. Notably, we confirmed that the angiogenic rescue in 16p11.2-deficient ECs was ATP specific, as extracellular treatment of adenosine, hydrolysis product of ATP, did not increase *in vitro* network branching in 16p11.2-deficient ECs. It can be suggested that adenosine had no rescue effect compared to ATP due to the difference in energy availability between these two molecules. ATP entails three phosphate groups which are absent on adenosine. During phosphate group removal from ATP, energy is released, becoming ADP, AMP

and lastly adenosine[341]. As such, adenosine is more stable and contains less energy to be released compared to ATP. Thus, adenosine is not sufficient to rescue the bioenergetic failure in 16p11.2-deficient ECs. In addition, adenosine binds to P1-class purinergic receptors which are not targets of ATP [341]. We can suggest that P2-class receptors are essential for the ATP-mediated angiogenic rescue in 16p11.2-deficient ECs.

While intracellular ATP also rescued 16p11.2-deficient angiogenic capacity, we further determined if it established the angiogenic rescue in a similar manner as the extracellular ATP treatment. Brain ECs express pannexin-1 channels which release intracellular ATP from cells[98]. Of note, 16p11.2-deficient ECs and WT ECs both expressed pannexin-1 at a similar level. Interestingly, P2 antagonist treatment *in vitro* also prevented the intracellular ATP rescue in 16p11.2-deficient ECs. Therefore, ATP presumably exits the cell from pannexin-1 channels and acts on adjacent purinergic P2 receptors. Further investigation of the involvement of pannexin-1 in this response is needed. For instance, inhibiting pannexin-1 would determine whether ATP exits the cells via these channels. If that is the case, inhibition of pannexin-1 should prevent ATP from leaving the cell, leading to no activation of P2-class receptors, and in turn no rescue of 16p11.2-deficient ECs angiogenic capacity.

ATP activation of P2-class receptors induced intracellular calcium transients[342]. We identified reduced calcium transients in 16p11.2-deficient ECs following ATP treatment. This result being paradoxical as we would expect an increase in calcium signaling following ATP treatment in 16p11.2-deficient ECs; however, the opposite was observed. Further studies will be required to confirm the involvement of calcium signaling in the 16p11.2-deficient angiogenic rescue. If in absence of calcium, following the use of a calcium chelator, the rescue does not take place, it supports the involvement of calcium signaling in the ATP mediated 16p11.2-deficient

angiogenic rescue. Currently, it is not known how calcium responses take part in the rescue with ATP. However, the change in calcium transients in 16p11.2-deficient ECs suggested the possible involvement of calcium signaling in the ATP-mediated rescue. We can hypothesize that the reduced calcium transients in 16p11.2-deficient ECs may be related to the reduced mitochondrial density in 16p11.2-deficient ECs. Mitochondria are one of the major organelles regulating calcium signaling in conjunction with the endoplasmic reticulum[343]. Further studies are needed to confirm this relationship in 16p11.2-deficient ECs.

While we identified that ATP acts on P2 purinergic receptors, brain ECs express both P2 receptor subtypes (P2X and P2Y). Each subtype entail multiple isoforms. Brain ECs express all isoforms of P2X receptors and 4 of the 8 P2Y receptor isoforms (P2Y1, P2Y2, P2Y4, and P2Y14)[98,344]. Of note, there are discrepancies in the expression of P2Y receptors on brain ECs, however, the listed isoforms are the most commonly found P2Y isoforms in brain ECs. From our 16p11.2-deficient and WT EC RNA-sequencing database, we identified P2Y2 receptors as being overly expressed in 16p11.2-deficient ECs. In addition, P2Y2 is also known to play a crucial role in the vasculature by controlling vascular tone, angiogenesis and proliferation[345]. Wang and colleagues confirmed the role of P2Y2 receptors in vascular function by completing a conditional knockout of this receptor in mice. This mouse model exhibited dysregulated and increased vascular tone[346].

Given the involvement of P2Y2 for vascular function and its overexpression in 16p11.2-deficient ECs, we targeted P2Y2 using a specific agonist. This P2Y2 agonist, known as diquafosol tetrasodium (DQS), is clinically available for Dry Eye Syndrome in Japan and South Korea. Strikingly, treating 16p11.2-deficient ECs with DQS rescued their angiogenic capacity. We identified increased network tubes in 16p11.2-deficient ECs with DQS treatment compared to

16p11.2-deficient ECs without DQS. P2Y2 may establish its effect by altering calcium signaling, in turn activating angiogenesis in 16p11.2-deficient ECs. In the literature, overexpression of P2Y2 in ECs has been demonstrated to induce expression of proangiogenic molecules including CXCR4, CD34 and angiopoietin-2 (*Angpt2*). Elevated P2Y2 expression has also been associated with the phosphorylation of ERK1/2. Interestingly, the 16p11.2 locus entails *MapK3*, which is important for the MAPK/ERK signaling cascade to modulate angiogenesis[344]. Therefore, in 16p11.2-deficient ECs, activation of P2Y2 receptors may increase MAPK/ERK activity to compensate for *Mapk3* heterozygosity, and so stimulating angiogenesis. Future studies will need to determine if P2Y2 activation involves activation of the MAPK/ERK signaling cascade in 16p11.2-deficient ECs. Nevertheless, this finding suggest that P2Y2 is a potential specific target in the context of ASD pathophysiology, at least in 16p11.2 deletion syndrome. Moreover, to further strengthen the involvement of P2Y2 receptors in 16p11.2-deficient ECs, a selective P2Y2 antagonist could be used. If the P2Y2 antagonist abolishes the ATP or DQS mediated rescue, this would provide further support for the involvement of P2Y2 receptors in the 16p11.2-deficient angiogenic rescue. Of note, P2Y2 has also been of interest in cardiovascular disease. Treatment of newborn mouse cardiomyocytes with a P2Y2 agonist, MRS2768, prevented ischemic damage following myocardial infarct induction suggesting that P2Y2 activation has beneficial effects in disease states[347]. Taken together, we revealed a mechanism that rescued 16p11.2-deficient ECs phenotypes which entailed modulating ATP signaling through P2-class receptors. We identified a broad therapeutic target in brain EC for ASD such as energy metabolism as well as a specific therapeutic avenue through P2Y2 receptors.

While we specifically targeted ECs with P2Y2, the next steps are to determine what are the systemic effects of this approach and whether it will improve ASD-related behaviors. We have to

keep in mind that the systemic approach when targeting P2Y2 activation may also affect other cell types. For instance, astrocytes also express P2Y2 receptors. Activation of P2Y2 in astrocytes by ATP has been shown to increase calcium signaling to enable gliotransmission in the CNS[348]. Therefore, P2Y2 could entail a multicellular effect, if used as a target in ASD.

5.4. *Rock2* expression is a potential mechanism of interest in ASD

The 16p11.2 locus comprises genes which could contribute to the identified endothelial dysfunction in the 16p11.2 deletion mouse model. For instance, *Mapk3* gene is important for angiogenesis through activation of the MAPK/ERK pathway to increase expression of VEGF. *Maz1* is also required for the expression of VEGF and angiogenesis. Therefore, the reduced expression of these genes may be forefront in the reduced angiogenesis in 16p11.2-deficient ECs. *Mapk3* mutation in drosophila has been characterized with abnormal innervation of neurons and altered axonal morphology, as commonly found in ASD[349]. *Maz1*, to our knowledge, has not been independently associated with ASD-related phenotypes. Future studies, will have to perform single gene deletion of *MapK3* and *Maz1* to determine if these genes contribute independently to the 16p11.2 deletion endothelial phenotypes.

In addition, a gene of interest in the 16p11.2 locus is *Kctd13*. This gene has been implicated as a major driver of neurological disorders. Reduced *Kctd13* expression is associated with elevated RhoA levels which is linked with disease pathogenesis[309]. RhoA involves the activation of Rho-associated coiled-coil containing protein kinases (ROCK). The activation of RhoA/ROCK pathway leads to changes in the cytoskeleton, cell migration and apoptosis[350,351]. Inhibition of ROCK2, the isoform mostly expressed in the brain and vasculature, has been shown to have beneficial vascular effects by increasing vascular stability. Considering the involvement of

ROCK2 in the vasculature and decreased expression of *Kctd13* in 16p11.2 deletion, we generated a mouse model of 16p11.2 deletion with *Rock2* heterozygosity in Manuscript III. Developmental *Rock2* heterozygosity improved angiogenic capacity (*in vitro*) and rescued recognition memory in 16p11.2-deficient ECs and mice, respectively. The improved cognitive behavior in Manuscript III was consistent with a model of 16p11.2 deletion syndrome in which pharmacological inhibition of ROCK by *Fasudil* rescued recognition memory[352]. Furthermore, Lorenzo and colleagues, demonstrated that a mouse model of *Kctd13* deletion had similar cognitive impairments, as found in 16p11.2-deficient mice, which were also rescued with ROCK inhibition[352]. This suggest that *Kctd13* may independently, at least partially, contribute to 16p11.2 deletion phenotypes.

Manuscript III has the additional component of modulating *Rock2* expression during development. Therefore, having an effect during key developmental processes including angiogenesis and neurogenesis. This brings into question the treatment window for ASD, especially if individuals have a high familial risk. However, this may be very difficult to manage as ASD can also be idiopathic, and a diagnosis is only made once symptoms emerge.

While *Rock2* heterozygosity improved angiogenic capacity of 16p11.2-deficient ECs, it was not as effective as treatment with a P2Y2 agonist and ATP. P2Y2 treatment may be more direct in treating the bioenergetic failure in 16p11.2-deficient ECs as this is at the core of endothelial dysfunction in 16p11.2 deletion syndrome. The P2Y2 agonist may directly replace the lack of ATP signaling that is required to maintain EC function. Conversely, *Rock2* heterozygosity may induce cytoskeletal reorganisation and cell motility in 16p11.2-deficient ECs to form networks *in vitro*, rather than directly target the lack of ATP signaling in 16p11.2-deficient ECs. Furthermore, elevated RhoA has been linked with impaired angiogenesis in cell lines of cerebral cavernous malformations. In this study, they demonstrated that *Rock2* knockdown rescued tube

formation in this model[353]. This falls in line with our findings and supports the involvement of *Rock2* heterozygosity in improving 16p11.2-deficient endothelial dysfunctions. Further research is required to understand the rescue mechanism following the reduced *Rock2* expression in 16p11.2-deficient ECs. Moreover, considering that reduced expression of *Kctd13* can lead to similar phenotypes as found in 16p11.2 deletion syndrome, the contributions (if any) of *Kctd13* heterozygosity to vascular phenotypes in 16p11.2 deletion warrants further investigation.

Given that ASD are characterized by a multitude of symptoms with a variability in the severity of symptom presentation, a multiangled approach may be needed to improve ASD pathophysiology. The already available treatments for ASD mostly target neuronal functions such as NMDA receptors (memantine), and neurotransmission (methylphenidate) to modulate ASD-behaviors (repetitive movements and cognition)[354]. However, these treatments are not always effective in improving ASD-related symptoms. Therefore, these approaches may require to be coupled with a vascular target such as a P2Y2 agonist or even a ROCK2 inhibitor to have a multifaceted effect.

5.5. Sex-related differences in the cerebrovasculature and ASD

Sex-specific differences are known in cerebrovascular biology[355]. The presence of steroid hormones have a strong effect on cerebral blood flow. Women tend to be associated with increased rate of perfusion at baseline as well as higher perfusion during cognitive activity compared to men [356,357]. Estrogen stimulates production and increases sensitivity to vasodilatory factors including K^+ induced vasodilation, NO and prostacyclin[358]. In addition, estrogen affects proteins such as caveolin-1, an endothelial scaffolding protein that anchors eNOS and increases expression of calmodulin. Activation of estrogen receptors via estrogen also shifts the prostanoid balance

towards vasodilator prostacyclin[358]. Testosterone, on the other hand, has a more vasoconstrictive effect by shifting the prostanoid balance towards vasoconstrictive thromboxane[356,359]. Interestingly, steroid hormones may modulate cerebrovascular reactivity by acting on endothelial mechanisms. For example, denuded endothelium of cerebral arteries from intact, gonadectomized and hormone-treated (estrogen and testosterone) animals exhibited no difference in vascular tone[360,361].

While Manuscripts II and III are focused on male 16p11.2-deficient and wild-type mice, Manuscript I did allude to sex-differences in the 16p11.2 deletion syndrome mouse model. In Manuscript I, we identified mostly male-specific differences in activity dependent regulation of cerebral blood flow, baseline cerebral blood flow and neuronal activity, vascular density *in vivo* when comparing 16p11.2-deficient and wild-type mice. This being the reasoning for the male-based investigation in Manuscripts II and III. While we showed sex-differences during behavioral assessment of 16p11.2 deficient mice, the direct causes of these differences are yet to be determined.

Furthermore, ASD have a strong male bias, where males are found to be 4 times more affected than females[217]. The mechanisms accounting for these differences are not known. However, there are theories that are starting to emerge to possibly explain these differences. The two theories for the sex bias in ASD are: 1) females require an increased genetic burden to present with symptoms of ASD, and 2) estrogen is considered to be protective against ASD[362-364]. Female cases of ASD are often associated with excessive deleterious copy number variations which disrupts more genes compared to mutations found in males. In example, certain sex chromosome genes are risk factors for ASD such as *Fmr1*, *MeCP2*, neuroligins 3 and 4 which are found on chromosome X[365]. In this case, it is suggested that both chromosome X would have to be affected

for females to have severe phenotypes. Males on the other hand, only carry one chromosome X, thus requiring less genetic burden for symptoms and insinuating a higher risk of ASD diagnosis. Moreover, estrogen is also associated with protective effects as it mediates neurodevelopment plasticity, cerebral blood flow and synaptic structure[364]. Postmortem brain samples from ASD and control individuals revealed that estrogen receptor protein levels are lower in ASD brains compared to sex-matched controls[364]. Therefore, level of steroid hormones could impact ASD characteristics. The differences identified in Manuscript I could be directly related to steroid hormones modulation; however, we have not confirmed this connection.

Finally, the diagnostic strategy for ASD also has a sex-specific bias. Often ASD are diagnosed based on the presence of behaviors and the diagnosis criteria are geared towards boys. Males with ASD present with more externalizing behaviors including aggressive behavior, hyperactivity, reduced sociability and increased stereotypic behaviors and interests[366]. These are considered as being the core behaviors associated with ASD. However, females with ASD, while they can present with similar behaviors but to a lesser extent, show greater internalizing symptoms such as anxiety and depression[366]. The difference in presentation of symptoms could be explained by changes in steroid hormones, however this is not known. Female presentation of ASD as well as its link to the cerebrovasculature are fields of research in need of more attention to understand the mechanisms leading to the observed differences.

5.6. Limitations and future directions

This work provided extensive findings on the contribution of the brain vasculature to ASD. However, the studies described in this thesis also present with limitations. First, a mouse model of 16p11.2 deletion syndrome was used to depict a syndrome of ASD. Although this model

recapitulated several characteristics identified in the human 16p11.2 deletion syndrome including ASD-related behavior, murine models cannot fully replicate human conditions. Given this, human induced endothelial cells from 16p11.2 deletion carriers were incorporated in Manuscript I to translate our findings to the human condition. Importantly, 16p11.2 deletion hiECs reiterated the findings identified in the 16p11.2 deletion mouse model. Second, the findings in Manuscript II were obtained *in vitro.* While this work provided an important first step in identifying the contributors to the 16p11.2 deletion endothelial phenotypes and a rescue strategy for 16p11.2 deletion associated endothelial cell dysfunction, future studies will be needed to validate these findings *in vivo*. To further strengthen this work, future studies could inject diquafosol tetrasodium, a P2Y2 agonist, in 16p11.2-deficient mice to determine if this compound will ameliorate ASD-related behaviors, cerebrovascular function and structure *in vivo*. In addition, this assessment can be repeated in the endothelial-specific 16p11.2 deletion mouse model. Third, function of 16p11.2-deficient ECs in this thesis was mainly assessed using the tube formation assay. This assay allows for short-term assessment of angiogenesis. At 24 hours post-seeding, branches will start to collapse due to the lack of available trophic support. Investigation of long-term or maintained angiogenic ability in 16p11.2-deficient ECs following ATP treatment would be an interesting avenue of research as it would allow to determine the extent of the ATP-mediated rescue of 16p11.2-deletion EC phenotypes. Fourth, future work will need to determine if ROCK2 heterozygosity in 16p11.2-deficient mice also improves *in vivo* phenotypes associated with the 16p11.2 deletion including altered cerebrovascular function and structure. Moreover, generating a mouse model with an endothelial-specific ROCK2 knockout would provide an additional understanding of the rescue limitations of ROCK2 heterozygosity on 16p11.2 deletion endothelial phenotypes. Fifth and lastly, this thesis identified two distinct players for improving 16p11.2 deletion associated phenotypes.

However, additional studies are required to determine if these two pathways are overlapping. While elevated RhoA levels have been associated with modulating the activity of pannexin-1 channels for ATP release of cells[367], the question remains if this relates to the reduced intracellular ATP identified in 16p11.2-deficient ECs. A main goal of this thesis was to determine whether the brain vasculature contributes to ASD. This thesis was successful in meeting this goal and therefore, provides a strong rational for the future study of the brain vasculature in neurodevelopmental disorders.

5.7. Concluding remarks

This thesis seeks to address critical gaps of knowledge surrounding the cerebrovascular contributions to ASD. We are first to establish a vascular link to ASD including the association of 16p11.2 deletion syndrome with endothelial dysfunctions. We revealed that dysfunctional ECs can cell-autonomously contribute to 16p11.2 deletion phenotypes. Furthermore, we showed that the 16p11.2-deficient endothelium is characterized with an bioenergetic failure. Targeting P2-class purinergic receptors, specifically P2Y2 receptors, rescued the angiogenic capacity of 16p11.2-deficient ECs. We further identified modulation of *Rock2* expression as a potential pathway to target in ASD. Altogether, this work provided an important first step in identifying novel vascular aspects and potential vascular targets in ASD. Future work will be needed to unravel the downstream impact of targeting P2-class purinergic receptors in ECs as well as the long-term impact of vascular discrepancies in ASD. Furthermore, this thesis should encourage the need to complete a full vascular assessment on other mutations associated with ASD to determine the commonality of these vascular alterations. As ASD incidences are on the rise, exploring novel avenues represents an urgent need. The research in this thesis is an essential prerequisite for

developing novel diagnostics and therapeutics that is desperately needed for patients and caregivers. Taken together, assessing the cerebrovasculature as opposed to neuronal networks is a much needed paradigm shift to have a more complete understanding of ASD pathogenesis.

References

1 Watts, M. E., Pocock, R. & Claudianos, C. Brain Energy and Oxygen Metabolism: Emerging Role in Normal Function and Disease. *Front Mol Neurosci* **11**, 216 (2018). https://doi.org:10.3389/fnmol.2018.00216

2 Attwell, D. *et al.* Glial and neuronal control of brain blood flow. *Nature* **468**, 232-243 (2010). https://doi.org:10.1038/nature09613

3 Attwell, D. a. & Laughlin, S. An Energy Budget for Signaling in the Grey Matter of the Brain. *Journal of Cerebral Blood Flow and Metabolism* **21**, 1133-1145 (2001).

4 Girouard, H. & Iadecola, C. Neurovascular coupling in the normal brain and in hypertension, stroke, and Alzheimer disease. *J Appl Physiol (1985)* **100**, 328-335 (2006). https://doi.org:10.1152/japplphysiol.00966.2005

5 Wong, A. D. *et al.* The blood-brain barrier: an engineering perspective. *Front Neuroeng* **6**, 7 (2013). https://doi.org:10.3389/fneng.2013.00007

6 Sweeney, M. D., Kisler, K., Montagne, A., Toga, A. W. & Zlokovic, B. V. The role of brain vasculature in neurodegenerative disorders. *Nat Neurosci* **21**, 1318-1331 (2018). https://doi.org:10.1038/s41593-018-0234-x

7 Ouellette, J. & Lacoste, B. From Neurodevelopmental to Neurodegenerative Disorders: The Vascular Continuum. *Front Aging Neurosci* **13**, 749026 (2021). https://doi.org:10.3389/fnagi.2021.749026

8 Andreone, B. J., Lacoste, B. & Gu, C. Neuronal and vascular interactions. *Annu Rev Neurosci* **38**, 25-46 (2015). https://doi.org:10.1146/annurev-neuro-071714-033835

9 Lacoste, B. & Gu, C. Control of cerebrovascular patterning by neural activity during postnatal development. *Mech Dev* **138 Pt 1**, 43-49 (2015). https://doi.org:10.1016/j.mod.2015.06.003

10 Camandola, S. & Mattson, M. P. Brain metabolism in health, aging, and neurodegeneration. *EMBO J* **36**, 1474-1492 (2017). https://doi.org:10.15252/embj.201695810

11 Grubb, S., Lauritzen, M. & Aalkjaer, C. Brain capillary pericytes and neurovascular coupling. *Comp Biochem Physiol A Mol Integr Physiol* **254**, 110893 (2021). https://doi.org:10.1016/j.cbpa.2020.110893

12 Hamel, E. Perivascular nerves and the regulation of cerebrovascular tone. *J Appl Physiol (1985)* **100**, 1059-1064 (2006). https://doi.org:10.1152/japplphysiol.00954.2005

13 Kaplan, L., Chow, B. W. & Gu, C. Neuronal regulation of the blood-brain barrier and neurovascular coupling. *Nat Rev Neurosci* **21**, 416-432 (2020). https://doi.org:10.1038/s41583-020-0322-2

14 Lecrux, C. & Hamel, E. The neurovascular unit in brain function and disease. *Acta Physiol (Oxf)* **203**, 47-59 (2011). https://doi.org:10.1111/j.1748-1716.2011.02256.x

15 Hillman, E. M. Coupling mechanism and significance of the BOLD signal: a status report. *Annu Rev Neurosci* **37**, 161-181 (2014). https://doi.org:10.1146/annurev-neuro-071013-014111

16 Huneau, C., Benali, H. & Chabriat, H. Investigating Human Neurovascular Coupling Using Functional Neuroimaging: A Critical Review of Dynamic Models. *Frontiers in Neuroscience* **9** (2015).

17 Bell, A. H., Miller, S. L., Castillo-Melendez, M. & Malhotra, A. The Neurovascular Unit: Effects of Brain Insults During the Perinatal Period. *Front Neurosci* **13**, 1452 (2019). https://doi.org:10.3389/fnins.2019.01452

18 Iadecola, C. Regulation of the cerebral microcirculation during neural activity: is nitric oxide the missing link? *Trends in Neurosciences* **16**, 206-214 (1993). https://doi.org:doi.org/10.1016/0166-2236(93)90156-G

19 Freygang, W. H. & Sokoloff, L. Quantitative Measurement of Regional Circulation in the Central Nervous System by the use of Radioactive Inert Gas. *Advances in biological and medical physics* **6**, 263-279 (1959). https://doi.org:doi.org/10.1016/B978-1-4832-3112-9.50011-6

20 Chaigneau, E., Oheim, M., Audinat, E. & Charpak, S. Two-photon imaging of capillary blood flow in olfactory bulb glomeruli. *PNAS* **100**, 13081-13086 (2003). https://doi.org:10.1073/pnas.2133652100

21 Yamada, H. *et al.* A milestone for normal development of the infantile brain detected by functional MRI. *Neurology* **55**, 218-223 (2000).

22 Kozberg, M. G., Ma, Y., Shaik, M. A., Kim, S. H. & Hillman, E. M. Rapid Postnatal Expansion of Neural Networks Occurs in an Environment of Altered Neurovascular and Neurometabolic Coupling. *J Neurosci* **36**, 6704-6717 (2016). https://doi.org:10.1523/JNEUROSCI.2363-15.2016

23 Costa, E. D., Rezende, B. A., Cortes, S. F. & Lemos, V. S. Neuronal Nitric Oxide Synthase in Vascular Physiology and Diseases. *Front Physiol* **7**, 206 (2016). https://doi.org:10.3389/fphys.2016.00206

24 Vaucher, E., Tong, X.-K., Cholet, N., Lantin, S. & Hamel, E. GABA neurons provide a rich input to microvessels but not nitric oxide neurons in the rat cerebral cortex: a means for direct regulation of local cerebral blood flow. *Journal of comparative neurology* **421**, 161-171 (2000). https://doi.org:doi.org/10.1002/(SICI)1096-9861(20000529)421:2<161::AID-CNE3>3.0.CO;2-F

25 Yamada, M. *et al.* Cholinergic dilation of cerebral blood vessels is abolished in M5 muscarinic acetylcholine receptor knockout mice. *PNAS* **98**, 14096-14101 (2001). https://doi.org:doi10.1073pnas.251542998

26 Ko, K. R., Ngai, A. C. & Winn, H. R. Role of adenosine in regulation of regional cerebral blood flow in sensory cortex. *American Journal of Physiology* **259**, H1703-1708 (1990). https://doi.org:10.1152/ajpheart.1990.259.6.H1703.

27 Muoio, V., Persson, P. B. & Sendeski, M. M. The neurovascular unit-concept review. *Acta Physiol (Oxf)* **210**, 790-798 (2014). https://doi.org:doi.org/10.1111/apha.12250

28 Fahrenkrug, J. Transmitter role of vasoactive intestinal peptide. *Pharmacology & Toxicology* **72**, 344-406 (1993). https://doi.org:doi.org/10.1111/j.1600-0773.1993.tb01344.x

29 Carmeliet, P. & Jain, R. K. Molecular mechanisms and clinical applications of angiogenesis. *Nat Review* **473**, 298-307 (2011). https://doi.org:10.1038/nature10144REVIEWDLL4

30 Rizzo, M. T. & Leaver, H. A. Brain endothelial cell death: modes, signaling pathways, and relevance to neural development, homeostasis, and disease. *Mol Neurobiol* **42**, 52-63 (2010). https://doi.org:10.1007/s12035-010-8132-6

31 Grasman, J. M. & Kaplan, D. L. Human endothelial cells secrete neurotropic factors to direct axonal growth of peripheral nerves. *Sci Rep* **7**, 4092 (2017). https://doi.org:10.1038/s41598-017-04460-8

32 Lacoste, B., Prat, A., Freitas-Andrade, M. & Gu, C. The Blood-Brain Barrier: Composition, Properties, and Roles in Brain Health. *Cold Spring Harb Perspect Biol.* (2024). https://doi.org:10.1101/cshperspect.a041422
33 Cauli, B. H., E. Revisiting the role of neurons in neurovascular coupling. *frontiers in neuroenergetics* **2** (2010). https://doi.org:10.3389/fnene.2010.00009
34 Vasile, F., Dossi, E. & Rouach, N. Human astrocytes: structure and functions in the healthy brain. *Brain Struct Funct* **222**, 2017-2029 (2017). https://doi.org:10.1007/s00429-017-1383-5
35 Oberheim, N. A., Goldman, S. A. & Nedergaard, M. Heterogeneity of astrocytic form and function. *Methods Mol Biol* **814**, 23-45 (2012). https://doi.org:10.1007/978-1-61779-452-0_3
36 Ransom, B. R. & Ransom, C. B. Astrocytes: Multitalented Stars of the Central Nervous System. *Methods Mol Biol* **814**, 3-7 (2011). https://doi.org:doi.org/10.1007/978-1-61779-452-0_1
37 Benarroch, E. E. Neuron-astrocyte interactions: partnership for normal function and disease in the central nervous system. *Mayo Clin Proc* **80**, 1326-1338 (2005). https://doi.org:10.4065/80.10.1326
38 Abbott, N. J., Ronnback, L. & Hansson, E. Astrocyte-endothelial interactions at the blood-brain barrier. *Nat Rev Neurosci* **7**, 41-53 (2006). https://doi.org:10.1038/nrn1824
39 Iadecola, C. & Nedergaard, M. Glial regulation of the cerebral microvasculature. *Nat Neurosci* **10**, 1369-1376 (2007). https://doi.org:10.1038/nn2003
40 Takano, T. *et al.* Astrocyte-mediated control of cerebral blood flow. *Nat Neurosci* **9**, 260-267 (2006). https://doi.org:10.1038/nn1623
41 Matsui, T. *et al.* Astrocytic glycogen-derived lactate fuels the brain during exhaustive exercise to maintain endurance capacity. *Proc Natl Acad Sci U S A* **114**, 6358-6363 (2017). https://doi.org:10.1073/pnas.1702739114
42 Mahmoud, S., Gharagozloo, M., Simard, C. & Gris, D. Astrocytes Maintain Glutamate Homeostasis in the CNS by Controlling the Balance between Glutamate Uptake and Release. *Cells* **8** (2019). https://doi.org:10.3390/cells8020184
43 Francesca, B. & Rezzani, R. Aquaporin and blood brain barrier. *Current Neuropharmacology* **8**, 92-96 (2010). https://doi.org:10.2174/157015910791233132
44 Zhao, Y., Xin, Y., He, Z. & Hu, W. Function of Connexins in the Interaction between Glial and Vascular Cells in the Central Nervous System and Related Neurological Diseases. *Neural Plast* **2018**, 6323901 (2018). https://doi.org:10.1155/2018/6323901
45 Menezes, M. J. *et al.* The extracellular matrix protein laminin alpha2 regulates the maturation and function of the blood-brain barrier. *J Neurosci* **34**, 15260-15280 (2014). https://doi.org:10.1523/JNEUROSCI.3678-13.2014
46 Cabezas, R. *et al.* Astrocytic modulation of blood brain barrier: perspectives on Parkinson's disease. *Front Cell Neurosci* **8**, 211 (2014). https://doi.org:10.3389/fncel.2014.00211
47 Liu, S. & Lin, Z. Vascular Smooth Muscle Cells Mechanosensitive Regulators and Vascular Remodeling. *J Vasc Res* **59**, 90-113 (2022). https://doi.org:10.1159/000519845
48 Hayes, G. *et al.* Vascular smooth muscle cell dysfunction in neurodegeneration. *Front Neurosci* **16**, 1010164 (2022). https://doi.org:10.3389/fnins.2022.1010164
49 Retailleau, K. *et al.* Piezo1 in Smooth Muscle Cells Is Involved in Hypertension-Dependent Arterial Remodeling. *Cell Rep* **13**, 1161-1171 (2015). https://doi.org:10.1016/j.celrep.2015.09.072

50 Amberg, G. C. & Navedo, M. F. Calcium dynamics in vascular smooth muscle. *Microcirculation* **20**, 281-289 (2013). https://doi.org:10.1111/micc.12046
51 Sweeney, M. D., Ayyadurai, S. & Zlokovic, B. V. Pericytes of the neurovascular unit: key functions and signaling pathways. *Nat Neurosci* **19**, 771-783 (2016). https://doi.org:10.1038/nn.4288
52 Bell, R. D. *et al.* Pericytes control key neurovascular functions and neuronal phenotype in the adult brain and during brain aging. *Neuron* **68**, 409-427 (2010). https://doi.org:10.1016/j.neuron.2010.09.043
53 Armulik, A. *et al.* Pericytes regulate the blood-brain barrier. *Nature* **468**, 557-561 (2010). https://doi.org:10.1038/nature09522
54 Daneman, R., Zhou, L., Kebede, A. A. & Barres, B. A. Pericytes are required for blood-brain barrier integrity during embryogenesis. *Nature* **468**, 562-566 (2010). https://doi.org:10.1038/nature09513
55 Ben-Zvi, A. *et al.* Mfsd2a is critical for the formation and function of the blood-brain barrier. *Nature* **509**, 507-511 (2014). https://doi.org:10.1038/nature13324
56 Mae, M. A. *et al.* Single-Cell Analysis of Blood-Brain Barrier Response to Pericyte Loss. *Circ Res* **128**, e46-e62 (2021). https://doi.org:10.1161/CIRCRESAHA.120.317473
57 Winkler, E. A., Bell, R. D. & Zlokovic, B. V. Central nervous system pericytes in health and disease. *Nat Neurosci* **14**, 1398-1405 (2011). https://doi.org:10.1038/nn.2946
58 Mishra, A. *et al.* Astrocytes mediate neurovascular signaling to capillary pericytes but not to arterioles. *Nat Neurosci* **19**, 1619-1627 (2016). https://doi.org:10.1038/nn.4428
59 Kisler, K., Nelson, A. R., Montagne, A. & Zlokovic, B. V. Cerebral blood flow regulation and neurovascular dysfunction in Alzheimer disease. *Nat Rev Neurosci* **18**, 419-434 (2017). https://doi.org:10.1038/nrn.2017.48
60 Alarcon-Martinez, L. *et al.* Capillary pericytes express alpha-smooth muscle actin, which requires prevention of filamentous-actin depolymerization for detection. *Elife* **7** (2018). https://doi.org:10.7554/eLife.34861
61 Attwell, D., Mishra, A., Hall, C. N., O'Farrell, F. M. & Dalkara, T. What is a pericyte? *J Cereb Blood Flow Metab* **36**, 451-455 (2016). https://doi.org:10.1177/0271678X15610340
62 Krueger, M. & Bechmann, I. CNS pericytes: Concepts, misconceptions, and a way out. *Glia* **58**, 1-10 (2010). https://doi.org:doi.org/10.1002/glia.20898
63 Armulik, A., Genove, G. & Betsholtz, C. Pericytes: developmental, physiological, and pathological perspectives, problems, and promises. *Dev Cell* **21**, 193-215 (2011). https://doi.org:10.1016/j.devcel.2011.07.001
64 Ribatti, D., Nico, B. & Crivellato, E. The role of pericytes in angiogenesis. *Int J Dev Biol* **55**, 261-268 (2011). https://doi.org:10.1387/ijdb.103167dr
65 Bergers, G. & Song, S. The role of pericytes in blood-vessel formation and maintenance. *Neuro Oncol* **7**, 452-464 (2005). https://doi.org:10.1215/S1152851705000232
66 Eilken, H. M. *et al.* Pericytes regulate VEGF-induced endothelial sprouting through VEGFR1. *Nat Commun* **8**, 1574 (2017). https://doi.org:10.1038/s41467-017-01738-3
67 Tang, M. *et al.* An early endothelial cell-specific requirement for Glut1 is revealed in Glut1 deficiency syndrome model mice. *JCI Insight* **6** (2021). https://doi.org:10.1172/jci.insight.145789
68 Betz, A. L. & Goldstein, G. W. Polarity of the Blood-Brain Barrier: Neutral Amino Acid Transport into Isolated Brain Capillaries. *Science* **202**, 225-227 (1978). https://doi.org:10.1126/science.211586

69 Salmon, A. H. & Satchell, S. C. Endothelial glycocalyx dysfunction in disease: albuminuria and increased microvascular permeability. *J Pathol* **226**, 562-574 (2012). https://doi.org:10.1002/path.3964
70 Ushiyama, A., Kataoka, H. & Iijima, T. Glycocalyx and its involvement in clinical pathophysiologies. *J Intensive Care* **4**, 59 (2016). https://doi.org:10.1186/s40560-016-0182-z
71 Thomsen, M. S., Routhe, L. J. & Moos, T. The vascular basement membrane in the healthy and pathological brain. *J Cereb Blood Flow Metab* **37**, 3300-3317 (2017). https://doi.org:10.1177/0271678X17722436
72 Weiss, N., Miller, F., Cazaubon, S. & Couraud, P. O. The blood-brain barrier in brain homeostasis and neurological diseases. *Biochim Biophys Acta* **1788**, 842-857 (2009). https://doi.org:10.1016/j.bbamem.2008.10.022
73 Larsen, J., Martin, D. R. & Byrne, M. Recent Advances in Delivery Through the Blood-Brain Barrier. *Current Topics in Medicinal Chemistry* **14** (2014). https://doi.org:10.2174/1568026614666140329230311
74 Daneman, R. & Prat, A. The blood-brain barrier. *Cold Spring Harb Perspect Biol* **7**, a020412 (2015). https://doi.org:10.1101/cshperspect.a020412
75 Van Dyken, P. & Lacoste, B. Impact of Metabolic Syndrome on Neuroinflammation and the Blood–Brain Barrier. *Frontiers in Neuroscience* **12** (2018). https://doi.org:10.3389/fnins.2018.00930
76 Caja, S. & Enriquez, J. A. Mitochondria in endothelial cells: Sensors and integrators of environmental cues. *Redox Biol* **12**, 821-827 (2017). https://doi.org:10.1016/j.redox.2017.04.021
77 Wei, H. *et al.* Vascular endothelial cells: a fundamental approach for brain waste clearance. *Brain* **146**, 1299-1315 (2023). https://doi.org:10.1093/brain/awac495
78 Kadry, H., Noorani, B. & Cucullo, L. A blood-brain barrier overview on structure, function, impairment, and biomarkers of integrity. *Fluids Barriers CNS* **17**, 69 (2020). https://doi.org:10.1186/s12987-020-00230-3
79 Van Itallie, C. M., Fanning, A. S., Bridges, A. & Anderson, J. M. ZO-1 Stabilizes the Tight Junction Solute Barrier through Coupling to the Perijunctional Cytoskeleton. *Molecular biology of the cell* **20**, 3930-3940 (2009). https://doi.org:10.1091/mbc.E09-04-0320
80 Siegenthaler, J. A., Sohet, F. & Daneman, R. 'Sealing off the CNS': cellular and molecular regulation of blood-brain barriergenesis. *Curr Opin Neurobiol* **23**, 1057-1064 (2013). https://doi.org:10.1016/j.conb.2013.06.006
81 Stamatovic, S. M., Johnson, A. M., Keep, R. F. & Andjelkovic, A. V. Junctional proteins of the blood-brain barrier: New insights into function and dysfunction. *Tissue Barriers* **4**, e1154641 (2016). https://doi.org:10.1080/21688370.2016.1154641
82 Jaishankar, D. *et al.* Connexins in endothelial cells as a therapeutic target for solid organ transplantation. *Am J Transplant* **22**, 2502-2508 (2022). https://doi.org:10.1111/ajt.17104
83 Zlokovic, B. V. The blood-brain barrier in health and chronic neurodegenerative disorders. *Neuron* **57**, 178-201 (2008). https://doi.org:10.1016/j.neuron.2008.01.003
84 Taslimifar, M., Buoso, S., Verrey, F. & Kurtcuoglu, V. Functional Polarity of Microvascular Brain Endothelial Cells Supported by Neurovascular Unit Computational Model of Large Neutral Amino Acid Homeostasis. *Front Physiol* **9**, 171 (2018). https://doi.org:10.3389/fphys.2018.00171

85 O'Kane, R. L. & Hawkins, R. A. Na+-dependent transport of large neutral amino acids occurs at the abluminal membrane of the blood-brain barrier. *American Journal of Physiology* **285** (2003). https://doi.org:doi.org/10.1152/ajpendo.00193.2003
86 Engelhardt, B. & Ransohoff, R. M. Capture, crawl, cross: the T cell code to breach the blood–brain barriers. *Trends in immunology* **33**, 579-589 (2012). https://doi.org:doi.org/10.1016/j.it.2012.07.004
87 Wu, J. Y. & Prentice, H. Role of taurine in the central nervous system. *J Biomed Sci* **17 Suppl 1**, S1 (2010). https://doi.org:10.1186/1423-0127-17-S1-S1
88 Loscher, W. & Potschka, H. Drug resistance in brain diseases and the role of drug efflux transporters. *Nat Rev Neurosci* **6**, 591-602 (2005). https://doi.org:10.1038/nrn1728
89 Qosa, H. *et al.* Transporters as Drug Targets in Neurological Diseases. *Clin Pharmacol Ther* **100**, 441-453 (2016). https://doi.org:10.1002/cpt.435
90 Daneman, R. *et al.* Wnt/ -catenin signaling is required for CNS, but not non-CNS, angiogenesis. *PNAS* **106**, 641-646 (2009).
91 Alvarez, J. I. *et al.* The Hedgehog Pathway Promotes Blood-Brain Barrier Integrity and CNS Immune Quiescence. *Science* **334**, 1727-1731 (2011). https://doi.org:10.1126/science.1206936
92 Ainslie, P. N. & Ogoh, S. Regulation of cerebral blood flow in mammals during chronic hypoxia: a matter of balance. *Exp Physiol* **95**, 251-262 (2010). https://doi.org:10.1113/expphysiol.2008.045575
93 Busse, R. *et al.* EDHF: bringing the concepts together. *Trends in Pharmacological Sciences* **23**, 374-380 (2002). https://doi.org:doi.org/10.1016/S0165-6147(02)02050-3
94 Serhan, C. N. Pro-resolving lipid mediators are leads for resolution physiology. *Nature* **510**, 92-101 (2014). https://doi.org:10.1038/nature13479
95 Choi, S. H., Aid, S. & Bosetti, F. The distinct roles of cyclooxygenase-1 and -2 in neuroinflammation: implications for translational research. *Trends Pharmacol Sci* **30**, 174-181 (2009). https://doi.org:10.1016/j.tips.2009.01.002
96 Dhaun, N. & Webb, D. J. Endothelins in cardiovascular biology and therapeutics. *Nat Rev Cardiol* **16**, 491-502 (2019). https://doi.org:10.1038/s41569-019-0176-3
97 Chatterjee, S. & Fisher, A. B. Mechanotransduction: forces, sensors, and redox signaling. *Antioxid Redox Signal* **20**, 868-871 (2014). https://doi.org:10.1089/ars.2013.5753
98 Thakore, P. *et al.* Brain endothelial cell TRPA1 channels initiate neurovascular coupling. *Elife* **10** (2021). https://doi.org:10.7554/eLife.63040
99 Iadecola, C. Neurovascular regulation in the normal brain and in Alzheimer's disease. *Nat Rev Neurosci* **5**, 347-360 (2004). https://doi.org:10.1038/nrn1387
100 Grant, R. I. *et al.* Organizational hierarchy and structural diversity of microvascular pericytes in adult mouse cortex. *J Cereb Blood Flow Metab* **39**, 411-425 (2019). https://doi.org:10.1177/0271678X17732229
101 Frosen, J. & Joutel, A. Smooth muscle cells of intracranial vessels: from development to disease. *Cardiovasc Res* **114**, 501-512 (2018). https://doi.org:10.1093/cvr/cvy002
102 Zlokovic, B. V. Neurovascular mechanisms of Alzheimer's neurodegeneration. *Trends Neurosci* **28**, 202-208 (2005). https://doi.org:10.1016/j.tins.2005.02.001
103 Klein, B., Kuschinsky, W., Schrock, H. & Vetterlein, F. Interdependency of local capillary density, blood flow, and metabolism in rat brains. *Am J Physiol* **251**, H1333-H1340 (1986).

104 Dunn, A. K., Hayrunnisa, B., Moskowitz, M. & Boas, D. Dynamic Imaging of Cerebral Blood Flow Using Laser Speckle. *Journal of Cerebral Blood Flow and Metabolism* **21**, 195-201 (2001).
105 Sokolova, I. A. *et al.* Rarefication of the Arterioles and Capillary Network in the Brain of Rats with Different Forms of Hypertension. *Microvascular research* **30**, 1-9 (1985).
106 Drew, P. J., Shih, A. Y. & Kleinfeld, D. Fluctuating and sensory-induced vasodynamics in rodent cortex extend arteriole capacity. *Proc Natl Acad Sci U S A* **108**, 8473-8478 (2011). https://doi.org:10.1073/pnas.1100428108
107 Vanlandewijck, M. *et al.* A molecular atlas of cell types and zonation in the brain vasculature. *Nature* **554**, 475-480 (2018). https://doi.org:10.1038/nature25739
108 Erdener, S. E. & Dalkara, T. Small Vessels Are a Big Problem in Neurodegeneration and Neuroprotection. *Front Neurol* **10**, 889 (2019). https://doi.org:10.3389/fneur.2019.00889
109 Hartmann, D. A. *et al.* Brain capillary pericytes exert a substantial but slow influence on blood flow. *Nat Neurosci* **24**, 633-645 (2021). https://doi.org:10.1038/s41593-020-00793-2
110 Tierney, A. & Nelson, C. A. Brain Development and the Role of Experience in the Early Years. *Zero Three* **30**, 9-13 (2009).
111 Stiles, J. & Jernigan, T. L. The basics of brain development. *Neuropsychol Rev* **20**, 327-348 (2010). https://doi.org:10.1007/s11065-010-9148-4
112 Mira, H. & Morante, J. Neurogenesis From Embryo to Adult - Lessons From Flies and Mice. *Front Cell Dev Biol* **8**, 533 (2020). https://doi.org:10.3389/fcell.2020.00533
113 Oyarzabal, A., Musokhranova, U., Barros, L. & Garcia-Cazorla, A. Energy metabolism in childhood neurodevelopmental disorders. *EBioMedicine* **69**, 103474 (2021). https://doi.org:10.1016/j.ebiom.2021.103474
114 Walchli, T. *et al.* Shaping the brain vasculature in development and disease in the single-cell era. *Nat Rev Neurosci* **24**, 271-298 (2023). https://doi.org:10.1038/s41583-023-00684-y
115 Cristancho, A. G. *et al.* Deficits in Seizure Threshold and Other Behaviors in Adult Mice without Gross Neuroanatomic Injury after Late Gestation Transient Prenatal Hypoxia. *Developmental Neuroscience* **44**, 246-265 (2022). https://doi.org:10.1159/000524045
116 Sarkar, A. *et al.* In utero exposure to protease inhibitor-based antiretroviral regimens delays growth and developmental milestones in mice. *PLoS One* **15**, e0242513 (2020). https://doi.org:10.1371/journal.pone.0242513
117 Schnoll, J. G. *et al.* Evaluating Neurodevelopmental Consequences of Perinatal Exposure to Antiretroviral Drugs: Current Challenges and New Approaches. *Journal of Neuroimmune Pharmacology* **16**, 113-129 (2019). https://doi.org:10.1007/s11481-019-09880-z
118 Vivi, E. & Di Benedetto, B. Brain stars take the lead during critical periods of early postnatal brain development: relevance of astrocytes in health and mental disorders. *Molecular Psychiatry* (2024). https://doi.org:10.1038/s41380-024-02534-4
119 Morimoto, K. & Nakajima, K. Role of the Immune System in the Development of the Central Nervous System. *Frontiers in Neuroscience* **13** (2019). https://doi.org:10.3389/fnins.2019.00916
120 Biswas, S., Cottarelli, A. & Agalliu, D. Neuronal and glial regulation of CNS angiogenesis and barriergenesis. *Development* **147** (2020). https://doi.org:10.1242/dev.182279

121 Zhou, Y., Song, H. & Ming, G.-l. Genetics of human brain development. *Nature Reviews Genetics* **25**, 26-45 (2023). https://doi.org:10.1038/s41576-023-00626-5
122 Vogenstahl, J., Parrilla, M., Acker-Palmer, A. & Segarra, M. Vascular Regulation of Developmental Neurogenesis. *Front Cell Dev Biol* **10**, 890852 (2022). https://doi.org:10.3389/fcell.2022.890852
123 Walchli, T. *et al.* Quantitative assessment of angiogenesis, perfused blood vessels and endothelial tip cells in the postnatal mouse brain. *Nat Protoc* **10**, 53-74 (2015). https://doi.org:10.1038/nprot.2015.002
124 Geudens, I. & Gerhardt, H. Coordinating cell behaviour during blood vessel formation. *Development* **138**, 4569-4583 (2011). https://doi.org:10.1242/dev.062323
125 Potente, M., Gerhardt, H. & Carmeliet, P. Basic and therapeutic aspects of angiogenesis. *Cell* **146**, 873-887 (2011). https://doi.org:10.1016/j.cell.2011.08.039
126 Lacoste, B. *et al.* Sensory-Related Neural Activity Regulates the Structure of Vascular Networks in the Cerebral Cortex. *Neuron* **83**, 1117-1130 (2014). https://doi.org:10.1016/j.neuron.2014.07.034
127 Tata, M. & Ruhrberg, C. Cross-talk between blood vessels and neural progenitors in the developing brain. *Neuronal Signaling* (2018). https://doi.org:10.1042/NS20170139
128 Rosenstein, J. M., Krum, J. M. & Ruhrberg, C. VEGF in the nervous system. *Organogenesis* **6**, 107-114 (2010).
129 Mancuso, M. R., Kuhnert, F. & Kuo, C. J. Developmental angiogenesis of the central nervous system. *Lymphat Res Biol* **6**, 173-180 (2008). https://doi.org:10.1089/lrb.2008.1014
130 Jakobsson, L. *et al.* Endothelial cells dynamically compete for the tip cell position during angiogenic sprouting. *Nat Cell Biol* **12**, 943-953 (2010). https://doi.org:10.1038/ncb2103
131 Blanco, R. & Gerhardt, H. VEGF and Notch in tip and stalk cell selection. *Cold Spring Harb Perspect Med* **3**, a006569 (2013). https://doi.org:10.1101/cshperspect.a006569
132 Phng, L. K. *et al.* Nrarp coordinates endothelial Notch and Wnt signaling to control vessel density in angiogenesis. *Dev Cell* **16**, 70-82 (2009). https://doi.org:10.1016/j.devcel.2008.12.009
133 Bierhansl, L., Conradi, L. C., Treps, L., Dewerchin, M. & Carmeliet, P. Central Role of Metabolism in Endothelial Cell Function and Vascular Disease. *Physiology (Bethesda)* **32**, 126-140 (2017). https://doi.org:10.1152/physiol.00031.2016
134 Li, S., Haigh, K., Haigh, J. & Vasudevan, A. Endothelial VEGF Sculpts Cortical Cytoarchitecture. *The Journal of Neuroscience* **33**, 14809-14815 (2013). https://doi.org:10.1523/JNEUROSCI.1368-13.2013
135 Segarra, M. *et al.* Endothelial Dab1 signaling orchestrates neuro-glia-vessel communication in the central nervous system. *Science* **361** (2018). https://doi.org:10.1126/science.aao2861
136 Rothman, J. Mechanisms of intracellular protein transport. *Nature* **372**, 55-63 (1994).
137 Belanger, M., Allaman, I. & Magistretti, P. J. Brain energy metabolism: focus on astrocyte-neuron metabolic cooperation. *Cell Metab* **14**, 724-738 (2011). https://doi.org:10.1016/j.cmet.2011.08.016
138 Kasischke, K., Vishwasrao, H., Fischer, P., Zipfel, W., Webb, W. Neural Activity Triggers Neuronal Oxidative Metabolism Followed by Astrocytic Glycolysis. *Science* **305**, 99-103 (2004).

139 Beltran, F., Acuna, A., Miro, M., Castro, M. Brain energy metabolism in health and disease. *Neuroscience-Dealing with Frontiers*, 331-362 (2011).
140 Sonnay, S., Gruetter, R. & Duarte, J. M. N. How Energy Metabolism Supports Cerebral Function: Insights from (13)C Magnetic Resonance Studies In vivo. *Front Neurosci* **11**, 288 (2017). https://doi.org:10.3389/fnins.2017.00288
141 Kotchetkov, P., Blakeley, N. & Lacoste, B. Involvement of brain metabolism in neurodevelopmental disorders. *Int Rev Neurobiol* **173**, 67-113 (2023). https://doi.org:10.1016/bs.irn.2023.08.004
142 Chaudhry, R. & Varacallo, M. *Biochemistry, Glycolysis*, <https://www.ncbi.nlm.nih.gov/books/NBK482303/> (2023).
143 Alabduladhem, T. O. & Bordoni, B. *Physiolgy, Krebs Cycle*, <https://www.ncbi.nlm.nih.gov/books/NBK556032/> (2023).
144 Ahmad, M., Wolberg, A. & Kahwaji, C. I. *Biochemistry, Electron Transport Chain*, <https://www.ncbi.nlm.nih.gov/books/NBK526105/#> (2023).
145 Benarroch, E. Brain glucose transporters. *Neurology* **82** (2014).
146 Wei, Y. *et al.* Aerobic glycolysis is the predominant means of glucose metabolism in neuronal somata, which protects against oxidative damage. *Nat Neurosci* **26**, 2081-2089 (2023). https://doi.org:10.1038/s41593-023-01476-4
147 Shetty, P. K., Galeffi, F. & Turner, D. A. Cellular Links between Neuronal Activity and Energy Homeostasis. *Front Pharmacol* **3**, 43 (2012). https://doi.org:10.3389/fphar.2012.00043
148 Magistretti, P. J. & Pellerin, L. Cellular mechanisms of brain energy metabolism and their relevance to functional brain imaging. *Philos Trans R Soc Lond B Biol Sci* **354**, 1155-1163 (1999).
149 Pellerin, L. & Magistretti, P. J. Glutamate uptake into astrocytes stimulates aerobic glycolysis: A mechanism coupling neuronal activity to glucose utilization. *Proc Natl Acad Sci U S A* **91**, 10625-10629 (1994).
150 Vergara, R. C. *et al.* The Energy Homeostasis Principle: Neuronal Energy Regulation Drives Local Network Dynamics Generating Behavior. *Front Comput Neurosci* **13**, 49 (2019). https://doi.org:10.3389/fncom.2019.00049
151 Chen, Z. *et al.* Brain Energy Metabolism: Astrocytes in Neurodegenerative Diseases. *CNS Neurosci Ther* **29**, 24-36 (2023). https://doi.org:10.1111/cns.13982
152 Bak, L. K. & Walls, A. B. CrossTalk opposing view: lack of evidence supporting an astrocyte-to-neuron lactate shuttle coupling neuronal activity to glucose utilisation in the brain. *J Physiol* **596**, 351-353 (2018). https://doi.org:10.1113/JP274945
153 Veys, K. *et al.* Role of the GLUT1 Glucose Transporter in Postnatal CNS Angiogenesis and Blood-Brain Barrier Integrity. *Circ Res* **127**, 466-482 (2020). https://doi.org:10.1161/CIRCRESAHA.119.316463
154 Lee, H. W. *et al.* Endothelium-derived lactate is required for pericyte function and blood-brain barrier maintenance. *EMBO J* **41**, e109890 (2022). https://doi.org:10.15252/embj.2021109890
155 Oldendorf, W. H., Cornford, M. E. & Brown, W. J. The large apparent work capability of the blood-brain barrier: a study of the mitochondrial content of capillary endothelial cells in brain and other tissues of the rat. *Ann Neurol* **1**, 409-417 (1977). https://doi.org:10.1002/ana.410010502

156 Rohlenova, K., Veys, K., Miranda-Santos, I., De Bock, K. & Carmeliet, P. Endothelial Cell Metabolism in Health and Disease. *Trends Cell Biol* **28**, 224-236 (2018). https://doi.org:10.1016/j.tcb.2017.10.010
157 Mcdonald, C. J., Blankenheim, Z. J. & Drewes, L. R. Brain Endothelial Cells: Metabolic Flux and Energy Metabolism. *Physiology, pharmacology, and pathology of the blood-brain barrier*, 59-79 (2021).
158 de Castro Abrantes, H. *et al.* The Lactate Receptor HCAR1 Modulates Neuronal Network Activity through the Activation of G(alpha) and G(betagamma) Subunits. *J Neurosci* **39**, 4422-4433 (2019). https://doi.org:10.1523/JNEUROSCI.2092-18.2019
159 Grammas, P., Martinez, J. & Miller, B. Cerebral microvascular endothelium and the pathogenesis of neurodegenerative diseases. *Expert Rev Mol Med* **13**, e19 (2011). https://doi.org:10.1017/S1462399411001918
160 Snowden, J. S. The Neuropsychology of Huntington's Disease. *Arch Clin Neuropsychol.* **32**, 876-887 (2017). https://doi.org:https://doi.org/10.1093/arclin/acx086
161 Derejko, M. *et al.* Regional cerebral blood flow in Parkinson's disease as an indicator of cognitive impairment. *Nucl Med Commun.* **27**, 945-951 (2006). https://doi.org:10.1097/01.mnm.0000243370.18883.62
162 Al-Bachari, S., Naish, J. H., Parker, G. J. M., Emsley, H. C. A. & Parkes, L. M. Blood-Brain Barrier Leakage Is Increased in Parkinson's Disease. *Front Physiol* **11**, 593026 (2020). https://doi.org:10.3389/fphys.2020.593026
163 Willis, K. J. & Hakim, A. M. Stroke prevention and cognitive reserve: emerging approaches to modifying risk and delaying onset of dementia. *Front Neurol* **4**, 13 (2013). https://doi.org:10.3389/fneur.2013.00013
164 Sweeney, M. D. *et al.* Vascular dysfunction-The disregarded partner of Alzheimer's disease. *Alzheimers Dement* **15**, 158-167 (2019). https://doi.org:10.1016/j.jalz.2018.07.222
165 D'Haeseleer, M., Cambron, M., Vanopdenbosch, L. & De Keyser, J. Vascular aspects of multiple sclerosis. *The Lancet Neurology* **10**, 657-666 (2011). https://doi.org:10.1016/s1474-4422(11)70105-3
166 D'Haeseleer, M. *et al.* Cerebral hypoperfusion in multiple sclerosis is reversible and mediated by endothelin-1. *Proc Natl Acad Sci U S A* **110**, 5654-5658 (2013). https://doi.org:10.1073/pnas.1222560110
167 Ge, Y. *et al.* Dynamic Susceptibility Contrast Perfusion MR Imaging of Multiple Sclerosis Lesions: Characterizing Hemodynamic Impairment and Inflammatory Activity. *AJNR* **26**, 1539-1547 (2005).
168 Peruzzo, D. *et al.* Heterogeneity of cortical lesions in multiple sclerosis: an MRI perfusion study. *J Cereb Blood Flow Metab* **33**, 457-463 (2013). https://doi.org:10.1038/jcbfm.2012.192
169 Hostenbach, S. *et al.* Role of cerebral hypoperfusion in multiple sclerosis (ROCHIMS): study protocol for a proof-of-concept randomized controlled trial with bosentan. *Trials* **20**, 164 (2019). https://doi.org:10.1186/s13063-019-3252-4
170 Varga, A. W. *et al.* White matter hemodynamic abnormalities precede sub-cortical gray matter changes in multiple sclerosis. *J Neurol Sci* **282**, 28-33 (2009). https://doi.org:10.1016/j.jns.2008.12.036
171 McQuaid, S., Cunnea, P., McMahon, J. & Fitzgerald, U. The effects of blood–brain barrier disruption on glial cell function in multiple sclerosis. *Biochem Soc Trans* **37** (2009). https://doi.org:10.1042/BST0370329

172 Papadaki, E. Z. *et al.* Regional MRI perfusion measures predict motor/executive function in patients with clinically isolated syndrome. *Behav Neurol* **2014**, 252419 (2014). https://doi.org:10.1155/2014/252419
173 Reid, I. C. *et al.* Imaging of cerebral blood flow markers in Huntington's disease using single photon emission computed tomography. *Journal of Neurology, Neurosurgery, and Psychiatry* **51**, 1264-1268 (1988). https://doi.org:10.1136/jnnp.51.10.1264
174 Sax, D. S. *et al.* Evidence of Cortical Metabolic Dysfunction in Early Huntington's Disease by Single-Photon-Emission Computed Tomography. *Movement Disorders* **11**, 671-677 (1996). https://doi.org: https://doi.org/10.1002/mds.870110612
175 Harris, G. J. *et al.* Reduced basal ganglia blood flow and volume in pre-sympotmatic, gene-tested persons at-risk for Huntington's disease. *Brain* **122**, 1667-1678 (1999). https://doi.org:https://doi.org/10.1093/brain/122.9.1667
176 Lim, R. G. *et al.* Huntington's Disease iPSC-Derived Brain Microvascular Endothelial Cells Reveal WNT-Mediated Angiogenic and Blood-Brain Barrier Deficits. *Cell Rep* **19**, 1365-1377 (2017). https://doi.org:10.1016/j.celrep.2017.04.021
177 Drouin-Ouellet, J. *et al.* Cerebrovascular and blood-brain barrier impairments in Huntington's disease: Potential implications for its pathophysiology. *Ann Neurol* **78**, 160-177 (2015). https://doi.org:10.1002/ana.24406
178 Antony, P. M., Diederich, N. J., Kruger, R. & Balling, R. The hallmarks of Parkinson's disease. *FEBS J* **280**, 5981-5993 (2013). https://doi.org:10.1111/febs.12335
179 Brown, W. R. A Review of String Vessels or Collapsed, Empty Basement Membrane Tubes. *Journal of Alzheimer's Disease* **21**, 725-739 (2010). https://doi.org:10.3233/jad-2010-100219
180 Gray, M. T. & Woulfe, J. M. Striatal blood-brain barrier permeability in Parkinson's disease. *J Cereb Blood Flow Metab* **35**, 747-750 (2015). https://doi.org:10.1038/jcbfm.2015.32
181 Yang, P. *et al.* String Vessel Formation is Increased in the Brain of Parkinson Disease. *J Parkinsons Dis* **5**, 821-836 (2015). https://doi.org:10.3233/JPD-140454
182 Farkas, E., De Jong, G. I., de Vos Ernst, R. A. I., Steur, J. N. H. & Luiten, P. G. M. Pathological features of cerebral cortical capillaries are doubled in Alzheimer's disease and Parkinson's disease. *Acta Neuropathol* **100**, 395-402 (2000). https://doi.org:10.1007/s004010000195
183 Wu, M. *et al.* Connecting the Dots Between Hypercholesterolemia and Alzheimer's Disease: A Potential Mechanism Based on 27-Hydroxycholesterol. *Front Neurosci* **16**, 842814 (2022). https://doi.org:10.3389/fnins.2022.842814
184 Sierra, C. Hypertension and the Risk of Dementia. *Front Cardiovasc Med* **7**, 5 (2020). https://doi.org:10.3389/fcvm.2020.00005
185 Montagne, A. *et al.* Brain imaging of neurovascular dysfunction in Alzheimer's disease. *Acta Neuropathol* **131**, 687-707 (2016). https://doi.org:10.1007/s00401-016-1570-0
186 Incalza, M. A. *et al.* Oxidative stress and reactive oxygen species in endothelial dysfunction associated with cardiovascular and metabolic diseases. *Vascul Pharmacol* **100**, 1-19 (2018). https://doi.org:10.1016/j.vph.2017.05.005
187 Benedictus, M. R. *et al.* Lower cerebral blood flow is associated with faster cognitive decline in Alzheimer's disease. *Eur Radiol* **27**, 1169-1175 (2017). https://doi.org:10.1007/s00330-016-4450-z

188 Korte, N., Nortley, R. & Attwell, D. Cerebral blood flow decrease as an early pathological mechanism in Alzheimer's disease. *Acta Neuropathol* **140**, 793-810 (2020). https://doi.org:10.1007/s00401-020-02215-w
189 Cruz Hernandez, J. C. *et al.* Neutrophil adhesion in brain capillaries reduces cortical blood flow and impairs memory function in Alzheimer's disease mouse models. *Nat Neurosci* **22**, 413-420 (2019). https://doi.org:10.1038/s41593-018-0329-4
190 Mughal, A., Harraz, O. F., Gonzales, A. L., Hill-Eubanks, D. & Nelson, M. T. PIP2 Improves Cerebral Blood Flow in a Mouse Model of Alzheimer's Disease. *Function (Oxf)* **2**, zqab010 (2021). https://doi.org:10.1093/function/zqab010
191 Kalaria, R. N. & Harik, S. I. Reduced Glucose Transporter at the Blood-Brain Barrier and in Cerebral Cortex in Alzheimer Disease. *Journal of Neurochemistry* **53** (1989). https://doi.org:https://doi.org/10.1111/j.1471-4159.1989.tb07399.x
192 Halliday, M. R. *et al.* Accelerated pericyte degeneration and blood-brain barrier breakdown in apolipoprotein E4 carriers with Alzheimer's disease. *J Cereb Blood Flow Metab* **36**, 216-227 (2016). https://doi.org:10.1038/jcbfm.2015.44
193 Grammas, P. Neurovascular dysfunction, inflammation and endothelial activation: implications for the pathogenesis of Alzheimer's disease. *J Neuroinflammation* **8** (2011). https://doi.org:10.1186/1742-2094-8-26
194 Quick, S., Moss, J., Rajani, R. M. & Williams, A. A Vessel for Change: Endothelial Dysfunction in Cerebral Small Vessel Disease. *Trends Neurosci* **44**, 289-305 (2021). https://doi.org:10.1016/j.tins.2020.11.003
195 Iadecola, C. The pathobiology of vascular dementia. *Neuron* **80**, 844-866 (2013). https://doi.org:10.1016/j.neuron.2013.10.008
196 Menard, C. *et al.* Social stress induces neurovascular pathology promoting depression. *Nat Neurosci* **20**, 1752-1760 (2017). https://doi.org:10.1038/s41593-017-0010-3
197 Dudek, K. A. *et al.* Molecular adaptations of the blood-brain barrier promote stress resilience vs. depression. *Proc Natl Acad Sci U S A* **117**, 3326-3336 (2020). https://doi.org:10.1073/pnas.1914655117
198 Dion-Albert, L. *et al.* Vascular and blood-brain barrier-related changes underlie stress responses and resilience in female mice and depression in human tissue. *Nature Communications* **13** (2022). https://doi.org:10.1038/s41467-021-27604-x
199 Morris-Rosendahl, D. J. & Crocq, M. A. Neurodevelopmental disorders-the history and future of a diagnostic concept. *Dialogues Clin Neurosci* **22**, 65-72 (2020). https://doi.org:10.31887/DCNS.2020.22.1/macrocq
200 Cainelli, E. & Bisiacchi, P. Neurodevelopmental Disorders: Past, Present, and Future. *Children (Basel)* **10** (2022). https://doi.org:10.3390/children10010031
201 Antolini, G. & Colizzi, M. Where Do Neurodevelopmental Disorders Go? Casting the Eye Away from Childhood towards Adulthood. *Healthcare (Basel)* **11** (2023). https://doi.org:10.3390/healthcare11071015
202 Lee, J. S. *et al.* Regional cerebral blood flow in children with attention deficit hyperactivity disorder: comparison before and after methylphenidate treatment. *Hum Brain Mapp* **24**, 157-164 (2005). https://doi.org:10.1002/hbm.20067
203 Lao, P. *et al.* Cerebrovascular disease emerges with age and Alzheimer's disease in adults with Down syndrome. *Sci Rep* **14**, 12334 (2024). https://doi.org:10.1038/s41598-024-61962-y

204 Stachowiak, M. K. *et al.* Schizophrenia: A neurodevelopmental disorder — Integrative genomic hypothesis and therapeutic implications from a transgenic mouse model. *Schizophrenia Research* **143**, 367-376 (2013). https://doi.org:https://doi.org/10.1016/j.schres.2012.11.004
205 Schuepbach, D. *et al.* Determinants of cerebral hemodynamics during the Trail Making Test in schizophrenia. *Brain Cogn* **109**, 96-104 (2016). https://doi.org:10.1016/j.bandc.2016.09.002
206 Stegmayer, K. *et al.* Specific cerebral perfusion patterns in three schizophrenia symptom dimensions. *Schizophr Res* **190**, 96-101 (2017). https://doi.org:10.1016/j.schres.2017.03.018
207 Pinkham, A. *et al.* Resting quantitative cerebral blood flow in schizophrenia measured by pulsed arterial spin labeling perfusion MRI. *Psychiatry Res* **194**, 64-72 (2011). https://doi.org:10.1016/j.pscychresns.2011.06.013
208 Malaspina, D. *et al.* Resting neural activity distinguishes subgroups of schizophrenia patients. *Biol Psychiatry* **56**, 931-937 (2004). https://doi.org:10.1016/j.biopsych.2004.09.013
209 Schultz, S. K. *et al.* Age and Regional Cerebral Blood Flow in Schizophrenia: Age Effects in Anterior Cingulate, Frontal, and Parietal Cortex. *The Journal of Neuropsychiatry and Clinical Neurosciences* **14**, 19-24 (2002). https://doi.org:https://doi.org/10.1176/jnp.14.1.19
210 Kawakami, K. *et al.* The Effects of Aging on Changes in Regional Cerebral Blood Flow in Schizophrenia. *Neuropsychobiology* **69**, 202-209 (2014). https://doi.org:https://doi.org/10.1159/000358840
211 Mathalon, D. H., Ford, J. M. & Pfefferbaum, A. Trait and state aspects of P300 amplitude reduction in schizophrenia: a retrospective longitudinal study. *Biol Psychiatry* **47**, 434-449 (2000). https://doi.org:10.1016/s0006-3223(99)00277-2
212 Pu, S. *et al.* Social cognition and prefrontal hemodynamic responses during a working memory task in schizophrenia. *Sci Rep* **6**, 22500 (2016). https://doi.org:10.1038/srep22500
213 Uranova, N. A. *et al.* Ultrastructural damage of capillaries in the neocortex in schizophrenia. *World J Biol Psychiatry* **11**, 567-578 (2010). https://doi.org:10.3109/15622970903414188
214 Carrier, M., Guilbert, J., Levesque, J. P., Tremblay, M. E. & Desjardins, M. Structural and Functional Features of Developing Brain Capillaries, and Their Alteration in Schizophrenia. *Front Cell Neurosci* **14**, 595002 (2020). https://doi.org:10.3389/fncel.2020.595002
215 Lai, M. C., Lombardo, M. V. & Baron-Cohen, S. Autism. *Lancet* **383**, 896-910 (2014). https://doi.org:10.1016/S0140-6736(13)61539-1
216 Vijayakumar, N. T. & Judy, M. V. Autism spectrum disorders: Integration of the genome, transcriptome and the environment. *J Neurol Sci* **364**, 167-176 (2016). https://doi.org:10.1016/j.jns.2016.03.026
217 Werling, D. M. & Geschwind, D. H. Sex differences in autism spectrum disorders. *Curr Opin Neurol* **26**, 146-153 (2013). https://doi.org:10.1097/WCO.0b013e32835ee548
218 Murphy, C. M. *et al.* Autism spectrum disorder in adults: diagnosis, management, and health services development. *Neuropsychiatr Dis Treat* **12**, 1669-1686 (2016). https://doi.org:10.2147/NDT.S65455

219 Wozniak, R. H., Leezenbaum, N. B., Northrup, J. B., West, K. L. & Iverson, J. M. The development of autism spectrum disorders: variability and causal complexity. *Wiley Interdiscip Rev Cogn Sci* **8** (2017). https://doi.org:10.1002/wcs.1426
220 Kanner, L. Autistic Disturbances of Affective Contact. *Acta Paedopsychiatr.* **35**, 100-136 (1943).
221 Al-Beltagi, M. Autism medical comorbidities. *World J Clin Pediatr* **10**, 15-28 (2021). https://doi.org:10.5409/wjcp.v10.i3.15
222 Kim, H., Lim, C. S. & Kaang, B. K. Neuronal mechanisms and circuits underlying repetitive behaviors in mouse models of autism spectrum disorder. *Behav Brain Funct* **12**, 3 (2016). https://doi.org:10.1186/s12993-016-0087-y
223 Hyman, S. L., Levy, S. E., Myers, S. M., Council On Children With Disabilities, S. O. D. & Behavioral, P. Identification, Evaluation, and Management of Children With Autism Spectrum Disorder. *Pediatrics* **145** (2020). https://doi.org:10.1542/peds.2019-3447
224 Ghanouni, P. & Seaker, L. What does receiving autism diagnosis in adulthood look like? Stakeholders' experiences and inputs. *Int J Ment Health Syst* **17**, 16 (2023). https://doi.org:10.1186/s13033-023-00587-6
225 Lord, C. *et al.* Autism From 2 to 9 Years of Age. *Arch Gen Psychiatry* **63**, 694-701 (2006). https://doi.org:10.1001/archpsyc.63.6.694
226 Croen, L. A. *et al.* The health status of adults on the autism spectrum. *Autism* **19**, 814-823 (2015). https://doi.org:10.1177/1362361315577517
227 Bishop, L. *et al.* Cardiovascular disease risk factors in autistic adults: The impact of sleep quality and antipsychotic medication use. *Autism Res* **16**, 569-579 (2023). https://doi.org:10.1002/aur.2872
228 Wang, L., Wang, B., Wu, C., Wang, J. & Sun, M. Autism Spectrum Disorder: Neurodevelopmental Risk Factors, Biological Mechanism, and Precision Therapy. *Int J Mol Sci* **24** (2023). https://doi.org:10.3390/ijms24031819
229 Pugsley, K., Scherer, S. W., Bellgrove, M. A. & Hawi, Z. Environmental exposures associated with elevated risk for autism spectrum disorder may augment the burden of deleterious de novo mutations among probands. *Mol Psychiatry* **27**, 710-730 (2022). https://doi.org:10.1038/s41380-021-01142-w
230 Rylaarsdam, L. & Guemez-Gamboa, A. Genetic Causes and Modifiers of Autism Spectrum Disorder. *Front Cell Neurosci* **13**, 385 (2019). https://doi.org:10.3389/fncel.2019.00385
231 Arora, A. *et al.* Screening autism-associated environmental factors in differentiating human neural progenitors with fractional factorial design-based transcriptomics. *Sci Rep* **13**, 10519 (2023). https://doi.org:10.1038/s41598-023-37488-0
232 Krakowiak, P. *et al.* Maternal metabolic conditions and risk for autism and other neurodevelopmental disorders. *Pediatrics* **129**, e1121-1128 (2012). https://doi.org:10.1542/peds.2011-2583
233 Kolozsi, E., Mackenzie, R. N., Roullet, F. I., Decatanzaro, D. & Foster, J. A. Prenatal exposure to valproic acid leads to reduced expression of synaptic adhesion molecule neuroligin 3 in mice. *Neuropharmacology* **163**, 1201-1210 (2009). https://doi.org:https://doi.org/10.1016/j.neuroscience.2009.07.021
234 Libbey, J. E., Sweeten, T. L., McMahon, W. M. & Fujinami, R. S. Autistic disorder and viral infections. *J Neurovirol* **11**, 1-10 (2005). https://doi.org:10.1080/13550280590900553
235 Cohen, D. J., Paul, R., Anderson, G. M. & Harcherik, D. F. Blood lead in autistic children. *The Lancet* **320**, 94-95 (1982).

236 Folstein, S. & Rutter, M. L. Genetic influences and infantile autism. *Nature* **265**, 726-728 (1977).
237 De Rubeis, S. *et al.* Synaptic, transcriptional and chromatin genes disrupted in autism. *Nature* **515**, 209-215 (2014). https://doi.org:10.1038/nature13772
238 Geschwind, D. H. Genetics of autism spectrum disorders. *Trends Cogn Sci* **15**, 409-416 (2011). https://doi.org:10.1016/j.tics.2011.07.003
239 Marshall, C. R. *et al.* Structural variation of chromosomes in autism spectrum disorder. *Am J Hum Genet* **82**, 477-488 (2008). https://doi.org:10.1016/j.ajhg.2007.12.009
240 Courchesne, E. C., R. Akshoomoff, N. Evidence of brain overgrowth in the first year of life in autism. *JAMA* **290**, 337-344 (2003). https://doi.org:10.1001/jama.290.3.337
241 Donovan, A. P. & Basson, M. A. The neuroanatomy of autism - a developmental perspective. *J Anat* **230**, 4-15 (2017). https://doi.org:10.1111/joa.12542
242 Ortiz-Mantilla, S., Choe, M.-S., Flax, J., Grant, E. & Benasich, A. A. Associations between the size of the amygdala in infancy and language abilities during the preschool years in normally developing children. *Neuroimage* **49**, 2791-2799 (2010). https://doi.org:doi.org/10.1016/j.neuroimage.2009.10.029
243 Kaushik, G. & Zarbalis, K. S. Prenatal Neurogenesis in Autism Spectrum Disorders. *Frontiers in Chemistry* **4** (2016).
244 Courchesne, E. *et al.* Neuron Number and Size in Prefrontal Cortex of Children With Autism. *JAMA* **306**, 2001-2010 (2011).
245 Ebert, D. H. & Greenberg, M. E. Activity-dependent neuronal signalling and autism spectrum disorder. *Nature* **493**, 327-337 (2013). https://doi.org:10.1038/nature11860
246 Emerson, R. W. *et al.* Functional neuroimaging of high-risk 6-month-old infants predicts a diagnosis of autism at 24 months of age. *Sci Transl Med* **9**, eaag2882 (2017). https://doi.org:10.1126/scitranslmed.aag2882
247 Zikopoulos, B. & Barbas, H. Changes in prefrontal axons may disrupt the network in autism. *J Neurosci* **30**, 14595-14609 (2010). https://doi.org:10.1523/JNEUROSCI.2257-10.2010
248 Cakar, M. E., Cummings, K. K., Bookheimer, S. Y., Dapretto, M. & Green, S. A. Age-related changes in neural responses to sensory stimulation in autism: a cross-sectional study. *Mol Autism* **14**, 38 (2023). https://doi.org:10.1186/s13229-023-00571-4
249 Fang, W.-Q., Chen, W.-W., Fu, A. K. Y. & Ip, N. Y. Overproduction of Upper-Layer Neurons in the Neocortex Leads to Autism-like Features in Mice. *Cell Rep* **9**, 1635-1643 (2014). https://doi.org:10.1016/j.celrep.2014.11.003
250 Hashem, S. *et al.* Genetics of structural and functional brain changes in autism spectrum disorder. *Transl Psychiatry* **10**, 229 (2020). https://doi.org:10.1038/s41398-020-00921-3
251 Beopoulos, A., Gea, M., Fasano, A. & Iris, F. Autism spectrum disorders pathogenesis: Toward a comprehensive model based on neuroanatomic and neurodevelopment considerations. *Front Neurosci* **16**, 988735 (2022). https://doi.org:10.3389/fnins.2022.988735
252 Courchesne, E. *et al.* The ASD Living Biology: from cell proliferation to clinical phenotype. *Mol Psychiatry* **24**, 88-107 (2019). https://doi.org:10.1038/s41380-018-0056-y
253 Bosl, W. J., Tager-Flusberg, H. & Nelson, C. A. EEG Analytics for Early Detection of Autism Spectrum Disorder: A data-driven approach. *Sci Rep* **8**, 6828 (2018). https://doi.org:10.1038/s41598-018-24318-x

254 Fatemi, S. H. *et al.* Glutamic acid decarboxylase 65 and 67 kDa proteins are reduced in autistic parietal and cerebellar cortices. *Biological Psychiatry* **52**, 805-810 (2002).
255 Purcell, A. E., Jeon, O. H., Zimmerman, A. W., Blue, M. E. & Pevsner, J. Postmortem brain abnormalities of the glutamate neurotransmitter system in autism. *Neurology* **57**, 1618-1628 (2001).
256 Barkovich, A. J., Kuzniecky, R., Jackson, G., Guerrini, R. & Dobyns, W. B. A developmental and genetic classification for malformations of cortical development. *65*, 1873-1887 (2005). https://doi.org:doi.org/10.1212/01.wnl.0000183747.05269.2d
257 Takarae, Y. & Sweeney, J. Neural Hyperexcitability in Autism Spectrum Disorders. *Brain Sci* **7** (2017). https://doi.org:10.3390/brainsci7100129
258 Hollestein, V. *et al.* Excitatory/inhibitory imbalance in autism: the role of glutamate and GABA gene-sets in symptoms and cortical brain structure. *Transl Psychiatry* **13**, 18 (2023). https://doi.org:10.1038/s41398-023-02317-5
259 Tang, G. *et al.* Loss of mTOR-dependent macroautophagy causes autistic-like synaptic pruning deficits. *Neuron* **83**, 1131-1143 (2014). https://doi.org:10.1016/j.neuron.2014.07.040
260 Bjørklund, G. *et al.* Cerebral hypoperfusion in autism spectrum disorder. *Acta Neurobiologiae Experimentalis* **78**, 21-29 (2018). https://doi.org:10.21307/ane-2018-005
261 Jann, K. *et al.* Altered resting perfusion and functional connectivity of default mode network in youth with autism spectrum disorder. *Brain Behav* **5**, e00358 (2015). https://doi.org:10.1002/brb3.358
262 Yerys, B. E. *et al.* Arterial spin labeling provides a reliable neurobiological marker of autism spectrum disorder. *J Neurodev Disord* **10**, 32 (2018). https://doi.org:10.1186/s11689-018-9250-0
263 Siegel, B. V. *et al.* Regional cerebral glucose metabolism and attention in adults with a history of childhood autism. *J Neuropsychiatry Clin Neurosci.* **4** (1992). https://doi.org:10.1176/jnp.4.4.406
264 Uratani, M. *et al.* Reduced prefrontal hemodynamic response in pediatric autism spectrum disorder measured with near-infrared spectroscopy. *Child Adolesc Psychiatry Ment Health* **13**, 29 (2019). https://doi.org:10.1186/s13034-019-0289-9
265 Peterson, B. S. *et al.* Hyperperfusion of Frontal White and Subcortical Gray Matter in Autism Spectrum Disorder. *Biol Psychiatry* **85**, 584-595 (2019). https://doi.org:10.1016/j.biopsych.2018.11.026
266 Azmitia, E. C., Saccomano, Z. T., Alzoobaee, M. F., Boldrini, M. & Whitaker-Azmitia, P. M. Persistent Angiogenesis in the Autism Brain: An Immunocytochemical Study of Postmortem Cortex, Brainstem and Cerebellum. *J Autism Dev Disord* **46**, 1307-1318 (2016). https://doi.org:10.1007/s10803-015-2672-6
267 Fiorentino, M. *et al.* Blood-brain barrier and intestinal epithelial barrier alterations in autism spectrum disorders. *Mol Autism* **7**, 49 (2016). https://doi.org:10.1186/s13229-016-0110-z
268 Onore, C., Careaga, M. & Ashwood, P. The role of immune dysfunction in the pathophysiology of autism. *Brain Behav Immun* **26**, 383-392 (2012). https://doi.org:10.1016/j.bbi.2011.08.007
269 Kostiukow, A. & Samborski, W. The effectiveness of hyperbaric oxygen therapy (HBOT) in children with autism spectrum disorders. *Pol Merkur Lekarski.* **48**, 15-18 (2020).

270 Rossignol, D. A. *et al.* Hyperbaric oxygen treatment in autism spectrum disorders. *Med Gas Res* **2** (2012). https://doi.org:0.1186/2045-9912-2-16
271 Abookasis, D., Lerman, D., Roth, H., Tfilin, M. & Turgeman, G. Optically derived metabolic and hemodynamic parameters predict hippocampal neurogenesis in the BTBR mouse model of autism. *Journal of Biophotonics* **11** (2018). https://doi.org: https://doi.org/10.1002/jbio.201600322
272 Tarlungeanu, D. C. *et al.* Impaired Amino Acid Transport at the Blood Brain Barrier Is a Cause of Autism Spectrum Disorder. *Cell* **167**, 1481-1494 e1418 (2016). https://doi.org:10.1016/j.cell.2016.11.013
273 Kumar, H., Sharma, B. M. & Sharma, B. Benefits of agomelatine in behavioral, neurochemical and blood brain barrier alterations in prenatal valproic acid induced autism spectrum disorder. *Neurochem Int* **91**, 34-45 (2015). https://doi.org:10.1016/j.neuint.2015.10.007
274 Cheng, N., Rho, J. M. & Masino, S. A. Metabolic Dysfunction Underlying Autism Spectrum Disorder and Potential Treatment Approaches. *Front Mol Neurosci* **10**, 34 (2017). https://doi.org:10.3389/fnmol.2017.00034
275 Boekema, E. J. & Braun, H.-P. Supramolecular Structure of the Mitochondrial Oxidative Phosphorylation System. *Journal of Biological Chemistry* **282**, 1-4 (2007). https://doi.org:10.1074/jbc.R600031200
276 Chauhan, A. *et al.* Brain region-specific deficit in mitochondrial electron transport chain complexes in children with autism. *J Neurochem* **117**, 209-220 (2011). https://doi.org:10.1111/j.1471-4159.2011.07189.x
277 Fernandez, A. *et al.* Mitochondrial Dysfunction Leads to Cortical Under-Connectivity and Cognitive Impairment. *Neuron* **102**, 1127-1142 e1123 (2019). https://doi.org:10.1016/j.neuron.2019.04.013
278 Filipek, P. A. *et al.* Mitochondrial dysfunction in autistic patients with 15q inverted duplication. *Annals of Neurology* **53**, 801-804 (2003). https://doi.org: https://doi.org/10.1002/ana.10596
279 Giulivi, C. *et al.* Mitochondrial Dysfunction in Autism. *JAMA* **304**, 2389-2396 (2010). https://doi.org: doi:10.1001/jama.2010.1706
280 Rossignol, D. A. & Frye, R. E. Mitochondrial dysfunction in autism spectrum disorders: a systematic review and meta-analysis. *Mol Psychiatry* **17**, 290-314 (2012). https://doi.org:10.1038/mp.2010.136
281 Nava, C. *et al.* Analysis of the chromosome X exome in patients with autism spectrum disorders identified novel candidate genes, including TMLHE. *Transl Psychiatry* **2**, e179 (2012). https://doi.org:10.1038/tp.2012.102
282 Féron, F. *et al.* Autism spectrum disorders: an impaired glycolysis induces an ATP deficiency and a reduced cell respiration. *bioRXiv* (2024). https://doi.org:10.1101/2024.01.22.576644
283 Frye, R. E. *et al.* Biomarkers of mitochondrial dysfunction in autism spectrum disorder: A systematic review and meta-analysis. *Neurobiology of Disease* **197** (2024). https://doi.org:10.1016/j.nbd.2024.106520
284 Siddiqui, M. F., Elwell, C. & Johnson, M. H. Mitochondrial Dysfunction in Autism Spectrum Disorders. *Autism Open Access* **6** (2016). https://doi.org:10.4172/2165-7890.1000190

285 Wang, Q. *et al.* Impaired calcium signaling in astrocytes modulates autism spectrum disorder-like behaviors in mice. *Nat Commun* **12**, 3321 (2021). https://doi.org:10.1038/s41467-021-23843-0
286 Lingampelly, S. S. *et al.* Metabolic network analysis of pre-ASD newborns and 5-year-old children with autism spectrum disorder. *Commun Biol* **7**, 536 (2024). https://doi.org:10.1038/s42003-024-06102-y
287 Dai, S. *et al.* Purine signaling pathway dysfunction in autism spectrum disorders: Evidence from multiple omics data. *Front Mol Neurosci* **16**, 1089871 (2023). https://doi.org:10.3389/fnmol.2023.1089871
288 Naviaux, R. K. Antipurinergic therapy for autism-An in-depth review. *Mitochondrion* **43**, 1-15 (2018). https://doi.org:10.1016/j.mito.2017.12.007
289 Babiec, L., Wilkaniec, A., Gawinek, E., Hilgier, W. & Adamczyk, A. Inhibition of purinergic P2 receptors prevents synaptic and behavioral alterations in a rodent model of autism spectrum disorders. *Research in Autism Spectrum Disorders* **112** (2024). https://doi.org:10.1016/j.rasd.2024.102353
290 Frye, R. E. Introduction to Part 1. *Semin Pediatr Neurol* **34**, 100802 (2020). https://doi.org:10.1016/j.spen.2020.100802
291 El-Rashidy, O. *et al.* Ketogenic diet versus gluten free casein free diet in autistic children: a case-control study. *Metab Brain Dis* **32**, 1935-1941 (2017). https://doi.org:10.1007/s11011-017-0088-z
292 Li, Q., Liang, J., Fu, N., Han, Y. & Qin, J. A Ketogenic Diet and the Treatment of Autism Spectrum Disorder. *Front Pediatr* **9**, 650624 (2021). https://doi.org:10.3389/fped.2021.650624
293 Jensen, N. J., Wodschow, H. Z., Nilsson, M. & Rungby, J. Effects of Ketone Bodies on Brain Metabolism and Function in Neurodegenerative Diseases. *Int J Mol Sci* **21** (2020). https://doi.org:10.3390/ijms21228767
294 Cermak, S. A., Curtin, C. & Bandini, L. G. Food selectivity and sensory sensitivity in children with autism spectrum disorders. *J Am Diet Assoc* **110**, 238-246 (2010). https://doi.org:10.1016/j.jada.2009.10.032
295 D'Angelo, D. *et al.* Defining the Effect of the 16p11.2 Duplication on Cognition, Behavior, and Medical Comorbidities. *JAMA Psychiatry* **73**, 20-30 (2016). https://doi.org:10.1001/jamapsychiatry.2015.2123
296 Rosenfeld, J. A. *et al.* Speech delays and behavioral problems are the predominant features in individuals with developmental delays and 16p11.2 microdeletions and microduplications. *J Neurodev Disord* **2**, 26-38 (2010). https://doi.org:10.1007/s11689-009-9037-4
297 Kumar, R. A. *et al.* Recurrent 16p11.2 microdeletions in autism. *Human Molecular Genetics* **17**, 628-638 (2007). https://doi.org:10.1093/hmg/ddm376
298 Weiss, L., Shen, Y., Korn, J. & al., e. Association between Microdeletion and Microduplication at 16p11.2 and Autism. *N Engl J Med* **358**, 667-675 (2008).
299 Fernandez, B. A. *et al.* Phenotypic spectrum associated with de novo and inherited deletions and duplications at 16p11.2 in individuals ascertained for diagnosis of autism spectrum disorder. *J Med Genet* **47**, 195-203 (2010). https://doi.org:10.1136/jmg.2009.069369
300 Niarchou, M. *et al.* Psychiatric disorders in children with 16p11.2 deletion and duplication. *Transl Psychiatry* **9**, 8 (2019). https://doi.org:10.1038/s41398-018-0339-8

301 Kostopoulos, E. *et al.* Hyperinsulinaemic hypoglycaemia: A new presentation of 16p11.2 deletion syndrome. *Clinical Endocrinology* **90**, 766-769 (2019).
302 Kamara, D., De Boeck, P., Lecavalier, L., Neuhaus, E. & Beauchaine, T. P. Characterizing Sleep Problems in 16p11.2 Deletion and Duplication. *J Autism Dev Disord* **53**, 1462-1475 (2023). https://doi.org:10.1007/s10803-021-05311-2
303 Zufferey, F. *et al.* A 600 kb deletion syndrome at 16p11.2 leads to energy imbalance and neuropsychiatric disorders. *J Med Genet* **49**, 660-668 (2012). https://doi.org:10.1136/jmedgenet-2012-101203
304 Wang, Y. *et al.* Prenatal Diagnosis of Chromosome 16p11.2 Microdeletion. *Genes (Basel)* **13** (2022). https://doi.org:10.3390/genes13122315
305 Qureshi, A. Y. *et al.* Opposing brain differences in 16p11.2 deletion and duplication carriers. *J Neurosci* **34**, 11199-11211 (2014). https://doi.org:10.1523/JNEUROSCI.1366-14.2014
306 Portmann, T. *et al.* Behavioral abnormalities and circuit defects in the basal ganglia of a mouse model of 16p11.2 deletion syndrome. *Cell Rep* **7**, 1077-1092 (2014). https://doi.org:10.1016/j.celrep.2014.03.036
307 Morson, S., Yang, Y., Price, D. J. & Pratt, T. Expression of Genes in the 16p11.2 Locus during Development of the Human Fetal Cerebral Cortex. *Cereb Cortex* **31**, 4038-4052 (2021). https://doi.org:10.1093/cercor/bhab067
308 Valtorta, F., Benfenati, F., Zara, F. & Meldolesi, J. PRRT2: from Paroxysmal Disorders to Regulation of Synaptic Function. . *Trends Neurosci* **39**, 668-679 (2014).
309 Escamilla, C. O. *et al.* Kctd13 deletion reduces synaptic transmission via increased RhoA. *Nature* **551**, 227-231 (2017). https://doi.org:10.1038/nature24470
310 Pietras, P. *et al.* MVP Expression Facilitates Tumor Cell Proliferation and Migration Supporting the Metastasis of Colorectal Cancer Cells. *Int J Mol Sci* **22** (2021). https://doi.org:10.3390/ijms222212121
311 Sobanski, T. *et al.* The fructose-bisphosphate, Aldolase A (ALDOA), facilitates DNA-PKcs and ATM kinase activity to regulate DNA double-strand break repair. *Sci Rep* **13**, 15171 (2023). https://doi.org:10.1038/s41598-023-41133-1
312 Hoefen, R. & Berk, B. The role of MAP kinases in endothelial activation. *Vascul Pharmacol* **38**, 271-273 (2002).
313 Smits M, Wurdinger T, van het Hof B & al., e. Myc-associated zinc finger protein (MAZ) is regulated by miR-125b and mediates VEGF-induced angiogenesis in glioblastoma. *FASEB journal : official publication of the Federation of American Societies for Experimental Biology* **26**, 2639-2647 (2012).
314 Sun, X. *et al.* Chitinase 3 like 1 contributes to the development of pulmonary vascular remodeling in pulmonary hypertension. *JCI Insight* **7** (2022). https://doi.org:10.1172/jci.insight.159578
315 Kim, G.-Y., Kim, H., Lim, H.-J. & Park, H.-Y. Coronin 1A depletion protects endothelial cells from TNFα-induced apoptosis by modulating p38β expression and activation. *Cellular signalling* **27**, 1688-1693 (2015).
316 Horev, G. *et al.* Dosage-dependent phenotypes in models of 16p11.2 lesions found in autism. *Proc Natl Acad Sci U S A* **108**, 17076-17081 (2011). https://doi.org:10.1073/pnas.1114042108

317 Fang, Y. C., Hsieh, Y. C., Hu, C. J. & Tu, Y. K. Endothelial Dysfunction in Neurodegenerative Diseases. *Int J Mol Sci* **24** (2023). https://doi.org:10.3390/ijms24032909
318 Wang, F. *et al.* Dysfunction of Cerebrovascular Endothelial Cells: Prelude to Vascular Dementia. *Front Aging Neurosci* **10**, 376 (2018). https://doi.org:10.3389/fnagi.2018.00376
319 Bai, T., Yu, S. & Feng, J. Advances in the Role of Endothelial Cells in Cerebral Small Vessel Disease. *Front Neurol* **13**, 861714 (2022). https://doi.org:10.3389/fneur.2022.861714
320 De Giorgis, V. *et al.* Overall cognitive profiles in patients with GLUT1 Deficiency Syndrome. *Brain Behav* **9**, e01224 (2019). https://doi.org:10.1002/brb3.1224
321 Stankovic, I. *et al.* Schizophrenia endothelial cells exhibit higher permeability and altered angiogenesis patterns in patient-derived organoids. *Transl Psychiatry* **14**, 53 (2024). https://doi.org:10.1038/s41398-024-02740-2
322 Hakanpaa, L. *et al.* Endothelial destabilization by angiopoietin-2 via integrin beta1 activation. *Nat Commun* **6**, 5962 (2015). https://doi.org:10.1038/ncomms6962
323 Gu, Q. *et al.* GREM1 overexpression inhibits proliferation, migration and angiogenesis of osteosarcoma. *Exp Cell Res* **384**, 111619 (2019). https://doi.org:10.1016/j.yexcr.2019.111619
324 Liu, Y., Li, Y., Hou, R. & Shu, Z. Knockdown GREM1 suppresses cell growth, angiogenesis, and epithelial-mesenchymal transition in colon cancer. *J Cell Biochem* **120**, 5583-5596 (2019). https://doi.org:10.1002/jcb.27842
325 Beland-Millar, A. *et al.* 16p11.2 haploinsufficiency reduces mitochondrial biogenesis in brain endothelial cells and alters brain metabolism in adult mice. *Cell Rep* **42**, 112485 (2023). https://doi.org:10.1016/j.celrep.2023.112485
326 Sender, R. & Milo, R. The distribution of cellular turnover in the human body. *Nat Med* **27**, 45-48 (2021). https://doi.org:10.1038/s41591-020-01182-9
327 Wen, Y. & Yao, Y. *Autism Spectrum Disorders: The Mitochondria Connection*, <https://www.ncbi.nlm.nih.gov/books/NBK573616/# doi: 10.36255/exonpublications.autismspectrumdisorders.2021.mitochondria> (2021).
328 Lin, R. Z. *et al.* Mitochondrial transfer mediates endothelial cell engraftment through mitophagy. *Nature* **629**, 660-668 (2024). https://doi.org:10.1038/s41586-024-07340-0
329 D'Souza, A. *et al.* Microvesicles transfer mitochondria and increase mitochondrial function in brain endothelial cells. *J Control Release* **338**, 505-526 (2021). https://doi.org:10.1016/j.jconrel.2021.08.038
330 You, W. *et al.* PGC-1a mediated mitochondrial biogenesis promotes recovery and survival of neuronal cells from cellular degeneration. *Cell Death Discov* **10**, 180 (2024). https://doi.org:10.1038/s41420-024-01953-0
331 Page, K. & Lange, Y. Cell adhesion to fibronectin regulates membrane lipid biosynthesis through 5'-AMP-activated protein kinase. *J Biol Chem* **272**, 19339-19342 (1997). https://doi.org:10.1074/jbc.272.31.19339
332 Owen, J. B. a. B., A. Measurement of Oxidized/Reduced Glutathione Ratio. *Protein Misfolding and Cellular Stress in Disease and Aging*, 269-277 (2010).
333 Bjorklund, G. *et al.* The role of glutathione redox imbalance in autism spectrum disorder: A review. *Free Radic Biol Med* **160**, 149-162 (2020). https://doi.org:10.1016/j.freeradbiomed.2020.07.017

334 Dome, P., Tombor, L., Lazary, J., Gonda, X. & Rihmer, Z. Natural health products, dietary minerals and over-the-counter medications as add-on therapies to antidepressants in the treatment of major depressive disorder: a review. *Brain Res Bull* **146**, 51-78 (2019). https://doi.org:10.1016/j.brainresbull.2018.12.015

335 Cameron, J. M. *et al.* Variability of Creatine Metabolism Genes in Children with Autism Spectrum Disorder. *Int J Mol Sci* **18** (2017). https://doi.org:10.3390/ijms18081665

336 Parra, M., Stahl, S. & Hellmann, H. Vitamin B(6) and Its Role in Cell Metabolism and Physiology. *Cells* **7** (2018). https://doi.org:10.3390/cells7070084

337 Menzies, C. *et al.* Distinct basal metabolism in three mouse models of neurodevelopmental disorders. *eNeuro* (2021). https://doi.org:10.1523/ENEURO.0292-20.2021

338 Castro, K., Baronio, D., Schweigert, I., dos Santos Riesgo, R. & Gottfried, C. The effect of ketogenic diet in an animal model of autism induced by prenatal exposure to valproic acid. *Nutritional Neuroscience* **20**, 343-350 (2017). https://doi.org:/10.1080/1028415X.2015.1133029

339 Losenkova, K. *et al.* Endothelial cells cope with hypoxia-induced depletion of ATP via activation of cellular purine turnover and phosphotransfer networks. *Biochim Biophys Acta Mol Basis Dis* **1864**, 1804-1815 (2018). https://doi.org:10.1016/j.bbadis.2018.03.001

340 Burnstock, G. & Ralevic, V. Purinergic signaling and blood vessels in health and disease. *Pharmacol Rev* **66**, 102-192 (2014). https://doi.org:10.1124/pr.113.008029

341 Dunn, J. G. & Grider, M. H. *Physiology, Adenosine Triphosphate*, <https://www.ncbi.nlm.nih.gov/books/NBK553175/> (2023).

342 Mikolajewicz, N., Smith, D., Komarova, S. V. & Khadra, A. High-affinity P2Y2 and low-affinity P2X7 receptor interaction modulates ATP-mediated calcium signaling in murine osteoblasts. *PLoS Comput Biol* **17**, e1008872 (2021). https://doi.org:10.1371/journal.pcbi.1008872

343 Nguyen, R. L., Medvedeva, Y. V., Ayyagari, T. E., Schmunk, G. & Gargus, J. J. Intracellular calcium dysregulation in autism spectrum disorder: An analysis of converging organelle signaling pathways. *Biochim Biophys Acta Mol Cell Res* **1865**, 1718-1732 (2018). https://doi.org:10.1016/j.bbamcr.2018.08.003

344 Muhleder, S. *et al.* Purinergic P2Y(2) receptors modulate endothelial sprouting. *Cell Mol Life Sci* **77**, 885-901 (2020). https://doi.org:10.1007/s00018-019-03213-2

345 Shihan, M., Novoyatleva, T., Lehmeyer, T., Sydykov, A. & Schermuly, R. T. Role of the Purinergic P2Y2 Receptor in Pulmonary Hypertension. *Int J Environ Res Public Health* **18** (2021). https://doi.org:10.3390/ijerph182111009

346 Wang, S. *et al.* P2Y(2) and Gq/G(1)(1) control blood pressure by mediating endothelial mechanotransduction. *J Clin Invest* **125**, 3077-3086 (2015). https://doi.org:10.1172/JCI81067

347 Hochhauser, E. *et al.* P2Y2 receptor agonist with enhanced stability protects the heart from ischemic damage in vitro and in vivo. *Purinergic Signal* **9**, 633-642 (2013). https://doi.org:10.1007/s11302-013-9374-3

348 Gallagher, C. J. & Salter, M. W. Differential Properties of Astrocyte Calcium Waves Mediated by P2Y1 and P2Y2 Receptors. *The Journal of Neuroscience* **23**, 6728-6739 (2003). https://doi.org:https://doi.org/10.1523/JNEUROSCI.23-17-06728.2003

349 Park, S. M., Park, H. R. & Lee, J. H. MAPK3 at the Autism-Linked Human 16p11.2 Locus Influences Precise Synaptic Target Selection at Drosophila Larval Neuromuscular Junctions. *Mol Cells* **40**, 151-161 (2017). https://doi.org:10.14348/molcells.2017.2307

350 Beckers, C. M. *et al.* ROCK2 primes the endothelium for vascular hyperpermeability responses by raising baseline junctional tension. *Vascul Pharmacol* **70**, 45-54 (2015). https://doi.org:10.1016/j.vph.2015.03.017
351 Fayed, H. S. *et al.* Selective ROCK Inhibitor Enhances Blood Flow Recovery after Hindlimb Ischemia. *Int J Mol Sci* **24** (2023). https://doi.org:10.3390/ijms241914410
352 Martin Lorenzo, S., Nalesso, V., Chevalier, C., Birling, M. C. & Herault, Y. Targeting the RHOA pathway improves learning and memory in adult Kctd13 and 16p11.2 deletion mouse models. *Mol Autism* **12**, 1 (2021). https://doi.org:10.1186/s13229-020-00405-7
353 Borikova, A. L. *et al.* Rho kinase inhibition rescues the endothelial cell cerebral cavernous malformation phenotype. *J Biol Chem* **285**, 11760-11764 (2010). https://doi.org:10.1074/jbc.C109.097220
354 Leclerc, S. & Easley, D. Pharmacological Therapies for Autism Spectrum Disorder: A Review. *Pharmacy and Therapeutics* **40** (2015).
355 McCarthy, M., Arnold, A., Ball, G., Blaustein, J. & De Vries, G. Sex differences in the brain: the not so inconvenient truth. *J Neurosci* **32**, 2241-2247 (2008).
356 Ghisleni C, Bollmann S & A, B.-L. Effects of Steroid Hormones on Sex Differences in Cerebral Perfusion. *PLoS One* **10**, e0135827 (2015).
357 Gur RC, Gur RE & WD, O. Sex and handedness differences in cerebral blood flow during rest and cognitive activity. *Science* **217**, 659-661 (1982).
358 Krause, D. N., Duckles, S. P. & Pelligrino, D. A. Influence of sex steroid hormones on cerebrovascular function. *J Appl Physiol (1985)* **101**, 1252-1261 (2006). https://doi.org:10.1152/japplphysiol.01095.2005
359 Ospina JA, Duckles SP & Krause DN. 17beta-estradiol decreases vascular tone in cerebral arteries by shifting COX-dependent vasoconstriction to vasodilation. *Am J Physiol Heart Circ Physiol* **285**, H241-250 (2003).
360 Gonzales, R. J., Krause, D. N. & Duckles, S. P. Testosterone suppresses endothelium-dependent dilation of rat middle cerebral arteries. *Am J Physiol Heart Circ Physiol* **286**, 552-560 (2004).
361 Geary, G. G., Krause, D. N. & Duckles, S. P. Estrogen reduces mouse cerebral artery tone through endothelial NOS- and cyclooxygenase-dependent mechanisms. *Am J Physiol Heart Circ Physiol* **279**, 511-519 (2000).
362 Jacquemont, S. *et al.* A higher mutational burden in females supports a "female protective model" in neurodevelopmental disorders. *Am J Hum Genet* **94**, 415-425 (2014). https://doi.org:10.1016/j.ajhg.2014.02.001
363 Robinson, E. B., Lichtenstein, P., Anckarsater, H., Happe, F. & Ronald, A. Examining and interpreting the female protective effect against autistic behavior. *Proc Natl Acad Sci U S A* **110**, 5258-5262 (2013). https://doi.org:10.1073/pnas.1211070110
364 Crider, A. & Pillai, A. Estrogen Signaling as a Therapeutic Target in Neurodevelopmental Disorders. *J Pharmacol Exp Ther* **360**, 48-58 (2017).
365 Gadad, B. S., Hewitson, L., Young, K. A. & German, D. C. Neuropathology and Animal Models of Autism: Genetic and Environmental Factors. *Autism Research and Treatment* **2013**, 1-12 (2013). https://doi.org:10.1155/2013/731935
366 Bauminger, N., Solomon, M. & Rogers, S. J. Externalizing and internalizing behaviors in ASD. *Autism Research* **3**, 101-112 (2010). https://doi.org:10.1002/aur.131

367 Seminario-Vidal, L. *et al.* Rho signaling regulates pannexin 1-mediated ATP release from airway epithelia. *J Biol Chem* **286**, 26277-26286 (2011). https://doi.org:10.1074/jbc.M111.260562

Appendices

Appendix A

Supplemental information for Manuscript I

Vascular contributions to 16p11.2 deletion autism syndrome modeled in mice

Julie Ouellette, Xavier Toussay, Cesar H. Comin, Luciano da F. Costa, Mirabelle Ho, María Lacalle-Aurioles, Moises Freitas-Andrade, Qing Yan Liu, Sonia Leclerc, Youlian Pan, Ziying Liu, Jean-François Thibodeau, Melissa Yin, Micael Carrier, Cameron J. Morse, Peter Van Dyken, Christopher J. Bergin, Sylvain Baillet, Christopher R. Kennedy, Marie-Ève Tremblay, Yannick D. Benoit, William L. Stanford, Dylan Burger, Duncan J. Stewart and Baptiste Lacoste

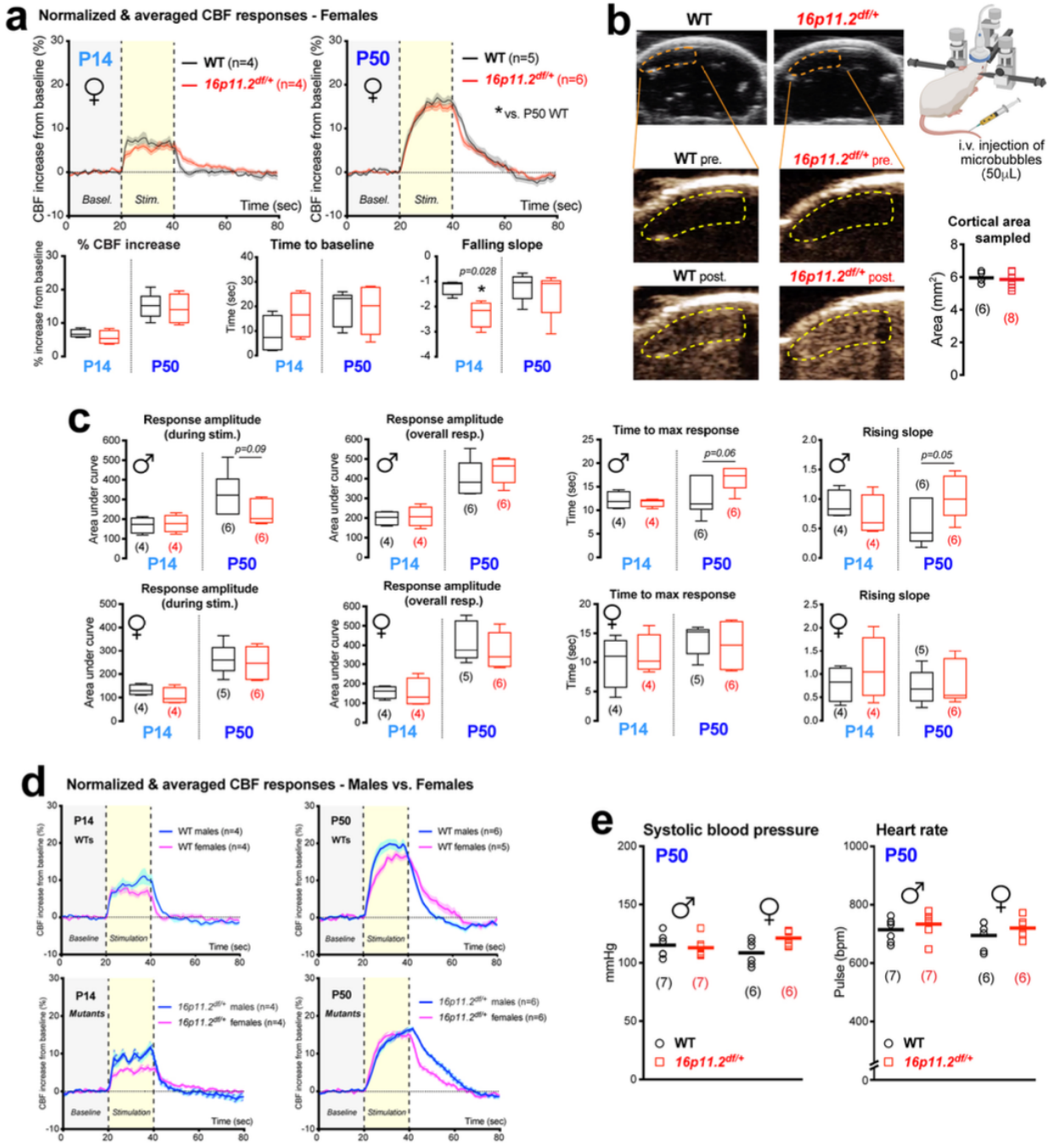

Extended Data Fig. 1 | Neurovascular parameters in *16p11.2*$^{df/+}$ and WT mice at P14 and P50. a, CBF assessment by LDF in *16p11.2*$^{df/+}$ and WT females at P14 and P50. Only falling slope appeared affected by genotype in females at P14. **b**, Additional representative images and a diagram for contrast imaging method, showing the region of interest (ROI, dotted lines) before (*pre.*) and after (*post.*) i.v. injection of microbubbles. The graph on the right shows identical ROI size in all animals. **c**, Additional CBF parameters in *16p11.2*$^{df/+}$ and WT males versus females. **d**, LDF traces (mean ± s.e.m.) obtained before, during, and after whisker stimulation in all mice (regrouped by genotype). **e**, Mean systolic blood pressure and heart rate measured over 5 days at P50 using tail cuffs. WT, Wild-Type. Data are whisker boxes (min to max, center line indicating median) in **a** and **c**, or mean with individual values in **b** and **e**. Traces in **a** and **d** are mean ± s.e.m. (n = 4-8 animals per group). *$P < 0.05$ (two tailed Mann-Whitney test). ♂: males; ♀: females.

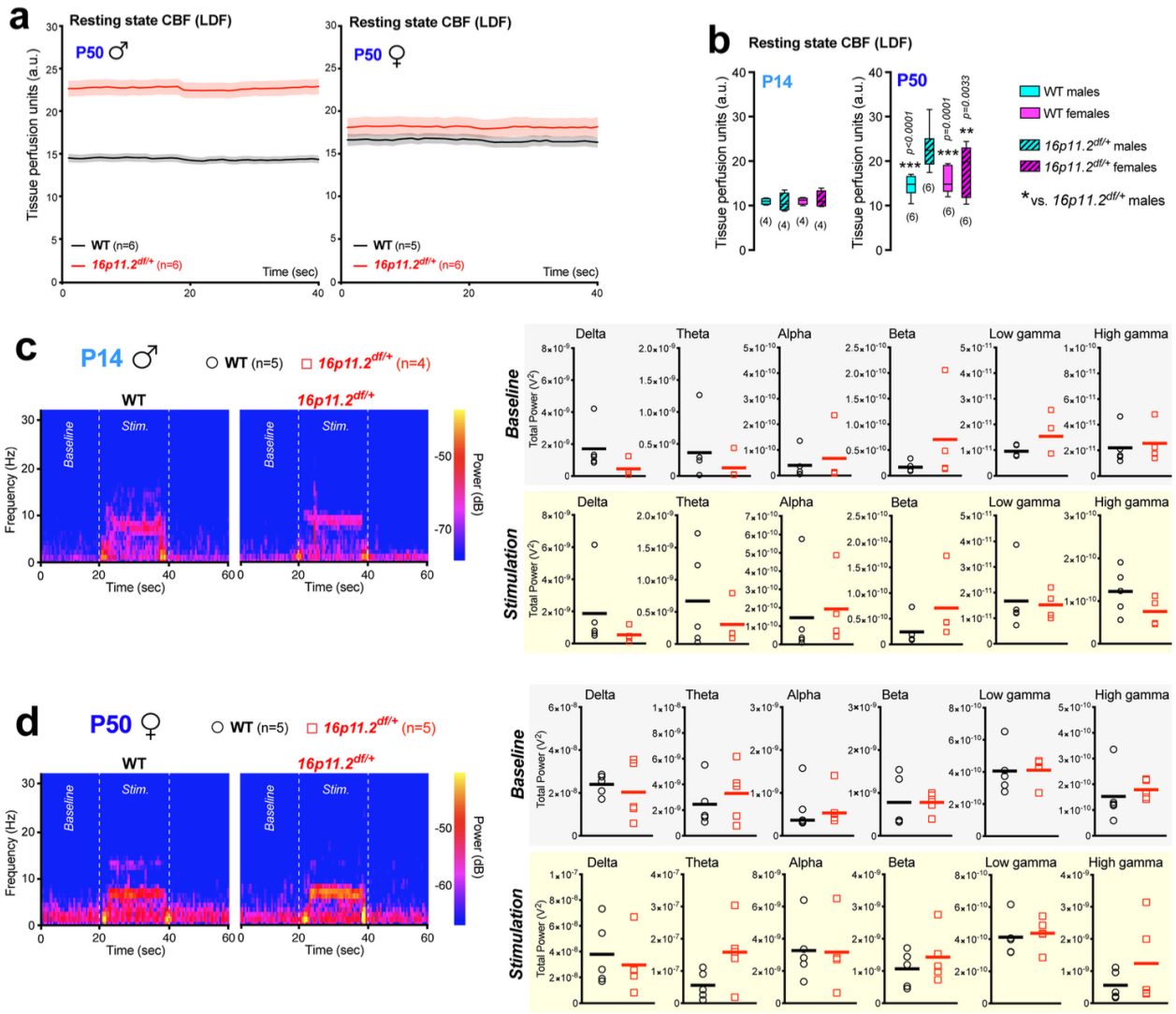

Extended Data Fig. 2 | Cerebrovascular and electrophysiological parameters in male and female *16p11.2*$^{df/+}$ and WT mice at P14 and P50. a, LDF recording (Tissue perfusion units, mean ± s.e.m.) of resting state CBF over the primary somatosensory cortex from anesthetized mice, averaged over 40 sec. **b**, Quantification and comparison of resting state CBF using LDF in all groups of mice. **c,d**, eCoG recordings in the primary somatosensory cortex from P14 male (**c**), and P50 female (**d**) *16p11.2*$^{df/+}$ and WT mice. In **c** and **d**: *Left*, Representative power spectral traces of low-frequency bands (n = 4-5 animals per group; 6 stimulations per animal). *Right*, Average absolute power in Delta (1-4 Hz), Theta (4-8 Hz), Alpha (8-13 Hz), Beta (13-30 Hz), Low Gamma (35-55 Hz) and High Gamma (65-100 Hz) frequency bands at resting-state (*upper panel*) and during stimulation (*lower panel*). Data (*right*) are mean with individual values (n = 4-5 animals per group; 6 stimulations per animal). Data are mean ± s.e.m. in **a**, whisker boxes (min to max, center line indicating median) in **b**, or mean with individual values in c,d (*right*) (n = 4-6 animals per group). $^{**}P < 0.01$, $^{***}P < 0.001$ (2-way ANOVA and Tukey's *post-hoc* test in **b**).

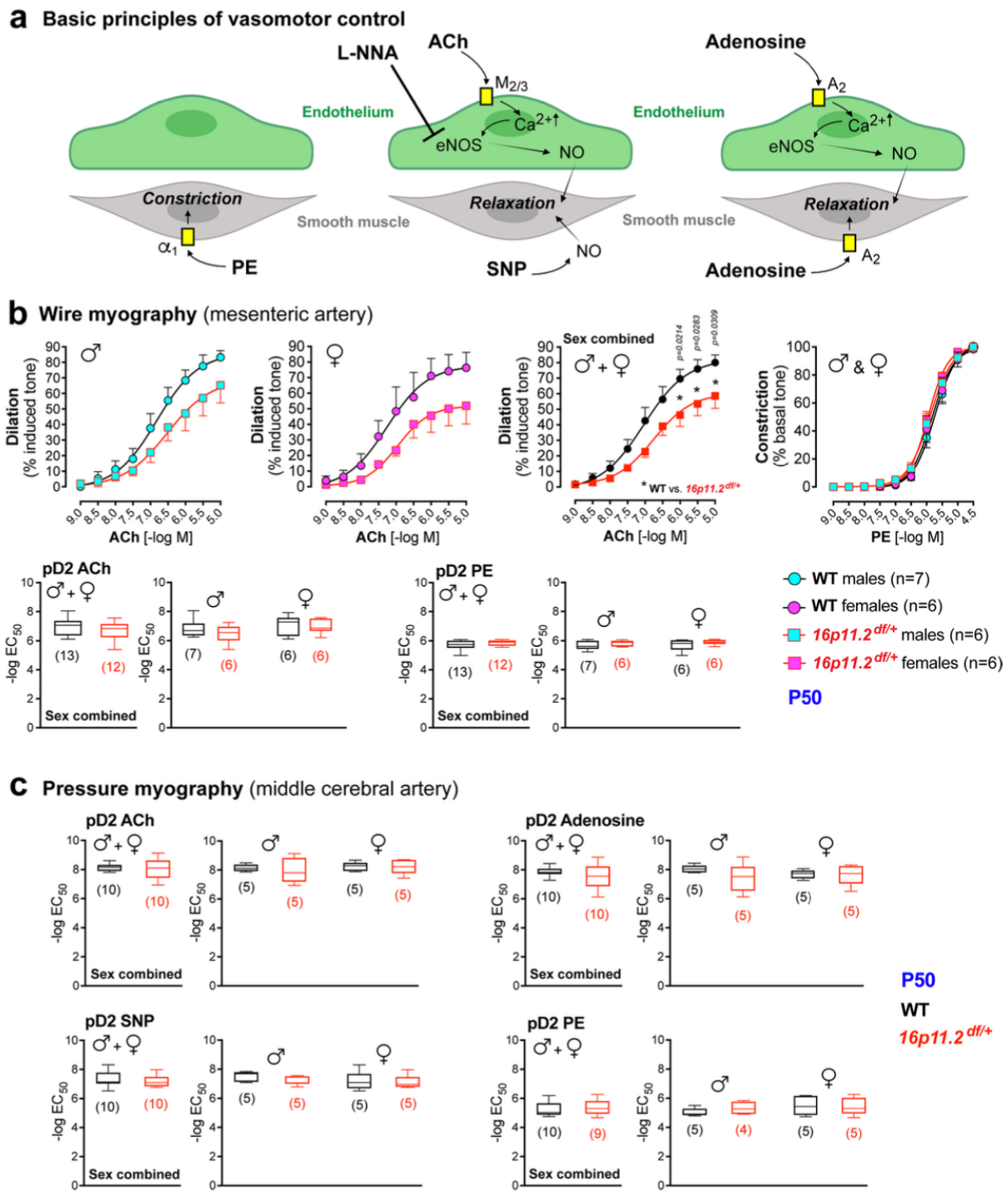

Extended Data Fig. 3 | *Ex vivo* vascular reactivity (VR) of middle cerebral and mesenteric arteries from *16p11.2*$^{df/+}$ and WT mice at P50. a, Schematic representation of cellular and molecular VR mechanisms. **b**, *Upper panels*, Wire myography of mesenteric arteries *ex vivo* confirming 16p11.2 deletion-induced endothelial dysfunction. Females and males display a similar endothelial-dependent deficit, but normal VSMC response. *Lower panels*, pD2 values obtained from the dose-response curves from male and female mice. **c**, pD2 values obtained from dose-response curves of male and female middle cerebral arteries (see Fig. 2). ACh, acetylcholine; L-NNA, NG-Nitro-L-arginine; Pe, phenylephrine; SNP, sodium nitroprusside; VSMC, vascular smooth muscle cell; WT, Wild-Type. Data are mean ± s.e.m. in **b** (*upper panel*), or whisker boxes (min to max, center line indicating median) in **b** (*lower panel*) and **c** (n = 5-7 animals per sex group). *$P < 0.05$ (2-way repeated measure ANOVA and Tukey's *post-hoc* test in **b**).

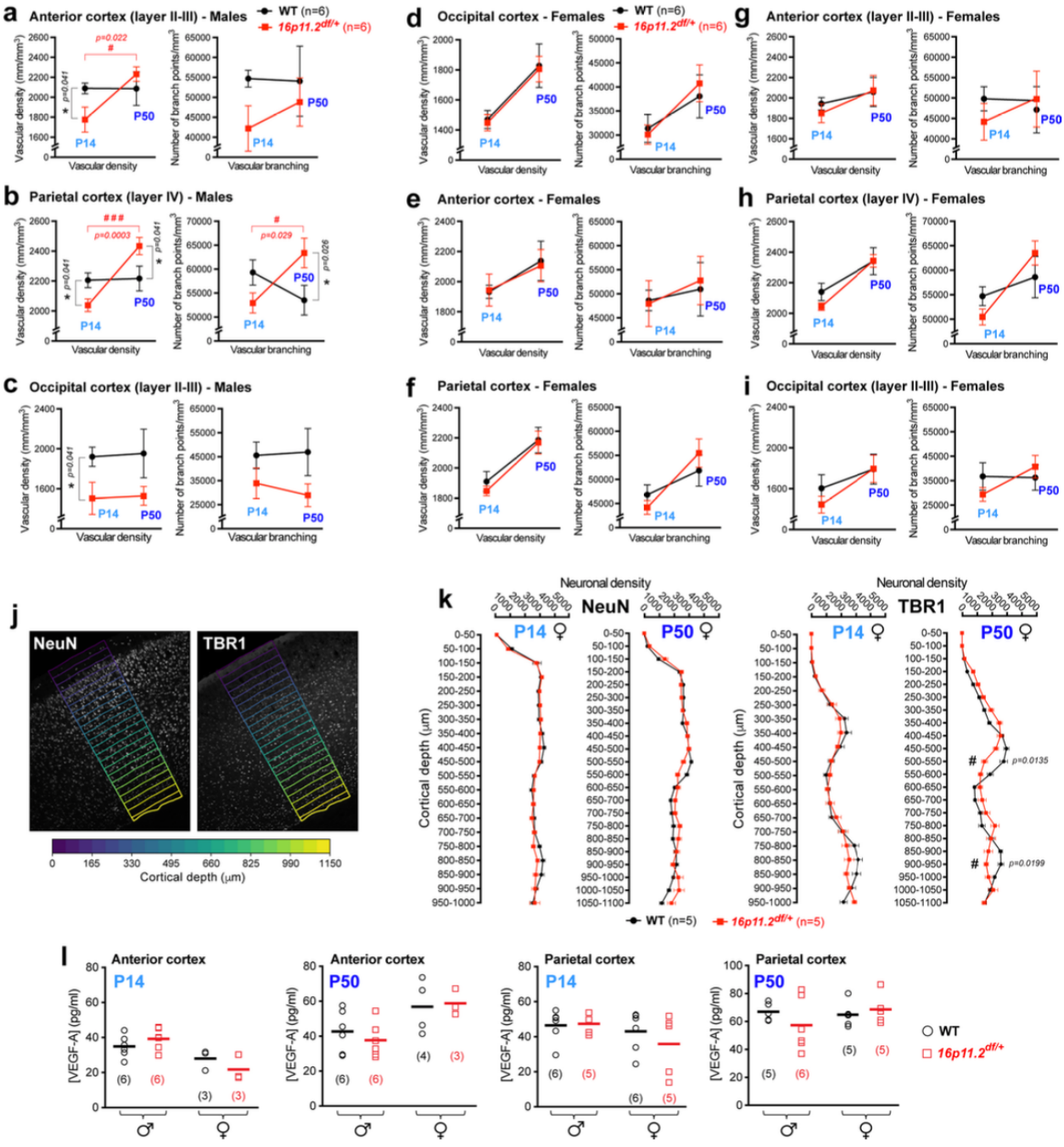

Extended Data Fig. 4 | Postnatal neurovascular maturation in the cerebral cortex of *16p11.2*$^{df/+}$ and WT mice. **a–c**, Postnatal developmental profile of cerebral cortex endothelial networks in *16p11.2*$^{df/+}$ and WT males (cortical layers where most significant differences were found). **d-i**, Postnatal developmental profile of cerebral cortex endothelial networks in *16p11.2*$^{df/+}$ and WT females. **j**, Sample image of the computational approach used to delineate ROIs in the cortex to quantify neuronal density (see methods for details). **k**, Quantification of neuronal density in the parietal (that is, somatosensory) cortex of female mice following immunostaining for neuronal markers NeuN and TBR1. **l**, Vascular endothelial growth factor-A (VEGF-A) levels measured by E.L.I.S.A. in protein extracts from cerebral cortex micro-dissected at P14 or P50 in male and female mice. WT, Wild-Type. Data are mean ± s.e.m. in **a-i** and **k**, or mean with individual values in **l** (n = 3-6 animals per group). *$P < 0.05$ (two tailed Mann-Whitney test). $^{\#}P < 0.05$, $^{\#\#\#}P < 0.001$ (2-way ANOVA and Sidak's *post-hoc* test).

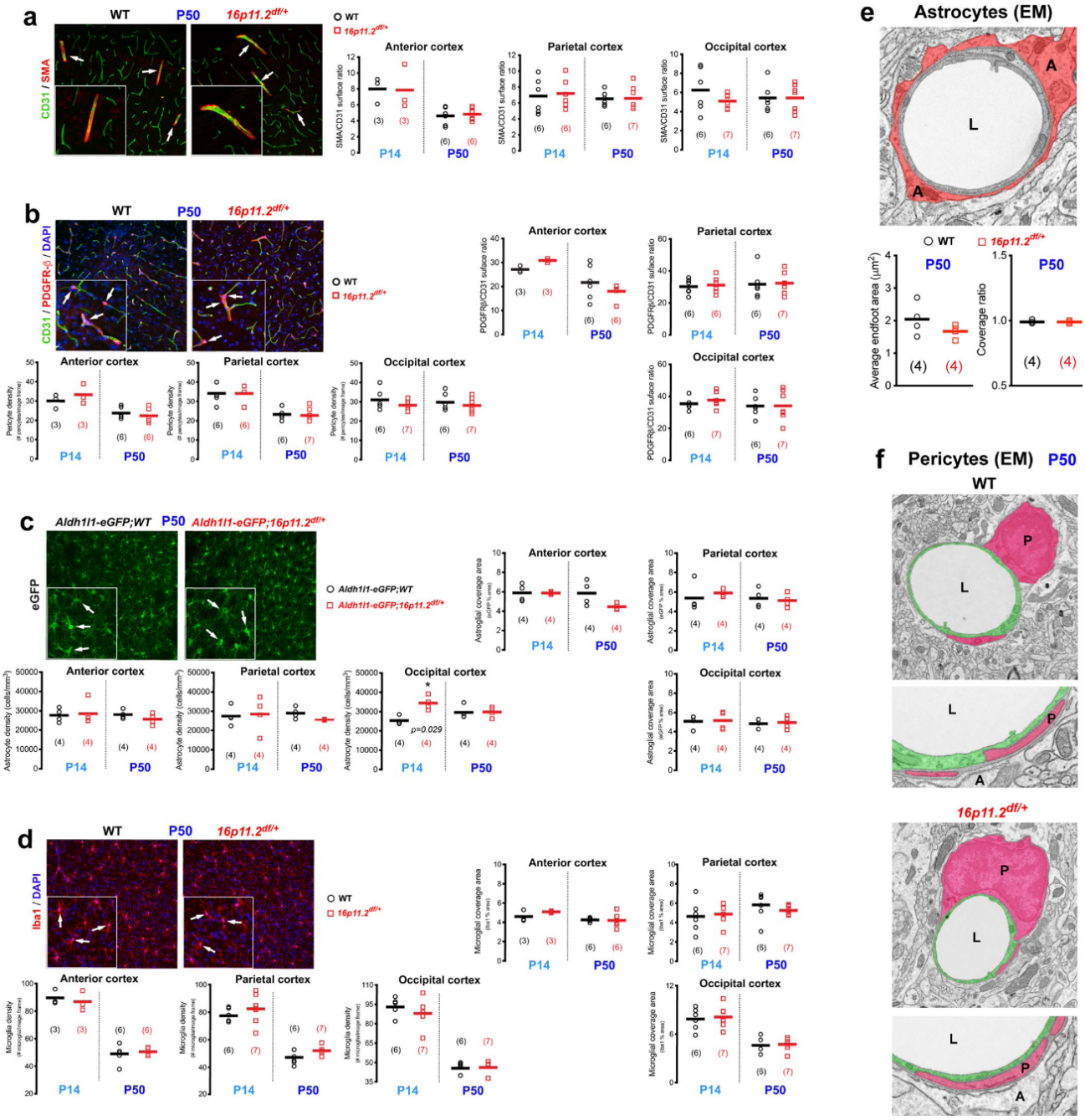

Extended Data Fig. 5 | Morphology of the neurovascular unit in male *16p11.2*$^{df/+}$ and WT mice at P14 and P50. Immunohistochemical analysis of vascular smooth muscle cells, VSMCs (**a**, SMA), pericytes (**b**, PDGFR-β), astrocytes (**c**, Aldh1l1-eGFP) and microglia (**d**, Iba1) in the cerebral cortex. **a**, endothelial coverage by VSMCs measured in the anterior, parietal and occipital cortex. **b**, Pericyte density and endothelial coverage measured in the anterior, parietal and occipital cortex. endothelial marker CD31 was used in **a** and **b** to stain vessels. **c**, Astrocyte density and surface coverage measured in the anterior, parietal and occipital cortex of mice expressing eGFP under the control of the pan-astrocytic *Aldh1l1* promotor. **d**, Microglia density and surface coverage measured in the anterior, parietal and occipital cortex. **e**, *Top*, Transmission electron micrograph showing astrocytic endfeet (red-pseudocolored) surrounding a brain capillary. *Bottom*, Quantification of average endfoot size (*left*) and endothelial coverage ratio by endfeet (*right*). **f**, Transmission electron micrographs showing pericytes (pink-pseudocolored) within the basement membrane around brain endothelial cells (green-pseudocolored). Images are representative of experiments repeated in 4 male mice per group, with similar results. Normal astrocyte coverage and pericyte attachment were observed in *16p11.2*$^{df/+}$ mice. A, astrocytes; L, lumen; P, pericyte; WT, Wild-Type. All data are mean with individual values (n = 3-7 animals per group). *$P < 0.05$ (two tailed Mann-Whitney test in **c**).

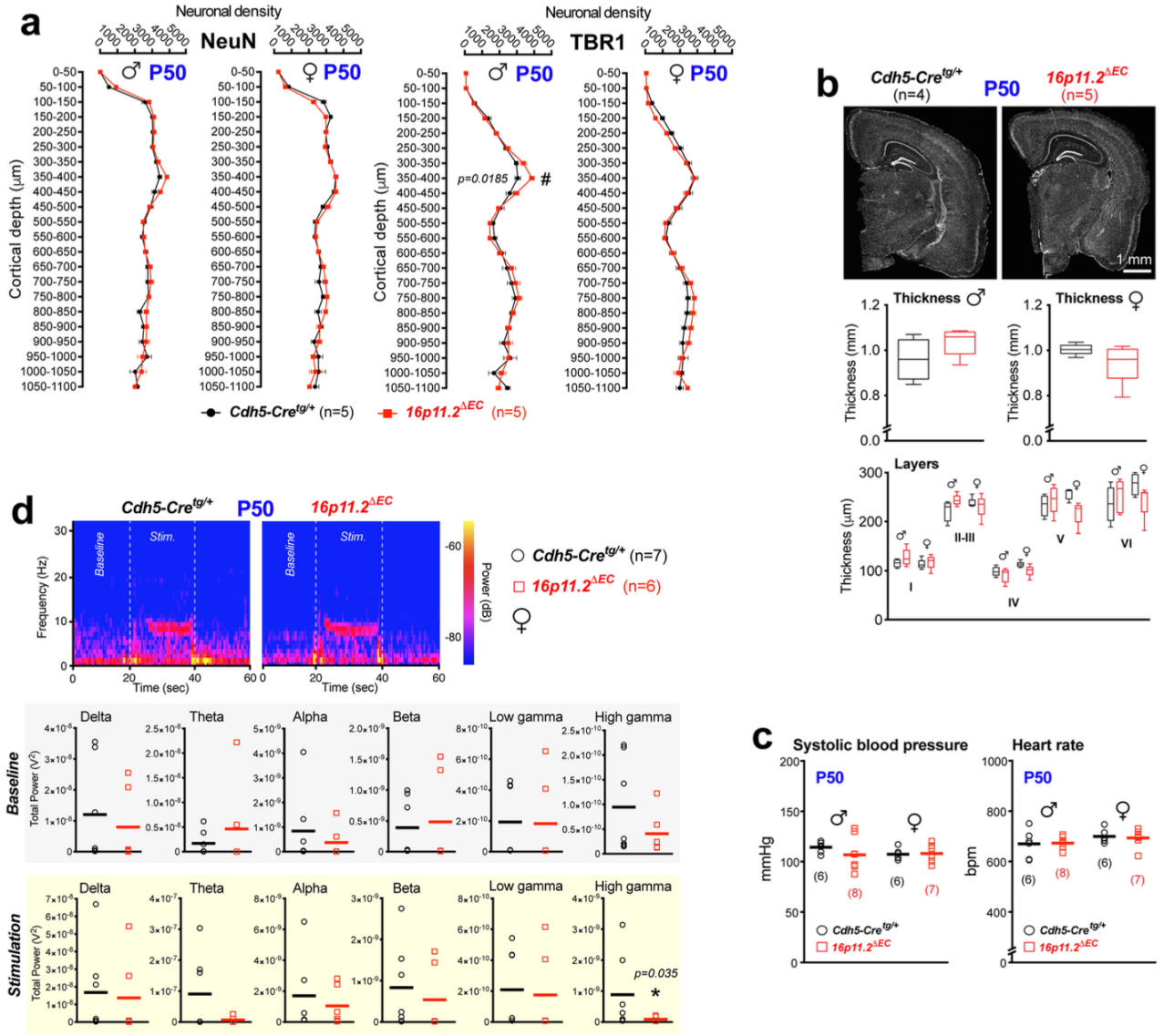

Extended Data Fig. 6 | Additional information on neurovascular features in conditional *16p11.2*$^{\Delta EC}$ mutants and *Cdh5-Cre*$^{tg/+}$ controls at P50. **a**, Quantification of neuronal density in the parietal (that is, somatosensory) cortex of P50 males and females following immunostaining for neuronal markers NeuN and TBR1. **b**, Quantification of cortical thickness and layering from micrographs of DAPI-stained brain sections from males and females. No difference was evidenced between *16p11.2*$^{\Delta EC}$ and control mice. **c**, Normal mean systolic blood pressure and heart rate in *16p11.2*$^{\Delta EC}$ as measured by tail cuffs. **d**, eCoG recordings in the primary somatosensory cortex from P50 female *16p11.2*$^{\Delta EC}$ and control mice. *Top panels*, representative power spectral traces of low-frequency bands. *Bottom graphs,* average absolute power in Delta (1-4 Hz), Theta (4-8 Hz), Alpha (8-13 Hz), Beta (13-30 Hz), Low Gamma (35-55 Hz) and High Gamma (65-100 Hz) frequency bands at resting-state (*upper graphs*) and during stimulation (*bottom graphs*). Data are mean ± s.e.m. in **a**, whisker boxes (min to max, center line indicating median) in **b**, or mean with individual values in **c** and **d** (n = 4-8 animals per group). $^{\#}P < 0.05$ (2-way ANOVA and Sidak's *post-hoc* test in **a**). $^{*}P < 0.05$ (Mann-Whitney test in **c**).

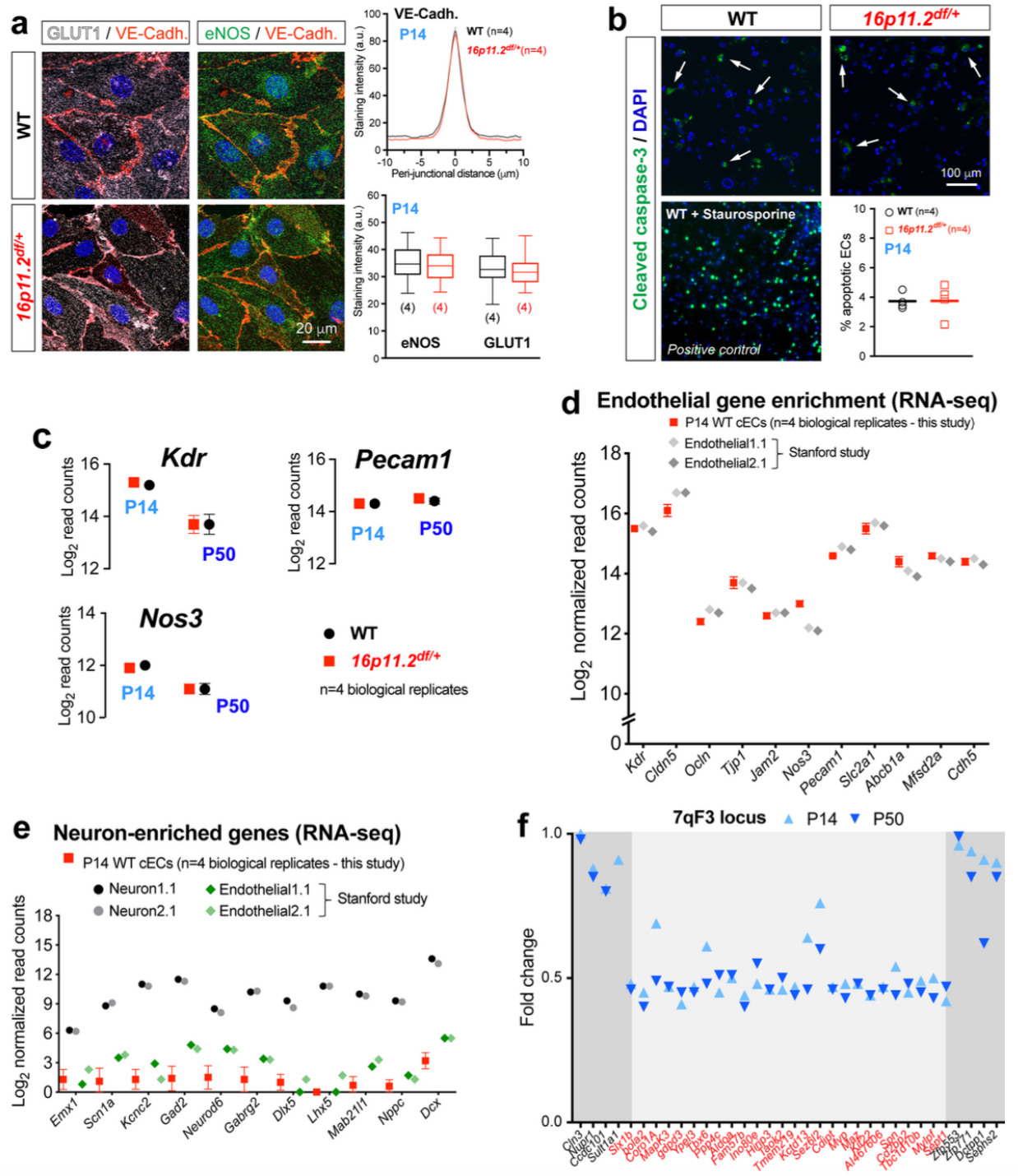

Extended Data Fig. 7 | See next page for caption.

Extended Data Fig. 7 | Characterization of primary mouse cerebral cortex ECs (cECs) from male WT and *16p11.2*$^{df/+}$ mice. a, Representative images and quantifications of immunocytochemical staining for ceC-specific markers GLUT-1, eNOS and Ve-Cadherin, showing no difference between WT and mutant ceCs isolated at P14 (blue: DAPI). **b**, Assessment of apoptosis in P14 ceC cultures. The Caspase-3/7 green assay revealed normal apoptotic rates in *16p11.2df/+* ceCs. **c**, qPCR validation on ceC RNA using mouse VeGFR-2, CD31 and eNOS as markers (a no reverse transcriptase control was used as negative control). **d**, Assessment of endothelial gene enrichment using RNAseq data normalized to a publicly-available database from Dr. Ben A. Barres lab, Stanford University, USA (Zhang *et al*. 2014, PMID 25186741; http://www.brainrnaseq.org/). **e**, Assessment of neuronal contamination using RNAseq data (as in **d)**. A very low level of contamination was achieved. examples given are from cortical endothelial cells (ceCs) isolated from male mice at P14. **f**, Confirmation of ceC 16p11.2 haploinsufficiency by RNAseq. Mapping of fold change (FC) to 7qF3 locus genes confirms a ~50% decrease in gene expression levels at both P14 and P50. Data are mean ± s.e.m in **a** (Ve-Cadh.) and **c,d,e**, whisker boxes (min to max, center line indicating median) in **a** (eNOS, GLUT1), or mean with individual values in **b**. CTL, control; WT, Wild-Type. For RNAseq, n = 3-4 biological replicates per group (2 mice per replicate).

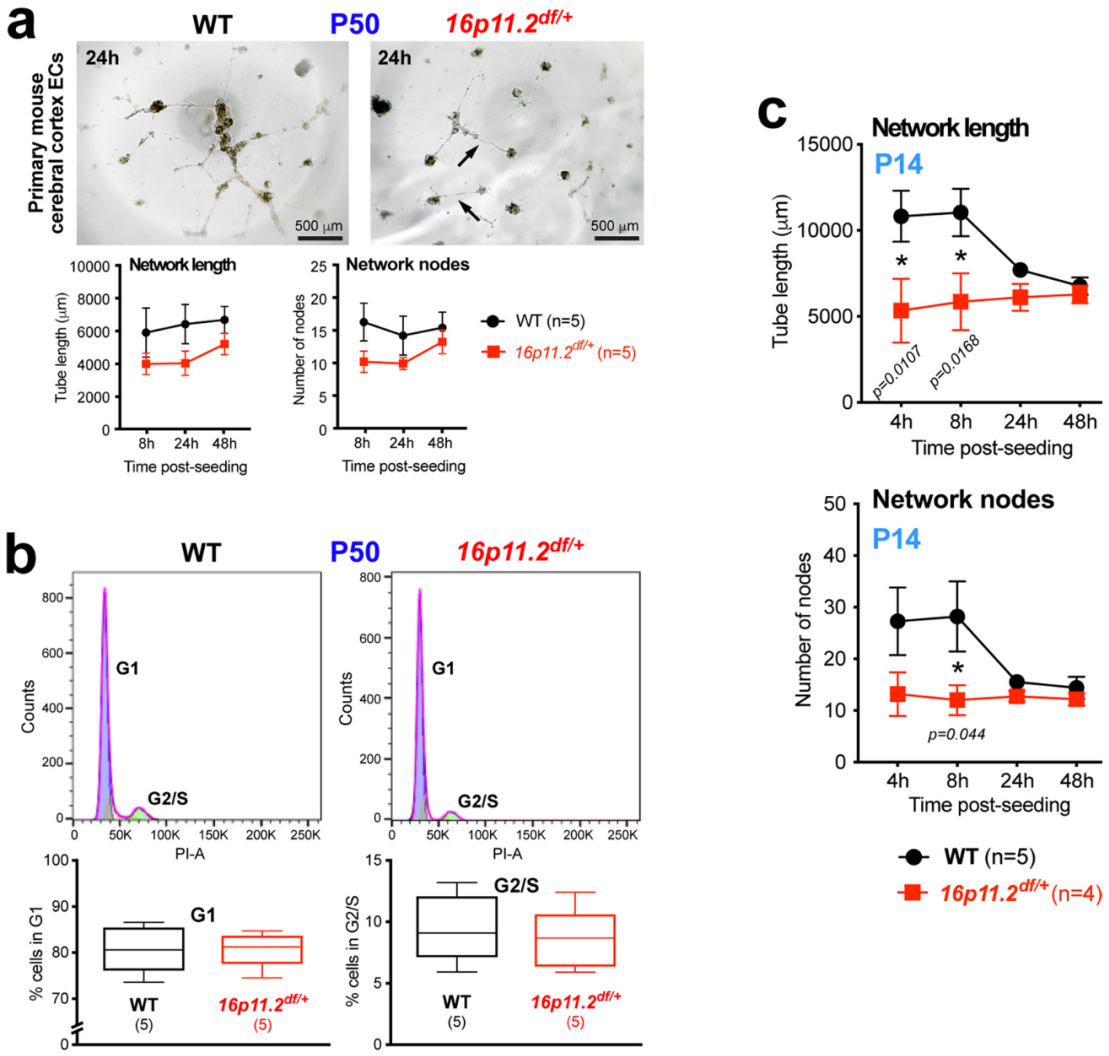

Extended Data Fig. 8 | *In vitro* network formation assay using primary cECs from P14 and P50 male mice. a, *In vitro* network formation assay using primary cECs from P50 brains to assess vascular network formation and remodeling over 48 hrs in a growth factor-reduced Matrigel® (eGF < 0.5 ng/mL; PDGF < 5 pg/mL; IGF-1 5 ng/mL; TGF-β 1.7 ng/mL). No significant difference was quantified between *16p11.2df/+* and WT cECs. **b**, Assessment of cell proliferation using cell cycle analysis with cECs from P50 brains. The proportion of cells in G2/S (proliferation) or G1 (growth) phases was identical between *16p11.2df/+* and WT cECs. **c**, Cultured P14 cECs were seeded in a growth-factor supplemented Matrigel® (eGF: 0.7 ng/mL; PDGF 12 pg/mL; IGF1 16 ng/mL; TGFβ 2.3 ng/mL). Impaired angiogenic activity of *16p11.2df/+* of cECs was only partly rescued in these conditions. Data are mean ± s.e.m. in **a** and **c**, or whisker boxes (min to max, center line indicating median) in **b** (n = 4-5 animals per group). **P* < 0.05 (2-way repeated measure ANOVA and Sidak's *post-hoc* test).

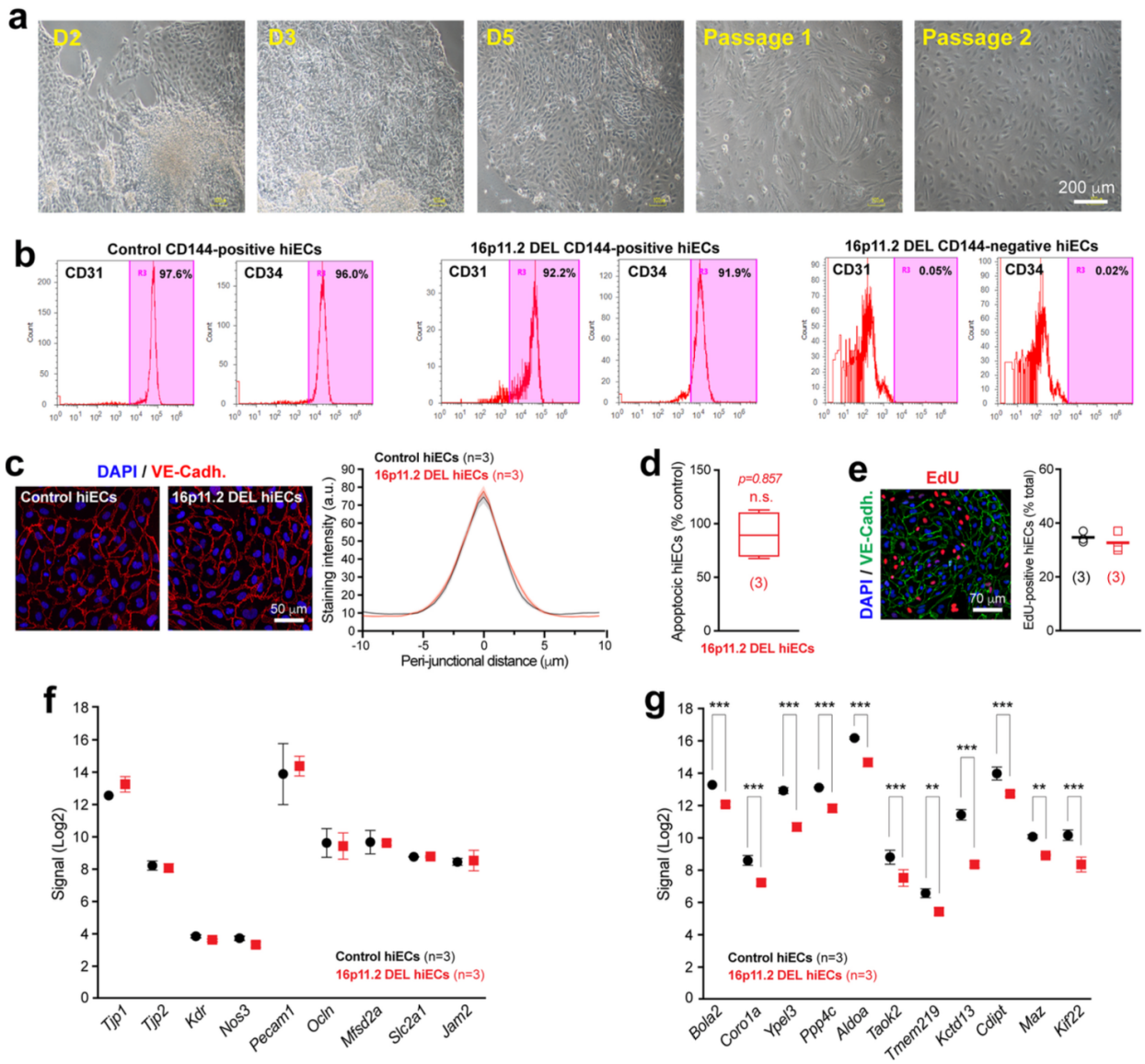

Extended Data Fig. 9 | Human iPSC lines used to derive endothelial cells, and the quality controls. a, Representative images of cell morphology from culture steps (D=day) involved in differentiating human iPSC into human-induced endothelial cells (hiECs). Images are representative of 3 experiments repeated independently with similar results. **b**, Representative flow cytometric plots of MAC-selected CD144- positive cells from both control (healthy) and 16p11.2 individuals, demonstrating similarly high expression of endothelial markers CD31 and CD34. Conversely, CD144-negative hiECs show negligible expression of endothelial markers. Flow cytometric plots displayed are representative of 4 experiments repeated independently with similar results. **c**, *Left*, Sample images of immunocytochemical staining for endothelial marker VE-Cadherin in hiECs cultures. *Right*, Quantification of Ve-Cadherin staining intensity across cell-cell junctions (total of 100 junctions/genotype) showing normal endothelial differentiation using 16p11.2 deletion iPSCs. **d**, Assessment of apoptotic rates in cell culture using a Caspase3/7 green assay shows no difference between control and 16p11.2 DEL hiECs.**e**, Assessment of proliferation in cell culture using an edU incorporation assay shows no difference between control and 16p11.2 DEL hieCs.**f**, Quantification of core endothelium-enriched genes using ClariomTM S shows no differences between control and 16p11.2 DEL hiECs. **g**, Quantification of 16p11.2 locus genes using ClariomTM S microarray confirms hemizygosity of 16p11.2 DEL hiECs compared to control hieCs. DeL, deletion. Data are mean ± s.e.m. in **c**, **f** and **g**, whisker boxes (min to max, center line indicating median) in **d**, or mean with individual values in **e** (n = 3 cell lines per group). $^{**}P < 0.01$, $^{***}P < 0.001$ (2-way ANOVA and Tukey's *post-hoc* test).

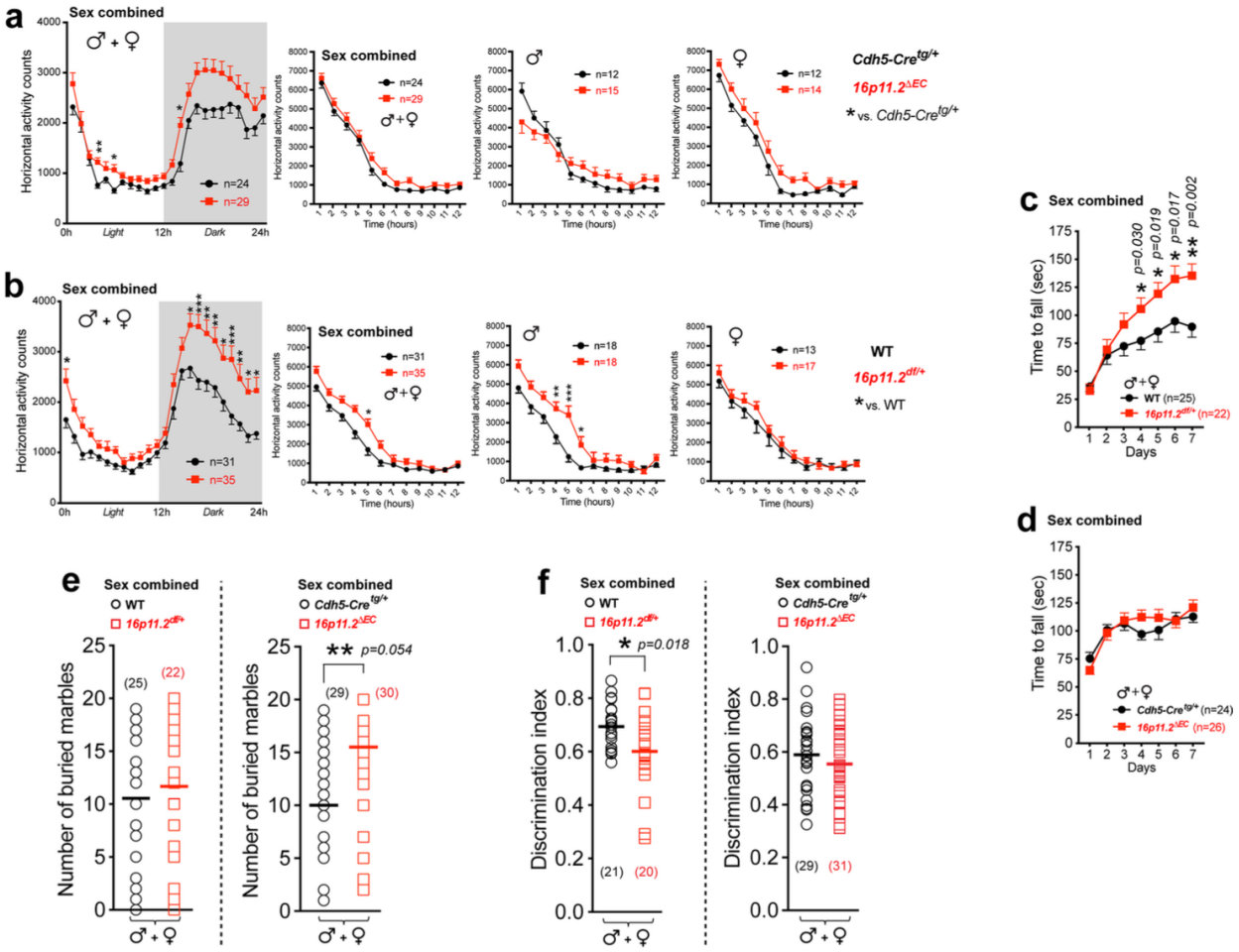

Extended Data Fig. 10 | Additional behavioral analysis of constitutive and conditional mutant mice and their controls. a, **b**, *Left*, Assessment of home cage activity in the beam break test for combined *16p11.2*$^{\Delta EC}$ and control littermates (**a**), or combined male and female *16p11.2*$^{df/+}$ and WT mice (**b**). *Right*, First 12hrs of habituation (from testing day 1) in the beam break test for male and female *16p11.2*$^{\Delta EC}$ and control littermates (**a**), or *16p11.2*$^{df/+}$ and WT mice (**b**). **c,d**, Assessment of motor learning/coordination in the rotarod test for combined male and female *16p11.2*$^{df/+}$ and WT mice (**c**), or *16p11.2*$^{\Delta EC}$ and control littermates (**d**). **e**, The marble burying test revealed a phenotype for combined sexes in *16p11.2*$^{\Delta EC}$ mice (*right*), but not *16p11.2*$^{df/+}$ mice (*left*). **f**, The novel object recognition test revealed a phenotype for combined sexes in *16p11.2df/+* mice (*left*), but not for *16p11.2*$^{\Delta EC}$ mice (*right*). Data are mean ± s.e.m. in **a-d**, or mean with individual values in **e** and **f** (n = 9-18 mice per sex group). *$P < 0.05$, **$P < 0.01$, ***$P < 0.001$ (2-way repeated measure ANOVA and Sidak's *post-hoc* test in **a-c**; Mann-Whitney test in **e** and **f**). ♂: males; ♀: females.

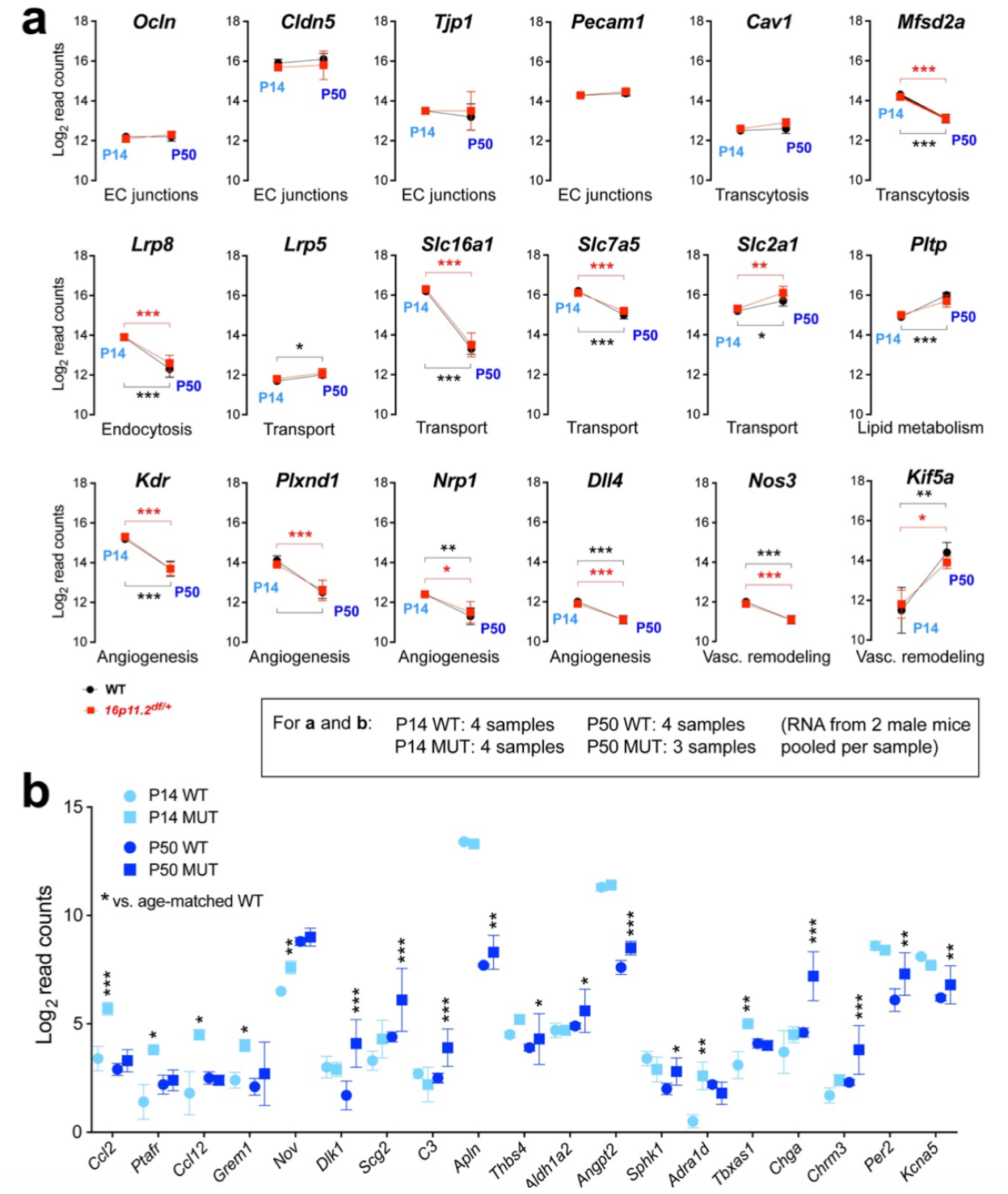

Supplementary Fig. 1 | Additional information on gene expression between male WT and *16p11.2*$^{df/+}$ brain endothelial cells. a, Effect of age (i.e. between P14 and P50) on brain endothelial gene expression. Examples of genes involved in blood-brain barrier function and maintenance, angiogenesis, transport, lipid metabolism and vascular remodeling are presented. **b,** Endothelial expression levels (Log2 of read counts) of 19 upregulated genes at P14 and P50. WT, Wild-Type; MUT, Mutant. Data are mean ± s.e.m. in **a**, or mean ± s.d. in **b** (n=3-4 samples per group, RNA from 2 mice pooled per sample). **P* < 0.05, ***P* < 0.01, ****P* < 0.001 (2-way ANOVA and Sidak's *post-hoc* test).

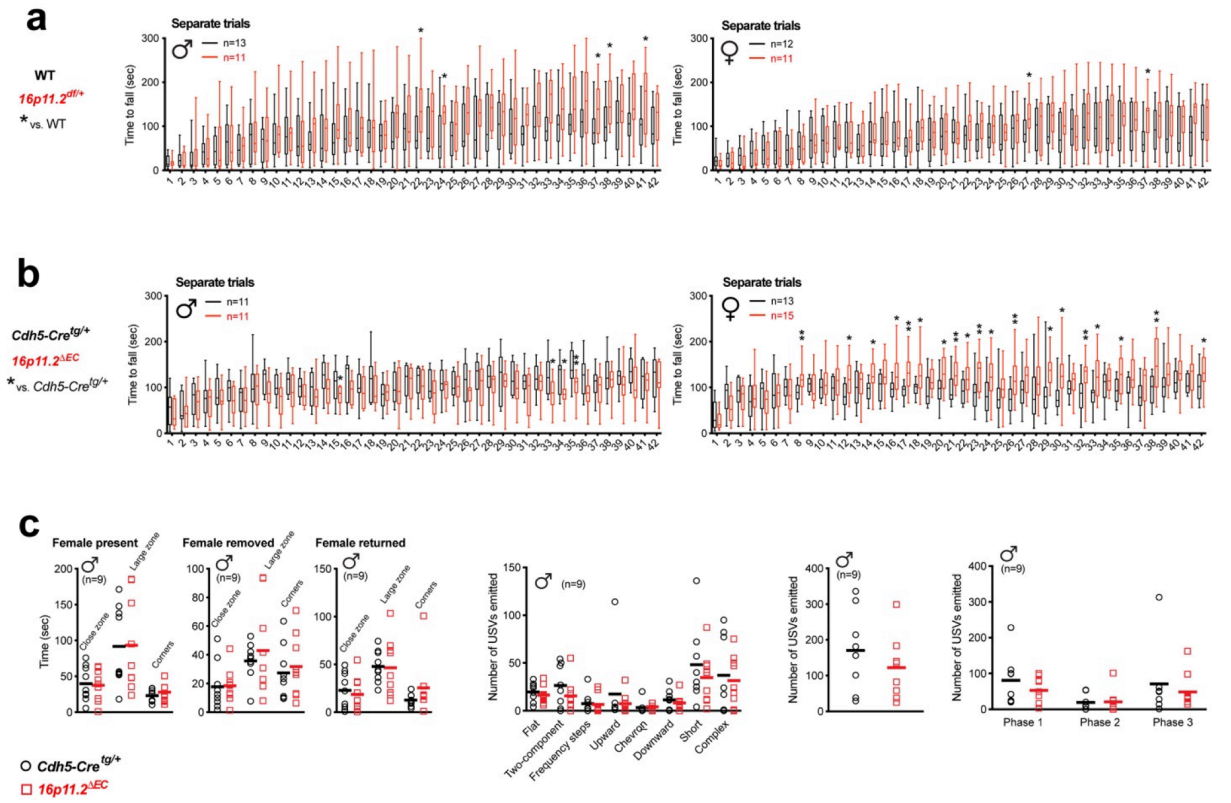

Supplementary Fig. 2 | Additional information on behavioral changes between WT and *16p11.2*$^{df/+}$ mice, and between control and in *16p11.2*$^{\Delta EC}$ mice. a,b, Separate trials across the entire duration of the rotarod test (7 days, 6 trials per day, total of 42 trials) are shown for WT vs. *16p11.2*$^{df/+}$ male and female mice (**a**), or *Cdh5-Cre*$^{tg/+}$ vs. *16p11.2*$^{\Delta EC}$ male and female mice (**b**). **c,** Male-female interaction test with ultrasonic vocalizations (USVs) in *16p11.2* $^{\Delta EC}$ and control mice. The *top* graph represents the time spent by males in the rectangular interaction zone (2cm from female enclosure), as well as time spent in two open field corners away from the female. The *bottom* graphs represent overall USVs, number of USVs during each phase (1,2,3) of the test, and the different categories of USVs based on their phonological signature. This test failed to reveal any difference between *16p11.2* $^{\Delta EC}$ and control males. Data are whisker boxes (min to max, center line indicating median) in **a** and **b**, or mean with individual values in **c** (n=9-18 mice per sex group). *$P < 0.05$, **$P < 0.01$ (2-way repeated measure ANOVA and Sidak's *post-hoc* test in **a** and **b**).

Supplementary Table 1 | Critical information on the iPSC lines used in this study.

iPSC line ID	Sex	Age (years)	Source cell type	Reprogramming	Genotype	Source	Laboratory
SV0001442	M	5	Fibroblast	Episomal	16p11.2 DEL	SFARI	Dolmetsch
SV0001453	M	7	Fibroblast	Episomal	16p11.2 DEL	SFARI	Dolmetsch
SV0001459	M	39	Fibroblast	Episomal	16p11.2 DEL	SFARI	Dolmetsch
SV0001455	M	12	Fibroblast	Episomal	16p11.2 DEL	SFARI	Dolmetsch
SV0001481	M	8	Fibroblast	Episomal	16p11.2 DEL	SFARI	Dolmetsch
090-iPSC	F	36	Fibroblast	Retroviral	Control	OHRI	Stanford
EPC-iPSC 106	M	24	EPC	Retroviral	Control	OHRI	Stanford
EPC-iPSC Clone B	M	45	EPC	Retroviral	Control	OHRI	Stanford
EPC-iPSC Clone C	M	45	EPC	Retroviral	Control	OHRI	Stanford
GM01650E	F	37	Fibroblast	Episomal	Control	OHRI	Stanford
BJ1D	M	0	Fibroblast	Retroviral	Control	OHRI	Stanford

Clones B and C originate from the same donor. All iPSC lines listed were used in the Matrigel- based assay presented in Figure 7. DEL, Deletion; EPC, Endothelial progenitor cell; OHRI, Ottawa Hospital Research Institute; SFARI, Simons Foundation Autism Research Initiative

Appendix B

Supplemental information for Manuscript II

P2 purinergic receptor activation rectifies autism-associated brain endothelial cell dysfunction

Julie Ouellette, Sareen Warsi, Purva Khare, Shama Naz, Leya Aubert-Tandon, Chantal Pileggi, Sozerko Yandiev, Moises Freitas-Andrade, Cesar H. Comin, Mary-Ellen Harper, Devika S. Manickam, Armen Saghatelyan, and Baptiste Lacoste

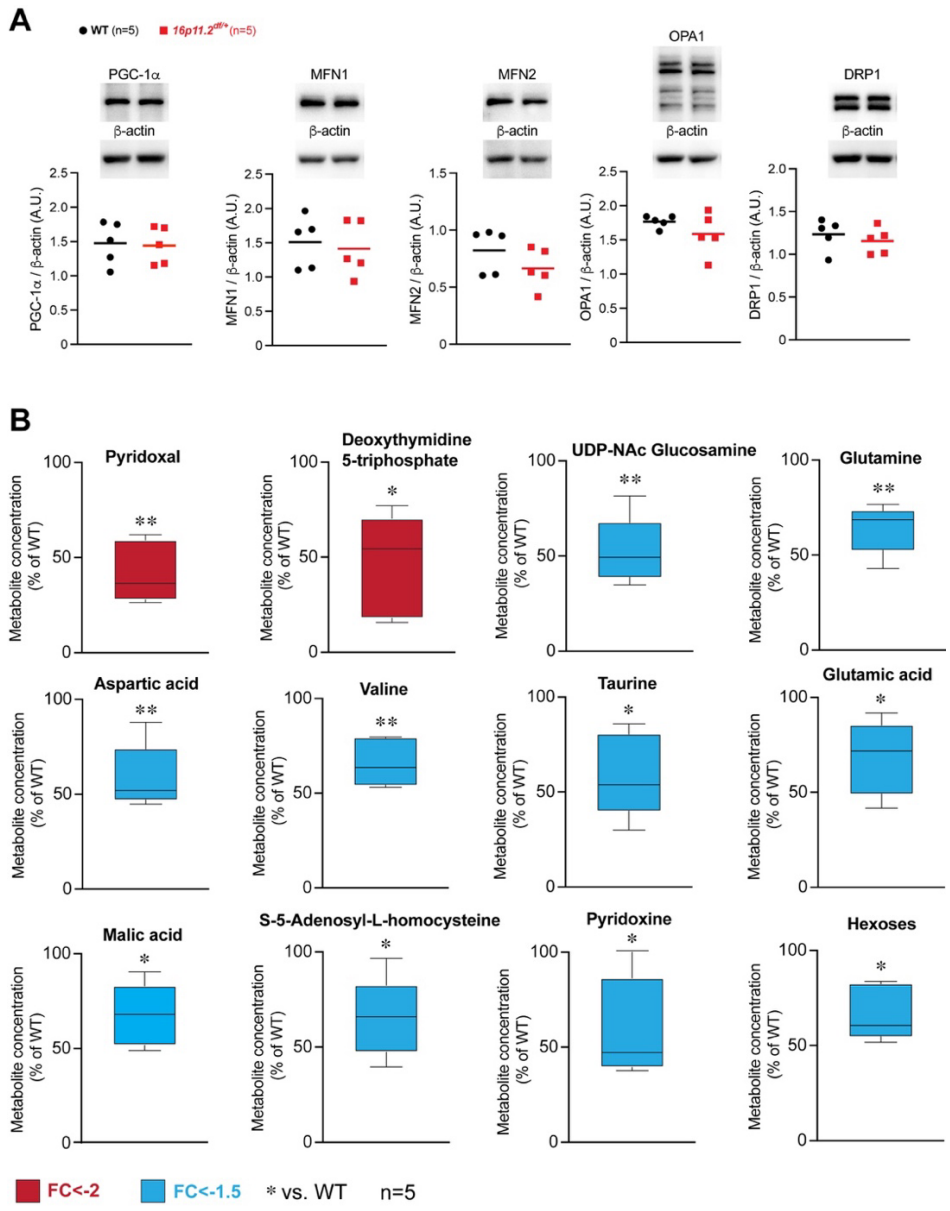

Fig S1. No change in mitochondrial dynamics and biogenesis in 16p11.2-deficient brain endothelial cells and additional altered metabolites. *(A)* Western blot quantification of relative levels of proteins associated with mitochondrial biogenesis (PGC-1α) as well as mitochondrial fusion and fission (OPA-1, DRP1, and MFN1 and -2) in primary mouse brain endothelial cells isolated from male *16p11.2*$^{df/+}$ and WT littermates (n=5 animals). *(B)* Additional metabolites found at a reduced abundance in 16p11.2-deficient ECs. Metabolites displayed consist of a fold-change (FC)<-2 (red) and FC<-1.5 (blue) (n=5 samples, ECs pooled from 3 mice per sample). All data shown are from ECs isolated from male mice. Data are mean with individual values (*A*) or whisker boxes in (*B*) (min to max, center line indicating median). *P< 0.05, **P<0.01 by a two-tailed paired *t* test in (*B*).

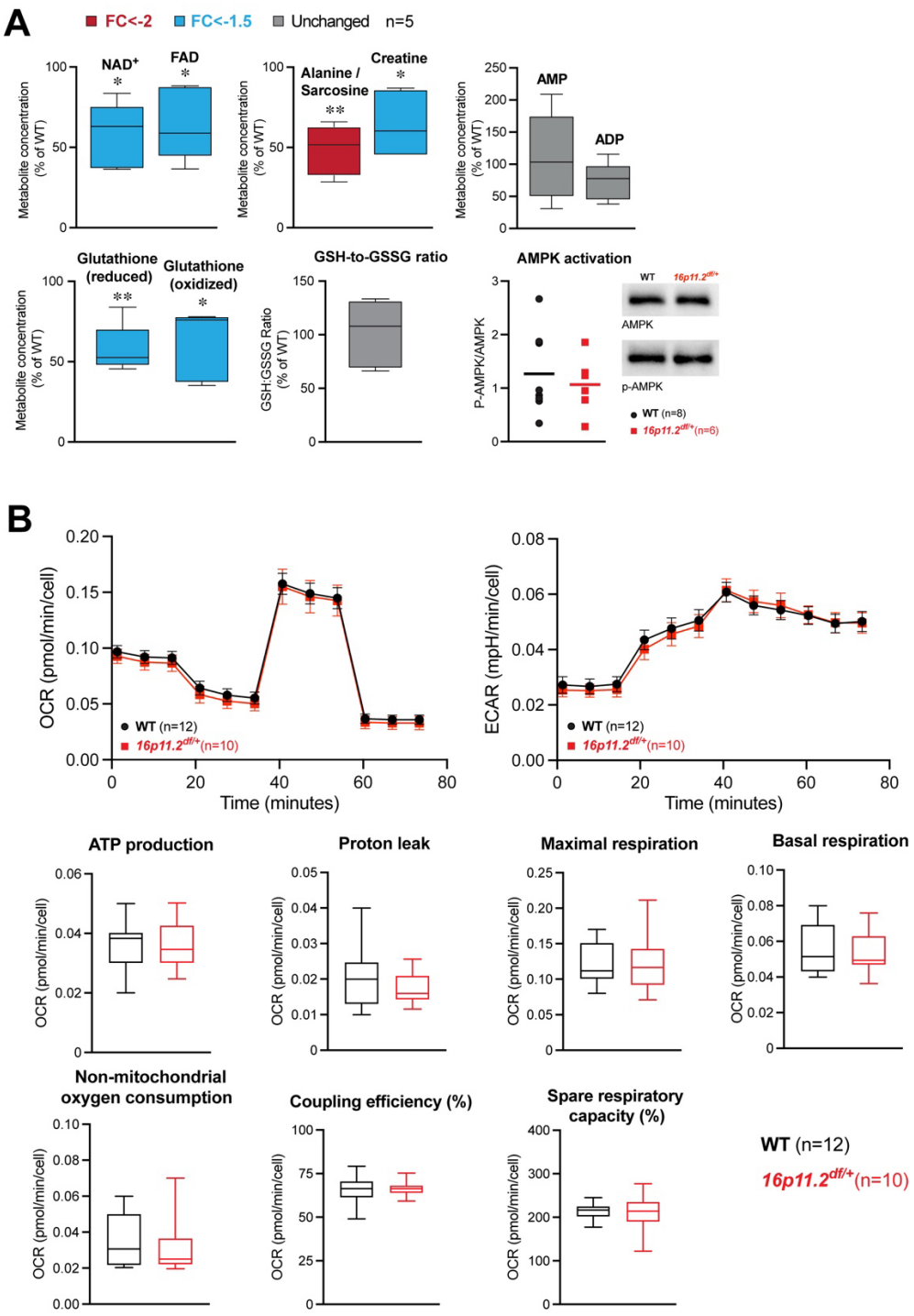

Fig S2. See next page for caption.

Fig S2. Additional altered energy-related metabolites and mitochondrial function assessment in 16p11.2-deficient brain endothelial cells. *(A) Top and bottom left*, additional energy-related metabolites detected by univariate statistical analysis. Metabolites displayed consist of a fold-change (FC)<-2 (red), FC<-1.5 (blue) or unchanged (gray) (n=5 samples, ECs pooled from 3 mice per sample). *Bottom right,* western blot quantification of relative levels of proteins associated with AMPK activation (AMPK and p-AMPK) in brain 16p11.2-deficient (n=6 animals) and WT (n=8 animals) ECs. *(B)* Assessment of mitochondrial function. *Top,* quantification of oxygen consumption rate (OCR, *left*) and extracellular acidification rate (ECAR, *right*) of WT (n=12 mice) and 16p11.2-deficient (n=10 mice) ECs. *Middle and bottom panels*, quantification of mitochondrial functional parameters. All data shown are from ECs isolated from male mice. Data are shown as whisker boxes in *A, B* (min to max, center line indicating median) and represented as percentage of Wild-type (WT in *A*), mean with individual values (*A*) or mean $\pm$ s.e.m. (*B*). *P<0.05, **P<0.01 (two-tailed paired t test in *A)*.

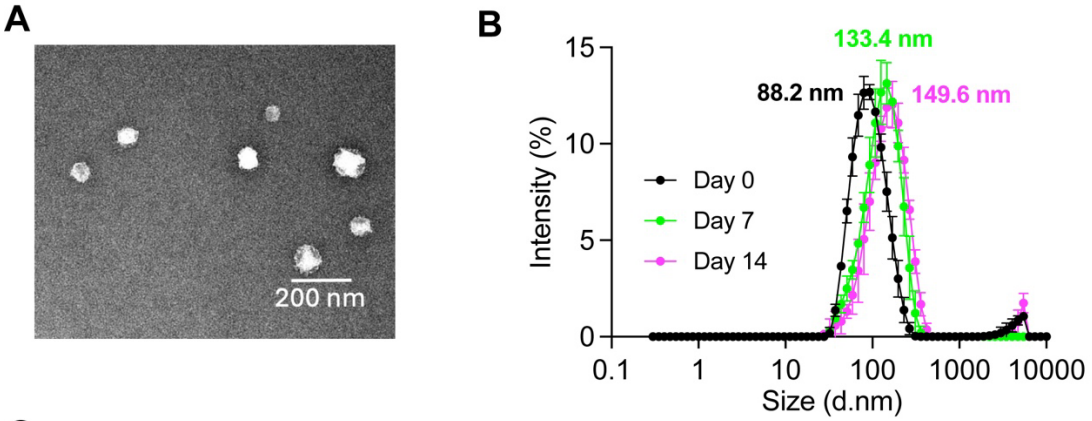

C

	Particle size (nm)	Dispersity index
Day 0	88.2 ± 1.8	0.22 ± 0
Day 7	133.4 ± 3.0	0.33 ± 0.03
Day 14	149.6 ± 0.7	0.34 ± 0.03

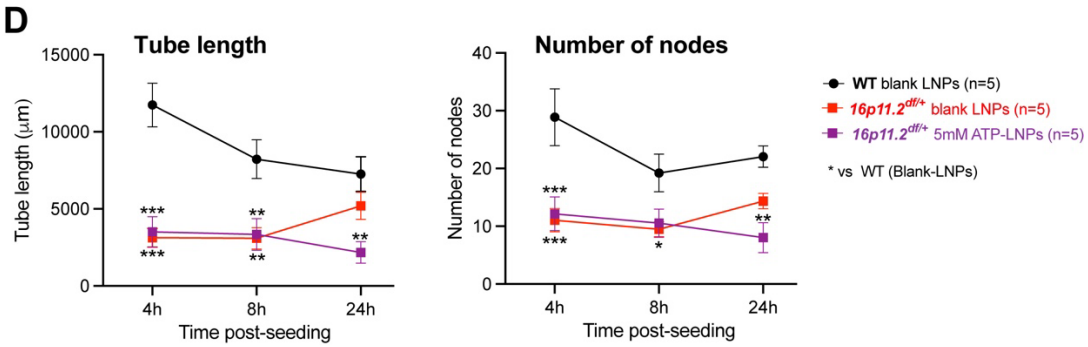

Fig S3. *In vitro* network formation assay of 16p11.2-deficient ECs with treatment of 5mM ATP-LNPs and confirmation of colloidal stability of ATP-LNPs. *(A)* Transmission electron microscopy image of ATP-LNPs. Negative-stain electron micrograph of ATP-LNPs was acquired using a Thermofisher TF20 electron microscope. Scale bar= 200 nm. *(B)* Intensity size distribution plots demonstrating the colloidal stability of ATP-LNPs upon storage at 4 °C for 14 days. *(C)* Particle size and dispersity index of LNPs using dynamic light scattering. *(D)* Quantifications of network densities (total endothelial tube length) and network nodes (total number of branching hubs) following treatment of 16p11.2-deficient ECs with 5mM ATP-LNPs. ATP-LNPs were prepared as described in Table 1. ATP-LNPs were prepared and diluted to a final ATP concentration of 40 mM using 1x PBS (pH 7.4) for *A,B,C*. Particle size and dispersity indices were measured using a Malvern Zetasizer Pro. Data are represented as mean ± SD of at least n=3 measurements in *B, C*. Data shown in *D* are from ECs isolated from male mice and are shown as the mean ± s.e.m. (n=5 animals per group) *P<0.05, **P<0.01, ***P<0.001 (two-way repeated measure ANOVA and Sidak's multicomparison *post hoc* test in *D*).

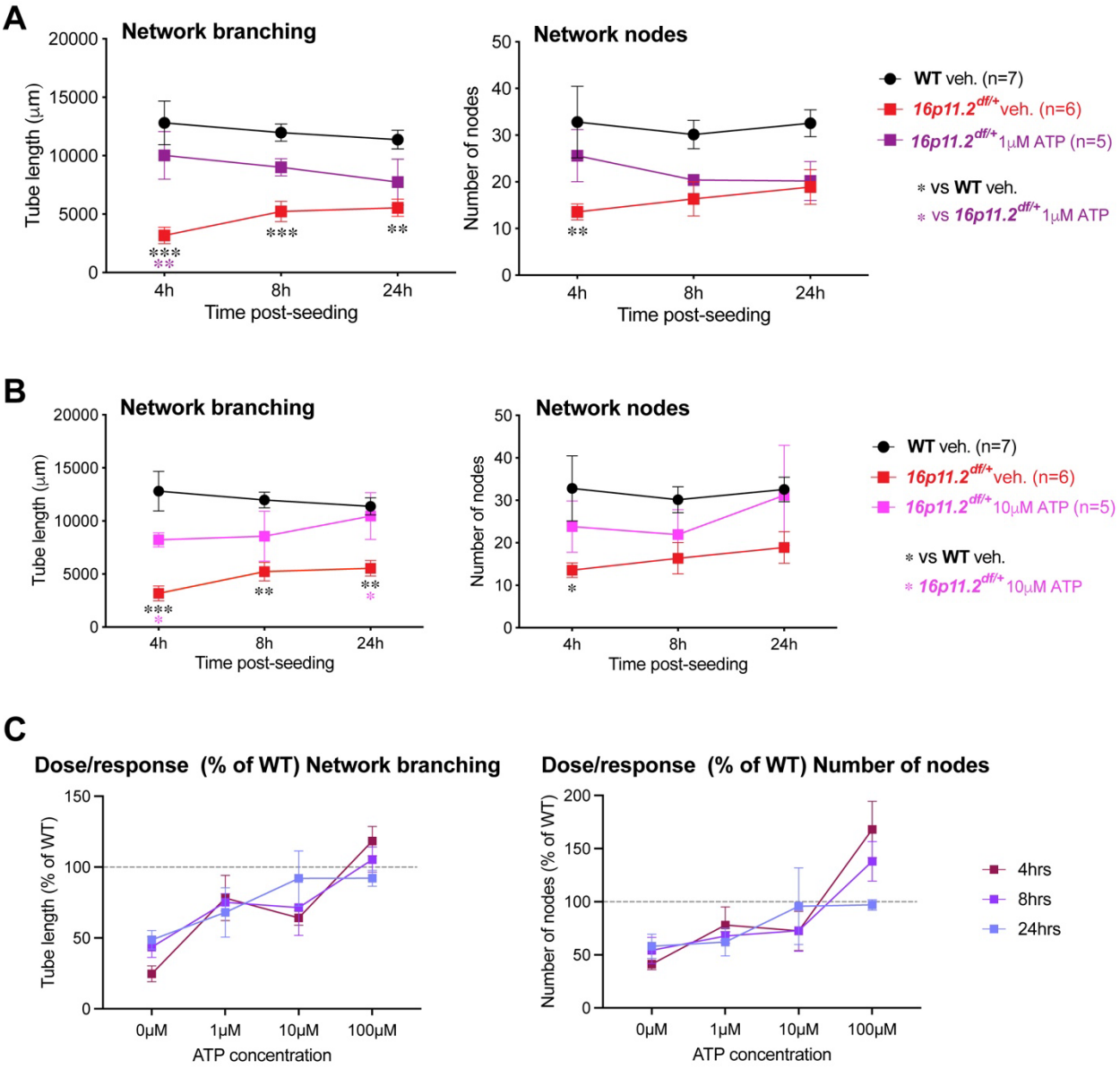

Fig S4. Additional treatment conditions of extracellular ATP in 16p11.2-deficient brain ECs. Network densities (total endothelial tube length) and network nodes (total number of branching hubs) following treatment of 1μM (*A*) and 10μM (*B*) extracellular ATP. (*C*) Dose response curves for network branching (*left*) and number of nodes (*right*) of 16p11.2-deficient ECs following extracellular ATP treatment (1μM, 10μM or 100μM) measured using an *in vitro* tube formation assay imaged at 4hrs, 8hrs and 24hrs post-seeding. Data are shown as the mean ± s.e.m with percent of WT in *C*. Dotted line represents 100 % of WT values in *C*. (n=5-7 animals per group); veh.= vehicle; *P<0.05, **P<0.01, ***P<0.001 (two-way repeated measure ANOVA and Sidak's multicomparison *post hoc* test in *A* and *B*).

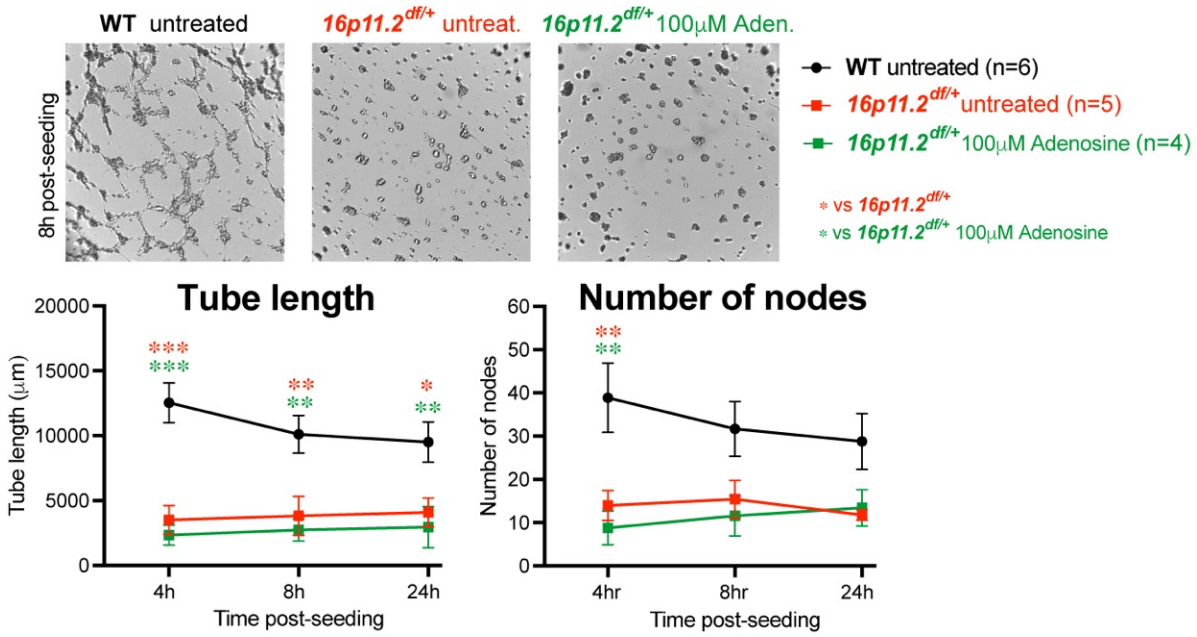

Fig S5. Adenosine supplementation does not improve 16p11.2-deficient primary brain ECs network formation *in vitro*. *Top,* representative images of capillary-like networks at the 8h post-seeding time point. *Bottom,* quantifications of network tube length and network nodes (total number of branching hubs). All data shown are from ECs isolated from male mice. Data are shown as the mean ± s.e.m. (n=4-6 animals per group); untreat.=untreated; Aden.=Adenosine; *P<0.05, **P<0.01, ***P<0.001 (two-way repeated measure ANOVA and Sidak's multicomparison *post hoc* test).

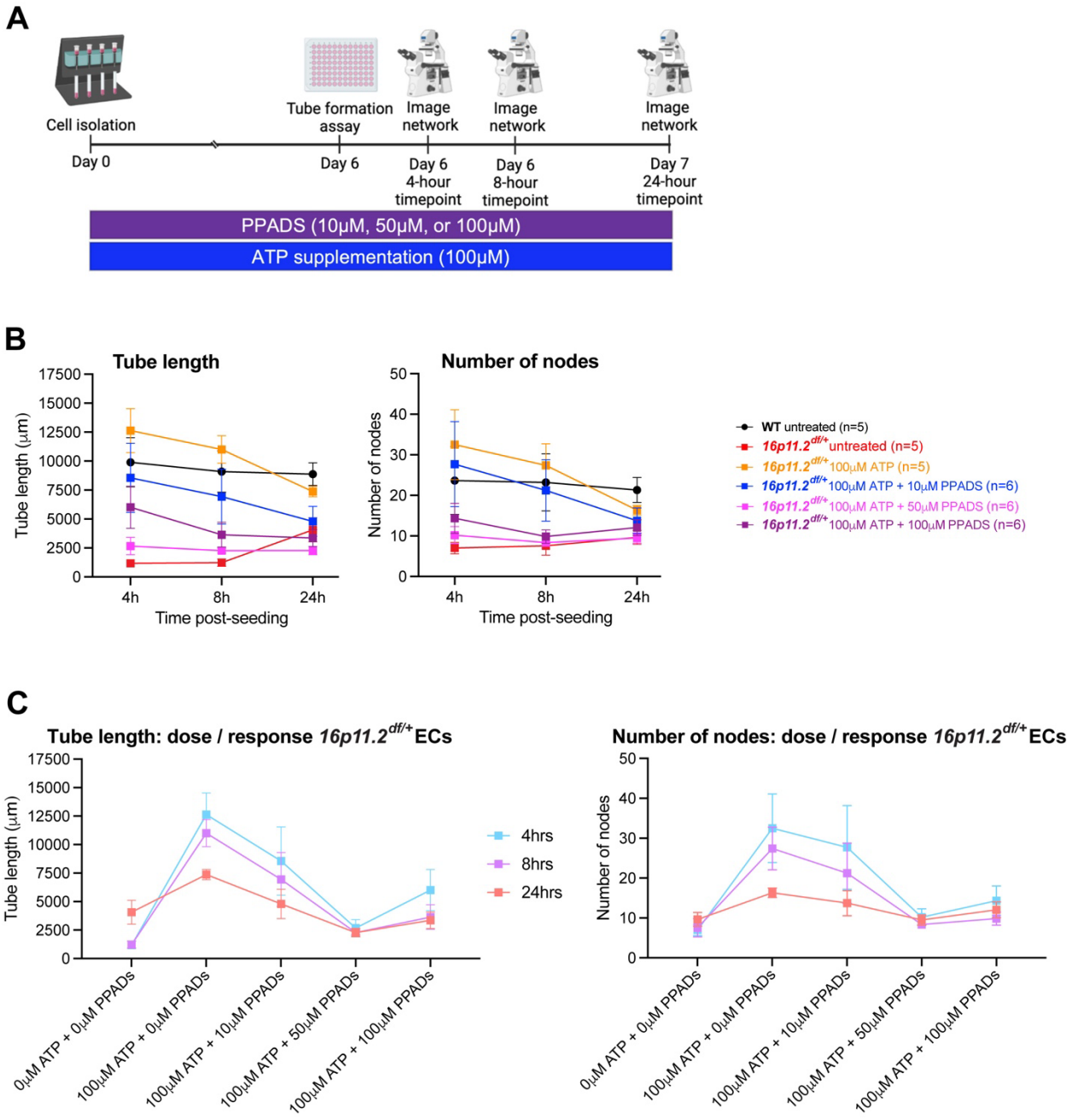

Fig S6. Additional treatment conditions of non-selective antagonist (PPADs) and representative dose response curves. *(A)* Experimental timeline for treatment of 16p11.2-deficient ECs with extracellular ATP and PPADs following cell isolation and during a 24-hour *in vitro* network formation assay. *(B)* Quantifications of network tube length and network nodes (total number of branching hubs) following co-administration of extracellular ATP (100μM) and PPADs (10μM, 50μM or 100μM). *(C)* Dose response curves of tube length (*left*) and number of nodes (*right*) of 16p11.2-deficient ECs following co-administration of extracellular ATP and PPADs measured using an *in vitro* tube formation assay imaged at 4hrs, 8hrs and 24hrs post-seeding.

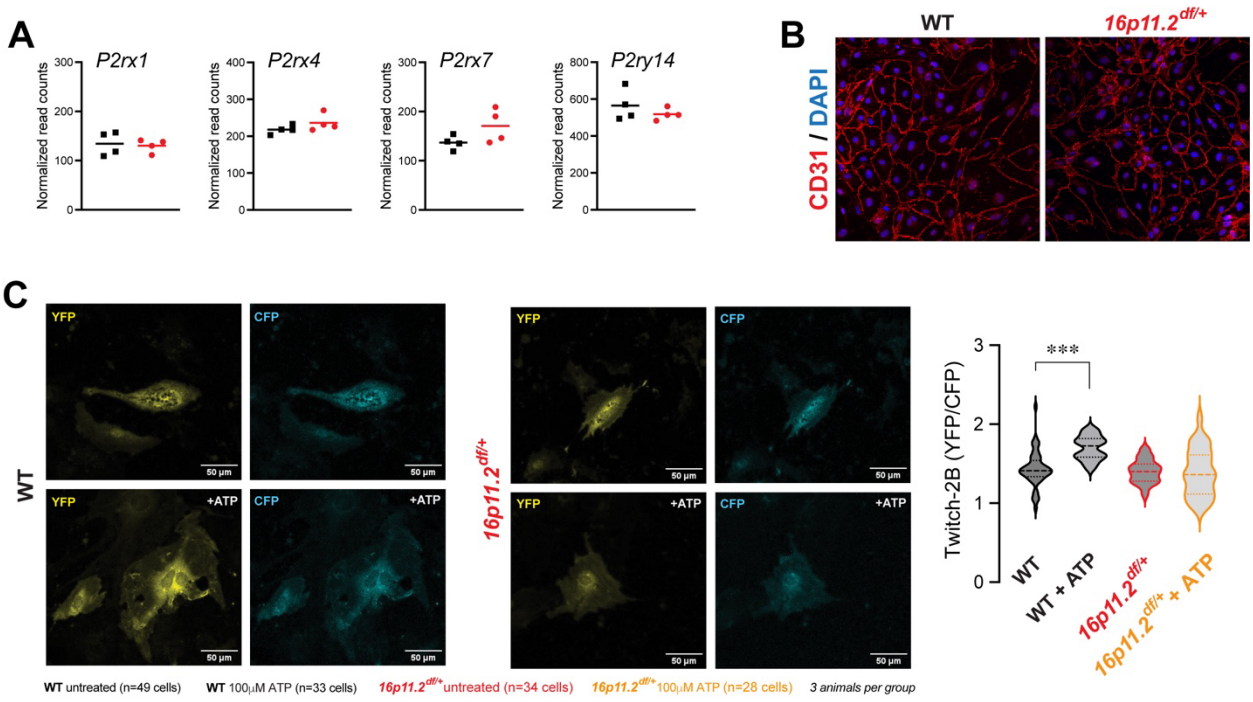

Fig S7. Gene expression level of other P2-class receptors and steady-calcium profile of 16p11.2-deficient brain endothelial cells. *(A)* Expression level of additional genes encoding P2-class receptors in WT and 16p11.2-deficient ECs from our previously generated RNAseq database (Ouellette et al., 2020). *(B)* Representative images of 16p11.2-deficient and WT ECs transfected with Twitch-2B, a FRET-based ratiometric Ca^{2+} indicator used to measure steady-state intracellular Ca^{2+} level. *(C) Left,* images of YFP and CFP for both 16p11.2-deficient and WT ECs, with and without ATP are shown. *Right,* quantification of YFP/CFP ratio in 16p11.2-deficient and WT ECs in the absence or presence of 100 µM of extracellular ATP. Note, the lack of effect of ATP supplementation on steady-state intracellular Ca^{2+} level in 16p11.2-deficient ECs. Data are violin plots (center line indicating median, n=3-4 animals per group). ***P<0.001 (on-way ANOVA and Tukey multicomparison *post hoc* test).

Appendix C - Manuscript IV

Association to hypothesis: This manuscript provides detailed methods for the isolation and characterization of primary brain endothelial cells (ECs). In addition, it describes techniques to assess functional properties of ECs. As brain ECs play a role in neurological disorder pathophysiology, including autism spectrum disorders, understanding the full complement of these cells in brain health is an essential tool. The protocols described in this manuscript were predominantly used in Manuscripts I-III which unraveled dysfunctional brain ECs in 16p11.2 deletion syndrome and highlighted mechanisms to target.

Current manuscript status: This manuscript was published in *Star Protocols* in 2021.

Statement of contribution: J.O. optimized and carried out experiments, wrote the manuscript draft and participated in figure generation. B.L. proofread the manuscript, provided guidance in writing, and participated in figure assembly.

STAR Protocols

CellPress
OPEN ACCESS

Protocol

Isolation and functional characterization of primary endothelial cells from mouse cerebral cortex

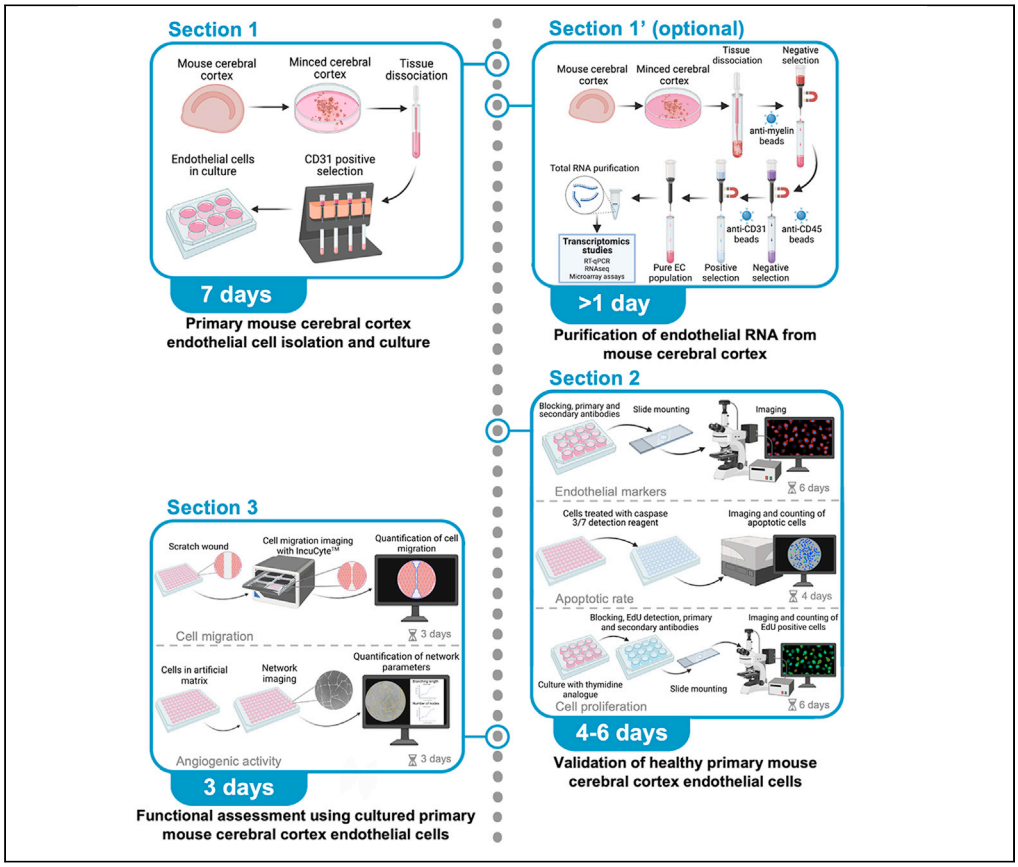

Endothelial cells (ECs) lining blood vessels are implicated in organ development, function, and maintenance. We present a detailed protocol enabling isolation and characterization of primary mouse brain ECs, including quality controls and functional assays. These procedures promote survival of primary brain ECs for the assessment of endothelial health. Since alterations in brain ECs are involved in the onset and progression of neurological disorders, this protocol represents a valuable tool to better understand the roles of ECs in brain health.

Julie Ouellette, Baptiste Lacoste

jouel100@uottawa.ca (J.O.)
blacoste@uottawa.ca (B.L.)

Highlights

Streamlined approach to determine the health of cultured mouse brain endothelial cells

Protocol focused on primary endothelial cell from mouse cerebral cortex

Complete procedures from molecular analysis to cell behavior including quality controls

Ouellette & Lacoste, STAR Protocols 2, 101019 December 17, 2021
https://doi.org/10.1016/j.xpro.2021.101019

STAR Protocols

CellPress
OPEN ACCESS

Protocol

Isolation and functional characterization of primary endothelial cells from mouse cerebral cortex

Julie Ouellette[1,2,4,*] and Baptiste Lacoste[1,2,3,5,*]

[1]Ottawa Hospital Research Institute, Neuroscience Program, Ottawa, ON K1H8M5, Canada

[2]University of Ottawa, Faculty of Medicine, Department of Cellular and Molecular Medicine, Ottawa, ON K1H8M5, Canada

[3]University of Ottawa Brain and Mind Research Institute, Ottawa, ON K1H8M5, Canada

[4]Technical contact

[5]Lead contact

*Correspondence: jouel100@uottawa.ca (J.O.), blacoste@uottawa.ca (B.L.)
https://doi.org/10.1016/j.xpro.2021.101019

SUMMARY

Endothelial cells (ECs) lining blood vessels are implicated in organ development, function, and maintenance. We present a detailed protocol enabling isolation and characterization of primary mouse brain ECs, including quality controls and functional assays. These procedures promote survival of primary brain ECs for the assessment of endothelial health. Since alterations in brain ECs are involved in the onset and progression of neurological disorders, this protocol represents a valuable tool to better understand the roles of ECs in brain health.

For complete details on the use and execution of this profile, please refer to Ouellette et al. (2020).

BEFORE YOU BEGIN

The following protocol describes the specific steps to isolate, purify, maintain and characterize primary mouse brain (cortical) endothelial cells (ECs). These procedures have been optimized for isolation of ECs from young mice at postnatal day (P) 14 of either sex. While the following protocols may be used for isolation of adult primary mouse brain ECs, adult ECs will grow significantly slower (please read the limitations section). Refer to the key resources table for a complete list of reagents and tools. All studies were approved by the University of Ottawa Animal Care Committee and conducted in accordance to guidelines of the Canadian Council on Animal Care.

KEY RESOURCES TABLE

REAGENT or RESOURCE	SOURCE	IDENTIFIER
Antibodies		
Rat anti-CD31 (use at 1:200)	BD Pharmingen	Cat#553370
Rabbit anti-VE-Cadherin (use at 1:500)	Abcam	Cat#ab33168
Goat anti-Iba1 (use at 1:1000)	Abcam	Cat#ab107159
Goat anti-PDGRβ (use at 1:200)	R&D systems	Cat#AF1042
Guinea pig anti-NeuN (use at 1:1500)	Millipore Sigma	Cat#ABN90
Guinea pig anti-GFAP (use at 1:1000)	Synaptic Systems	Cat#173004
Mouse anti-αSMA (use at 1:200)	Sigma-Aldrich	Cat#A2547

(*Continued on next page*)

STAR Protocols *2*, 101019, December 17, 2021

Continued

REAGENT or RESOURCE	SOURCE	IDENTIFIER
Donkey anti-Rat IgG (H+L) Highly Cross-Adsorbed Secondary Antibody, Alexa Fluor 488 (use at 1:300)	Invitrogen	Cat#A-21208
Donkey anti-Rabbit IgG (H+L) Highly Cross-Adsorbed Secondary Antibody, Alexa Fluor 568 (use at 1:300)	Invitrogen	Cat#A-10042
Donkey anti-Rabbit IgG (H+L) Highly Cross-Adsorbed Secondary Antibody, Alexa Fluor 647 (use at 1:300)	Invitrogen	Cat#A-31573
Donkey anti-goat IgG (H+L) cross-absorbed secondary antibody, Alexa Fluor 568 (use at 1:300)	Invitrogen	Cat#A-11057
Goat anti-guinea pig IgG (H+L) Highly cross-absorbed secondary antibody, Alexa Fluor 488 (use at 1:300)	Invitrogen	Cat#A-11073
Goat anti-guinea pig IgG (H+L) Highly cross-absorbed secondary antibody, Alexa Fluor 647 (use at 1:300)	Invitrogen	Cat#A-21450
Donkey anti-mouse IgG (H+L) cross-absorbed secondary antibody, Alexa Fluor 568 (use at 1:300)	Invitrogen	Cat#A10037
Alexa Fluor™ 488 Phalloidin (use at 1:40)	Invitrogen	Cat#A12379
Chemicals, peptides, and recombinant proteins		
EGM™-2 MV Microvascular Endothelial Cell Growth Medium-2 BulletKit™	Lonza	Cat#CC-3202
Penicillin-Streptomycin (10,000 U/mL)	Thermo Fisher Scientific	Cat#15140122
HBSS without calcium/magnesium	Gibco	Cat#14170-120
HBSS with calcium/magnesium	Gibco	Cat#14025-092
Attachment factor 1×	Gibco	Cat#S-006-100
Albumin, Bovine (BSA)	VWR	Cat#0332-100G
CD31 MicroBeads, Mouse	Miltenyi Biotec	Cat#130-097-418
Myelin Removal Beads II, human, mouse, rat	Miltenyi Biotec	Cat#130-096-733
CD45 MicroBeads, Mouse	Miltenyi Biotec	Cat#130-052-301
Sterile 1× PBS	Wisent BioProducts	Cat#311-011-CL
TrypLE™ Express Enzyme (1×), no phenol red	Thermo Fisher Scientific	Cat#12604013
Alconox detergent	VWR	Cat#21835-032
Virkon® S Disinfectant and Virucide	Fisher Scientific	Cat#NC9549979
CellEvent™ Caspase-3/7 Green Detection	Thermo Fisher Scientific	Cat#C10423
Staurosporine	Thermo Fisher Scientific	Cat# BP2541100
Hoechst 33342, Trihydrochloride, Trihydrate-10 mg/mL Solution in Water	Invitrogen	Cat#H3570
Paraformaldehyde 20% Solution, EM grade	Electron Microscopy Sciences	Cat#15713-S
Fluoromount-G™	Electron Microscopy Sciences	Cat#17984-25
Triton-X-100	VWR	Cat#0694-1L
Fish gelatin blocking buffer, 10%	VWR	Cat#M319-500mL
Donkey serum, sterile filtered	Wisent Bioproducts	Cat#035-150
Dimethyl sulfoxide,DMSO	sigma-Aldrich	Cat#D8418-100mL
DAPI	Invitrogen	Cat#D1306
Matrigel® Matrix Basement Membrane, Growth Factor Reduced	Fisher Scientific	Cat#354230
Sodium chloride (NaCl)	VWR	Cat#0241-5KG
Sodium phosphate dibasic anhydrous (Na_2HPO_4)	VWR	Cat#0404-1KG
Sodium phosphate monobasic ($NaH_2PO_4H_2O$)	VWR	Cat#BDH9298.2.5
β-mercaptoethanol, Molecular biology grade	Merck Millipore	Cat#444203
Critical commercial assays		
Neural Tissue Dissociation Kit (P)	Miltenyi Biotec	Cat#130-092-628
Click-iT™EdU Alexa Fluor™ 594 Imaging Kit	Invitrogen	Cat#C10339

(*Continued on next page*)

Continued		
REAGENT or RESOURCE	SOURCE	IDENTIFIER
E.Z.N.A.® HP Total RNA Kit	OMEGA bio-tek	Cat#R6812-01
RNase-free DNase I Set	OMEGA bio-tek	Cat#E1091
Experimental models: Organisms/strains		
Mouse: B6129SF1/J (14 days old, male or female)	The Jackson Laboratory	Cat#101043
Software and algorithms		
IncuCyte® ZOOM Software	Essen Bioscience	N/A
Fiji Image J	Schindelin et al., 2012	https://imagej.net/software/fiji/
Angiogenesis Analyzer for Image J	Carpentier, 2012	https://imagej.nih.gov/ij/macros/toolsets/Angiogenesis%20Analyzer.txt
Other		
70 μM pore size strainer	VWR	Cat#76327-100
LS columns	Miltenyi Biotec	Cat#130-042-401
LD columns	Miltenyi Biotec	Cat#130-042-901
MACS® MultiStand	Miltenyi Biotec	Cat#130-042-303
QuadroMACS™ separator	Miltenyi Biotec	Cat#130-090-976
IncuCyte® ImageLock Plates	Essen Bioscience	Cat#4379
IncuCyte® 96-well WoundMaker Tool	Essen Bioscience	Cat#4563
German glass coverslips, 12 mm round, #1 thickness	Mandel	Cat#NEU-GG-12-1.5-OZ
Corning® cryogenic vials, internal thread	Millipore sigma	Cat#CLS431386
Mr. Frosty™ Freezing Container	Thermo Fisher Scientific	Cat#5100-0001
Superfrost Plus Microscope Slides	Fisher Scientific	Cat#12-550-15
96-Well Tissue Culture Plate, Non-treated, Sterilized, Non-Pyrogenic	VWR	Cat#10861-562
IncuCyte™ Zoom® Apparatus	Essen Bioscience	N/A
Nikon Eclipse TE2000-E inverted microscope	Nikon	N/A
Zeiss Axio Imager M2 microscope	Zeiss	N/A
Axiocam 506 mono	Zeiss	N/A
ApoTome.2 module	Zeiss	N/A

STEP-BY-STEP METHOD DETAILS

Section 1: Primary mouse cerebral cortex endothelial cell isolation and culture

Preparation of reagents and medium for primary mouse cerebral cortex endothelial cell isolation

Timing: 20 min (on the day prior to cell isolation)

1. Reagent preparation
   a. Enzyme P [included in the "Neural Dissociation Kit (P)"] is ready to use. Prepare aliquots of 200 μL to avoid repeated freeze-thaw cycles. Store aliquots at −20°C. This kit contains buffers and enzymes for 50 isolations.
   b. Resuspend lyophilized Enzyme A with 1 mL of Buffer A in provided vial labeled Enzyme A (included in the same kit). Do not vortex. The final Enzyme A solution is clear when fully resuspended. Prepare aliquots of 40 μL and store at −20°C.

   Note: To resuspend Enzyme A, slowly pipette up and down (~5–10 times) using a 1 mL pipette until powder is no longer visible.

2. Endothelial cell medium preparation
   a. Thaw SingleQuots™ Kit (included in EGM™-2 MV Microvascular Endothelial Cell Growth Medium-2 BulletKit™). Add SingleQuots™ Kit to basal medium. Do not refreeze.
   b. Add 1% penicillin/streptomycin to prepared BulletKit™ medium.

3. Autoclave all dissection tools (curved forceps, straight forceps, large scissors, curved small scissors).

⚠ CRITICAL: Once thawed, SingleQuots™ Kit must be mixed with basal medium within 72 h. After BulletKit™ medium is prepared, use within 1 month.

Mouse cerebral cortex dissection

Two cortical hemispheres (i.e., one mouse brain) are ideal for plating endothelial cells in 2 wells of a 6-well plate to promote cell survival and growth following isolation.

Timing: 90 min (the day of cell isolation)

4. Clean dissection bench using 70% or 100% ethanol.
5. Submerge dissection tools and razor blade in 100% ethanol for a minimum of 30 min prior to dissection.
6. Cortical dissection (Figures 1A–1H)
   a. Prepare a 12-well plate with 1 mL of cold HBSS (without calcium/magnesium).
   b. Sacrifice the mouse by cervical dislocation.

   Note: No anesthesia or carbon dioxide overdose is recommended before the cervical dislocation. This might disrupt endothelial cell health. A guillotine can be used for quick euthanasia.

   c. Decapitate mouse and extract brain rapidly from the skull (Collins et al., 2018; Meyerhoff et al., 2021).
   d. Transfer the brain into a petri dish containing cold HBSS without calcium/magnesium. Remove the cerebellum and brain stem, leaving cerebral hemispheres intact.
   e. Bisect cerebral hemispheres along midline using a sterile razor blade. Repeat with the other hemisphere.
   f. Place each hemisphere with the medial side facing up. Using curved forceps remove striatum, hippocampus and thalamus, leaving the cortex intact. Repeat with the other hemisphere.
   g. Using a razor blade, mince cortex in small pieces and delicately transfer fragments using a sterile 3 mL plastic transfer pipette to a 12-well plate containing 1 mL of cold HBSS without calcium/magnesium.
   h. Repeat with next mouse.
   i. Once dissections are complete, delicately transfer each pair of minced cortex submerged in cold HBSS (without calcium/magnesium) from the 12-well plate into a 15 mL conical tube placed on ice, using a 3 mL transfer pipette.

Primary endothelial cell isolation

Timing: 4 h

All following steps are performed in sterile conditions in a biosafety cabinet. These steps have been adapted from the Miltenyi biotec "Neural Dissociation Kit (P)" and CD31 MicroBeads protocols found on Miltenyi biotec website. The volumes described below are for the isolation of one mouse brain (i.e., two cerebral cortices). The end result consists of a semi-pure endothelial cell culture. A pure endothelial cell culture will be reached after 48 h in culture (see steps 33–34).

7. Prepare a 6-well plate for endothelial cell culture.
   a. Add 2 mL of 100% ethanol per well of a 6-well plate. Let plate incubate at room temperature in the biosafety cabinet for 1 h. Aspirate 100% ethanol and let plate dry.

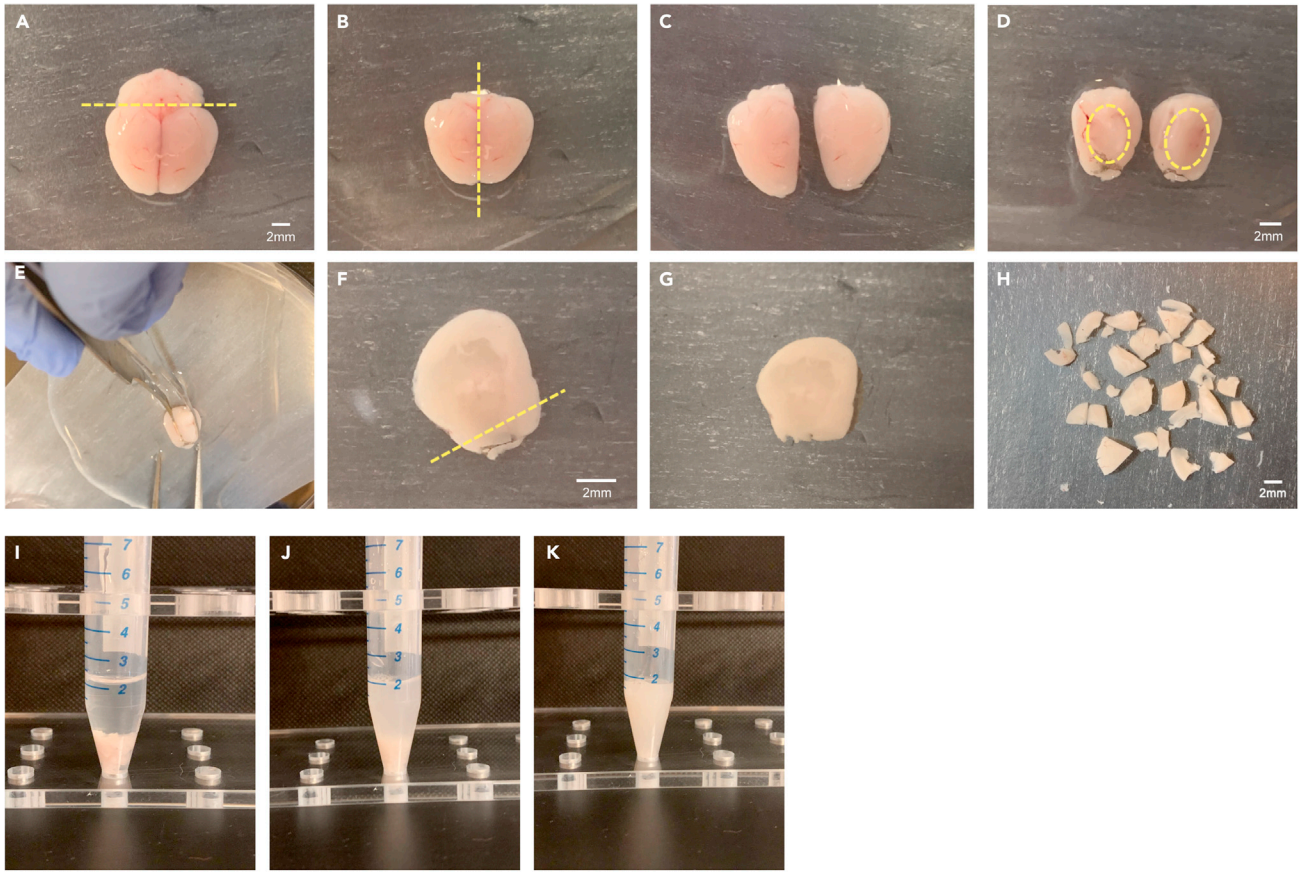

Figure 1. Mouse cerebral cortex dissection from freshly extracted brain

(A) The brain is removed fresh from skull, and the cerebellum is discarded (dotted line depicts cut). Scale bar: 2 mm.

(B and C) Cerebral hemispheres are separated using a razor blade or scalpel (dotted midline shows cut axis). Dorsal view is shown in C (i.e., cortex surface up).

(D) Hemispheres are placed medial side facing up. Dotted line depicts the interior of the cortical 'cup' (i.e., striatum, hippocampus and thalamus) that will be scooped out. Scale bar: 2 mm.

(E) Using curved forceps, remove striatum, hippocampus and thalamus from cortical cup (see D). Straight forceps may be used to stabilize the brain during dissection.

(F and G) Remove leftover olfactory bulb including pigmented vessels using razor blade or scalpel (dotted line in F depicts cut). Scale bar: 2 mm.

(H) Using a razor blade, mince cortical pair in medium-to-small pieces to facilitate ensuing tissue dissociation (avoid mincing too small and for too long to limit damage to endothelial cells). Scale bar: 2 mm.

(I–K) Tissue dissociation steps for cell isolation. (I) Enzyme mix 1 and 2 have been added to minced tissue. (J) Cortical pair is dissociated after being pipetted up and down ~10 times with a 3mL transfer pipette. (K) Cortical pair is fully dissociated after being pipetted up and down ~10 times with a glass Pasteur pipette.

Note: Prepare 2 wells of a 6-well plate for each pair of cortical hemispheres.

b. Add 1 mL of 1× attachment factor (Gibco, Cat#S-006-100) to each well and let sit at room temperature for 30 min. Aspirate 1× attachment factor and let plate dry.

Note: The attachment factor contains gelatin which promotes the growth of microvascular endothelial cells.

8. Prepare PEB buffer (see Table 1).

Note: Steps 7 and 8 may be completed at the same time as the following steps of the cell isolation.

Table 1. PEB buffer

Reagent	Final concentration	Amount
Albumin, bovine (BSA)	0.5%	0.25 g
HBSS without calcium/magnesium	n/a	50 mL
Total	**n/a**	**50 mL**

Store at −20°C for up to 4 weeks.

9. Prepare enzyme mix 1.
   a. Mix 1900 μL of buffer X with 50 μL of enzyme P [included in "Neural dissociation kit (P)"] for a final volume of 1950 μL. Do not vortex.
   b. Pre-heat mixture at 37°C for 15 min.

Note: Prepare separate tubes of enzyme mix 1 for each mouse.

10. Centrifuge minced cortex at 300×*g* for 2 min at room temperature and aspirate supernatant.
11. Add 1950 μL of pre-heated enzyme mix 1 to each tube containing minced cortex.
12. Incubate minced cortex for 15 min at 37°C. Tap and gently swirl the tube (~5 times) to dislodge tissue every 5 min.
13. Prepare enzyme mix 2.
   a. Mix 20 μL of buffer Y with 10 μL of enzyme A [included in "Neural dissociation kit (P)"] for a final volume of 30 μL. Do not vortex.

Note: Prepare separate tubes of enzyme mix 2 for each mouse.

14. Add 30 μL of enzyme mix 2 to each tube containing minced cortex following 15 min incubation (Figure 1I). Invert gently.
15. Dissociate cortical pair mechanically using a sterile 3 mL plastic transfer pipette, pipetting up and down slowly (~10 times; Figure 1J). Avoid forming air bubbles.
16. Incubate tissue at 37°C for 10 min. Tap and gently swirl the tube every 5 min.
17. Dissociate tissue mechanically using a glass Pasteur pipette (Figure 1K). Avoid forming air bubbles.

Note: Continue with dissociation until tissue can be pipetted up and down without difficulty (~10 times). Pieces of tissue may still be visible following second dissociation.

18. Incubate dissociated tissue at 37°C for 10 min. Tap and gently swirl the tube every 5 min.
19. Place a 70 μM strainer on a 50 mL tube and wash strainer with 1 mL of HBSS with calcium/magnesium.
20. Apply cell suspension to prepared 70 μM strainer and add 10 mL of HBSS with calcium/magnesium to strainer.
21. Discard 70 μM strainer and centrifuge cell suspension at 300×*g* for 10 min at room temperature. Aspirate supernatant.
22. Resuspend cells with 1 mL of PEB buffer. Transfer to a 1.5 mL tube.
23. Centrifuge cell suspension at 300×*g* for 5 min at 4°C and aspirate supernatant.
24. Resuspend cell pellet in 270 μL of PEB buffer.
25. Prepare CD31 MicroBeads
   a. Vortex CD31 MicroBeads bottle.
   b. Add 30 μL of CD31 MicroBeads to cell suspension.

Note: CD31 MicroBeads have been designed for the positive selection of endothelial cells from mouse tissues.

26. Incubate cell suspension containing CD31 MicroBeads for 20 min at 4°C while being agitated on a rotator.

27. Add 1 mL of PEB buffer to cell suspension and centrifuge at 300×*g* for 5 min at 4°C. Aspirate supernatant.
28. Resuspend pellet with 1 mL of PEB buffer.
29. Preparation for positive selection
    a. Place LS columns on magnetic separator (MACS® MultiStand and QuadroMACS™ Separator) with a 15 mL collection tube. One LS column per mouse is required.
    b. Add 2 mL of PEB buffer to each LS column.
    c. Warm 50 mL of endothelial cell culture medium at room temperature.
30. Apply cell suspension to LS column and wash columns 3 times with 0.5 mL of PEB buffer. Discard total effluent.

Note: Following positive selection, endothelial cells are trapped within the LS column.

31. Endothelial cell collection
    a. Label 15 mL conical tubes.
    b. Remove LS column from magnetic separator and place on labelled 15 mL conical tube.
    c. Add 2 mL of endothelial cell culture medium to each LS column. Immediately flush out endothelial cells by firmly pushing the plunger into the LS column.
32. Add 1 mL of endothelial cells to the 1× attachment factor coated 6-well plate and 1 mL of endothelial cell medium to each well. Place plate in a 37°C incubator at 5% CO_2.

Note: Each mouse cortex will yield 2 wells of a 6-well plate using this protocol. Elution volume may be increased to plate endothelial cells in additional wells. However, caution must be taken when doing this approach as endothelial cells in culture require to be at a high density to assure attachment when first plated following isolation. This cell isolation protocol results in a semi-pure endothelial cell culture. A pure endothelial cell population will be achieved within 48 h of culture (see steps 33–34).

Maintenance of primary mouse cerebral cortex ECs

Timing: 1 week

Endothelial cells may require up to 7 days to reach confluency. However, growth rate will depend on initial endothelial cell plating density. Culture medium must be changed 48 h after isolation to remove non-adherent cells and replenish nutrients. After 48 h of culture a pure endothelial cell population is achieved.

33. Aliquot endothelial cell medium. A total of 2 mL is required per well. Let medium warm up at room temperature for 15 min. Slowly aspirate endothelial medium from wells containing cells and replace with fresh medium.
34. Endothelial cell medium must be replaced every second day up until 80% confluence is reached (~7 days). Troubleshooting 1

Pause point: Once endothelial cells are 70%–80% confluent, they may be used for subsequent quality controls and functional assessment. Conversely, cells may be frozen for later use using 10% DMSO.

Freezing stocks of primary mouse cerebral cortex ECs

Timing: 1 h

35. Harvest primary endothelial cells

a. Aliquot TrypLE™ Express Enzyme (1×) in a 15 mL conical tube (1 mL per well of a 6-well plate). Incubate at 37°C for 30 min. Aliquot endothelial cell medium [same volume as TrypLE™ Express Enzyme (1×)].
b. Aspirate old culture medium from endothelial cells and wash twice with sterile 1× PBS. Aspirate 1× PBS.
c. Add 1 mL of TrypLE™ Express Enzyme (1×) per well containing cells and place in the 37°C, 5% CO_2 incubator for 5 min.

⚠ CRITICAL: After 5 minute incubation tap plate. Most cells should be detached. If several cells are still attached to the plate, place plate back in the 37°C, 5% CO_2 incubator for 2 min.

d. After incubation, add 1 mL of endothelial cell medium to each well and tap plate to detach cells.

36. Transfer cells to a 15 mL conical tube and centrifuge for 5 min at 500×*g*. Aspirate supernatant. Resuspend cell pellet using endothelial cell medium.

Note: Cells from one well should be frozen in one cryovial.

37. Add 900 μL of resuspended cells to each cryovial.
38. Slowly add 100 μL of sterile DMSO to each cryovial. Slowly pipette cells up and down to mix DMSO.
39. Place cryovials containing cells in Mr. Frosty™ freezing container.

Note: This container ensures optimal cooling rate for cell preservation.

40. Place container at −80°C for 24 h.
41. Transfer cryovials from Mr. Frosty™ freezing container to liquid nitrogen for long term storage.

Thawing stocks of primary mouse cerebral cortex ECs

Timing: 1 h

42. Prepare 6-well plate coated with 1× attachment factor as described for cell isolation. Warm 10 mL of endothelial cell medium at room temperature.
43. Aliquot 2 mL of pre-heated endothelial cell medium in a 15 mL conical tube.
44. Remove cryovial from liquid nitrogen and place in 37°C water bath for 1–2 min.

Note: A small piece of frozen cells should still be visible after cryovial is removed from 37°C water bath.

45. Transfer cells to prepared 15 mL conical tube containing 2 mL of endothelial cell medium.
46. Centrifuge cells for 5 min at 500×*g*. Aspirate supernatant.
47. Resuspend pellet in endothelial cell medium.

Note: One cryovial should be separated into two wells of a 6-well plate with a final volume of 2 mL per well.

48. Place cells in a 37°C, 5% CO_2 incubator.
49. Endothelial cell medium must be replaced every second day up until 80% confluence is reached. Cells may be used for subsequent quality controls and experiments.

Section 1': Purification of endothelial RNA from mouse cerebral cortex

The described cell isolation protocol in steps 1–32 yields a semi-pure population of ECs (purified passively through changes of culture medium). Indeed, after 48 h of culture, a pure EC population is reached (Figure 2). However, in order to perform the acute purification of endothelial RNA following EC isolation from mouse cerebral cortex, additional selection steps must be completed to ensure optimal purity of isolated ECs. Note that with the preparation below, a lower cell density is obtained compared to the isolation protocol described in steps 4–32.

Acute isolation of primary cerebral cortex endothelial cells

Timing: 2 h [Start from step 21 of the primary EC isolation]

50. Prepare 50 mL of sterile 1× PBS and 0.5% BSA buffer (Table 2).
51. Resuspend cells with 180 µL of prepared sterile 1× PBS and 0.5% BSA buffer and transfer to a 1.5 mL tube.
52. Add 20 µL of myelin removal beads to each tube.
53. Incubate at 4°C for 15 min while being agitated on a rotator.
54. Preparation for negative selection
    a. Place LS columns on magnetic separator (MACS® MultiStand and QuadroMACS™ Separator) with a 15 mL collection tube. One LS column per mouse is required.
    b. Add 3 mL of sterile 1× PBS and 0.5% BSA buffer to each LS column.
55. Apply cell suspension to LS column and wash columns 2 times with 1 mL of sterile 1× PBS and 0.5% BSA buffer. Collect unlabeled cells that pass through the column.

⚠ CRITICAL: Do not throw out effluent, this is the unlabeled cell fraction.

56. Centrifuge cell suspension in 15 mL collection tube at 300×*g* for 10 min. Aspirate supernatant completely.
57. Resuspend cell pellet in 270 µL of PEB buffer (Table 1) and transfer to a new 1.5 mL tube.
58. Prepare CD45 MicroBeads for negative selection
    a. Vortex CD45 MicroBeads bottle.
    b. Add 30 µL of CD45 MicroBeads to cell suspension.
59. Incubate cell suspension containing CD45 MicroBeads for 20 min at 4°C while being agitated on a rotator.
60. Add 1 mL of PEB buffer to cell suspension and centrifuge at 300×*g* for 10 min at 4°C. Aspirate supernatant.
61. Resuspend pellet with 500 µL of PEB buffer.
62. Preparation for negative selection
    a. Place LD columns on magnetic separator (MACS® MultiStand and QuadroMACS™ Separator) with a 15 mL collection tube. One LD column per mouse is required.
    b. Add 2 mL of PEB buffer to each LD column.
63. Apply cell suspension to LD column and wash columns 2 times with 1 mL of PEB buffer. Collect unlabeled cells that pass through the column.

⚠ CRITICAL: Do not throw out effluent, this is the unlabeled cell fraction.

64. Continue with step 23–31 in primary endothelial cell isolation protocol.

Note: Elution may be performed using PEB buffer instead of endothelial cell culture medium only for acute RNA extraction.

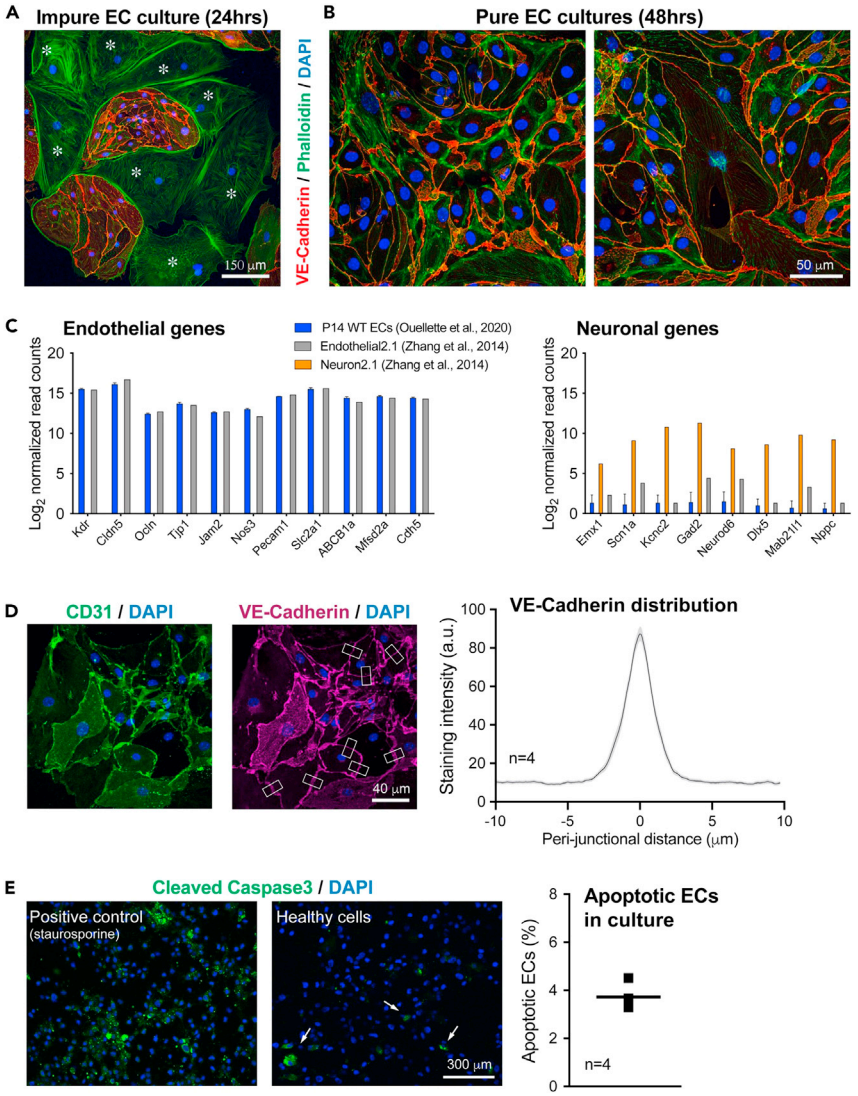

Figure 2. Quality controls with primary mouse cortical ECs isolated from P14 male animals

(A and B) Control of endothelial culture purity using double staining for phalloidin and VE-Cadherin, at two time points. At 24 h, VE-Cadherin-negative contaminating cells (*) can be observed, scale bar: 150µM (A). At 48 h, endothelial culture purity is achieved, as all cells display VE-Cadherin immunoreactivity, scale bar: 50µM (B).

(C) *Left*, Assessment of endothelial gene enrichment using RNAseq data (Ouellette et al., 2020) normalized to a publicly available database (Zhang et al., 2014; http://www.brainrnaseq.org/). *Right*, Assessment of neuronal contamination (same as *Left*). These data show that a very low level of contamination was achieved.

(D) Representative images (*left*) and quantification (*right*) of immunocytochemical staining for endothelial markers CD31 or VE-Cadherin. Distribution of VE-Cadherin fluorescence intensity is shown as example (10 µM × 20 µM white boxes represent areas of quantified staining). Scale bar: 40µM.

(E) Representative images (*left*) and quantification (*right*) for the assessment of apoptosis in EC cultures. The Caspase-3/7 green assay reveals apoptotic rates. Scale bar: 300µM.

In (A, B, D, and E), stained endothelial cells were imaged with a Zeiss Axio Imager M2 microscope equipped with a digital camera (Axiocam 506 mono) and the ApoTome.2 module.

RNA purification

All following steps have been adapted from the OMEGA bio-tek "E.Z.N.A.® HP Total RNA kit" protocol.

Timing: 1 h

Table 2. Sterile 1× PBS (50 mM, pH 7.4) and 0.5% BSA buffer

Reagent	Final concentration	Amount
Albumin, bovine (BSA)	0.5%	0.25 g
Sterile 1× PBS	n/a	50 mL
Total	**n/a**	**50 mL**

Store at −20°C for up to 4 weeks.

65. Add 20 μL β-mercaptoethanol in 1 mL of GTC Lysis buffer found in OMEGA bio-tek E.Z.N.A.® HP Total RNA kit. Prepare 1 mL 70% ethanol.

Note: Volume of prepared β-mercaptoethanol mixed with GTC Lysis buffer and 70% ethanol depends on number of samples to undergo the RNA purification (350 μL of buffer and 70% ethanol/sample is required).

66. Centrifuge 15 mL tubes containing ECs at 500×*g* for 5 min and aspirate supernatant.
67. Resuspend cells in 350 μL of GTC Lysis buffer mixed with β-mercaptoethanol. Vortex to mix thoroughly.
68. Insert a RNA homogenizer mini columns into a 2 mL collection tube.
69. Transfer lysate (from step 67) to the RNA homogenizer mini column. Centrifuge at 13,000×*g* for 1 min. Save filtrate and discard RNA homogenizer mini column.
70. Add 350 μL of 70% ethanol to filtrate. Vortex to mix thoroughly.

Note: Using scissors cut the cap from a 2 mL tube in order to close the 2 mL collection tube. The kit does not provide caps for vortexing.

71. Insert a HiBlind® RNA mini column into a new 2 mL collection tube.
72. Transfer 700 μL sample to the HiBlind® RNA mini column. Centrifuge at 10,000×*g* for 1 min. Discard filtrate and reuse collection tube.
73. Prepare DNase I digestion mixture
    a. Add 73.5 μL of E.Z.N.A.® DNase I digestion buffer and 1.5 μL of RNase-free DNase I (20Kunitz/ μL) to a 1.5 mL tube.

Note: Volume describe in step 73 is for one sample. Adjust volumes accordingly for total number of samples.

74. Add 250 μL of RNA wash buffer I to HiBlind® RNA mini column of each sample. Centrifuge at 10,000×*g* for 1 min. Discard the filtrate and reuse collection tube.
75. Add 75 μL of DNase I digestion mixture directly to the surface of the membrane of the HiBlind® RNA mini column.

Note: Mixture must be added on the membrane to ensure DNA digestion is complete.

76. Let sit at room temperature for 15 min.
77. Add 250 μL RNA wash buffer I. Let sit at room temperature for 2 min. Centrifuge at 10,000×*g* for 1 min. Discard filtrate and reuse collection tube.
78. Add 500 μL of RNA wash buffer II prepared with 100% ethanol (preparation according to manufacturer's protocol). Centrifuge at 10,000×*g* for 1 min. Discard filtrate and reuse collection tube.
79. Repeat step 78.
80. Centrifuge the empty HiBlind® RNA mini column at maximum speed for 2 min to dry the column.

81. Transfer HiBlind® RNA mini column to a clean 1.5 mL tube.
82. Add 60 μL of DNase-free water to HiBlind® RNA mini column. Centrifuge at maximum speed for 2 min.
83. Pass eluted sample (60 μL) through HiBlind® RNA mini column a second time. Centrifuge at maximum speed for 2 min.
84. Measure RNA concentration using Nanodrop. Troubleshooting 2
85. Store eluted RNA at −80°C.
86. Extracted RNA may be used for subsequent reverse transcription- quantitative polymerase chain reaction (RT-qPCR), RNA deep-sequencing or microarray technologies.

Section 2: Validation of healthy primary mouse cerebral cortex endothelial cells

The following steps are essentially completed before starting any assessment on endothelial cells. The quality controls are required when experiments involve cells isolated from mice with different genotypes or receiving treatments. This will identify any basic alterations between groups. These additional steps consist at a minimum confirmation of a pure endothelial cell population using immunocytochemistry, transcriptomics technologies, number of apoptotic cells, as well as endothelial cell proliferation.

Quality control #1: Confirmation of the endothelial identity of primary ECs in culture

Timing: ~6 days

This quality control step consists of confirming the identity of the isolated cells. Here, immunocytochemistry is performed using endothelial cell markers (Figures 2A, 2B, and 2D).

87. Preparation of 12-well plate.
    a. Add a 12 mm glass coverslip to each well of a 12-well plate.
    b. Add 1 mL of 100% ethanol to each well containing a 12 mm glass coverslip and let incubate for 1 h in sterile conditions. This is to sterilize glass coverslips.
    c. After incubation, aspirate 100% ethanol and let dry.
    d. Coat 12-well plate containing 12 mm glass coverslip with 500 μL of 1× attachment factor and let incubate for 30 min at room temperature in sterile conditions.
    e. After incubation, aspirate 1× attachment factor and let dry.
88. Harvest primary endothelial cells
    a. Aliquot TrypLE™ Express Enzyme (1×) in a 15 mL conical tube (1 mL per well of 6-well plate). Incubate at 37°C for 30 min. Aliquot endothelial cell medium [same volume as TrypLE™ Express Enzyme (1×)].

Note: One confluent well of a 6-well plate contains approximately 8 × 10^4 cells to 1 × 10^5 cells. A total of 2–3 confluent wells of a 6-well plate is required to seed 12 wells of a 12-well plate with 1 × 10^4 cells per well.

    b. Aspirate old culture medium from endothelial cells and wash twice with sterile 1× PBS. Aspirate 1× PBS.
    c. Add 1 mL of TrypLE™ Express Enzyme (1×) per well containing cells and place in a 37°C, 5% CO_2 incubator for 5 min.

⚠ CRITICAL: After 5 minute incubation tap plate. Most cells should be detached. If several cells are still attached to the plate, place the plate back in the 37°C, 5% CO_2 incubator for 2 min.

    d. After incubation, add 1 mL of endothelial cell medium to each well and tap plate to detach cells.
    e. Transfer cells to a 15 mL conical tube and centrifuge for 5 min at 500×*g*. Aspirate supernatant. Resuspend cells in 1 mL of endothelial cell medium.

89. Count cells using a hemocytometer.

    Optional: Cells may be counted using an automated cell counter.

90. Seed cells at a density of 1 × 10^4 cells per well in a coated 12-well plate with a final volume of 1 mL per well.

    Note: Cells are added directly to the coverslip to encourage attachment of cells. Once all cells have been seeded, medium is added.

91. Place 12-well plate containing cells in a 37°C, 5% CO_2 incubator for 3–4 days.

    Note: Endothelial cell media requires to be replaced every second day until 40%–60% confluence is reached.

92. Once cells have reached required confluency on glass coverslips, aspirate endothelial culture medium from 12-well plate containing cells. Wash cells twice with 1 mL sterile 1× PBS.
93. Fixation of endothelial cells
    a. Prepare 4% PFA in 1× PBS.
    b. Add 500 μL of 4% PFA to 12-well plate containing 12 mm glass coverslips and cells. Let incubate for 10 min at room temperature.
    c. Aspirate 4% PFA from cells and wash twice with 1 mL sterile 1× PBS. After second wash, add 1 mL of sterile 1× PBS to each well.

    Note: Once cells are fixed, the next steps do not need to be performed under a biosafety cabinet but can be continued at the bench.

94. Immunocytochemistry of endothelial cells.
    a. Prepare blocking solution [10% donkey serum, 0.5% fish gelatin mixed in 0.1% PBST (see Tables 3 and 4)]. A total of 1.5 mL per well is required for entire experiment.

    Note: We use donkey serum because secondary antibody used here were raised in donkey. In general, the serum contained in the blocking solution should match species of the secondary antibodies.

    b. Add 500 μL of blocking solution to each well containing cells and let incubate at room temperature for 60 min. Aspirate blocking solution.
    c. Add 500 μL primary antibodies diluted in blocking solution to each well. We used endothelial markers, rabbit anti-VE-Cadherin at a concentration of 1:500 and rat anti-CD31 at a concentration of 1:200.

    Note: A combination of additional non-endothelial markers is suggested to confirm the purity of isolated cells when initially establishing this protocol. These markers include primary antibodies for neurons (guinea-pig anti-NeuN, 1:1500), pericytes (goat anti-PDGFRß, 1:200), astrocytes (guinea-pig anti-GFAP, 1:1000), microglia (goat anti-Iba1, 1:1000) and smooth muscle cells (mouse anti-αSMA, 1:200).

    d. Incubate at room temperature for 2 h while being slowly agitated on an orbital shaker.
    e. Wash cells 3 × 5 min with 2 mL of 0.2% PBST (see Tables 3 and 5). Aspirate 0.2% PBST.
    f. Add 500 μL of secondary antibodies diluted in blocking solution to each well. We used donkey anti-rabbit IgG (H+L) highly cross-absorbed secondary antibody, Alexa Fluor 568 at a concentration of 1:300 and donkey anti-rat IgG (H+L) highly cross-absorbed secondary antibody, Alexa Fluor 488 at a concentration of 1:300.

Note: For non-endothelial markers, suggested secondary antibodies consist of donkey anti-goat IgG (H+L) cross-absorbed secondary antibody Alexa Fluor 568 at a concentration of 1:300 for pericytes or microglia, goat anti-guinea pig IgG (H+L) highly cross-absorbed secondary antibody Alexa Fluor 488 at a concentration of 1:300 for astrocytes, goat anti-guinea pig IgG (H+L) highly cross-absorbed secondary antibody Alexa Fluor 647 at a concentration of 1:300 for neurons and donkey anti-mouse IgG (H+L) cross-absorbed secondary antibody Alexa Fluor 568 at a concentration of 1:300 for smooth muscle cells. Another suggested antibody to confirm pure EC population includes Alexa Fluor 488-Phalloidin for staining F-actin. This stain may be added to the wells following the 2 washes of 0.2% PBST (step 94h). Dilute Phalloidin at a concentration of 1:40 in the blocking solution and add to cells for 1 h. After incubation, proceed with step 94i.

g. Incubate at room temperature for 60 min while protected from light and slowly agitated on an orbital shaker. Troubleshooting 3
h. Wash cells twice for 5 min with 2 mL of 0.2% PBST. Aspirate 0.2% PBST.
i. Add 1 mL of DAPI in 0.1M PB solution (see Table 6) at a concentration of 1:20,000 to each well. Incubate for 5 min while protected from light. Aspirate DAPI solution.
j. Wash cells twice for 5 min with 1 mL of 0.1M PB.
k. Mounting slides
    i. Add ~10 µL of Fluoromount-G™ media on a slide.
    ii. Using forceps remove glass coverslip with cells from 12-well plate.

⚠ CRITICAL: Glass coverslips are extremely fragile. Do not apply too much pressure with forceps as they will break. Practice removal of glass coverslip from 12-well plate before attempting with cells. If glass coverslip breaks and falls on bench, it can still be imaged.

    iii. Dip coverslip in water and place face down on slide with Fluoromount-G™ drop.
    iv. Let slide dry at room temperature for 1 h while being protected from light. Place slides at 4°C overnight to dry.
    v. Image cells.

Quality control #2: Measure the expression of signature endothelial genes and non-endothelial genes from purified RNA

Additional gene expression assays such as RT-qPCR, RNA deep sequencing (RNAseq) or microarray technologies (Ouellette et al., 2020) can be used to confirm EC population purity following the acute purification of RNA described in purification of endothelial RNA from mouse cerebral cortex (Figure 2C).

Quality control #3: Evaluation of apoptotic rate in cultured primary mouse cerebral cortex endothelial cells

Timing: 4 days

Table 3. 1× PBS (50 mM, pH 7.4) buffer

Reagent	Final concentration	Amount
Na_2HPO_4	41.34 mM	5.87 g
$NaH_2PO_4H_2O$	8.69 mM	1.20 g
NaCl	154 mM	9.00 g
Sterile water	n/a	Fill up to 1 L
Total	**n/a**	**1 L**

Store at room temperature (20°C–22°C) for up to 1 year.

Table 4. 0.1% PBST buffer

Reagent	Final concentration	Amount
Triton® X-100	0.1%	250 µL
1× PBS	n/a	249.75 mL
Total	**n/a**	**250 mL**

Store at room temperature (20°C–22°C) for up to 1 year.

The following step consist of a third quality control. This assay allows for the detection and quantification of programmed cell death following caspase activation (Figure 2E).

95. Preparation of 96-well plate.
    a. Coat a 96-well plate with 100 µL of 1× attachment factor.
    b. Let plate incubate for 30 min at room temperature in sterile conditions.
    c. Aspirate 1× attachment factor and let dry.
96. Harvest primary endothelial cells.
    a. Aliquot TrypLE™ Express Enzyme (1×) in a 15 mL conical tube (1 mL per well of 6-well plate). Incubate at 37°C for 30 min. Aliquot endothelial cell medium [same volume as TrypLE™ Express Enzyme (1×)].

Note: One confluent well of a 6-well plate contains approximately 8 × 10^4 cells to 1 × 10^5 cells. One confluent well can seed up to one 96-well plate.

    b. Aspirate old culture medium from endothelial cells and wash twice with sterile 1× PBS. Aspirate 1× PBS.
    c. Add 1 mL of TrypLE™ Express Enzyme (1×) per well containing cells and place in a 37°C, 5% CO_2 incubator for 5 min.

⚠ CRITICAL: After 5 minute incubation tap plate. Most cells should be detached. If several cells are still attached to the plate, place the plate back in the 37°C, 5% CO_2 incubator for 2 min.

    d. After incubation, add 1 mL of endothelial cell medium to each well and tap plate to detach cells.
    e. Transfer cells to a 15 mL conical tube and centrifuge for 5 min at 500×*g*. Aspirate supernatant. Resuspend cells in 1 mL of endothelial cell medium.
97. Count cells using a hemocytometer.

Optional: Cells may be counted using an automated cell counter.

98. Seed cells at a density of 5 × 10^3 cells per well in coated 96-well plate with a final volume of 200 µL per well.
99. Place 96-well plate containing cells in a 37°C, 5% CO_2 incubator for 48 h.
100. Visually confirm that cells have attached to plate with 70%–80% confluence.
101. Treat 3–4 wells with 1 µM staurosporine for 6 h to act as the positive control.

Table 5. 0.2% PBST buffer

Reagent	Final concentration	Amount
Triton® X-100	0.2%	500 µL
1× PBS	n/a	249.5 mL
Total	**n/a**	**250 mL**

Store at room temperature (20°C–22°C) for up to 1 year.

Table 6. PB (0.1M, pH 7.4) buffer

Reagent	Final concentration	Amount
Na_2HPO_4	82.7 mM	11.74 g
$NaH_2PO_4H_2O$	17.39 mM	2.40 g
Sterile water	n/a	Fill up to 1 L
Total	**n/a**	**1 L**

Store at room temperature (20°C–22°C) for up to 1 year.

Note: Number of wells for positive control depends on available cells.

102. Remove media and replace with 5 μM of CellEvent™ Caspase-3/7 Green Detection Reagent diluted in endothelial cell medium to each well and incubate for 30 min in a 37°C, 5% CO_2 incubator.
103. Wash cells twice using 100 μL sterile 1× PBS.
104. Fix endothelial cells using 100 μL of 2% paraformaldehyde for 30 min and wash cells twice using 100 μL sterile 1× PBS.
105. Stain nuclei using Hoechst 33342 following manufacturers protocol.
106. Image cells.

Note: Cellomics ArrayScan VTI high-content imaging platform running on HCS Studio software was used to image caspase-3 positive cells.

107. Following imaging, count caspase-3 positive cells (green) using Fiji-Image J (Schindelin et al., 2012).

Quality control #4: Quantification of endothelial cell proliferation in culture using a thymidine analogue

Timing: ~6 days

This fourth quality control step consist of the assessment of proliferation in cell culture using an 5-Ethynyl-2′-deoxyuridine (EdU) incorporation assay.

108. Preparation of 12-well plate.
    a. Add a 12 mm glass coverslip to each well of a 12-well plate.
    b. Add 1 mL of 100% ethanol to each well containing a 12 mm glass coverslip and let incubate for 1 h in sterile conditions. This is to sterilize glass coverslips.
    c. After incubation, aspirate 100% ethanol and let dry.
    d. Coat 12-well plate containing 12 mm glass coverslip with 500 μL of 1× attachment factor and let incubate for 30 min at room temperature in sterile conditions.
    e. After incubation, aspirate 1× attachment factor and let dry.
109. Harvest primary endothelial cells.
    a. Aliquot TrypLE™ Express Enzyme (1×) in a 15 mL conical tube (1 mL per well of 6-well plate). Incubate at 37°C for 30 min. Aliquot endothelial cell medium [same volume as TrypLE™ Express Enzyme (1×)].
    b. Aspirate old culture medium from endothelial cells and wash twice with sterile 1× PBS. Aspirate 1× PBS.
    c. Add 1 mL of TrypLE™ Express Enzyme (1×) per well containing cells and place in a 37°C, 5% CO_2 incubator for 5 min.

⚠ CRITICAL: After 5 minute incubation tap plate. Most cells should be detached. If several cells are still attached to the plate, place the plate back in the 37°C, 5% CO_2 incubator for 2 min.

d. After incubation, add 1 mL of endothelial cell medium to each well and tap plate to detach cells.
e. Transfer cells to a 15 mL conical tube and centrifuge for 5 min at 500×*g*. Aspirate supernatant. Resuspend cells in 1 mL of endothelial cell medium.

110. Count cells using a hemocytometer.

Optional: Cells may be counted using an automated cell counter.

111. Seed cells at a density of 5 × 10^3 cells per well in coated 12-well plate with a final volume of 1 mL per well.
112. Place 12-well plate containing cells in a 37°C, 5% CO_2 incubator for 3–4 days.

Note: Endothelial cell media requires to be replaced every second day until ~60% confluence is reached.

113. Rates of endothelial cell proliferation was determined using a Click-iT 5-ethynyl-2′-deoxyuridine (EdU) assay. Protocol was adapted from the manufacturer's instructions.
    a. Prepare 20 mM stock solution of EdU (5 mg of EdU in 1 mL of sterile 1× PBS).
    b. Dilute 20 mM EdU in 1/10 endothelial cell medium (5 μL of 20 mM EdU in 45 μL of endothelial cell medium).
    c. Add 10 μL of diluted EdU in 490 μL of endothelial cell medium (final concentration 20 μM in 500 μL).

Note: This volume is for 1 well of a 12-well plate. Volume will need to be modified accordingly for more wells containing cells.

    d. Remove 500 μL of endothelial cell medium of each well of 12-well plate containing cells.
    e. Add 500 μL of EdU at 20 μM to each well containing cells.

Note: A final volume of 1 mL is in each well containing cells. Therefore, final concentration of EdU in well is 10 μM.

    f. Incubate cells in a 37°C, 5% CO_2 incubator for 48 h without changing endothelial cell medium.
    g. Fixation of endothelial cells
        i. Prepare 4% PFA in 1× PBS.
        ii. Add 500 μL of 4% PFA to 12-well plate containing 12 mm glass coverslips and cells. Let incubate for 10 min at room temperature.
        iii. Aspirate 4% PFA from cells and wash twice with 1 mL of 3% BSA in 1× PBS.

Note: Once cells are fixed, the next steps do not need to be performed under a biosafety cabinet but may be continued at the bench.

        iv. Aspirate washing solution. Add 1 mL of 0.5% Triton® X-100 in 1× PBS to each well. Incubate at room temperature for 20 min.
    h. EdU detection
        i. Prepare 1× Click-iT® reaction cocktail according to manufacturer's protocol (found in Click-iT™ EdU Alexa Fluor™ 594 Imaging Kit).
        ii. Remove 0.5% Triton® X-100 in 1× PBS solution from each well. Wash cells twice with 1 mL of 3% BSA in 1× PBS.
        iii. Add 0.5 mL of 1× Click-iT® reaction cocktail to each well containing cells.
        iv. Incubate plate for 30 min at room temperature, while protected from light.
        v. Remove reaction cocktail and wash cells once with 1 mL of 3% BSA in 1× PBS.

vi. Proceed to immunocytochemistry. Follow protocol as of step 94c.

Note: Primary antibody and secondary antibody used following EdU incorporation assay are rabbit anti-VE-Cadherin at a concentration of 1:500 and donkey anti-rabbit IgG (H+L) highly cross-absorbed secondary antibody, Alexa Fluor 647 at a concentration of 1:300. Troubleshooting 4

114. Image cells.
    a. Take ten images using 20× objective.
    b. Count EdU positive cells using the Cell Counter plugin in Fiji-Image J (Schindelin et al., 2012).

Section 3: Functional assessment using cultured primary mouse cerebral cortex endothelial cells

Assessment of endothelial cell migration

Timing: 3 days

Cells must have reached 70%–80% confluence before completing scratch wound assay. This assay is a convenient method for analysis of cell migration (Figure 3A). This protocol is adapted from the Incucyte ZOOM® 96-Well Scratch Wound Cell Migration & Invasion Assays User Manual. Troubleshooting 5

115. Prepare 96-well ImageLock plate.
    a. Coat a 96-well ImageLock plate with 100 µL of 1× attachment factor.
    b. Let plate incubate for 30 min at room temperature in sterile conditions.
    c. Aspirate 1× attachment factor and let dry.
116. Harvest primary endothelial cells.
    a. Aliquot TrypLE™ Express Enzyme (1×) in a 15 mL conical tube (1 mL per well of 6-well plate). Incubate at 37°C for 30 min. Aliquot endothelial cell medium [same volume as TrypLE™ Express Enzyme (1×)].
    b. Aspirate old culture medium from endothelial cells and wash twice with sterile 1× PBS. Aspirate 1× PBS.
    c. Add 1 mL of TrypLE™ Express Enzyme (1×) per well containing cells and place in a 37°C, 5% CO_2 incubator for 5 min.

⚠ CRITICAL: After 5 minute incubation tap plate. Most cells should be detached. If several cells are still attached to the plate, place the plate back in the 37°C, 5% CO_2 incubator for 2 min.

    d. After incubation, add 1 mL of endothelial cell medium to each well and tap plate to detach cells.
    e. Transfer cells to a 15 mL conical tube and centrifuge for 5 min at 500×*g*. Aspirate supernatant. Resuspend cells in 1 mL of endothelial cell medium.

117. Count cells using a hemocytometer.

Optional: Cells may be counted using an automated cell counter.

118. Seed cells at a density of 2 × 10^4 cells per well in coated 96-well ImageLock plate with a final volume of 100 µL per well.

Note: All wells of 96-well ImageLock plate must have 100 µL, even if there are no cells in wells. Do not write on top of the plate.

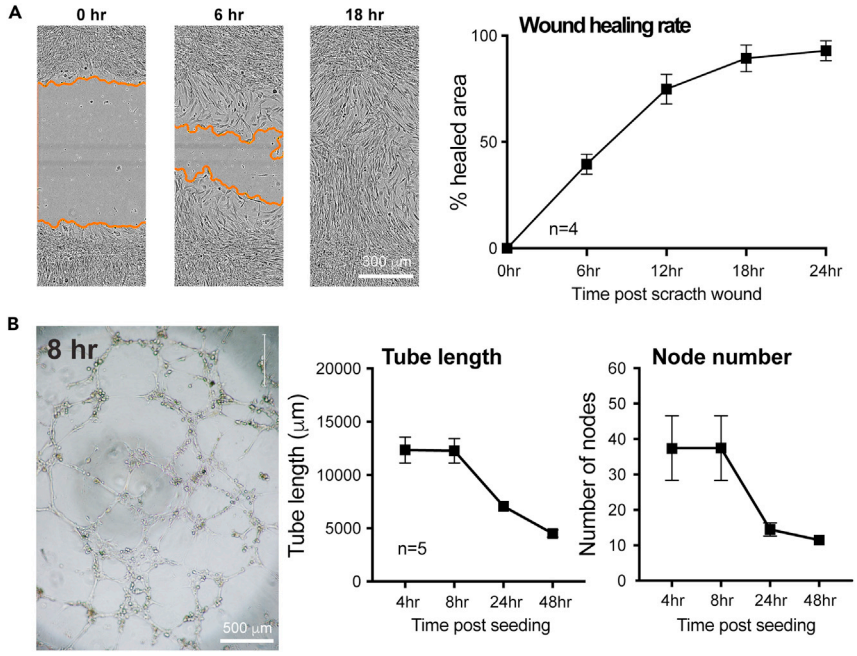

Figure 3. Expected outcomes with primary mouse cerebral cortex ECs isolated from P14 male animals

(A) Representative images (*left*) and quantification (*right*) for a scratch wound-healing assays used to measure migration of primary mouse brain ECs. The orange lines indicate cellular migration fronts. Scale bar: 300µM.

(B) *In vitro* network formation assay using primary mouse brain ECs from P14 brains to assess vascular network formation and remodeling over 48 h in a growth factor-reduced Matrigel®. *Left*, representative images at the 8hr time point, scale bar: 500µM. *Right*, Quantifications of network density (i.e., total endothelial tube length) and network nodes (i.e., total number of branching hubs). Image in (B) was captured using a Nikon Eclipse TE2000- E inverted microscope. All data displayed are mean ± S.E.M.

119. Place 96-well ImageLock plate containing cells in a 37°C, 5% CO_2 incubator for 48 h.
120. Preparing and creating wounds using WoundMaker™
    a. Fill wash boat 1 with 45 mL of sterile water and place WoundMaker™ pin block in water for 5 min.
    b. Fill wash boat 2 with 45 mL of 70% ethanol and place WoundMaker™ pin block in the solution for 5 min.
    c. Place WoundMaker™ pin block on an empty wash boat.
    d. Insert 96-well ImageLock plate containing cells and media into the base plate holder. Remove plate cover.
    e. Place WoundMaker™ pin block onto the base plate holding the cells. Push and hold lever.

⚠ CRITICAL: If cells are too confluent, large sheets of cells will be removed and wound will not be uniform between wells. Troubleshooting 6

    f. Lift WoundMaker™ pin block and replace with 96-well ImageLock plate cover.
    g. Aspirate and replace endothelial cell culture medium to remove floating cells.
121. Place 96-well ImageLock plate containing cells and 100 µL fresh media into the IncuCyte™ Zoom® Apparatus to record cell migration.

Note: ZOOM software is scheduled for repeat scanning with images taken every 2 h for 24 h. In the software make sure 'scan type' is set to Scratch Wound and Wide Mode.

122. Clean WoundMaker™ after use.
    a. Fill wash boat 4 with 45 mL of 0.5% Alconox and place WoundMaker™ pin block in solution for 5 min.

b. Fill wash boat 5 with 45 mL of 1% Virkon S. and place WoundMaker™ pin block in the solution for 5 min.
c. Fill wash boat 1 with 45 mL of sterile water and place WoundMaker™ pin block in water for 5 min.
d. Fill wash boat 2 with 45 mL of 70% ethanol and place WoundMaker™ pin block in the solution for 5 min.
e. Place WoundMaker™ on its base and store at room temperature.

123. Quantification of migration assay is performed using IncuCyte® ZOOM Software. More detailed information on data analysis can be found at the Essen BioScience website.

Assessment of endothelial cell angiogenic activity

Timing: 3 days

The following steps are to be completed after cell isolation and 70%–80% confluence has been reached. This endothelial cell tube formation assay measures the ability of endothelial cells to form capillary-like structures in a extracellular matrix (Matrigel®; Figure 3B).

Day prior to tube formation assay

124. Place a 96-well plate and 200 μL pipette tips at −20°C overnight.
125. Reduced growth factor Matrigel® should be at 4°C overnight to ensure slow thawing.

⚠ CRITICAL: Reduced growth factor Matrigel® must be handled with care. Rapid thawing will lead to polymerization of matrix. Matrix must always be on ice or at 4°C.

Day of tube formation assay

126. Harvest primary endothelial cells and preparation of growth factor reduced Matrigel® plate
    a. Aliquot TrypLE™ Express Enzyme (1×) in a 15 mL conical tube (1 mL per well of 6-well plate). Incubate at 37°C for 30 min. Aliquot endothelial cell medium [same volume as TrypLE™ Express Enzyme (1×)].
    b. Place 96-well plate and 200 μL pipette tips (from the −20°C freezer) as well as growth factor reduced Matrigel on ice in the biosafety cabinet.
    c. Aspirate old culture medium from endothelial cells and wash twice with sterile 1× PBS. Aspirate 1× PBS.
    d. Add 1 mL of TrypLE™ Express Enzyme (1×) per well containing cells and place in a 37°C, 5% CO_2 incubator for 5 min.

⚠ CRITICAL: After 5 minute incubation, tap plate. Most cells should be detached. If several cells are still attached to the plate, return plate to the 37°C, 5% CO_2 incubator for 2 min.

    e. During 5 min incubation, add 50 μL of growth factor reduced Matrigel® per well of cold 96-well plate. Quickly remove any visible bubbles in wells containing growth factor reduced Matrigel®. After removing bubbles, a minimum of 40 μL growth factor reduced Matrigel® must be left in the well for assay. Place 96-well plate containing growth factor reduced Matrigel in a 37°C, 5% CO_2 incubator for 30 min.

Note: Hold the neck of the Matrigel® bottle to reduce heat transfer. Prepare 3 wells of growth factor reduced Matrigel per mouse for accurate assessment of angiogenic capacity. Always leave the 96-well plate on ice to prevent Matrigel® polymerization until all wells are ready to be transferred to the incubator.

f. After incubation, add 1 mL of endothelial cell medium to each well of 6-well plate and tap plate to detach cells.
g. Transfer cells to a 15 mL conical tube and centrifuge for 5 min at 500×*g*. Aspirate supernatant. Resuspend cells in 1 mL of endothelial cell medium.

127. Count cells using a hemocytometer.

Optional: Cells may be counted using an automated cell counter.

128. A total of 6×10^4 cells is required per mouse in a final volume of 450 µL of endothelial cell medium.

Note: For each mouse, 3 wells of a 96-well plate will be prepared. A total of 6×10^4 cells per mouse is needed. Each well of the 96-well plate will contain 2×10^4 cells. One confluent well of a 6-well plate is needed to prepare 3 wells of a 96-well plate with matrigel (one confluent well contains approximately 8×10^4 cells to 1×10^5 cells).

129. After the 30 min incubation of the 96-well plate containing growth factor reduced Matrigel®, seed 2×10^4 cells (150 µL) per well containing matrix.
130. Place 96-well plate containing matrix and endothelial cells in a 37°C, 5% CO_2 incubator until imaging time points (4 h, 8 h, 24 h, 48 h). Troubleshooting 7

Note: Imaging was completed with a Nikon Eclipse TE2000-E inverted microscope.

131. Quantification of tube formation assay using Fiji-image J (Schindelin et al., 2012).
a. Download macro: Angiogenesis Analyzer for ImageJ (Carpentier, 2012)
b. Install and open macro in Fiji-image J.
c. Choose file containing all tube formation images and select "Analyze HUVECS Phase Contrast" and let macro run.
d. Once analysis is complete, export file in Excel. Branching length is found under "Total branching length" column and number of nodes is found under "Nb master junction" column. Using this data angiogenic activity differences between may be determined.

EXPECTED OUTCOMES

Our protocol yields pure primary mouse brain EC cultures, whereby ECs can be utilized for subsequent characterization and functional assays. In culture, ECs will reach a pure population within 48 h of culture, and confluence within 7 days. Using a double staining of phalloidin and VE-Cadherin revealed a pure EC population after 48 h in culture as all cells are VE-Cadherin positive (Figures 2A and 2B). As of this stage, population purity and health can be confirmed, and assessment of functional characteristics can be completed. Of note, endothelial behavior will start to change after two passages. Therefore, cell isolation from multiple mice may be required to complete the entirety of this protocol, in order to eliminate the need of additional passaging of cells. We emphasize the importance of validating the nature of ECs and of confirming their health in culture prior to any functional assessment. Additional transcriptomics assays can confirm EC population purity following acute cell isolation. Using deep RNA sequencing, we confirmed endothelial gene enrichment from purified endothelial RNA as well as a very low neuronal contamination (Figure 2C). Following immunocytochemical staining for endothelial markers CD31 and VE-cadherin (other markers can be used), intercellular junctions can be delineated and their distribution quantified. For instance, normal distribution of staining can be quantified across cell-cell junctions using the profile plot tool in ImageJ. A peak in staining intensity should be observed at cell-cell junctions (Figure 2D). Using the caspase-3/7 green assay to assess apoptotic rates of cortical ECs allows direct count of the proportion of apoptotic cells. Number of apoptotic cells (green) are counted and expressed as % of

total cells in each image. In our hands, healthy WT mouse brain ECs isolated at P14 yield ~4% of apoptotic ECs (Figure 2E). Our protocol also describes a fourth quality control with the measure of EC proliferation. The number of EdU positive cells is counted and expressed as % of total cells. For more information, please consult our recent publication Ouellette et al. (2020) in which this experiment was performed using human-derived endothelial cells. Once EC identity and health are confirmed, these cells can undergo various functional assays. This protocol describes two assays: a cell migration assay and an angiogenic activity assay. For cell migration assessment, a scratch wound is imaged and measured during 24 h. Imaging at different time points during this period allows to measure the percent of healed area throughout time (Figure 3A). To measure angiogenic activity of ECs, a Matrigel®-based network formation assay is used. Imaging at different time points allows to quantify the formation of new endothelial networks. At 8 h post-seeding, branching and nodes can be readily identified in this 3D matrix. An extensive network will be formed until ~12 h, after which the network will collapse due to nutrient depletion within the well (Figure 3B).

LIMITATIONS

This protocol has been optimized for the isolation and characterization of primary mouse cerebral cortex endothelial cells (ECs) isolated from P14 pups. While these steps can be applied to younger (e.g., embryos, <P14) or adult (≥P50) mice, note that cell isolations from adult mice are more challenging and yield a lower number of ECs. Thus, adult mice cortices may need to be pooled to get a higher cell density. Moreover, adult primary brain ECs are more sensitive to manipulations and require an extended amount of time for growth before functional assays.

The cell isolation procedure described in primary mouse cerebral cortex endothelial cell isolation and culture yields a semi-pure EC population, in part contaminated by myelin debris; therefore, the precise number of ECs following this isolation cannot be determined. However, once EC colonies grow and expand, a total of 80,000–100,000 confluent cells can be counted in one well from a 6-well plate. With acute isolation of ECs for gene expression studies (purification of endothelial RNA from mouse cerebral cortex), the number of cells is not counted to preserve cell population integrity by reducing manipulations. As noted in Ouellette et al. (2020), ECs from two P14 brains (four cerebral cortices) are pooled into one biological replicate to obtain a sufficient amount of total RNA for transcriptomic studies.

TROUBLESHOOTING

Problem 1

Low number cells have attached to culture plate (step 34).

Potential solution

Following cell isolation decrease elution volume in order to have a higher density of endothelial cells for initial plating. Plate all cells within one well of a coated 6-well plate.

Problem 2

Low RNA concentration (step 84).

Potential solution

To increase RNA concentration, pool ECs from 4 cortices (2 mice) following ECs elution from LS column. This will increase the number of cells prior to the RNA extraction. Therefore, yield a higher concentration of RNA.

Problem 3

Endothelial cells have detached during immunocytochemistry (step 94g).

Potential solution

During all incubations, plates containing cells may be slowly agitated. However, if cells are being washed away during incubation or washing steps, leave plate on the bench without being agitated during incubations. During washing steps, a plastic transfer pipette with a 200 μL tip can be used to aspirate buffers to decrease the chance of disturbing the cells.

Problem 4

Emission bleed between A594 and A647 (step 113h).

Potential solution

An alternate fluorophore may be used for immunocytochemistry. Secondary antibody donkey anti-rabbit IgG (H+L) highly cross-absorbed secondary antibody, Alexa Fluor 488 at a concentration of 1: 300 is recommended instead of Alexa Fluor 647.

Problem 5

Incucyte ZOOM® equipment is not available (steps 115–123).

Potential solution

A traditional scratch wound assay can be used in this quality control protocol. In this case, the plate is prepared as described in step 95. Endothelial cells are seeded at a density 2×10^4 cells per well of a coated 96-well plate. The plate containing the cells is placed in a 37°C, 5% CO_2 incubator for 48 h. A sterile 200 μL pipette tip is used to create a straight wound withing each well. Cell migration imaging at time points of interest can be completed using an inverted phase contrast microscope attached to a camera until the wound is closed.

Problem 6

Large cell sheets have been removed following wound (step 120e).

Potential solution

If cells are too confluent, large cell sheets will be removed during wound creating: 1) decrease seeding density of endothelial cells, or 2) create wound after 24 h of plating instead of 48 h. By decreasing cell seeding density and time before assay, a single layer of cells will be formed. This single layer of cells will lead to a defined wound.

Problem 7

Cells within matrix appear round and no branching has formed after 24 h (step 130).

Potential solution

If cells are dying within the matrix, it is possible that the amount of time allotted for cell counting is too long. Thus, it would be beneficial to harvest cells in batches that way they are out of an optimal growing environment for a shorter amount of time increasing their chance of survival.

RESOURCE AVAILABILITY

Lead contact

Further information and requests for resources and reagents should be directed to and will be fulfilled by the lead contact, Baptiste Lacoste: blacoste@uottawa.ca

Materials availability

This study did not generate new unique reagents.

Data and code availability

Data and codes are available from the lead contact upon request as well as from supplementary material from Ouellette et al. (2020) *Nat. Neurosci.*

ACKNOWLEDGMENTS

For this work, J.O. was supported by Ph.D. scholarship awards from the Canadian Institutes of Health Research (CIHR) and the Canadian Vascular Network (CVN), and B.L. by a research grant from the CIHR (grant #388805). We thank the Cell Biology and Image Acquisition (CBIA) Core Facility at Faculty of Medicine at University of Ottawa.

AUTHOR CONTRIBUTIONS

J.O. optimized and carried out experiments, wrote the manuscript draft and participated in figure generation. B.L. proofread the manuscript, provided guidance in writing, and participated in figure assembly.

DECLARATION OF INTERESTS

Authors declare no competing interest.

REFERENCES

Carpentier, G. (2012). Contribution: Angiogenesis Analyzer (ImageJ News).

Collins, S., Wagner, C., Gagliardi, L., Kretz, P., Fischer, M.-C., Kessler, P., Kannan, M., and Yalcin, B. (2018). A method for parasagittal sectioning for neuroanatomical quantification of brain structures in the adult mouse. Curr. Protoc. Mouse Biol. *8*, e48.

Meyerhoff, J., Muhie, S., Chakraborty, N., Naidu, L., Sowe, B., Hammamieh, R., Jett, M., and Gautam, A. (2021). Microdissection of mouse brain into functionally and anatomically different regions. J. Vis. Exp. *168*, e61941.

Ouellette, J., Toussay, X., Comin, C.H., Costa, L.D.F., Ho, M., Lacalle-Aurioles, M., Freitas-Andrade, M., Liu, Q.Y., Leclerc, S., Pan, Y., et al. (2020). Vascular contributions to 16p11.2 deletion autism syndrome modeled in mice. Nat. Neurosci. *23*, 1090–1101.

Schindelin, J., Arganda-Carreras, I., Frise, E., Kaynig, V., Longair, M., Pietzsch, T., Preibisch, S., Rueden, C., Saalfeld, S., Schmid, B., et al. (2012). Fiji: an open-source platform for biological-image analysis. Nat. Methods *9*, 676–682.

Zhang, Y., Chen, K., Sloan, S.A., Bennett, M.L., Scholze, A.R., O'Keeffe, S., Phatnani, H.P., Guarnieri, P., Caneda, C., Ruderisch, N., et al. (2014). An RNA-sequencing transcriptome and splicing database of glia, neurons, and vascular cells of the cerebral cortex. J. Neurosci. *34*, 11929–11947.

Appendix D - Manuscript V

Association to hypothesis: This manuscript provides evidence of vascular discrepancies in neurodevelopmental and neurodegenerative disorders found in the literature, highlighting the importance in understanding the vascular contributions to neurological disorders. Furthermore, this manuscript emphasized that early vascular alterations can lead to long-term impacts.

Current manuscript status: This manuscript was published in *Frontiers in Aging Neuroscience* in 2021.

Author contributions : JO wrote the draft following BL's instructions. BL chose the theme and edited the manuscript. Both authors contributed to the article and approved the submitted version.

frontiers in Aging Neuroscience

REVIEW
published: 20 October 2021
doi: 10.3389/fnagi.2021.749026

From Neurodevelopmental to Neurodegenerative Disorders: The Vascular Continuum

Julie Ouellette[1,2] *and Baptiste Lacoste*[1,2,3]*

[1] Ottawa Hospital Research Institute, Neuroscience Program, Ottawa, ON, Canada, [2] Department of Cellular and Molecular Medicine, Faculty of Medicine, University of Ottawa, Ottawa, ON, Canada, [3] University of Ottawa Brain and Mind Research Institute, Ottawa, ON, Canada

Structural and functional integrity of the cerebral vasculature ensures proper brain development and function, as well as healthy aging. The inability of the brain to store energy makes it exceptionally dependent on an adequate supply of oxygen and nutrients from the blood stream for matching colossal demands of neural and glial cells. Key vascular features including a dense vasculature, a tightly controlled environment, and the regulation of cerebral blood flow (CBF) all take part in brain health throughout life. As such, healthy brain development and aging are both ensured by the anatomical and functional interaction between the vascular and nervous systems that are established during brain development and maintained throughout the lifespan. During critical periods of brain development, vascular networks remodel until they can actively respond to increases in neural activity through neurovascular coupling, which makes the brain particularly vulnerable to neurovascular alterations. The brain vasculature has been strongly associated with the onset and/or progression of conditions associated with aging, and more recently with neurodevelopmental disorders. Our understanding of cerebrovascular contributions to neurological disorders is rapidly evolving, and increasing evidence shows that deficits in angiogenesis, CBF and the blood-brain barrier (BBB) are causally linked to cognitive impairment. Moreover, it is of utmost curiosity that although neurodevelopmental and neurodegenerative disorders express different clinical features at different stages of life, they share similar vascular abnormalities. In this review, we present an overview of vascular dysfunctions associated with neurodevelopmental (autism spectrum disorders, schizophrenia, Down Syndrome) and neurodegenerative (multiple sclerosis, Huntington's, Parkinson's, and Alzheimer's diseases) disorders, with a focus on impairments in angiogenesis, CBF and the BBB. Finally, we discuss the impact of early vascular impairments on the expression of neurodegenerative diseases.

Keywords: cerebrovascular abnormalities, neurodevelopment and intellectual disabilities, aging, neurodegeneration, cerebral blood flow, angiogenesis, blood-brain barrier

OPEN ACCESS

Edited by:
Anusha Mishra,
Oregon Health and Science University, United States

Reviewed by:
Barbara Lykke Lind,
University of Copenhagen, Denmark
Ravi L. Rungta,
Université de Montréal, Canada
Vanessa Coelho-Santos,
Seattle Children's Research Institute, United States

***Correspondence:**
Baptiste Lacoste
blacoste@uottawa.ca

Received: *28 July 2021*
Accepted: *13 September 2021*
Published: *20 October 2021*

Citation:
Ouellette J and Lacoste B (2021) From Neurodevelopmental to Neurodegenerative Disorders: The Vascular Continuum. Front. Aging Neurosci. 13:749026. doi: 10.3389/fnagi.2021.749026

INTRODUCTION

The human brain contains approximately 100 billion vessels (∼600 km), all of which are critical for the delivery of nutrients and oxygen to neural cells (Quaegebeur et al., 2011). Although the brain accounts for only 2% of the body's mass, it consumes about a quarter of the body energy produced at rest (Attwell et al., 2010). This colossal energy consumption is elemental to maintain normal functioning of the brain. Such energy requirements make the brain heavily reliant on key vascular features: (i) a dense vasculature to sustain adequate perfusion, (ii) a functional blood-brain barrier (BBB) to maintain brain homeostasis, and (iii) the proper regulation of cerebral blood flow (CBF) to match metabolic demands (**Figure 1**). Thus, a healthy brain vasculature is essential to support neural cells and ensure normal brain maturation, function and aging (Attwell and Laughlin, 2001; Girouard and Iadecola, 2006; Andreone et al., 2015; Lacoste and Gu, 2015). This is accomplished in part via neurovascular coupling (NVC) mechanisms that regulate CBF to support energetic demands of brain cells (Hamel, 2006; Attwell et al., 2010; Kaplan et al., 2020). While most studies are describing neurovascular signaling at the level of the microvasculature, other vascular segments have received very little attention. There is evidence suggesting that different vascular segments play different roles during vascular responses which is involved in maintaining brain homeostasis. The concept of heterogeneous vascular modules has been extensively reviewed in Schaeffer and Iadecola (2021).

The close anatomical apposition between the nervous and vascular systems supports a functionally integrated network (Attwell et al., 2010; Lecrux and Hamel, 2011; Hillman, 2014; Huneau et al., 2015; Kaplan et al., 2020). This involves modulating vascular tone by secretion of vasoconstrictor and vasodilator molecules. Initially, it was proposed that local metabolic factors released by neurons modulate local CBF (Sherrington, 1890; Friedland and Iadecola, 1991). Since then, several studies have introduced other cellular mediators of NVC which altogether form the neurovascular unit (NVU). This anatomical substrate of NVC indeed involves a multicellular system consisting of neurons, pericytes, smooth muscle cells, astrocytes, microglia and endothelial cells (ECs) that together orchestrate CBF, and thus brain function (Attwell et al., 2010; Andreone et al., 2015; Grubb et al., 2021; **Figure 1**). The cerebral cortex is innervated by projection neurons that release neurotransmitters including, but not limited to, acetylcholine, noradrenaline, serotonin and glutamate, involved in the regulation of vessel diameter (Sandoo et al., 2010). Pericytes, while having debated roles in NVC, possess contractile properties and regulate blood flow around capillaries (Attwell et al., 2010, 2016; Fernandez-Klett and Priller, 2015; Sweeney et al., 2018; Watson et al., 2020; Hartmann et al., 2021). Capillary pericytes are α-smooth muscle actin (SMA)-negative and only partially cover the vessel, while ensheathing pericytes are α-SMA-positive, occupy proximal branches of penetrating arteriole offshoots, and fully cover the vessels. However, they are classified as different from smooth muscle cells as they display an ovoid cell body (Grant et al., 2019). Vascular smooth muscle cells (SMCs), found on intracerebral arterioles and arteries, are absent from intracerebral capillaries. These cells are short, densely packed, ring-shaped, and essential for regulating vessel tone (Lacoste and Gu, 2015; Frosen and Joutel, 2018; Grant et al., 2019). Astrocytes occupy a critical position between blood vessels and neurons. They can modulate vessel tone via receptor-mediated increase in astrocytic Ca^{2+}, resulting in the release of astrocyte-derived prostaglandins (PGE_2), nitric oxide (NO), epoxyeicosatrienoic acids (EETs), glutamate, or adenosine, all of which can alter vascular diameter and tone (Attwell et al., 2010; Cauli and Hamel, 2010; Filosa and Iddings, 2013; Harada et al., 2015; Haidey et al., 2021), as reviewed in detailed elsewhere (Filosa and Iddings, 2013; Howarth, 2014; MacVicar and Newman, 2015; Mishra, 2017; McConnell et al., 2019; Stackhouse and Mishra, 2021). Whereas microglia are the main regulators of inflammatory processes in the brain, their role in NVC is not well defined. However, recently, they were suggested as essential in regulating CBF during neural activation (Császár et al., 2021). Brain ECs have unique morphological and functional features such as a lack of fenestration, the presence of tight junctions between cells, a low number of pinocytic vesicles that limit transcytosis, hence forming the first limiting layer of the BBB (Reese and Karnovsky, 1967; Stamatovic et al., 2008; Rizzo and Leaver, 2010; Salmina et al., 2014; Andreone et al., 2015). This highly selective barrier promotes a tightly regulated brain homeostasis to ensure proper neuronal function, protecting the brain from toxins, pathogens, inflammation, and injury (Weiss et al., 2009; Larsen et al., 2014; Daneman and Prat, 2015; Van Dyken and Lacoste, 2018). Furthermore, brain ECs regulate vascular tone by releasing vasodilators including endothelial-derived NO, endothelium-derived EETs, PGE_2 and prostacyclin, as well as vasoconstrictors such as endothelin-1, thromboxane A_2 and prostaglandin $F_{2\alpha}$ (Mohan et al., 2012; Filosa and Iddings, 2013; Andreone et al., 2015; Kisler et al., 2016, 2017; Dabertrand et al., 2021). While the endothelium regulates vascular permeability and tone, it is also the main target of small vessel disease (SVD), which refers to a pathological process that damages arterioles, venules and brain capillaries. SVD has a major impact on CBF and cognition (Hakim, 2019). The NVU as a whole is also responsible for maintaining BBB integrity (Abbott et al., 2006; Zlokovic, 2008; Daneman, 2012; Kadry et al., 2020). Alterations in vascular patterning, CBF and BBB, either during development or later in life, contribute to the onset and/or progression of early- or late-onset neurological disorders (**Figure 2**).

Well-balanced vascular and neuronal interactions are required to support brain function from early life. The shared spatial and temporal patterns of vascular and neuronal networks suggest an integrative role for vessels in neural development, and *vice versa* (Gu et al., 2005; Carmeliet and Jain, 2011; Andreone et al., 2015; Lacoste and Gu, 2015). Neurovascular crosstalk, which initially takes place during embryogenesis, supports the rising oxygen and nutrient demand of immature neurons as they require extensive energy to maintain normal course of development (De Filippis and Delia, 2011). The increased energy consumption by neurons creates a hypoxic environment acting as a signal for boosting blood vessel production to upsurge delivery of oxygen and metabolic substrates to the brain (Stone et al., 1995;

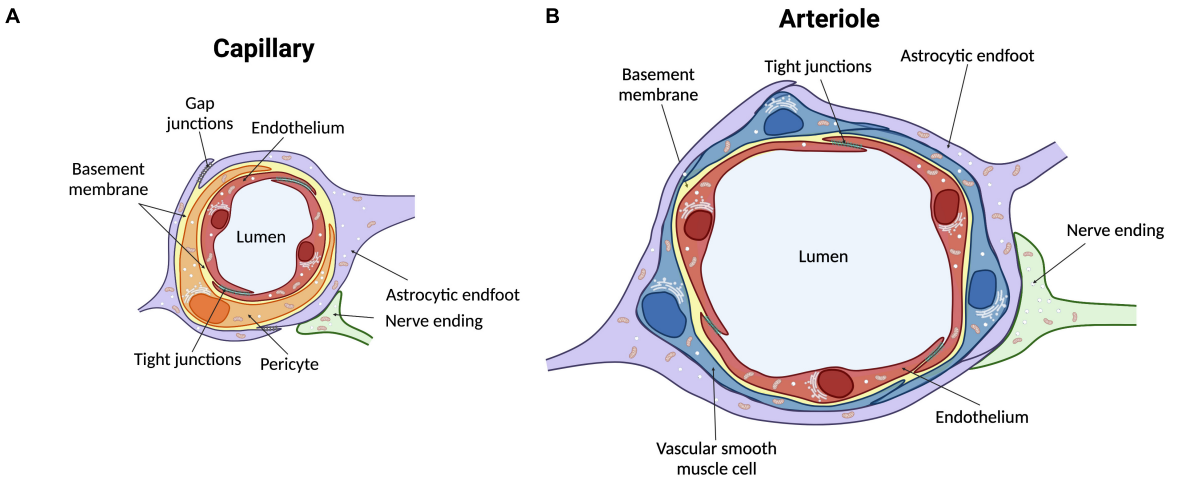

FIGURE 1 | Summary of structures and functions of the neurovascular unit (NVU). The anatomical substrate for regulation of cerebral blood flow and the blood-brain barrier is a multicellular system consisting of neurons, pericytes, smooth muscle cells, astrocytes and endothelial cells known as the NVU. **(A)** Intracerebral capillaries lack vascular smooth muscle cells but are partly covered by contractile pericytes. **(B)** At the level of intracerebral arterioles, the endothelium is fully covered by a single layer of vascular smooth muscle cells, which provide contractile properties to the arteriole. Astrocytes send their processes called endfeet around both capillaries and arterioles, providing support as well as a functional connection to surrounding parenchyma. **(C)** Summary of functions of the blood-brain barrier and neurovascular coupling. Arrows point to neurovascular unit components. *Figure made using BioRender*.

Lacoste and Gu, 2015; Peguera et al., 2021). Hypoxia initiates vessel ingression into deep brain structures, followed by usage of vascular patterning cues (Lacoste and Gu, 2015; Tata et al., 2015; Tata and Ruhrberg, 2018; Okabe et al., 2020). Comparably, ECs instruct neural progenitors into dividing, differentiating or migrating through release of paracrine signals that regulate neuronal development in vascular niches (Hogan et al., 2004; Shen et al., 2004; Daneman et al., 2009; Goldman and Chen, 2011; Delgado et al., 2014; Lacoste and Gu, 2015; Licht and Keshet, 2015; Walchli et al., 2015; Tata and Ruhrberg, 2018; Peguera et al., 2021). Moreover, neuronal activity plays important roles in modulating postnatal brain angiogenesis (Lacoste et al., 2014; Whiteus et al., 2014; Biswas et al., 2020). As the brain matures, vascular networks remodel until the system consists of an extensive network that actively regulates blood flow to adequately sustain energy demands. The functional relationships between neurons and blood vessels ensures that NVC mechanisms progressively develop (Lacoste and Gu, 2015; Coelho-Santos and Shih, 2020). NVC becomes fully functional ∼3–4 weeks after birth in rodents, and 7–8 weeks in humans (Yamada et al., 2000; Muramuto et al., 2002; Kozberg et al., 2016).

These vascular features can become defective early in life, affecting brain maturation. Vascular susceptibilities can also emerge later in life, taking part in neurodegenerative processes. Indeed, NVU deficits play a role in both early- and late-onset neurological disorders (**Figure 2**). Mounting evidence shows that vascular impairments contribute to the pathophysiology of neurological conditions throughout life, including neurodevelopmental, metabolic, and neurodegenerative disorders (Nicolakakis and Hamel, 2011; Van Dyken and Lacoste, 2018; McConnell et al., 2019; Ouellette et al., 2020; Sharma and Brown, 2021). This suggests the existence of a vascular continuum between developmental conditions and illnesses of aging, which will be the focus of this review (**Figure 3**). A better understanding of mechanisms and key players involved in cerebrovascular impairments may lead to transformative therapeutic strategies at different stages of life.

CEREBROVASCULAR DEFICITS ASSOCIATED WITH NEURODEVELOPMENTAL DISORDERS

Neurodevelopmental disorders are considered a group of conditions with onset/diagnosis during infancy, childhood, or adolescence (Morris-Rosendahl and Crocq, 2020). They are

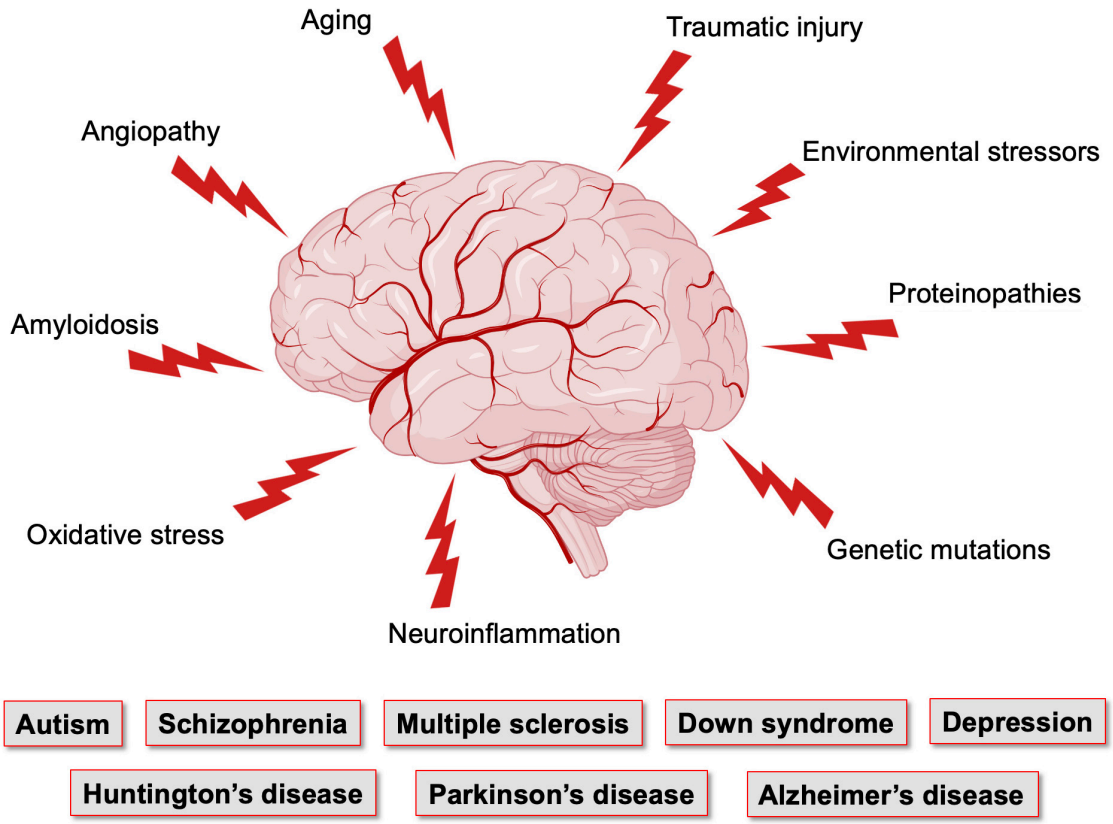

FIGURE 2 | Factors affecting the brain vasculature and leading to neurological conditions. The brain, which has elevated metabolic needs but poor energy storage, is highly dependent on a continuous supply of nutrients and oxygen from the blood stream, and is thus dependent on the integrity of its vasculature. Vasculature of the brain is the most complex and dense in the human body. Yet, it is maintaining a very fragile equilibrium and is the target of numerous pathological conditions that affect neuronal maturation and function. *Figure made using BioRender*.

defined by impairments in motor, social, cognitive, academic, and/or occupational functioning. Most studies focused on the neuronal contributions to these disorders; however, concomitant vascular impairments are starting to emerge (Ouellette et al., 2020). Here, we highlight vascular impairments identified in autism spectrum disorders (ASD) and schizophrenia.

Vascular Links to Autism Spectrum Disorders

ASD are pervasive neurodevelopmental disorders associated with social interaction deficits, speech and language impairments, as well as repetitive behaviors and restricted interests (Vijayakumar and Judy, 2016). These disorders have a prevalence of 1–2% in the general population and affect four times more boys than girls (Hogan et al., 2004; Daneman et al., 2009). Individuals with ASD show atypical behaviors associated with visual attention, imitation, social responses, and motor control by 12 months of age. By the age of 3, a child can be efficiently diagnosed with ASD (Park et al., 2016). While the underlying causes of ASD are enigmatic, both environmental and genetic origins have been found, leading to the identification of gene mutations within the ASD population (Hogan et al., 2004; James et al., 2009; Emerson et al., 2017). Although most studies have been neurocentric, ASD are now being associated with vascular vulnerabilities.

Altered Cerebral Blood Flow in Autism Spectrum Disorders

Neuroimaging techniques can map changes in CBF or blood oxygenation during various activities. Morphological and functional investigations using functional magnetic resonance imaging (fMRI), positron emission tomography (PET), single-photon emission computed tomography (SPECT), or Arterial Spin Labeling (ASL) are used to measure CBF changes in ASD children. CBF disruptions have been demonstrated in ASD patients when compared to healthy controls in different regions of the brain (Bjørklund et al., 2018). It has also been suggested that perfusion alterations are more pronounced in older children diagnosed with ASD. Cerebral hypoperfusion has been detected in nearly 75% of ASD children (Zilbovicius et al., 2000). As CBF impacts the delivery of oxygen and nutrients to neurons, hypoperfusion in ASD children has been associated with key ASD-related behaviors such as language deficits, impaired executive function and abnormal responses to sensory stimuli, as well as difficulty in facial perception (Siegel et al., 1992;

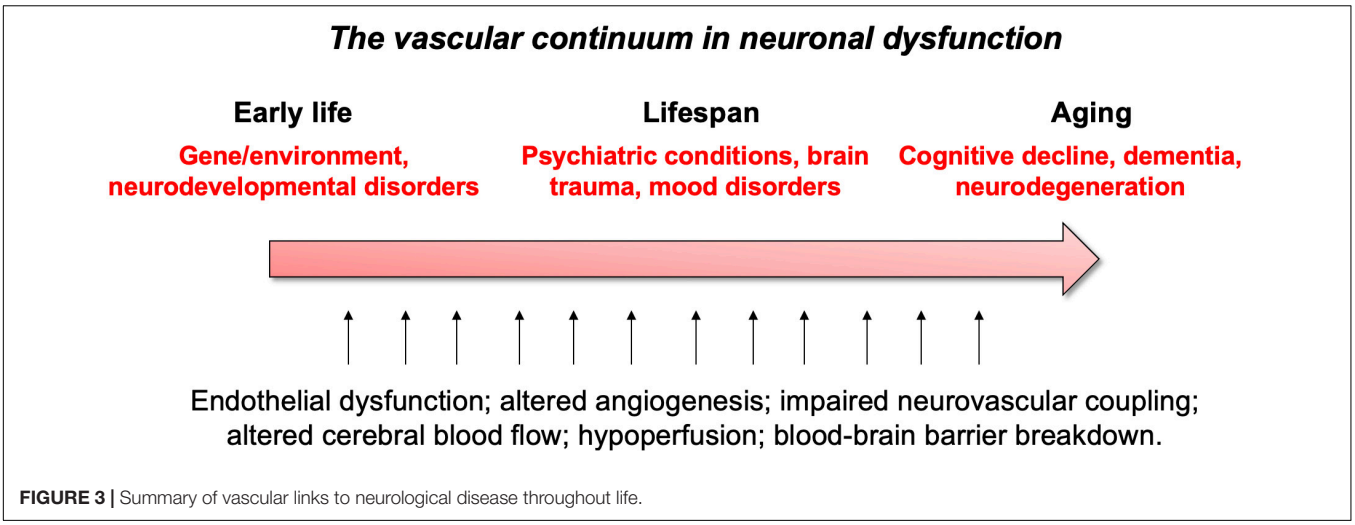

FIGURE 3 | Summary of vascular links to neurological disease throughout life.

Chiron et al., 1995; Ohnishi et al., 2000; Burroni et al., 2008; Reynell and Harris, 2013; Bjørklund et al., 2018; Yerys et al., 2018). These behaviors correlate with abnormal regional cerebral blood flow (rCBF) in the bilateral insula, superior temporal gyri and left prefrontal cortices, medial temporal lobe, supramarginal gyrus, right fusiform gyrus, and dorsal anterior cingulate cortex (Ohnishi et al., 2000; Zilbovicius et al., 2000; Burroni et al., 2008; Jann et al., 2015; Yerys et al., 2018). Studies are attempting to ameliorate these behavioral abnormalities using hyperbaric oxygen treatment (HBOT) to counteract cerebral hypoperfusion in children with ASD. There is some evidence that children who undertook 40 HBOT sessions of 60 min each showed improvements on selected psychosomatic parameters in the Autism Treatment Evaluation Checklist (ATEC) and Childhood Autism Rating Scale (CARS) (Kostiukow and Samborski, 2020). Currently, there is insufficient evidence to support the use of HBOT to treat children with ASD as there are many contradicting studies claiming no improvement in behaviors. Nevertheless, each study followed different protocols, consisted of patients with a large spectrum of behavioral impairments, and some lacked proper control groups, which could explain discrepancies. More research is required to determine if specific groups of children could benefit from HBOT treatment (Rossignol et al., 2012; Sakulchit et al., 2017).

ASL-based measurements of cerebral perfusion showed that children with ASD presented a pattern of widespread hyperperfusion in frontotemporal regions including medial orbitofrontal cortex, bilateral inferior frontal operculum, left inferior/middle temporal gyrus and the right precentral gyrus (Jann et al., 2015). The medial orbitofrontal cortex is known to have extensive connections with the limbic system involved in socio-emotional cognition. Furthermore, hyperperfusion was detected throughout the frontal white matter and subcortical gray matter in ASD children, which correlated positively with severity of social deficits (Peterson et al., 2019). As shown by these studies, CBF abnormalities appear linked to clinical manifestations. Although opposing observations of CBF in ASD patients were reported, these further support the complexity of these disorders (Jann et al., 2015).

Neurovascular coupling alterations were also observed in ASD patients. Hemodynamic responses in children with ASD during a color-word task were significantly lower than the control group, especially in the dorsolateral prefrontal cortex (Uratani et al., 2019). Conversely, children displayed no difference in hemoglobin concentrations in the prefrontal cortex during a letter fluency task, while adults showed reduced responses (Kawakubo et al., 2009). Despite inter-study variability, there seems to be a consensus on the impact of altered CBF on the expression of behavioral impairments (Zilbovicius et al., 2000; Jann et al., 2015). But as ASD are heterogeneous, with various behavioral traits, genetic causes, medical co-morbidities and medications, these variables may have impacted neuroimaging results, which led to inconsistencies. Importantly, these studies take an important step toward the identification of key players in ASD pathophysiology, opening new opportunities for early diagnosis and treatment.

The relationship between CBF alterations and symptom profiles in ASD children provides insight into disease mechanisms that can be tested in animal models. As most pre-clinical studies have also focused on the neuronal aspects of ASD, very few have considered vascular contributions to these disorders in laboratory models. Recent studies using different ASD mouse models have reported alteration in CBF. A study by Abookasis et al. (2018) using inbred Black and Tan Brachyury (BTBR) *T+tf/J* reported decreased CBF in mutant mice using laser speckle imaging and laser Doppler flowmetry (LDF). Subsequently, work by Ouellette et al. (2020) using the 16p11.2 deletion mouse model of ASD (*16p11.2*$^{df/+}$; Horev et al., 2011) demonstrated an increase in resting CBF as well as neurovascular uncoupling in adult (P50) *16p11.2*$^{df/+}$ mice compared to WT littermates using a combination of ultrasound imaging and LDF. No difference in CBF or NVC were observed between younger (P14) mutant and control mice (Ouellette et al., 2020). Results from this study in *16p11.2*$^{df/+}$ mice revealed the cause of these functional cerebrovascular impairments: an endothelial

deficit. While normal vascular smooth muscle cell function was measured, defective endothelium-dependent vasodilation was found *ex vivo* following exposure to specific vasomodulators (Ouellette et al., 2020). This suggests that endothelial health plays an important role in the etiology of the 16p11.2 deletion ASD syndrome. Understanding the molecular and cellular factors that mediate CBF alterations in ASD could help design rescue approaches in animal models, as well as therapeutic approaches down the line.

Since MRI studies rely on Blood Oxygen Level Dependent (BOLD) signals as surrogates for neuronal activity (Hillman, 2014; Howarth et al., 2021; Moon et al., 2021), it is possible that changes in rCBF reflect changes in underlying neuronal activity. For instance, cerebral cortex hypoperfusion in ASD patients could reflect lower metabolic demands (Schifter et al., 1994). In the case *16p11.2*$^{df/+}$ mice, however, it is interesting to note that a neurovascular uncoupling was measured, with enhanced neuronal activation yet reduced vascular responses to whisker stimulations, which led to the discovery of endothelium-dependent deficits (Ouellette et al., 2020).

Altered Blood-Brain Barrier and Angiogenesis in Autism Spectrum Disorders

Cerebral vessels are central for the maintenance of brain homeostasis, sustaining proper neuronal function, and providing an effective protection against toxins and pathogens (Profaci et al., 2020). The BBB consists of specialized ECs lining the vessel wall to separate the peripheral blood from cerebral tissue. Brain (central) ECs are distinct from peripheral ECs, as they produce specific proteins to control the flux (entry and exit) of metabolites across vessels, to maintain low rates of trans-endothelial vesicular transport, and to form tight junctions to limit the para-cellular flow of material between adjacent ECs (Andreone et al., 2015; Chow and Gu, 2015; Kealy et al., 2020). Alterations in the BBB are at the core of the onset and/or progression of numerous neurological disorders (Daneman and Prat, 2015; Van Dyken and Lacoste, 2018; Profaci et al., 2020). Only few studies have investigated the components of the BBB in the context of ASD. Children diagnosed with ASD have been associated with reduced levels of adhesion molecules such as soluble Platelet Endothelial Cell Adhesion Molecule-1 (PECAM-1, or CD31) and P-selectin. Since these molecules are essential to modulate BBB permeability through signaling and leukocyte infiltration, it suggests that crucial BBB components may be at play in ASD pathophysiology (Onore et al., 2012). Furthermore, a post-mortem study, with a small sample size, demonstrated altered BBB integrity in ASD with increased gene expression of matrix metalloproteinase (MMP)-9 (Fiorentino et al., 2016). Studies have shown that MMP-9 regulates cell proliferation, adhesion, degradation of laminin and collagen, angiogenesis, oxidative injury, and is implicated in BBB breakdown (Lepeta and Kaczmarek, 2015; Turner and Sharp, 2016). Additionally, important components of BBB integrity displayed altered expression in ASD patients, including claudin-5 (*CLDN5*) and claudin-12 (*CLDN12*), as well as tricellulin (*MARVD2*), a component of tight junctions involved in decreased permeability to macromolecules in brain ECs (Fiorentino et al., 2016). In an older study, a small subset of ASD participants demonstrated higher levels of autoantibodies against brain ECs in the serum compared to typically developing individuals, suggesting an impact on the BBB (Connolly et al., 1999). Animal models have facilitated the study of BBB integrity in ASD. In a valproic acid rat model of autism, increased BBB permeability to Evans blue was found in the cerebellum, a phenotype attenuated by treatment with memantine, an NMDA receptor modulator. This BBB alteration was also attenuated using minocycline (antibiotic) and agomelatine (melatonin receptor) treatment (Kumar et al., 2015; Kumar and Sharma, 2016). Animal studies have investigated transendothelial transport mechanisms in ASD mouse models. Tarlungeanu et al. (2016) demonstrated that the large neutral amino acid transporter (LAT1, *Slc7a5*) localized at the BBB to maintain normal levels of brain branched chain amino acid (BCAA) was required for neurotypical development. Mice harboring an endothelial-specific deletion of *Slc7a5* (*Slc7a5*$^{\Delta EC}$) displayed behaviors reminiscent of ASD, including motor dysfunctions consistent with a study in human patients harboring the constitutive mutation (Novarino et al., 2012; Tarlungeanu et al., 2016). Interestingly, administration of BCAA rescued ASD-like behaviors in *Slc7a5*$^{\Delta EC}$ mice (Tarlungeanu et al., 2016).

Recently, a post-mortem analysis of brain tissue from individuals diagnosed with ASD revealed significantly higher levels of markers associated with pericytes, as well as increased vascular tortuosity, indirectly suggesting impairments in angiogenesis, a process through which new blood vessels are formed (Azmitia et al., 2016). A more recent study in *16p11.2*$^{df/+}$ mice revealed impaired cerebral angiogenesis in young (P14) *16p11.2*$^{df/+}$ male mice compared to sex-/age-matched littermates, a phenotype which was absent in adult mice. Defective angiogenic activity was also measured using primary brain ECs from P14 *16p11.2*$^{df/+}$ males or ECs derived from human-induced pluripotent stem cells (hiPSCs) of 16p11.2 deletion carriers (Ouellette et al., 2020). Moreover, RNA-sequencing analysis of *16p11.2*$^{df/+}$ mouse brain EC transcriptome revealed changes in the expression of genes involved in angiogenesis (e.g., *Grem1*, *Apln*, *Angpt2*), while key genes involved in BBB regulation (e.g., *Pecam1*, *Mfsd2a*, *Cldn5*, *Slc2a1*) were not affected by the 16p11.2 deletion (Ouellette et al., 2020). Finally, this study generated a mouse model with endothelial-specific 16p11.2 haploinsufficiency which recapitulated ASD-related phenotypes, revealing a causal relationship between endothelial dysfunction and neuronal aspects of the 16p11.2 deletion syndrome (Ouellette et al., 2020).

Overall, these studies allude to the contribution (structural and functional) of a defective BBB and NVU in ASD, with an important role for endothelial impairments.

Vascular Links to Schizophrenia

Schizophrenia is a debilitating neurodevelopmental disorder affecting ∼1% of the population. It is associated with behavioral and cognitive symptoms that arise progressively. Memory and attention deficits appear in childhood, while positive symptoms (psychotic episodes) and negative symptoms (social and motivational deficits) emerge later in adolescence or early adulthood (Stachowiak et al., 2013). Although the incidence of

schizophrenia is higher in men, women have a slightly later disease onset (Gogtay et al., 2011; Ochoa et al., 2012). While the behavioral aspects of schizophrenia have been described, the causes of this disorder are poorly known. As in ASD, both genetic and environmental origins are involved. Schizophrenia has been associated with genes essential for a wide range of functions including neuronal connectivity and patterning of brain structures, cell proliferation and differentiation, as well as cytoskeleton reorganization (Stachowiak et al., 2013; Clifton et al., 2019). As in most neurological disorders, the implication of neuronal alterations has been extensively studied, but research on vascular impairments in schizophrenia is starting to emerge.

Altered Cerebral Blood Flow in Schizophrenia

Cognitive impairments are often present before the first psychotic episode in patients with schizophrenia (Keefe and Harvey, 2012; Schuepbach et al., 2016) and deficits in executive functions are often parallel to changes in CBF. Several studies have linked altered CBF with schizophrenia-related symptoms (Sabri et al., 1997; Malaspina et al., 1999, 2004; Pinkham et al., 2011; Fujiki et al., 2013; Schuepbach et al., 2016; Stegmayer et al., 2017; Zhu et al., 2017). Interestingly, the manifestations of negative or positive symptoms correlate with different rCBF changes. In a study by Pinkham et al. (2011), CBF of 30 schizophrenia patients was measured using ASL perfusion MRI, which revealed a positive correlation between increased severity of positive symptoms and higher CBF in the cingulate and superior frontal gyri, but decreased CBF in precentral and middle frontal gyri. Patients who presented with severe negative symptoms also displayed reduced CBF in the superior temporal gyrus bilaterally, cingulate and left middle frontal gyri (Malaspina et al., 2004; Scheef et al., 2010; Pinkham et al., 2011; Liu et al., 2012). Most studies investigating CBF alterations in schizophrenia considered perfusion rates from medicated patients, and a small number of studies have measured CBF rates in neuroleptic-naïve patients. Using ASL in non-medicated patients, the schizophrenia group displayed resting-state hypoperfusion in the frontal lobes, anterior and medial cingulate gyri, as well as in the parietal lobes, while increased perfusion was measured in the cerebellum, brainstem and thalamus (Scheef et al., 2010). Sabri et al. (1997) measured rCBF using SPECT in non-medicated patients that have experienced positive symptoms, revealing that rCBF values varied depending on the severity of positive symptoms. Hyperperfusion was detected in the frontal, anterior cingulate as well as in both parietal and temporal cortices in patients who had scored high in severity for formal thought disorder (disturbance of the organization and expression of thought). In contrast, patients who scored high for delusions, hallucinations or distrust, with low scores for formal thought, displayed hypoperfusion in the same brain regions. No difference in rCBF was identified between control and schizophrenia groups after treatment (Andreasen et al., 1997; Sabri et al., 1997; Horn et al., 2009). Recent studies have detected hyperperfusion and hypoperfusion in brain regions from individuals with hallucinations. For instance, CBF increase was found in the right superior temporal gyrus and caudate nucleus, while CBF decrease was found bilaterally in the occipital and left parietal cortices (Zhuo et al., 2017). In another study, patients were classified based on the severity of three behavioral dimensions (language, affectivity, and motor) according to the Bern Psychopathology scale. Patients with altered affectivity were associated with increased CBF in the amygdala, while changes in language dimension were linked to increased CBF in Heschl's gyrus (Stegmayer et al., 2017). While schizophrenia is classified as a neurodevelopmental disorder, its symptoms persist with age. Studies have identified significant bilateral temporal hypoperfusion related to aging and disease course. It has been suggested that this decrease in CBF with aging is paralleled with the degenerative changes observed in patients with schizophrenia (Schultz et al., 2002; Kawakami et al., 2014).

The polygenic risk of schizophrenia is an important dimension of this syndrome, and changes in CBF have been identified in patients diagnosed for either familial or sporadic schizophrenia. Sporadic schizophrenia patients were associated with hypofrontality (left frontal gyrus, orbitofrontal cortex, anterior cingulate, and paracingulate cortices), while familial schizophrenia patients had left temporoparietal hypoperfusion (posterior Sylvian fissure at the superior and inferior parietal lobules, angular, and supramarginal gyri). In both groups, positive symptoms are often associated with increased rCBF in the parahippocampal gyrus, cerebellum, and pons (Malaspina et al., 2004). Sporadic patients showed additional hyperperfusion in the fusiform gyrus, and familial patients the hippocampus, dentate, amygdala, thalamus, and putamen (Malaspina et al., 2004). In addition, the prefrontal cortex in schizophrenia has been associated with deficits of pericapillary oligodendrocytes, which could contribute to changes in CBF (Vostrikov et al., 2008; Uranova et al., 2010). Altogether, these studies support the idea that altered CBF is involved in schizophrenia pathophysiology.

In addition to studies investigating resting state CBF, there is evidence of altered NVC in schizophrenia whereby many reports demonstrate reduced hemodynamic response, reflecting reduced neuronal activity during processing of cognitive tasks, especially in the lateral prefrontal cortex and temporal regions (Ford et al., 1999, 2005; Mathalon et al., 2000; Carter et al., 2001; Hanlon et al., 2016; Pu et al., 2016). As with CBF reports, there are inconsistent hemodynamic responses associated with schizophrenia since increased hemodynamic responses in hippocampus, thalamus and prefrontal cortex have been identified (Tregellas et al., 2007). These conflicting results are translating to rodent models of schizophrenia whereby some models have revealed overall hypofrontality, hypoperfusion in the hippocampus or hyperperfusion in the somatosensory cortex (Finnerty et al., 2013; Song et al., 2013; Drazanova et al., 2019).

Altogether, these studies support the idea that altered CBF regulation is involved in schizophrenia pathophysiology. Moreover, it appears critical to consider the polygenic risk of disease, the category and severity of symptoms, as well as the age of patients when comparing CBF rates in schizophrenia. Although many studies have detected altered CBF using various methods, results thus far remain conflicting based on various stages of disease and pharmacological treatment (Drazanova et al., 2019).

Altered Blood-Brain Barrier and Angiogenesis in Schizophrenia

A dysfunctional BBB has been reported in schizophrenia, with increased permeability to damaging proteins (Müller and Ackenheil, 1995; Shcherbakova et al., 1999; Crockett et al., 2021). Studies are starting to decipher changes in cells associated with the BBB (for a detailed review, see Carrier et al., 2020). Briefly, evidence of schizophrenia-associated microvascular abnormalities in the neocortex include thickening and deformation of basal lamina, vacuolation of cytoplasm in ECs, basal lamina and astrocytic end-feet, swelling of astrocyte end-feet, activation of microglial cells in the prefrontal and visual cortex, as well as atypical vascular arborization (Uranova et al., 2010; Carrier et al., 2020).

Moreover, specific mutations are associated with schizophrenia, including alterations in the 22q11.2 deletion syndrome (22qDS) -strongest monogenic risk allele for this disorder, and polymorphisms in claudin-5, a densely expressed tight junction molecule (Gur et al., 2017; Greene et al., 2018; Carrier et al., 2020) altogether revealing barrier dysfunction in schizophrenia patients (Greene et al., 2018; Crockett et al., 2021). Post-mortem brain sections from 22qDS patients and animal models of 22qDS both demonstrate reduced claudin-5 expression in the BBB, which in turn compromised BBB function (Nishiura et al., 2017; Guo et al., 2020; Crockett et al., 2021; Usta et al., 2021). Additionally, altered levels of vascular endothelial (VE)-cadherin and occludin in ECs were identified in schizophrenia. These molecules regulate adherence of ECs and restrict movement of substances across the BBB (Cai et al., 2020). Furthermore, BBB hyperpermeability has been associated with another risk allele for schizophrenia. *NDST3*, expressed in the brain, encodes an enzyme involved in the metabolism of heparan sulfate, a component of basal lamina extracellular matrix that is required for BBB integrity (Khandaker et al., 2015).

Studies have documented primary vascular endothelial dysfunction in schizophrenia. Individuals carrying *MTHER T* and/or *COMT Val* risk allele have been associated with cerebrovascular endotheliopathy, as well as lower frontal executive functions (Grove et al., 2015). While endothelial dysfunction is possibly associated with schizophrenia, many studies are using peripheral endotheliopathy as a surrogate marker for endothelial dysfunction. For example, studies are using non-invasive peripheral arterial tonometry (RH-PAT) to assess peripheral arteriole endothelial-dependent vasodilation and revealed impaired peripheral arterial vasodilation in schizophrenia (Ellingrod et al., 2011; Burghardt et al., 2014). Notably, brain ECs have unique properties to maintain BBB integrity and brain homeostasis. Although altered endothelial function was found in the periphery, it does not represent a definite marker of brain (central) endothelial dysfunction. A critical regulator of angiogenesis, *vascular endothelial growth factor* (VEGF), and its receptor (VEGFR2) have been found upregulated in the prefrontal cortex of individuals diagnosed with schizophrenia (Hino et al., 2016). Findings of elevated VEGF could also be linked to vascular hyperpermeability, as VEGF not only regulates angiogenesis but increases BBB leakage (Mayhan, 1999; Zhang et al., 2000). Conversely, a different group revealed that a decreased production of VEGF predisposed individuals to develop this disorder and contributed to the severity of symptoms (Saoud et al., 2021). Another study investigated the impact of hiPSC-derived neural stem cells from schizophrenia patients on angiogenesis (Casas et al., 2018). This study found an imbalance in the expression and secretion of several angiogenic factors and non-canonical neuro-angiogenic guidance cues from neural stem cells from schizophrenic patients. Conditioned media from these cells induced impaired angiogenesis as evidenced by reduced number of sprouts and tubes formed in *in vivo* and *in vitro* models, as well as decreased neural stem cell migration compared to control conditioned media (Casas et al., 2018).

CEREBROVASCULAR DEFICITS ASSOCIATED WITH NEURODEGENERATIVE DISORDERS

CNS disorders are dichotomized as early onset neurodevelopmental disorders and late-onset neurodegenerative diseases (Taoufik et al., 2018). Neurodegenerative diseases consist of a group of heterogeneous disorders characterized by the progressive degeneration of structure and function in the CNS (Gitler et al., 2017). Although neurodegenerative and neurodevelopmental disorders are differentially classified, an accumulating body of work demonstrates significant similarities between these two groups of conditions. Here below, we cover cerebrovascular impairments reported in four neurodegenerative diseases that emerge throughout lifespan: multiple sclerosis (MS), Huntington's disease (HD), Parkinson's disease (PD), and Alzheimer's disease (AD).

Vascular Links to Multiple Sclerosis

MS is a chronic autoimmune disease of the CNS, occurring when the immune system attacks its own nerve fibers and myelin sheaths (D'Haeseleer et al., 2013). The pathological hallmark of MS consists of perivenular inflammatory lesions, leading to demyelinating plaques and diffuse axonal degeneration throughout the CNS (Dobson and Giovannoni, 2019). It is characterized by the infiltration of T cells reactive against myelin in the CNS (Schwartz and Kipnis, 2005). This demyelinating disease has key features including inflammation, BBB disruption and neurodegeneration. MS has a prevalence of 0.5–1.5 per 100,000 individuals, whereby women are three times more affected than men (Harbo et al., 2013). The age of MS onset is situated between 20 and 40 years of age (Ortiz et al., 2014). General symptoms related to MS include, but are not limited to, tremors, lack of coordination as well as weakness in limbs. There are various types of MS including relapsing-remitting MS (RR-MS), secondary progressive MS (SP-MS) and primary progressive MS (PP-MS). RR-MS consists of unpredictable relapses or inflammatory flare-ups during which new symptoms appear or existing ones worsen (Adhya et al., 2006). Most people with RR-MS, transition to a disease phase known as SP-MS. In this phase, there is progressive worsening and fewer relapses. Active lesions with profound lymphocytic inflammation are mostly found in RR-MS (Dobson and Giovannoni, 2019). PP-MS is

considered as a slow accumulation of disability without defined relapses. In this case, PP-MS is associated with an inactive lesion core surrounded by activated microglia and macrophages (Dobson and Giovannoni, 2019).

Altered Cerebral Blood Flow in Multiple Sclerosis

MS has been associated with functional cerebrovascular abnormalities including decreased cerebral perfusion and reduced CNS venous blood drainage, known as chronic cerebrospinal venous insufficiency (D'Haeseleer et al., 2011). SPECT, PET, and ASL imaging studies have reported decreased CBF in both gray and white matter of MS patients (Ge et al., 2005; D'Haeseleer et al., 2011). Widespread cerebral hypoperfusion has been revealed in SP-MS, RR-MS and PP-MS patients, while an ischemic threshold was not reached (Adhya et al., 2006; Ota et al., 2013; Monti et al., 2018). Gray matter hypoperfusion in MS suggests a reduction of metabolism due to the loss of cortical neurons (Peruzzo et al., 2013). Furthermore, studies have reported that CBF is globally impaired in normal appearing white matter (NAWM) of patients with early RR-MS (Law et al., 2004; Adhya et al., 2006). Of note, CBF was generally lower in PP-MS than in RR-MS in the periventricular and frontal white matter (Adhya et al., 2006). In the contrary, other studies have measured elevation of CBF and cerebral blood volume (CBV) in NAWM of patients with early RR-MS several weeks before signs of increased BBB permeability (Wuerfel et al., 2004). Although studies on different types of MS revealed changes in CBF, general active demyelinating lesion regions are associated with hyperperfusion while the more stable forms show hypoperfusion (Monti et al., 2018). Decreased CBF in cerebral NAWM, thalamus, and putamen was identified in patients whose symptoms emerged within the first 5 years of onset. This suggests that CBF alterations are present in the very early stages of the disease (Varga et al., 2009). Different mechanisms have been proposed to explain hypoperfusion in MS. A study suggested that decreased CBF is secondary to axonal degeneration, which leads to a decreased metabolic demand (Saindane et al., 2007). However, this hypothesis is yet to receive experimental support. A second mechanism that has been proposed is an impaired energy metabolism of astrocytes (De Keyser et al., 1999). In MS, astrocytes are deficient in β2-adrenergic receptors which regulate high energy-consuming activities, such as glycogenolysis and phosphocreatine metabolism (De Keyser et al., 1999). Reduced energy production in astrocytes could be contributing to altered CBF. A third mechanism suggested was increased release of vasoconstrictor endothelin-1 (ET-1) from reactive astrocytes, found in a post-mortem study on white matter samples of RR-MS patients (D'Haeseleer et al., 2013; Hostenbach et al., 2019). Hence, elevated levels of ET-1 could be involved in dysregulating CBF in MS. Interestingly, administration of ET-1 antagonist Bosentan restored CBF to control levels in MS patients (D'Haeseleer et al., 2013).

Impaired cerebral vascular reactivity was evidenced in MS patients exposed to hypercapnia, which has been suggested to contribute to neuronal death identified in this disorder (Marshall et al., 2014). This global deficit is thought to be associated with elevated levels of NO reported in MS (Trapp and Stys, 2009; Juurlink, 2013). These studies suggest that the overproduction of NO may desensitize endothelial and smooth muscle cell function, causing decreased vasodilatory capacity and limited blood supply for neurons that perform demanding tasks. Increased NO in MS may lead to neuronal activity-induced hypoxia leading to neurodegeneration (Marshall et al., 2014). Interestingly, high inflammatory MS lesion load has been associated with increased CBF. Therefore, perfusion changes may be sensitive to active inflammation (Bester et al., 2015). However, it remains unclear whether abnormal perfusion in MS is a precursor of lesions or occurs independently of lesion development (Marshall et al., 2014).

Notably, MS has been associated with cerebral SVD. It was demonstrated that younger MS cases are more severely impacted by cerebral SVD compared to older individuals (Geraldes et al., 2020). This suggests that the interaction between MS and cerebral SVD is affected by age, an assumption still under investigation (Geraldes et al., 2020).

Altered Blood-Brain Barrier and Angiogenesis in Multiple Sclerosis

BBB dysfunction is considered a major hallmark of MS and is deemed a trigger of disease onset (McQuaid et al., 2009; Cramer et al., 2014). Intense focal disruption of the BBB associated with inflammation (identified by gadolinium-enhanced MRI at acute and chronic MS lesion sites; Saade et al., 2018) and diffuse extensive BBB disruption with a long-term pathological activity, are both found in MS patients (Bennett et al., 2010). Hyperpermeability of the BBB was evidenced by leukocyte passage across the BBB (Cramer et al., 2014). Increased BBB leakage was associated with decreased expression of tight junction proteins in brain capillary ECs in patients with active lesions, inactive lesions, as well as NAWM associated with fibrinogen leakage (Kirk et al., 2003; McQuaid et al., 2009; Bennett et al., 2010). More specifically, dysregulation of tight junction adaptor protein ZO-1, occludin and claudin-5 have been reported in both primary progressive and secondary progressive disease states (Kirk et al., 2003; Leech et al., 2007). Experimental autoimmune encephalomyelitis (EAE) in rodents is a disease model with clinical and pathological characteristics relevant to the study of MS. This model revealed reorganization of ZO-1 and actin in the presence of inflammatory factors *in vitro*, associated with increased permeability of an endothelial monolayer (Bennett et al., 2010). The EAE model also revealed increased expression of VEGF in ECs, astrocytes, monocytes and activated TH1 lymphocytes, all of which contribute to BBB permeability during the early phase of disease, while decreased expression VEGF was evident in the late phase (Girolamo et al., 2014). The increase in VEGF expression was also found in the brain of MS patients (Girolamo et al., 2014). Furthermore, junctional adhesion molecule-A, a component of tight junctions, was found abnormally distributed in active and inactive MS lesions, although adherent junction proteins were normally expressed and localized in MS tissue (Padden et al., 2007). In addition, levels of PECAM-1 were found increased in active gadolinium-enhancing MS lesions (Ortiz et al., 2014). While BBB leakage is evident in MS, the complex network of cellular

and molecular players that lead to this dysfunction have yet to be fully understood. Targeting BBB defects in MS represent a therapeutic opportunity, for instance with MMP inhibitors, interferons, and corticosteroids (Minn et al., 2002; Ross et al., 2004; Pardridge, 2012; Ortiz et al., 2014). However, no current therapy addresses BBB deficits (Ortiz et al., 2014). For more details on BBB dysfunction in MS, the following reviews can be consulted (Girolamo et al., 2014; Kamphuis et al., 2015; Xiao et al., 2020).

ECs proliferation as well as an increase in vascular network density has been reported (Ludwin, 2006; Holley et al., 2010). Increased angiogenesis was suggested to contribute to disease progression as well as remission after relapses (Papadaki et al., 2014). In addition to increased VEGF levels, VEGFR2 is also expressed on ECs in active MS lesions (Seabrook et al., 2010). Other molecules, such as basic fibroblast growth factor, were increased in MS patients and involved in angiogenesis (Su et al., 2006). MS patients with activated lesions and NAWM show blood vessels with a glomeruloid morphology, hemorrhages and vessel wall hyalinization (Girolamo et al., 2014). Immunosuppressive therapies have been used in aggressive MS as they not only impact neuroinflammation but also have an anti-angiogenic effect. Further research is warranted to elucidate the vascular links to MS and identify new therapeutic targets, as disease modifying drugs have unfortunately little to no impact on MS progression (Girolamo et al., 2014).

Vascular Links to Huntington's Disease

HD is an hereditary, autosomal dominant and neurodegenerative disorder (Davenport, 1915; Wasmuth et al., 1988; Bano et al., 2011) leading to altered muscle coordination and declined mental abilities (Paulsen, 2011; Ha and Fung, 2012). An expansion of trinucleotide CAG repeats on chromosome 4 within the Huntingtin gene (*HTT)* results in the production of an altered Huntingtin (Htt) protein which accumulates in specific brain regions. Aggregation of mutant Htt (mHtt) leads to increased neurotoxicity (Zheng and Diamond, 2012), particularly in subcortical brain structures such as the neostriatum (caudate and putamen) where GABAergic medium-spiny neurons are particularly vulnerable (Sieradzan and Mann, 2001; Walker, 2007; Ross and Tabrizi, 2011; Drouin-Ouellet et al., 2015; McColgan and Tabrizi, 2018). At the cellular level, mHtt results in neuronal dysfunction and death through disrupted mechanisms involved in proteostasis, transcription and mitochondrial function as well as toxicity from the mutant protein (McColgan and Tabrizi, 2018). Worldwide, 2.71 per 100,000 individuals suffer from HD (Rawlins et al., 2016; Kounidas et al., 2021). Both men and women are affected equally, and heterogeneous symptoms emerge at around 40 years of age. However, functional and structural brain alterations emerge a decade before symptoms manifest (Snowden, 2017). Carriers of CAG repeat expansions in *HTT* can be identified decades before clinical manifestation, allowing researchers to identify possible biomarkers in the premanifest stage of HD (preHD). With this comes the increasing interest to study cerebrovascular abnormalities in HD (Snowden, 2017).

Altered Cerebral Blood Flow in Huntington's Disease

HD-related perfusion deficits have been mostly associated with cerebral hypoperfusion (Reid et al., 1988; Sotrel et al., 1991; Hasselbalch et al., 1992; Harris et al., 1999; Deckel and Duffy, 2000; Wild and Fox, 2009). There is evidence of reduced CBF in the basal ganglia in early HD, prior to gross structural changes and to motor symptoms. In these cases, severity of cortical hypoperfusion correlated with decreased functional capabilities (Sax et al., 1996; Harris et al., 1999). In preHD patients, classified as either near or far from motor symptom onset, displayed altered rCBF by MR-based perfusion imaging. Participants with preHDfar and preHDnear had lower rCBF in the medial prefrontal cortex and increased rCBF in the left precuneus. Of note, structure and function of the precuneus and hippocampus can be abnormal in very early HD (Feigin et al., 2006). PreHDnear participants had additional regions showing altered rCBF, including hypoperfusion in the medial and lateral prefrontal cortex and hyperperfusion in the right hippocampus (Wolf et al., 2011).

While resting CBF is affected, early manifest and premanifest HD patients also display altered neurovascular coupling during visual stimulation (Klinkmueller et al., 2021). After HD onset, a significant hypoperfusion in the HD group was identified in most of the cerebral cortex. During problem-solving activities, such as solving a maze or resting their eyes open while looking at a modified maze, patients with HD showed increased CBF in the caudate nucleus (Deckel and Duffy, 2000; Deckel et al., 2000). Following physical activity, HD patients were associated with CBF hyperperfusion compared to the control group (Steventon et al., 2020).

Animal models of HD (e.g., gene knock-in of a human exon 1 CAG_{140} expansion repeat) also revealed altered rCBF. In mice as in humans, different brain regions displayed either hypoperfusion (basal ganglia motor circuit, hippocampus and prefrontal area) or hyperperfusion (cerebellar-thalamic and somatosensory regions). This altered CBF was apparent at a presymptomatic stage (Wang et al., 2016).

While CBF is starting to emerge as a biomarker for HD, mounting evidence supports the utilization of CBV as an additional metric. Several studies have reported elevated CBV in preHD patients (Hua et al., 2014; Liu et al., 2020). In addition, there is evidence of increased CBV in cortical gray matter after HD onset (Drouin-Ouellet et al., 2015), suggesting that arteriolar CBV may be a sensitive biomarker for premanifest HD (Hua et al., 2014; Liu et al., 2020). From these studies it was suggest that imaging of CBF may be used to detect widespread functional abnormalities in HD, and possibly predict HD symptoms onset during premanifest stages.

Altered Blood-Brain Barrier and Angiogenesis in Huntington's Disease

Increases in vessel density, BBB permeability and VEGF-A release were observed in HD patients and animal models of HD (Steventon et al., 2020). There is evidence that BBB leakage increases alongside disease progression (Drouin-Ouellet et al., 2015). Despite these observations, there seems to be discrepancies between mouse models of HD. For instance, the BACHD

transgenic mice, a well-known model of HD expressing the full-length mutant human *HTT*, failed to develop BBB breakdown at 12 months of age despite robust motor deficits (Lin et al., 2013; Mantovani et al., 2016). BBB dysfunction in HD patients has been associated with decreased tight junction molecules such as occludin and claudin-5 (Drouin-Ouellet et al., 2015). Moreover, other markers associated with BBB permeability, including hepatocyte growth factor, interleukin-8 and tissue inhibitor of MMP-1, were found elevated in HD patients (Drouin-Ouellet et al., 2015). A transgenic mouse model of HD (R6/2 mice) confirmed elevated tight junction molecules similar to HD patients. The R6/2 mouse model of HD is the most commonly studied and harbors a mutant *Htt* with CAG repeat expansion in exon 1 (Li et al., 2005). R6/2 mice also displayed increased transcytosis and paracellular transport across the brain endothelium compared to control mice (Drouin-Ouellet et al., 2015). In R6/2 mice, tight junction imbalance and perturbed BBB homeostasis were perceptible at very early stage of the disease, in absence of symptoms (Di Pardo et al., 2017). At the structural level, mHtt aggregates were found in the basal membrane of cerebral blood vessels in HD patients (Drouin-Ouellet et al., 2015). Interestingly, mHtt aggregates were localized in ECs, smooth muscle cells and perivascular macrophages, consistent with observations in R6/2 mice.

Further research is needed to determine BBB impairments in preHD patients. Lim et al. (2017) reported that iPSCs-derived brain microvascular endothelial cells (BMECs) from HD patients exhibit increased angiogenesis and altered barrier properties associated with elevated transcytosis and paracellular permeability. An increased and unregulated angiogenic activity may lead blood vessels to become more permeable with a potential role in neurovascular dysfunction in HD. RNA-seq analysis revealed a significant number of affected gene that regulate both clathrin- and caveolin- mediated endocytosis, which could lead to changes in endo- and transcytosis across the brain endothelium. These genes include *FABP4*, *DYNAMIN*, and *FILAMIN* that play a role in vesicle formation and scission. In addition, higher levels of transcytosis-related genes such as *CAV1* was detected in HD iPSCs-derived BMECs that also displayed impaired Wnt/β-catenin signaling (Lim et al., 2017). The Wnt/β-catenin pathway is essential for regulation of cell proliferation, cell determination and tissue homeostasis (Silva-Garcia et al., 2019). Furthermore, astrocytes from both HD patients and mouse models were associated with higher levels of VEGF-A, which may trigger proliferation of ECs and contributes to neurovascular changes in HD (Hsiao et al., 2015). Of note, sustained delivery of VEGF into the rat striatum via injectable hydrogels was neuroprotective in a lesioned model of HD; VEGF implants significantly protected against the quinolinic acid-induced loss of striatal neurons (Emerich et al., 2010). Moreover, neuroprotection induced by inhibition of hypoxia inducible factor (HIF) prolyl-4-hydroxylases in HD mice has been correlated with enhanced VEGF expression (Niatsetskaya et al., 2010). In post-mortem tissue, cerebral blood vessel density was greater in HD patients while no differences in diameter of small- or medium sized blood vessels have been observed (Drouin-Ouellet et al., 2015). Post-mortem tissue of HD patients revealed a higher proportion of small compared to medium-sized blood vessels in the putamen, an effect occurring in parallel with putamen degeneration. Notably, altered density of small blood vessels in HD patients was consistent with the R6/2 mouse model when brain vascular anomalies were restricted to smaller vessels (Drouin-Ouellet et al., 2015; St-Amour et al., 2015).

Vascular Links to Parkinson's Disease

PD is the second most common neurodegenerative disorder after AD (Antony et al., 2013). It is characterized by the progressive degeneration of the nigrostriatal system, resulting in rigidity, bradykinesia, postural instability, and resting tremor (Antony et al., 2013; Pagano et al., 2016). The most affected cells are dopaminergic neurons from the substantia nigra pars compacta (SNc). The pathological hallmark of PD is the formation of Lewy bodies containing aggregated α-synuclein (Hijaz and Volpicelli-Daley, 2020). While increasing age is a risk factor for PD, the average age of onset is after 60 years old (Hindle, 2010; Parkinson Canada, 2010). The etiology of PD is multifactorial where genetics (familial PD) and environmental (sporadic PD) factors take part in disease onset (Klein and Westenberger, 2012). Familial PD accounts for 10–15% of all PD cases whereas the remainder is classified as sporadic PD (Verstraeten et al., 2015). Genetically linked PD is inherited in an autosomal dominant or recessive fashion (Ball et al., 2019). Research has identified seven causal genes for familial PD including phosphatase and tensing homolog-induced Kinase-1 (PINK1), Parkinson protein 7 (PARK7), parkin RBR E3 ubiquitin protein ligase (PARK2), vacuolar protein sorting-associated protein 35 (VPS35), alpha-synuclein (SNCA), glucocerebrosidase (GBA) and leucine-rich repeat Kinase 2 (LRRK2) (Verstraeten et al., 2015; Kalinderi et al., 2016; Ball et al., 2019). Conversely, sporadic PD may develop from gene-environment interactions (Benmoyal-Segal and Soreq, 2006). Environmental factors associated with PD includes but are not limited to pesticides, heavy metals, and illicit drugs (Kwakye et al., 2017). Notably, individuals may respond differently to environmental factors which results in diverse symptomology of PD, thus adding to the complexity of the disease (Ball et al., 2019).

Altered Cerebral Blood Flow in Parkinson's Disease

Using non-invasive MRI in an heterogeneous PD patient population, studies revealed decreased CBF in the frontal, parietal and occipital areas, more specifically the posterior parieto-occipital cortex, cuneus, middle frontal gyri, putamen, anterior cingulate and post- and pre-central gyri (Kamagata et al., 2011; Melzer et al., 2011; Fernandez-Seara et al., 2012; Madhyastha et al., 2015). A study by Fernandez-Seara et al. (2012) reported a 20–40% decrease in CBF in PD patients compared to a control group. Studies are trying to determine if CBF changes are related to the presence of dementia in PD, or if it can be considered as a biomarker. Derejko et al. (2006) used SPECT in PD patients with dementia and demonstrated left temporo-parietal hypoperfusion compared to the group without dementia. This suggested that CBF differences between PD patients with or without dementia could represent a clinical biomarker for discriminating PD patients (Derejko et al., 2006). Another study revealed hypoperfusion in PD patients without dementia in posterior

cortical regions (posterior cingulate/precuneus) compared to healthy individuals (Syrimi et al., 2017). Hypoperfusion was positively correlated with global cognitive performance and the level of motor impairment (Madhyastha et al., 2015; Syrimi et al., 2017). Melzer et al. (2011) and Fernandez-Seara et al. (2012) reported CBF reduction with parietal cortex thinning in mild PD patients without dementia and proposed that CBF alterations occur in the early stages of PD.

Although studies have identified hypoperfusion in PD patients, the mechanisms underlying these changes are unknown (Biju et al., 2020). One study used a mouse model of PD (α-synuclein transgenic mice), which overexpress human WT α-synuclein. α-synuclein pathology develops before clinical symptoms and is present in both sporadic and familial forms. Using ASL-MRI analysis in this PD mouse model, authors reported a 36.6% reduction in cortical CBF in mutant mice accompanied by motor coordination impairments and olfactory bulb atrophy/dysfunction (Biju et al., 2020).

Altered Blood-Brain Barrier and Angiogenesis in Parkinson's Disease

The association of PD with altered vascular function has led studies to investigate possible players contributing to BBB (Al-Bachari et al., 2020). In animal studies, BBB disruption in the SNc has been reported (Barcia et al., 2005; Rite et al., 2007; Chao et al., 2009). While human studies investigating BBB in PD patients are sparse, there is evidence of BBB dysfunction with increased permeability in the post commissural putamen of PD patients (Kortekaas et al., 2005; Gray and Woulfe, 2015). Wardlaw et al. (2008) and Al-Bachari et al. (2020) revealed increased leakage of the BBB in PD using ASL and dynamic contrast enhanced -MRI (DCE-MRI). Authors compared PD patients with two other control groups: one with and one without known cerebrovascular disease. This comparison could determine if BBB changes are attributable to co-existing cerebrovascular disease in an aging population, or if a pattern of BBB alteration is specific to PD. Authors reported increased BBB leakage in the group with cerebrovascular disease compared to the group without cerebrovascular disease in regions previously associated with PD, including the substantia nigra, white matter, and posterior cortical regions (Al-Bachari et al., 2020).

Accumulation of α-synuclein in ECs may also contribute to BBB dysfunction and increased permeability (Elabi et al., 2021). Higher number of EC nuclei was found in the SNc of PD patients (Faucheux et al., 1999). Other EC dysfunctions were reported, such as down regulation of tight junction proteins (Kuan et al., 2016). In the 1-methyl-4-phenyl-1,2,3,6-tetrahydropyridine (MPTP) mouse model of PD, down-regulation of tight junction protein ZO-1 and BBB leakage were measured in the substantia nigra (Patel et al., 2011). There is also evidence of string vessel formation in brain capillaries from human PD. String vessels are described as collapsed basement membrane without endothelium and no circulatory function. An altered basement membrane was also observed in PD mice (Yang et al., 2015). VEGF, a prominent growth factor promoting angiogenesis and BBB permeability, was upregulated in the substantia nigra, but not the striatum, of PD patients, while animal models of PD displayed parkinsonian traits following administration of exogenous VEGF into the substantia nigra (Barcia et al., 2005; Wada et al., 2006; Rite et al., 2007).

Guan et al. (2013) reported vascular degeneration in human PD, with formation of endothelial clusters, capillary network damage, and loss of capillary connections in the substantia nigra and brain stem nuclei. Authors found a larger vessel size in PD patients, while capillaries were shorter in average length, less in number and had fewer branches. These observations were also confirmed in an MPTP mouse model of PD (Guan et al., 2013; Sarkar et al., 2014). Furthermore, ultrastructural abnormalities were identified in cerebro-cortical microvessels of PD patients, including basement membrane thickening, vacuolization and pericyte degradation (Farkas et al., 2000). Structural alterations of the basement membrane can lead to pathophysiological consequences including compromised nutrient transport and cognitive disturbances (Farkas et al., 2000). Recently, a PD mouse model of α-synuclein overexpression was associated with altered vascular density at different stages of the disease (Elabi et al., 2021). The study reported that 8 month-old animals had increased vessel density compared to control mice, while 13 month-old PD mice displayed decreased vessel density, suggesting compensatory angiogenesis in the younger group (Elabi et al., 2021). Increased angiogenesis is considered an adaptative response to pathological conditions and is regulated by basement membrane proteins and their integrin receptors. These studies postulate that immature nascent vessels in PD could contribute to increased BBB permeability, as reviewed recently (Bogale et al., 2021).

Vascular Links to Alzheimer's Disease

AD accounts for 60–80% of all diagnoses of dementia (Alzheimer's Association, 2021). This progressive and debilitating neurodegenerative disease manifests with memory, attention, executive, visuospatial and perceptual impairments. AD is not only characterized by amyloid deposition, neuroinflammation, neurodegeneration and cognitive deficits, but also by cerebrovascular pathology. Indeed, an inadequate brain perfusion has been identified as an early event in the development and progression of AD (Nicolakakis and Hamel, 2011). The risk of developing AD is increased by age-associated vascular diseases such as hypercholesterolemia, hypertension, ischemic stroke, and diabetes (Kalaria, 1996; Roher et al., 2003; Casserly and Topol, 2004; Gorelick, 2004; Luchsinger et al., 2005). The AD brain is characterized by increased levels of soluble and insoluble amyloid-beta peptide (Aβ), derived from the amyloid protein precursor (APP), neurofibrillary tangles of hyperphosphorylated *tau* protein, neurodegeneration and neuroinflammation, and also linked with a cerebrovascular pathology (Selkoe, 2002; Iadecola, 2004; Querfurth and LaFerla, 2010). The latter is identified post-mortem by Aβ deposition in brain vessels (cerebral amyloid angiopathy, CAA), Aβ-induced oxidative stress, and alterations of the vessel wall that included fibrosis and degeneration of ECs (Buee et al., 1994; Vinters et al., 1994; Zarow et al., 1997; Farkas and Luiten, 2001; Humpel and Marksteiner, 2005). Various mouse models of AD have been developed, most mimicking

the overproduction of Aβ through transgene expression of mutated human APP (hAPP) combined or not with the amyloidogenic presenilin (PS1) or the pathologic *tau* (Mucke et al., 2000; Oddo et al., 2003; Gotz and Ittner, 2008). These models recapitulate AD's cerebrovascular pathology in addition to the cognitive deficits, senile plaques, Aβ-induced oxidative stress, neuroinflammation, cholinergic denervation, synaptic failure, and cerebral hypometabolism (Hsia et al., 1999; Palop et al., 2003; Aucoin et al., 2005; Tong et al., 2005; Nicolakakis et al., 2008; Iturria-Medina et al., 2016; Love and Miners, 2016; Liu et al., 2018; Czako et al., 2020). It is in fact estimated that up to 45% of all dementias worldwide are partly, or wholly, due to age-related SVD of the brain (Montagne et al., 2016; Clancy et al., 2021). This suggests that AD and vascular dementia share common grounds, which complicates their stratification. As such, it is of utmost importance to improve our understanding of vascular underpinnings of AD (Willis and Hakim, 2013). Clinical studies that attempted to reduce plaque load by blocking Aβ production, removing Aβ with antibodies, or preventing tau phosphorylation, have all failed to alleviate AD symptoms (Korte et al., 2020). However, mounting evidence demonstrates that the brain vasculature is the missing link (Sweeney et al., 2019). Early cerebrovascular dysfunction in AD leads to decreased Aβ clearance, vascular oxidative stress, inflammatory damage and impaired BBB function (Zlokovic, 2005). Here below we will succinctly describe vascular underpinnings of AD, from alterations in CBF to BBB dysfunction, topics that have been extensively reviewed elsewhere (Bell and Zlokovic, 2009; Zlokovic, 2011; Hamel, 2015; Hays et al., 2016; Nelson et al., 2016; Kisler et al., 2017; Korte et al., 2020; Solis et al., 2020; Soto-Rojas et al., 2021).

Cerebral Blood Flow Alterations in Alzheimer's Disease

Numerous investigations on individuals diagnosed with AD observed reduced CBF (Prohovnik et al., 1988; Montaldi et al., 1990; Bressi et al., 1992; O'Brien et al., 1992; Smith et al., 1992; Minoshima et al., 1997; Mattsson et al., 2014; Mielke et al., 2014; Smith and Verkman, 2018). CBF decline can be detected prior to cognitive decline, but also before plaque deposition. The accumulation of soluble Aβ prior to plaque deposition has early pathogenic consequences in AD (Suo et al., 1998). Studies have demonstrated increased levels of soluble amyloid species including $A\beta_{1-40}$ and $A\beta_{1-42}$ in AD cases compared to age-matched controls (Suo et al., 1998; Smith and Greenberg, 2009). Both soluble $A\beta_{1-40}$ and $A\beta_{1-42}$ have been associated to abnormal vascular reactivity in the absence of plaque deposition or vessel wall dysfunction (Smith and Greenberg, 2009; Dietrich et al., 2010). In particular, studies have revealed that application of exogenous $A\beta_{1-40}$ to mouse neocortex *in vivo,* or to healthy bovine blood vessels *ex vivo,* leads to endothelium-dependent vasoconstriction (Thomas et al., 1996; Niwa et al., 2000). In addition, increased levels of soluble amyloid species ($A\beta_{1-40}$ and $A\beta_{1-42}$) are associated with significantly reduced CBF, increased cerebral vascular resistance, decrease myogenic and vasodilator responses (Suo et al., 1998; Dietrich et al., 2010), where $A\beta_{1-42}$ is equally potent to $A\beta_{1-40}$ except at a higher concentration (Dietrich et al., 2010). Soluble Aβ impacts vascular function through increased production of reactive oxygen species (ROS). The reaction of ROS superoxide and excess NO produces peroxynitrite. Peroxynitrite is commonly known as a toxic oxidant which contributes to endothelial dysfunction, a mechanism relevant to AD but also to other neuroinflammatory and metabolic conditions (Beckman et al., 1990; Paris et al., 1998; Tan et al., 2004; Dietrich et al., 2010; Kelleher and Soiza, 2013; Salisbury and Bronas, 2015; Incalza et al., 2018). Both $A\beta_{1-40}$ and $A\beta_{1-42}$ have been shown to acutely increase ROS production in cultured rat cerebral microvascular endothelial and smooth muscle cells in a dose dependent manner (Dietrich et al., 2010). Interestingly, this response was inhibited by the ROS scavenger MnTBAP (Dietrich et al., 2010). Notably, $A\beta_{1-40}$ is the predominant isoform found in cerebral vessel walls and is commonly associated with vascular deposits in CAA, which will be discussed later, while $A\beta_{1-42}$ is the major isoform deposited in senile plaques (Suo et al., 1998). Although this concept is still controversial, it is thought that $A\beta_{1-42}$ acts as a "seed" which initiates the formation of vascular Aβ deposit in CAA (McGowan et al., 2005; Gireud-Goss et al., 2020).

Following Aβ deposition, reduction of CBF was found in the frontal, parietal and temporal cortices from individuals carrying Apolipoprotein E4 (*APOE4*) gene, most prevalent genetic risk factor for AD (Thambisetty et al., 2010; Michels et al., 2016). In addition, ApoE4 allele carriers displayed early impairments in cerebrovascular reactivity to a memory task (Suri et al., 2015). BOLD-fMRI, which uses blood flow changes as a surrogate to neuronal activity, detected decreased activation in areas engaged during naming and fluency tasks in AD patients compared to individuals with no risk factors (Smith et al., 1999). Decreased BOLD-fMRI responses to different cognitive tasks in early stage of AD are region-specific (Kisler et al., 2017). Most studies investigating perfusion in AD reported either CBF or CBV alterations. However, CBF alterations appear before CBV deficits during AD progression (Lacalle-Aurioles et al., 2014).

Decreased CBF is associated with poor cognitive function, and evidence suggested that lower CBF is linked with faster cognitive decline in patients with AD (Benedictus et al., 2017). Zheng et al. (2019) investigated rCBF, functional activity and connectivity in AD by combining resting-state BOLD fMRI and ASL techniques. ASL revealed decreased rCBF in AD patients in the left posterior cingulate cortex, bilateral dorsolateral prefrontal cortex, left interior parietal lobule, right middle temporal gyrus, left middle occipital gyrus and left precuneus. In addition, they revealed decreased connectivity between regions in AD patients, which was associated with impaired cognitive performances (Alsop et al., 2000; Zheng et al., 2019). Brain regions affected by a reduction of CBF in AD patients (parietal, frontal, temporal and occipital cortices) are associated with cognitive impairment in all domains (language, global cognition, memory, attention, executive functioning and visuospatial functioning) (Leeuwis et al., 2017).

Blood flow reductions have also been identified in early preclinical AD, before Aβ plaque deposition (Nicolakakis and Hamel, 2011; Iturria-Medina et al., 2016; Szu and Obenaus, 2021).

Early reduction of CBF has been reported in mouse models of AD, such as mice overexpressing mutant forms of APP (Niwa et al., 2002; Ongali et al., 2010; Lacoste et al., 2013) and in mice expressing the *ApoE4* gene allele (Lin et al., 2017). In some brain areas, CBF reduction can reach over 50%. This CBF reduction has been associated with cognitive changes in mice, including a loss of ability to sustain attention (Marshall et al., 2001). Both *ApoE4* transgenic and APP/PS1 mice revealed CBF reduction prior to neuronal and synaptic dysfunctions (Guo et al., 2019; Montagne et al., 2021).

While decreased CBF in AD is widely accepted, studies are only starting to identify underlying mechanisms, for example the involvement of pericytes. Pericytes have been linked to hypoperfusion and increased capillary constriction in AD (Bell et al., 2010; Korte et al., 2020). Pericyte-deficient transgenic mice with no Aβ pathology develop early CBF reduction in the gray matter, even with normal neuronal activity, endothelial-dependent vasodilation, astrocyte number and blood vessels coverage (Bell et al., 2010; Kisler et al., 2017). As these pericyte-deficient mice age, neuronal dysfunction and degeneration start to emerge. Another underlying mechanism was reported by Cruz Hernandez et al. (2019), demonstrating that capillaries become blocked by neutrophils, while another study revealed increased formation of occlusive thrombi in AD mice (Cortes-Canteli et al., 2019). Inhibiting neutrophils adhesion using an antibody against neutrophil-specific protein Ly6G in the APP/PSI mouse model led to rapid improvements in CBF (Cruz Hernandez et al., 2019). In a follow-up study, the same group assessed the impact of one treatment of anti-Ly6G on short-term memory function and reported increased CBF by 17% in 21–22 months old APP/PSI mice. Furthermore, they suggested that increased CBF improved cognition into late stages of AD mice (Bracko et al., 2020). Reduced neurovascular coupling and cerebrovascular reactivity have also been reported in AD mice (Girouard and Iadecola, 2006; Tong et al., 2019). Recently, impaired capillary endothelial inward rectifying Kir2.1 channel, playing a role in mediating blood delivery, has been associated with AD (Mughal et al., 2021). In a model of familial AD (5xFAD) where Kir2.1 channel function is impaired, systemic administration of the co-factor phosphatidylinositol 4,5-bisphosphate (PIP_2), required for Kir2.1 activity, led to increased CBF and functional neurovascular coupling in 5xFAD mice (Mughal et al., 2021).

AD patients are often (80–90%) diagnosed with CAA, a vessel disorder (Gireud-Goss et al., 2020) and an important risk factor for intracerebral hemorrhage and cognitive impairment (Reijmer et al., 2016). CAA consist of vascular amyloid deposits similar to senile plaques in AD (Kumar-Singh et al., 2005). Neuropathological studies have revealed that CAA affects the outer leptomeningeal vessels on the surface of the brain as well as distal intraparenchymal arteries, arterioles, and capillaries (Gireud-Goss et al., 2020; Howe et al., 2020). APP23 mouse model and human AD brain revealed an association between CAA-related capillary occlusion with CBF disturbances, hypoperfusion, detected by magnetic resonance angiopathy (MRA), which could explain in part the changes in CBF measured in AD patients (Thal et al., 2009; Milner et al., 2014). As in AD, patients with CAA have been linked to altered hemodynamics during visual stimulation as evidenced by reduced amplitude of BOLD response (Smith et al., 2008; Dumas et al., 2012; Switzer et al., 2020).

Altered Blood-Brain Barrier and Angiogenesis in Alzheimer's Disease

Early signs of BBB leakage in AD have been detected before dementia onset (Montagne et al., 2016). Neuroimaging techniques have evidenced BBB breakdown in AD in gray and white matter brain regions (Montagne et al., 2016; van de Haar et al., 2016). Aβ and tau pathologies contribute to increased BBB permeability in AD patients and mouse models (Park et al., 2011; Sagare et al., 2013; Alata et al., 2015). Several players involved in Aβ clearance, and closely related to the BBB, are reduced in AD patients, including phosphatidylinositol-binding clathrin assembly protein (PICALM, allows for Aβ exocytosis across the luminal part of the BBB), P-glycoprotein (expressed on both sided of the BBB) and glucose transporter (GLUT)1 (Mooradian et al., 1997; Chiu et al., 2015; Zhao et al., 2015). AD brain microvessel show diminished expression of LRP1, a major Aβ clearance receptor at the BBB (Deane et al., 2004; Donahue et al., 2006). LRP1 is an ApoE receptor and is expressed at the abluminal side of brain ECs and mediates the internalization of soluble Aβ (Deane et al., 2004). Endothelium-specific deletion of LRP1 leads to the acceleration of Aβ pathology in APP-overexpressing $APP_{sw/0}$ mice (Storck et al., 2016). Moreover, studies have demonstrated low levels of GLUT1 in AD brain endothelium, which alters glucose transport (Kalaria and Harik, 1989; Simpson et al., 1994).

Several features lead to increased BBB permeability in AD, including reduced expression of tight junctions, perivascular accumulation of blood-derived products, degeneration of pericytes and ECs, as well as infiltration of circulating leukocytes (Sweeney et al., 2018; Huang et al., 2020). It was demonstrated that Aβ disrupts tight junctions and increases vascular permeability by suppressing expression of ZO-1, claudin-5 and occludin while increasing expression of MMP-2 and MMP-9 (Kook et al., 2012; Blair et al., 2015; Wan et al., 2015; Huang et al., 2020). Isolated rat cerebral cortical ECs treated with $A\beta_{1-42}$ displayed decreased expression of occludin and redistribution of claudin-5 and ZO-2 in the cytoplasm while in untreated cells, both claudin-5 and ZO-2 were distributed along the plasma membrane at cell-cell contacts (Marco and Skaper, 2006). In addition, studies have reported leakage of blood-derived proteins (fibrinogen, thrombin, albumin, and IgG) around capillaries from post-mortem brain tissue in the prefrontal and entorhinal cortex as well as in hippocampus of AD patients (Ryu and McLarnon, 2009; Hultman et al., 2013; Sengillo et al., 2013). Furthermore, animal studies revealed that lacking pericyte-derived soluble factors, required for a healthy endothelium, can contribute to endothelial degeneration in AD (Bell et al., 2010). Finally, mouse models of AD have demonstrated that pericyte reduction is associated with BBB dysfunction as well as accelerated buildup of Aβ and tau pathology (Sagare et al., 2013). In human studies, there is also evidence of pericyte loss in the hippocampus and cortex of AD

patients due in part to prolonged exposure to Aβ peptides (Sagare et al., 2013; Sengillo et al., 2013; Huang et al., 2020). Of note, pericytes play a role in Aβ clearance by internalizing different Aβ peptides using the LRP1 pathway (Sagare et al., 2013).

Evidence of reduced capillary length and basement membrane changes in AD patients have been reported (Salloway et al., 2002; Sengillo et al., 2013; Halliday et al., 2016). It was shown that AD patients display abnormal angiogenesis due to low expression of MEOX2, a regulator of vascular differentiation, as well as premature pruning of capillary networks resulting in reductions of CBF (Wu et al., 2005; Grammas, 2011). Endothelial degeneration including reduction of EC thickness, length and density of blood vessels were reported in brain tissue from AD patients (Sweeney et al., 2018). An increase of pro-angiogenic factors in the AD brain, without the increase in vasculature, was also reported (Grammas, 2011). Notably, the increased Aβ species and plaques in AD have anti-angiogenic effects (Parodi-Rullan et al., 2020), and impaired angiogenesis was identified in transgenic AD mice (Grammas, 2011). Emerging evidence suggest that dysfunction of the VEGF-A/VEGFR2 pathway may play an aggravating role in neurodegeneration and AD. For instance, sustained brain delivery of VEGF via injectable hydrogels was protective against quinolinic acid-induced neurodegeneration (Emerich et al., 2010), and low VEGF levels have been associated to another debilitating neurological disorder, spinocerebellar ataxia type 1 (Cvetanovic et al., 2011). Aβ acts as an antagonist of VEGF signaling via sequestration of VEGF-A in senile plaques, and also via inhibition of VEGFR2 tyrosine phosphorylation (Patel et al., 2010). Moreover, implantation of VEGF secreting microcapsules on the cerebral cortex of APP/PS1 mice attenuated both brain Aβ burden and cognitive impairments (Spuch et al., 2010). Whether impaired neural perfusion and increased neurotoxicity in AD correlate to a loss of VEGF function, and whether VEGF overexpression is neuroprotective in transgenic AD mice remains to be explored.

CAA is associated with increased BBB permeability and arterial stiffness (Magaki et al., 2018; Gireud-Goss et al., 2020). Aβ deposition in CAA has been found to occur on the cerebrovascular basement membrane of arteries, arterioles and on the basal lamina of capillaries as shown by electron microscopy (Gireud-Goss et al., 2020). Moreover, ultrastructural studies of CAA demonstrated a thinned endothelium, shrinkage and degeneration of ECs, as well as vessel occlusion, all of which can lead to CBF disturbances and microinfarcts (Attems and Jellinger, 2004; Thal et al., 2009; Magaki et al., 2018). Tight junction proteins in CAA-laden vessels are found decreased (Tai et al., 2010). After exposure to exogenous Aβ, human ECs showed decreased expression of occludin, while post-mortem brain tissue of CAA patients revealed decreased expression of claudin-5, ZO-1, CD31 and basement protein collagen IV (Tai et al., 2010; Carrano et al., 2011; Magaki et al., 2018). In addition, CAA patients displayed increased expression of MMP-2 and MMP-9, which may lead to basement membrane degradation and increased BBB permeability (Carrano et al., 2011). In the Tg2576 mouse model of CAA, BBB integrity was compromised due to decreased expression of claudin-5 and claudin-1 (Carrano et al., 2011). Moreover, TgSwDI mice, another model of CAA, revealed spontaneous hemorrhage and loss of BBB integrity (Davis et al., 2004). Soluble $A\beta_{1-40}$, predominant amyloid isoform in vessel walls, also leads to tight junction redistribution at the BBB and decreased transendothelial electric resistance (Hartz et al., 2012; Gireud-Goss et al., 2020). Understanding the impact of Aβ in CAA and AD is essential for slowing cerebrovascular disease progression.

ADDITIONAL REMARKS: VASCULAR DEFICITS IN DOWN SYNDROME, TRAUMATIC BRAIN INJURY AND DEPRESSION

In addition to neurodevelopmental disorders discussed earlier in this review, Down syndrome (DS), which results from trisomy of human chromosome 21, is a cause of early onset Alzheimer's disease-dementia (AD-DS) (Ballard et al., 2016; Tosh et al., 2021). Two-thirds of individuals with DS will develop dementia by the age of 65 (Tosh et al., 2021). The onset of AD in DS patients parallels the development of the classic brain pathological lesions seen in AD patients without DS (Salehi et al., 2016). DS and AD disorders have genetic similarities, as individuals with DS possess a triplication of the gene encoding APP, while patients with familial AD have an extra copy of the APP gene (Salehi et al., 2016). In rodent studies of DS-AD, triplication of chromosome 21 genes other than *APP* demonstrated increased Aβ aggregation deposition and cognitive deficits (Wiseman et al., 2018). A recent study, focused on a model of DS comprising of a mutation in a Down syndrome critical region (Hsa21) on chromosome 21 encompassing 21q21–21q22.3 (Li et al., 2016; Tosh et al., 2021). This study crossed an Hsa21 mouse model of DS with partial trisomies other than *APP* with a transgenic APP mouse model and revealed that an additional copy of genes of the Hsa21 region modulates APP/Aβ biology, including Aβ aggregation and mortality (Tosh et al., 2021). Despite striking similarities between AD and DS in terms of genetics and symptoms onset, neurovascular impairments in DS have been largely overlooked. As such, studies aimed at elucidating vascular abnormalities in DS represent an unmet clinical need.

Early vascular insults following a traumatic brain injury (TBI) can also increase the risk of late-onset neurological diseases (Brett et al., 2021). TBI is a significant public health problem associated with long-term disabilities. Early chronic TBI may lead to secondary injury with pathophysiological changes similar to those observed in neurodegenerative diseases (Impellizzeri et al., 2016). For instance, neuroinflammation plays a fundamental role in TBI, including reactive microglia and astrocytes, as well as release of pro-inflammatory cytokines and chemokines that may hinder the brain's ability to repair itself and lead to neurodegeneration following prolonged activation of these processes (Impellizzeri et al., 2016; Brett et al., 2021). Severe or repeated mild TBI can initiate long-term neurodegeneration with signs of AD (Mendez, 2017). For example, various contact-sport players developed TBI-associated dementia or parkinsonism years after retiring. TBI can induce acute BBB disruption through

TABLE 1 | Major altered features associated with CBF, BBB, and angiogenesis in neurodevelopmental and neurodegenerative disorders.

Disorder	Key features	Selected references
ASD		
Altered CBF	– Widespread cerebral hypoperfusion in 75% of ASD children associated with language deficits, impaired executive function and abnormal response to sensory stimuli. – Hyperperfusion identified in frontotemporal regions. – Reduced hemodynamic responses. – Cerebral hypoperfusion also identified in rodent models of ASD. – Increased resting CBF and decreased NVC in an adult mouse model of ASD associated with endothelial dysfunction.	Ohnishi et al., 2000; Zilbovicius et al., 2000; Burroni et al., 2008; Reynell and Harris, 2013; Jann et al., 2015; Ouellette et al., 2020; Uratani et al., 2019
Altered BBB and angiogenesis	– Reduced level of adhesion molecules (CD31 and P-selectin). – Increased MMP-9 which regulates cell proliferation, adhesion, angiogenesis, oxidative injury and BBB breakdown. – Altered expression of claudin-5 and claudin-12. – Increased BBB permeability and impaired angiogenesis in animal models. – Reduced angiogenesis found in a mouse model of ASD.	Onore et al., 2012; Kumar et al., 2015; Azmitia et al., 2016; Fiorentino et al., 2016; Turner and Sharp, 2016; Ouellette et al., 2020
Schizophrenia		
Altered CBF	– Increased CBF in the cingulate gyrus and superior frontal gyrus associated with positive symptoms. – Negative symptoms associated with hypoperfusion in the superior temporal gyrus bilaterally and left middle frontal gyrus. – rCBF alterations depend on severity of positive symptoms. – Increased CBF in the right superior temporal gyrus and caudate nucleus. – Decreased CBF in the occipital and left parietal cortices. – Altered NVC including reduced amplitude of response and delayed hemodynamics.	Sabri et al., 1997; Carter et al., 2001; Schultz et al., 2002; Malaspina et al., 2004; Ford et al., 2005; Pinkham et al., 2011; Liu et al., 2012; Kawakami et al., 2014; Pu et al., 2016; Zhuo et al., 2017
Altered BBB and angiogenesis	– Increased BBB permeability. – Thickening and deformation of basal lamina, vacuolation of EC cytoplasm, swelling of astrocyte end-feet, activation of microglial cells and atypical vascular arborization in prefrontal and visual cortices. – Decreased claudin-5 expression, altered level of VE-cadherin and occludin in ECs. – Impaired angiogenesis and VEGF upregulation in the prefrontal cortex linked to vascular hyperpermeability.	Grove et al., 2015; Hino et al., 2016; Casas et al., 2018; Carrier et al., 2020; Cai et al., 2020; Guo et al., 2020; Crockett et al., 2021; Usta et al., 2021
MS		
Altered CBF	– Hypoperfusion in SP-MS, RR-MS and PP-MS patients. – Active demyelinating lesions associated with hyperperfusion and stable lesions linked to hypoperfusion. – CBF alterations present in early stages of disease. – Impaired cerebral vascular reactivity leads to neuronal death. – Overproduction of NO desensitize EC and smooth muscle cell function, leading to decreased vasodilatory capacity and limited blood supply to neurons.	Ge et al., 2005; Varga et al., 2009; D'Haeseleer et al., 2011; Ota et al., 2013; Marshall et al., 2014; Bester et al., 2015; Monti et al., 2018; Hostenbach et al., 2019
Altered BBB and angiogenesis	– BBB hyperpermeability. – Decreased expression of TJ proteins (ZO-1, occludin and claudin-5) in ECs in patients with active and inactive lesions. – Rodent model of MS show increased expression of VEGF in ECs, astrocytes and monocytes. – Increased vascular network density and angiogenesis.	Kirk et al., 2003; Bennett et al., 2010; Holley et al., 2010; Cramer et al., 2014; Girolamo et al., 2014; Papadaki et al., 2014
HD		
Altered CBF	– Altered CBF prior to structural changes and motor symptoms. – Cerebral hypoperfusion in the basal ganglia, medial and lateral prefrontal cortex. – Cerebral hyperperfusion in the cerebellar-thalamic and somatosensory regions. – Altered neurovascular coupling during visual stimulation.	Hasselbalch et al., 1992; Sax et al., 1996; Deckel and Duffy, 2000; Wang et al., 2016; Klinkmueller et al., 2021

(Continued)

TABLE 1 | (Continued)

Disorder	Key features	Selected references
Altered BBB and angiogenesis	– Increased vessel density, BBB leakage and VEGF-A release. – Decreased TJ molecules including occludin and claudin-5. – Rodent model of HD revealed increased transcytosis and paracellular transport in brain ECs with TJ imbalance. – mHtt aggregates localized in ECs, smooth muscle cells and perivascular macrophages. – iPSCs-derived HD BMECs show increased angiogenesis, altered barrier properties and impaired Wnt/β-catenin signaling.	Steventon et al., 2020; Drouin-Ouellet et al., 2015; Di Pardo et al., 2017; Lim et al., 2017
PD		
Altered CBF	– Decreased CBF in frontal, parietal and occipital areas. – PD patients with dementia show left temporo-parietal hypoperfusion. – PD patients without dementia display hypoperfusion in the posterior cortical regions. – Hypoperfusion is positively correlated with cognitive performance and motor impairment.	Derejko et al., 2006; Kamagata et al., 2011; Fernandez-Seara et al., 2012; Madhyastha et al., 2015; Syrimi et al., 2017
Altered BBB and angiogenesis	– BBB disruption in the SNc with increased permeability in the post-commissural putamen. – Down regulation of TJ proteins (ZO-1) and higher number of EC nuclei in the SNc. – String vessel formation in brain capillary networks. – Upregulation of VEGF, and parkinsonian traits following VEGF administration in rodent models. – Formation of endothelial clusters, capillary network damage, loss of capillary connections in the SN, basement membrane thickening, vacuolization, and pericyte degradation.	Farkas et al., 2000; Barcia et al., 2005; Kortekaas et al., 2005; Wada et al., 2006; Rite et al., 2007; Chao et al., 2009; Patel et al., 2011; Guan et al., 2013; Yang et al., 2015; Kuan et al., 2016
AD		
Altered CBF	– Reduced CBF prior to cognitive decline and plaque deposition. – Soluble $A\beta_{1-40}$ and $A\beta_{1-42}$ are associated with abnormal vascular reactivity and decreased myogenic responses in absence of plaque deposition. – Hypoperfusion detected following Aβ deposition in the frontal, parietal and temporal cortices and poor cognitive function. – BOLD-fMRI detected decreased activation in regions involved in naming and fluency tasks. – Hypoperfusion identified in rodent models overexpressing mutant forms of APP. – Rodent models show reduced NVC and cerebrovascular reactivity. – Parallel diagnosis of CAA linked with altered hemodynamics, capillary occlusion and hypoperfusion.	Montaldi et al., 1990; Bressi et al., 1992; Smith et al., 1999; Marshall et al., 2001; Girouard and Iadecola, 2006; Smith and Greenberg, 2009; Dietrich et al., 2010; Ongali et al., 2010; Dumas et al., 2012; Lacoste et al., 2013; Mattsson et al., 2014; Milner et al., 2014; Benedictus et al., 2017; Smith and Verkman, 2018
Altered BBB and angiogenesis	– Aβ and tau pathologies contribute to BBB breakdown, reduced expression of TJ (ZO-1, claudin-5, occludin) and degeneration of pericytes and ECs. – Brain microvessel with diminished expression of LRP1. – Reduced level of GLUT1 in brain endothelium. – Reduced capillary length with basement membrane alterations. – Abnormal angiogenesis related to low expression of MEOX2. – Reduced EC thickness, and lower length/density of blood vessels. – Dysfunction of the VEGF-A/VEGFR2 pathway aggravates neurodegeneration. – Rodent models show pericyte loss. – Aβ deposition in CAA linked to decreased TJ proteins, increased expression of MMP-2 and MMP-9, thinned endothelium, degeneration of ECs and leaky BBB.	Kalaria and Harik, 1989; Simpson et al., 1994; Emerich et al., 2010; Tai et al., 2010; Grammas, 2011; Carrano et al., 2011; Sagare et al., 2013; Halliday et al., 2016; Montagne et al., 2016; van de Haar et al., 2016; Magaki et al., 2018; Sweeney et al., 2018; Huang et al., 2020

Selected references are displayed. Aβ, β-amyloid peptide; AD, Alzheimer's disease; APP, amyloid precursor protein; ASD, autism spectrum disorders; BBB, blood brain barrier; BMECs, brain microvascular endothelial cells; BOLD-FMRI, blood oxygen level dependent imaging-functional magnetic resonance imaging; CAA, cerebral amyloid angiopathy; CBF, cerebral blood flow; ECs, endothelial cells; GLUT1, glucose transporter 1; HD, Huntington's disease; iPSC, induced pluripotent stem cells; LRP1, low-density lipoprotein receptor-related protein 1; MEOX2, Mesenchyme Homeobox 2; mHtt, mutant huntingtin; MMP, matrix metalloproteinases; MS, multiple sclerosis; NO, nitric oxide; NVC, neurovascular coupling; PD, Parkinson's disease; PP-MS, primary progressive-multiple sclerosis; rCBF, regional cerebral blood flow; RR-MS, relapsing remitting-multiple sclerosis; SN, substantia nigra; SNc, substantia nigra pars compacta; SP-MS, secondary progressive-multiple sclerosis; TJ, tight junctions; VE-cadherin, vascular endothelial cadherin; VEGF, vascular endothelial growth factor; VEGFR2, vascular endothelial growth factor receptor 2; Wnt/β-catenin, Wingless-related integration site β- catenin; ZO-1, Zonula occludens-1.

vascular shear stress, hemorrhages, edema, alterations in CBF and chronic inflammation, which is known to contribute to Aβ deposition and tau pathology (Iadecola, 2013; De Silva and Faraci, 2016). Autopsies of TBI patients show diffuse Aβ plaques similar to those identified in AD, as reviewed by Perry et al. (2016). The formation of Aβ in perivascular spaces following TBI may lead to an injury cascade consisting of cerebrovascular damage, oxidative stress and ECs dysfunction (Ramos-Cejudo et al., 2018). Interestingly, alterations in EC survival, BBB integrity and neuroinflammation are considered early events after TBI, all of which are characteristic of cerebrovascular damage involved in the progression of AD and impairment of Aβ clearance. Thus, these early vascular impairments promote the onset of neurodegenerative diseases (Ramos-Cejudo et al., 2018). Considering early vascular injuries in TBI, biomarker studies are integrating a variety of neuroimaging and molecular techniques to better understand the incidence of cerebrovascular dysfunction and the onset of neurodegenerative diseases, and therapeutic investigations have looked at ways to improve cerebrovascular function (Graham and Sharp, 2019; Martinez and Stabenfeldt, 2019).

One of the leading causes of mental illness worldwide, depression, has a tremendous impact on psychosocial behaviors and vascular health (Knight and Baune, 2017; Menard et al., 2017). Chronic stress is the primary environmental risk factor for depression. The nucleus accumbens (NAc) is one of the main players in regulating stress response (Russo and Nestler, 2013). Menard et al. (2017) have demonstrated that chronic social stress induces BBB leakiness in the NAc of mice, which leads to circulating proinflammatory mediators and depression-like behaviors such as helplessness, social avoidance and anhedonia. As seen in neurodevelopmental and neurodegenerative disorders, the increase in BBB permeability in the rodent model of chronic social stress was facilitated by the loss of tight junction protein claudin-5 (Menard et al., 2017). Furthermore, stress-induced BBB permeability has been linked to inflammation of the endothelium and up-regulation of an epigenetic repressor, *hdac1*, which is involved in reducing claudin-5 expression and loosening of tight junctions (Dudek et al., 2020). Consequently, these studies are highlighting mechanisms by which chronic stress impacts vascular health, which could have long-term consequences on brain maturation and aging.

The vascular system, as any other system, undergoes aging. It has been hypothesized that vascular aging leads to a progressive functional deterioration (Grunewald et al., 2021). During aging, the brain vasculature undergoes several changes including decreased capillary density, attenuation of neovascularization potential, increased BBB permeability and decreased CBF as reviewed in Watanabe et al. (2020) and Banks et al. (2021). A suggested mechanism of typical vascular aging consist of the inability of VEGF to replenish vessel loss. The mechanisms by which VEGF is involved in vascular aging are unknown. However, mice treated with VEGF have been shown to live longer, with extended multiorgan functionality (Grunewald et al., 2021). Furthermore, aging is associated with several vascular changes including aortic stiffness which has been linked to reduced blood flow in tissues leading to increased neuroinflammation and neurodegeneration later in life (Moore et al., 2021). Therefore, age-related changes in key vascular features may predispose to age-associated diseases (Banks et al., 2021). Improving early pathological conditions by protecting the brain vasculature is essential in preventing or modulating disease progression.

CONCLUSION

Vascular risk factors and co-morbidities take part in disease onset and/or exacerbate disease progression (Sweeney et al., 2018; Clancy et al., 2021). When it comes to alterations in CBF, BBB, and vascular patterning, neurodevelopmental and neurodegenerative disorders share interesting similarities (**Table 1**). While these disorders are siloed, mainly due to the age of onset, the commonalities in vascular alterations force to question the implication of early life vascular impairments on the expression of age-related neurodegenerative diseases. The vascular implications in middle-aged autistic adults have been largely overlooked, 10% of individuals diagnosed with ASD age between 40 and 60 years old will develop dementia, including AD within 15 years (Plana-Ripoll et al., 2019). In addition, there is a high frequency of parkinsonism among older ASD patients (Starkstein et al., 2015). The impact of altered brain perfusion and BBB integrity in ASD may contribute to the onset of neurodegenerative diseases due to the continuous vascular impairments associated with these diseases. Likewise, schizophrenia is associated with an elevated risk for developing Alzheimer's and Parkinson's diseases as they share core features including white matter abnormalities and cognitive deficits (Ribe et al., 2015; Kochunov et al., 2021; Kuusimaki et al., 2021).

Since fast-growing evidence demonstrates the role of early vascular impairments in the onset and/or progression of numerous neurological conditions, more work is needed to identify therapeutic targets to promote healthy cerebrovascular maturation and aging, as well as hinder the progression of age-related dementia and neurodegeneration. This is primordial considering recent findings that ECs show limited turnover compared to other cells in the human body (Sender and Milo, 2021). For instance, it was estimated that the turnover rate of ECs is 0.1% per day, as opposed to much higher rates for erythrocytes (65%), neutrophils (18%) or gastrointestinal epithelial cells (12%). In addition, the turnover rates of cellular mass in the human body were estimated at 0.4% for ECs, 4% for skin cells and adipocytes, and 42% for gastrointestinal epithelial cells (Sender and Milo, 2021). Hence, as ECs are long-lived, they may carry on early structural and functional impairments into adulthood and throughout aging, altering organ function in the long term. This concept emphasizes the importance of infant screening for cerebrovascular abnormalities, and of continuous management of vascular risk factors during lifespan. As such, the vascular continuum between neurodevelopmental and neurodegenerative disease should represent a growing focus in modern neuroscience (**Figure 3**).

AUTHOR CONTRIBUTIONS

JO wrote the draft following BL's instructions. BL chose the theme and edited the manuscript. Both authors contributed to the article and approved the submitted version.

FUNDING

This publication was possible thanks to funding by the Canadian Institutes for Health Research (grant #388805) to BL and a Canadian Vascular Network scholarship to JO.

REFERENCES

Abbott, N. J., Ronnback, L., and Hansson, E. (2006). Astrocyte-endothelial interactions at the blood-brain barrier. *Nat. Rev. Neurosci.* 7, 41–53. doi: 10.1038/nrn1824

Abookasis, D., Lerman, D., Roth, H., Tfilin, M., and Turgeman, G. (2018). Optically derived metabolic and hemodynamic parameters predict hippocampal neurogenesis in the BTBR mouse model of autism. *J. Biophotonics* 11:e201600322. doi: 10.1002/jbio.201600322

Adhya, S., Johnson, G., Herbet, J., Jaggi, H., Babb, J. S., Grossman, R. I., et al. (2006). Pattern of hemodynamic impairment in multiple sclerosis: dynamic susceptibility contrast perfusion MR imaging at 3.0 T. *Neuroimage* 33, 1029–1035. doi: 10.1016/j.neuroimage.2006.08.008

Al-Bachari, S., Naish, J. H., Parker, G. J. M., Emsley, H. C. A., and Parkes, L. M. (2020). Blood-Brain Barrier Leakage Is Increased in Parkinson's Disease. *Front. Physiol.* 11:593026. doi: 10.3389/fphys.2020.593026

Alata, W., Ye, Y., St-Amour, I., Vandal, M., and Calon, F. (2015). Human apolipoprotein E varepsilon4 expression impairs cerebral vascularization and blood-brain barrier function in mice. *J. Cereb. Blood Flow Metab.* 35, 86–94. doi: 10.1038/jcbfm.2014.172

Alsop, D. C., Detre, J. A., and Grossman, M. (2000). Assessment of cerebral blood flow in Alzheimer's disease by spin-labeled magnetic resonance imaging. *Ann. Neurol.* 47, 93–100.

Alzheimer's Association (2021). 2021 Alzheimer's disease facts and figures. *Alzheimers Dement.* 17, 327–406. doi: 10.1002/alz.12328

Andreasen, N. C., O'Leary, D. S., Flaum, M., Nopoulos, P., Watkins, G. L., Boles Ponto, L. L., et al. (1997). Hypofrontality in schizophrenia: distributed dysfunctional circuits in neuroleptic-naïve patients. *Lancet* 349, 1730–1734. doi: 10.1016/s0140-6736(96)08258-x

Andreone, B. J., Lacoste, B., and Gu, C. (2015). Neuronal and vascular interactions. *Annu. Rev. Neurosci.* 38, 25–46. doi: 10.1146/annurev-neuro-071714-033835

Antony, P. M., Diederich, N. J., Kruger, R., and Balling, R. (2013). The hallmarks of Parkinson's disease. *FEBS J.* 280, 5981–5993. doi: 10.1111/febs.12335

Attems, J., and Jellinger, K. A. (2004). Only cerebral capillary amyloid angiopathy correlates with Alzheimer pathology–a pilot study. *Acta Neuropathol.* 107, 83–90. doi: 10.1007/s00401-003-0796-9

Attwell, D., Buchan, A. M., Charpak, S., Lauritzen, M., Macvicar, B. A., and Newman, E. A. (2010). Glial and neuronal control of brain blood flow. *Nature* 468, 232–243. doi: 10.1038/nature09613

Attwell, D., Mishra, A., Hall, C. N., O'Farrell, F. M., and Dalkara, T. (2016). What is a pericyte? *J. Cereb. Blood Flow Metab.* 36, 451–455. doi: 10.1177/0271678X15610340

Attwell, D. A., and Laughlin, S. (2001). An energy budget for signaling in the grey matter of the brain. *J. Cereb. Blood Flow Metab.* 21, 1133–1145.

Aucoin, J. S., Jiang, P., Aznavour, N., Tong, X. K., Buttini, M., Descarries, L., et al. (2005). Selective cholinergic denervation, independent from oxidative stress, in a mouse model of Alzheimer's disease. *Neuroscience* 132, 73–86. doi: 10.1016/j.neuroscience.2004.11.047

Azmitia, E. C., Saccomano, Z. T., Alzoobaee, M. F., Boldrini, M., and Whitaker-Azmitia, P. M. (2016). Persistent angiogenesis in the autism brain: an immunocytochemical study of postmortem cortex, brainstem and cerebellum. *J. Autism Dev. Disord.* 46, 1307–1318. doi: 10.1007/s10803-015-2672-6

Ball, N., Teo, W. P., Chandra, S., and Chapman, J. (2019). Parkinson's disease and the environment. *Front. Neurol.* 10:218. doi: 10.3389/fneur.2019.00218

Ballard, C., Mobley, W., Hardy, J., Williams, G., and Corbett, A. (2016). Dementia in Down's syndrome. *Lancet Neurol.* 15, 622–636. doi: 10.1016/s1474-4422(16)00063-6

Banks, W. A., Reed, M. J., Logsdon, A. F., Rhea, E. M., and Erickson, M. A. (2021). Healthy aging and the blood-brain barrier. *Nat. Aging* 1, 243–254. doi: 10.1038/s43587-021-00043-5

Bano, D., Zanetti, F., Mende, Y., and Nicotera, P. (2011). Neurodegenerative processes in Huntington's disease [Review]. *Cell Death Dis.* 2:e228. doi: 10.1038/cddis.2011.112

Barcia, C., Bautista, V., Sanchez-Bahillo, A., Fernandez-Villalba, E., Faucheux, B., Poza y Poza, M., et al. (2005). Changes in vascularization in substantia nigra pars compacta of monkeys rendered parkinsonian. *J Neural Transm. (Vienna)* 112, 1237–1248. doi: 10.1007/s00702-004-0256-2

Beckman, J. S., Beckman, T. W., Chen, J., Marshall, P. A., and Freeman, B. A. (1990). Apparent hydroxyl radical production by peroxynitrite: implications for endothelial injury from nitric oxide and superoxide. *Proc. Natl. Acad. Sci. U.S.A.* 87, 1620–1624. doi: 10.1073/pnas.87.4.1620

Bell, R. D., Winkler, E. A., Sagare, A. P., Singh, I., LaRue, B., Deane, R., et al. (2010). Pericytes control key neurovascular functions and neuronal phenotype in the adult brain and during brain aging. *Neuron* 68, 409–427. doi: 10.1016/j.neuron.2010.09.043

Bell, R. D., and Zlokovic, B. V. (2009). Neurovascular mechanisms and blood-brain barrier disorder in Alzheimer's disease. *Acta Neuropathol.* 118, 103–113. doi: 10.1007/s00401-009-0522-3

Benedictus, M. R., Leeuwis, A. E., Binnewijzend, M. A., Kuijer, J. P., Scheltens, P., Barkhof, F., et al. (2017). Lower cerebral blood flow is associated with faster cognitive decline in Alzheimer's disease. *Eur. Radiol.* 27, 1169–1175. doi: 10.1007/s00330-016-4450-z

Benmoyal-Segal, L., and Soreq, H. (2006). Gene-environment interactions in sporadic Parkinson's disease. *J. Neurochem.* 97, 1740–1755. doi: 10.1111/j.1471-4159.2006.03937.x

Bennett, J., Basivireddy, J., Kollar, A., Biron, K. E., Reickmann, P., Jefferies, W. A., et al. (2010). Blood-brain barrier disruption and enhanced vascular permeability in the multiple sclerosis model EAE. *J. Neuroimmunol.* 229, 180–191. doi: 10.1016/j.jneuroim.2010.08.011

Bester, M., Forkert, N. D., Stellmann, J. P., Sturner, K., Aly, L., Drabik, A., et al. (2015). Increased perfusion in normal appearing white matter in high inflammatory multiple sclerosis patients. *PLoS One* 10:e0119356. doi: 10.1371/journal.pone.0119356

Biju, K. C., Shen, Q., Hernandez, E. T., Mader, M. J., and Clark, R. A. (2020). Reduced cerebral blood flow in an alpha-synuclein transgenic mouse model of Parkinson's disease. *J. Cereb. Blood Flow Metab.* 40, 2441–2453. doi: 10.1177/0271678X19895432

Biswas, S., Cottarelli, A., and Agalliu, D. (2020). Neuronal and glial regulation of CNS angiogenesis and barriergenesis. *Development* 147:dev182279. doi: 10.1242/dev.182279

Bjørklund, G., Kern, J. K., Urbina, M. A., Saad, K., El-Houfey, A. A., Geier, D. A., et al. (2018). Cerebral hypoperfusion in autism spectrum disorder. *Acta Neurobiol. Exp.* 78, 21–29. doi: 10.21307/ane-2018-005

Blair, L. J., Frauen, H. D., Zhang, B., Nordhues, B. A., Bijan, S., Lin, Y. C., et al. (2015). Tau depletion prevents progressive blood-brain barrier damage in a mouse model of tauopathy. *Acta Neuropathol. Commun.* 3:8. doi: 10.1186/s40478-015-0186-2

Bogale, T. A., Faustini, G., Longhena, F., Mitola, S., Pizzi, M., and Bellucci, A. (2021). Alpha-Synuclein in the regulation of brain endothelial and perivascular cells: gaps and future perspectives. *Front. Immunol.* 12:611761. doi: 10.3389/fimmu.2021.611761

Bracko, O., Njiru, B. N., Swallow, M., Ali, M., Haft-Javaherian, M., and Schaffer, C. B. (2020). Increasing cerebral blood flow improves cognition into late stages in Alzheimer's disease mice. *J. Cereb. Blood Flow Metab.* 40, 1441–1452. doi: 10.1177/0271678X19873658

Bressi, S., Volontè, M. A., Alberoni, M., Canal, N., and Franceschi, M. (1992). Transcranial doppler sonography in the early phase of Alzheimer's disease. *Dement. Geriatr. Cogn. Disord.* 3, 25–31. doi: 10.1159/000106990

Brett, B. L., Gardner, R. C., Godbout, J., Dams-O'Connor, K., and Keene, C. D. (2021). Traumatic brain injury and risk of neurodegenerative disorder. *Biol. Psychiatry* (in press). doi: 10.1016/j.biopsych.2021.05.025

Buee, L., Hof, P. R., Bouras, C., Delacourte, A., Perl, D. P., Morrison, J. H., et al. (1994).). Pathological alterations of the cerebral microvasculature in Alzheimer's disease and related dementing disorders [Research Support, Non-U.S. Gov't Research Support, U.S. Gov't, P.H.S.]. *Acta Neuropathol.* 87, 469–480.

Burghardt, K., Grove, T., and Ellingrod, V. (2014). Endothelial nitric oxide synthetase genetic variants, metabolic syndrome and endothelial function in schizophrenia. *J. Psychopharmacol.* 28, 349–356. doi: 10.1177/0269881113516200

Burroni, L., Orsi, A., Monti, L., Hayek, Y., Rocchi, R., and Vattimo, A. (2008). Regional cerebral blood flow in childhood autism: a SPET study with SPM evaluation. *Nucl. Med. Commun.* 29, 150–156. doi: 10.1097/MNM.0b013e3282f1bb8e

Cai, H. Q., Catts, V. S., Webster, M. J., Galletly, C., Liu, D., O'Donnell, M., et al. (2020). Increased macrophages and changed brain endothelial cell gene expression in the frontal cortex of people with schizophrenia displaying inflammation. *Mol. Psychiatry* 25, 761–775. doi: 10.1038/s41380-018-0235-x

Carmeliet, P., and Jain, R. K. (2011). Molecular mechanisms and clinical applications of angiogenesis. *Nat. Review* 473, 298–307. doi: 10.1038/nature10144REVIEWDLL4

Carrano, A., Hoozemans, J., van der Vies, S., Rozemuller, A., van Horssen, J., and de Vries, H. E. (2011). Amyloid beta induces oxidative stress-mediated blood–brain barrier changes in capillary amyloid angiopathy. *Antioxid. Redox Signal.* 15, 1167–1178. doi: 10.1089/ars.2011.3895

Carrier, M., Guilbert, J., Levesque, J. P., Tremblay, M. E., and Desjardins, M. (2020). Structural and functional features of developing brain capillaries, and their alteration in schizophrenia. *Front. Cell. Neurosci.* 14:595002. doi: 10.3389/fncel.2020.595002

Carter, C. S., MacDonald, A. W., Ross, L. L., and Stenger, V. A. (2001). Anterior cingulate cortex activity and impaired self-monitoring of performance in patients with schizophrenia: an event-related fMRI study. *Am. J. Psychiatry* 158, 1423–1428. doi: 10.1176/appi.ajp.158.9.1423

Casas, B. S., Vitoria, G., do Costa, M. N., Madeiro da Costa, R., Trindade, P., Maciel, R., et al. (2018). hiPSC-derived neural stem cells from patients with schizophrenia induce an impaired angiogenesis. *Transl. Psychiatry* 8:48. doi: 10.1038/s41398-018-0095-9

Casserly, I., and Topol, E. (2004). Convergence of atherosclerosis and Alzheimer's disease: inflammation, cholesterol, and misfolded proteins [Review]. *Lancet* 363, 1139–1146. doi: 10.1016/S0140-6736(04)15900-X

Cauli, B., and Hamel, E. (2010). Revisiting the role of neurons in neurovascular coupling. *Front. Neuroenergetics* 2:9. doi: 10.3389/fnene.2010.00009

Chao, Y.-X., He, B.-P., and Wah Tay, S. S. (2009). Mesenchymal stem cell transplantation attenuates blood brain barrier damage and neuroinflammation and protects dopaminergic neurons against MPTP toxicity in the substantia nigra in a model of Parkinson's disease. *J. Neuroimmunol.* 216, 39–50. doi: 10.1016/j.jneuroim.2009.09.003

Chiron, C., Leboyer, M., Leon, F., Jambaque, L., Nuttin, C., and Syrota, A. (1995). SPECT of the Brain in childhood autism: evidence for a lack of normal hemispheric asymmetry. *Dev. Med. Child Neurol.* 37, 849–860. doi: 10.1111/j.1469-8749.1995.tb11938.x

Chiu, C., Miller, M. C., Monahan, R., Osgood, D. P., Stopa, E. G., and Silverberg, G. D. (2015). P-glycoprotein expression and amyloid accumulation in human aging and Alzheimer's disease: preliminary observations. *Neurobiol. Aging* 36, 2475–2482. doi: 10.1016/j.neurobiolaging.2015.05.020

Chow, B. W., and Gu, C. (2015). The molecular constituents of the blood-brain barrier. *Trends Neurosci.* 38, 598–608. doi: 10.1016/j.tins.2015.08.003

Clancy, U., Gilmartin, D., Jochems, A. C. C., Knox, L., Doubal, F. N., and Wardlaw, J. M. (2021). Neuropsychiatric symptoms associated with cerebral small vessel disease: a systematic review and meta-analysis. *Lancet Psychiatry* 8, 225–236. doi: 10.1016/S2215-0366(20)30431-4

Clifton, N. E., Hannon, E., Harwood, J. C., Di Florio, A., Thomas, K. L., Holmans, P. A., et al. (2019). Dynamic expression of genes associated with schizophrenia and bipolar disorder across development. *Transl. Psychiatry* 9:74. doi: 10.1038/s41398-019-0405-x

Coelho-Santos, V., and Shih, A. Y. (2020). Postnatal development of cerebrovascular structure and the neurogliovascular unit. *Wiley Interdiscip. Rev. Dev. Biol.* 9:e363. doi: 10.1002/wdev.363

Connolly, A. M., Chez, M. G., Pestronk, A., Arnold, S. T., Mehta, S., and Deuel, R. K. (1999). Serum autoantibodies to brain in Landau-Kleffner variant, autism, and other neurologic disorders. *J. Pediatr.* 134, 607–613. doi: 10.1016/s0022-3476(99)70248-9

Cortes-Canteli, M., Kruyer, A., Fernandez-Nueda, I., Marcos-Diaz, A., Ceron, C., Richards, A. T., et al. (2019). Long-Term dabigatran treatment delays Alzheimer's disease pathogenesis in the tgcrnd8 mouse model. *J. Am. Coll. Cardiol.* 74, 1910–1923. doi: 10.1016/j.jacc.2019.07.081

Cramer, S. P., Simonsen, H., Frederiksen, J. L., Rostrup, E., and Larsson, H. B. (2014). Abnormal blood-brain barrier permeability in normal appearing white matter in multiple sclerosis investigated by MRI. *Neuroimage Clin.* 4, 182–189. doi: 10.1016/j.nicl.2013.12.001

Crockett, A. M., Ryan, S. K., Vasquez, A. H., Canning, C., Kanyuch, N., Kebir, H., et al. (2021). Disruption of the blood-brain barrier in 22q11.2 deletion syndrome. *Brain* 144, 1351–1360. doi: 10.1093/brain/awab055

Cruz Hernandez, J. C., Bracko, O., Kersbergen, C. J., Muse, V., Haft-Javaherian, M., Berg, M., et al. (2019). Neutrophil adhesion in brain capillaries reduces cortical blood flow and impairs memory function in Alzheimer's disease mouse models. *Nat. Neurosci.* 22, 413–420. doi: 10.1038/s41593-018-0329-4

Császár, E., Lénárt, N., Cserép, C., Környei, Z., Fekete, R., Pósfai, B., et al. (2021). Microglia control cerebral blood flow and neurovascular coupling via P2Y12R-mediated actions. *bioRXiv* [Preprint] doi: 10.1101/2021.02.04.429741

Cvetanovic, M., Patel, J. M., Marti, H. H., Kini, A. R., and Opal, P. (2011). Vascular endothelial growth factor ameliorates the ataxic phenotype in a mouse model of spinocerebellar ataxia type 1 [Research Support, N.I.H., Extramural Research Support, Non-U.S. Gov't]. *Nat. Med.* 17, 1445–1447. doi: 10.1038/nm.2494

Czako, C., Kovacs, T., Ungvari, Z., Csiszar, A., Yabluchanskiy, A., Conley, S., et al. (2020). Retinal biomarkers for Alzheimer's disease and vascular cognitive impairment and dementia (VCID): implication for early diagnosis and prognosis. *Geroscience* 42, 1499–1525. doi: 10.1007/s11357-020-00252-7

D'Haeseleer, M., Beelen, R., Fierens, Y., Cambron, M., Vanbinst, A. M., Verborgh, C., et al. (2013). Cerebral hypoperfusion in multiple sclerosis is reversible and mediated by endothelin-1. *Proc. Natl. Acad. Sci. U.S.A.* 110, 5654–5658. doi: 10.1073/pnas.1222560110

D'Haeseleer, M., Cambron, M., Vanopdenbosch, L., and De Keyser, J. (2011). Vascular aspects of multiple sclerosis. *Lancet Neurol.* 10, 657–666. doi: 10.1016/s1474-4422(11)70105-3

Dabertrand, F., Harraz, O. F., Masayo, K., Longden, T. A., Rosehart, A. C., Hill-Eubanks, D., et al. (2021). PIP 2 corrects cerebral blood flow deficits in small vessel disease by rescuing capillary Kir2.1 activity. *Proc. Natl. Acad. Sci. U.S.A.* 118:e2025998118. doi: 10.1073/pnas.2025998118

Daneman, R. (2012). The blood–brain barrier in health and disease. *Ann. Neurol.* 72, 648–672. doi: 10.1002/ana.23648

Daneman, R., Agalliu, D., Zhou, L., Kuhnert, F., Kuo, C., and Barres, B. (2009). Wnt/ -catenin signaling is required for CNS, but not non-CNS, angiogenesis. *Proc. Natl. Acad. Sci. U.S.A.* 106, 641–646.

Daneman, R., and Prat, A. (2015). The blood-brain barrier. *Cold Spring Harb. Perspect. Biol.* 7:a020412. doi: 10.1101/cshperspect.a020412

Davenport, C. B. (1915). Huntington's Chorea in relation to heredity and eugenics. *Proc. Natl. Acad. Sci. U.S.A.* 1, 283–285.

Davis, J., Xu, F., Deane, R., Romanov, G., Previti, M. L., Zeigler, K., et al. (2004). Early-onset and robust cerebral microvascular accumulation of amyloid beta-protein in transgenic mice expressing low levels of a vasculotropic Dutch/Iowa mutant form of amyloid beta-protein precursor. *J. Biol. Chem.* 279, 20296–20306. doi: 10.1074/jbc.M312946200

De Filippis, L., and Delia, D. (2011). Hypoxia in the regulation of neural stem cells. *Cell. Mol. Life Sci.* 68, 2831–2844. doi: 10.1007/s00018-011-0723-5

De Keyser, J., Wilczak, N., Leta, R., and Streetland, C. (1999). Astrocytes in multiple sclerosis lack beta-2 adrenergic receptors. *Neurology* 53, 1628–1633. doi: 10.1212/WNL.53.8.1628

De Silva, T. M., and Faraci, F. M. (2016). Microvascular dysfunction and cognitive impairment. *Cell. Mol. Neurobiol.* 36, 241–258. doi: 10.1007/s10571-015-0308-1

Deane, R., Wu, Z., Sagare, A., Davis, J., Du Yan, S., Hamm, K., et al. (2004). LRP/amyloid beta-peptide interaction mediates differential brain efflux of Abeta isoforms. *Neuron* 43, 333–344. doi: 10.1016/j.neuron.2004.07.017

Deckel, A. W., and Duffy, J. D. (2000). Vasomotor hyporeactivity in the anterior cerebral artery during motor activation in Huntington's disease patients. *Brain Res.* 872, 258–261. doi: 10.1016/S0006-8993(00)02506-3

Deckel, A. W., Weiner, R., Szigeti, D., Claark, V., and Vento, J. (2000). Altered patterns of regional cerebral blood flow in patients with Huntington's disease: a SPECT study during rest and cognitive or motor activation. *J. Nucl. Med.* 41, 773–780.

Delgado, A. C., Ferron, S. R., Vicente, D., Porlan, E., Perez-Villalba, A., Trujillo, C. M., et al. (2014). Endothelial NT-3 delivered by vasculature and CSF promotes quiescence of subependymal neural stem cells through nitric oxide induction. *Neuron* 83, 572–585. doi: 10.1016/j.neuron.2014.06.015

Derejko, M., Sławek, J., Wieczorek, D., Brockhuis, B., Dubaniewicz, M., and Lass, P. (2006). Regional cerebral blood flow in Parkinson's disease as an indicator of cognitive impairment. *Nucl. Med. Commun.* 27, 945–951. doi: 10.1097/01.mnm.0000243370.18883.62

Di Pardo, A., Amico, E., Scalabri, F., Pepe, G., Castaldo, S., Elifani, F., et al. (2017). Impairment of blood-brain barrier is an early event in R6/2 mouse model of Huntington Disease. *Sci. Rep.* 7:41316. doi: 10.1038/srep41316

Dietrich, H. H., Xiang, C., Han, B. H., Zipfel, G. J., and Holtzman, D. M. (2010). Soluble amyloid-beta, effect on cerebral arteriolar regulation and vascular cells. *Mol. Neurodegener.* 5:15. doi: 10.1186/1750-1326-5-15

Dobson, R., and Giovannoni, G. (2019). Multiple sclerosis – a review. *Eur. J. Neurol.* 26, 27–40. doi: 10.1111/ene.13819

Donahue, J. E., Flaherty, S. L., Johanson, C. E., Duncan, J. A. III, Silverberg, G. D., Miller, M. C., et al. (2006). RAGE, LRP-1, and amyloid-beta protein in Alzheimer's disease. *Acta Neuropathol.* 112, 405–415. doi: 10.1007/s00401-006-0115-3

Drazanova, E., Ruda-Kucerova, J., Kratka, L., Stark, T., Kuchar, M., Maryska, M., et al. (2019). Different effects of prenatal MAM vs. perinatal THC exposure on regional cerebral blood perfusion detected by Arterial Spin Labelling MRI in rats. *Sci. Rep.* 9:6062. doi: 10.1038/s41598-019-42532-z

Drouin-Ouellet, J., Sawiak, S. J., Cisbani, G., Lagace, M., Kuan, W. L., Saint-Pierre, M., et al. (2015). Cerebrovascular and blood-brain barrier impairments in Huntington's disease: potential implications for its pathophysiology. *Ann. Neurol.* 78, 160–177. doi: 10.1002/ana.24406

Dudek, K. A., Dion-Albert, L., Lebel, M., LeClair, K., Labrecque, S., Tuck, E., et al. (2020). Molecular adaptations of the blood-brain barrier promote stress resilience vs. depression. *Proc. Natl. Acad. Sci. U.S.A.* 117, 3326–3336. doi: 10.1073/pnas.1914655117

Dumas, A., Dierksen, G. A., Gurol, M. E., Halpin, A., Martinez-Ramirez, S., Schwab, K., et al. (2012). Functional magnetic resonance imaging detection of vascular reactivity in cerebral amyloid angiopathy. *Ann. Neurol.* 72, 76–81. doi: 10.1002/ana.23566

Elabi, O., Gaceb, A., Carlsson, R., Padel, T., Soylu-Kucharz, R., Cortijo, I., et al. (2021). Human alpha-synuclein overexpression in a mouse model of Parkinson's disease leads to vascular pathology, blood brain barrier leakage and pericyte activation. *Sci. Rep.* 11:1120. doi: 10.1038/s41598-020-80889-8

Ellingrod, V. L., Taylor, S. F., Brook, R. D., Evans, S. J., Zollner, S. K., Grove, T. B., et al. (2011). Dietary, lifestyle and pharmacogenetic factors associated with arteriole endothelial-dependent vasodilatation in schizophrenia patients treated with atypical antipsychotics (AAPs). *Schizophr. Res.* 130, 20–26. doi: 10.1016/j.schres.2011.03.031

Emerich, D. F., Mooney, D. J., Storrie, H., Babu, R. S., and Kordower, J. H. (2010). Injectable hydrogels providing sustained delivery of vascular endothelial growth factor are neuroprotective in a rat model of Huntington's disease. *Neurotox. Res.* 17, 66–74. doi: 10.1007/s12640-009-9079-0

Emerson, R. W., Adams, C., Nishino, T., Hazlett, H. C., Wolff, J. J., Zwaigenbaum, L., et al. (2017). Functional neuroimaging of high-risk 6-month-old infants predicts a diagnosis of autism at 24 months of age. *Sci. Transl. Med.* 9:eaag2882. doi: 10.1126/scitranslmed.aag2882

Farkas, E., De Jong, G. I., de Vos Ernst, R. A. I., Steur, J. N. H., and Luiten, P. G. M. (2000). Pathological features of cerebral cortical capillaries are doubled in Alzheimer's disease and Parkinson's disease. *Acta Neuropathol.* 100, 395–402. doi: 10.1007/s004010000195

Farkas, E., and Luiten, P. G. (2001). Cerebral microvascular pathology in aging and Alzheimer's disease [Review]. *Prog. Neurobiol.* 64, 575–611.

Faucheux, B. A., Agid, Y., Hirsch, E. C., and Bonnet, A.-M. (1999). Blood vessels change in the mesencephalon of patients with Parkinson's disease. *Lancet* 353, 981–982. doi: 10.1016/s0140-6736(99)00641-8

Feigin, A., Ghilardi, M. F., Huang, C., Ma, Y., Carbon, M., Guttman, M., et al. (2006). Preclinical Huntington's disease: compensatory brain responses during learning. *Ann. Neurol.* 59, 53–59. doi: 10.1002/ana.20684

Fernandez-Klett, F., and Priller, J. (2015). Diverse functions of pericytes in cerebral blood flow regulation and ischemia. *J. Cereb. Blood Flow Metab.* 35, 883–887. doi: 10.1038/jcbfm.2015.60

Fernandez-Seara, M. A., Mengual, E., Vidorreta, M., Aznarez-Sanado, M., Loayza, F. R., Villagra, F., et al. (2012). Cortical hypoperfusion in Parkinson's disease assessed using arterial spin labeled perfusion MRI. *Neuroimage* 59, 2743–2750. doi: 10.1016/j.neuroimage.2011.10.033

Filosa, J. A., and Iddings, J. A. (2013). Astrocyte regulation of cerebral vascular tone. *Am. J. Physiol. Heart Circ. Physiol.* 305, H609–H619. doi: 10.1152/ajpheart.00359.2013

Finnerty, N. J., Bolger, F. B., Palsson, E., and Lowry, J. P. (2013). An investigation of hypofrontality in an animal model of schizophrenia using real-time microelectrochemical sensors for glucose, oxygen, and nitric oxide. *ACS Chem. Neurosci.* 4, 825–831. doi: 10.1021/cn4000567

Fiorentino, M., Sapone, A., Senger, S., Camhi, S. S., Kadzielski, S. M., Buie, T. M., et al. (2016). Blood-brain barrier and intestinal epithelial barrier alterations in autism spectrum disorders. *Mol. Autism* 7:49. doi: 10.1186/s13229-016-0110-z

Ford, J. M., Johnson, M. B., Whitfield, S. L., Faustman, W. O., and Mathalon, D. H. (2005). Delayed hemodynamic responses in schizophrenia. *Neuroimage* 26, 922–931. doi: 10.1016/j.neuroimage.2005.03.001

Ford, J. M., Roth, W. T., Menon, V., and Pfefferbaum, A. (1999). Failures of automatic and strategic processing in schizophrenia: comparisons of event-related brain potential and startle blink modification. *Schizophr. Res.* 37, 149–163. doi: 10.1016/s0920-9964(98)00148-0

Friedland, R. P., and Iadecola, C. (1991). Roy and Sherrington (1890): a centennial reexamination of "On the regulation of the blood-supply of the brain". *Neurology* 41, 10–14. doi: 10.1212/wnl.41.1.10

Frosen, J., and Joutel, A. (2018). Smooth muscle cells of intracranial vessels: from development to disease. *Cardiovasc. Res.* 114, 501–512. doi: 10.1093/cvr/cvy002

Fujiki, R., Morita, K., Sato, M., Kamada, Y., Kato, Y., Inoue, M., et al. (2013). Reduced prefrontal cortex activation using the Trail Making Test in schizophrenia. *Neuropsychiatr. Dis. Treat.* 9, 675–685. doi: 10.2147/NDT.S43137

Ge, Y., Law, M., Johnson, G., Herbert, J., Babb, J. S., Mannon, L. J., et al. (2005). Dynamic susceptibility contrast perfusion MR imaging of multiple sclerosis lesions: characterizing hemodynamic impairment and inflammatory activity. *AJNR Am. J. Neuroradiol.* 26, 1539–1547.

Geraldes, R., Esiri, M. M., Perera, R., Yee, S. A., Jenkins, D., Palace, J., et al. (2020). Vascular disease and multiple sclerosis: a post-mortem study exploring their relationships. *Brain* 143, 2998–3012. doi: 10.1093/brain/awaa255

Gireud-Goss, M., Mack, A. F., McCullough, L. D., and Urayama, A. (2020). Cerebral amyloid angiopathy and blood-brain barrier dysfunction. *Neuroscientist* doi: 10.1177/1073858420954811 [Epub ahead of print].

Girolamo, F., Coppola, C., Ribatti, D., and Trojano, M. (2014). Angiogenesis in multiple sclerosis and experimental autoimmune encephalomyelitis. *Acta Neuropathol. Commun.* 2:84. doi: 10.1186/s40478-014-0084-z

Girouard, H., and Iadecola, C. (2006). Neurovascular coupling in the normal brain and in hypertension, stroke, and Alzheimer disease. *J. Appl. Physiol. (1985)* 100, 328–335. doi: 10.1152/japplphysiol.00966.2005

Gitler, A. D., Dhillon, P., and Shorter, J. (2017). Neurodegenerative disease: models, mechanisms, and a new hope. *Dis. Model. Mech.* 10, 499–502. doi: 10.1242/dmm.030205

Gogtay, N., Vyas, N. S., Testa, R., Wood, S. J., and Pantelis, C. (2011). Age of onset of schizophrenia: perspectives from structural neuroimaging studies. *Schizophr. Bull.* 37, 504–513. doi: 10.1093/schbul/sbr030

Goldman, S. A., and Chen, Z. (2011). Perivascular instruction of cell genesis and fate in the adult brain. *Nat. Neurosci.* 14, 1382–1389. doi: 10.1038/nn.2963

Gorelick, P. B. (2004). Risk factors for vascular dementia and Alzheimer disease. *Stroke* 35(11 Suppl. 1), 2620–2622.

Gotz, J., and Ittner, L. M. (2008). Animal models of Alzheimer's disease and frontotemporal dementia. *Nat. Rev. Neurosci.* 9, 532–544.

Graham, N. S., and Sharp, D. J. (2019). Understanding neurodegeneration after traumatic brain injury: from mechanisms to clinical trials in dementia. *J. Neurol. Neurosurg. Psychiatry* 90, 1221–1233. doi: 10.1136/jnnp-2017-317557

Grammas, P. (2011). Neurovascular dysfunction, inflammation and endothelial activation: implications for the pathogenesis of Alzheimer's disease. *J. Neuroinflammation* 8:26. doi: 10.1186/1742-2094-8-26

Grant, R. I., Hartmann, D. A., Underly, R. G., Berthiaume, A. A., Bhat, N. R., and Shih, A. Y. (2019). Organizational hierarchy and structural diversity of microvascular pericytes in adult mouse cortex. *J. Cereb. Blood Flow Metab.* 39, 411–425. doi: 10.1177/0271678X17732229

Gray, M. T., and Woulfe, J. M. (2015). Striatal blood-brain barrier permeability in Parkinson's disease. *J. Cereb. Blood Flow Metab.* 35, 747–750. doi: 10.1038/jcbfm.2015.32

Greene, C., Kealy, J., Humphries, M. M., Gong, Y., Hou, J., Hudson, N., et al. (2018). Dose-dependent expression of claudin-5 is a modifying factor in schizophrenia. *Mol. Psychiatry* 23, 2156–2166. doi: 10.1038/mp.2017.156

Grove, T., Taylor, S., Dalack, G., and Ellingrod, V. (2015). Endothelial function, folate pharmacogenomics, and neurocognition in psychotic disorders. *Schizophr. Res.* 164, 115–121. doi: 10.1016/j.schres.2015.02.006

Grubb, S., Lauritzen, M., and Aalkjaer, C. (2021). Brain capillary pericytes and neurovascular coupling. *Comp. Biochem. Physiol. A Mol. Integr. Physiol.* 254:110893. doi: 10.1016/j.cbpa.2020.110893

Grunewald, M., Kumar, S., Sharife, H., Volinsky, E., Gileles-Hillel, A., Licht, T., et al. (2021). Counteracting age-related VEGF signaling insufficiency promotes healthy aging and extends life span. *Science* 373:eabc8479. doi: 10.1126/science.abc8479

Gu, C., Yoshida, Y., Livet, J., Reimert, D., Mann, F., Merte, J., et al. (2005). Semaphorin 3E and Plexin-D1 control vascular pattern independently of neuropilins. *Science* 307, 265–268. doi: 10.1126/science.1105416

Guan, J., Pavlovic, D., Dalkie, N., Waldvogel, H., O'Carroll, S. J., Green, C. R., et al. (2013). Vascular degeneration in Parkinson's disease. *Brain Pathol.* 23, 154–164. doi: 10.1111/j.1750-3639.2012.00628.x

Guo, Y., Li, X., Zhang, M., Chen, N., Wu, S., Lei, J., et al. (2019). Age and brain regionassociated alterations of cerebral blood flow in early Alzheimer's disease assessed in AbetaPPSWE/PS1DeltaE9 transgenic mice using arterial spin labeling. *Mol. Med. Rep.* 19, 3045–3052. doi: 10.3892/mmr.2019.9950

Guo, Y., Singh, L. N., Zhu, Y., Gur, R. E., Resnick, A., Anderson, S. A., et al. (2020). Association of a functional Claudin-5 variant with schizophrenia in female patients with the 22q11.2 deletion syndrome. *Schizophr. Res.* 215, 451–452. doi: 10.1016/j.schres.2019.09.014

Gur, R. E., Bassett, A. S., McDonald-McGinn, D. M., Bearden, C. E., Chow, E., Emanuel, B. S., et al. (2017). A neurogenetic model for the study of schizophrenia spectrum disorders: the International 22q11.2 Deletion Syndrome Brain Behavior Consortium. *Mol. Psychiatry* 22, 1664–1672. doi: 10.1038/mp.2017.161

Ha, A. D., and Fung, V. S. (2012). Huntington's disease. *Curr. Opin. Neurol.* 25, 491–498. doi: 10.1097/WCO.0b013e3283550c97

Haidey, J. N., Peringod, G., Institoris, A., Gorzo, K. A., Nicola, W., Vandal, M., et al. (2021). Astrocytes regulate ultra-slow arteriole oscillations via stretch-mediated TRPV4-COX-1 feedback. *Cell Rep.* 36:109405. doi: 10.1016/j.celrep.2021.109405

Hakim, A. M. (2019). Small vessel disease. *Front. Neurol.* 10:1020. doi: 10.3389/fneur.2019.01020

Halliday, M. R., Rege, S. V., Ma, Q., Zhao, Z., Miller, C. A., Winkler, E. A., et al. (2016). Accelerated pericyte degeneration and blood-brain barrier breakdown in apolipoprotein E4 carriers with Alzheimer's disease. *J. Cereb. Blood Flow Metab.* 36, 216–227. doi: 10.1038/jcbfm.2015.44

Hamel, E. (2006). Perivascular nerves and the regulation of cerebrovascular tone. *J. Appl. Physiol.* 100, 1059–1064. doi: 10.1152/japplphysiol.00954.2005

Hamel, E. (2015). Cerebral circulation function and dysfunction in Alzheimer's disease. *J. Cardiovasc. Pharmacol.* 65, 317–324. doi: 10.1097/FJC.0000000000000177

Hanlon, F. M., Shaff, N. A., Dodd, A. B., Ling, J. M., Bustillo, J. R., Abbott, C. C., et al. (2016). Hemodynamic response function abnormalities in schizophrenia during a multisensory detection task. *Hum. Brain Mapp.* 37, 745–755. doi: 10.1002/hbm.23063

Harada, K., Kamiya, T., and Tsuboi, T. (2015). Gliotransmitter release from astrocytes: functional, developmental, and pathological implications in the brain. *Front. Neurosci.* 9:499. doi: 10.3389/fnins.2015.00499

Harbo, H. F., Gold, R., and Tintore, M. (2013). Sex and gender issues in multiple sclerosis. *Ther. Adv. Neurol. Disord.* 6, 237–248. doi: 10.1177/1756285613488434

Harris, G. J., Codoris, A. M., Lewis, R. F., Schmidt, E., Bedi, A., and Brandt, J. (1999). Reduced basal ganglia blood flow and volume in pre-sympotmatic, gene-tested persons at-risk for Huntington's disease. *Brain* 122, 1667–1678. doi: 10.1093/brain/122.9.1667

Hartmann, D. A., Berthiaume, A. A., Grant, R. I., Harrill, S. A., Koski, T., Tieu, T., et al. (2021). Brain capillary pericytes exert a substantial but slow influence on blood flow. *Nat. Neurosci.* 24, 633–645. doi: 10.1038/s41593-020-00793-2

Hartz, A. M., Bauer, B., Soldner, E. L., Wolf, A., Boy, S., Backhaus, R., et al. (2012). Amyloid-beta contributes to blood-brain barrier leakage in transgenic human amyloid precursor protein mice and in humans with cerebral amyloid angiopathy. *Stroke* 43, 514–523. doi: 10.1161/STROKEAHA.111.627562

Hasselbalch, S. G., Øberg, G., Sørensen, S. A., Andersen, A. R., Waldemar, G., Schmidt, J. F., et al. (1992). Reduced regional cerebral blood flow in Huntington's disease studied by SPECT. *J. Neurol. Neurosurg. Psychiatry* 55, 1018–1023. doi: 10.1136/jnnp.55.11.1018

Hays, C. C., Zlatar, Z. Z., and Wierenga, C. E. (2016). The utility of cerebral blood flow as a biomarker of preclinical Alzheimer's disease. *Cell. Mol. Neurobiol.* 36, 167–179. doi: 10.1007/s10571-015-0261-z

Hijaz, B. A., and Volpicelli-Daley, L. A. (2020). Initiation and propagation of alpha-synuclein aggregation in the nervous system. *Mol. Neurodegener.* 15:19. doi: 10.1186/s13024-020-00368-6

Hillman, E. M. (2014). Coupling mechanism and significance of the BOLD signal: a status report. *Annu. Rev. Neurosci.* 37, 161–181. doi: 10.1146/annurev-neuro-071013-014111

Hindle, J. V. (2010). Ageing, neurodegeneration and Parkinson's disease. *Age Ageing* 39, 156–161. doi: 10.1093/ageing/afp223

Hino, M., Kunii, Y., Matsumoto, J., Wada, A., Nagaoka, A., Niwa, S., et al. (2016). Decreased VEGFR2 expression and increased phosphorylated Akt1 in the prefrontal cortex of individuals with schizophrenia. *J. Psychiatry Res.* 82, 100–108. doi: 10.1016/j.jpsychires.2016.07.018

Hogan, K. A., Ambler, C. A., Chapman, D. L., and Bautch, V. L. (2004). The neural tube patterns vessels developmentally using the VEGF signaling pathway. *Development* 131, 1503–1513. doi: 10.1242/dev.01039

Holley, J. E., Newcombe, J., Whatmore, J. L., and Gutowski, N. J. (2010). Increased blood vessel density and endothelial cell proliferation in multiple sclerosis cerebral white matter. *Neurosci. Lett.* 470, 65–70. doi: 10.1016/j.neulet.2009.12.059

Horev, G., Ellegood, J., Lerch, J. P., Son, Y. E., Muthuswamy, L., Vogel, H., et al. (2011). Dosage-dependent phenotypes in models of 16p11.2 lesions found in autism. *Proc. Natl. Acad. Sci. U.S.A.* 108, 17076–17081. doi: 10.1073/pnas.1114042108

Horn, H., Federspiel, A., Wirth, M., Muller, T. J., Wiest, R., Wang, J. J., et al. (2009). Structural and metabolic changes in language areas linked to formal thought disorder. *Br. J. Psychiatry* 194, 130–138. doi: 10.1192/bjp.bp.107.045633

Hostenbach, S., Pauwels, A., Michiels, V., Raeymaekers, H., Van Binst, A. M., Van Merhaeghen-Wieleman, A., et al. (2019). Role of cerebral hypoperfusion in multiple sclerosis (ROCHIMS): study protocol for a proof-of-concept randomized controlled trial with bosentan. *Trials* 20:164. doi: 10.1186/s13063-019-3252-4

Howarth, C. (2014). The contribution of astrocytes to the regulation of cerebral blood flow. *Front. Neurosci.* 8:103. doi: 10.3389/fnins.2014.00103

Howarth, C., Mishra, A., and Hall, C. N. (2021). More than just summed neuronal activity: how multiple cell types shape the BOLD response. *Philos. Trans. R. Soc. Lond. B Biol. Sci.* 376:20190630. doi: 10.1098/rstb.2019.0630

Howe, M. D., McCullough, L. D., and Urayama, A. (2020). The role of basement membranes in cerebral amyloid angiopathy. *Front. Physiol.* 11:601320. doi: 10.3389/fphys.2020.601320

Hsia, A. Y., Masliah, E., McConlogue, L., Yu, G. Q., Tatsuno, G., Hu, K., et al. (1999). Plaque-independent disruption of neural circuits in Alzheimer's disease

mouse models [Research Support, Non-U.S. Gov't Research Support, U.S. Gov't, P.H.S.]. *Proc. Natl. Acad. Sci. U.S.A.* 96, 3228–3233.

Hsiao, H.-Y., Chen, Y.-C., Huang, C.-H., Chen, C.-C., Hsu, Y.-H., Chen, H.-M., et al. (2015). Aberrant astrocytes impair vascular reactivity in Huntington disease. *Ann. Neurol.* 78, 178–192. doi: 10.1002/ana.24428

Hua, J., Unschuld, P. G., Margolis, R. L., van Zijl, P. C., and Ross, C. A. (2014). Elevated arteriolar cerebral blood volume in prodromal Huntington's disease. *Mov. Disord.* 29, 396–401. doi: 10.1002/mds.25591

Huang, Z., Wong, L. W., Su, Y., Huang, X., Wang, N., Chen, H., et al. (2020). Blood-brain barrier integrity in the pathogenesis of Alzheimer's disease. *Front. Neuroendocrinol.* 59:100857. doi: 10.1016/j.yfrne.2020.100857

Hultman, K., Strickland, S., and Norris, E. H. (2013). The APOE varepsilon4/varepsilon4 genotype potentiates vascular fibrin(ogen) deposition in amyloid-laden vessels in the brains of Alzheimer's disease patients. *J. Cereb. Blood Flow Metab.* 33, 1251–1258. doi: 10.1038/jcbfm.2013.76

Humpel, C., and Marksteiner, J. (2005).). Cerebrovascular damage as a cause for Alzheimer's disease [Research Support, Non-U.S. Gov't Review]. *Curr. Neurovasc. Res.* 2, 341–347.

Huneau, C., Benali, H., and Chabriat, H. (2015). Investigating human neurovascular coupling using functional neuroimaging: a critical review of dynamic models. *Front. Neurosci.* 9:467. doi: 10.3389/fnins.2015.00467

Iadecola, C. (2004). Neurovascular regulation in the normal brain and in Alzheimer's disease. *Nat. Rev. Neurosci.* 5, 347–360. doi: 10.1038/nrn1387

Iadecola, C. (2013). The pathobiology of vascular dementia. *Neuron* 80, 844–866. doi: 10.1016/j.neuron.2013.10.008

Impellizzeri, D., Campolo, M., Bruschetta, G., Crupi, R., Cordaro, M., Paterniti, I., et al. (2016). Traumatic brain injury leads to development of Parkinson's disease related pathology in mice. *Front. Neurosci.* 10:458. doi: 10.3389/fnins.2016.00458

Incalza, M. A., D'Oria, R., Natalicchio, A., Perrini, S., Laviola, L., and Giorgino, F. (2018). Oxidative stress and reactive oxygen species in endothelial dysfunction associated with cardiovascular and metabolic diseases. *Vascul. Pharmacol.* 100, 1–19. doi: 10.1016/j.vph.2017.05.005

Iturria-Medina, Y., Sotero, R. C., Toussaint, P. J., Mateos-Perez, J. M., Evans, A. C., and Alzheimer's Disease Neuroimaging Initiative (2016). Early role of vascular dysregulation on late-onset Alzheimer's disease based on multifactorial data-driven analysis. *Nat. Commun.* 7:11934. doi: 10.1038/ncomms11934

James, J. M., Gewolb, C., and Bautch, V. L. (2009). Neurovascular development uses VEGF-A signaling to regulate blood vessel ingression into the neural tube. *Development* 136, 833–841. doi: 10.1242/dev.028845

Jann, K., Hernandez, L. M., Beck-Pancer, D., McCarron, R., Smith, R. X., Dapretto, M., et al. (2015). Altered resting perfusion and functional connectivity of default mode network in youth with autism spectrum disorder. *Brain Behav.* 5:e00358. doi: 10.1002/brb3.358

Juurlink, B. H. (2013). The evidence for hypoperfusion as a factor in multiple sclerosis lesion development. *Mult. Scler. Int.* 2013:598093. doi: 10.1155/2013/598093

Kadry, H., Noorani, B., and Cucullo, L. (2020). A blood-brain barrier overview on structure, function, impairment, and biomarkers of integrity. *Fluids Barriers CNS* 17:69. doi: 10.1186/s12987-020-00230-3

Kalaria, R. N. (1996). Cerebral vessels in ageing and Alzheimer's disease [Research Support, Non-U.S. Gov't Research Support, U.S. Gov't, P.H.S. Review]. *Pharmacol. Ther.* 72, 193–214.

Kalaria, R. N., and Harik, S. I. (1989). Reduced glucose transporter at the blood-brain barrier and in cerebral cortex in Alzheimer disease. *J. Neurochem.* 53, 1083–1088. doi: 10.1111/j.1471-4159.1989.tb07399.x

Kalinderi, K., Bostantjopoulou, S., and Fidani, L. (2016). The genetic background of Parkinson's disease: current progress and future prospects. *Acta Neurol. Scand.* 134, 314–326. doi: 10.1111/ane.12563

Kamagata, K., Motoi, Y., Hori, M., Suzuki, M., Nakanishi, A., Shimoji, K., et al. (2011). Posterior hypoperfusion in Parkinson's disease with and without dementia measured with arterial spin labeling MRI. *J. Magn. Reson. Imaging* 33, 803–807. doi: 10.1002/jmri.22515

Kamphuis, W. W., Derada Troletti, C., Reijerkerk, A., Romero, I. A., and de Vries, H. E. (2015). The blood-brain barrier in multiple sclerosis: microRNAs as key regulators. *CNS Neurol. Disord. Drug Targets* 14, 157–167. doi: 10.2174/1871527314666150116125246

Kaplan, L., Chow, B. W., and Gu, C. (2020). Neuronal regulation of the blood-brain barrier and neurovascular coupling. *Nat. Rev. Neurosci.* 21, 416–432. doi: 10.1038/s41583-020-0322-2

Kawakami, K., Wake, R., Miyaoka, T., Furuya, M., Liaury, K., and Horiguchi, J. (2014). The effects of aging on changes in regional cerebral blood flow in schizophrenia. *Neuropsychobiology* 69, 202–209. doi: 10.1159/000358840

Kawakubo, Y., Kuwabara, H., Watanabe, K., Minowa, M., Someya, T., Minowa, I., et al. (2009). Impaired prefrontal hemodynamic maturation in autism and unaffected siblings. *PLoS One* 4:e6881. doi: 10.1371/journal.pone.0006881

Kealy, J., Greene, C., and Campbell, M. (2020). Blood-brain barrier regulation in psychiatric disorders. *Neurosci. Lett.* 726:133664. doi: 10.1016/j.neulet.2018.06.033

Keefe, R. S. E., and Harvey, P. D. (2012). *Cognitive Impairment in Schizophrenia*, Vol. 213. Berlin: Springer, doi: 10.1007/978-3-642-25758-2_2

Kelleher, R. J., and Soiza, R. L. (2013). Evidence of endothelial dysfunction in the development of Alzheimer's disease: Is Alzheimer's a vascular disorder? *Am. J. Cardiovasc. Dis.* 3, 197–226.

Khandaker, G. M., Cousins, L., Deakin, J., Lennox, B. R., Yolken, R., and Jones, P. B. (2015). Inflammation and immunity in schizophrenia: implications for pathophysiology and treatment. *Lancet Psychiatry* 2, 258–270. doi: 10.1016/s2215-0366(14)00122-9

Kirk, J., Plumb, J., Mirakhur, M., and McQuaid, S. (2003). Tight junctional abnormality in multiple sclerosis white matter affects all calibres of vessel and is associated with blood–brain barrier leakage and active demyelination. *J. Pathol.* 201, 319–327. doi: 10.1002/path.1434

Kisler, K., Nelson, A. R., Montagne, A., and Zlokovic, B. V. (2017). Cerebral blood flow regulation and neurovascular dysfunction in Alzheimer disease. *Nat. Rev. Neurosci.* 18, 419–434. doi: 10.1038/nrn.2017.48

Kisler, K., Nelson, A. R., Rege, S. V., Ramanathan, A., Wang, Y., Ahuja, A., et al. (2016). Pericyte degeneration leads to neurovascular uncoupling and limits oxygen supply to brain. *Nat. Neurosci.* 20, 406–420. doi: 10.1038/nn.4489A

Klein, C., and Westenberger, A. (2012). Genetics of Parkinson's disease. *Cold Spring Harb. Perspect. Med.* 2:a008888. doi: 10.1101/cshperspect.a008888

Klinkmueller, P., Kronenbuerger, M., Miao, X., Bang, J., Ultz, K. E., Paez, A., et al. (2021). Impaired response of cerebral oxygen metabolism to visual stimulation in Huntington's disease. *J. Cereb. Blood Flow Metab.* 41, 1119–1130. doi: 10.1177/0271678X20949286

Knight, M. J., and Baune, B. T. (2017). Psychosocial dysfunction in major depressive disorder-rationale, design, and characteristics of the cognitive and emotional recovery training program for depression (CERT-D). *Front. Psychiatry* 8:280. doi: 10.3389/fpsyt.2017.00280

Kochunov, P., Zavaliangos-Petropulu, A., Jahanshad, N., Thompson, P. M., Ryan, M. C., Chiappelli, J., et al. (2021). A white matter connection of schizophrenia and Alzheimer's disease. *Schizophr. Bull.* 47, 197–206. doi: 10.1093/schbul/sbaa078

Kook, S. Y., Hong, H. S., Moon, M., Ha, C. M., Chang, S., and Mook-Jung, I. (2012). Abeta(1)(-)(4)(2)-RAGE interaction disrupts tight junctions of the blood-brain barrier via Ca(2)(+)-calcineurin signaling. *J. Neurosci.* 32, 8845–8854. doi: 10.1523/JNEUROSCI.6102-11.2012

Korte, N., Nortley, R., and Attwell, D. (2020). Cerebral blood flow decrease as an early pathological mechanism in Alzheimer's disease. *Acta Neuropathol.* 140, 793–810. doi: 10.1007/s00401-020-02215-w

Kortekaas, R., Leenders, K. L., van Oostrom, J. C. H., Vaalburg, W., Bart, J., Willemsen, A. T. M., et al. (2005). Blood–brain barrier dysfunction in parkinsonian midbrain in vivo. *Ann. Neurol.* 57, 176–179. doi: 10.1002/ana.20369

Kostiukow, A., and Samborski, W. (2020). The effectiveness of hyperbaric oxygen therapy (HBOT) in children with autism spectrum disorders. *Pol. Merkur. Lekarski.* 48, 15–18.

Kounidas, G., Cruickshank, H., Kastora, S., Sihlabela, S., and Miedzybrodzka, Z. (2021). The known burden of Huntington disease in the North of Scotland: prevalence of manifest and identified pre-symptomatic gene expansion carriers in the molecular era. *J. Neurol.* doi: 10.1007/s00415-021-10505-w

Kozberg, M. G., Ma, Y., Shaik, M. A., Kim, S. H., and Hillman, E. M. (2016). Rapid postnatal expansion of neural networks occurs in an environment of altered neurovascular and neurometabolic coupling. *J. Neurosci.* 36, 6704–6717. doi: 10.1523/JNEUROSCI.2363-15.2016

Kuan, W. L., Bennett, N., He, X., Skepper, J. N., Martynyuk, N., Wijeyekoon, R., et al. (2016). α-Synuclein pre-formed fibrils impair tight junction protein expression without affecting cerebral endothelial cell function. *Exp. Neurol.* 285(Pt A), 72–81. doi: 10.1016/j.expneurol.2016.09.003

Kumar, H., and Sharma, B. (2016). Memantine ameliorates autistic behavior, biochemistry & blood brain barrier impairments in rats. *Brain Res. Bull.* 124, 27–39. doi: 10.1016/j.brainresbull.2016.03.013

Kumar, H., Sharma, B. M., and Sharma, B. (2015). Benefits of agomelatine in behavioral, neurochemical and blood brain barrier alterations in prenatal valproic acid induced autism spectrum disorder. *Neurochem. Int.* 91, 34–45. doi: 10.1016/j.neuint.2015.10.007

Kumar-Singh, S., Pirici, D., McGowan, E., Serneels, S., Ceuterick, C., Hardy, J., et al. (2005). Dense-Core plaques in Tg2576 and PSAPP mouse models of Alzheimer's disease are centered on vessel walls. *Am. J. Pathol.* 167, 527–543. doi: 10.1016/S0002-9440(10)62995-1

Kuusimaki, T., Al-Abdulrasul, H., Kurki, S., Hietala, J., Hartikainen, S., Koponen, M., et al. (2021). Increased risk of Parkinson's disease in patients with schizophrenia spectrum disorders. *Mov. Disord.* 36, 1353–1361. doi: 10.1002/mds.28484

Kwakye, G. F., McMinimy, R. A., and Aschner, M. (2017). Disease-Toxicant interactions in Parkinson's disease neuropathology. *Neurochem. Res.* 42, 1772–1786. doi: 10.1007/s11064-016-2052-4

Lacalle-Aurioles, M., Mateos-Perez, J. M., Guzman-De-Villoria, J. A., Olazaran, J., Cruz-Orduna, I., Aleman-Gomez, Y., et al. (2014). Cerebral blood flow is an earlier indicator of perfusion abnormalities than cerebral blood volume in Alzheimer's disease. *J. Cereb. Blood Flow Metab.* 34, 654–659. doi: 10.1038/jcbfm.2013.241

Lacoste, B., Comin, C. H., Ben-Zvi, A., Kaeser, P. S., Xu, X., Costa, L. F., et al. (2014). Sensory-Related neural activity regulates the structure of vascular networks in the cerebral cortex. *Neuron* 83, 1117–1130. doi: 10.1016/j.neuron.2014.07.034

Lacoste, B., and Gu, C. (2015). Control of cerebrovascular patterning by neural activity during postnatal development. *Mech. Dev.* 138(Pt 1), 43–49. doi: 10.1016/j.mod.2015.06.003

Lacoste, B., Tong, X. K., Lahjouji, K., Couture, R., and Hamel, E. (2013). Cognitive and cerebrovascular improvements following kinin B1 receptor blockade in Alzheimer's disease mice. *J. Neuroinflammation* 10:57.

Larsen, J., Martin, D. R., and Byrne, M. (2014). Recent advances in delivery through the blood-brain barrier. *Curr. Top. Med. Chem.* 14, 1148–1160. doi: 10.2174/1568026614666140329230311

Law, M., Saindane, A. M., Ge, Y., Babb, J. S., Johnson, G., Mannon, L. J., et al. (2004). Microvascular abnormality in relapsing-remitting multiple sclerosis: perfusion MR imaging findings in normal-appearing white matter. *Radiology* 231, 645–652. doi: 10.1148/radiol.2313030996

Lecrux, C., and Hamel, E. (2011). The neurovascular unit in brain function and disease. *Acta Physiol. (Oxf.)* 203, 47–59. doi: 10.1111/j.1748-1716.2011.02256.x

Leech, S., Kirk, J., Plumb, J., and McQuaid, S. (2007). Persistent endothelial abnormalities and blood-brain barrier leak in primary and secondary progressive multiple sclerosis. *Neuropathol. Appl. Neurobiol.* 33, 86–98. doi: 10.1111/j.1365-2990.2006.00781.x

Leeuwis, A. E., Benedictus, M. R., Kuijer, J. P. A., Binnewijzend, M. A. A., Hooghiemstra, A. M., Verfaillie, S. C. J., et al. (2017). Lower cerebral blood flow is associated with impairment in multiple cognitive domains in Alzheimer's disease. *Alzheimers Dement.* 13, 531–540. doi: 10.1016/j.jalz.2016.08.013

Lepeta, K., and Kaczmarek, L. (2015). Matrix Metalloproteinase-9 as a Novel Player in Synaptic Plasticity and Schizophrenia. *Schizophr. Bull.* 41, 1003–1009. doi: 10.1093/schbul/sbv036

Li, J. Y., Popovic, N., and Brundin, P. (2005). The use of the R6 transgenic mouse models of Huntington's disease in attempts to develop novel therapeutic strategies. *NeuroTherapeutics* 2, 447–464. doi: 10.1602/neurorx.2.3.447

Li, S. S., Qu, Z., Haas, M., Ngo, L., Heo, Y. J., Kang, H. J., et al. (2016). The HSA21 gene EURL/C21ORF91 controls neurogenesis within the cerebral cortex and is implicated in the pathogenesis of Down Syndrome. *Sci. Rep.* 6:29514. doi: 10.1038/srep29514

Licht, T., and Keshet, E. (2015). The vascular niche in adult neurogenesis. *Mech. Dev.* 138(Pt 1), 56–62. doi: 10.1016/j.mod.2015.06.001

Lim, R. G., Quan, C., Reyes-Ortiz, A. M., Lutz, S. E., Kedaigle, A. J., Gipson, T. A., et al. (2017). Huntington's disease iPSC-derived brain microvascular endothelial cells reveal WNT-mediated angiogenic and blood-brain barrier deficits. *Cell Rep.* 19, 1365–1377. doi: 10.1016/j.celrep.2017.04.021

Lin, A. L., Jahrling, J. B., Zhang, W., DeRosa, N., Bakshi, V., Romero, P., et al. (2017). Rapamycin rescues vascular, metabolic and learning deficits in apolipoprotein E4 transgenic mice with pre-symptomatic Alzheimer's disease. *J. Cereb. Blood Flow Metab.* 37, 217–226. doi: 10.1177/0271678X15621575

Lin, C.-Y., Hsu, Y.-H., Lin, M.-H., Yang, T.-H., Chen, H.-M., Chen, Y.-C., et al. (2013). Neurovascular abnormalities in humans and mice with Huntington's disease. *Exp. Neurol.* 250, 20–30. doi: 10.1016/j.expneurol.2013.08.019

Liu, H., Zhang, C., Xu, J., Jin, J., Cheng, L., Wu, Q., et al. (2020). HTT silencing delays onset and slows progression of Huntington's disease like phenotype: monitoring with a novel neurovascular biomarker. *bioRXiv* [Preprint] doi: 10.1101/2020.11.17.386631

Liu, Y., Braidy, N., Poljak, A., Chan, D. K. Y., and Sachdev, P. (2018). Cerebral small vessel disease and the risk of Alzheimer's disease: a systematic review. *Ageing Res. Rev.* 47, 41–48. doi: 10.1016/j.arr.2018.06.002

Liu, Y., Cao, Y., Zhang, W., Bergmeier, S., Qian, Y., Akbar, H., et al. (2012). A small-molecule inhibitor of glucose transporter 1 downregulates glycolysis, induces cell-cycle arrest, and inhibits cancer cell growth in vitro and in vivo. *Mol. Cancer Ther.* 11, 1672–1682. doi: 10.1158/1535-7163.MCT-12-0131

Love, S., and Miners, J. S. (2016). Cerebral Hypoperfusion and the Energy Deficit in Alzheimer's Disease. *Brain Pathol.* 26, 607–617. doi: 10.1111/bpa.12401

Luchsinger, J. A., Reitz, C., Honig, L. S., Tang, M. X., Shea, S., and Mayeux, R. (2005). Aggregation of vascular risk factors and risk of incident Alzheimer disease [Research Support, N.I.H., Extramural Research Support, Non-U.S. Gov't Research Support, U.S. Gov't, P.H.S.]. *Neurology* 65, 545–551. doi: 10.1212/01.wnl.0000172914.08967.dc

Ludwin, S. K. (2006). The pathogenesis of multiple sclerosis: relating human pathology to experimental studies. *J. Neuropathol. Exp. Neurol.* 65, 305–318. doi: 10.1097/01.jnen.0000225024.12074.80

MacVicar, B. A., and Newman, E. A. (2015). Astrocyte regulation of blood flow in the brain. *Cold Spring Harb. Perspect. Biol.* 7:a020388. doi: 10.1101/cshperspect.a020388

Madhyastha, T. M., Askren, M. K., Boord, P., Zhang, J., Leverenz, J. B., and Grabowski, T. J. (2015). Cerebral perfusion and cortical thickness indicate cortical involvement in mild Parkinson's disease. *Mov. Disord.* 30, 1893–1900. doi: 10.1002/mds.26128

Magaki, S., Tang, Z., Tung, S., Williams, C. K., Lo, D., Yong, W. H., et al. (2018). The effects of cerebral amyloid angiopathy on integrity of the blood-brain barrier. *Neurobiol. Aging* 70, 70–77. doi: 10.1016/j.neurobiolaging.2018.06.004

Malaspina, D., Harkavy-Friedman, J., Corcoran, C., Mujica-Parodi, L., Printz, D., Gorman, J. M., et al. (2004). Resting neural activity distinguishes subgroups of schizophrenia patients. *Biol. Psychiatry* 56, 931–937. doi: 10.1016/j.biopsych.2004.09.013

Malaspina, D., Storer, S., Furman, V., Esser, P., Printz, D., Berman, A., et al. (1999). SPECT study of visual fixation in schizophrenia and comparison subjects. *Soc. Biol. Psychiatry* 46, 89–93. doi: 10.1016/s0006-3223(98)00306-0

Mantovani, S., Gordon, R., Li, R., Christie, D. C., Kumar, V., and Woodruff, T. M. (2016). Motor deficits associated with Huntington's disease occur in the absence of striatal degeneration in BACHD transgenic mice. *Hum. Mol. Genet.* 25, 1780–1791. doi: 10.1093/hmg/ddw050

Marco, S., and Skaper, S. D. (2006). Amyloid beta-peptide1-42 alters tight junction protein distribution and expression in brain microvessel endothelial cells. *Neurosci. Lett.* 401, 219–224. doi: 10.1016/j.neulet.2006.03.047

Marshall, O., Lu, H., Brisset, J. C., Xu, F., Liu, P., Herbert, J., et al. (2014). Impaired cerebrovascular reactivity in multiple sclerosis. *JAMA Neurol.* 71, 1275–1281. doi: 10.1001/jamaneurol.2014.1668

Marshall, R. S., Lazar, R. M., Pile-Spellman, J., Young, W. L., Hoang Duong, D., Joshi, S., et al. (2001). Recovery of brain function during induced cerebral hypoperfusion. *Brain* 124, 1208–1217. doi: 10.1093/brain/124.6.1208

Martinez, B. I., and Stabenfeldt, S. E. (2019). Current trends in biomarker discovery and analysis tools for traumatic brain injury. *J. Biol. Eng.* 13:16. doi: 10.1186/s13036-019-0145-8

Mathalon, D. H., Ford, J. M., and Pfefferbaum, A. (2000). Trait and state aspects of P300 amplitude reduction in schizophrenia: a retrospective longitudinal study. *Biol. Psychiatry* 47, 434–449. doi: 10.1016/s0006-3223(99)00277-2

Mattsson, N., Tosun, D., Insel, P. S., Simonson, A., Jack, C. R. Jr., Beckett, L. A., et al. (2014). Association of brain amyloid-beta with cerebral perfusion and structure in Alzheimer's disease and mild cognitive impairment. *Brain* 137(Pt 5), 1550–1561. doi: 10.1093/brain/awu043

Mayhan, W. G. (1999). VEGF increases permeability of the blood-brain barrier via a nitric oxide synthase/cGMP-dependent pathway. *Am. J. Physiol.* 276, C1148–C1153. doi: 10.1152/ajpcell.1999.276.5.C1148

McColgan, P., and Tabrizi, S. J. (2018). Huntington's disease: a clinical review. *Eur. J. Neurol.* 25, 24–34. doi: 10.1111/ene.13413

McConnell, H. L., Li, Z., Woltjer, R. L., and Mishra, A. (2019). Astrocyte dysfunction and neurovascular impairment in neurological disorders: correlation or causation? *Neurochem. Int.* 128, 70–84. doi: 10.1016/j.neuint.2019.04.005

McGowan, E., Pickford, F., Kim, J., Onstead, L., Eriksen, J., Yu, C., et al. (2005). Aβ42 is essential for parenchymal and vascular amyloid deposition in mice. *Neuron* 47, 191–199. doi: 10.1016/j.neuron.2005.06.030

McQuaid, S., Cunnea, P., McMahon, J., and Fitzgerald, U. (2009). The effects of blood–brain barrier disruption on glial cell function in multiple sclerosis. *Biochem. Soc. Trans.* 37(Pt 1), 329–331. doi: 10.1042/BST0370329

Melzer, T. R., Watts, R., MacAskill, M. R., Pearson, J. F., Rueger, S., Pitcher, T. L., et al. (2011). Arterial spin labelling reveals an abnormal cerebral perfusion pattern in Parkinson's disease. *Brain* 134(Pt 3), 845–855. doi: 10.1093/brain/awq377

Menard, C., Pfau, M. L., Hodes, G. E., Kana, V., Wang, V. X., Bouchard, S., et al. (2017). Social stress induces neurovascular pathology promoting depression. *Nat. Neurosci.* 20, 1752–1760. doi: 10.1038/s41593-017-0010-3

Mendez, M. F. (2017). What is the relationship of traumatic brain injury to dementia? *J. Alzheimers Dis.* 57, 667–681. doi: 10.3233/JAD-161002

Michels, L., Warnock, G., Buck, A., Macauda, G., Leh, S. E., Kaelin, A. M., et al. (2016). Arterial spin labeling imaging reveals widespread and Abeta-independent reductions in cerebral blood flow in elderly apolipoprotein epsilon-4 carriers. *J. Cereb. Blood Flow Metab.* 36, 581–595. doi: 10.1177/0271678X15605847

Mielke, M. M., Vemuri, P., and Rocca, W. A. (2014). Clinical epidemiology of Alzheimer's disease: assessing sex and gender differences. *Clin. Epidemiol.* 6, 37–48. doi: 10.2147/CLEP.S37929

Milner, E., Zhou, M. L., Johnson, A. W., Vellimana, A. K., Greenberg, J. K., Holtzman, D. M., et al. (2014). Cerebral amyloid angiopathy increases susceptibility to infarction after focal cerebral ischemia in Tg2576 mice. *Stroke* 45, 3064–3069. doi: 10.1161/STROKEAHA.114.006078

Minn, A., Leclerc, S., Heydel, J.-M., Minn, A.-L., Denizcot, C., Cattarelli, M., et al. (2002). Drug transport into the mammalian brain: the nasal pathway and its specific metabolic barrier. *J. Drug Target* 10, 285–296. doi: 10.1080/713714452

Minoshima, S., Giordani, B., Berent, S., Frey, K. A., Foster, N. L., and Kuhl, D. E. (1997). Metabolic reduction in the posterior cingulate cortex in very early Alzheimer's disease. *Ann. Neurol.* 42, 85–94. doi: 10.1002/ana.410420114

Mishra, A. (2017). Binaural blood flow control by astrocytes: listening to synapses and the vasculature. *J. Physiol.* 595, 1885–1902. doi: 10.1113/JP270979

Mohan, S., Ahmad, A. S., Glushakov, A. V., Chambers, C., and Dore, S. (2012). Putative role of prostaglandin receptor in intracerebral hemorrhage. *Front. Neurol.* 3:145. doi: 10.3389/fneur.2012.00145

Montagne, A., Nation, D. A., Pa, J., Sweeney, M. D., Toga, A. W., and Zlokovic, B. V. (2016). Brain imaging of neurovascular dysfunction in Alzheimer's disease. *Acta Neuropathol.* 131, 687–707. doi: 10.1007/s00401-016-1570-0

Montagne, A., Nikolakopoulou, A. M., Huuskonen, M. T., Sagare, A. P., Lawson, E. J., Lazic, D., et al. (2021). APOE4 accelerates advanced-stage vascular and neurodegenerative disorder in old Alzheimer's mice via cyclophilin A independently of amyloid-β. *Nat. Aging* 1, 506–520. doi: 10.1038/s43587-021-00073-z

Montaldi, D., Brooks, D. N., McColl, J. H., Wyper, D., Patterson, J., Barron, E., et al. (1990). Measurement of regional cerebral blood flow and cognitive performance in Alzheimer's disease. *J. Neurol. Neurosurg. Psychiatry* 53, 33–38. doi: 10.1136/jnnp.53.1.33

Monti, L., Morbidelli, L., and Rossi, A. (2018). Impaired cerebral perfusion in multiple sclerosis: relevance of endothelial factors. *Biomark. Insights* 13, 1–10. doi: 10.1177/1177271918774800

Moon, H. S., Jiang, H., Vo, T. T., Jung, W. B., Vazquez, A. L., and Kim, S. G. (2021). Contribution of excitatory and inhibitory neuronal activity to BOLD fMRI. *Cereb. Cortex* 31, 4053–4067. doi: 10.1093/cercor/bhab068

Mooradian, A. D., Chung, H. C., and Shah, G. N. (1997). GLUT-1 expression in the cerebra of patients with Alzheimer's disease. *Neurobiol. Aging* 18, 469–474. doi: 10.1016/s0197-4580(97)00111-5

Moore, E. E., Liu, D., Li, J., Schimmel, S. J., Cambronero, F. E., Terry, J. G., et al. (2021). Association of aortic stiffness with biomarkers of neuroinflammation, synaptic dysfunction, and neurodegeneration. *Neurology* 97, e329–e340. doi: 10.1212/WNL.0000000000012257

Morris-Rosendahl, D. J., and Crocq, M. A. (2020). Neurodevelopmental disorders-the history and future of a diagnostic concept. *Dialogues Clin. Neurosci.* 22, 65–72. doi: 10.31887/DCNS.2020.22.1/macrocq

Mucke, L., Masliah, E., Yu, G. Q., Mallory, M., Rockenstein, E. M., Tatsuno, G., et al. (2000). High-level neuronal expression of abeta 1-42 in wild-type human amyloid protein precursor transgenic mice: synaptotoxicity without plaque formation. *J. Neurosci.* 20, 4050–4058.

Mughal, A., Harraz, O. F., Gonzales, A. L., Hill-Eubanks, D., and Nelson, M. T. (2021). PIP2 improves cerebral blood flow in a mouse model of Alzheimer's disease. *Function (Oxf)* 2:zqab010. doi: 10.1093/function/zqab010

Müller, N., and Ackenheil, M. (1995). Immunoglobulin and albumin content of cerebrospinal fluid in schizophrenic patients: relationship to negative symptomatology. *Schizophr. Res.* 14, 223–228. doi: 10.1016/0920-9964(94)00045-a

Muramuto, S., Yamada, H., Sadato, N., Kimura, H., Konishi, Y., Kimura, K., et al. (2002). Age-dependent change in metabolic re- sponse to photic stimulation of the primary visual cortex in infants: functional mag- netic resonance imaging study. *J. Comput. Assist. Tomogr.* 26, 894–901.

Nelson, A. R., Sweeney, M. D., Sagare, A. P., and Zlokovic, B. V. (2016). Neurovascular dysfunction and neurodegeneration in dementia and Alzheimer's disease. *Biochim. Biophys. Acta* 1862, 887–900. doi: 10.1016/j.bbadis.2015.12.016

Niatsetskaya, Z., Basso, M., Speer, R. E., McConoughey, S. J., Coppola, G., Ma, T. C., et al. (2010). HIF prolyl hydroxylase inhibitors prevent neuronal death induced by mitochondrial toxins: therapeutic implications for Huntington's disease and Alzheimer's disease [Research Support, N.I.H., Extramural Research Support, Non-U.S. Gov't]. *Antioxid. Redox Signal.* 12, 435–443. doi: 10.1089/ars.2009.2800

Nicolakakis, N., Aboulkassim, T., Ongali, B., Lecrux, C., Fernandes, P., Rosa-Neto, P., et al. (2008). Complete rescue of cerebrovascular function in aged Alzheimer's disease transgenic mice by antioxidants and pioglitazone, a peroxisome proliferator-activated receptor gamma agonist. *J. Neurosci.* 28, 9287–9296.

Nicolakakis, N., and Hamel, E. (2011). Neurovascular function in Alzheimer's disease patients and experimental models. *J. Cereb. Blood Flow Metab.* 31, 1354–1370. doi: 10.1038/jcbfm.2011.43

Nishiura, K., Ichikawa-Tomikawa, N., Sugimoto, K., Kunii, Y., Kashiwagi, K., Tanaka, M., et al. (2017). PKA activation and endothelial claudin-5 breakdown in the schizophrenic prefrontal cortex. *Oncotarget* 7, 93382–93391. doi: 10.18632/oncotarget.21850

Niwa, K., Carlson, G. A., and Iadecola, C. (2000). Exogenous Ab1-40 reproduces cerebrovascular alterations resulting from amyloid precursor protein overexpression in mice. *J. Cereb. Blood Flow Metab.* 20, 1659–1668. doi: 10.1097/00004647-200012000-00005

Niwa, K., Kazama, K., Younkin, S. G., Carlson, G. A., and Iadecola, C. (2002). Alterations in cerebral blood flow and glucose utilization in mice overexpressing the amyloid precursor protein. *Neurobiol. Dis.* 9, 61–68. doi: 10.1006/nbdi.2001.0460

Novarino, G., El-Fishawy, P., Kayserili, H., Meguid, N. A., Scott, E. M., Schroth, J., et al. (2012). Mutations in BCKD-kinase lead to a potentially treatable form of autism with epilepsy. *Science* 338, 394–397. doi: 10.1126/science.1224631

O'Brien, J. T., Eagger, S., Syed, G. M., Sahakian, B. J., and Levy, R. (1992). A study of regional cerebral blood flow and cognitive performance in Alzheimer's disease. *J. Neurol. Neurosurg. Psychiatry* 55, 1182–1187. doi: 10.1136/jnnp.55.12.1182

Ochoa, S., Usall, J., Cobo, J., Labad, X., and Kulkarni, J. (2012). Gender differences in schizophrenia and first-episode psychosis: a comprehensive literature review. *Schizophr. Res. Treat.* 2012:916198. doi: 10.1155/2012/916198

Oddo, S., Caccamo, A., Shepherd, J. D., Murphy, M. P., Golde, T. E., Kayed, R., et al. (2003). Triple-transgenic model of Alzheimer's disease with plaques and tangles: intracellular Abeta and synaptic dysfunction [Comparative Study Research Support, Non-U.S. Gov't Research Support, U.S. Gov't, P.H.S.]. *Neuron* 39, 409–421.

Ohnishi, T., Matsuda, H., Hashimoto, T., Kunihiro, T., Nishikawa, M., Uema, T., et al. (2000). Abnormal regional cerebral blood flow in childhood autism. *Brain* 123(Pt 9), 1838–1844.

Okabe, K., Fukada, H., Tai-Nagara, I., Ando, T., Honda, T., Nakajima, K., et al. (2020). Neuron-derived VEGF contributes to cortical and hippocampal development independently of VEGFR1/2-mediated neurotrophism. *Dev. Biol.* 459, 65–71. doi: 10.1016/j.ydbio.2019.11.016

Ongali, B., Nicolakakis, N., Lecrux, C., Aboulkassim, T., Rosa-Neto, P., Papadopoulos, P., et al. (2010). Transgenic mice overexpressing APP and transforming growth factor-beta1 feature cognitive and vascular hallmarks of Alzheimer's disease. *Am. J. Pathol.* 177, 3071–3080. doi: 10.2353/ajpath.2010.100339

Onore, C., Careaga, M., and Ashwood, P. (2012). The role of immune dysfunction in the pathophysiology of autism. *Brain Behav. Immun.* 26, 383–392. doi: 10.1016/j.bbi.2011.08.007

Ortiz, G. G., Pacheco-Moises, F. P., Macias-Islas, M. A., Flores-Alvarado, L. J., Mireles-Ramirez, M. A., Gonzalez-Renovato, E. D., et al. (2014). Role of the blood-brain barrier in multiple sclerosis. *Arch. Med. Res.* 45, 687–697. doi: 10.1016/j.arcmed.2014.11.013

Ota, T., Sato, N., Nakata, Y., Ito, K., Kamiya, K., Maikusa, N., et al. (2013). Abnormalities of cerebral blood flow in multiple sclerosis: a pseudocontinuous arterial spin labeling MRI study. *Magn. Reson. Imaging* 31, 990–995. doi: 10.1016/j.mri.2013.03.016

Ouellette, J., Toussay, X., Comin, C. H., Costa, L. D. F., Ho, M., Lacalle-Aurioles, M., et al. (2020). Vascular contributions to 16p11.2 deletion autism syndrome modeled in mice. *Nat. Neurosci.* 23, 1090–1101. doi: 10.1038/s41593-020-0663-1

Padden, M., Leech, S., Craig, B., Kirk, J., Brankin, B., and McQuaid, S. (2007). Differences in expression of junctional adhesion molecule-A and beta-catenin in multiple sclerosis brain tissue: increasing evidence for the role of tight junction pathology. *Acta Neuropathol.* 113, 177–186. doi: 10.1007/s00401-006-0145-x

Pagano, G., Ferrara, N., Brooks, D. J., and Pavese, N. (2016). Age at onset and Parkinson disease phenotype. *Neurology* 86, 1400–1407. doi: 10.1212/WNL.0000000000002461

Palop, J. J., Jones, B., Kekonius, L., Chin, J., Yu, G. Q., Raber, J., et al. (2003). Neuronal depletion of calcium-dependent proteins in the dentate gyrus is tightly linked to Alzheimer's disease-related cognitive deficits. *Proc. Natl. Acad. Sci. U.S.A.* 100, 9572–9577.

Papadaki, E. Z., Simos, P. G., Mastorodemos, V. C., Panou, T., Maris, T. G., Karantanas, A. H., et al. (2014). Regional MRI perfusion measures predict motor/executive function in patients with clinically isolated syndrome. *Behav. Neurol.* 2014:252419. doi: 10.1155/2014/252419

Pardridge, W. M. (2012). Drug transport across the blood-brain barrier. *J. Cereb. Blood Flow Metab.* 32, 1959–1972. doi: 10.1038/jcbfm.2012.126

Paris, D., Parker, T. A., Suo, Z., Fang, C., Humphrey, J., Crawford, F., et al. (1998). Role of peroxynitrite in the vasoactive and cytotoxic effects of Alzheimer's beta-amyloid1-40 peptide. *Exp. Neurol.* 152, 116–122. doi: 10.1006/exnr.1998.6828

Park, H. R., Lee, J. M., Moon, H. E., Lee, D. S., Kim, B. N., Kim, J., et al. (2016). A short review on the current understanding of autism spectrum disorders. *Exp. Neurobiol.* 25, 1–13. doi: 10.5607/en.2016.25.1.1

Park, L., Wang, G., Zhou, P., Zhou, J., Pitstick, R., Previti, M. L., et al. (2011). Scavenger receptor CD36 is essential for the cerebrovascular oxidative stress and neurovascular dysfunction induced by amyloid-beta. *Proc. Natl. Acad. Sci. U.S.A.* 108, 5063–5068. doi: 10.1073/pnas.1015413108

Parkinson Canada (2010). *A Manual for People Living with Parkinson's Disease*. Available online at: https://www.parkinson.ca/gated/parkinsons-disease-an-introductory-guide/ (accessed July 5, 2021).

Parodi-Rullan, R., Ghiso, J., Cabrera, E., Rostagno, A., and Fossati, S. (2020). Alzheimer's amyloid beta heterogeneous species differentially affect brain endothelial cell viability, blood-brain barrier integrity, and angiogenesis. *Aging Cell* 19:e13258. doi: 10.1111/acel.13258

Patel, A., Toia, G. V., Colletta, K., Bradaric, B. D., Carvey, P. M., and Hendey, B. (2011). An angiogenic inhibitor, cyclic RGDfV, attenuates MPTP-induced dopamine neuron toxicity. *Exp. Neurol.* 231, 160–170. doi: 10.1016/j.expneurol.2011.06.004

Patel, N. S., Mathura, V. S., Bachmeier, C., Beaulieu-Abdelahad, D., Laporte, V., Weeks, O., et al. (2010). Alzheimer's beta-amyloid peptide blocks vascular endothelial growth factor mediated signaling via direct interaction with VEGFR-2. *J. Neurochem.* 112, 66–76. doi: 10.1111/j.1471-4159.2009.06426.x

Paulsen, J. S. (2011). Cognitive impairment in Huntington disease: diagnosis and treatment [Research Support, N.I.H., Extramural Research Support, Non-U.S. Gov't Review]. *Curr. Neurol. Neurosci. Rep.* 11, 474–483. doi: 10.1007/s11910-011-0215-x

Peguera, B., Segarra, M., and Acker-Palmer, A. (2021). Neurovascular crosstalk coordinates the central nervous system development. *Curr. Opin. Neurobiol.* 69, 202–213. doi: 10.1016/j.conb.2021.04.005

Perry, D. C., Sturm, V. E., Peterson, M. J., Pieper, C. F., Bullock, T., Boeve, B. F., et al. (2016). Association of traumatic brain injury with subsequent neurological and psychiatric disease: a meta-analysis. *J. Neurosurg.* 124, 511–526. doi: 10.3171/2015.2.JNS14503

Peruzzo, D., Castellaro, M., Calabrese, M., Veronese, E., Rinaldi, F., Bernardi, V., et al. (2013). Heterogeneity of cortical lesions in multiple sclerosis: an MRI perfusion study. *J. Cereb. Blood Flow Metab.* 33, 457–463. doi: 10.1038/jcbfm.2012.192

Peterson, B. S., Zargarian, A., Peterson, J. B., Goh, S., Sawardekar, S., Williams, S. C. R., et al. (2019). Hyperperfusion of frontal white and subcortical gray matter in autism spectrum disorder. *Biol. Psychiatry* 85, 584–595. doi: 10.1016/j.biopsych.2018.11.026

Pinkham, A., Loughead, J., Ruparel, K., Wu, W. C., Overton, E., Gur, R., et al. (2011). Resting quantitative cerebral blood flow in schizophrenia measured by pulsed arterial spin labeling perfusion MRI. *Psychiatry Res.* 194, 64–72. doi: 10.1016/j.pscychresns.2011.06.013

Plana-Ripoll, O., Pedersen, C. B., Holtz, Y., Benros, M. E., Dalsgaard, S., de Jonge, P., et al. (2019). Exploring comorbidity within mental disorders among a danish national population. *JAMA Psychiatry* 76, 259–270. doi: 10.1001/jamapsychiatry.2018.3658

Profaci, C. P., Munji, R. N., Pulido, R. S., and Daneman, R. (2020). The blood-brain barrier in health and disease: important unanswered questions. *J. Exp. Med.* 217:e20190062. doi: 10.1084/jem.20190062

Prohovnik, I., Mayeux, R., Sackeim, H. A., Smith, G., Stern, Y., and Alderson, P. O. (1988). Cerebral perfusion as a diagnostic marker of early Alzheimer's disease. *Neurology* 38, 931–937. doi: 10.1212/WNL.38.6.931

Pu, S., Nakagome, K., Yamada, T., Itakura, M., Yamanashi, T., Yamada, S., et al. (2016). Social cognition and prefrontal hemodynamic responses during a working memory task in schizophrenia. *Sci. Rep.* 6:22500. doi: 10.1038/srep22500

Quaegebeur, A., Lange, C., and Carmeliet, P. (2011). The neurovascular link in health and disease: molecular mechanisms and therapeutic implications. *Neuron* 71, 406–424. doi: 10.1016/j.neuron.2011.07.013

Querfurth, H. W., and LaFerla, F. M. (2010). Alzheimer's disease. *N. Engl. J. Med.* 362, 329–344.

Ramos-Cejudo, J., Wisniewski, T., Marmar, C., Zetterberg, H., Blennow, K., de Leon, M. J., et al. (2018). Traumatic brain injury and Alzheimer's disease: the cerebrovascular link. *EBioMedicine* 28, 21–30. doi: 10.1016/j.ebiom.2018.01.021

Rawlins, M. D., Wexler, N. S., Wexler, A. R., Tabrizi, S. J., Douglas, I., Evans, S. J., et al. (2016). The prevalence of Huntington's disease. *Neuroepidemiology* 46, 144–153. doi: 10.1159/000443738

Reese, T. S., and Karnovsky, M. (1967). Fine structural localization of a blood-brain barrier to exogenous peroxidase. *J. Cell Biol.* 34, 207–217. doi: 10.1083/jcb.34.1.207

Reid, I. C., Besson, J. A. O., Best, P. V., Sharp, P. F., Gemmell, H. G., and Smith, F. W. (1988). Imaging of cerebral blood flow markers in Huntington's disease

using single photon emission computed tomography. *J. Neurol. Neurosurg. Psychiatry* 51, 1264–1268. doi: 10.1136/jnnp.51.10.1264

Reijmer, Y. D., van Veluw, S. J., and Greenberg, S. M. (2016). Ischemic brain injury in cerebral amyloid angiopathy. *J. Cereb. Blood Flow Metab.* 36, 40–54. doi: 10.1038/jcbfm.2015.88

Reynell, C., and Harris, J. J. (2013). The BOLD signal and neurovascular coupling in autism. *Dev. Cogn. Neurosci.* 6, 72–79. doi: 10.1016/j.dcn.2013.07.003

Ribe, A. R., Laursen, T. M., Charles, M., Katon, W., Fenger-Gron, M., Davydow, D., et al. (2015). Long-term Risk of dementia in persons with Schizophrenia: a Danish population-based cohort study. *JAMA Psychiatry* 72, 1095–1101. doi: 10.1001/jamapsychiatry.2015.1546

Rite, I., Machado, A., Cano, J., and Venero, J. L. (2007). Blood-brain barrier disruption induces in vivo degeneration of nigral dopaminergic neurons. *J. Neurochem.* 101, 1567–1582. doi: 10.1111/j.1471-4159.2007.04567.x

Rizzo, M. T., and Leaver, H. A. (2010). Brain endothelial cell death: modes, signaling pathways, and relevance to neural development, homeostasis, and disease. *Mol. Neurobiol.* 42, 52–63. doi: 10.1007/s12035-010-8132-6

Roher, A. E., Esh, C., Kokjohn, T. A., Kalback, W., Luehrs, D. C., Seward, J. D., et al. (2003). Circle of willis atherosclerosis is a risk factor for sporadic Alzheimer's disease. *Arterioscler. Thromb. Vasc. Biol.* 23, 2055–2062.

Ross, C. A., and Tabrizi, S. J. (2011). Huntington's disease: from molecular pathogenesis to clinical treatment. *Lancet Neurol.* 10, 83–98. doi: 10.1016/S1474-4422(10)70245-3

Ross, T. M., Martinez, P. M., Renner, J. C., Thorne, R. G., Hanson, L. R., and Frey, W. H. II (2004). Intranasal administration of interferon beta bypasses the blood–brain barrier to target the central nervous system and cervical lymph nodes: a non-invasive treatment strategy for multiple sclerosis. *J. Neuroinflammation* 151, 66–77. doi: 10.1016/j.jneuroim.2004.02.011

Rossignol, D. A., Bradstreet, J. J., Van Dyke, K., Schneider, C., Freedenfeld, S. H., O'Hara, N., et al. (2012). Hyperbaric oxygen treatment in autism spectrum disorders. *Med. Gas Res.* 2:16.

Russo, S. J., and Nestler, E. J. (2013). The brain reward circuitry in mood disorders. *Nat. Rev. Neurosci.* 14, 609–625. doi: 10.1038/nrn3381

Ryu, J. K., and McLarnon, J. G. (2009). A leaky blood-brain barrier, fibrinogen infiltration and microglial reactivity in inflamed Alzheimer's disease brain. *J. Cell. Mol. Med.* 13, 2911–2925. doi: 10.1111/j.1582-4934.2008.00434.x

Saade, C., Bou-Fakhredin, R., Yousem, D. M., Asmar, K., Naffaa, L., and El-Merhi, F. (2018). Gadolinium and multiple sclerosis: vessels, barriers of the brain, and glymphatics. *AJNR Am. J. Neuroradiol.* 39, 2168–2176. doi: 10.3174/ajnr.A5773

Sabri, O., Erkwoh, R., Schreckenberger, M., Owega, A., Sass, H., and Buell, U. (1997). Correlation of positive symptoms exclusively to hyperperfusion or hypoperfusion of cerebral cortex in never-treated schizophrenics. *Lancet* 349, 1735–1739. doi: 10.1016/s0140-6736(96)08380-8

Sagare, A. P., Bell, R. D., Zhao, Z., Ma, Q., Winkler, E. A., Ramanathan, A., et al. (2013). Pericyte loss influences Alzheimer-like neurodegeneration in mice. *Nat. Commun.* 4:2932. doi: 10.1038/ncomms3932

Saindane, A. M., Law, M., Ge, Y., Johnson, G., Babb, J. S., and Grossman, R. I. (2007). Correlation of diffusion tensor and dynamic perfusion MR imaging metrics in normal- appearing corpus callosum: support for primary hypoperfusion in multiple sclerosis. *Am. J. Neuroradiol.* 28, 767–772.

Sakulchit, T., Ladish, C., and Goldman, R. D. (2017). Hyperbaric oxygen therapy for children with autism spectrum disorder. *Can. Fam. Physician* 63, 446–448.

Salehi, A., Ashford, J. W., and Mufson, E. J. (2016). The link between Alzheimer's disease and down syndrome. a historical perspective. *Curr. Alzheimer Res.* 13, 2–6. doi: 10.2174/1567205012999151021102914

Salisbury, D., and Bronas, U. (2015). Reactive oxygen and nitrogen species: impact on endothelial dysfunction. *Nurs. Res.* 64, 53–66. doi: 10.1097/NNR.0000000000000068

Salloway, S., Gur, T., Berzin, T., Zipser, B., Correia, S., Hovanesian, V., et al. (2002). Effect of APOE genotype on microvascular basement membrane in Alzheimer's disease. *J. Neurol. Sci.* 203-204, 183–187. doi: 10.1016/s0022-510x(02)00288-5

Salmina, A. B., Morgun, A. V., Kuvacheva, N. V., Pozhilenkova, E. A., Solonchuk, Y. R., Lopatina, O. L., et al. (2014). Endothelial progenitor cells in cerebral endothelium development and repair. *Curr. Technol. Med.* 6, 213–221. doi: 10.1186/s13041-016-0193-7

Sandoo, A., Veldhuijzen van Zanten, J., Metsios, G., Carroll, D., and Kitas, G. (2010). The endothelium and its role in regulating vascular tone. *Open Cardiovasc. Med. J.* 4, 302–312.

Saoud, H., Aflouk, Y., Ben Afia, A., Gaha, L., and Bel Hadj Jrad, B. (2021). Association of VEGF and KDR polymorphisms with the development of schizophrenia. *medRxiv* [preprint] doi: 10.1101/2021.08.06.21261566

Sarkar, S., Raymick, J., Mann, D., Bowyer, J. F., Hanig, J. P., Schmued, L. C., et al. (2014). Neurovascular changes in acute, sub-acute and chronic mouse models of Parkinson's disease. *Curr. Neurovasc. Res.* 11, 48–61. doi: 10.2174/1567202610666131124234506

Sax, D. S., Powsner, R., Kim, A., Tilak, S., Bhatia, R., Cupples, L. A., et al. (1996). Evidence of cortical metabolic dysfunction in early Huntington's disease by single-photon-emission computed tomography. *Mov. Disord.* 11, 671–677. doi: 10.1002/mds.870110612

Schaeffer, S., and Iadecola, C. (2021). Revisiting the neurovascular unit. *Nat. Neurosci.* 24, 1198–1209. doi: 10.1038/s41593-021-00904-7

Scheef, L., Manka, C., Daamen, M., Kühn, K., Maier, W., Schild, H., et al. (2010). Resting-State perfusion in nonmedicated schizophrenic patients: a continuous arterial spin-labeling 3.0-T MR study. *Radiology* 256, 253–260. doi: 10.1148/radiol.10091224

Schifter, T., Hoffman, J. M., Hatten, P. Jr., Hanson, M. W., Coleman, E., and DeLong, R. (1994). Neuroimaging in infantile autism. *J. Child Neurol.* 9, 155–161. doi: 10.1177/088307389400900210

Schuepbach, D., Egger, S. T., Boeker, H., Duschek, S., Vetter, S., Seifritz, E., et al. (2016). Determinants of cerebral hemodynamics during the Trail Making Test in schizophrenia. *Brain Cogn.* 109, 96–104. doi: 10.1016/j.bandc.2016.09.002

Schultz, S. K., O'Leary, D. S., Boles Ponto, L. L., Arndt, S., Magnotta, V., Leonard Watkins, G., et al. (2002). Age and regional cerebral blood flow in schizophrenia: age effects in anterior cingulate, frontal, and parietal cortex. *J. Neuropsychiatry Clin. Neurosci.* 14, 19–24. doi: 10.1176/jnp.14.1.19

Schwartz, M., and Kipnis, J. (2005). Protective autoimmunity and neuroprotection in inflammatory and noninflammatory neurodegenerative diseases. *J. Neurol. Sci.* 233, 163–166. doi: 10.1016/j.jns.2005.03.014

Seabrook, T. J., Littlewood-Evans, A., Brinkmann, V., Pöllinger, B., Schnell, C., and Hiestand, P. C. (2010). Angiogenesis is present in experimental autoimmune encephalomyelitis and pro- angiogenic factors are increased in multiple sclerosis lesions. *J. Neuroinflammation* 7:95. doi: 10.1186/1742-2094-7-95

Selkoe, D. J. (2002). Alzheimer's disease is a synaptic failure. *Science* 298, 789–791.

Sender, R., and Milo, R. (2021). The distribution of cellular turnover in the human body. *Nat. Med.* 27, 45–48. doi: 10.1038/s41591-020-01182-9

Sengillo, J. D., Winkler, E. A., Walker, C. T., Sullivan, J. S., Johnson, M., and Zlokovic, B. V. (2013). Deficiency in mural vascular cells coincides with blood-brain barrier disruption in Alzheimer's disease. *Brain Pathol.* 23, 303–310. doi: 10.1111/bpa.12004

Sharma, S., and Brown, C. E. (2021). Microvascular basis of cognitive impairment in type 1 diabetes. *Pharmacol. Therap.* 107929. doi: 10.1016/j.pharmthera.2021.107929

Shcherbakova, I., Neshkova, E., Dotsenko, V., Platonova, T., Shcherbakova, E., and Yarovaya, G. (1999). The possible role of plasma kallikrein-kinin system and leukocyte elastase in pathogenesis of schizophrenia. *Immunopharmacology* 43, 273–279. doi: 10.1016/s0162-3109(99)00099-5

Shen, Q., Goderie, S. K., Jin, L., Karanth, N., Sun, Y., Abramova, N., et al. (2004). Endothelial cells stimulate self-renewal and expand neurogenesis of neural stem cells. *Science* 304, 1338–1340. doi: 10.1126/science.1095505

Sherrington, R. A. (1890). On the regulation of the blood-supply of the brain. *Neurology* 41, 10–14.

Siegel, B. V., Tanguay, P., Call, J. D., Abel, L., Ho, A., Lott, I., et al. (1992). Regional cerebral glucose metabolism and attention in adults with a history of childhood autism. *J. Neuropsychiatry Clin. Neurosci.* 4, 406–414. doi: 10.1176/jnp.4.4.406

Sieradzan, K. A., and Mann, D. M. (2001). The selective vulnerability of nerve cells in Huntington's disease [Review]. *Neuropathol. Appl. Neurobiol.* 27, 1–21.

Silva-Garcia, O., Valdez-Alarcon, J. J., and Baizabal-Aguirre, V. M. (2019). Wnt/beta-Catenin signaling as a molecular target by pathogenic bacteria. *Front. Immunol.* 10:2135. doi: 10.3389/fimmu.2019.02135

Simpson, I. A., Chundu, K., Davies-Hill, T., Honer, W., and Davies, P. (1994). Decreased concentrations of GLUT1 and GLUT3 glucose transporters in the brains of patients with Alzheimer's diseas. *Ann. Neurol.* 35, 546–551. doi: 10.1002/ana.410350507

Smith, A. J., and Verkman, A. S. (2018). The "glymphatic" mechanism for solute clearance in Alzheimer's disease: game changer or unproven speculation? *FASEB J.* 32, 543–551. doi: 10.1096/fj.201700999

Smith, C. D., Andersen, A. H., Kryscio, R. J., Schmitt, F. A., Kindy, M. S., Blonder, L. X., et al. (1999). Altered brain activation in cognitively intact individuals at high risk for Alzheimer's disease. *Neurology* 53, 581–595.

Smith, E. E., and Greenberg, S. M. (2009). Beta-amyloid, blood vessels, and brain function. *Stroke* 40, 2601–2606. doi: 10.1161/STROKEAHA.108.536839

Smith, E. E., Vijayappa, M., Lima, F., Delgado, P., Wendell, L., Rosand, J., et al. (2008). Impaired visual evoked flow velocity response in cerebral amyloid angiopathy. *Neurology* 71, 1424–1430. doi: 10.1212/01.wnl.0000327887.64299.a4

Smith, G. S., de Leon, M. J., George, A. E., Kluger, A., Volkow, N. D., McRae, T., et al. (1992). Topography of cross-sectional and longitudinal glucose metabolic deficits in Alzheimer's disease. *Arch. Neurol.* 49, 1142–1150. doi: 10.1001/archneur.1992.00530350056020

Snowden, J. S. (2017). The neuropsychology of Huntington's disease. *Arch. Clin. Neuropsychol.* 32, 876–887. doi: 10.1093/arclin/acx086

Solis, E. Jr., Hascup, K. N., and Hascup, E. R. (2020). Alzheimer's disease: the link between amyloid-beta and neurovascular dysfunction. *J. Alzheimers Dis.* 76, 1179–1198. doi: 10.3233/JAD-200473

Song, C., Schwarzkopf, D. S., Lutti, A., Li, B., Kanai, R., and Rees, G. (2013). Effective connectivity within human primary visual cortex predicts interindividual diversity in illusory perception. *J. Neurosci.* 33, 18781–18791. doi: 10.1523/JNEUROSCI.4201-12.2013

Soto-Rojas, L. O., Pacheco-Herrero, M., Martinez-Gomez, P. A., Campa-Cordoba, B. B., Apatiga-Perez, R., Villegas-Rojas, M. M., et al. (2021). The neurovascular unit dysfunction in Alzheimer's disease. *Int. J. Mol. Sci.* 22:2022. doi: 10.3390/ijms22042022

Sotrel, A., Paskevich, P. A., Kiely, D. K., Bird, E. D., Williams, R. S., and Myers, R. H. (1991). Morphometric analysis of the prefrontal cortex in Huntington's disease. *Neurology* 41, 1117–1123. doi: 10.1212/wnl.41.7.1117

Spuch, C., Antequera, D., Portero, A., Orive, G., Hernandez, R. M., Molina, J. A., et al. (2010). The effect of encapsulated VEGF-secreting cells on brain amyloid load and behavioral impairment in a mouse model of Alzheimer's disease [Research Support, Non-U.S. Gov't]. *Biomaterials* 31, 5608–5618. doi: 10.1016/j.biomaterials.2010.03.042

St-Amour, I., Aubé, B., Rieux, M., and Cicchetti, F. (2015). Targeting cerebrovascular impairments in Huntington's disease: a novel treatment perspective. *Future Med.* 5, 389–393. doi: 10.2217/nmt.15.41

Stachowiak, M. K., Kucinski, A., Curl, R., Syposs, C., Yang, Y., Narla, S., et al. (2013). Schizophrenia: a neurodevelopmental disorder — Integrative genomic hypothesis and therapeutic implications from a transgenic mouse model. *Schizophr. Res.* 143, 367–376. doi: 10.1016/j.schres.2012.11.004

Stackhouse, T. L., and Mishra, A. (2021). Neurovascular coupling in development and disease: focus on astrocytes. *Front. Cell Dev. Biol.* 9:702832. doi: 10.3389/fcell.2021.702832

Stamatovic, S., Keep, R., and Andjelkovic, A. (2008). Brain endothelial cell-cell junctions: how to "open" the blood brain barrier. *Curr. Neuropharmacol.* 6, 179–192. doi: 10.2174/157015908785777210

Starkstein, S., Gellar, S., Parlier, M., Payne, L., and Piven, J. (2015). High rates of parkinsonism in adults with autism. *J. Neurodev. Disord.* 7:29. doi: 10.1186/s11689-015-9125-6

Stegmayer, K., Strik, W., Federspiel, A., Wiest, R., Bohlhalter, S., and Walther, S. (2017). Specific cerebral perfusion patterns in three schizophrenia symptom dimensions. *Schizophr. Res.* 190, 96–101. doi: 10.1016/j.schres.2017.03.018

Steventon, J. J., Furby, H., Ralph, J., O'Callaghan, P., Rosser, A. E., Wise, R. G., et al. (2020). Altered cerebrovascular response to acute exercise in patients with Huntington's disease. *Brain Commun.* 2:fcaa044. doi: 10.1093/braincomms/fcaa044

Stone, J., Itin, A., Alon, T., Pe'er, J., Gnessin, H., Chan-Ling, T., et al. (1995). Development of retinal vasculature is mediated by hypoxia- induced vascular endothelial growth factor (VEGF) expression by neuroglia. *J. Neurosci.* 15, 4738–4747.

Storck, S. E., Meister, S., Nahrath, J., Meissner, J. N., Schubert, N., Di Spiezio, A., et al. (2016). Endothelial LRP1 transports amyloid-beta(1-42) across the blood-brain barrier. *J. Clin. Invest.* 126, 123–136. doi: 10.1172/JCI81108

Su, J. J., Osoegawa, M., Matsuoka, T., Minohara, M., Tanaka, M., Ishizu, T., et al. (2006). Upregulation of vascular growth factors in multiple sclerosis: correlation with MRI findings. *J. Neurol. Sci.* 243, 21–30. doi: 10.1016/j.jns.2005.11.006

Suo, Z., Humphrey, J., Kundtz, A., Sethi, F., Placzek, A., Crawford, F., et al. (1998). Soluble Alzheimers beta-amyloid constricts the cerebral vasculature in vivo. *Neurosci. Lett.* 257, 77–80. doi: 10.1016/s0304-3940(98)00814-3

Suri, S., Mackay, C. E., Kelly, M. E., Germuska, M., Tunbridge, E. M., Frisoni, G. B., et al. (2015). Reduced cerebrovascular reactivity in young adults carrying the APOE epsilon4 allele. *Alzheimers Dement.* 11, 648–657 e641. doi: 10.1016/j.jalz.2014.05.1755

Sweeney, M. D., Kisler, K., Montagne, A., Toga, A. W., and Zlokovic, B. V. (2018). The role of brain vasculature in neurodegenerative disorders. *Nat. Neurosci.* 21, 1318–1331. doi: 10.1038/s41593-018-0234-x

Sweeney, M. D., Montagne, A., Sagare, A. P., Nation, D. A., Schneider, L. S., Chui, H. C., et al. (2019). Vascular dysfunction-The disregarded partner of Alzheimer's disease. *Alzheimers Dement.* 15, 158–167. doi: 10.1016/j.jalz.2018.07.222

Switzer, A. R., Cheema, I., McCreary, C. R., Zwiers, A., Charlton, A., Alvarez-Veronesi, A., et al. (2020). Cerebrovascular reactivity in cerebral amyloid angiopathy, Alzheimer disease, and mild cognitive impairment. *Neurology* 95, e1333–e1340. doi: 10.1212/WNL.0000000000010201

Syrimi, Z. J., Vojtisek, L., Eliasova, I., Viskova, J., Svatkova, A., Vanicek, J., et al. (2017). Arterial spin labelling detects posterior cortical hypoperfusion in non-demented patients with Parkinson's disease. *J. Neural Transm. (Vienna)* 124, 551–557. doi: 10.1007/s00702-017-1703-1

Szu, J. I., and Obenaus, A. (2021). Cerebrovascular phenotypes in mouse models of Alzheimer's disease. *J. Cereb. Blood Flow Metab.* 41, 1821–1841. doi: 10.1177/0271678X21992462

Tai, L. M., Holloway, K. A., Male, D. K., Loughlin, A. J., and Romero, I. A. (2010). Amyloid-beta-induced occludin down-regulation and increased permeability in human brain endothelial cells is mediated by MAPK activation. *J. Cell. Mol. Med.* 14, 1101–1112. doi: 10.1111/j.1582-4934.2009.00717.x

Tan, K. H., Harrington, S., Purcell, W. M., and Hurst, R. D. (2004). Peroxynitrite mediates nitric oxide–induced blood–brain barrier damage. *Neurochem. Res.* 29, 579–587. doi: 10.1023/b:nere.0000014828.32200.bd

Taoufik, E., Kouroupi, G., Zygogianni, O., and Matsas, R. (2018). Synaptic dysfunction in neurodegenerative and neurodevelopmental diseases: an overview of induced pluripotent stem-cell-based disease models. *Open Biol.* 8:180138. doi: 10.1098/rsob.180138

Tarlungeanu, D. C., Deliu, E., Dotter, C. P., Kara, M., Janiesch, P. C., Scalise, M., et al. (2016). Impaired amino acid transport at the blood brain barrier is a cause of autism spectrum disorder. *Cell* 167, 1481–1494 e1418. doi: 10.1016/j.cell.2016.11.013

Tata, M., and Ruhrberg, C. (2018). Cross-talk between blood vessels and neural progenitors in the developing brain. *Neuronal Signal.* 2:NS20170139. doi: 10.1042/NS20170139

Tata, M., Ruhrberg, C., and Fantin, A. (2015). Vascularisation of the central nervous system. *Mech. Dev.* 138(Pt 1), 26–36. doi: 10.1016/j.mod.2015.07.001

Thal, D. R., Capetillo-Zarate, E., Larionov, S., Staufenbiel, M., Zurbruegg, S., and Beckmann, N. (2009). Capillary cerebral amyloid angiopathy is associated with vessel occlusion and cerebral blood flow disturbances. *Neurobiol. Aging* 30, 1936–1948. doi: 10.1016/j.neurobiolaging.2008.01.017

Thambisetty, M., Beason-Held, L., An, Y., Kraut, M. A., and Resnick, S. M. (2010). APOE epsilon4 genotype and longitudinal changes in cerebral blood flow in normal aging. *Arch. Neurol.* 67, 93–98. doi: 10.1001/archneurol.2009.913

Thomas, T., Thomas, G., McLendon, C., Sutton, T., and Mullan, M. (1996). β-Amyloid-mediated vasoactivity and vascular endothelial damage. *Nature* 380, 168–171. doi: 10.1038/380168a0

Tong, X. K., Nicolakakis, N., Kocharyan, A., and Hamel, E. (2005). Vascular remodeling versus amyloid beta-induced oxidative stress in the cerebrovascular dysfunctions associated with Alzheimer's disease. *J. Neurosci* 25, 11165–11174.

Tong, Y., Hocke, L. M., and Frederick, B. B. (2019). Low frequency systemic hemodynamic "noise" in resting state BOLD fMRI: characteristics, causes, implications, mitigation strategies, and applications. *Front. Neurosci.* 13:787. doi: 10.3389/fnins.2019.00787

Tosh, J. L., Rhymes, E. R., Mumford, P., Whittaker, H. T., Pulford, L. J., Noy, S. J., et al. (2021). Genetic dissection of down syndrome-associated alterations in APP/amyloid-beta biology using mouse models. *Sci. Rep.* 11:5736. doi: 10.1038/s41598-021-85062-3

Trapp, B. D., and Stys, P. K. (2009). Virtual hypoxia and chronic necrosis of demyelinated axons in multiple sclerosis. *Lancet Neurol.* 8, 280–291. doi: 10.1016/S1474-4422(09)70043-2

Tregellas, J. R., Davalos, D. B., Rojas, D. C., Waldo, M. C., Gibson, L., Wylie, K., et al. (2007). Increased hemodynamic response in the hippocampus, thalamus and prefrontal cortex during abnormal sensory gating in schizophrenia. *Schizophr. Res.* 92, 262–272. doi: 10.1016/j.schres.2006.12.033

Turner, R. J., and Sharp, F. R. (2016). Implications of MMP9 for blood brain barrier disruption and hemorrhagic transformation following ischemic stroke. *Front. Cell. Neurosci.* 10:56. doi: 10.3389/fncel.2016.00056

Uranova, N. A., Zimina, I. S., Vikhreva, O. V., Krukov, N. O., Rachmanova, V. I., and Orlovskaya, D. D. (2010). Ultrastructural damage of capillaries in the neocortex in schizophrenia. *World J. Biol. Psychiatry* 11, 567–578. doi: 10.3109/15622970903414188

Uratani, M., Ota, T., Iida, J., Okazaki, K., Yamamuro, K., Nakanishi, Y., et al. (2019). Reduced prefrontal hemodynamic response in pediatric autism spectrum disorder measured with near-infrared spectroscopy. *Child Adolesc. Psychiatry Ment. Health* 13:29. doi: 10.1186/s13034-019-0289-9

Usta, A., Kilic, F., Demirdas, A., Isik, U., Doguc, D. K., and Bozkurt, M. (2021). Serum zonulin and claudin-5 levels in patients with schizophrenia. *Eur. Arch. Psychiatry Clin. Neurosci.* 271, 767–773. doi: 10.1007/s00406-020-01152-9

van de Haar, H., Burgmans, S., Jansen, J., van Osch, M., van Buchem, M., Muller, M., et al. (2016). Blood-Brain barrier leakage in patients with early Alzheimer disease. *Radiology* 281, 527–535. doi: 10.1148/radiol.2016152244

Van Dyken, P., and Lacoste, B. (2018). Impact of metabolic syndrome on neuroinflammation and the blood–brain barrier. *Front. Neurosci.* 12:930. doi: 10.3389/fnins.2018.00930

Varga, A. W., Johnson, G., Babb, J. S., Herbert, J., Grossman, R. I., and Inglese, M. (2009). White matter hemodynamic abnormalities precede sub-cortical gray matter changes in multiple sclerosis. *J. Neurol. Sci.* 282, 28–33. doi: 10.1016/j.jns.2008.12.036

Verstraeten, A., Theuns, J., and Van Broeckhoven, C. (2015). Progress in unraveling the genetic etiology of Parkinson disease in a genomic era. *Trends Genet.* 31, 140–149. doi: 10.1016/j.tig.2015.01.004

Vijayakumar, N. T., and Judy, M. V. (2016). Autism spectrum disorders: integration of the genome, transcriptome and the environment. *J. Neurol. Sci.* 364, 167–176. doi: 10.1016/j.jns.2016.03.026

Vinters, H. V., Secor, D. L., Read, S. L., Frazee, J. G., Tomiyasu, U., Stanley, T. M., et al. (1994). Microvasculature in brain biopsy specimens from patients with Alzheimer's disease: an immunohistochemical and ultrastructural study [Research Support, U.S. Gov't, P.H.S.]. *Ultrastruct. Pathol.* 18, 333–348.

Vostrikov, V., Orlovskaya, D. D., and Uranova, N. A. (2008). Deficit of pericapillary oligodendrocytes in the prefrontal cortex in schizophrenia. *World J. Biol. Psychiatry* 9, 34–42. doi: 10.1080/15622970701210247

Wada, K., Arai, H., Takahashi, M., Fukae, J., Oizumi, H., Yasuda, T., et al. (2006). Expression levels of vascular endothelial growth factor and its receptors in Parkinson's disease. *Neuroreport* 17, 705–709. doi: 10.1097/01.wnr.0000215769.71657.65

Walchli, T., Wacker, A., Frei, K., Regli, L., Schwab, M. E., Hoerstrup, S. P., et al. (2015). Wiring the vascular network with neural cues: a CNS perspective. *Neuron* 87, 271–296. doi: 10.1016/j.neuron.2015.06.038

Walker, F. O. (2007). Huntington's disease [Review]. *Lancet* 369, 218–228. doi: 10.1016/S0140-6736(07)60111-1

Wan, W., Cao, L., Liu, L., Zhang, C., Kalionis, B., Tai, X., et al. (2015). Abeta(1-42) oligomer-induced leakage in an in vitro blood-brain barrier model is associated with up-regulation of RAGE and metalloproteinases, and down-regulation of tight junction scaffold proteins. *J. Neurochem.* 134, 382–393. doi: 10.1111/jnc.13122

Wang, T., Zhan, W., Chen, Q., Chen, N., Zhang, J., Liu, Q., et al. (2016). Altered resting-state ascending/descending pathways associated with the posterior thalamus in migraine without aura. *Neuroreport* 27, 257–263. doi: 10.1097/WNR.0000000000000529

Wardlaw, J. M., Farrall, A., Armitage, P. A., Carpenter, T., Chappell, F., Doubal, F., et al. (2008). Changes in background blood-brain barrier integrity between lacunar and cortical ischemic stroke subtypes. *Stroke* 39, 1327–1332. doi: 10.1161/STROKEAHA.107.500124

Wasmuth, J. J., Hewitt, J., Smith, B., Allard, D., Haines, J. L., Skarecky, D., et al. (1988). A highly polymorphic locus very tightly linked to the Huntington's disease gene [Research Support, Non-U.S. Gov't Research Support, U.S. Gov't, P.H.S.]. *Nature* 332, 734–736. doi: 10.1038/332734a0

Watanabe, C., Imaizumi, T., Kawai, H., Suda, K., Honma, Y., Ichihashi, M., et al. (2020). Aging of the vascular system and neural diseases. *Front. Aging Neurosci.* 12:557384. doi: 10.3389/fnagi.2020.557384

Watson, A. N., Berthiaume, A.-A., Faino, A. V., McDowell, K. P., Bhat, N. R., Hartmann, D. A., et al. (2020). Mild pericyte deficiency is associated with aberrant brain microvascular flow in aged PDGFRβ+/- mice. *J. Cereb. Blood Flow Metab.* 40, 2387–2400. doi: 10.1177/0271678X19900543

Weiss, N., Miller, F., Cazaubon, S., and Couraud, P. O. (2009). The blood-brain barrier in brain homeostasis and neurological diseases. *Biochim. Biophys. Acta* 1788, 842–857. doi: 10.1016/j.bbamem.2008.10.022

Whiteus, C., Freitas, C., and Grutzendler, J. (2014). Perturbed neural activity disrupts cerebral angiogenesis during a postnatal critical period. *Nature* 505, 407–411. doi: 10.1038/nature12821

Wild, E. J., and Fox, N. C. (2009). Serial volumetric MRI in Parkinsonian disorders. *Mov. Disord.* 24(Suppl. 2), S691–S698. doi: 10.1002/mds.22500

Willis, K. J., and Hakim, A. M. (2013). Stroke prevention and cognitive reserve: emerging approaches to modifying risk and delaying onset of dementia. *Front. Neurol.* 4:13. doi: 10.3389/fneur.2013.00013

Wiseman, F. K., Pulford, L. J., Barkus, C., Liao, F., Portelius, E., Webb, R., et al. (2018). Trisomy of human chromosome 21 enhances amyloid-beta deposition independently of an extra copy of APP. *Brain* 141, 2457–2474. doi: 10.1093/brain/awy159

Wolf, R. C., Gron, G., Sambataro, F., Vasic, N., Wolf, N. D., Thomann, P. A., et al. (2011). Magnetic resonance perfusion imaging of resting-state cerebral blood flow in preclinical Huntington's disease. *J. Cereb. Blood Flow Metab.* 31, 1908–1918. doi: 10.1038/jcbfm.2011.60

Wu, Z., Guo, H., Chow, N., Sallstrom, J., Bell, R. D., Deane, R., et al. (2005). Role of the MEOX2 homeobox gene in neurovascular dysfunction in Alzheimer disease. *Nat. Med.* 11, 959–965. doi: 10.1038/nm1287

Wuerfel, J., Bellmann-Strobl, J., Brunecker, P., Aktas, O., McFarland, H., Villringer, A., et al. (2004). Changes in cerebral perfusion precede plaque formation in multiple sclerosis: a longitudinal perfusion MRI study. *Brain* 127(Pt 1), 111–119. doi: 10.1093/brain/awh007

Xiao, M., Xiao, Z. J., Yang, B., Lan, Z., and Fang, F. (2020). Blood-Brain barrier: more contributor to disruption of central nervous system homeostasis than victim in neurological disorders. *Front. Neurosci.* 14:764. doi: 10.3389/fnins.2020.00764

Yamada, H., Sadato, N., Konishi, Y., Muramuto, S., Kimura, K., Tanaka, M., et al. (2000). A milestone for normal development of the infantile brain detected by functional MRI. *Neurology* 55, 218–223.

Yang, P., Pavlovic, D., Waldvogel, H., Dragunow, M., Synek, B., Turner, C., et al. (2015). String vessel formation is increased in the brain of Parkinson disease. *J. Parkinsons Dis.* 5, 821–836. doi: 10.3233/JPD-140454

Yerys, B. E., Herrington, J. D., Bartley, G. K., Liu, H. S., Detre, J. A., and Schultz, R. T. (2018). Arterial spin labeling provides a reliable neurobiological marker of autism spectrum disorder. *J. Neurodev. Disord.* 10:32. doi: 10.1186/s11689-018-9250-0

Zarow, C., Barron, E., Chui, H. C., and Perlmutter, L. S. (1997). Vascular basement membrane pathology and Alzheimer's disease. *Ann. N. Y. Acad. Sci.* 826, 147–160.

Zhang, Z. G., Zhang, L., Jiang, Q., Zhang, R., Davies, K., Powers, C., et al. (2000). VEGF enhances angiogenesis and promotes blood-brain barrier leakage in the ischemic brain. *J. Clin. Invest.* 106, 829–838. doi: 10.1172/JCI9369

Zhao, Z., Sagare, A. P., Ma, Q., Halliday, M. R., Kong, P., Kisler, K., et al. (2015). Central role for PICALM in amyloid-beta blood-brain barrier transcytosis and clearance. *Nat. Neurosci.* 18, 978–987. doi: 10.1038/nn.4025

Zheng, W., Cui, B., Han, Y., Song, H., Li, K., He, Y., et al. (2019). Disrupted regional cerebral blood flow, functional activity and connectivity in Alzheimer's disease:

a combined ASL perfusion and resting state fMRI Study. *Front. Neurosci.* 13:738. doi: 10.3389/fnins.2019.00738

Zheng, Z., and Diamond, M. I. (2012). Huntington disease and the huntingtin protein [Review]. *Prog. Mol. Biol. Transl. Sci.* 107, 189–214. doi: 10.1016/B978-0-12-385883-2.00010-2

Zhu, J., Zhuo, C., Xu, L., Liu, F., Qin, W., and Yu, C. (2017). Altered coupling between resting-state cerebral blood flow and functional connectivity in schizophrenia. *Schizophr. Bull.* 43, 1363–1374. doi: 10.1093/schbul/sbx051

Zhuo, C., Zhu, J., Qin, W., Qu, H., Ma, X., and Yu, C. (2017). Cerebral blood flow alterations specific to auditory verbal hallucinations in schizophrenia. *Br. J. Psychiatry* 210, 209–215. doi: 10.1192/bjp.bp.115.174961

Zilbovicius, M., Boddaert, N., Belin, P., Poline, J.-B., Remy, P., Mangin, J.-F., et al. (2000). Temporal lobe dysfunction in childhood autism: a PET study. *Am. J. Psychiatry* 157, 1988–1993.

Zlokovic, B. V. (2005). Neurovascular mechanisms of Alzheimer's neurodegeneration. *Trends Neurosci.* 28, 202–208. doi: 10.1016/j.tins.2005.02.001

Zlokovic, B. V. (2008). The blood-brain barrier in health and chronic neurodegenerative disorders. *Neuron* 57, 178–201. doi: 10.1016/j.neuron.2008.01.003

Zlokovic, B. V. (2011). Neurovascular pathways to neurodegeneration in Alzheimer's disease and other disorders. *Nat. Rev. Neurosci.* 12, 723–738. doi: 10.1038/nrn3114

Conflict of Interest: The authors declare that the research was conducted in the absence of any commercial or financial relationships that could be construed as a potential conflict of interest.

Publisher's Note: All claims expressed in this article are solely those of the authors and do not necessarily represent those of their affiliated organizations, or those of the publisher, the editors and the reviewers. Any product that may be evaluated in this article, or claim that may be made by its manufacturer, is not guaranteed or endorsed by the publisher.

Appendix E- Manuscript VI

Association to hypothesis: This manuscript puts in perspective the need to identify other targets than neurons in the context of ASD. It emphasized the requirement of having a full picture of these disorders by unraveling the vascular components of ASD and their involvement in brain development. This manuscript summarized the current cerebrovascular knowledge on ASD.

Current manuscript status: This manuscript was published in *Neuroscience Insights* in 2024.

Author Contributions : B.L. and J.O. conceived the idea. All authors participated in drafting and editing the manuscript.

A Vascular-Centric Approach to Autism Spectrum Disorders

Neuroscience Insights
Volume 19: 1–4

DOI: 10.1177/26331055241235921

Julie Ouellette[1,2], Elizabeth E Crouch[3,4], Jean-Luc Morel[5,6], Vanessa Coelho-Santos[7,8,9] and Baptiste Lacoste[1,2,10]

[1]Neuroscience Program, Ottawa Hospital Research Institute, Ottawa, ON, Canada. [2]Faculty of Medicine, Department of Cellular and Molecular Medicine, University of Ottawa, Ottawa, ON, Canada. [3]Department of Pediatrics, University of California San Francisco, San Francisco, CA, USA. [4]The Eli and Edythe Broad Center of Regeneration Medicine and Stem Cell Research, University of California San Francisco, San Francisco, CA, USA. [5]University Bordeaux, CNRS, INCIA, UMR 5287, Bordeaux, France. [6]University Bordeaux, CNRS, IMN, UMR 5293, Bordeaux, France. [7]Institute for Nuclear Sciences Applied to Health, University of Coimbra, Coimbra, Portugal. [8]Coimbra Institute for Biomedical Imaging and Translational Research, University of Coimbra, Coimbra, Portugal. [9]Faculty of Medicine, Institute of Physiology, University of Coimbra, Coimbra, Portugal. [10]University of Ottawa Brain and Mind Research Institute, Ottawa, ON, Canada.

ABSTRACT: Brain development and function are highly reliant on adequate establishment and maintenance of vascular networks. Early impairments in vascular health can impact brain maturation and energy metabolism, which may lead to neurodevelopmental anomalies. Our recent work not only provides novel insights into the development of cerebrovascular networks but also emphasizes the importance of their well-being for proper brain maturation. In particular, we have demonstrated that endothelial dysfunction in autism spectrum disorders (ASD) mouse models is causally related to altered behavior and brain metabolism. In the prenatal human brain, vascular cells change metabolic states in the second trimester. Such findings highlight the need to identify new cellular and molecular players in neurodevelopmental disorders, raising awareness about the importance of a healthy vasculature for brain development. It is thus essential to shift the mostly neuronal point of view in research on ASD and other neurodevelopmental disorders to also include vascular and metabolic features.

KEYWORDS: Autism, cerebrovascular, metabolism, neurodevelopment, angiogenesis, endothelium

RECEIVED: December 18, 2023. **ACCEPTED:** February 13, 2024.

TYPE: Perspective

FUNDING: J.O. is supported by a CIHR Doctoral Research Award.

DECLARATION OF CONFLICTING INTERESTS: The author(s) declared no potential conflicts of interest with respect to the research, authorship, and/or publication of this article.

CORRESPONDING AUTHOR: Baptiste Lacoste, Faculty of Medicine, Department of Cellular and Molecular Medicine, University of Ottawa, 451 Smyth Rd, Ottawa, ON K1H 8M5, Canada. Email: blacoste@uottawa.ca

Brain Health Relies on Neurovascular Interactions

The brain is a relatively small organ, approximately 2% of body mass, yet it consumes close to one-quarter of the total body energy available at rest. In other words, about 25% of the cardiac output is dedicated to the brain's energy needs for sustaining function of neural circuits.[1] The elevated energy demands, and low capacity to store energy fuel, together imply that the maturing brain becomes reliant on an uninterrupted supply of oxygen and nutrients from the bloodstream and in turn must efficiently use energy substrates as well as remove waste products. The ensemble of biological processes put in place to regulate delivery, intake, and utilization of energy sources is known as metabolism. During brain development, the formation and maturation of neurons, blood vessels, and glial cells are precisely orchestrated to ensure proper blood supply to withstand healthy brain growth. These "neuro-vascular" interactions actively regulate energy allocation for daily brain functioning, orchestrating a tight balance known as metabolic homeostasis. The synergistic function of vascular endothelial cells (lining the blood vessel wall), glial cells (eg, astrocytes and microglia), smooth muscle cells, pericytes, and neurons is required to uphold brain metabolism. The anatomical substrate of these multicellular interactions is known as the neurovascular unit (NVU), or neuro-glio-vascular unit, which regulates energy import and utilization. Healthy brain growth and function rely not only on the establishment of neuronal networks, but also on key vascular features: (i) The establishment of dense vascular networks (through neovascularization and angiogenesis) for effective brain blood perfusion; (ii) The formation and function of a tight blood-brain barrier to maintain a controlled environment, providing suitable conditions for cellular health; and (iii) The regulation of cerebral blood flow to match the demands of neural cells through the phenomenon of neurovascular coupling (whereby increases in neural network activity lead to increased regional cerebral blood flow). However, neurovascular coupling is not functional until approximately 3 weeks of age in rodents and at full term birth in humans.[2] It is hypothesized that the developing brain exists in a state of relative hypoxia, where metabolic demands are not satisfied by a corresponding increase in blood flow.[2] Hence, it must rely on alternative mechanisms to support demands imposed by its rapid expansion. In both humans and mice, developing brain vessels also arise from veins and venules.[3,4] Overall, genetic programs and hypoxia must act as major drivers for vascular

growth during embryonic development, and neuronal activity promotes brain angiogenesis early after birth.[1,5]

Consequently, common rules apply for guiding neuronal and vascular development, and molecules secreted by endothelial cells modulate the genesis and fate of neuronal and glial progenitors.[4,6] In this context, it becomes intuitive that early abnormalities in the establishment and function of the NVU will affect brain function in the long term. This emphasizes the need of investigating non-neuronal cells in the context of neurodevelopmental disorders, and the importance of shifting the neuronal point of view when studying the brain.

Neurodevelopmental Disorders Are Not Just About Neurons

Several inherited or acquired neurological disorders can originate from, or be perpetuated by, a defective brain vasculature. For instance, CADASIL (cerebral autosomal dominant arteriopathy with subcortical infarcts and leukoencephalopathy) and *COL4A1* mutations, small vessel diseases, lead to cerebrovascular dysregulation and in turn to cognitive impairment.[7] In addition, onset and/or progression of various neurological disorders have been associated with anomalies in cerebrovascular networks, including schizophrenia, dementia, and neurodegenerative disorders like multiple sclerosis or Alzheimer's disease.[8] Moreover, as reviewed recently,[8] neurodevelopmental and neurodegenerative diseases share similar vascular abnormalities despite emerging at different stages of life. However, the links between cerebrovascular deficits and neurodevelopmental disorders are only starting to emerge.

Considering the tightly regulated metabolism of proper brain development, disruption of energy supply and/or utilization during critical developmental periods can irreversibly impact brain maturation. The young brain is indeed particularly vulnerable to shortfalls in blood supply or defects in energy metabolism, and early metabolic disturbances may lead to atypical brain maturation and altered cognitive development, such as in autism spectrum disorders (ASD). ASD represent a set of complex neurodevelopmental disorders that impact attention, memory, motor coordination, language, speech, and social interactions. While ASD have environmental and genetic origins, the underlying causes remain largely unknown. The ASD brain has been characterized with exaggerated rates of growth in the first year of life, altered neuronal patterning, increased prevalence of seizures, and enhanced expression of neurotransmitter receptors. The development of genetically engineered rodent models have made it possible to characterize mutations linked to ASD such as in *Shank3, Neurexin1, Syngap1*, or *Mecp2* genes known to normally control synaptic transmission, neuronal morphology, and excitability, as well as animal behavior. These mouse models of ASD have demonstrated abnormal corticogenesis during postnatal development, cortical neuronal asynchrony, spontaneous seizures, and synaptic defects. While these models enable the clarification of neuronal underpinnings of ASD symptoms, the contribution of vascular and metabolic features to ASD pathophysiology have been largely overlooked. This critical knowledge gap now represents a growing focus in neuroscience.

Recent studies have obtained strong evidence demonstrating structural and functional cerebrovascular deficits in ASD patients and mouse models. In humans, evaluations by functional magnetic resonance imaging, positron emission tomography, or arterial spin labeling revealed cerebral hypoperfusion in approximately 75% of children with ASD compared with healthy individuals.[8] In a mouse model, we revealed a surprising contribution of vascular deficits to the pathogenesis of 16p11.2 deletion syndrome,[9] one of the most common genetic causes of human ASD. Copy number variations associated with psychiatric conditions are found at a higher frequency in the human 16p11.2 locus. The 16p11.2 deletion (heterozygous) comprises loss of approximately 30 highly conserved genes, and carriers display intellectual disabilities, learning and communication deficits, large head size, an increased prevalence of seizures, as well as metabolic problems. Among the conserved genes found in the human 16p11.2 locus, several genes are involved in maintaining cell function and metabolism. For instance, the genes *Taok2* and *Kctd13* regulate neuronal differentiation and maturation, while *Doc2A* and *Prrt2* control neuronal excitability. *Mapk3* regulates endothelial cell proliferation and migration, *Tmem219* and *Coro1A* negatively modulate endothelial cell apoptosis, and *Maz1* potentiates vascular growth. In addition, *AldoA* regulates glycolysis and gluconeogenesis. Working with the widely accepted *16p11.2*$^{df/+}$ mouse model[10] of 16p11.2 deletion syndrome, we revealed a causal relationship between cerebrovascular endothelial deficits and neuronal/behavioral abnormalities.[9] Neurovascular coupling was attenuated in adult *16p11.2*$^{df/+}$ male mice, which was attributed to endothelial dysfunction following quantification of cerebral artery responses to vasomodulators. Although adult vessel density was unchanged in *16p11.2*$^{df/+}$ mice, two-week old *16p11.2*$^{df/+}$ male mice displayed impaired brain angiogenesis compared with control littermates, which was confirmed in vitro as an endothelial cell autonomous deficit. Deep RNA-sequencing analysis of the *16p11.2*$^{df/+}$ mouse brain endothelial transcriptome revealed important changes in the expression of genes involved in the regulation of angiogenesis such as *Angpt2* and *Apln*. These results altogether demonstrated altered endothelial function caused by 16p11.2 haploinsufficiency. From this, we suggested that vascular factors may participate in the onset of ASD, at least in mice. To test this, we generated a mouse model with an endothelial-specific 16p11.2 haploinsufficiency. Notably, brain endothelial cells have essential roles in brain health including regulating vessel tone, chemical exchange with astrocytes and neurons, protecting the brain via the blood brain barrier, as well as releasing vesicles as Weibel-Palade bodies to regulate hemostasis, inflammation and angiogenesis through trophic factors. The endothelial-specific

16p11.2 deletion model displayed ASD-related behaviors,[9] highlighting the necessity of functional endothelial cells for maintaining proper brain function.

Brain Metabolism in ASD

Glucose transporter-1 deficiency syndrome (GLUT-1 DS) is an infantile-onset neurodevelopmental disorder characterized by pediatric epileptic encephalopathy and a movement disorder comprised of ataxia and spasticity. Brain hypometabolism in GLUT-1 DS has been compared to the Alzheimer's disease brain, with the latter also showing signs of reduced GLUT-1 function.[11] Intriguingly, *16p11.2$^{df/+}$* mice displayed striking similarities with mouse models of GLUT-1 DS, including reduced brain angiogenesis, enhanced evoked neuronal activity, and altered behaviors with hyperactivity.[9,11] Anomalies in brain metabolism have been identified in Alzheimer's disease, schizophrenia, and ASD[8] but the underlying mechanisms in ASD remain to be defined. As neuronal, vascular, and glial cells are metabolically interdependent to ensure proper brain maturation, it is expected that constitutive genetic mutations associated with ASD lead to perturbed cellular machinery and to brain metabolic imbalance. While we have identified that *16p11.2$^{df/+}$* mice display striking sex-specific differences in body composition, energy expenditure, and concentrations of circulating plasma metabolites related to mitochondrial function, suggesting that constitutive 16p11.2 haploinsufficiency also affects whole-body metabolism,[12] we have recently demonstrated brain metabolism alterations in adult *16p11.2$^{df/+}$* males. These include increased glucose uptake, changes in glucose and lactate utilization, as well as altered cortical metabolite profiles.[13]

Often, metabolic discrepancies in ASD rodent models are associated with concurrent mitochondrial dysfunction. In endothelial cells from adult *16p11.2$^{df/+}$* males, we revealed a reduced number of mitochondria and a lack of transcription factor NT-PGC-1α, a truncated variant of Peroxisome proliferator-activated receptor gamma coactivator 1-alpha (PGC-1α), a master regulator of mitochondrial biogenesis.[13] In mice with endothelial-specific 16p11.2 haploinsufficiency, brain glucose metabolism alterations were also observed, suggesting that these alterations are secondary to (or compensatory to) endothelial dysfunction. Nevertheless, the cellular and molecular mechanisms of these alterations remain to be fully elucidated. These findings open new questions in ASD brain metabolism research field: How are metabolites utilized during the activation of these compensatory mechanisms? When can these changes be detected during brain development? What is the long-term impact of metabolic shifts on brain function? Can these metabolic changes be targeted for future therapeutic solutions? With such metabolic link to ASD in mind, existence of vascular and metabolic players must be taken into consideration when investigating ASD risk factors.[13]

Prematurity and Perinatal Hypoxia as Risk Factors for ASD

Separate from genetic etiologies, prematurity is an independent risk factor for ASD.[14] Germinal matrix hemorrhage (GMH), a feared complication of extremely premature birth, can cause hydrocephalus and stroke immediately, cerebral palsy, intellectual disability, ASD, and/or psychiatric disorders in the long-term.[15] While the exact cause of GMH remains elusive, it is hypothesized to occur due to a combination of disturbed oxygen delivery and vascular immaturity in this particular brain region.[16] With emerging evidence, another way to frame GMH may reflect metabolic failure in neurovascular coupling. For example, brain vascular cells were shown to be exquisitely sensitive to changes in oxygen tension during development in a mouse model of GMH.[17] Importantly, periventricular blood vessels were the last to mature. Typically, brain endothelial cells are thought to primarily use glycolysis as an energy source.[11] In human brain development, endothelial cells may switch from oxidative phosphorylation to glycolysis during the second trimester.[4] These differential metabolic states may underlie this vulnerable window for GMH and the subsequent ASD. Future investigations will need to map out the temporal and spatial metabolic programs of neurovascular dependence in the human brain to address germinal matrix hemorrhage.

Perinatal hypoxia is another environmental condition significantly contributing to dysfunction in the central nervous system and leading to neurodevelopmental disorders.[18] It is characterized by insufficient oxygen delivery to the fetus before, during, or after birth. Chronic intermittent hypoxia (CIH), more prevalent than continuous hypoxia in early postnatal life (often stemming from sleep-disordered breathing), emerges as a notable contributor to disability in neonates. This impact is particularly noteworthy in premature infants, especially those with extremely low birth weight. Evidence indicates that CIH is associated with heightened neuroinflammation and oxidative stress, impacting the integrity of both gray and white matter and contributing to cognitive impairment. While the specific effects of CIH on cerebrovascular development remain poorly understood, CIH may induce enduring alterations in cerebrovascular structure and function, possibly by disrupting the finely regulated process of developmental angiogenesis.[19]

Concluding Remarks

Worldwide, 1 in 160 children has been diagnosed with ASD (World Health Organization [WHO] fact sheet on ASD, 2021). As ASD incidences are on the rise, exploring novel avenues for care represents an urgent clinical and economic need. Outcomes of innovative ASD research will promote the identification of new players in its pathogenesis, which is an essential prerequisite for developing the novel diagnostics and therapeutics that are desperately needed for patients, their relatives, and caregivers. Since most studies have focused on neuronal aspects of ASD, looking at neurodevelopmental disorders through the

vascular lens is a much-needed paradigm shift. Insight from such game-changing studies will allow scientists to gain novel understanding into how the vasculature control critical features of brain organization and function.

Author Contributions

B.L. and J.O. conceived the idea. All authors participated in drafting and editing the manuscript.

ORCID iD

Baptiste Lacoste https://orcid.org/0000-0002-1922-8801

REFERENCES

1. Lacoste B, Gu C. Control of cerebrovascular patterning by neural activity during postnatal development. *Mech Dev*. 2015;138 Pt 1:43-49.
2. Kozberg MG, Ma Y, Shaik MA, Kim SH, Hillman EMC. Rapid postnatal expansion of neural networks occurs in an environment of altered neurovascular and neurometabolic coupling. *J Neurosci*. 2016;36:6704-6717.
3. Coelho-Santos V, Berthiaume AA, Ornelas S, Stuhlmann H, Shih AY. Imaging the construction of capillary networks in the neonatal mouse brain. *Proc Natl Acad Sci USA*. 2021;118:e2100866118. doi:10.1073/pnas.2100866118
4. Crouch EE, Bhaduri A, Andrews MG, et al. Ensembles of endothelial and mural cells promote angiogenesis in prenatal human brain. *Cell*. 2022;185:3753-3769.e18.
5. Lacoste B, Comin CH, Ben-Zvi A, et al. Sensory-related neural activity regulates the structure of vascular networks in the cerebral cortex. *Neuron*. 2014;83:1117-1130.
6. Carmeliet P, Tessier-Lavigne M. Common mechanisms of nerve and blood vessel wiring. *Nature*. 2005;436:193-200.
7. Lanfranconi S, Markus HS. COL4A1 mutations as a monogenic cause of cerebral small vessel disease: a systematic review. *Stroke*. 2010;41:e513-e518.
8. Ouellette J, Lacoste B. From neurodevelopmental to neurodegenerative disorders: the vascular continuum. *Front Aging Neurosci*. 2021;13:749026.
9. Ouellette J, Toussay X, Comin CH, et al. Vascular contributions to 16p11.2 deletion autism syndrome modeled in mice. *Nat Neurosci*. 2020;23:1090-1101.
10. Horev G, Ellegood J, Lerch JP, et al. Dosage-dependent phenotypes in models of 16p11.2 lesions found in autism. *Proc Natl Acad Sci USA*. 2011;108:17076-17081.
11. Tang M, Monani UR. Glut1 deficiency syndrome: new and emerging insights into a prototypical brain energy failure disorder. *Neurosci Insights*. 2021;16:1-7.
12. Menzies C, Naz S, Patten D, et al. Distinct basal metabolism in three mouse models of neurodevelopmental disorders. *eNeuro*. 2021;8:ENEURO.0292-20.2021.
13. Béland-Millar A, Kirby A, Truong Y, et al. 16p11.2 haploinsufficiency reduces mitochondrial biogenesis in brain endothelial cells and alters brain metabolism in adult mice. *Cell Rep*. 2023;42:112485.
14. Limperopoulos C, Bassan H, Sullivan NR, et al. Positive screening for autism in ex-preterm infants: prevalence and risk factors. *Pediatrics*. 2008;121:758-765.
15. Whitaker AH, Feldman JF, Lorenz JM, et al. Neonatal head ultrasound abnormalities in preterm infants and adolescent psychiatric disorders. *Arch Gen Psychiatry*. 2011;68:742-752.
16. Ballabh P. Intraventricular hemorrhage in premature infants: mechanism of disease. *Pediatr Res*. 2010;67:1-8.
17. Licht T, Dor-Wollman T, Ben-Zvi A, Rothe G, Keshet E. Vessel maturation schedule determines vulnerability to neuronal injuries of prematurity. *J Clin Investig*. 2015;125:1319-1328.
18. Pașca AM, Park JY, Shin HW, et al. Human 3D cellular model of hypoxic brain injury of prematurity. *Nat Med*. 2019;25:784-791.
19. Coelho-Santos V, Cruz AN, Shih AY. Does perinatal intermittent hypoxia affect cerebrovascular network development? *Dev Neurosci*. 2024;46:44-54.